MICROBIAL CONTROL OF THE NITROGEN CYCLE

EDITED BY: Lourdes Girard, Juan Sanjuan and Maria J. Delgado
PUBLISHED IN: Frontiers in Microbiology

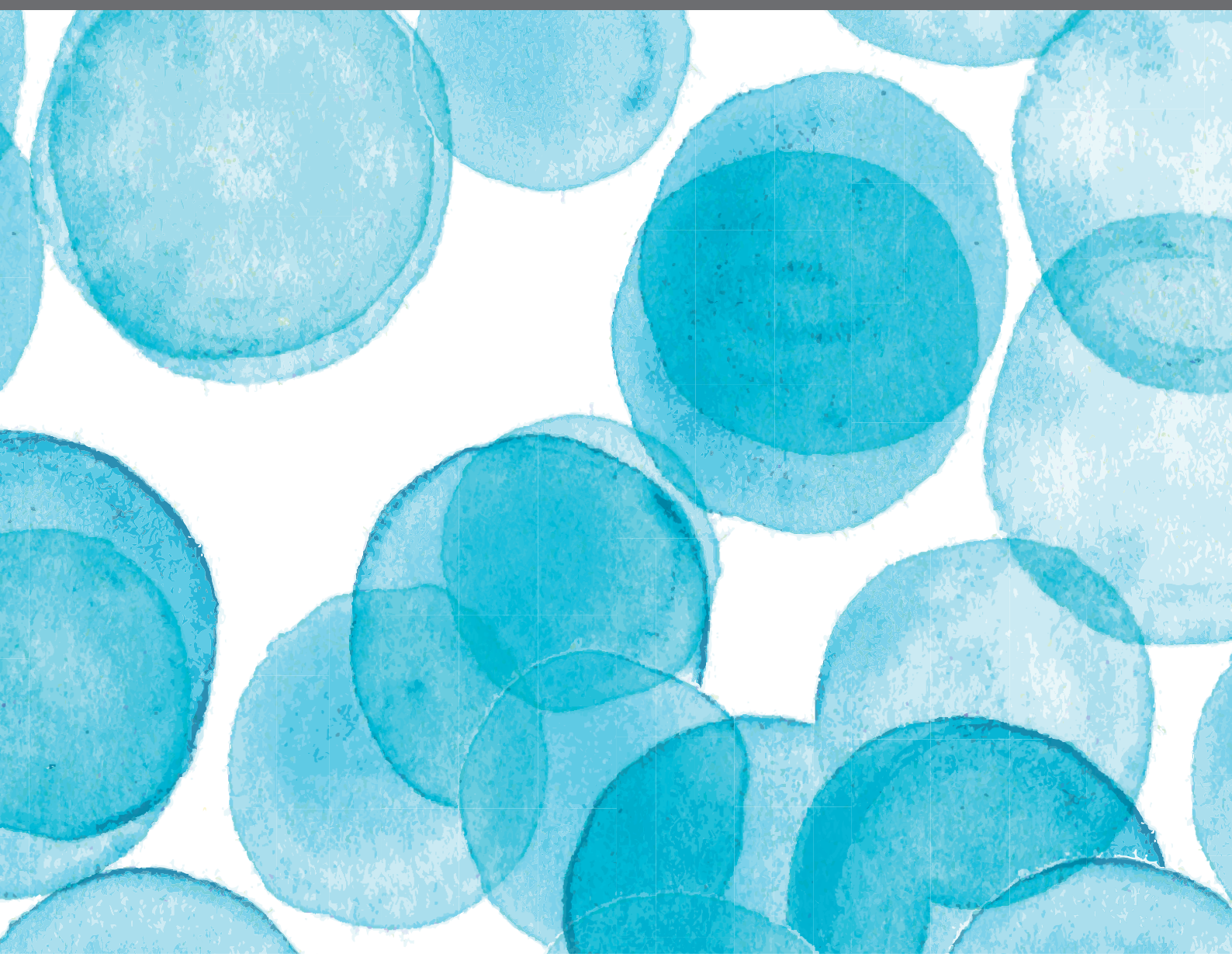

frontiers Research Topics

ISSN 1664-8714
ISBN 978-2-88963-816-1
DOI 10.3389/978-2-88963-816-1

About Frontiers

Frontiers is more than just an open-access publisher of scholarly articles: it is a pioneering approach to the world of academia, radically improving the way scholarly research is managed. The grand vision of Frontiers is a world where all people have an equal opportunity to seek, share and generate knowledge. Frontiers provides immediate and permanent online open access to all its publications, but this alone is not enough to realize our grand goals.

Frontiers Journal Series

The Frontiers Journal Series is a multi-tier and interdisciplinary set of open-access, online journals, promising a paradigm shift from the current review, selection and dissemination processes in academic publishing. All Frontiers journals are driven by researchers for researchers; therefore, they constitute a service to the scholarly community. At the same time, the Frontiers Journal Series operates on a revolutionary invention, the tiered publishing system, initially addressing specific communities of scholars, and gradually climbing up to broader public understanding, thus serving the interests of the lay society, too.

Dedication to Quality

Each Frontiers article is a landmark of the highest quality, thanks to genuinely collaborative interactions between authors and review editors, who include some of the world's best academicians. Research must be certified by peers before entering a stream of knowledge that may eventually reach the public - and shape society; therefore, Frontiers only applies the most rigorous and unbiased reviews.
Frontiers revolutionizes research publishing by freely delivering the most outstanding research, evaluated with no bias from both the academic and social point of view. By applying the most advanced information technologies, Frontiers is catapulting scholarly publishing into a new generation.

What are Frontiers Research Topics?

Frontiers Research Topics are very popular trademarks of the Frontiers Journals Series: they are collections of at least ten articles, all centered on a particular subject. With their unique mix of varied contributions from Original Research to Review Articles, Frontiers Research Topics unify the most influential researchers, the latest key findings and historical advances in a hot research area! Find out more on how to host your own Frontiers Research Topic or contribute to one as an author by contacting the Frontiers Editorial Office: researchtopics@frontiersin.org

MICROBIAL CONTROL OF THE NITROGEN CYCLE

Topic Editors:
Lourdes Girard, National Autonomous University of Mexico, Mexico
Juan Sanjuan, Consejo Superior de Investigaciones Científicas (CSIC), Spain
Maria J. Delgado, Consejo Superior de Investigaciones Científicas (CSIC), Spain

Citation: Girard, L., Sanjuan, J., Delgado, M. J., eds. (2020). Microbial Control of the Nitrogen Cycle. Lausanne: Frontiers Media SA. doi: 10.3389/978-2-88963-816-1

Table of Contents

frontiers in Microbiology

EDITORIAL
published: 14 May 2020
doi: 10.3389/fmicb.2020.00950

Editorial: Microbial Control of the Nitrogen Cycle

Juan Sanjuan[1]*, *María J. Delgado*[1] and *Lourdes Girard*[2]

[1] Departamento de Microbiología del Suelo y Sistemas Simbióticos, Estación Experimental del Zaidín, CSIC, Granada, Spain,
[2] Programa de Biología de Sistemas y Biología Sintética, Centro de Ciencias Genómicas, UNAM, Cuernavaca, Mexico

Keywords: nitrogen oxides, environmental pollution, climate change, sustainable food production, nitrogen fixation

Editorial on the Research Topic

Microbial Control of the Nitrogen Cycle

Plant biomass and productivity of many ecosystems are limited by the availability of reactive nitrogen, this is reduced or oxidized forms of N. Over the last century synthetic N fertilizers have undoubtedly helped to enhance crop yields, thus allowing an unprecedented growth of the world population. Despite this, nearly 80% of N fertilizer applied to crops does not reach human mouths but is lost to the environment in water run-off from fields, animal waste, and gas emissions. This N fertilizer abuse, particularly in rich countries, has strongly perturbed the biogeochemical N cycle with an unprecedented production and accumulation of reactive N in the biosphere that threatens human health and ecosystems biodiversity, and contributes to climate change. Optimizing N use and minimizing its negative impacts is a major challenge for the next decades (Galloway et al., 2013).

Microbes (bacteria and fungi) are main protagonists of all the major reactions in the N-cycle. Microbial activities that process nitrogen in soils and sediments are complex and highly challenging. Better understanding of these processes is important for improving the efficiency of agricultural practices that are essential for food production and environmental quality across the globe. Therefore, any technologies aiming at reducing the N problem must recognize the roles and potential applications of these N-cycle microbes, from diazotrophs to denitrifiers. These microbiotechnologies are necessary if we want to bring reactive N levels back within planet safety boundaries while ensuring crop productivity and food security (Steffen et al., 2015).

This Research Topic focused on the biotechnology of microbes and microbial processes which can directly or indirectly contribute to alleviate the N problem at local and/or global scales. Fifteen of 20 submitted manuscripts have been accepted for publication.

Five articles dealt with various aspects of nitrogenase and biological nitrogen fixation (BNF), the key bacterial process that converts atmospheric N_2 into reactive nitrogen accessible for living organisms. Three papers were on the nitrogen fixing symbioses between legume plants and soil rhizobia. Temprano-Vera et al. analyzed differences among *Sinorhizobium fredii* strains at nodulating various genotypes of *Glycine max* (soybean, the most widely produced legume) and *Glycine soja* (the wild ancestor of soybeans). Their results illustrate the complexity of genetic determinants of the soybean-rhizobia compatibility. Also concerning soybeans, Fernández et al. reported the importance of adaptation of the soybean symbiont *Bradyrhizobium japonicum* to microxic conditions for efficient nitrogen fixation, and identified novel genes subjected to posttranscriptional regulation during microxia which are important for symbiosis. Tsyganov et al. reported on the contribution of a legume nitrogen-fixing symbiosis to the plant tolerance to Cd, as well as its potential applications for phytoremediation and phytostabilization of soils with high Cd contents. Two other studies identified novel functions which are important for optimal nitrogen fixation in free-living diazotrophs, and therefore should be considered in current and future studies aiming at obtaining nitrogen-fixing plants by genetic engineering. Navarro-Rodríguez et al.

OPEN ACCESS

Edited by:
Marcus A. Horn,
Leibniz University Hannover, Germany

Reviewed by:
Peter Groffman,
The City University of New York, United States

****Correspondence:***
Juan Sanjuan
juan.sanjuan@eez.csic.es

Specialty section:
This article was submitted to Terrestrial Microbiology, a section of the journal Frontiers in Microbiology

Received: *05 February 2020*
Accepted: *21 April 2020*
Published: *14 May 2020*

Citation:
Sanjuan J, Delgado MJ and Girard L (2020) Editorial: Microbial Control of the Nitrogen Cycle. Front. Microbiol. 11:950. doi: 10.3389/fmicb.2020.00950

reported on the importance of the molybdenum storage protein MoSto for nitrogen fixation by *Azotobacter vinelandii* under Mo-limiting conditions. On another hand, Nonaka et al. described the essentiality of several proteins required for nitrogenase assembly during diazotrophic growth by the cyanobacterium *Leptolyngbya boryana*.

Another key process in the N cycle is denitrification, which has a strong impact in the environment through the production of reactive nitric oxide (NO) and the powerful greenhouse gas nitrous oxide (N_2O), with a strong potential to drive climate change. Olaya-Abril et al. have explored this process in *Paracoccus denitrificans* PD1222 through a quantitative proteomic analysis and have established key features of the denitrification metabolism, particularly the induction of enzymes of the TCA and glyoxylate cycles, together with enzymes that synthesize acetyl-CoA. On another hand, Liu B. et al. have monitored the kinetics of denitrification gene expression and NO, N_2O, and N_2 production in soils exposed to microxia. They concluded that regulatory strategies observed in individual isolates are also displayed in complex communities, emphasizing the need for successive sampling when identifying active key organisms. Two other manuscripts showed that in addition to denitrification, other microbial processes such as nitrate assimilation can be sources of NO and N_2O. Ruiz et al. reported that the pathway involving the assimilatory nitrate (NarB) and nitrite (NirB) reductases indirectly contribute to NO synthesis by cooperating with the denitrification pathway in *Sinorhizobium meliloti*. Hidalgo-García et al. demonstrated that in addition to its involvement in nitrate assimilation, NarB is also required for NO and N_2O production in *Rhizobium etli*. Nitrite produced by NarB from assimilatory nitrate reduction is detoxified by NirK and cNor denitrifying enzymes that convert nitrite into NO which in turn is reduced to N_2O, respectively.

Nitrification linked to denitrification constitutes an important biotic source of N_2O emissions from soils. The aerobic oxidation of ammonia (NH_3) to nitrite (NO_2^-) is carried out by ammonia oxidizing bacteria (AOB) or archaea (AOA) that also possess the enzymatic pathway to reduce NO_2^- to N_2O (Hu et al., 2015). In this regard, the changes in the microbial communities and N_2O emissions due to common soil management practices were investigated in various papers. The impact of urea fertilization on the nitrifier microbial populations was evaluated by Staley et al. in eight contrasting agricultural soil types. Their results indicate that while bacterial and archeal diversity is negatively affected, high urea applications favor particular strains or species of nitrifying genera such as *Nitrobacter*, *Nitrospira,* and *Nitrosospira*, regardless the soil type. In the same line, Lourenço et al. reported that soil amendments with organic vinasses and inorganic N fertilizer lead to increased N_2O emissions which correlate with enhanced abundance of AOB, particularly *Nitrosospira*. On another hand, Fang et al. reported that application of dazomet, a microbicide used to control soil pathogens, causes reversible changes in bacterial community compositions and reduces the abundance of N-cycle functional genes, however N_2O production rates increased in correlation with NH_3, dissolved amino acids and microbial biomass nitrogen contents. Tomasek et al. provided evidence that inundation drives shifts in both the microbial community and the denitrification rates, suggesting that approaches such as periodic flooding can be an effective management strategy to remediate nitrate pollution. Finally, Black and Just reported the influence that river mussels communities have on the abundance of N-cycling microbial species. Mussels filtration and biodeposition determine a sediment habitat that favors the mixotrophic coexistence of nitrite-oxidizing (NOB) and ammonia-oxiding (comammox) *Nitrospira* species, what impacts N-cycling in river backwaters. Another important group of microorganisms that play a significant role in the N cycle are AOA. Liu L. et al. explored a new strategy for the rapid enrichment of high abundance *Nitrosocosmicus*-like AOA from soil, providing a new solution to the enrichment and cultivation of AOA in short periods.

In summary, these articles have brought novel knowledge on the diversity, genetics, and physiology of microbes from terrestrial and aquatic ecosystems that participate in the N cycle. Potential applications of this knowledge can be envisaged that will contribute to alleviate the nitrogen problem to achieve a healthier planet and a sustainable food production.

AUTHOR CONTRIBUTIONS

JS initiated the Research Topic and invited editors MD and LG. The editorial was written jointly by the editors of the topic.

ACKNOWLEDGMENTS

The aim of this topic was to collect latest insights on the biology and biotechnology of microorganisms involved in the N cycle in diverse ecosystems. The editors express their gratitude to all the researchers who contributed their valuable work to this topic, as well as the reviewers who provided their constructive criticisms to improve the articles and the topic work.

REFERENCES

Galloway, J. N., Leach, A. M., Bleeker, A., Erisman, J. W. (2013). A chronology of human understanding of the nitrogen cycle. *Phil. Trans. R. Soc. B.* 368:20130120. doi: 10.1098/rstb.2013.0120

Hu, H.-W., Chen, D., He, J.-Z. (2015). Microbial regulation of terrestrial nitrous oxide formation: understanding the biological pathways for prediction of emission rates. *FEMS Microbiol. Rev*. 39, 729–749. doi: 10.1093/femsre/fuv021

Steffen, W., Richardson, K., Rockström, J., Cornell, S. E., Fetzer, I., Bennett, E.M., et al. (2015). Planetary boundaries: guiding human development on a changing planet. *Science* 347:1259855 doi: 10.1126/science.1259855

Conflict of Interest: The authors declare that the research was conducted in the absence of any commercial or financial relationships that could be construed as a potential conflict of interest.

frontiers in Microbiology

ORIGINAL RESEARCH
published: 22 November 2017
doi: 10.3389/fmicb.2017.02304

Increased Denitrification Rates Associated with Shifts in Prokaryotic Community Composition Caused by Varying Hydrologic Connectivity

Abigail Tomasek[1, 2†], Christopher Staley[3†], Ping Wang[3], Thomas Kaiser[3], Nicole Lurndahl[4], Jessica L. Kozarek[1], Miki Hondzo[1, 2] and Michael J. Sadowsky[3, 5]*

[1] St. Anthony Falls Laboratory, University of Minnesota, Minneapolis, MN, United States, [2] Department of Civil, Environmental, and Geo-Engineering, University of Minnesota, Minneapolis, MN, United States, [3] BioTechnology Institute, University of Minnesota, St. Paul, MN, United States, [4] Water Resources Science, University of Minnesota, St. Paul, MN, United States, [5] Department of Soil, Water, and Climate, University of Minnesota, St. Paul, MN, United States

OPEN ACCESS

Edited by:
Lourdes Girard, Centro de Ciencias Genomicas, UNAM, Mexico

Reviewed by:
Pablo Vinuesa, Universidad Nacional Autónoma de México, Mexico
Lluís Bañeras, University of Girona, Spain

***Correspondence:**
Michael J. Sadowsky
sadowsky@umn.edu

[†] *Share first authorship.*

Specialty section:
This article was submitted to Terrestrial Microbiology, a section of the journal Frontiers in Microbiology

Received: *13 August 2017*
Accepted: *08 November 2017*
Published: *22 November 2017*

Citation:
Tomasek A, Staley C, Wang P, Kaiser T, Lurndahl N, Kozarek JL, Hondzo M and Sadowsky MJ (2017) Increased Denitrification Rates Associated with Shifts in Prokaryotic Community Composition Caused by Varying Hydrologic Connectivity. Front. Microbiol. 8:2304. doi: 10.3389/fmicb.2017.02304

While modern developments in agriculture have allowed for increases in crop yields and rapid human population growth, they have also drastically altered biogeochemical cycles, including the biotransformation of nitrogen. Denitrification is a critical process performed by bacteria and fungi that removes nitrate in surface waters, thereby serving as a potential natural remediation strategy. We previously reported that constant inundation resulted in a coupling of denitrification gene abundances with denitrification rates in sediments, but these relationships were not maintained in periodically-inundated or non-inundated environments. In this study, we utilized Illumina next-generation sequencing to further evaluate how the microbial community responds to these hydrologic regimes and how this community is related to denitrification rates at three sites along a creek in an agricultural watershed over 2 years. The hydrologic connectivity of the sampling location had a significantly greater influence on the denitrification rate ($P = 0.010$), denitrification gene abundances ($P < 0.001$), and the prokaryotic community ($P < 0.001$), than did other spatiotemporal factors (e.g., creek sample site or sample month) within the same year. However, annual variability among denitrification rates was also observed ($P < 0.001$). Furthermore, the denitrification rate was significantly positively correlated with water nitrate concentration (Spearman's $\rho = 0.56$, $P < 0.0001$), denitrification gene abundances ($\rho = 0.23$–0.47, $P \leq 0.006$), and the abundances of members of the families *Burkholderiaceae*, *Anaerolinaceae*, *Microbacteriaceae*, *Acidimicrobineae incertae sedis*, *Cytophagaceae*, and *Hyphomicrobiaceae* ($\rho = 0.17$–0.25, $P \leq 0.041$). Prokaryotic community composition accounted for the least amount of variation in denitrification rates (22%), while the collective influence of spatiotemporal factors and gene abundances accounted for 37%, with 40% of the variation related to interactions among all parameters. Results of this study suggest that the hydrologic connectivity at each location had a greater effect on the prokaryotic community than did spatiotemporal differences, where inundation is associated with shifts favoring increased denitrification

potential. We further establish that while complex interactions among the prokaryotic community influence denitrification, the link between hydrologic connectivity, microbial community composition, and genetic potential for biogeochemical cycling is a promising avenue to explore hydrologic remediation strategies such as periodic flooding.

Keywords: sequencing, bacterial community structure, denitrification, hydrology, qPCR, soil

INTRODUCTION

The expansion of modern agricultural practices and the use of synthetic nitrogen (N) fertilizers have resulted in several environmental and ecological consequences. Approximately, 45% of total fixed nitrogen [as ammonia (NH_3)] produced annually originates from chemical fertilizers (Canfield et al., 2010), and 50–70% of the fixed nitrogen applied to soils is lost to the atmosphere or through soil leaching (Masclaux-Daubresse et al., 2010). Fixed nitrogen in soils is converted to nitrate (NO_3–) by nitrification, and in tile-drained systems, such as those in the Midwestern United States, the leached NO_3– is transported directly to water bodies via tile or field drainage. Nitrate loading leads to eutrophication, decreased dissolved oxygen levels, and negative ecological and health effects (Rabalais et al., 2007; Powlson et al., 2008). Specifically, nitrate export in the Mississippi River contributes to the annual formation of the hypoxic dead zone in the Gulf of Mexico (Rabalais et al., 2007). Anthropogenic alteration of the nitrogen cycle also leads to increased emissions of the greenhouse gas nitrous oxide (N_2O) through incomplete denitrification (Davidson, 2009; Venterea et al., 2012). While only a small fraction (3–5%) of N applied in fertilizers is lost as N_2O (Crutzen et al., 2016), this still accounts for 50–60% of global N_2O emissions (USEPA, 2010). Nitrous oxide gas has a considerably greater global warming potential than other greenhouse gases (Forster et al., 2007).

Nitrate is removed from ecosystems through assimilation into biomass by plants, algae, and microbes or through anaerobic oxidation of ammonia (anammox) processes and microbiologically-driven denitrification (Shapleigh, 2006; Kuenen, 2008). Anammox involves the anaerobic oxidation of ammonium (NH_{4+}) to nitrogen gas (N_2), via nitrite (NO_{2-}) or nitrate (NO_3–), and is carried out by a diverse group of bacteria within the phylum *Planctomycetes* (Kuenen, 2008; Humbert et al., 2010). Denitrification is the step-wise reduction of nitrate to NO_{2-}, nitric oxide (·NO), N_2O, and finally to N_2. Denitrification is performed by a broad range of prokaryotic species (Shapleigh, 2006) and fungi, and while it is primarily an anaerobic process, it has also been observed in microaerophilic and aerobic environments (Zumft, 1997).

The extent of hydrologic connectivity has been shown to have important ecological impacts related to the transfer of organisms as well as biogeochemical cycling (Pringle, 2003). For example, increased biogeochemical cycling has been demonstrated at the interface between terrestrial and aquatic ecosystems (riparian zones; McClain et al., 2003; Hefting et al., 2006; Wang et al., 2012; Zhu et al., 2013). This results in the formation of "hot spots" of nutrient conversion, including increased rates of denitrification (McClain et al., 2003; Hefting et al., 2006; Wang et al., 2012; Zhu et al., 2013; Tomasek et al., 2017). Organic carbon (Perryman et al., 2011), oxygen concentration (Inwood et al., 2007), as well as soil water content (Pinay et al., 2007), nitrate concentration (Inwood et al., 2007), and water velocity (Arnon et al., 2007; O'Connor and Hondzo, 2008) have been shown to affect denitrification rates among soils. Furthermore, floodplain location and hydrologic connectivity to surface waters significantly impacts denitrification rates (Roley et al., 2012a,b; Mahl et al., 2015; Tomasek et al., 2017).

Previous studies have measured the relationship between physiochemical parameters, denitrification rates, and bacterial community structure (Cao et al., 2008; Harvey et al., 2013; Tatariw et al., 2013; Shrewsbury et al., 2016). However, these studies usually targeted only a few genes in the denitrification pathway. These largely included the gene encoding nitrite reductase (*nirS* or *nirK*), which is specific to denitrifiers (Zumft, 1997), or *nosZ*, encoding nitrous oxide reductase that is important for N_2O production and shows broad distribution among prokaryotes (Philippot et al., 2011; Domeignoz-Horta et al., 2016). A recent study modeling the effects of physicochemical parameters on N_2O production found that the addition of nitrification gene abundances, rather than solely soil properties, improved predictive accuracy (Breuillin-Sessoms et al., 2017). Inconsistent trends have been observed relating abundances of denitrification genes with actual process rates (Song et al., 2010; Guentzel et al., 2014; Tomasek et al., 2017), and a broader meta-analysis revealed only a weak correlation between gene abundances and process rates when both were measured (Rocca et al., 2015). These results suggest that the ability to significantly associate gene abundances with process rates may depend upon the specific environment sampled.

Advances in next-generation sequencing technology have allowed for more thorough characterization of prokaryotic communities in the environment (Staley and Sadowsky, 2016). However, due to greater diversity (species richness) in soil and sediment communities, as well as microscale variation in community composition, leveraging a whole community profile to assess potentially functionally relevant shifts remains challenging (Robertson et al., 1997; Blackwood et al., 2006; Schmidt and Waldron, 2015). Thus, in order to determine how community-level variation is related to process rates and functional gene abundances, the three components must be measured simultaneously. We previously reported a relationship between gene abundances and denitrification rates at samples collected from in-channel locations of an agricultural watershed, containing Seven Mile creek, located in the Minnesota River Basin (Tomasek et al., 2017). In contrast, we found limited to no coupling between process rates and gene abundances

at intermittently-inundated or never-inundated hydrologic regimes.

In the current study, we expand upon our previous studies relating denitrification rates, physicochemical parameters, and denitrification gene abundances by incorporating prokaryotic community compositions, determined using Illumina next-generation sequencing of the V4 hypervariable region of the 16S rRNA gene. Samples were collected from three sites in the agriculturally-dominated Seven Mile Creek (SMC) watershed over 2 years. The hydrologic connectivity of sampling locations varied over the course of the study (ranging from constantly inundated to never inundated) due to large differences in precipitation as well as sample location. We hypothesized that the hydrologic connectivity of a sampling location would have a greater influence on denitrification rates, gene abundances, and bacterial communities than variation in sampling date and site location in SMC. Furthermore, we suspected that community composition would be associated with denitrification rates due to the relatively broad distribution of denitrification genes. Results of this study reveal how varying hydrologic connectivity affects denitrification rates and further provide novel information regarding the interaction and influence of the prokaryotic community at large on denitrification rates resulting from these hydrologic conditions.

MATERIALS AND METHODS

Sample Collection

Soil samples were collected from three sites in the Seven Mile Creek (SMC) watershed, located in the Minnesota River basin in southern Minnesota (Tomasek et al., 2017). Sites SMC1 (44.2925 N, 94.0759 W) and SMC2 (44.3117 N, 94.0614 W) are located in an agricultural ditch and are surrounded by predominantly agricultural land use, and SMC3 (44.2633 N, 94.0320 W) is located in a nearby county park (Figure S1). At SMC1 and SMC2, three positions with differing hydrologic connectivity were sampled along a transect that included the channel, which was constantly inundated, the floodzone, which was periodically inundated, and the nonfloodzone which was in the riparian region, but never inundated. Samples were only collected from the channel position at SMC3.

Samples were collected on June 12, August 20, and October 20 in 2014 and on May 12, June 15, July 27, August 18, and November 9 in 2015. Triplicate samples were collected for DNA extraction, within 5 cm of each other, using a 5 ml syringe with the top removed. Samples were immediately stored on dry ice, and held at −80°C prior to extraction. Triplicate samples were collected using a 35 ml syringe for measurement of soil nitrate, bulk density, soil organic matter, and moisture content. For measurement of denitrification rates, a 60 ml syringe was used to collect soil to a depth of 5 cm (Inwood et al., 2007). Soil cores were transferred to plastic bags, transported on ice, stored at 4°C, and denitrification rates were determined within 2 days of collection (Findlay et al., 2011). Water width and depth were also measured, as was water velocity using a SonTek Flowtracker (Xylem, Inc., Rye Brook, NY, USA). Triplicate, 1 L, water samples were also collected to determine nitrate concentrations.

Determination of Physicochemical Parameters

Environmental parameters, including nitrate concentration, were measured as described previously (Tomasek et al., 2017). Water samples were filtered through pre-combusted 0.7 μm GF/F filters (Whatman, Marlborough, MA, USA). Nitrate concentrations were determined using the cadmium reduction method on a Lachat QC800 Autoanalyzer (Hach Company, Loveland, CO, USA). Shear velocities were calculated from the time-averaged velocity at varying water depths (Biron et al., 2004). Bulk density and moisture content were determined by drying soil cores for 24 h at 110°C and normalizing the difference between dry and wet weight by soil volume. Soil organic matter was determined using the loss on ignition method (LOI), where dried soil was passed through a 2 mm sieve and approximately 5 g was burned at 550°C for 4 h (Heiri et al., 2001). Soil nitrate was measured through water extractions, where the nitrate concentration of the extracted water was measured as described above and the concentration was normalized by the dry soil weight of the sample.

Denitrification rates were determined using a modified acetylene block method (Groffman et al., 2006; Loken et al., 2016; Tomasek et al., 2017). To determine unamended denitrification potential (DN_U), site-specific water samples were treated with 10 mg L^{-1} chloramphenicol. N_2O concentrations were analyzed using a 5890 series II gas chromatograph (Hewlett-Packard Enterprise, Palo Alto, CA, USA) equipped with an electron capture detector and headspace autosampler (Hewlett-Packard, 7694) as described previously (Loken et al., 2016). Accumulation of N_2O over the incubation period was corrected using the Bunsen solubility coefficient (Tiedje, 1982). Denitrification rates were calculated as a function of bulk density and reported as an areal rate (Tomasek et al., 2017). Amended denitrification rates were determined as described previously (Tomasek et al., 2017) following amendment with nitrate (100 mg N L^{-1} as potassium nitrate), carbon (40 mg C L^{-1} as glucose), and phosphate (13.84 mg P L^{-1} as potassium dihydrogen phosphate).

Denitrification Gene Abundances

DNA was extracted from triplicate 500 mg soil samples using the DNeasy PowerSoil Kit (QIAGEN, Hilden, Germany) according to the manufacturer's instructions, and DNA was used as template for quantitative PCR (qPCR) assays to determine gene abundances, as described previously (Tomasek et al., 2017). Denitrification gene abundances were determined for *narG* (encoding nitrate reductase, primers narG-1960m2fE/narG2050m2R; Kandeler et al., 2006), *nirK* (encoding nitrite reductase, primers nirK876F/1040R; Petersen et al., 2012), *nirS* (encoding nitrite reductase, primers m-cd3AF/m-R3cd; Petersen et al., 2012), *cnorB* (encoding nitric oxide reductase, primers cnorB-BF/cnorB-BR; Dandie et al., 2007), *nosZ1* (encoding nitrous oxide reductase, primers nosZ_F/nosZ_1622R; Rösch et al., 2002), and *nosZ3* (encoding nitrous oxide reductase, primers nosZ2F/nosZ2R; Petersen et al., 2012). Laboratory triplicates were run for all field triplicate

samples. Standard curves were generated using gBlocks® Gene Fragments (Integrated DNA Technologies, Inc., Coralville, IA, USA; Svec et al., 2015; Tomasek et al., 2017), except for *nirS*, for which a plasmid standard was used. Tests for inhibition were not performed, and efficiencies for all targets ranged from 80 to 110 with $r^2 > 0.99$. Negative, no-template controls were included with each qPCR run. Gene abundances were normalized per g dry soil for analysis.

Illumina Sequencing and Bioinformatics

The V4 hypervariable region of 16S rRNA was amplified from triplicate DNA extracts per sample using the 515F/806R primer set (Caporaso et al., 2012) and sequenced using the dual index method by the University of Minnesota Genomics Center (UMGC, Minneapolis, MN, USA) (Gohl et al., 2016). Samples from 2014 were paired-end sequenced on the Illumina HiSeq2500 (Illumina, Inc., San Diego, CA, USA) at a read length of 150 nucleotides (nt) and samples from 2015 were paired-end sequenced on the Illumina MiSeq at a read length of 300 nt. The use of different sequencing platforms has been previously shown not to bias biological conclusions drawn (Caporaso et al., 2012). Raw data are deposited in the Sequence Read Archive of the National Center for Biotechnology Information under BioProject accession number SRP113317.

Sequence data were processed and analyzed using mothur version 1.35.1 (Schloss et al., 2009), as described previously for V6 and V5V6 hypervariable regions (Staley et al., 2015b). Samples were trimmed to 150 nt and paired-end joined using fastq-join software with an average join length of approximately 10 nt (Aronesty, 2013), trimmed for quality based on quality score (>35 over a 50 nt window), ambiguous bases (0), homopolymer length (≤8), and primer mismatches (≤2). High quality sequences were aligned against the SILVA database version 123 (Pruesse et al., 2007), subjected to a 2% pre-cluster (Huse et al., 2010), and UCHIME was used to remove chimeric sequences (Edgar et al., 2011). Following quality trimming, the average sequence length was approximately 174 nt. For statistical comparisons, all samples were rarefied by random subsampling to 38,000 sequence reads per sample to reduce statistical bias due to varying numbers of sequences reads (Gihring et al., 2012). Operational taxonomic units (OTUs) were assigned at 97% similarity using complete-linkage clustering and taxonomic classifications were assigned against the Ribosomal Database Project, version 14 (Cole et al., 2009). Different databases were used for alignment and OTU classification due to considerations described previously (Schloss, 2009).

Statistical Analyses

ANOVA analyses with Tukey's *post-hoc* test, Spearman rank correlations, and canonical correspondence analysis were performed using XLSTAT version 2015.6 (Addinsoft, Belmont, MA, USA). Shannon indices, beta diversity calculations, and ordination plots were calculated using mothur. Beta diversity analysis and ordination were performed using Bray-Curtis dissimilarity matrices (Bray and Curtis, 1957). Differences in community composition were evaluated by analysis of molecular variance (ANOSIM; Clarke, 1993) and sample clustering was evaluated by analysis of molecular variance (AMOVA; Excoffier et al., 1992). Ordination was performed by principal coordinate analysis (PCoA; Anderson and Willis, 2003) and Spearman correlations of family abundances associated with ordination were calculated using the corr.axes command in mothur. Variance partitioning was performed by partial redundancy analysis using the vegan package in R, as described previously (Borcard et al., 1992; R Core Team, 2012; Oksanen et al., 2015). All statistics were calculated at $\alpha = 0.05$ with Bonferroni correction for multiple comparisons.

RESULTS

Denitrification Rates and Physicochemical Parameters

Among samples collected at channel locations from all sites (those constantly inundated), large differences were observed among hydrologic parameters (shear velocity, discharge, and depth), both unamended denitrification potential (DN_U) as well as denitrification potential following amendment with nutrients (DN_A), and nitrate (NO_3–) concentrations over the study period

TABLE 1 | Hydrologic parameters, nitrate concentration, and denitrification potential among channel sites.

Year	Site	*n*	Shear velocity (m s^{-1})	Discharge (m^3 s^{-1})	Depth (m)	NO_3 as N (mg L^{-1})	DN_U (mg N m^{-2} h^{-1})	DN_A (mg N m^{-2} h^{-1})
2014	SMC1	9	0.004 ± 0.000	0.28 ± 0.4	0.57 ± 0.05	13.51 ± 20.24	7.70 ± 14.64	15.24 ± 13.03
	SMC2	9	0.003 ± 0.004 B		0.31 ± 0.24 B	11.43 ± 16.88	4.29 ± 6.14 B	28.69 ± 9.77 AB
	SMC3	9	0.018 ± 0.010 B		0.13 ± 0.02 B	13.16 ± 10.69	4.66 ± 5.20 B	5.49 ± 6.37 B
2015	SMC1	15	0.012 ± 0.009 B	0.89 ± 1.1	0.64 ± 0.08 A	17.18 ± 10.81	14.23 ± 11.79 B	24.48 ± 15.83 B
	SMC2	15	0.016 ± 0.009 B		0.52 ± 0.23 A	17.79 ± 11.29	30.16 ± 27.77 A	47.79 ± 40.22 A
	SMC3	15	0.043 ± 0.025 A		0.18 ± 0.07 B	14.00 ± 5.43	4.24 ± 4.76 B	5.30 ± 5.45 B
Fisher's *F**			<0.0001	0.196	<0.001	0.796	<0.001	<0.001

Values as mean ± standard deviation are shown, and n represents the number of samples for each site. Data from site SMC1 in 2014 were excluded from analyses due to multicolinearity.
**Fisher's F statistics for the ANOVA model. Separate models were calculated for each variable.*
A,B Values sharing the same letter did not vary significantly by Tukey's post-hoc test ($P > 0.05$).

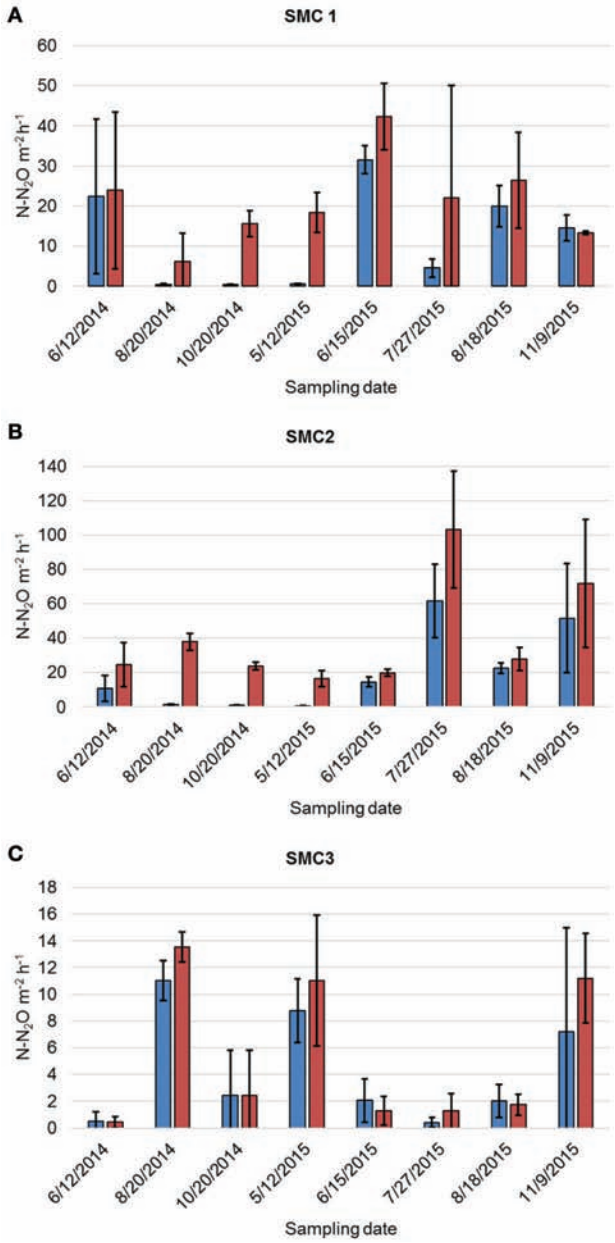

FIGURE 1 | Mean denitrification rates of triplicate samples collected from channel positions at **(A)** SMC1, **(B)** SMC2, and **(C)** SMC3. Error bars reflect standard deviation. Blue bars represent DN_U and red bars represent DN_A.

(**Table 1**). Hydrologic parameters were greater in 2015 (0.024 ± 0.021 m s^{-1}, 0.45 ± 0.24 m, and 0.89 ± 1.1 m^3 s^{-1}, respective to shear velocity, depth, and discharge (Figure S2) than those observed in 2014 (0.009 ± 0.009 m s^{-1}, 0.34 ± 0.23 m, 0.28 ± 0.37 m^3 s^{-1}) at all sites. Similarly DN_U was greater in 2015 (16.48 ± 20.47 mg N m^{-2} h^{-1} vs. 5.55 ± 9.39 N m^{-2} h^{-1} in 2014) than in 2014, while DN_A was significantly greater at the SMC2 site during both years of sampling (**Table 1**). Furthermore, water discharge was significantly and positively correlated with NO_3– concentration (Spearman's $\rho = 0.690$, $P < 0.0001$) and DN_u ($\rho = 0.389$, $P = 0.001$), and DN_u was also positively correlated with NO_3– ($\rho = 0.561$, $P < 0.0001$) and DN_A ($\rho = 0.636$, $P < 0.0001$).

Denitrification rates varied between sampling years, as well as among sampling months within the same year, spatial position (i.e., channel, floodzone, or nonfloodzone), and sampling site (ANOVA $P < 0.0001$, **Figure 1**, Tables S1, S2). The unamended denitrification rate (DN_U) was significantly greater in 2015 than in 2014 (Tukey's *post-hoc* $P < 0.0001$), greater among channel samples than samples collected in the nonfloodzone ($P = 0.010$), and greater at SMC2 than the other sites ($P < 0.001$). Similarly, DN_A was greater in 2015 ($P = 0.005$), greater among channel samples than those from the nonfloodzone ($P = 0.028$), and significantly different among all sites in the order of: SMC2 > SMC1 > SMC3 ($P < 0.001$). In addition, physicochemical measurements, including the dry weight:wet weight ratio, volumetric water content, bulk density, organic matter, and soil nitrate (Table S3), also showed significant variation among sampling sites and positions, but showed less temporal variability.

Denitrification Gene Abundances

Gene abundances quantified by qPCR (**Figure 2**) were significantly different due to variability in time, hydrologic connectivity, and site location along SMC (ANOVA Fisher's $F < 0.0001$ for all genes). The 16S rRNA gene abundances were significantly greater in 2014 compared to 2015 (Tukey's $P = 0.008$), at the floodzone relative to the nonfloodzone ($P < 0.001$), and at SMC1 and SMC2 relative to SMC3 ($P < 0.001$). Among denitrification genes, significantly lower relative abundances of genes were also typically observed in nonfloodzone samples (**Table 2**).

Abundances of all genes except *nirS* were significantly and positively correlated with DN_U ($\rho = 0.231$–0.469, $P \leq 0.006$), and the abundances of all genes were significantly correlated with DN_A ($\rho = 0.325$–0.516, $P < 0.0001$), among all samples. When samples were analyzed by sampling position, among both years and all samples sites (Table S4), significant positive correlations among denitrification rates and gene abundances were only found among samples collected from the channel and floodzone positions, with one exception. Furthermore, these correlations were generally stronger ($\rho \geq 0.490$) than those found when samples from all positions were combined.

Alpha Diversity and Community Composition

The number of OTUs varied from 385 to 8,160 OTUs per sample, with a mean Good's coverage of $96.3 \pm 0.3\%$, among all samples. Samples collected in 2014 had significantly lower alpha diversity, measured by the Shannon index, compared to those collected in 2015 (mean 4.07 ± 0.23 in 2014 and 7.26 ± 0.40, $P < 0.0001$). Among samples collected in 2014 (Figure S3A), Shannon indices among samples collected at SMC2 were significantly greater than those at SMC3 (Tukey's $P = 0.010$), and diversity decreased by position as: channel > floodzone > nonfloodzone ($P \leq 0.002$). Similar patterns were observed in 2015 (Figure S3B), except there was no significant difference between samples collected in the channel and floodzone ($P = 0.546$) and samples collected in

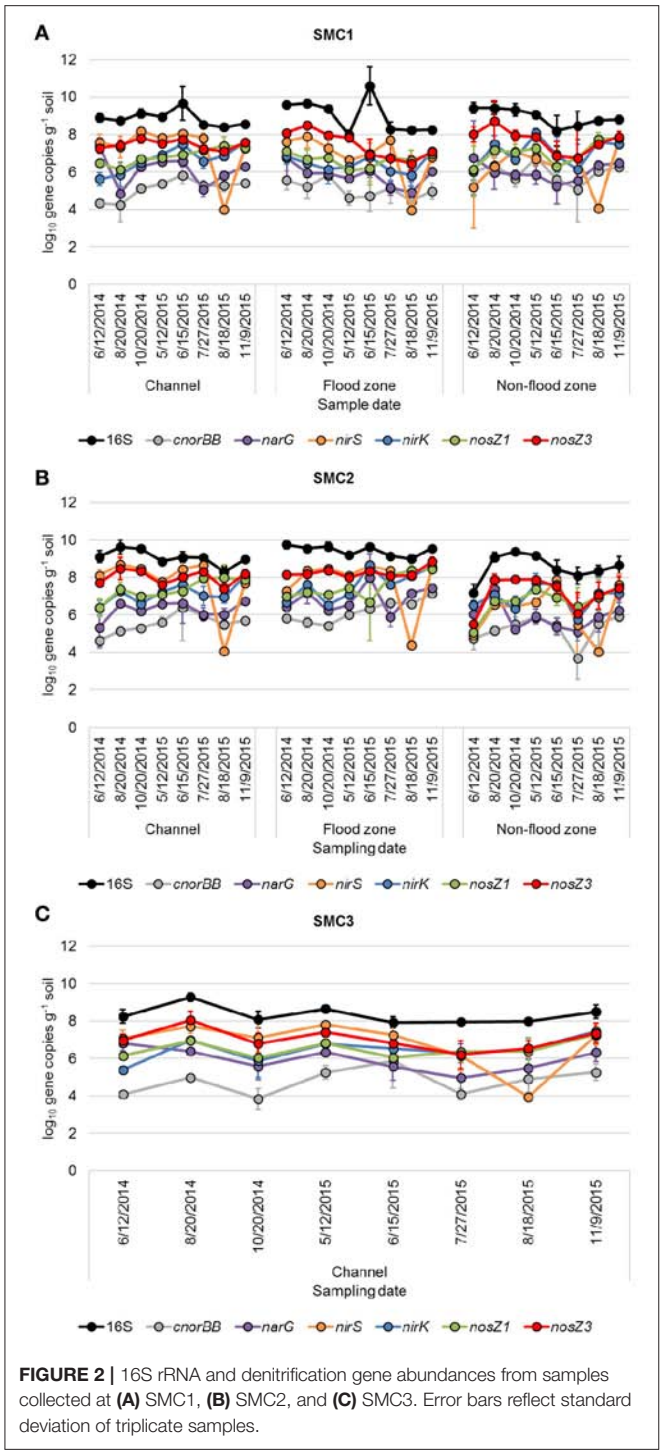

FIGURE 2 | 16S rRNA and denitrification gene abundances from samples collected at **(A)** SMC1, **(B)** SMC2, and **(C)** SMC3. Error bars reflect standard deviation of triplicate samples.

July and August had significantly greater diversity than those collected in May ($P = 0.013$ and 0.018, respectively).

During both years of sampling, communities from all sampling sites were predominantly comprised of members of the Actinobacteria, α- and β-Proteobacteria, and Acidobacteria classes (**Figure 3**). Family-level classification (Figure S4) revealed that communities were predominantly comprised of many low-abundance families, and approximately 20–30% of sequence reads could not be assigned at this taxonomic level.

Beta Diversity

Prokaryotic community composition (beta diversity) among samples differed significantly between sampling years (ANOSIM $R = 1.000$, $P < 0.001$, Figure S5). During both sampling years (taken together), differences in beta diversity varied significantly, more due to hydrologic connectivity associated with sample positions ($R = 0.271$, *post-hoc* $P < 0.001$) than to sampling sites ($R = 0.066$, $P \leq 0.013$). These trends were maintained when individual sampling years were evaluated separately. Moreover, prokaryotic communities did not vary significantly by sampling month in either year ($r = 0.031$, $P = 0.117$ and $r = -0.004$, $P = 0.498$, in 2014 and 2015, respectively).

Similar to ANOSIM results, ordination of Bray-Curtis dissimilarity matrices by PCoA revealed clustering of samples primarily based on sample position (AMOVA $F_s = 19.8$, $P < 0.001$ and $F_s = 16.8$, $P < 0.001$ for 2014 and 2015, respectively; **Figure 4**). Spearman correlation analyses relating family abundances to ordination position revealed similar trends during both years of sampling ($P \leq 0.006$; **Figure 4**). For example, abundances of members of the family *Anaerolineaceae* were significantly related to samples collected from the channel, as indicated by similar ordination position. Similarly, members of the families *Cytophagaceae*, *Gemmatimonadaceae*, and *Xanthomonadaceae* were generally associated with floodzone samples, and the *Gaiellaceae* were found at greater abundances in nonfloodzone samples.

Associations Among Prokaryotic Communities and Denitrification

Variance partitioning was performed using constrained redundancy analyses to determine how the prokaryotic community influenced denitrification rates (DN_U and DN_A) in conjunction with temporal, spatial, physicochemical parameters, and denitrification gene abundances. By using this method, the prokaryotic community composition alone, taken as abundances of predominant families (those present at a mean of at least 1.0% of sequence reads), accounted for 21.8% of variation in denitrification rates (DN_U and DN_A). Non-community factors (including abundances of denitrification genes) accounted for 37.1% of the variation in denitrification rates, and interactions among all parameters accounted for 41.1%.

The relationships among all parameters modeled were further evaluated by canonical correspondence analysis (CCA; **Figure 5**). Denitrification gene abundances were found to cluster closely and were similarly all significantly positively inter-correlated by Spearman correlation ($\rho = 0.221$–0.826, median $= 0.452$, $P \leq 0.004$). Similarly, abundances of bacterial families were found to associate with channel and nonfloodzone features, as observed in the PCoA analyses (above). In contrast, families associated with the floodzone by PCoA showed inconsistent relationships by CCA. No consistent trends were observed for correlations among family abundances and denitrification genes (e.g., abundances of the archaeal nitrifier *Nitrososphaera* were not significantly correlated

TABLE 2 | Differences in denitrification gene abundances due to temporal, spatial, and geographic features.

Gene	Year	Location	Site
cnorBB	2015 > 2014 (0.020)	NS*	SMC2 > SMC3 (0.005)
narG	2015 > 2014 (0.010)	floodzone > nonfloodzone (0.037)	SMC2 > SMC3 (0.012)
nirS	NS	nonfloodzone < others (< 0.001)	SMC2 > SMC1 > SMC3 (≤ 0.035)
nirK	2015 > 2014 (< 0.0001)	NS	SMC2 > others (< 0.001)
nosZ1	2015 > 2014 (< 0.0001)	NS	SMC2 > SMC1 > SMC3 (≤ 0.039)
nosZ3	NS	Nonfloodzone < others (≤ 0.047)	SMC2 > SMC1 > SMC3 (≤ 0.032)

Tukey's post-hoc P values are shown in parentheses, where significant (P < 0.05). Only the abundances of cnorBB did not show some significant variation among months of sampling (P ≥ 0.105).

**NS: no significant differences were observed in relation to the variable.*

with gene abundances by traditional Spearman correlation). Abundances of members of the families *Burkholderiaceae*, *Anaerolinaceae*, *Microbacteriaceae*, *Acidimicrobineae incertae sedis*, *Cytophagaceae*, and *Hyphomicrobiaceae* (in order of abundance) were positively correlated with DN_U ($\rho = 0.169$–0.251, $P \leq 0.041$), while the abundances of members of the families *Gaiellaceae*, *Comamonadaceae*, and *Sinobacteraceae* were negatively correlated ($\rho = -0.291$ to -0.168, $P \leq 0.042$).

DISCUSSION

In this study, denitrification rates under site conditions (DN_u) and under non-limiting nutrient concentrations (DN_A) varied in response to spatiotemporal parameters as well as hydrologic connectivity. Differences between DN_U and DN_A rates can provide insight into environmental parameters limiting denitrification under field conditions, and allow for comparisons of the potential of sites to denitrify under optimal conditions. Under unfavorable field conditions, for instance low nitrate concentrations, denitrification will be limited even if denitrifying bacteria are present. Therefore DN_A rates are valuable when correlating denitrification rates and gene abundances. The measured DN_u rates were similar to those found in previous studies in agricultural systems (Roley et al., 2012a; Mahl et al., 2015; Tomasek et al., 2017). In August and October 2014, and May 2015, when nitrate concentrations were lowest, the low DN_u and the large differences between DN_u and DN_A implied that channel locations at SMC1 and SMC2 were likely nitrate-limited on these dates. At the nonfloodzone locations of both SMC1 and SMC2, DN_U and DN_A remained relatively constant throughout the study period. SMC3 had much lower DN_U and DN_A compared to SMC1 and SMC2 channel locations, which may be due to site characteristics including sandy sediment and greater shear velocities, leading to a potentially less stable microbial community due to increased bedload transport (Arnon et al., 2007; Tomasek et al., 2017). This supposition is further supported by the significantly lower abundances of the 16S rRNA gene and the next-generation sequencing data, where significantly lower diversity was observed at SMC3 relative to SMC2.

Previous research has shown that reconnecting channels with riparian areas can enhance denitrification (Kaushal et al., 2008; Klocker et al., 2009; Roley et al., 2012a; Mahl et al., 2015). The two agricultural sites in this study, SMC1 and SMC2, had differing ditch geometry. SMC1 had a traditional trapezoidal configuration, whereas SMC2 had an inset depositional floodplain at the floodzone location (Tomasek et al., 2017). Therefore, the floodzone location at SMC2 would have a larger reactive surface area, more sediment-water contact time, a larger hyporheic zone, and would likely favor greater rates of nitrogen cycling (McClain et al., 2003; Hefting et al., 2006; Wang et al., 2012; Woodward et al., 2015). Precipitation during the summer of 2014 occurred largely in one rain event in late June, whereas the rest of the summer was relatively dry. In comparison, precipitation was greater and occurred more frequently throughout the summer in 2015. The increased precipitation in 2015 caused inundation at the floodzone location, particularly at SMC2. This likely caused the differential correlations between denitrification rates, environmental parameters, and gene abundances in 2015 compared to 2014 at floodzone locations. The floodzone location at SMC2 had significantly greater soil moisture content and DN_u in 2015 than in 2014. However, there was no significant difference between 2015 and 2014 in soil water content or DN_U at the floodzone location of SMC1. Denitrifying gene abundances were also significantly greater at the floodzone location of SMC2 compared to SMC1 in 2015.

Abundances of nearly all denitrification genes investigated were significantly and positively correlated with DN_U and DN_A, suggesting that, in this ecosystem, these abundances are related to active transcription and process rates (Rocca et al., 2015). We previously reported the gene abundances were coupled with denitrification rates at only channel positions among 2014 samples (Tomasek et al., 2017). In the current study, when samples were grouped by hydrologic regime, denitrification rates were significantly correlated with gene abundances for the channel and floodzone positions; however, there was only one significant correlation between *nirS* and DN_A among nonfloodzone samples. This may explain why similar denitrification rates were observed across sampling dates at the nonfloodzone locations, where unfavorable environmental conditions limit denitrification rates, even when denitrifying bacteria are present. Our data may suggest that inundation is one method that may induce a denitrification response by providing more favorable environmental conditions (Tomasek et al., 2017). Furthermore,

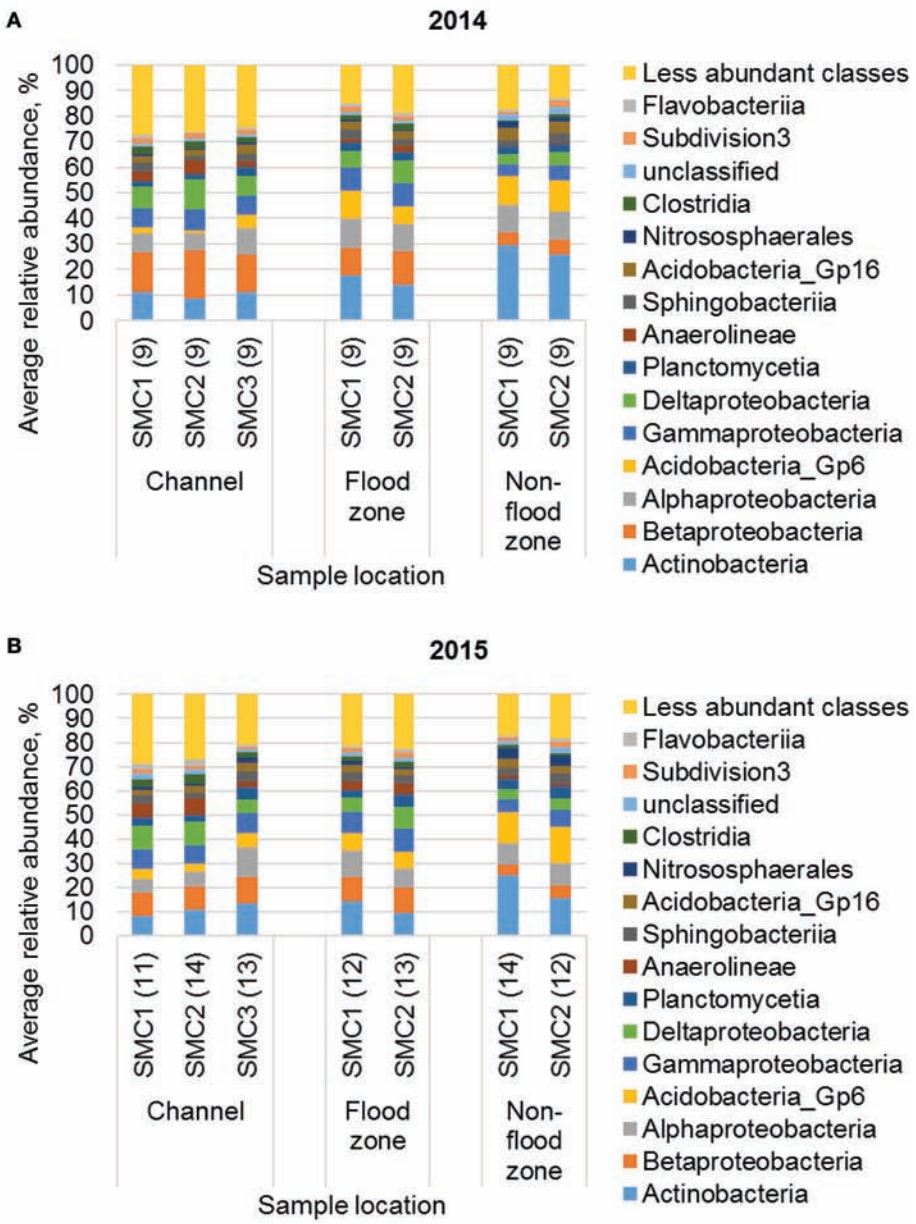

FIGURE 3 | Distribution of the 15 most abundant classes from samples collected in **(A)** 2014 and **(B)** 2015. Numbers in parentheses reflect sample size. Samples in 2015 that did not meet the rarefaction depth of 38,000 sequence reads were excluded from the dataset. Less abundant classes were present at a mean ≤1.6% of sequence reads, among all samples.

a previous study similarly suggested that flooding induced a physiological response among denitrifiers (Manis et al., 2014).

Legacy effects associated with soil moisture have recently been shown to significantly impact the microbial community composition and N_2O flux (Banerjee et al., 2016). While early inundation shaped a community favoring *Burkholderiaceae* in 2014, only a short-term increase in denitrification was observed in June, while a more sustained response was observed during 2015, when soil moisture and precipitation were greater throughout the sampling period. Recent work has similarly suggested that hydroecology during Spring is likely to help shape the microbial community (Esposito et al., 2016). However, samples between years were also sequenced on different instruments. While differences in sequencing platform may have had minor effects on the communities characterized, results using different sequencing platforms have previously been shown to be comparable (Caporaso et al., 2012), especially among environmental samples processed using a pipeline similar to that used in this study (Staley et al., 2015a).

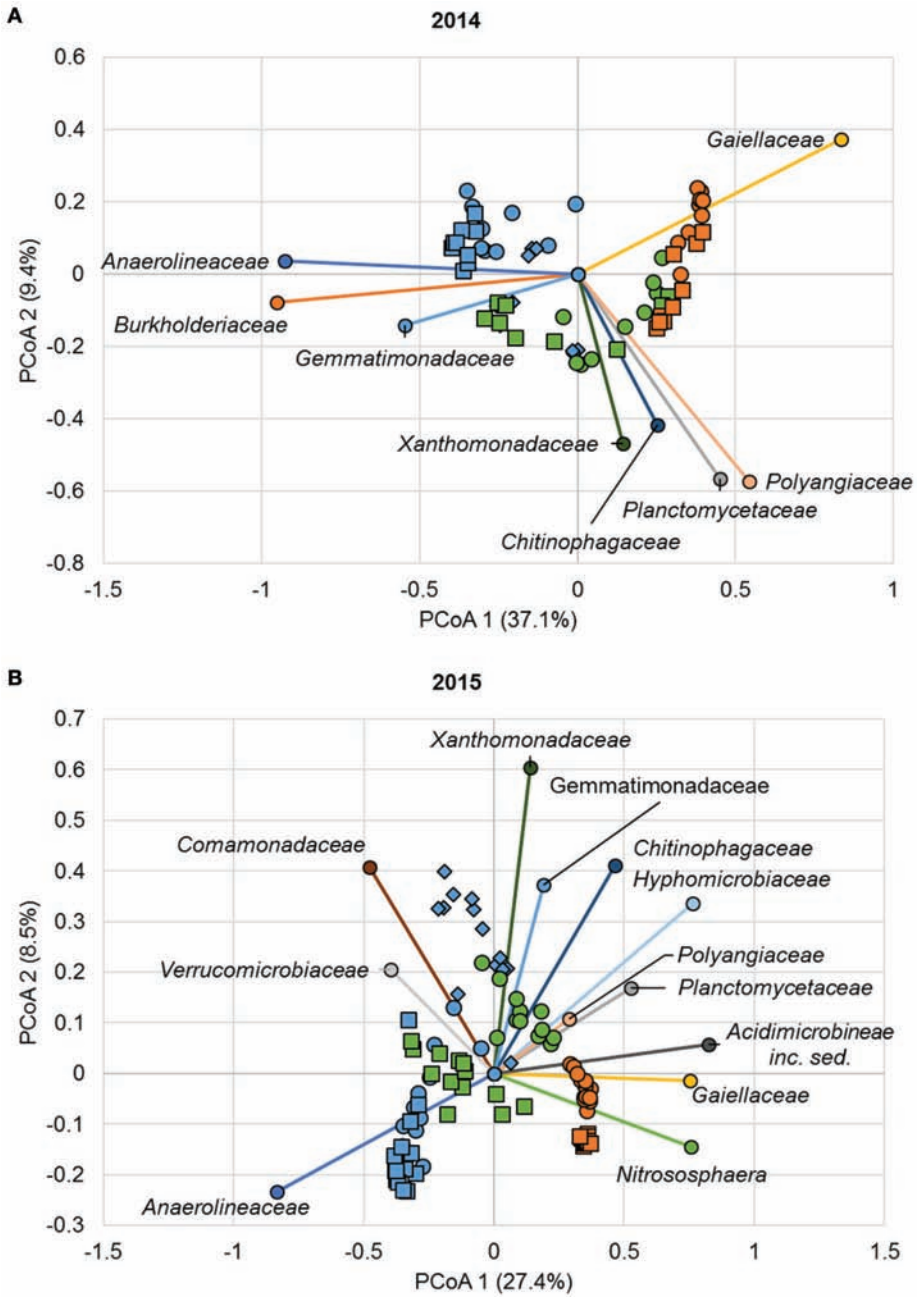

FIGURE 4 | Principal coordinate analysis of Bray-Curtis dissimilarity matrices from samples collected in **(A)** 2014 ($r^2 = 0.82$) and **(B)** 2015 ($r^2 = 0.73$). Legend: SMC1 (•), SMC2 (■), SMC3 (♦), channel (blue), floodzone (green), nonfloodzone (orange). Relative abundances of families shown (among the 15 most abundant shown in Figure S4) were significantly correlated with ordination position ($P < 0.05$). Families that were not significantly correlated are not shown.

Inclusion of next-generation bacterial community characterization further elucidates how microbial community structure changed as a result of hydrologic connectivity, and how this community influenced denitrification rates. Soil microbial communities have previously been shown to vary more as a result of site than specific treatments (Fernandez et al., 2016a,b). Here we also reported differences in community composition between sampling years as well as between sampling sites, but, interestingly, the hydrologic regime more strongly drove differences in community composition than did geographic variation. Similar to a previous report (Argiroff et al., 2017), increased hydrologic connectivity corresponded with an increase in the abundances of Proteobacteria and significantly separated communities characterized by both

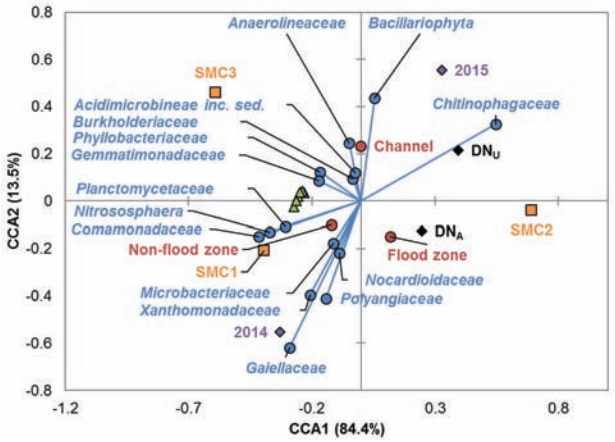

FIGURE 5 | Canonical correspondence analysis of sampling sites, years, and positions; denitrification rates; denitrification gene abundances; and family abundances (among the 10 most abundant). Legend: sampling sites (■), years (♦), positions (•), denitrification rates (■), denitrification genes (▲), and prokaryotic families (•).

family-level abundances, as well as functional gene categories. Not surprisingly, more frequent inundation favored more highly anaerobic communities, but genes associated with denitrification were more evenly spread across three soils with varying hydrologic connectivity (Argiroff et al., 2017). We found few correlations between family-level abundances and either denitrification rates or gene abundances, which is not surprising given the functional redundancy resulting from the wide distribution of these genes (Zumft, 1997; Shapleigh, 2006). Furthermore, prokaryotic community composition and its interaction with other spatiotemporal and physicochemical parameters caused a considerable amount of variation in denitrification rates. Several of the families correlated with denitrification rate were significantly associated with inundation, such as *Anaerolinaceae* and *Microbacteriaceae*, suggesting these families potentially play an important role in denitrification.

CONCLUSIONS

Results of this study reveal how varying hydrologic regimes associated with differences in hydrologic connectivity influence both denitrification rates as well as prokaryotic community composition. Frequent inundation increases both denitrification gene abundances and denitrification rates, and indirectly influences the composition of the microbial community. Abundances of the families *Burkholderiaceae*, *Anaerolinaceae*, *Microbacteriaceae*, *Acidimicrobineae incertae sedis*, *Cytophagaceae*, and *Hyphomicrobiaceae* were significantly correlated with DN_U and may be among the most active in denitrification under the varying hydrological conditions tested. Further study is necessary to determine which environmental parameters are most likely to shift microbial communities to stimulate biogeochemical processes including denitrification. However, this study provides novel evidence that inundation drives shifts in the microbial community that increase denitrification rates. Thus, changing patterns of hydrologic connectivity, for example by periodic flooding, may serve as an effective management strategy to remediate nitrate pollution by causing corresponding shifts in the microbial community.

AUTHOR CONTRIBUTIONS

AT, CS, MH, JK, and MS help conceive and guide the study. AT, CS, PW, TK, and NL helped carry-out experiments. AT, CS, JK, MH and MS helped write the manuscript.

ACKNOWLEDGMENTS

Funding was provided in part by the Clean Water Research Program through the Minnesota Department of Agriculture with funding from the Minnesota Clean Water, Land, and Legacy Amendment. This project was also supported by Agriculture and Food Research Initiative Competitive Grant no. 2015-06019-23600 from the USDA National Institute of Food and Agriculture. Processing and analysis of sequence data were performed using the resources of the Minnesota Supercomputing Institute. We gratefully acknowledge the assistance of Jacques Finlay, Martin du Saire, and Kurt Spokas for laboratory use in denitrification assays, along with the technical staff and student help at the St. Anthony Falls Laboratory.

SUPPLEMENTARY MATERIAL

The Supplementary Material for this article can be found online at: https://www.frontiersin.org/articles/10.3389/fmicb.2017.02304/full#supplementary-material

REFERENCES

Anderson, M. J., and Willis, T. J. (2003). Canonical analysis of principal coordinates: a useful method of constrained ordination for ecology. *Ecology* 84, 511–525. doi: 10.1890/0012-9658(2003)084[0511:CAOPCA]2.0.CO;2

Argiroff, W. A., Zak, D. R., Lanser, C. M., and Wiley, M. J. (2017). Microbial community functional potential and composition are shaped by hydrologic connectivity in riverine floodplain soils. *Microb. Ecol.* 73, 630–644. doi: 10.1007/s00248-016-0883-9

Arnon, S., Gray, K. A., and Packman, A. I. (2007). Biophysicochemical process coupling controls nitrogen use by benthic biofilms. *Limnol. Oceanogr.* 52, 1665–1671. doi: 10.4319/lo.2007.52.4.1665

Aronesty, E. (2013). Comparison of sequencing utility programs. *Open Bioinforma. J.* 7, 1–8. doi: 10.2174/1875036201307010001

Banerjee, S., Helgason, B., Wang, L., Winsley, T., Ferrari, B. C., and Siciliano, S. D. (2016). Legacy effects of soil moisture on microbial community structure and N2O emissions. *Soil Biol. Biochem.* 95, 40–50. doi: 10.1016/j.soilbio.2015.12.004

Biron, P. M., Robson, C., Lapointe, M. F., and Gaskin, S. J. (2004). Comparing different methods of bed shear stress estimates in simple and complex flow fields. *Earth Surf. Process. Landforms* 29, 1403–1415. doi: 10.1002/esp.1111

Blackwood, C. B., Dell, C. J., Smucker, A. J. M., and Paul, E. A. (2006). Eubacterial communities in different soil macroaggregate environments and cropping systems. *Soil Biol. Biochem.* 38, 720–728. doi: 10.1016/j.soilbio.2005.07.006

Borcard, D., Legendre, P., and Drapeau, P. (1992). Partialling out the spatial component of ecological variation. *Ecology* 73, 1045–1055.

Bray, J. R., and Curtis, J. T. (1957). An ordination of the upland forest communities of southern Wisconsin. *Ecol. Monogr.* 27, 325–349.

Breuillin-Sessoms, F., Venterea, R. T., Sadowsky, M. J., Coulter, J. A., Clough, T. J., and Wang, P. (2017). Nitrification gene ratio and free ammonia explain nitrite and nitrous oxide production in urea-amended soils. *Soil Biol. Biochem.* 111, 143–153. doi: 10.1016/j.soilbio.2017.04.007

Canfield, D. E., Glazer, A. N., and Falkowski, P. G. (2010). The evolution and future of Earth's nitrogen cycle. *Science* 330, 192–196. doi: 10.1126/science.1186120

Cao, Y., Green, P. G., and Holden, P. A. (2008). Microbial community composition and denitrifying enzyme activities in salt marsh sediments. *Appl. Environ. Microbiol.* 74, 7585–7595. doi: 10.1128/AEM.01221-08

Caporaso, J. G., Lauber, C. L., Walters, W. A., Berg-Lyons, D., Huntley, J., Fierer, N., et al. (2012). Ultra-high-throughput microbial community analysis on the Illumina HiSeq and MiSeq platforms. *ISME J.* 6, 1621–1624. doi: 10.1038/ismej.2012.8

Clarke, K. R. (1993). Non-parametric multivariate analyses of changes in community structure. *Aust. J. Ecol.* 18, 117–143.

Cole, J. R., Wang, Q., Cardenas, E., Fish, J., Chai, B., Farris, R. J., et al. (2009). The Ribosomal Database Project: improved alignments and new tools for rRNA analysis. *Nucleic Acids Res.* 37, D141–D145. doi: 10.1093/nar/gkn879

Crutzen, P. J., Mosier, A. R., Smith, K. A., and Winiwarter, W. (2016). "N_2O release from agro-biofuel production negates global warming reduction by replacing fossil fuels," in *Paul J. Crutzen: A Pioneer on Atmospheric Chemistry and Climate Change in the Anthropocene,* eds P. J. Crutzen and H. G. Brauch (Cham: Springer International Publishing), 227–238.

Dandie, C. E., Burton, D. L., Zebarth, B. J., Trevors, J. T., and Goyer, C. (2007). Analysis of denitrification genes and comparison of *nosZ*, *cnorB* and 16S rDNA from culturable denitrifying bacteria in potato cropping systems. *Syst. Appl. Microbiol.* 30, 128–138. doi: 10.1016/j.syapm.2006.05.002

Davidson, E. A. (2009). The contribution of manure and fertilizer nitrogen to atmospheric nitrous oxide since 1860. *Nat. Geosci.* 2, 659–662. doi: 10.1038/ngeo608

Domeignoz-Horta, L. A., Putz, M., Spor, A., Bru, D., Breuil, M. C., Hallin, S., et al. (2016). Non-denitrifying nitrous oxide-reducing bacteria - An effective N_2O sink in soil. *Soil Biol. Biochem.* 103, 376–379. doi: 10.1016/j.soilbio.2016.09.010

Edgar, R. C., Haas, B. J., Clemente, J. C., Quince, C., and Knight, R. (2011). UCHIME improves sensitivity and speed of chimera detection. *Bioinformatics* 27, 2194–2200. doi: 10.1093/bioinformatics/btr381

Esposito, A., Engel, M., Ciccazzo, S., Daprà, L., Penna, D., Comiti, F., et al. (2016). Spatial and temporal variability of bacterial communities in high alpine water spring sediments. *Res. Microbiol.* 167, 325–333. doi: 10.1016/j.resmic.2015.12.006

Excoffier, L., Smouse, P. E., and Quattro, J. M. (1992). Analysis of molecular variance inferred from metric distances among DNA haplotypes - application to human mitochondrial DNA restriction data. *Genetics* 131, 479–491.

Fernandez, A. L., Sheaffer, C. C., Wyse, D. L., Staley, C., Gould, T. J., and Sadowsky, M. J. (2016a). Associations between soil bacterial community structure and nutrient cycling functions in long-term organic farm soils following cover crop and organic fertilizer amendment. *Sci. Total Environ.* 566–567, 949–959. doi: 10.1016/j.scitotenv.2016.05.073

Fernandez, A. L., Sheaffer, C. C., Wyse, D. L., Staley, C., Gould, T. J., and Sadowsky, M. J. (2016b). Structure of bacterial communities in soil following cover crop and organic fertilizer incorporation. *Appl. Microbiol. Biotechnol.* 100, 9331–9341. doi: 10.1007/s00253-016-7736-9

Findlay, S. E. G., Mulholland, P. J., Hamilton, S. K., Tank, J. L., Bernot, M. J., Burgin, A. J., et al. (2011). Cross-stream comparison of substrate-specific denitrification potential. *Biogeochemistry* 104, 381–392. doi: 10.1007/s10533-010-9512-8

Forster, P., Ramaswamy, V., Artaxo, P., Berntsen, T., Betts, R., Fahey, D. W., et al. (2007). "Changes in atmospheric constituents and in radiative forcing," in *Climate Change 2007: The Physical Science Basis,* eds S. Solomon, D. Qin, M. Manning, Z. Chen, M. Marquis, K. B. Averyt, et al. (New York, NY: Cambridge University Press), 129–234.

Gihring, T. M., Green, S. J., and Schadt, C. W. (2012). Massively parallel rRNA gene sequencing exacerbates the potential for biased community diversity comparisons due to variable library sizes. *Environ. Microbiol.* 14, 285–290. doi: 10.1111/j.1462-2920.2011.02550.x

Gohl, D. M., Vangay, P., Garbe, J., MacLean, A., Hauge, A., Becker, A., et al. (2016). Systematic improvement of amplicon marker gene methods for increased accuracy in microbiome studies. *Nat. Biotechnol.* 34, 942–949. doi: 10.1038/nbt.3601

Groffman, P. M., Altabet, M. A., Böhlke, J. K., Butterbach-Bahl, K., David, M. B., Firestone, M. K., et al. (2006). Methods for measuring denitrification: diverse approaches to a difficult problem. *Ecol. Appl.* 16, 2091–2122. doi: 10.1890/1051-0761(2006)016[2091:MFMDDA]2.0.CO;2

Guentzel, K. S., Hondzo, M., Badgley, B. D., Finlay, J. C., Sadowsky, M. J., and Kozarek, J. L. (2014). Measurement and modeling of denitrification in sand-bed streams under various land uses. *J. Environ. Qual.* 43, 1013–1023. doi: 10.2134/jeq2013.06.0249

Harvey, J. W., Böhlke, J. K., Voytek, M. A., Scott, D., and Tobias, C. R. (2013). Hyporheic zone denitrification: controls on effective reaction depth and contribution to whole-stream mass balance. *Water Res. Res.* 49, 6298–6316. doi: 10.1002/wrcr.20492

Hefting, M. M., Bobbink, R., and Janssens, M. P. (2006). Spatial variation in denitrification and N_2O emission in relation to nitrate removal efficiency in a N-stressed riparian buffer zone. *Ecosystems* 9, 550–563. doi: 10.1007/s10021-006-0160-8

Heiri, O., Lotter, A. F., and Lemcke, G. (2001). Loss on ignition as a method for estimating organic and carbonate content in sediments: reproducibility and comparability of results. *J. Paleolimnol.* 25, 101–110. doi: 10.1023/A:1008119611481

Humbert, S., Tarnawski, S., Fromin, N., Mallet, M.-P., Aragno, M., and Zopfi, J. (2010). Molecular detection of anammox bacteria in terrestrial ecosystems: distribution and diversity. *ISME J.* 4, 450–454. doi: 10.1038/ismej.2009.125

Huse, S. M., Welch, D. M., Morrison, H. G., and Sogin, M. L. (2010). Ironing out the wrinkles in the rare biosphere through improved OTU clustering. *Environ. Microbiol.* 12, 1889–1898. doi: 10.1111/j.1462-2920.2010.02193.x

Inwood, S. E., Tank, J. L., and Bernot, M. J. (2007). Factors controlling sediment denitrification in midwestern streams of varying land use. *Microb. Ecol.* 53, 247–258. doi: 10.1007/s00248-006-9104-2

Kandeler, E., Deiglmayr, K., Tscherko, D., Bru, D., and Philippot, L. (2006). Abundance of *narG*, *nirS*, *nirK*, and *nosZ* genes of denitrifying bacteria during primary successions of a glacier foreland. *Appl. Environ. Microbiol.* 72, 5957–5962. doi: 10.1128/AEM.00439-06

Kaushal, S. S., Groffman, P. M., Mayer, P. M., Striz, E., and Gold, A. J. (2008). Effects of stream restoration on denitrification in an urbanizing watershed. *Ecol. Appl.* 18, 789–804. doi: 10.1890/07-1159.1

Klocker, C. A., Kaushal, S. S., Groffman, P. M., Mayer, P. M., and Morgan, R. P. (2009). Nitrogen uptake and denitrification in restored and unrestored streams in urban Maryland, USA. *Aquat. Sci.* 71, 411–424. doi: 10.1007/s00027-009-0118-y

Kuenen, J. G. (2008). Anammox bacteria: from discovery to application. *Nat. Rev. Microbiol.* 6, 320–326. doi: 10.1038/nrmicro1857

Loken, L. C., Small, G. E., Finlay, J. C., Sterner, R. W., and Stanley, E. H. (2016). Nitrogen cycling in a freshwater estuary. *Biogeochemistry* 127, 199–216. doi: 10.1007/s10533-015-0175-3

Mahl, U. H., Tank, J. L., Roley, S. S., and Davis, R. T. (2015). Two-stage ditch floodplains enhance N-removal capacity and reduce turbidity and dissolved P in agricultural streams. *J. Am. Water Res. Assoc.* 51, 923–940. doi: 10.1111/1752-1688.12340

Manis, E., Royer, T. V., Johnson, L. T., Leff, L. G., and Hein, T. (2014). Denitrification in agriculturally impacted streams: seasonal changes in structure and function of the bacterial community. *PLoS ONE* 9:e105149. doi: 10.1371/journal.pone.0105149

Masclaux-Daubresse, C., Daniel-Vedele, F., Dechorgnat, J., Chardon, F., Gaufichon, L., and Suzuki, A. (2010). Nitrogen uptake, assimilation and remobilization in plants: challenges for sustainable and productive agriculture. *Ann. Bot.* 105, 1141–1157. doi: 10.1093/aob/mcq028

McClain, M. E., Boyer, E. W., Dent, C. L., Gergel, S. E., Grimm, N. B., Groffman, P. M., et al. (2003). Biogeochemical hot spots and hot moments at the interface of terrestrial and Aquatic Ecosystems. *Ecosystems* 6, 301–312. doi: 10.1007/s10021-003-0161-9

O'Connor, B. L., and Hondzo, M. (2008). Enhancement and inhibition of denitrification by fluid-flow and dissolved oxygen flux to stream sediments. *Environ. Sci. Technol.* 42, 119–125. doi: 10.1021/es071173s

Oksanen, J., Blanchet, F. G., Kindt, R., Legendre, P., Minchin, P. R., O'Hara, R. B., et al. (2015). *Vegan: Commity Ecology Package.*

Perryman, S. E., Rees, G. N., Walsh, C. J., and Grace, M. R. (2011). Urban stormwater runoff drives denitrifying community composition through changes in sediment texture and carbon content. *Microb. Ecol.* 61, 932–940. doi: 10.1007/s00248-011-9833-8

Petersen, D. G., Blazewicz, S. J., Firestone, M., Herman, D. J., Turetsky, M., and Waldrop, M. (2012). Abundance of microbial genes associated with nitrogen cycling as indices of biogeochemical process rates across a vegetation gradient in Alaska. *Environ. Microbiol.* 14, 993–1008. doi: 10.1111/j.1462-2920.2011.02679.x

Philippot, L., Andert, J., Jones, C. M., Bru, D., and Hallin, S. (2011). Importance of denitrifiers lacking the genes encoding the nitrous oxide reductase for N_2O emissions from soil. *Glob. Chang. Biol.* 17, 1497–1504. doi: 10.1111/j.1365-2486.2010.02334.x

Pinay, G., Gumiero, B., Tabacchi, E., Gimenez, O., Tabacchi-Planty, A. M., Hefting, M. M., et al. (2007). Patterns of denitrification rates in European alluvial soils under various hydrological regimes. *Freshw. Biol.* 52, 252–266. doi: 10.1111/j.1365-2427.2006.01680.x

Powlson, D. S., Addiscott, T. M., Benjamin, N., Cassman, K. G., de Kok, T. M., van Grinsven, H., et al. (2008). When does nitrate become a risk for humans? *J. Environ. Qual.* 37:291. doi: 10.2134/jeq2007.0177

Pringle, C. (2003). What is hydrologic connectivity and why is it ecologically important? *Hydrol. Process.* 17, 2685–2689. doi: 10.1002/hyp.5145

Pruesse, E., Quast, C., Knittel, K., Fuchs, B. M., Ludwig, W. G., Peplies, J., et al. (2007). SILVA: a comprehensive online resource for quality checked and aligned ribosomal RNA sequence data compatible with ARB. *Nucleic Acids Res.* 35, 7188–7196. doi: 10.1093/nar/gkm864

Rabalais, N. N., Turner, R. E., Sen Gupta, B. K., Boesch, D. F., Chapman, P., and Murrell, M. C. (2007). Hypoxia in the northern Gulf of Mexico: does the science support the plan to reduce, mitigate, and control hypoxia? *Estuar. Coasts* 30, 753–772. doi: 10.1007/B. F.02841332

R Core Team (2012). *R: A Language and Environment for Statistical Computing*. Vienna: R Foundation for Statistical Computing.

Robertson, G. P., Klingensmith, K. M., Klug, M. J., Paul, E. A., Crum, J. R., and Ellis, B. G. (1997). Soil resources, microbial activity, and primary production across an agricultural ecosystem. *Ecol. Appl.* 7, 158–170. doi: 10.1890/1051-0761(1997)007[0158:SRMAAP]2.0.CO;2

Rocca, J. D., Hall, E. K., Lennon, J. T., Evans, S. E., Waldrop, M. P., Cotner, J. B., et al. (2015). Relationships between protein-encoding gene abundance and corresponding process are commonly assumed yet rarely observed. *ISME J.* 9, 1693–1699. doi: 10.1038/ismej.2014.252

Roley, S. S., Tank, J. L., Stephen, M. L., Johnson, L. T., Beaulieu, J. J., and Witter, J. D. (2012a). Floodplain restoration enhances denitrification and reach-scale nitrogen removal in an agricultural stream. *Ecol. Appl.* 22, 281–297. doi: 10.1890/11-0381.1

Roley, S. S., Tank, J. L., and Williams, M. A. (2012b). Hydrologic connectivity increases denitrification in the hyporheic zone and restored floodplains of an agricultural stream. *J. Geophys. Res. Biogeosci.* 117:G00N04. doi: 10.1029/2012JG001950

Rösch, C., Mergel, A., and Bothe, H. (2002). Biodiversity of denitrifying and dinitrogen-fixing bacteria in an acid forest soil. *Appl. Environ. Microbiol.* 68, 3818–3829. doi: 10.1128/AEM.68.8.3818-3829.2002

Schloss, P. D., Westcott, S. L., Ryabin, T., Hall, J. R., Hartmann, M., Hollister, E. B., et al. (2009). Introducing mothur: open-source, platform-independent, community-supported software for describing and comparing microbial communities. *Appl. Environ. Microbiol.* 75, 7537–7541. doi: 10.1128/AEM.01541-09

Schloss, P. D. (2009). A high-throughput DNA sequence aligner for microbial ecology studies. *PLoS ONE* 4:e8230. doi: 10.1371/journal.pone.0008230

Schmidt, T. M., and Waldron, C. (2015). "Microbial diversity in soils of agricultural landscapes and its relation to ecosystem function," in *The Ecology of Agricultural Landscapes: Long-Term Research on the Path to Sustainability*, eds S. K. Hamilton, J. E. Doll, and G. P. Robertson (New York, NY: Oxford University Press), 135–157.

Shapleigh, J. P. (2006). "The denitrifying prokaryotes," in *The Prokaryotes*, eds M. Dworkin, S. Falkow, E. Rosenberg, K.-H. Schlieger, and E. Stackebrant (New York, NY: Springer), 769–792.

Shrewsbury, L. H., Smith, J. L., Huggins, D. R., Carpenter-Boggs, L., and Reardon, C. L. (2016). Denitrifier abundance has a greater influence on denitrification rates at larger landscape scales but is a lesser driver than environmental variables. *Soil Biol. Biochem.* 103, 221–231. doi: 10.1016/j.soilbio.2016.08.016

Song, K., Lee, S.-H., Mitsch, W. J., and Kang, H. (2010). Different responses of denitrification rates and denitrifying bacterial communities to hydrologic pulsing in created wetlands. *Soil Biol. Biochem.* 42, 1721–1727. doi: 10.1016/j.soilbio.2010.06.007

Staley, C., and Sadowsky, M. J. (2016). Application of metagenomics to assess microbial communities in water and other environmental matrices. *J. Mar. Biol. Assoc. U.K.* 96, 121–129. doi: 10.1017/S0025315415001496

Staley, C., Gould, T. J., Wang, P., Phillips, J., Cotner, J. B., and Sadowsky, M. J. (2015a). Species sorting and seasonal dynamics primarily shape bacterial communities in the Upper Mississippi River. *Sci. Total Environ.* 505, 435–445. doi: 10.1016/j.scitotenv.2014.10.012

Staley, C., Gould, T. J., Wang, P., Phillips, J., Cotner, J. B., and Sadowsky, M. J. (2015b). Evaluation of water sampling methodologies for amplicon-based characterization of bacterial community structure. *J. Microbiol. Methods* 114, 43–50. doi: 10.1016/j.mimet.2015.05.003

Svec, D., Tichopad, A., Novosadova, V., Pfaffl, M. W., and Kubista, M. (2015). How good is a PCR efficiency estimate: recommendations for precise and robust qPCR efficiency assessments. *Biomol. Detect. Quantif.* 3, 9–16. doi: 10.1016/j.bdq.2015.01.005

Tatariw, C., Chapman, E. L., Sponseller, R. A., Mortazavi, B., and Edmonds, J. W. (2013). Denitrification in a large river: consideration of geomorphic controls on microbial activity and community structure. *Ecology* 94, 2249–2262. doi: 10.1890/12-1765.1

Tiedje, J. (1982). "Denitrification," in *Methods of Soil Analysis, Part 2: Chemical and Microbiological Properties,* ed A. L. Page (Madison, WI: American Society of Agronomy: Soil Science Society of America), 1011–1026.

Tomasek, A., Kozarek, J., Hondzo, M., Lurndahl, N., Sadowsky, M., Wang, P., et al. (2017). Environmental drivers of denitrification rates and gene abundances in channels and riparian areas. *Water Res. Res.* 53, 6523–6538. doi: 10.1002/2016WR019566

USEPA (2010). *Methane and Nitrous Oxide Emissions from Natural Sources*. Washington, DC:USEPA.

Venterea, R. T., Halvorson, A. D., Kitchen, N., Liebig, M. A., Cavigelli, M. A., Del Grosso, S. J., et al. (2012). Challenges and opportunities for mitigating nitrous oxide emissions from fertilized cropping systems. *Front. Ecol. Environ.* 10, 562–570. doi: 10.1890/120062

Wang, Y., Zhu, G., Ye, L., Feng, X., Op den Camp, H. J. M., and Yin, C. (2012). Spatial distribution of archaeal and bacterial ammonia oxidizers in the littoral buffer zone of a nitrogen-rich lake. *J. Environ. Sci.* 24, 790–799. doi: 10.1016/S1001-0742(11)60861-9

Woodward, K. B., Fellows, C. S., Mitrovic, S. M., and Sheldon, F. (2015). Patterns and bioavailability of soil nutrients and carbon across a gradient of inundation frequencies in a lowland river channel, Murray–Darling Basin, Australia. *Agric. Ecosyst. Environ.* 205, 1–8. doi: 10.1016/j.agee.2015.02.019

Zhu, G., Wang, S., Wang, W., Wang, Y., Zhou, L., Jiang, B., et al. (2013). Hotspots of anaerobic ammonium oxidation at land-freshwater interfaces. *Nat. Geosci.* 6, 103–107. doi: 10.1038/ngeo1683

Zumft, W. G. (1997). Cell biology and molecular basis of denitrification. *Microbiol. Mol. Biol. Rev.* 61, 533–616.

Conflict of Interest Statement: The authors declare that the research was conducted in the absence of any commercial or financial relationships that could be construed as a potential conflict of interest.

The reviewer PV and handling Editor declared their shared affiliation.

frontiers in Microbiology

ORIGINAL RESEARCH
published: 04 April 2018
doi: 10.3389/fmicb.2018.00634

Urea Amendment Decreases Microbial Diversity and Selects for Specific Nitrifying Strains in Eight Contrasting Agricultural Soils

*Christopher Staley[1], Florence Breuillin-Sessoms[1], Ping Wang[1], Thomas Kaiser[1], Rodney T. Venterea[2,3] and Michael J. Sadowsky[1,2,4]**

[1] The BioTechnology Institute, University of Minnesota, St. Paul, MN, United States, [2] Department of Soil, Water, and Climate, University of Minnesota, St. Paul, MN, United States, [3] Soil and Water Management Research Unit, United States Department of Agriculture-Agricultural Research Service, St. Paul, MN, United States, [4] Department of Plant and Microbial Biology, University of Minnesota, St. Paul, MN, United States

OPEN ACCESS

Edited by:
Lourdes Girard,
Centro de Ciencias Genómicas, UNAM, Mexico

Reviewed by:
Christopher L. Hemme,
University of Rhode Island, United States
Annette Bollmann,
Miami University, United States

***Correspondence:**
Michael J. Sadowsky
sadowsky@umn.edu

Specialty section:
This article was submitted to Terrestrial Microbiology, a section of the journal Frontiers in Microbiology

Received: 02 November 2017
Accepted: 19 March 2018
Published: 04 April 2018

Citation:
Staley C, Breuillin-Sessoms F, Wang P, Kaiser T, Venterea RT and Sadowsky MJ (2018) Urea Amendment Decreases Microbial Diversity and Selects for Specific Nitrifying Strains in Eight Contrasting Agricultural Soils. Front. Microbiol. 9:634. doi: 10.3389/fmicb.2018.00634

Application of nitrogen (N) fertilizers, predominantly as urea, is a major source of reactive N in the environment, with wide ranging effects including increased greenhouse gas accumulation in the atmosphere and aquatic eutrophication. The soil microbial community is the principal driver of soil N cycling; thus, improved understanding of microbial community responses to urea addition has widespread implications. We used next-generation amplicon sequencing of the 16S rRNA gene to characterize bacterial and archaeal communities in eight contrasting agricultural soil types amended with 0, 100, or 500 μg N g^{-1} of urea and incubated for 21 days. We hypothesized that urea amendment would have common, direct effects on the abundance and diversity of members of the microbial community associated with nitrification, across all soils, and would further affect the broader heterotrophic community resulting in decreased diversity and variation in abundances of specific taxa. Significant ($P < 0.001$) differences in bacterial community diversity and composition were observed by site, but amendment with only the greatest urea concentration significantly decreased Shannon indices. Expansion in the abundances of members of the families *Microbacteriaceae*, *Chitinophagaceae*, *Comamonadaceae*, *Xanthomonadaceae*, and *Nitrosomonadaceae* were also consistently observed among all soils (linear discriminant analysis score ≥ 3.0). Analysis of nitrifier genera revealed diverse, soil-specific distributions of oligotypes (strains), but few were correlated with nitrification gene abundances that were reported in a previous study. Our results suggest that the majority of the bacterial and archaeal community are likely unassociated with N cycling, but are significantly negatively impacted by urea application. Furthermore, these results reveal that amendment with high concentrations of urea may reduce nitrifier diversity, favoring specific strains, specifically those within the nitrifying genera *Nitrobacter, Nitrospira,* and *Nitrosospira*, that may play significant roles related to N cycling in soils receiving intensive urea inputs.

Keywords: agriculture, microbial community, nitrogen cycle, soil, urea

INTRODUCTION

Worldwide demand for nitrogen (N) fertilizer is projected to increase at a rate of approximately 1.6 Tg (160,000 metric tons) of N per year, with much of the increase expected to occur in China (18%), India (17%) and Latin America (18%) (FAO, 2015). Production of N fertilizer via the Haber-Bosch process accounts for approximately 45% of global terrestrial N_2 fixation annually (Canfield et al., 2010). Due to its relative ease of transport and use, urea ($CO[NH_2]_2$) is the most dominant chemical form of N fertilizer used in the United States Corn Belt and across the world. Recent reporting by the United Nations Food and Agriculture Organization[1] indicated that approximately 80% of the total N fertilizer used worldwide in 2014 (113 Tg N) was in the form of urea (FAO, 2017). It is well known that application of N fertilizers is a major source of reactive N in the environment and contributes to several deleterious ecological outcomes. Negative effects include increased greenhouse gas composition of the atmosphere, stratospheric ozone depletion due to nitrous oxide (N_2O) emissions, water quality impairment due to nitrate (NO_3^-) entering ground and surface waters, and various impacts of atmospheric N deposition to terrestrial ecosystems (Galloway et al., 2003). The N fertilizer inputs to soil also support the increased production of cereals and other crops, which are needed to support a growing world population. Thus, improved understanding of the response of the soil microbial community, which drives N cycling, to urea addition has widespread implications and applications.

Once applied to soil, urea first undergoes hydrolytic reactions that produce ammonia (NH_3) which is then converted to nitrite (NO_2^-) and NO_3^- via nitrification processes (Prosser, 1990). These latter substrates can be further transformed to other by-products, including N_2O, by several processes including chemo-denitrification, nitrification, heterotrophic denitrification, and nitrifier-denitrification (Venterea et al., 2012). Denitrification is carried out under anaerobic conditions by a large variety of heterotrophic taxa, but only a few, such as *Pseudomonas* spp. and *Alcaligenes* spp., are numerically dominant in soils (Firestone and Davidson, 1989; Shoda, 2017), as are other members of the Alpha-, Beta-, and Gamma-proteobacteria (Jones et al., 2008). During nitrification, ammonia-oxidizing bacteria (AOB), such as those in the genera *Nitrosomonas* and *Nitrosospira,* as well as others, convert NH_3 to NO_2^-, followed by oxidation of NO_2^- to NO_3^- by nitrite-oxidizing bacteria (NOB), predominantly within the genera *Nitrobacter* and *Nitrospira* in soils (Robertson and Groffman, 2007; Klotz et al., 2011; Ruser and Schulz, 2015; Heil et al., 2016). Ammonia-oxidizing archaea (AOA) have also been reported, although their relative abundance and overall contribution to the formation of NO_2^- vary based on the environment studied (Leininger et al., 2006; Di et al., 2009; Zhang et al., 2012; Giguere et al., 2015; Ouyang et al., 2016). Furthermore, members of the genus *Nitrospira* have recently been reported to be capable of oxidizing both NH_3 and NO_2^-, in effect performing complete oxidation of NH_3 to NO_3^- (Daims et al., 2015; van Kessel et al., 2015).

[1] http://www.fao.org/faostat/en/#data/RF

Addition of N fertilizers to soil, in various chemical forms, has been shown to reduce heterotrophic respiration due to a variety of factors that may include soil acidification and impacts on carbon cycling (Janssens et al., 2010; Ramirez et al., 2010). It has been further postulated that increasing soil N availability may favor nitrogen-limited species that utilize carbon sources more efficiently (Ågren et al., 2001). Moreover, according to the subsidy-stress hypothesis, moderate levels of N addition may increase microbial diversity while greater amendment concentrations may have a more negative toxic effect resulting in decreased diversity (Odum et al., 1979; Odum, 1985). Changes in microbial community function and biomass in response to N addition have been characterized (Compton et al., 2004; Frey et al., 2004), and discrete changes in community composition are hypothesized to be soil-specific (Geisseler and Scow, 2014). Recent studies have reported how different soil types can respond differently to urea addition in their accumulation of intermediate N substrates (i.e., NO_2^- and NH_3) which are known to be toxic or inhibitory to a range of organisms, including AOB and NOB (Venterea et al., 2015; Breuillin-Sessoms et al., 2017). However, there remains a paucity of evidence regarding how the amendment of soil with N fertilizers, or with urea specifically, influences the soil microbial community at large.

Advances in next-generation sequencing have enabled an unprecedented assessment of bacterial diversity in a variety of environments (Sogin et al., 2006; Staley and Sadowsky, 2016). However, characterization of entire bacterial and archaeal communities in soils has remained a challenge due to a high degree of variability across very small spatial scales (Robertson et al., 1997; Blackwood et al., 2006; Schmidt and Waldron, 2015). For example, analyses done using Illumina next-generation sequencing indicated that soil bacterial communities from organic farms were shaped more by location than by specific treatment effects (Fernandez et al., 2016a). Quantification of some bacterial species related to nitrification and denitrification processes has been possible due to the development of polymerase chain reaction (PCR) assays (Geets et al., 2007). However, little is known about the diversity of species or strains associated with these gene targets or how abundances of these species might be related to the microbial community as a whole.

In this study, we used an Illumina next-generation sequencing approach to characterize the bacterial and archaeal communities in eight soil types with a range of chemical and physical properties collected from research fields distributed across the state of Minnesota. These soils were subsequently amended with varying concentrations of urea, as was described previously (Breuillin-Sessoms et al., 2017). We hypothesized that, despite site-specific differences in bacterial and archaeal communities, urea amendment would have a common effect on the abundance and diversity of members of the microbial community associated with nitrification processes, as well as potentially related taxa, across all soils. Furthermore, we hypothesized that urea amendment would further affect the broader heterotrophic community resulting in decreased diversity and variation in abundances of specific taxa. Results of this study provide novel insights into the response of the total bacterial and archaeal community to urea amendment

and describe specific shifts in populations of nitrifiers associated with N cycling.

MATERIALS AND METHODS

Sampling Sites and Soil Characterization

Agricultural soil samples were collected from eight research fields at University of Minnesota Research and Outreach centers distributed throughout the state, as previously described (Breuillin-Sessoms et al., 2017). Sites included Becker, Crookston, Lamberton, Waseca, Rosemount (two sites, tilled and non-tilled) (Venterea et al., 2006), and Saint Paul (two sites, cropped with either corn or soybeans). Samples were collected in 2014 following the autumn crop harvest from treatments receiving no N fertilizer addition. Soils were dried at room temperature for 7–10 days, sieved (2 mm), homogenized, and stored at 4°C until used. Initial soil composition and edaphic parameters are reported in Supplementary Table S1 as previously described (Breuillin-Sessoms et al., 2017).

Microcosm Design and Chemical Analyses

Microcosm experiments were performed in sterile 250-mL glass microcosm jars as previously described (Breuillin-Sessoms et al., 2017). Briefly, 10–13 g soil from a single sampling site was added to a series of replicated microcosms and the moisture content was adjusted to 85% water holding capacity containing reagent grade urea [$CO(NH_2)_2$] and purified water at treatment levels of 0 (water only), 100, and 500 $\mu g\ N\ g^{-1}$ dry soil. These urea concentrations were selected to cover a range of soil chemical conditions following different N fertilizer application practices, with the greater concentration (500 $\mu g\ N\ g^{-1}$) representing potential conditions within fertilizer bands and/or within close proximity to urea granules (Wetselaar et al., 1972; Yadvinger-Singh and Beauchamp, 1988), whereas the lower (100 $\mu g\ N\ g^{-1}$) concentration is more representative of uniform (broadcast) application methods. Microcosms were maintained under aerobic conditions in the dark at 22°C through a 21-day sample collection. A destructive sampling method was used, with triplicate jars per soil type and urea amendment sacrificed at 0, 4, 14, and 21 days for next-generation sequence analysis. Analyses of several chemical variables were performed as described previously (Breuillin-Sessoms et al., 2017) (summarized here briefly in Supplementary Methods) and values used in the present study are summarized in Supplementary Table S2. Effects of drying/re-wetting soils were not specifically evaluated in this study, although these physical dynamics may also impact changes in the microbial community composition in a soil-specific manner (Fierer et al., 2003).

DNA Extraction and Quantitative PCR Assays

DNA was extracted from 250 mg (wet weight) of soil using the DNeasy® PowerSoil Kit® (QIAGEN, Hilden, Germany) according to the manufacturer's instructions, with the final elution performed twice. The DNA extracts were subjected to qPCR analysis of abundances for *amoA*, *nxrA*, and *nxrB* genes that were previously reported (Breuillin-Sessoms et al., 2017). These qPCR data are included in the current study only as metadata to offer some contextualization of 16S rRNA amplicon sequencing results. Quantitative PCR (qPCR) analyses were performed on 1:10 dilutions of DNA extracts in PCR-grade water using the 7500 Fast Real Time PCR system (Applied Biosystems, Foster City, CA, United States) and iTaq Universal SYBR Green Supermix (Bio-Rad Laboratories, Inc., Hercules, CA, United States) as described previously (Breuillin-Sessoms et al., 2017). For enumeration of the 16S rRNA gene, the 515F/806R primer set targeting the V4 hypervariable region was used (Caporaso et al., 2012). For all assays, samples were run in triplicate, with no-template-added negative controls. Standard curves were used to estimate gene copy number, with r^2 values $\geq$ 0.99 and efficiencies between 80 and 95%. Quantitative PCR data used in the present study are summarized in Supplementary Table S3.

Next-Generation Sequencing

Undiluted DNA (see above) was also used as a template for amplification and Illumina next-generation sequencing of the V4 hypervariable region using the dual index method by the University of Minnesota Genomics Center [UMGC, (Gohl et al., 2016)]. Briefly, samples were amplified using 25 cycles with primers without full adapter sequences or barcoding indices, followed by addition of adapters and barcodes with an additional 10 cycles of PCR. Amplicons were size-selected, pooled, and paired-end sequenced at a read length of 250 nucleotides (nt) on the Illumina HiSeq2500 platform (Illumina, Inc., San Diego, CA, United States) by UMGC. Sequence data were returned as fastq files and are deposited in the Sequence Read Archive of the National Center for Biotechnology Information under BioProject accession number SRP106784.

Bioinformatics

Sequence data were processed and analyzed using mothur ver. 1.35.1 (Schloss et al., 2009), and processed as described previously (Staley et al., 2015). Briefly, samples were trimmed to 160 nt, paired-end joined using fastq-join software (Aronesty, 2013), and trimmed for quality based on quality score (>35), homopolymer length (8 nt), ambiguous bases, and primer mismatches (2 nt). Samples were aligned against the SILVA database ver. 123 (Pruesse et al., 2007), subjected to a 2% pre-cluster step to remove sequence errors (Huse et al., 2010), and chimeras were identified and removed using UCHIME (Edgar et al., 2011). Operational taxonomic units (OTUs) were identified at 97% similarity using the complete-linkage algorithm and taxonomic classifications were made using the version 14 release from the Ribosomal Database Project (Cole et al., 2009).

Alpha diversity indices, as well as Good's coverage, were calculated using the Shannon index and abundance-based coverage estimate (ACE) using mothur. Differences in beta diversity were evaluated using Bray–Curtis dissimilarity matrices (Bray and Curtis, 1957), which accounts for differences in abundance of OTUs. Differences in community

composition were evaluated by analysis of similarity (ANOSIM) (Clarke, 1993), while differences in sample clustering were evaluated by analysis of molecular variance (AMOVA) (Excoffier et al., 1992). Ordination of samples was performed by principal coordinate analysis (PCoA) (Anderson and Willis, 2003). Operational taxonomic units that differed significantly in abundance by treatment were determined using linear discriminant analysis of effect sizes (LEfSe) (Segata and Huttenhower, 2011), and were subsequently classified to families. Oligotyping analyses were used to determine potential species- and strain-level distributions among nitrifiers, according to recommended best practices (Eren et al., 2013). An oligotype was defined as present in more than 1% of reads, present in at least three samples, the most abundant unique sequence occurred at a minimum of 50 reads, and if the minimum read abundance throughout the dataset was at least 250.

Statistical Analyses

For statistical analyses, chemical analyte and qPCR data were $\log_{10}$ transformed, as performed previously (Breuillin-Sessoms et al., 2017), and bacterial and archaeal abundances were evaluated as percentages of total sequence reads. For statistical comparisons, all samples were rarefied to 50,000 reads per sample by random subsampling (Gihring et al., 2012). Statistics were calculated using XLSTAT ver. 2015.5.01 (Addinsoft, Belmont, MA, United States). ANOVA analyses were performed with Tukey's *post hoc* test and correlations were determined using Spearman rank correlations. Canonical correspondence analysis was used to describe multivariate analyses. Variance partitioning was performed using partial redundancy analysis as described previously (Borcard et al., 1992), using the vegan package in R ver. 3.2.2 (R Core Team, 2012; Oksanen et al., 2015). All statistics were evaluated at $\alpha = 0.05$ with Bonferroni correction for multiple comparisons.

RESULTS

Bacterial and Archaeal Community Alpha Diversity

Bacterial and archaeal communities showed high species richness among all samples, with a mean abundance-based coverage estimate (ACE) of 11,179 ± 2,570 (mean ± standard deviation, range: 5,564–20,216). The mean estimated Good's coverage, after rarefaction, was 95.1 ± 0.8%, among all samples. Samples from Becker, both the Rosemount sites, and the St. Paul (soybean) soil had significantly greater Shannon indices (means 6.94 – 6.96, **Table 1**) than did the Crookston, Lamberton, and St. Paul (corn) soils (means 6.71 – 6.79; Tukey's *post hoc* $P < 0.05$). Samples from St. Paul (corn) and Waseca had intermediate Shannon indices among all sites (6.79 ± 0.30 and 6.90 ± 0.10, respectively), while those from Crookston and Lamberton were significantly lower than all the other sites (6.71 ± 0.22 and 6.72 ± 0.09, respectively; $P < 0.05$), except St. Paul (corn).

Variation in alpha diversity resulting from urea amendment and time post-treatment showed soil-specific patterns (**Table 1**). Samples from soils amended with 500 μg N g^{-1} soil (6.71 ± 0.25)

TABLE 1 | Shannon indices (mean ± standard deviation) of microbial communities in triplicate soil samples.

Urea (μg N g^{-1})	Day	Becker	Crookston	Lamberton	Waseca	Rosemount (tilled)	Rosemount (non-tilled)	St. Paul (corn)	St. Paul (soybean)
0	0	7.24 ± 0.19^{A}	$6.78 \pm 0.03^{A-K}$	$6.77 \pm 0.08^{B-K}$	$6.94 \pm 0.01^{A-I}$	$7.04 \pm 0.04^{*,A-F}$	$7.09 \pm 0.05^{A-D}$	$7.06 \pm 0.03^{A-F}$	$7.09 \pm 0.04^{A-E}$
0	4	$6.97 \pm 0.21^{A-I}$	$6.83 \pm 0.07^{A-K}$	$6.65 \pm 0.07^{C-K}$	6.94 ± 0.01^{ABC}	$7.01 \pm 0.04^{A-F}$	$6.96 \pm 0.05^{A-I}$	$6.94 \pm 0.08^{A-I}$	$6.98 \pm 0.05^{A-I}$
0	14	7.22 ± 0.06^{AB}	$6.80 \pm 0.06^{A-K}$	$6.85 \pm 0.10^{A-K}$	$6.93^{\dagger,A-F}$	$6.99 \pm 0.05^{A-H}$	$6.98 \pm 0.07^{A-I}$	$7.01 \pm 0.00^{A-F}$	$6.97 \pm 0.02^{A-I}$
0	21	$7.14 \pm 0.01^{A-I}$	$6.80 \pm 0.01^{C-K}$	$6.78 \pm 0.07^{A-K}$	$6.87 \pm 0.04^{*,A-I}$	$7.07 \pm 0.06^{A-F}$	$6.97 \pm 0.05^{A-F}$	$6.93 \pm 0.04^{B-K}$	$6.99 \pm 0.03^{A-F}$
100	4	$7.00 \pm 0.05^{A-H}$	$6.80 \pm 0.01^{A-K}$	$6.69 \pm 0.03^{C-K}$	$7.04 \pm 0.10^{A-F}$	$6.89 \pm 0.04^{A-K}$	$6.90 \pm 0.08^{A-J}$	$6.89 \pm 0.01^{A-K}$	$6.95 \pm 0.03^{A-I}$
100	14	$7.03 \pm 0.11^{A-F}$	$6.85 \pm 0.01^{A-K}$	$6.69 \pm 0.03^{C-K}$	$6.87 \pm 0.01^{A-I}$	$6.98 \pm 0.02^{A-I}$	$6.98 \pm 0.03^{A-I}$	$6.91 \pm 0.02^{A-J}$	$6.95 \pm 0.04^{*,A-I}$
100	21	$7.09 \pm 0.06^{A-I}$	$6.77 \pm 0.05^{C-K}$	$6.76 \pm 0.08^{A-K}$	$6.94 \pm 0.17^{A-K}$	$7.00 \pm 0.06^{A-G}$	$6.91 \pm 0.04^{A-F}$	$6.88 \pm 0.01^{C-K}$	$6.96 \pm 0.05^{A-F}$
500	4	$6.63 \pm 0.07^{A-K}$	$6.78 \pm 0.04^{F-K}$	$6.63 \pm 0.04^{C-K}$	$6.87 \pm 0.01^{A-K}$	$6.92 \pm 0.03^{A-J}$	$6.97 \pm 0.08^{A-I}$	$6.88 \pm 0.09^{D-K}$	$6.96 \pm 0.02^{A-I}$
500	14	$6.85 \pm 0.14^{B-K}$	6.55 ± 0.02^{IJK}	$6.69 \pm 0.06^{E-K}$	$6.81 \pm 0.05^{C-K}$	$6.86 \pm 0.02^{A-K}$	$6.89 \pm 0.09^{A-K}$	$6.23 \pm 0.08^{G-K}$	$6.92 \pm 0.05^{A-K}$
500	21	$6.46 \pm 0.11^{C-K}$	6.10 ± 0.02^{K}	$6.67 \pm 0.07^{H-K}$	$6.77 \pm 0.09^{F-K}$	$6.65 \pm 0.30^{C-K}$	$6.88 \pm 0.05^{B-K}$	6.20 ± 0.07^{JK}	$6.86 \pm 0.06^{B-K}$

*$^{A-K}$Samples sharing the same superscript did not differ significantly by Tukey's post hoc test ($P > 0.05$). *Only two samples returned sufficient sequence reads for analysis. †Only one sample returned sufficient sequence reads for analysis.*

had significantly lower Shannon indices than unamended or 100-μg-N-treated soils ($P < 0.0001$). The most significant shifts in Shannon indices (e.g., in the 500 μg N g^{-1} treatment at Becker on day 21) represented a loss of up to 2,800 OTUs following treatment, as estimated by ACE richness. At the 14 and 21 days post-treatment (6.86 ± 0.20 and 6.81 ± 0.26, respectively) experimental conditions resulted in significantly lower Shannon diversity than that observed prior to any treatment (7.00 ± 0.17; $P \leq 0.037$). In contrast, there were no differences in Shannon indices in samples collected from unamended soil or soil amended with 100 μg N g^{-1} soil (means 6.96 ± 0.14 and 6.90 ± 0.12, respectively; $P = 0.259$), among all sites.

Bacterial and Archaeal Community Composition and Beta Diversity

Bacterial communities among all soils were primarily comprised of members of the bacterial phyla *Actinobacteria, Proteobacteria*, and *Acidobacteria*, which together represented more than 65% of sequence reads in all samples and time points (Supplementary Figure S1). Several sites also showed abundances of members of the archaeal phylum *Thaumarchaeota* that represented up to 13% of sequence reads. When classified to families (Supplementary Figure S2), members of the *Gaiellaceae* and *Sphingomonadaceae* were among the predominant bacteria classified, while nearly all archaeal taxa were classified within the genus *Nitrososphaera* in the family *Nitrososphaeraceae*. Taxa representing approximately 20–30% of sequence reads could not be further classified to bacterial and archaeal families, and members of low abundance families (consolidated in Supplementary Figure S1 and found at mean abundances < 1.5% of sequence reads) accounted for another 30–40% of sequence reads.

Linear discriminant analysis (LDA) of effect sizes (LEfSe) showed that OTUs classified within the families *Microbacteriaceae*, *Chitinophagaceae*, *Comamonadaceae*, *Xanthomonadaceae*, and *Nitrosomonadaceae* were predominantly identified as taxa with greater abundances in soils receiving more concentrated urea amendments (LDA score ≥ 3.0), in individual soils among all time points (data not shown). When LEfSe analysis was applied to all samples and time points, only five OTUs were identified as having greater abundance in the 500 μg N g^{-1} soil amendment, and the OTUs were similarly classified to these same families (Supplementary Figure S3). Changes in abundance of these families reflected an increase at greater urea amendment through the 21-day time point (**Figure 1**), although we did observe site-specific differences in the magnitude of shifts among families. When all samples were analyzed to determine consistent variation by time, only two OTUs within the *Xanthomonadaceae* were identified as indicators of the 4- and 21-day time points (one OTU per time point).

Ordination of Bray–Curtis dissimilarity matrices (a measure of difference in abundances of OTUs) by principal coordinate analysis (PCoA, **Figure 2**) revealed independent clustering of samples by soil, as evaluated by analysis of molecular variance (AMOVA, $P < 0.001$). Grouping of samples based on urea treatment or time-post-treatment were not significant ($P = 0.110$ and 0.744, respectively), among all samples. These groupings were also supported by differences in community composition, evaluated by analysis of similarity (ANOSIM, $P < 0.001$ for pairwise soil comparisons and $P = 0.078$ and 0.595 for treatment and time, respectively).

Within a site-specific soil type (Supplementary Figure S4), significant temporal shifts in community composition were generally observed between the 4-day time point and those taken 14 or 21 days following treatment ($P < 0.008$), although significant temporal shifts were not observed in the Waseca or Rosemount (tilled) soils. However, urea amendments had more significant effects than did temporal variation on community composition (ANOSIM $R = 0.32 \pm 0.14$ and 0.22 ± 0.07, respectively; **Table 2**).

Variation in Edaphic Parameters, Community Composition, and Nitrification Genes

Variance partitioning by partial redundancy analysis was used to evaluate drivers of community variation at the 21-day time point. This was taken as the relative abundances of all bacterial and archaeal families ($n = 348$) that was attributable to initial edaphic parameters prior to amendment (Supplementary Table S1), soil chemical properties following treatment (Supplementary Table S2), along with urea amendment, or both initial and treatment effects. The initial edaphic properties, including soil composition, pH, organic matter, organic N, organic C, cation exchange capacity, K, and moisture content accounted for 17.7% of community variation, among all soils. Furthermore, only 22.0% of variation was explained by concentrations of N-chemical analytes, H, CO_2, and urea. The remaining 60.3% of variation was constrained by these variables interacting in some combination to influence the bacterial and archaeal communities.

Canonical correspondence analysis (**Figure 3**) showed strong and significant correlations between the urea amendment concentrations and N-analytes or CO_2 at 21 days post-treatment (Spearman's $\rho = 0.363$ – 0.886, $P < 0.05$), and the majority of N-analytes were significantly and positively correlated amongst each other. Urea amendment concentration was also positively correlated with gene abundances of bacterial *amoA* and *nxrA* ($\rho = 0.923$ and 0.513, $P < 0.0001$). Conversely, the relative abundances of all members of the *Microbacteriaceae*, *Chitinophagaceae*, *Comamonadaceae*, and *Xanthomonadaceae* were significantly negatively correlated with the concentrations of many N-analytes, including N_2O, and gene abundances of *amoA* and *nxrA*. Soil pH was significantly and positively correlated with abundances of *Microbacteriaceae* ($\rho = 0.679$, $P < 0.0001$), but was negatively correlated with abundances of the *Chitinophagaceae, Comamonadaceae*, and *Nitrosomonadaceae* ($\rho = -0.561$ to -0.394, $P \leq 0.001$). Other soil edaphic parameters tended to be positively inter-correlated with fewer significant relationships to N-analytes, relative abundances of bacterial families, or nitrification gene abundances.

Oligotyping of Nitrifying Prokaryotes

Oligotyping analyses were done to determine the distribution of likely species or strains among the nitrifying genera *Nitrosospira,*

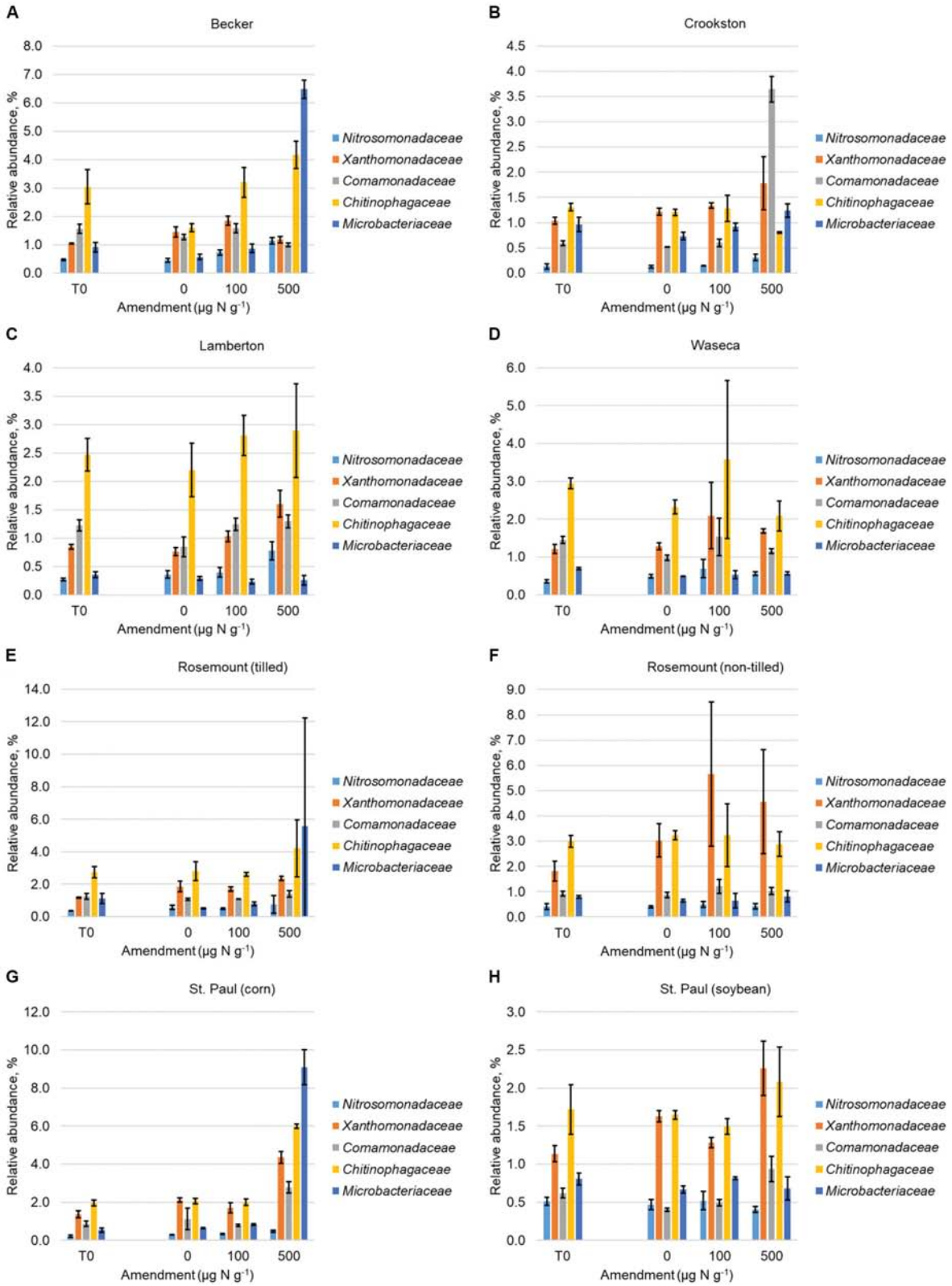

FIGURE 1 | Abundances (mean ± standard deviation) of families to which OTUs that were discriminatory for urea amendment (Supplementary Figure S3) were classified. Abundances are shown prior to urea amendment and at the 21-day time point for each amendment at **(A)** Becker, **(B)** Crookston, **(C)** Lamberton, **(D)** Waseca, **(E)** Rosemount (tilled), **(F)** Rosemount (non-tilled), **(G)** St. Paul (corn), **(H)** St. Paul (soybean).

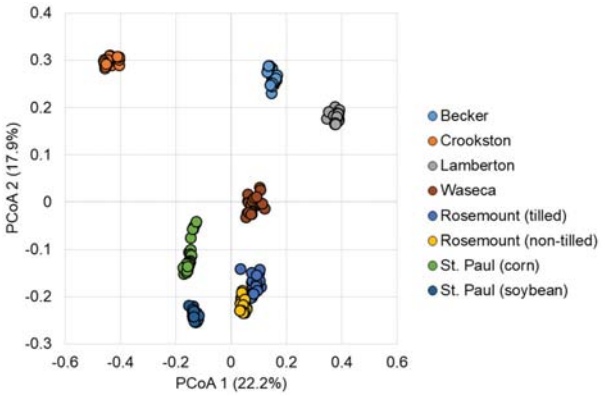

FIGURE 2 | Principal coordinate analysis of Bray–Curtis dissimilarity matrices among all samples (r^2 = 0.76).

Nitrospira, *Nitrobacter,* and *Nitrososphaera* (**Table 3**, **Figure 4**, and Supplementary Figures S5–S7), as well as their relationships to urea amendment and nitrification gene abundances (**Figure 5**). The distributions of oligotypes within the bacterial genera showed considerably greater, soil-specific shifts due to urea amendment concentration through the 21-day time point (**Figure 4** and Supplementary Figures S5–S7), relative to the archaeal genus *Nitrososphaera* (Supplementary Figure S7). Importantly, the relative abundances of only two oligotypes within the *Nitrobacter* or *Nitrospira* were significantly ($P < 0.05$) correlated with urea amendment concentration. In both genera, one oligotype was positively correlated, while the other was negatively correlated with amendment concentration. Similarly, among *Nitrosospira*, only the abundance of one oligotype was significantly positively correlated with urea concentration, while four were negatively correlated. Oligotyping was not performed on *Nitrosomonas* due to a low number of OTUs classified ($n = 7$, compared to >100 for other genera oligotyped).

The *Nitrobacter* oligotypes that were significantly related to nitrification gene abundances tended also to be positively correlated with abundances of *nxrA* and negatively correlated with *nxrB*. The oligotype 1 was also significantly positively correlated with bacterial *amoA* abundances (**Figure 5A**). Conversely, while several of the *Nitrospira* were positively correlated with abundances of *nxrB*, others showed positive correlations with *nxrA*, but only one (oligotype 1) showed a significant negative correlation with *amoA* (**Figure 5B**). Among the *Nitrosospira*, oligotype 1 was significantly positively correlated with *amoA* while other oligotypes that showed significant correlations with nitrification genes were positively correlated with *nxrB* (**Figure 5C**). Among the *Nitrososphaera* (**Figure 5D**), significant positive correlations were observed with oligotype abundances and *nxrA* or *nxrB*, but few showed significant relationships with more than one gene target.

TABLE 2 | Beta diversity statistics relating communities by urea treatment at each sampling site.

Site	Urea add (μg N/g soil)	0	100	500
Becker	**0**		**0.35, 0.003**	**0.85, <0.001**
	100	**2.48, 0.004**		**0.74, <0.001**
	500	**8.36, <0.001**	**6.47, <0.001**	
Crookston	**0**		<−0.01, 0.44	**0.40, 0.001**
	100	1.23, 0.051		**0.29, 0.007**
	500	**4.71, <0.001**	**3.93, 0.004**	
Lamberton	**0**		0.07, 0.118	**0.25, 0.003**
	100	1.28, 0.106		0.16, 0.020
	500	**2.40, 0.006**	**1.94, 0.004**	
Waseca	**0**		**0.35, 0.005**	**0.25, 0.001**
	100	**3.62, 0.005**		0.12, 0.082
	500	1.96, 0.068	1.35, 0.198	
Rosemount (tilled)	**0**		**0.33, 0.002**	**0.42, <0.001**
	100	**2.83, 0.001**		**0.25, <0.001**
	500	**3.78, <0.001**	**2.25, <0.001**	
Rosemount (non-tilled)	**0**		**0.20, 0.008**	**0.60, <0.001**
	100	**1.92, 0.004**		0.10, 0.048
	500	**3.61, <0.001**	1.42, 0.075	
St. Paul (corn)	**0**		0.05, 0.167	**0.64, <0.001**
	100	**1.55, 0.015**		**0.56, <0.001**
	500	**8.03, <0.001**	**6.91, <0.001**	
St. Paul (soybean)	**0**		0.20, 0.026	**0.56, <0.001**
	100	**1.53, 0.006**		**0.23, 0.008**
	500	**3.13, <0.001**	1.77, 0.033	

ANOSIM R-values and P-values are presented in the top matrix for each soil type. AMOVA F-statistic and P-values are presented in the bottom matrix for each soil type. Significance values are shown in bold. All statistics were evaluated at Bonferroni-corrected α = 0.02.

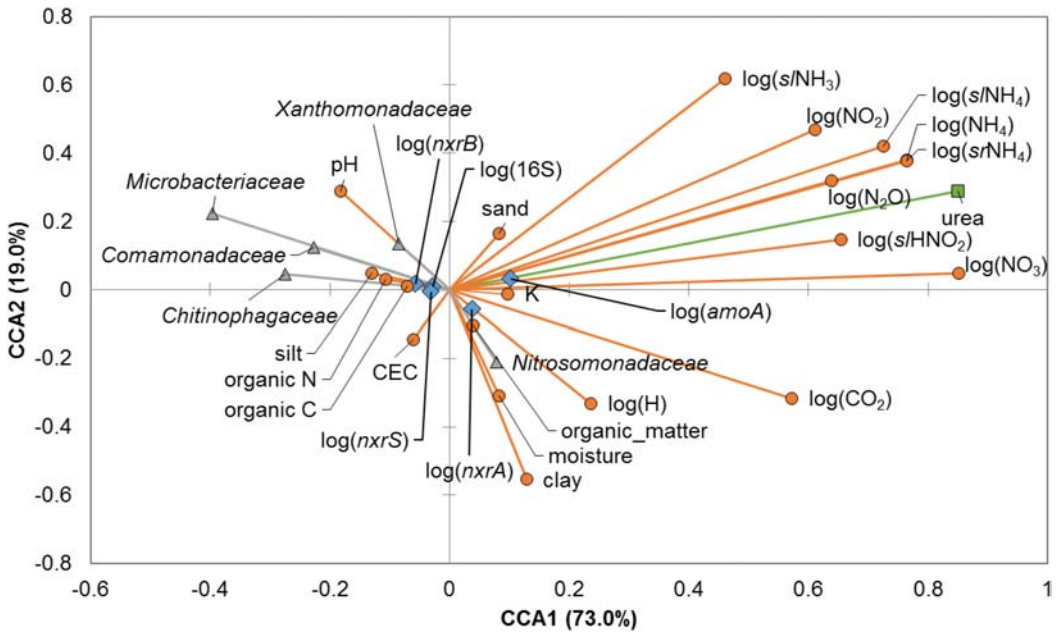

FIGURE 3 | Canonical correspondence analysis (CCA) relating bacterial families, edaphic and physicochemical parameters, and abundances of nitrification genes at 21 days post-treatment. Bacterial families presented are those in which OTUs determined to differ significantly due to nitrogen treatment by LEfSe analysis were classified. Relative abundances of all members of the families were used for CCA. Edaphic parameters and N-chemical analytes are shown as orange circles, abundances of bacterial families are shown as gray triangles, urea amendment is shown as a green square, and nitrification genes are shown as blue diamonds.

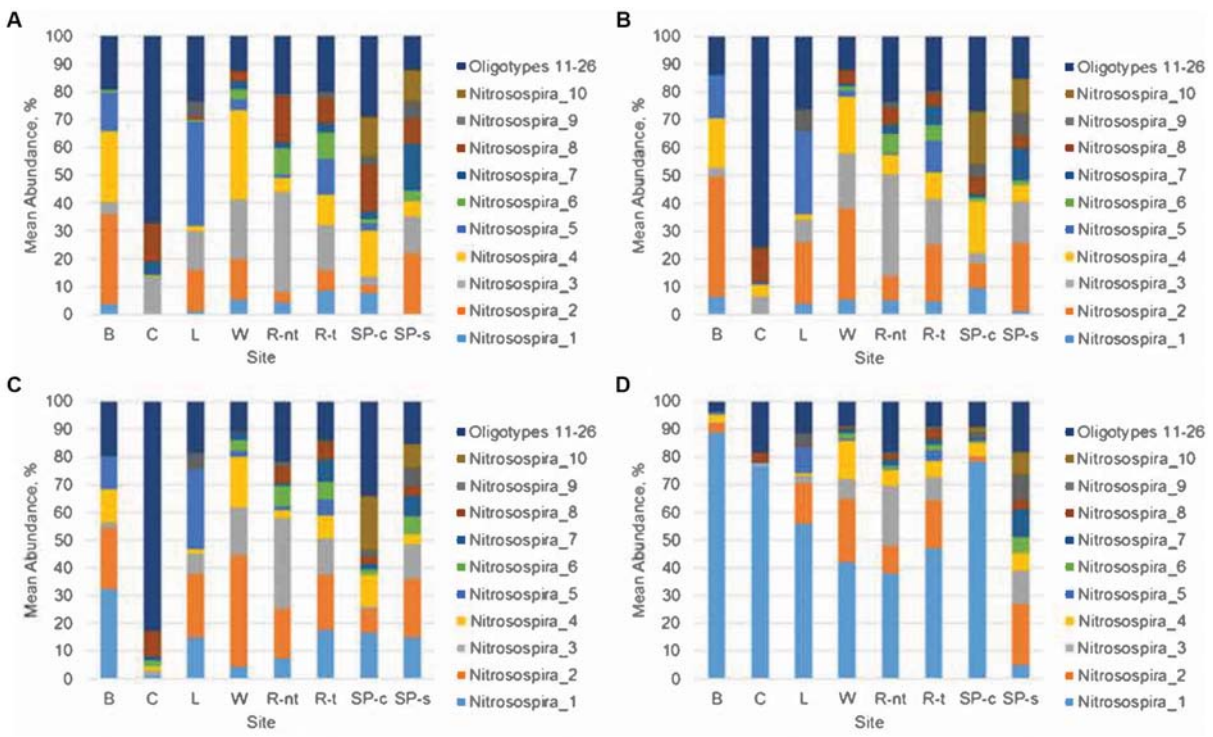

FIGURE 4 | Distribution of oligotypes within the genus *Nitrosospira*. **(A)** Initial sampling, prior to treatment, **(B)** no urea amendment, day 21, **(C)** 100 μg N g^{-1} soil amendment, day 21, **(D)** 500 μg N g^{-1} soil amendment, day 21. Sampling sites include Becker (B); Crookston (C); Lamberton (L); Waseca (W); Rosemount (non-tilled, R-nt); Rosemount (tilled, R-t), St. Paul (corn, SP-c), and St. Paul (soybean, SP-s).

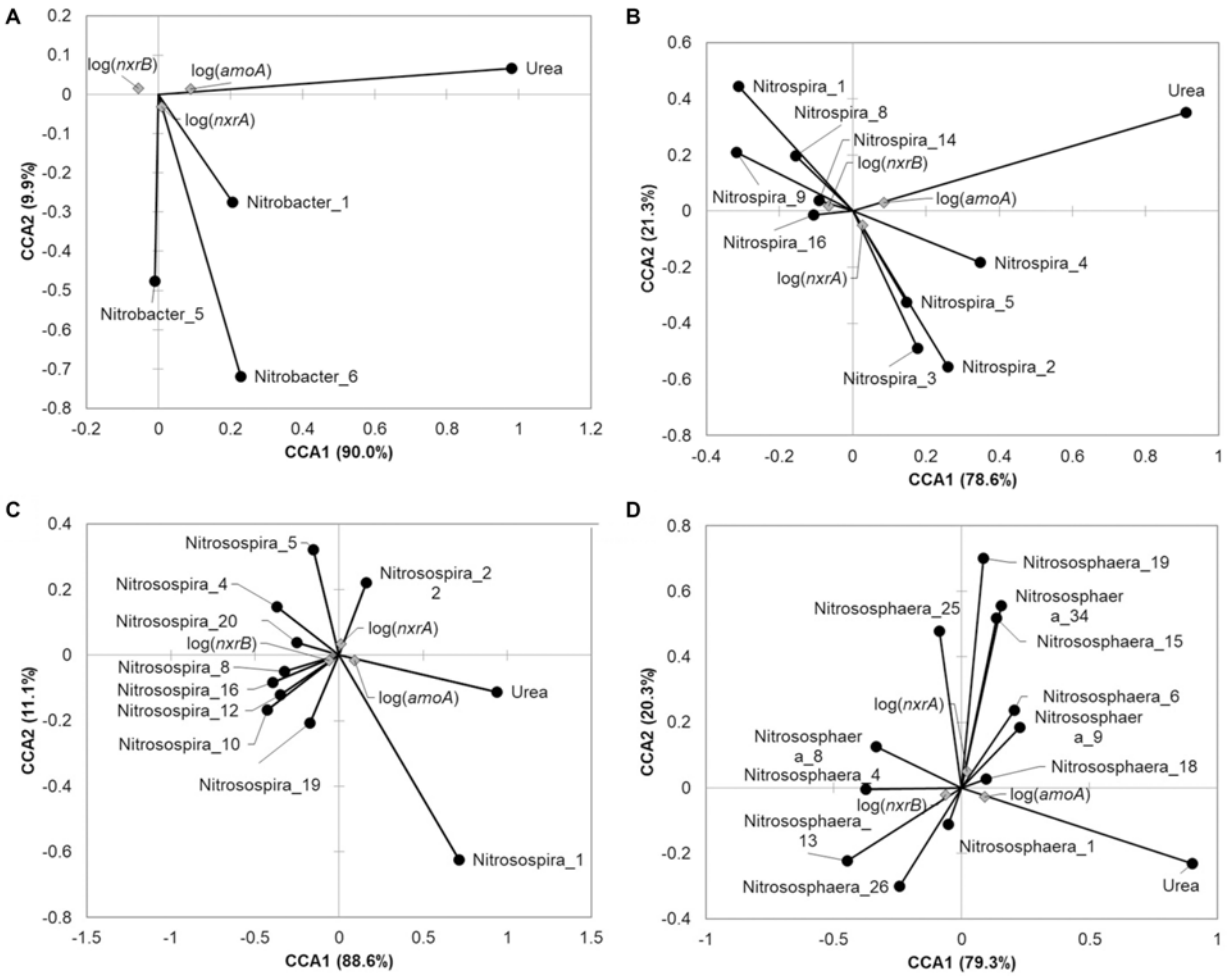

FIGURE 5 | Canonical correspondence analysis relating oligotypes and urea amendment concentration to abundance of nitrification genes at 21 days post-treatment. Relative abundance of the oligotype within the genus was used for analysis for **(A)** *Nitrobacter*, **(B)** *Nitrospira*, **(C)** *Nitrosospira*, or **(D)** *Nitrososphaera.* Only those oligotypes that showed significant Spearman correlations ($P < 0.05$) with nitrification genes are shown.

TABLE 3 | Mean abundances (±standard deviation, as %) of nitrifying prokaryotic taxa interrogated by oligotyping.

Site	Nitrosospira	Nitrospira	Nitrobacter	Nitrososphaera
Becker	0.61 ± 0.27 (0.20 – 1.27)	0.39 ± 0.17 (0.13 – 0.67)	0.10 ± 0.04 (0.05 – 0.25)	1.48 ± 0.51 (0.67 – 2.89)
Crookston	0.21 ± 0.14 (0.07 – 0.74)	0.48 ± 0.09 (0.27 – 0.66)	0.14 ± 0.03 (0.07 – 0.21)	12.18 ± 1.16 (10.05 – 14.49)
Lamberton	0.50 ± 0.26 (0.25 – 1.42)	0.32 ± 0.06 (0.21 – 0.48)	0.16 ± 0.03 (0.11 – 0.22)	3.97 ± 0.94 (1.68 – 5.82)
Waseca	0.67 ± 0.26 (0.32 – 1.34)	0.32 ± 0.07 (0.19 – 0.43)	0.07 ± 0.02 (0.04 – 0.11)	4.86 ± 1.64 (1.83 – 7.17)
Rosemount (tilled)	0.58 ± 0.25 (0.21 – 1.28)	0.43 ± 0.11 (0.20 – 0.57)	0.09 ± 0.03 (0.04 – 0.15)	6.85 ± 1.47 (3.29 – 9.74)
Rosemount (non-tilled)	0.41 ± 0.09 (0.26 – 0.63)	0.29 ± 0.07 (0.14 – 0.46)	0.14 ± 0.03 (0.09 – 0.20)	4.87 ± 1.11 (2.45 – 8.51)
St. Paul (corn)	0.36 ± 0.11 (0.16 – 0.58)	0.42 ± 0.10 (0.20 – 0.56)	0.02 ± 0.01 (0.00 – 0.05)	5.13 ± 1.45 (2.19 – 7.08)
St. Paul (soybean)	0.56 ± 0.25 (0.36 – 1.55)	0.50 ± 0.07 (0.35 – 0.64)	0.32 ± 0.42 (0.07 – 1.26)	5.41 ± 0.74 (3.05 – 6.41)

Range is shown in parentheses. All samples from each site are summarized, regardless of time point or treatment.

DISCUSSION

Bacterial and archaeal communities characterized in this study primarily showed variation as a result of sample location, similar to previous findings using Illumina sequencing in organic agricultural soils (Fernandez et al., 2016a,b). Soil-specific communities were further supported by variance partitioning and the initial soil characteristics explained 18% of the community, consistent with previous studies that demonstrated legacy effects of moisture on both soil community composition and N_2O flux (Banerjee et al., 2016). Among all sites and soils, the amendment with 500 μg N g^{-1} resulted in declines

in alpha diversity and consistent expansions in abundances of members of the families *Microbacteriaceae*, *Chitinophagaceae*, *Comamonadaceae*, *Xanthomonadaceae*, and *Nitrosomonadaceae*, typically by 14 days following amendment. The rapidity and extent of these changes, however, varied in a soil-dependent manner. In contrast, amendment with 100 μg N g^{-1} soil did not greatly affect overall alpha diversity in soils, but did result in significant community shifts in most of the tested soils that could not be attributed to specific taxa. This decrease in diversity is consistent with meta-analyses showing decreased microbial diversity in response to urea, but not other mineral fertilizers (Geisseler and Scow, 2014). Results of our study align well with the previous postulated subsidy-stress hypothesis, where low levels of urea amendment may stimulate N cycling in the communities, by either increasing microbial diversity or activity. In contrast, greater levels prove toxic to members of the microbial community resulting in decreased diversity (Odum et al., 1979; Odum, 1985). Similarly, in rice paddy soils amended with 200 μg N g^{-1} soil, urea amendment did not significantly affect alpha diversity, but also had no significant impact on community composition (Wang et al., 2015), although a more shallow sequencing depth (∼13,000 reads) was used in the previous study.

We hypothesized that urea amendments would result in consistent shifts in the bacterial and archaeal soil communities, despite high diversity and soil-specific variation in community composition and edaphic parameters, potentially due to a direct effect of this chemical amendment or changes in physicochemical parameters associated with reduced heterotrophic respiration (Janssens et al., 2010; Ramirez et al., 2010). Among all the soils examined, OTUs that classified to five families (*Microbacteriaceae*, *Chitinophagaceae*, *Comamonadaceae*, *Xanthomonadaceae*, and *Nitrosomonadaceae*) were consistently found to be indicators of greater urea amendment concentrations. Members of these families have recently been reported to be highly ubiquitous and relatively abundant in soils globally (Delgado-Baquerizo et al., 2018). Increases in their relative abundances may reflect some resistance to changes in soil chemistry as a result of urea application (e.g., increased pH and NH_3 concentrations) that are otherwise inhibitory to microorganisms (Geisseler and Scow, 2014). Further research will be required to determine if these families are associated with the decline in heterotrophic respiration that is typically observed (Janssens et al., 2010). Although a previous study did not find significant differences in rice paddy bacterial communities associated with urea addition (Wang et al., 2015), another noted an increase in AOB following short-term urea amendment in an alpine grassland (Xiang et al., 2017). Similarly, we previously observed a positive correlation between bacterial *amoA* abundances and N_2O (Pearson's $r = 0.62$) and NO_2^- ($r = 0.66$) (Breuillin-Sessoms et al., 2017). In contrast, AOB were found to respond to inorganic N, while AOA abundances increased in response to organic N following chronic application in clay loam soils, and this suggested that soil type and temporal dynamics may affect shifts in communities (Zhou et al., 2015). Taken together, these results suggest that the decline in abundance of these families is likely associated with more general species sorting dynamics (e.g., changes in pH and/or nutrient availability) rather than specific chemical toxicity, among all conditions tested.

Taxa within the family *Nitrosomonadaceae*, specifically the genus *Nitrosospira*, were also observed in this study to be responsive to urea amendment, although the relative abundance of this family showed weak and insignificant correlations with both urea amendment rate and N_2O production ($\rho = -0.054$ and 0.031). Since the microbial community composition was too diverse among all soils to resolve many specific trends related to taxa abundances, we performed oligotyping on the predominant nitrifiers found in the dataset. Oligotyping analyses of nitrifiers revealed diverse oligotypes (species or strains) within the genera *Nitrobacter*, *Nitrospira*, *Nitrosospira*, and *Nitrososphaera*. Typically, only one oligotype within each genus was strongly correlated with nitrification gene abundances, suggesting that only one or a few strains within nitrifier families plays an active role in response to N fertilization. Furthermore, these strain level differences in relation to nitrification genes may explain why taxonomic resolution at the family level did not reveal more discrete trends, in part due to the high diversity of potential nitrifiers (Hayatsu et al., 2008). Future work will be necessary to characterize these specific strains to evaluate their roles in N cycling.

While correlation analyses typically revealed the expected associations between abundances of gene targets and genus-specific oligotype (e.g., positive correlation between *Nitrobacter* and *nxrA* abundances), the implications of potentially greater strain-specific proficiency in carrying out processes of nitrification remains unknown. This finding may reflect a coincidental spatial benefit allowing more efficient cross-talk between AOB and NOB (Mobarry et al., 1996), or could reflect differences in competitive ability of certain strains (D'Costa et al., 2006). Similar to previous findings (Di et al., 2009; Giguere et al., 2017), abundances of *Nitrososphaera* showed considerably less variation due to urea amendment, which may suggest that the contribution of AOA to NH_3 oxidation in these agricultural soils is less than that of AOB. Stable populations within the *Nitrososphaera,* however, may also reflect a stable and consistent contribution of AOA to nitrification, although exhaustive determination of specific functional shifts was beyond the scope of the current work. Future research will be necessary to assess the contribution of AOA in these soils, since *amoA* of archaea was not measured in this study. Nevertheless, several communities were comprised of relatively large fractions (up to 13%) of *Nitrososphaera*, suggesting that AOA may play a more prominent role in some soils.

Nitrifying bacteria were found to be the dominant participants in N-metabolism, based on relationships with gene abundances, which is most likely due to the oxic conditions in which the study was carried out. Under more anoxic conditions, such as incidences of water inundation or at deeper depths, it is likely that denitrification plays a more significant role (Wang et al., 2015). As described previously (Breuillin-Sessoms et al., 2017), abundances of bacterial *amoA* were moderately to strongly correlated with N_2O, NO_2^-, and NH_3. The abundances of *nxrA* showed weaker correlations with N_2O and NO_2^-, but not with NH_3. This likely suggests that NH_3 toxicity had a

stronger inhibitory effect on NOB than AOB, as was previously suggested (Venterea et al., 2015). Despite significant declines in alpha diversity and community composition, few other taxa that were unaffiliated with nitrification and denitrification processes showed consistent directional responses to urea amendment, suggesting that total community composition minimally impacted N-cycling. However, soil-specific, significant shifts in community composition in response to greater concentrations of urea may have important longer-term implications in overall soil productivity and pathogen resistance (Bailey and Lazarovits, 2003; Otto-Hanson et al., 2013). These effects cannot be addressed in the present study due to the relatively short period of sample collection and *in vitro* nature of the present work.

In this study, we found that site-specific dynamics more strongly shape bacterial and archaeal communities than did urea addition, despite microscale variability among soil communities (Robertson et al., 1997; Blackwood et al., 2006). Urea addition, however, also had significant, but soil-specific, impacts on bacterial and archaeal community composition, although consistent shifts in abundances of *Microbacteriaceae*, *Chitinophagaceae*, *Comamonadaceae*, *Xanthomonadaceae*, and *Nitrosomonadacea* were observed. In the soils tested, bacterial genes associated with nitrification were found to be strongly associated with nitrogen intermediates, suggesting that nitrifiers were predominantly active in N-cycling under the oxic conditions used in this experiment. Oligotyping of the abundant nitrifiers revealed potentially strain-level differences in correlations with nitrification gene abundances and soil-specific variation in the relative abundances of oligotypes in response to urea application. These results provide novel insights regarding the shift in bacterial and archaeal community structure in response to urea application, and reveal previously unreported diversity among nitrifiers as well as strain selectivity in response to urea amendment within predominant nitrifier genera in various agricultural soils.

AUTHOR CONTRIBUTIONS

CS performed all data analysis and drafted the manuscript. FB-S, RV, and MS conceived of the study design. FB-S performed the sampling and chemical analyses. PW and FB-S performed the qPCR assays. TK assisted with the sequence data processing and analysis. All authors read, edited, and approved the final version of the manuscript.

FUNDING

Sequence data were processed and analyzed using the resources of the Minnesota Supercomputing Institute. This work was supported, in part, by a grant from the Agricultural Fertilizer Research & Education Council of the Minnesota Department of Agriculture, contract no. 89688.

SUPPLEMENTARY MATERIAL

The Supplementary Material for this article can be found online at: https://www.frontiersin.org/articles/10.3389/fmicb.2018.00634/full#supplementary-material

REFERENCES

Ågren, G. I., Bosatta, E., and Magill, A. H. (2001). Combining theory and experiment to understand effects of inorganic nitrogen on litter decomposition. *Oecologia* 128, 94–98. doi: 10.1007/s004420100646

Anderson, M. J., and Willis, T. J. (2003). Canonical analysis of principal coordinates: a useful method of constrained ordination for ecology. *Ecology* 84, 511–525. doi: 10.1890/0012-9658(2003)084[0511:CAOPCA]2.0.CO;2

Aronesty, E. (2013). Comparison of sequencing utility programs. *Open Bioinforma. J.* 7, 1–8. doi: 10.2174/1875036201307010001

Bailey, K., and Lazarovits, G. (2003). Suppressing soil-borne diseases with residue management and organic amendments. *Soil Tillage Res.* 72, 169–180. doi: 10.1016/S0167-1987(03)00086-2

Banerjee, S., Helgason, B., Wang, L., Winsley, T., Ferrari, B. C., and Siciliano, S. D. (2016). Legacy effects of soil moisture on microbial community structure and N_2O emissions. *Soil Biol. Biochem.* 95, 40–50. doi: 10.1016/j.soilbio.2015.12.004

Blackwood, C. B., Dell, C. J., Smucker, A. J. M., and Paul, E. A. (2006). Eubacterial communities in different soil macroaggregate environments and cropping systems. *Soil Biol. Biochem.* 38, 720–728. doi: 10.1016/j.soilbio.2005.07.006

Borcard, D., Legendre, P., and Drapeau, P. (1992). Partialling out the spatial component of ecological variation. *Ecology* 73, 1045–1055. doi: 10.2307/1940179

Bray, J. R., and Curtis, J. T. (1957). An ordination of the upland forest communities of southern Wisconsin. *Ecol. Monogr.* 27, 325–349. doi: 10.2307/1942268

Breuillin-Sessoms, F., Venterea, R. T., Sadowsky, M. J., Coulter, J. A., Clough, T. J., and Wang, P. (2017). Nitrification gene ratio and free ammonia explain nitrite and nitrous oxide production in urea-amended soils. *Soil Biol. Biochem.* 111, 143–153. doi: 10.1016/j.soilbio.2017.04.007

Canfield, D. E., Glazer, A. N., and Falkowski, P. G. (2010). The evolution and future of Earth's nitrogen cycle. *Science* 330, 192–196. doi: 10.1126/science.1186120

Caporaso, J. G., Lauber, C. L., Walters, W. A., Berg-Lyons, D., Huntley, J., Fierer, N., et al. (2012). Ultra-high-throughput microbial community analysis on the Illumina HiSeq and MiSeq platforms. *ISME J.* 6, 1621–1624. doi: 10.1038/ismej.2012.8

Clarke, K. R. (1993). Non-parametric multivariate analyses of changes in community structure. *Aust. J. Ecol.* 18, 117–143. doi: 10.1111/j.1442-9993.1993.tb00438.x

Cole, J. R., Wang, Q., Cardenas, E., Fish, J., Chai, B., Farris, R. J., et al. (2009). The ribosomal database project: improved alignments and new tools for rRNA analysis. *Nucleic Acids Res.* 37, D141–D145. doi: 10.1093/nar/gkn879

Compton, J. E., Watrud, L. S., Porteous, L. A., and DeGrood, S. (2004). Response of soil microbial biomass and community composition to chronic nitrogen additions at Harvard forest. *For. Ecol. Manage.* 196, 143–158. doi: 10.1016/j.foreco.2004.03.017

Daims, H., Lebedeva, E. V., Pjevac, P., Han, P., Herbold, C., Albertsen, M., et al. (2015). Complete nitrification by *Nitrospira* bacteria. *Nature* 528, 504–509. doi: 10.1038/nature16461

D'Costa, V. M., McGrann, K. M., Hughes, D. W., and Wright, G. D. (2006). Sampling the antibiotic resistome. *Science* 311, 374–377. doi: 10.1126/science.1120800

Delgado-Baquerizo, M., Oliverio, A. M., Brewer, T. E., Benavent-González, A., Eldridge, D. J., Bardgett, R. D., et al. (2018). A global atlas of the dominant bacteria found in soil. *Science* 359, 320–325. doi: 10.1126/science.aap9516

Di, H. J., Cameron, K. C., Shen, J. P., Winefield, C. S., O'Callaghan, M., Bowatte, S., et al. (2009). Nitrification driven by bacteria and not archaea in nitrogen-rich grassland soils. *Nat. Geosci.* 2, 621–624. doi: 10.1038/ngeo613

Edgar, R. C., Haas, B. J., Clemente, J. C., Quince, C., and Knight, R. (2011). UCHIME improves sensitivity and speed of chimera detection. *Bioinformatics* 27, 2194–2200. doi: 10.1093/bioinformatics/btr381

Eren, A. M., Maignien, L., Sul, W. J., Murphy, L. G., Grim, S. L., Morrison, H. G., et al. (2013). Oligotyping: differentiating between closely related microbial taxa using 16S rRNA gene data. *Methods Ecol. Evol.* 4, 1111–1119. doi: 10.1111/2041-210X.12114

Excoffier, L., Smouse, P. E., and Quattro, J. M. (1992). Analysis of molecular variance inferred from metric distances among DNA haplotypes - application to human mitochondrial DNA restriction data. *Genetics* 131, 479–491.

FAO (2015). *World Fertilizer Trends and Outlook to 2018*. Rome: Food and Agriculture Organization of the United Nations.

FAO (2017). *FAOSTAT*. Available at: http://www.fao.org/faostat/en/#data/RF

Fernandez, A. L., Sheaffer, C. C., Wyse, D. L., Staley, C., Gould, T. J., and Sadowsky, M. J. (2016a). Associations between soil bacterial community structure and nutrient cycling functions in long-term organic farm soils following cover crop and organic fertilizer amendment. *Sci. Total Environ.* 56, 949–959. doi: 10.1016/j.scitotenv.2016.05.073

Fernandez, A. L., Sheaffer, C. C., Wyse, D. L., Staley, C., Gould, T. J., and Sadowsky, M. J. (2016b). Structure of bacterial communities in soil following cover crop and organic fertilizer incorporation. *Appl. Microbiol. Biotechnol.* 100, 9331–9341. doi: 10.1007/s00253-016-7736-9

Fierer, N., Schimel, J. P., and Holden, P. A. (2003). Influence of drying-rewetting frequency on soil bacterial community structure. *Microb. Ecol.* 45, 63–71. doi: 10.1007/s00248-002-1007-2

Firestone, M. K., and Davidson, E. A. (1989). "Microbiological basis of NO and N_2O production and consumption in soil," in *Exchange of Trace Gases between Terrestrial Ecosystems and the Atmosphere*, eds M. O. Andreae and D. S. Schimel (Hoboken, NJ: John Wiley & Sons, Ltd.), 7–21.

Frey, S. D., Knorr, M., Parrent, J. L., and Simpson, R. T. (2004). Chronic nitrogen enrichment affects the structure and function of the soil microbial community in temperate hardwood and pine forests. *For. Ecol. Manage.* 196, 159–171. doi: 10.1016/j.foreco.2004.03.018

Galloway, J. N., Aber, J. D., Erisman, J. W., Seitzinger, S. P., Howarth, R. W., Cowling, E. B., et al. (2003). The nitrogen cascade. *Bioscience* 53, 341–356. doi: 10.1641/0006-3568(2003)053[0341:TNC]2.0.CO;2

Geets, J., de Cooman, M., Wittebolle, L., Heylen, K., Vanparys, B., De Vos, P., et al. (2007). Real-time PCR assay for the simultaneous quantification of nitrifying and denitrifying bacteria in activated sludge. *Appl. Microbiol. Biotechnol.* 75, 211–221. doi: 10.1007/s00253-006-0805-8

Geisseler, D., and Scow, K. M. (2014). Long-term effects of mineral fertilizers on soil microorganisms - a review. *Soil Biol. Biochem.* 75, 54–63. doi: 10.1016/j.soilbio.2014.03.023

Giguere, A. T., Taylor, A. E., Myrold, D. D., and Bottomley, P. J. (2015). Nitrification responses of soil ammonia-oxidizing archaea and bacteria to ammonium concentrations. *Soil Sci. Soc. Am. J.* 79, 1366–1374. doi: 10.2136/sssaj2015.03.0107

Giguere, A. T., Taylor, A. E., Suwa, Y., Myrold, D. D., and Bottomley, P. J. (2017). Uncoupling of ammonia oxidation from nitrite oxidation: impact upon nitrous oxide production in non-cropped Oregon soils. *Soil Biol. Biochem.* 104, 30–38. doi: 10.1016/j.soilbio.2016.10.011

Gihring, T. M., Green, S. J., and Schadt, C. W. (2012). Massively parallel rRNA gene sequencing exacerbates the potential for biased community diversity comparisons due to variable library sizes. *Environ. Microbiol.* 14, 285–290. doi: 10.1111/j.1462-2920.2011.02550.x

Gohl, D. M., Vangay, P., Garbe, J., MacLean, A., Hauge, A., Becker, A., et al. (2016). Systematic improvement of amplicon marker gene methods for increased accuracy in microbiome studies. *Nat. Biotechnol.* 34, 942–949. doi: 10.1038/nbt.3601

Hayatsu, M., Tago, K., and Saito, M. (2008). Various players in the nitrogen cycle: diversity and functions of the microorganisms involved in nitrification and denitrification. *Soil Sci. Plant Nutr.* 54, 33–45. doi: 10.1111/j.1747-0765.2007.00195.x

Heil, J., Vereecken, H., and Brüggemann, N. (2016). A review of chemical reactions of nitrification intermediates and their role in nitrogen cycling and nitrogen trace gas formation in soil. *Eur. J. Soil Sci.* 67, 23–39. doi: 10.1111/ejss.12306

Huse, S. M., Welch, D. M., Morrison, H. G., and Sogin, M. L. (2010). Ironing out the wrinkles in the rare biosphere through improved OTU clustering. *Environ. Microbiol.* 12, 1889–1898. doi: 10.1111/j.1462-2920.2010.02193.x

Janssens, I. A., Dieleman, W., Luyssaert, S., Subke, J.-A., Reichstein, M., Ceulemans, R., et al. (2010). Reduction of forest soil respiration in response to nitrogen deposition. *Nat. Geosci.* 3, 315–322. doi: 10.1038/ngeo844

Jones, C. M., Stres, B., Rosenquist, M., and Hallin, S. (2008). Phylogenetic analysis of nitrite, nitric oxide, and nitrous oxide respiratory enzymes reveal a complex evolutionary history for denitrification. *Mol. Biol. Evol.* 25, 1955–1966. doi: 10.1093/molbev/msn146

Klotz, M. G., Ward, B. B., and Arp, D. J. (eds). (2011). *Nitrification*. Washington, DC: ASM Press. doi: 10.1128/9781555817145

Leininger, S., Urich, T., Schloter, M., Schwark, L., Qi, J., Nicol, G. W., et al. (2006). Archaea predominate among ammonia-oxidizing prokaryotes in soils. *Nature* 442, 806–809. doi: 10.1038/nature04983

Mobarry, B. K., Wagner, M., Urbain, V., Rittmann, B. E., and Stahl, D. A. (1996). Phylogenetic probes for analyzing abundance and spatial organization of nitrifying bacteria. *Appl. Environ. Microbiol.* 62, 2156–2162.

Odum, E. P. (1985). Trends expected in stressed ecosystems. *Bioscience* 35, 419–422. doi: 10.2307/1310021

Odum, E. P., Finn, J. T., and Franz, E. H. (1979). Perturbation theory and the subsidy-stress gradient. *Bioscience* 29, 349–352. doi: 10.2307/1307690

Oksanen, J., Blanchet, F. G., Kindt, R., Legendre, P., Minchin, P. R., O'Hara, R. B., et al. (2015). *vegan: Community Ecology Package. R Package Version 2.0-8*. Available at: http://CRAN.R-project.org/package=vegan

Otto-Hanson, L. K., Grabau, Z., Rosen, C., Salomon, C. E., and Kinkel, L. L. (2013). Pathogen variation and urea influence selection and success of *Streptomyces* mixtures in biological control. *Phytopathology* 103, 34–42. doi: 10.1094/PHYTO-06-12-0129-R

Ouyang, Y., Norton, J. M., Stark, J. M., Reeve, J. R., and Habteselassie, M. Y. (2016). Ammonia-oxidizing bacteria are more responsive than archaea to nitrogen source in an agricultural soil. *Soil Biol. Biochem.* 96, 4–15. doi: 10.1016/j.soilbio.2016.01.012

Prosser, J. I. (1990). Autotrophic nitrification in bacteria. *Adv. Microb. Physiol.* 30, 125–181. doi: 10.1016/S0065-2911(08)60112-5

Pruesse, E., Quast, C., Knittel, K., Fuchs, B. M., Ludwig, W. G., Peplies, J., et al. (2007). SILVA: a comprehensive online resource for quality checked and aligned ribosomal RNA sequence data compatible with ARB. *Nucleic Acids Res.* 35, 7188–7196. doi: 10.1093/nar/gkm864

R Core Team (2012). *R: A Language and Environment for Statistical Computing*. Vienna: R Foundation for Statistical Computing.

Ramirez, K. S., Craine, J. M., and Fierer, N. (2010). Nitrogen fertilization inhibits soil microbial respiration regardless of the form of nitrogen applied. *Soil Biol. Biochem.* 42, 2336–2338. doi: 10.1016/j.soilbio.2010.08.032

Robertson, G. P., and Groffman, P. M. (2007). "Nitrogen transformations," in *Soil Microbiology, Ecology, and Biochemistry*, ed. E. A. Paul (Amsterdam: Elsevier), 341–364. doi: 10.1016/B978-0-08-047514-1.50017-2

Robertson, G. P., Klingensmith, K. M., Klug, M. J., Paul, E. A., Crum, J. R., and Ellis, B. G. (1997). Soil resources, microbial activity, and primary production across an agricultural ecosystem. *Ecol. Appl.* 7, 158–170. doi: 10.1890/1051-0761(1997)007[0158:SRMAAP]2.0.CO;2

Ruser, R., and Schulz, R. (2015). The effect of nitrification inhibitors on the nitrous oxide (N_2O) release from agricultural soils-a review. *J. Plant Nutr. Soil Sci.* 178, 171–188. doi: 10.1002/jpln.201400251

Schloss, P. D., Westcott, S. L., Ryabin, T., Hall, J. R., Hartmann, M., Hollister, E. B., et al. (2009). Introducing mothur: open-source, platform-independent, community-supported software for describing and comparing microbial communities. *Appl. Environ. Microbiol.* 75, 7537–7541. doi: 10.1128/AEM.01541-09

Schmidt, T. T. M., and Waldron, C. (2015). "Microbial diversity in soils of agricultural landscapes and its relation to ecosystem function," in *The Ecology of Agricultural Landscapes: Long-term Research on the Path to Sustainability*, eds S. Hamilton, J. Doll, and G. Robertson (New York, NY: Oxford University Press), 135–157.

Segata, N., and Huttenhower, C. (2011). Toward an efficient method of identifying core genes for evolutionary and functional microbial phylogenies. *PLoS One* 6:e24704. doi: 10.1371/journal.pone.0024704

Shoda, M. (2017). "Heterotrophic nitrification and aerobic denitrification by *Alcaligenes faecalis* No. 4," in *Nitrification and Denitrification*, ed. I. X. Zhu (Rijeka: InTech). doi: 10.5772/68052

Sogin, M. L., Morrison, H. G., Huber, J. A., Mark Welch, D., Huse, S. M., Neal, P. R., et al. (2006). Microbial diversity in the deep sea and the underexplored "rare biosphere". *Proc. Natl. Acad. Sci. U.S.A.* 103, 12115–12120. doi: 10.1073/pnas.0605127103

Staley, C., Gould, T. J., Wang, P., Phillips, J., Cotner, J. B., and Sadowsky, M. J. (2015). Evaluation of water sampling methodologies for amplicon-based characterization of bacterial community structure. *J. Microbiol. Methods* 114, 43–50. doi: 10.1016/j.mimet.2015.05.003

Staley, C., and Sadowsky, M. J. (2016). Application of metagenomics to assess microbial communities in water and other environmental matrices. *J. Mar. Biol. Assoc. U. K.* 96, 121–129. doi: 10.1017/S0025315415001496

van Kessel, M. A., Speth, D. R., Albertsen, M., Nielsen, P. H., Op den Camp, H. J., Kartal, B., et al. (2015). Complete nitrification by a single microorganism. *Nature* 528, 555–559. doi: 10.1038/nature16459

Venterea, R. T., Baker, J. M., Dolan, M. S., and Spokas, K. A. (2006). Carbon and nitrogen storage are greater under biennial tillage in a Minnesota corn–soybean rotation. *Soil Sci. Soc. Am. J.* 70, 1752–1762. doi: 10.2136/sssaj2006.0010

Venterea, R. T., Clough, T. J., Coulter, J. A., Breuillin-Sessoms, F., Wang, P., and Sadowsky, M. J. (2015). Ammonium sorption and ammonia inhibition of nitrite-oxidizing bacteria explain contrasting soil N_2O production. *Sci. Rep.* 5:12153. doi: 10.1038/srep12153

Venterea, R. T., Halvorson, A. D., Kitchen, N., Liebig, M. A., Cavigelli, M. A., Del Grosso, S. J., et al. (2012). Challenges and opportunities for mitigating nitrous oxide emissions from fertilized cropping systems. *Front. Ecol. Environ.* 10, 562–570. doi: 10.1890/120062

Wang, N., Ding, L. J., Xu, H. J., Li, H. B., Su, J. Q., and Zhu, Y. G. (2015). Variability in responses of bacterial communities and nitrogen oxide emission to urea fertilization among various flooded paddy soils. *FEMS Microbiol. Ecol.* 91, 1–11. doi: 10.1093/femsec/fiv013

Wetselaar, R., Passioura, J. B., and Singh, B. R. (1972). Consequences of banding nitrogen fertilizers in soil. *Plant Soil* 36, 159–175. doi: 10.1007/BF01373466

Xiang, X., He, D., He, J., Myrold, D. D., and Chu, H. (2017). Ammonia-oxidizing bacteria rather than archaea respond to short- term urea amendment in an alpine grassland. *Soil Biol. Biochem.* 107, 218–225. doi: 10.1016/j.soilbio.2017.01.012

Yadvinger-Singh, and Beauchamp, E. G. (1988). Nitrogen transformations near urea in soil: effects of nitrification inhibition, nitrifier activity and liming. *Fertil. Res.* 18, 201–212. doi: 10.1007/BF01049570

Zhang, L.-M., Hu, H.-W., Shen, J.-P., and He, J.-Z. (2012). Ammonia-oxidizing archaea have more important role than ammonia-oxidizing bacteria in ammonia oxidation of strongly acidic soils. *ISME J.* 6, 1032–1045. doi: 10.1038/ismej.2011.168

Zhou, X., Fornara, D., Wasson, E. A., Wang, D., Ren, G., Christie, P., et al. (2015). Effects of 44 years of chronic nitrogen fertilization on the soil nitrifying community of permanent grassland. *Soil Biol. Biochem.* 91, 76–83. doi: 10.1016/j.soilbio.2015.08.031

Conflict of Interest Statement: The authors declare that the research was conducted in the absence of any commercial or financial relationships that could be construed as a potential conflict of interest.

frontiers in Microbiology

ORIGINAL RESEARCH
published: 10 April 2018
doi: 10.3389/fmicb.2018.00674

Nitrosospira sp. Govern Nitrous Oxide Emissions in a Tropical Soil Amended With Residues of Bioenergy Crop

*Késia S. Lourenço[1,2,3], Noriko A. Cassman[1,3], Agata S. Pijl[1], Johannes A. van Veen[1,3], Heitor Cantarella[2] and Eiko E. Kuramae[1]**

[1] Department of Microbial Ecology, Netherlands Institute of Ecology, Wageningen, Netherlands, [2] Soils and Environmental Resources Center, Agronomic Institute of Campinas, Campinas, Brazil, [3] Institute of Biology Leiden, Leiden University, Leiden, Netherlands

Organic vinasse, a residue produced during bioethanol production, increases nitrous oxide (N_2O) emissions when applied with inorganic nitrogen (N) fertilizer in soil. The present study investigated the role of the ammonia-oxidizing bacteria (AOB) community on the N_2O emissions in soils amended with organic vinasse (CV: concentrated and V: non-concentrated) plus inorganic N fertilizer. Soil samples and N_2O emissions were evaluated at 11, 19, and 45 days after fertilizer application, and the bacterial and archaea gene (*amo*A) encoding the ammonia monooxygenase enzyme, bacterial denitrifier (*nir*K, *nir*S, and *nos*Z) genes and total bacteria were quantified by real time PCR. We also employed a deep *amo*A amplicon sequencing approach to evaluate the effect of treatment on the community structure and diversity of the soil AOB community. Both vinasse types applied with inorganic N application increased the total N_2O emissions and the abundance of AOB. *Nitrosospira* sp. was the dominant AOB in the soil and was correlated with N_2O emissions. However, the diversity and the community structure of AOB did not change with vinasse and inorganic N fertilizer amendment. The results highlight the importance of residues and fertilizer management in sustainable agriculture and can be used as a reference and an input tool to determine good management practices for organic fertilization.

Keywords: nitrogen and carbon biochemical cycles, recycling, vinasse, quantitative real time PCR, *amo*A gene, sugarcane

OPEN ACCESS

Edited by:
Maria J. Delgado, Consejo Superior de Investigaciones Científicas (CSIC), Spain

Reviewed by:
Xuesong Luo, Huazhong Agricultural University, China
Muhammad Ali, King Abdullah University of Science and Technology, Saudi Arabia

****Correspondence:***
Eiko E. Kuramae
E.Kuramae@nioo.knaw.nl

Specialty section:
This article was submitted to Terrestrial Microbiology, a section of the journal Frontiers in Microbiology

Received: *09 December 2017*
Accepted: *22 March 2018*
Published: *10 April 2018*

Citation:
Lourenço KS, Cassman NA, Pijl AS, van Veen JA, Cantarella H and Kuramae EE (2018) Nitrosospira sp. Govern Nitrous Oxide Emissions in a Tropical Soil Amended With Residues of Bioenergy Crop. Front. Microbiol. 9:674. doi: 10.3389/fmicb.2018.00674

INTRODUCTION

Brazil is the world's largest producer of sugarcane, with about 685 million tons of sugarcane produced from an area of 9 million hectares in 2016/2017 (CONAB, 2017). Roughly 53% of sugarcane production is directed toward bioethanol production, which is considered a sustainable biofuel (CONAB, 2017). Studies conducted by Macedo et al. (2008) and Seabra et al. (2011) indicated that ethanol production from sugarcane emits about 80% less greenhouse (GHG) gasses than the production of fossil fuels. These benefits are reduced during the practice of recycling sugarcane straw and bioethanol production residues (Galdos et al., 2010; De Figueiredo and La Scala, 2011; Carmo et al., 2013; Pitombo et al., 2015; Siqueira Neto et al., 2016; Soares et al., 2016).

For each liter of ethanol produced, 10–15 liters of the liquid waste, called vinasse, are generated, which totals roughly 360 billion liters of vinasse per year. Vinasse is the major residue generated during the production of ethanol from sugarcane. Vinasse is rich in organic content, carbon (10,000–20,000 mg C L^{-1}), nitrogen (357 mg N L^{-1}), and especially potassium (2056 mg L^{-1}) (Elia-Neto and Nakahodo, 1995; Macedo et al., 2008; Christofoletti et al., 2013; Fuess and Garcia, 2014). To recycle these nutrients, vinasse is directly applied on sugarcane fields as a fertilizer. Recently the use of concentrated vinasse fertilizer, made by reducing the water volume of vinasse, has become popular due to the overall reduced cost associated with transporting the fertilizer to the field. Thus, both types concentrated and non-concentrated vinasse are currently used as organic fertilizer (Rodrigues Reis and Hu, 2017). However, when vinasse is applied with N fertilizer in the soil, high nitrous oxide (N_2O) emission occur (Carmo et al., 2013; Paredes et al., 2014, 2015; Pitombo et al., 2015).

Nitrous oxide is one of the molecules of the nitrogen (N) cycle with major environmental and ecological impacts. N_2O is both an ozone-depletion substance (Ravishankara et al., 2009) and a GHG with global warming potential 298 times higher than carbon dioxide (CO_2) (IPCC, 2013). Agricultural soils account for an estimated 65% of global N_2O emissions (IPCC, 2013). N_2O is produced in soil via biotic and abiotic processes. Chemodenitrification is an abiotic process and it is carried out in low pH (<4.5) by the chemical decomposition of hydroxylamine (NH_2OH), nitroxyl hydride (HNO) or NO_2^- with organic and inorganic compounds. Biotic N_2O production processes are widely distributed over the soil microbiota and have been observed in more than 60 bacterial and archaeal genera (Philippot et al., 2007; Canfield et al., 2010; Nelson et al., 2016). N_2O can be emitted as a byproduct of nitrification or denitrification, which are the main biotic processes contributing to N_2O emissions in soil (Goreau et al., 1980; Wrage et al., 2001; Bakken and Frostegård, 2017). Denitrification is widely responsible for soil N_2O emissions at high water contents while nitrification has often been assumed to be the principal source of N_2O in soil under aerobic conditions (Mathieu et al., 2006; Soares et al., 2016).

Nitrification is the aerobic oxidation of ammonia (NH_3) to nitrate (NO_3^-), which occurs in two phases mediated mainly by autotrophic microorganisms. In the first phase, ammonia-oxidizing bacteria (AOB) or archaea (AOA) oxidize NH_3 to nitrite (NO_2^-); in the second phase, nitrite-oxidizing bacteria (NOB) oxidize NO_2^- to NO_3^-. The ammonia oxidation phase ($NH_3 \rightarrow NH_2OH/HNO \rightarrow NO_2^-$) is catalyzed by the ammonia monooxygenase enzyme encoded by the *amo*A gene, which is carried by β- or γ-proteobacteria (AOB) and the newly described *Thaumarchaeota* phylum (AOA). The *nxr*B gene encodes the enzyme nitrite oxidoreductase and regulates the second phase of nitrification. The N_2O production by AOB is the result of incomplete oxidation of NH_2OH to either nitroxyl (HNO) or NO (Smith and Hein, 1960; Hu et al., 2015) which occurs under aerobic conditions. The second N_2O^- yielding route related to nitrifiers is termed nitrifier denitrification and occurs under both high and low oxygen concentrations. In this process, AOB possess machinery that reduces NO_2^- to N_2O via a nitric oxide (NO) intermediate (Ritchie and Nicholas, 1972; Shaw et al., 2006). Shi et al. (2017) showed that nitrifier denitrification is an important pathway leading to high N_2O production (10.5–54.5%) in alkaline cropping soils (pH 7.2); however, heterotrophic denitrification accounted for a the largest proportion of total N_2O production (∼83%) in acid soils (pH 4.9). Recently, Caranto et al. (2016) demonstrated another direct enzymatic pathway from NH_2OH to N_2O under anaerobic conditions, which is mediated by cytochrome P460. Furthermore, nitrification can also occur during a single step as performed by bacteria of the genus *Nitrospira* sp. (Daims et al., 2015; van Kessel et al., 2015); however, it is not yet known if N_2O emissions occur during this process.

Denitrification is a multistep reaction performed by a variety of bacteria and fungi. During denitrification, oxidized mineral forms of N (NO_3^- and NO_2^-) are reduced to the gaseous products NO, N_2O, and N_2 under oxygen-limited conditions ($NO_3^- \rightarrow NO_2^- \rightarrow NO \rightarrow N_2O \rightarrow N_2$). The sequential processes of bacterial denitrification are regulated by divergent reductases encoded by distinct functional genes: the *nar*G or *nap*A genes encode nitrate reductase, the *nirK* or *nirS* genes encode two entirely different types of nitrite reductase, the *nor*B encode nitric oxide reductase and the *nos*Z gene encodes N_2O reductase (Philippot et al., 2007; Jones et al., 2013).

In a recent study conducted in sugarcane fields in Brazil, AOB rather than AOA or denitrifier bacteria were associated with N_2O emissions (Soares et al., 2016), suggesting that nitrification is the dominant N_2O-producing process in these soils. While it is known that using vinasse plus inorganic N fertilizers increases N_2O emissions, there are no studies to date on the effects of these treatments on the AOB communities in these soils. Therefore, the aim of the current study was to evaluate the effects of vinasse plus inorganic nitrogen fertilization on the ammonia-oxidizing bacterial community abundance, structure, and diversity of the AOB in a tropical soil planted with sugarcane. We hypothesized that the abundance and community structure of the AOB would respond to organic and inorganic, i.e., vinasse and fertilization.

MATERIALS AND METHODS

Experimental Setup and Soil Sampling

The field experiment was situated in Piracicaba, Brazil at APTA (Paulista Agency for Agribusiness Technology). The mean annual air temperature and precipitation of the region are 21°C and 1,390 mm, respectively. Precipitation and daily temperature measurements during the experiment were obtained from a meteorological station located nearby the experimental field. The soil was classified as Ferrasol (FAO, 2015) with pH of 5.0, organic matter of 21.1 g dm^{-3}, P of 14.6 mg dm^{-3}, K^+ of 0.7 $mmol_c$ dm^{-3}, Ca^{+2} of 17.4 $mmol_c$ dm^{-3}, Mg^{+2} of 11.9 $mmol_c$ dm^{-3}, $H^+ + Al^{+3}$ of 34.9 $mmol_c$ dm^{-3}, CEC of 65.1 $mmol_c$ dm^{-3}, and soil bulk density of 1.49 g cm^{-3}. The experiment was carried out in a field planted with the sugarcane variety RB86-7515. The sugarcane was mechanically harvested and the straw was left on top of the soil (16 Mg ha^{-1}).

The experiment was conducted in a randomized block design with three replicate blocks. The treatments were: (1) Control: plot without inorganic N fertilization or vinasse; (2) N: inorganic N fertilizer only; (3) CV+N: concentrated vinasse plus inorganic N fertilizer; and (4) V+N: non-concentrated vinasse plus inorganic N fertilizer.

The inorganic fertilizers and concentrated vinasse (CV) were surface-applied in a 0.2-m wide row, close to the plant (0.1 m) in agreement with common practices in commercial sugarcane production. The N fertilizer rate was 100 kg N ha^{-1} of ammonium nitrate (NH_4NO_3). Volumes of 1.0×10^5 l ha^{-1} of non-concentrated vinasse (V) were sprayed over the experimental plots using a motorized pump fit with a flow regulator. This amount of V corresponded with recommended average application rates to sugarcane plantations in Sao Paulo. Concentrated vinasse was applied in fertilization rows at rate of 1.7×10^5 l ha^{-1}. CV was produced by concentrating vinasse by a factor of 5.8, which is the average of sugar mill vinasse concentration processes. The chemical characteristics of the vinasses are listed in Supplementary Table S1.

The experiment started on August 15, 2014 and 6 soil samplings per plot were carried out on three time points: 11, 19, and 45 days after inorganic N and vinasse applications. For each treatment, soil samples were collected from the 0–10 cm layer for measurements of moisture content, concentrations of NO_3^--N and NH_4^+-N, and pH. Soil subsamples (30 g) were stored at −80°C for molecular analyses. In parallel, for each soil sample air and soil temperatures were measured. Soil temperatures were collected from the 0–10 cm layer with a digital thermometer. Soil moisture was determined gravimetrically by drying the soil at 105°C for 24 h and the water-filled pore space (WFPS) was calculated considering soil moisture and bulk density. Soil mineral N (NH_4^+-N, NO_3^--N) was measured with a continuous flow analytical system (FIAlab-2500 System) (Kamphake et al., 1967; Krom, 1980).

Nitrous Oxide Measurements

Fluxes of N_2O were measured using PVC static chambers with 20 cm height and 30 cm diameter, according to the method described in Pitombo et al. (2015) and Soares et al. (2016). The gases were sampled with plastic syringes (60 mL) at three time intervals (1, 15, and 30 min) after the chambers were closed (Soares et al., 2016). The samples were transferred and stored in pre-evacuated 12 mL glass vials and analyzed in a gas chromatograph with an electron capture detector for N_2O and with flame ionization detector for CO_2 determination (model GC-2014, Shimadzu Co.). Gas and soil samples were collected in the morning between 7:00 and 12:00 AM GMT-3. Overall N_2O flux was calculated by linear interpolation over the three sampling times.

DNA Extraction and Real-Time PCR

Total soil DNA was extracted using the MoBio PowerSoil DNA Isolation Kit (MoBio, Solana Beach, CA, United States). Of each soil sample, 0.30 g was used for DNA extraction according to the manufacturer's instructions. The quantity and quality of DNA were quantified and checked using a Qubit 2.0 Fluorometer (Life Technologies, Carlsbad, CA, United States), as well as visualized on 1% (w/v) agarose gel under UV light. The abundance of the *amo*A-AOB gene and total bacterial community was quantified by real-time PCR with a BIO-RAD CFX96 Touch™ Real-Time PCR Detection System. Amplification of the *amo*A-AOB gene was performed in total volume of 12 μL, containing 6 μL SYBR Green Bioline SensiFAST SYBR® No-ROX mix, 0.125 μL of each primer (10 pmol) and 4 μL of DNA (40 ng); the primer used was amoA1F (5′-GGGGTTTCTACTGGTGGT-3′) and amoA2R (5′-CCCCT CKGSAAAGCCTTCTTC-3′) (Rotthauwe et al., 1997). The thermal cycler conditions were 95°C-10 min; 40 times 95°C-10 s, 65°C-25 s; last, acquisition was done at 65°C. The qPCR amplicon products (491 bp) were checked by melting curve analysis and agarose gel electrophoresis. The efficiency of the *amo*A-AOB qPCR was 87% (R^2 = 0.99). Assessment of the abundance of the total bacterial community was based on 16S rRNA gene qPCR was performed in total volume of 12 μL, containing 6 μL SYBR Green iQ™ SYBR® Green Supermix (Bio-Rad), 0.125 μL of each primer (10 pmol), 0.30 μL of bovine serum albumin (BSA), and 4 μL of DNA (5 ng); the primer sets were Eub338 (5′-ACTCCTACGGGAGGCAGC AG-3′) and Eub518 (5′-ATTACCGCGGCTGCTGG-3′) (Fierer et al., 2005). The thermal cycler conditions were 95°C-3 min; 40 times 95°C-30 s, 59°C-35 s; 72°C-20 s, and acquisition was done at 59°C. The qPCR amplicon products (200 bp) were checked by melting curve analysis and agarose gel electrophoresis. The efficiency of the 16S rDNA qPCR was 96% (R^2 = 0.99). Plasmid DNA containing fragments of bacterial *amo*A and 16S rRNA genes were used as standards. Each qPCR run, in triplicate, included a DNA template, the standard positive control, and a negative control. The primers used for the archaea *amo*A and bacteria *nir*S, *nir*K, and *nos*Z and the, PCR conditions are described in the Supplementary Table S2.

Sequencing of *amo*A Amplicons for Ammonia-Oxidizing Bacteria

Primer sets amoA-1F/amoA-2R (Rotthauwe et al., 1997) for AOB (same primers used in the qPCR) were used to amplify the *amo*A gene fragment for sequencing with Illumina MiSeq sequencing platform. The PCR was carried out in 20 μl reaction containing each 2 μl of deoxynucleoside triphosphate at a concentration of 2.0 mM, 0.25 μl of forward and reverse primers (10 pmol), 0.1 μl of FastStart Taq DNA Polymerase, 2 μl of $MgCl_2$ buffer, and 0.5 μl of BSA (4 mg ml^{-1}). Each reaction mix received 1 μl of genomic DNA as a template. The PCR conditions for the amplicons were: preheating at 95°C for 5 min, then 35 cycles (95°C for 30 s, 53°C for 30 s, and 72°C for 30 s), with a final extension at 72°C for 10 min. Triplicate reaction mixtures per sample were pooled together, purified with the Agarose Gel DNA purification kit (TaKaRa), and quantified using the NanoDrop ND-1000 spectrophotometer (NanoDrop Technologies, Montchanin, DE, United States). The bar-coded PCR products from all samples were normalized in equimolar amounts before sequencing. The amplicon library was prepared by adaptor ligation and PCR using the TruSeq Nano

DNA Library Prep Kit (Illumina, CatFC-121-4001) according to the TruSeq nano protocol (Illumina, FC-121-4003). Paired-end MiSeq sequencing was carried out by BGI Inc. (China). The raw *amo*A sequence data are available at the European Nucleotide Archive (ENA)[1] under the study accession number PRJEB25428.

Clustering and Taxonomic Classification of *amo*A OTUs

The raw data of *amo*A sequences were preprocessed using MOTHUR v 1.3.3 (Schloss et al., 2009). Raw sequences were merged (make.contigs command), then trimmed and sorted simultaneously (trim.seqs). Sequences were filtered out if average read quality was less than 25, there were more than two N's or if the read length was less than 150 bp; remaining sequences were filtered based on primer quality ($\leq$ 2 errors), spacers ($\leq$2 errors), and barcodes ($\leq$1 error). Barcodes and primers were removed. Further, the sequences were processed using the UCLUST pipeline implemented in a Snakemake workflow which is available upon request (Edgar, 2010). In summary, the *amo*A-AOB sequences were truncated to 480 bp, clustered into 90% OTUs and singletons and chimeras were removed (Norton et al., 2002). An OTU table was created at the 90% cutoff level. The OTUs were checked by comparison to the March 17, 2014 KEGG database using UProC version 1.2.0 with the uproc-dna command (Meinicke, 2015); those OTUs that did not match the *pmo*A-*amo*A (Particulate methane monooxygenase-ammonia monooxygenase) pathway K10944 were removed (5 of 236 OTUs). To further validate the OTUs, centroids were compared to the October 04, 2016 NCBI-nr database using Diamond version 0.8.20 with the command blastx (Buchfink et al., 2015). The OTUs that were classified by the Last Common Ancestor algorithm from MEGAN version 6.5.8 as Eukaryote were removed (3 of 236 OTUs) (Huson and Weber, 2013). The centroid OTUs were finally classified using BLASTN (evalue cutoff of 0.02) against a custom *amo*A FunGene database described below which comprised 136 records (Fish et al., 2013). Last, the classification was added to the OTU table using a custom Perl script.

Due to poor classification results from blastx classification against the NCBI-nr database, a custom *amo*A database was created from FunGene *amo*A sequences as follows. High-quality *amo*A sequences with score above 350, size greater than 200 amino acids in length, HMM coverage of more than 85% and defined organism name were downloaded. The NCBI taxonomy of each unique record was obtained using a custom Perl script. The custom *amo*A sequences were aligned using ClustalW in MEGA7 (Kumar et al., 2016). A neighbor-joining tree (Saitou and Nei, 1987) was created to examine the phylogenetic relationships between the 138 records using as outgroup a *Nitrosococcus oceani amo*A sequence as shown in Supplementary Figure S2. Distances were computed using the Maximum Composite Likelihood method and a bootstrap test with 1000 replicates was conducted (Felsenstein, 1985). Because the *amo*A sequences clustered together at least at the Beta-proteobacteria level, the taxonomy of the records originally noted as unclassified Bacteria were updated as unclassified Beta-proteobacteria (see Supplementary Figure S2). We used the Interactive Tree of Life (iTOL) (Letunic and Bork, 2016) to visualize the tree containing the 30 most abundant *amo*A-AOB OTUs and their nearest neighbors in the custom FunGene *amo*A sequence database.

Statistical Analyses of Gas Fluxes, Gene Abundances, and *amo*A OTUs

All statistical analyses, except Spearman correlations, were carried out in RStudio version 1.0.136 running R version 3.3.1. Generalized linear models (Bolker et al., 2009) were used to test the effect of different treatments on N_2O fluxes and *amo*A gene copy numbers using the multcomp package (Hothorn et al., 2008) in R. The differences between treatments were analyzed within each sampling event. Treatments were considered statically significant using $p < 0.01$ as the criterion. To account for the increasing variation with the increase in the mean, we used Gamma (N_2O emission) and Poisson family (*amo*A and 16S gene copy number) distributions as criteria to the generalized linear models. Subsequently the glht function was used to evaluate the differences among treatments (Tukey $p \leq 0.01$). The correlation between N_2O flux and *amo*A-AOB gene abundances were calculated by Spearman correlation analysis in Sigma Plot, version 13.0 (Systatsoftware, 2014).

The phyloseq package was used to handle the *amo*A-AOB OTU abundance data (McMurdie and Holmes, 2013). The *amo*A data were rarified to the size of the smallest sample (12,978 sequences) prior to alpha and beta diversity analyses. To determine whether AOB bacterial community diversity differed by treatment or day, Renyi indexes were calculated using the BiodiversityR package and the values for average, normally distributed Shannon and Inverse Simpson indexes were compared between treatments (Tukey's HSD test with alpha of 0.05) using the multcomp package (Simpson, 1949; Kindt and Kindt, 2015). To test the effect of treatments on AOB bacterial community compositions, the rarified AOB data was ordinated using PCoA using the Bray distance measure. The PERMANOVA test in the vegan package was used to ascertain group significance with 9999 permutations (Oksanen et al., 2015). In parallel, the data was ordinated using correspondence analysis and group significance was assessed with between-groups analysis applying a random permutation test (999 repetitions) from the ade4 package (Dray and Dufour, 2007). Last, a permutation test for homogeneity of multivariate dispersions was run using the "betadisp" function from the vegan package. Group tests were applied for treatment (Control, N, CV+N, and V+N) and day (11, 19, and 45) groups. We also used multivariate regression tree (MRT) analyses (De'ath, 2002) in the R 'mvpart' package (Therneau and Atkinson, 1997; De'ath, 2007) to identify the effect of the temporal variation (time) on AOB community composition (Ouellette et al., 2012). For the MRT analysis, the rarified AOB data was log-transformed, and the tree was plotted after 500 cross-validations (Breiman et al., 1984), avoiding overfitting. Subsequently, the function rpart.pca from the mvpart package was used to plot a PCoA of the MTR.

[1] https://www.ebi.ac.uk/ena/

RESULTS

Weather Conditions, Greenhouse Gas Emission, and Soil Analysis

The climatic conditions during the experimental period were shown in Supplementary Figure S1A. The lowest air temperature was 7°C in the beginning of the experiment and the highest 35°C. The mean temperature during the 45-day experiment was 22°C (Supplementary Figure S1A). A similar pattern was observed in soil temperature; the temperature increased throughout the experimental period from 17 to 22°C.

Treatments with inorganic N plus vinasse application (CV or V) had higher N_2O emission rates than treatments with only inorganic N and control. At day 11 the emission rate was low due to lack of rain during the previous period, with consumption of N_2O in the control treatment (**Table 1**). The CO_2 emissions were similar to N_2O emissions, with lower emission at day 11 than in days 19 and 45. The CO_2 emissions were higher for treatments with inorganic N plus vinasse in comparison to the control and only N (Supplementary Figure S1B).

Within treatments, the total NH_4^+-N content decreased through the time, while NO_3^--N content increased (Supplementary Figures S3A,B). The soil pH had overall low variation across treatments; in the CV+N treatment the pH slightly increased while in the inorganic N and V+N treatments the pH decreased through the time (Supplementary Figure S3C). In field conditions where the spatial variation is high, the N_2O emissions were correlated with CO_2 emissions and other environmental parameters, including soil temperature, WFPS and NO_3-N (R^2 = 0.87; R^2 = 0.37; R^2 = 0.51; and R^2 = 0.63, respectively) (**Figure 1**).

Gene Abundance and AOB Community Composition Over Time

Inorganic N plus organic vinasse (CV and V) significantly increased AOB *amo*A gene copy numbers by more than 2, 8, and 51-fold at days 11, 19, and 45, respectively, compared to the control (**Table 1**). In contrast, the total bacteria (16S rDNA) gene copy number was similar for all treatments. The ratio between the abundance of the total bacteria and the *amo*A-AOB differed between treatments, and treatments with V or CV had the lowest ratio (**Table 2**). This suggested that vinasse (CV and V) plus inorganic N treatment increased the *amo*A gene copies compared with total bacteria. Furthermore, the abundance of *amo*A genes was significantly correlated with N_2O (R^2 = 0.39) and CO_2 (R^2 = 0.30) emissions; in addition, *amo*A gene abundances increased significantly with WFPS (R^2 = 0.28) and soil NO_3^--N (R^2 = 0.38) values (**Figure 1**). However, no correlation was found between N_2O emission and *amo*A-AOA and bacterial denitrifier (*nir*S, *nir*K, and *nos*Z) genes copy numbers (**Figure 1**).

TABLE 2 | Ratios between the gene copy numbers (per gram of dry soil) of ammonia-oxidizing bacteria (*amoA*-AOB) and total bacteria 16S rDNA (n = 3).

	Ratio (16S rDNA/*amo*A-AOB)		
Treatments[a]	**Day 11**	**Day 19**	**Day 45**
Control	13891 ± 13289c	4565 ± 2029d	478 ± 169d
N	18332 ± 17408d	2974 ± 2823c	180 ± 123c
CV+N	1351 ± 847b	2005 ± 865b	89 ± 43b
V+N	998 ± 582a	1197 ± 796a	26 ± 3a

The treatments were: Control; N, inorganic fertilizer; CV+N, mineral fertilizer plus concentrated vinasse; V+N, mineral fertilizer plus non-concentrated vinasse. [a] *Values followed by the same lowercase letter in the column are not significantly different at $p \leq 0.05$ using the Tukey test.*

Due to positive correlation between *amo*A-AOB gene copy numbers and N_2O emissions, the AOB community was sequenced. A total of 1,661,482 high quality *amo*A-AOB sequences from 36 samples (4 treatments × 3 time points × 3 replicates) with an average of 46,152 reads (13,213–202,908 reads) per sample were clustered into 236 OTUs for *amo*A-AOB community analysis. Rarefaction curves indicated that the community diversity was well captured with our sequencing depth (Supplementary Figure S4).

In order to assess the effects of the treatments or day on the *amo*A-AOB community structure, the taxonomic profiles were compared at different time points using a combination of ordination techniques and dissimilarity tests. Comparative analysis of the AOB community structure revealed no clear separation at the OTU level by treatment. The PERMANOVA and correspondence analysis-between class analysis revealed no differences between treatments based on OTU-level abundances (PERMANOVA: p = 0.54); furthermore, the interaction between treatment and time was not significant (PERMANOVA: p = 0.32) (Supplementary Table S3 and Supplementary Figure S5).

TABLE 1 | Ammonia-oxidizing bacteria (*amoA*-AOB) gene copy numbers (g^{-1} dry soil) and nitrous oxide (N_2O) fluxes (n = 3) for different treatments including Control; N, inorganic N fertilizer; CV+N, concentrated vinasse plus inorganic N fertilizer; V+N, non-concentrated vinasse plus inorganic N fertilizer.

	Day 11		Day 19		Day 45	
Treatment[a]	***amo*A[b]**	**N_2O-N[c]**	***amo*A**	**N_2O-N**	***amo*A**	**N_2O-N**
Control	7.1 ± 2.8a	−0.07 ± 0.12a	2.8 ± 1.1a	0.11 ± 0.03a	2.4 ± 0.5a	0.24 ± 0.10a
N	12.8 ± 6.5c	0.11 ± 0.03a	738.6 ± 12.4d	0.35 ± 0.09a	41.4 ± 22.1b	8.34 ± 2.60b
CV+N	15.0 ± 6.6d	0.33 ± 0.05a	15.4 ± 8.6c	40.22 ± 7.04b	247.4 ± 146.9d	27.54 ± 14.65b
V+N	12.3 ± 5.1b	0.70 ± 0.09b	11.6 ± 3.5b	23.71 ± 7.95b	71.5 ± 14.0c	8.93 ± 1.09b

[a] *Means followed by the same letter in the column at each treatment do not differ significantly by the Tukey's test ($p < 0.05$);* [b] *$\times 10^6$ gene copies g^{-1} dry soil;* [c] *mg N m^{-2} d^{-1}; Values followed by different letters are significantly different at $p \leq 0.05$ using the Tukey test.*

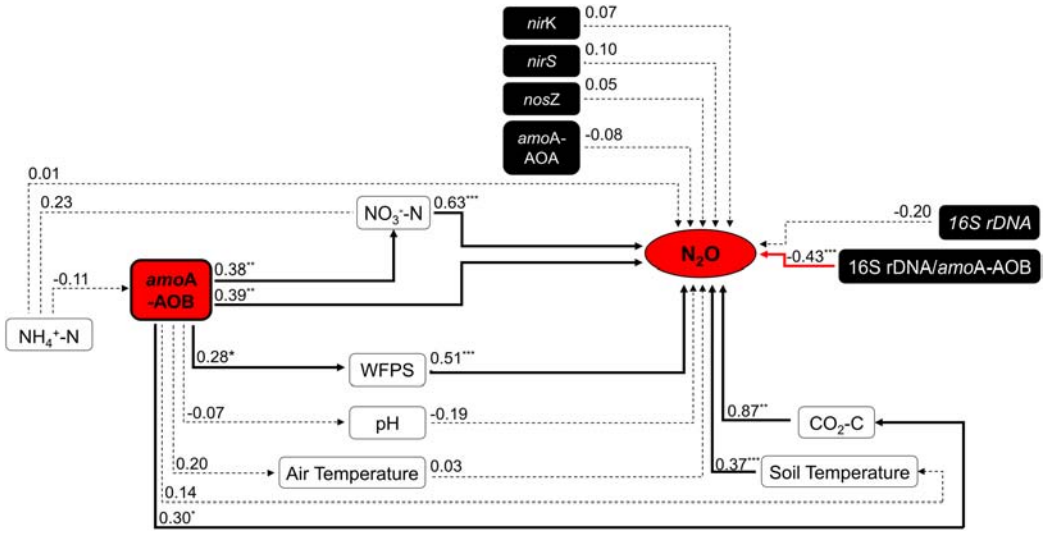

FIGURE 1 | Summary of Spearman's correlations between N_2O emission flux (mg N m^{-2} d^{-1}) and environmental variables, the abundance of bacterial *amo*A-AOB gene (gene copy g^{-1} dry soil) and the 16S rDNA/*amo*A ratio (n = 36). Black bold lines mean significant correlation, red bold lines significant negative correlation, and dotted lines no correlation between variables (n = 36). Significant difference: *$p \leq 0.10$, ** $p \leq 0.05$, and ***$p \leq 0.01$. Abbreviations: WFPS, Water-filled pore space; AOB, *amo*A belonging to ammonia-oxidizing bacteria (AOB).

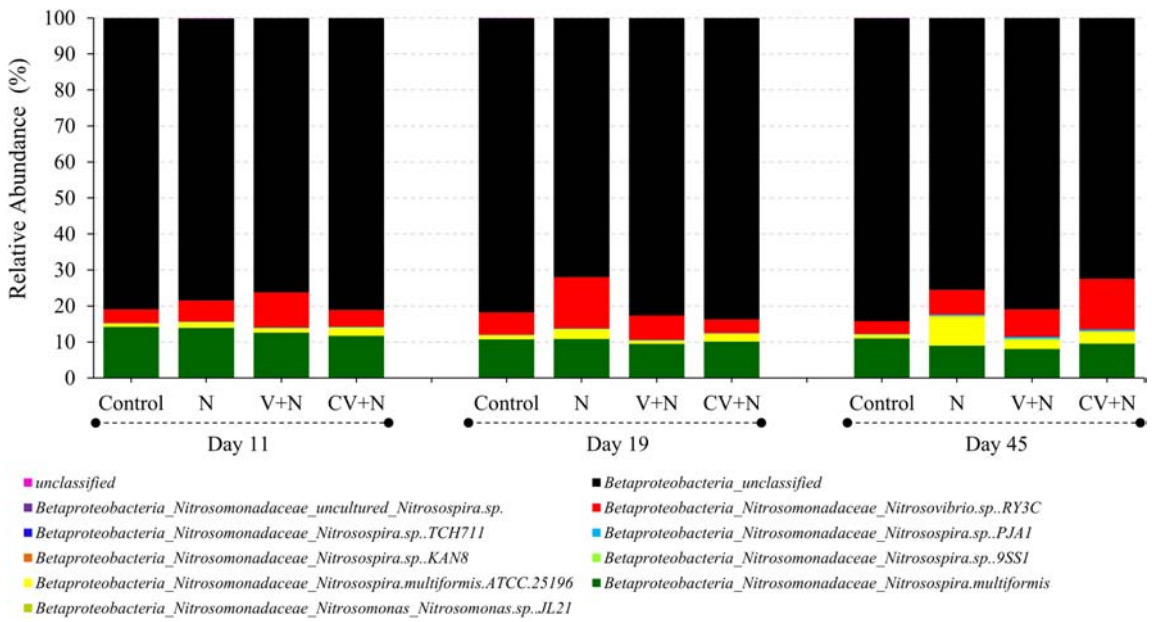

FIGURE 2 | Average relative abundances of the AOB community (n = 36) at the level of species. The sequencing reads of *amoA*-AOB genes were assigned to their taxonomic affiliations of nitrifying bacteria that oxidize ammonia, by comparison to the *amoA* database in FunGene.

To further explore temporal effects, we used a multivariate regression tree (MRT) approach and PCA ordination of the by MRT analysis which further showed that the microbial community composition did not change over time (Error = 0.92) (Supplementary Figure S6). Moreover, the factors treatment or time did not affect alpha-diversity of the AOB communities (OTU richness, Chao1, Simpson, and Shannon) (Supplementary Table S4).

The AOB community present in the soil was composed mainly of the β-Proteobacteria phylum and the *Nitrosomonadaceae* family, of which 20.8 % belonged to the genus *Nitrosospira* and 79.2% to unclassified β-proteobacteria (**Figure 2**). Based on these results, the phylogenetic tree was constructed and all OTUs clustered with *Nitrosospira* and *Nitrosovibrio* (now included in the Nitrosospira genus) genus, except 2 OTUs (OTU 23 and OTU165) which clustered with the *Nitrosomonas* genus

(**Figure 3**). *Nitrosospira* sp. PJA1 and *Nitrosovibrio* sp. RY3C were significantly positively correlated ($p \leq 0.10$) with N_2O-N, NO_3-N and the number of *amo*A gene copies (**Table 3**). Surprisingly, *Nitrosospira multiformis* abundances showed significant negative correlations with N_2O-N, NO_3-N and the *amo*A gene copy number ($p \leq 0.10$).

DISCUSSION

Here we investigated the effect of bioenergy residues (CV and V) plus inorganic N on the abundance of bacteria and nitrifier and denitrifier genes related with N_2O emissions, and the structure, composition and diversity of the AOB community in a tropical soil under sugarcane. Nitrification by AOB was previously determined to be the major process contributing to higher N_2O emissions in similar tropical soil (Soares et al., 2016) planted with sugarcane due to high drainage capacity. Soares et al. (2016) showed that a NO_3^- - based fertilizers had similar emission to the control treatment but neither vinasse nor straw were applied in the soil, however, the application of nitrification inhibitor together with urea decreased the N_2O emission in 94%. The results showed that denitrification by heterotrophic microbes are not relevant in that condition. In the current study, which was carried out on the same soil type, the addition of inorganic N plus vinasse application (CV and V) boosted high N_2O emissions. Vinasse is an organic residue rich in organic compounds with high biological oxygen demand (Fuess and Garcia, 2014). The input of labeled carbon from vinasse in the soils increases soil microbial activities

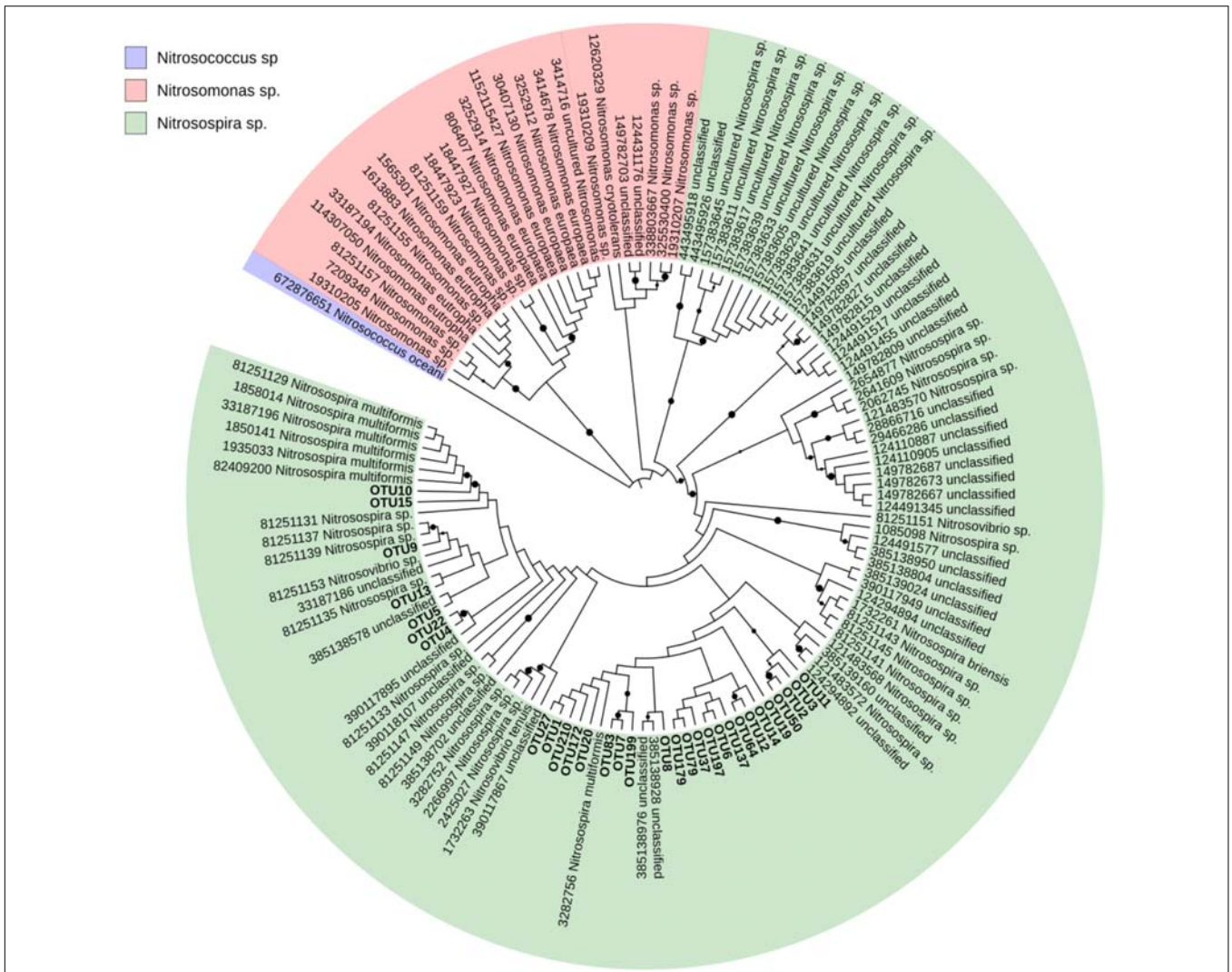

FIGURE 3 | Neighbor-joining tree of the 30 most abundant sample *amo*A-AOB OTUs and their nearest neighbors in the custom FunGene *amoA* sequence database. The NCBI taxonomic classification of the database entries is included. The outgroup is *Nitrosococcus oceani*. The percentage of replicate trees in which the associated taxa clustered together in the bootstrap test (1000 replicates) are shown next to the branches (black points mean bootstrap value >75%). Evolutionary distances were computed using the Maximum Composite Likelihood method. The analysis involved 131 sequences and 305 positions and was conducted in MEGA7.

TABLE 3 | Spearman's correlation coefficients between the *amoA* OTUs (classified at the species level) and *amoA* gene copy number (determined by qPCR), N_2O emission flux and mineral N (NH_4^+-N and NO_3^--N) values.

Speciel-level classification[a]	N_2O-N[b]	NO_3^--N	NH_4^+-N	*amoA* gene copy number
Betaproteobacteria_Nitrosomonadaceae_Nitrosomonas_Nitrosomonas sp. JL21	−0.1	−0.02	**0.36****	−0.01
Betaproteobacteria_Nitrosomonadaceae_Nitrosospira multiformis	**−0.43*****	**−0.32***	0.20	**−0.47*****
Betaproteobacteria_Nitrosomonadaceae_Nitrosospira multiformis ATCC.25196	0.05	0.12	−0.00	**0.75*****
Betaproteobacteria_Nitrosomonadaceae_Nitrosospira sp. 9SS1	0.19	0.25	−0.14	**0.76*****
Betaproteobacteria_Nitrosomonadaceae_Nitrosospira sp. KAN8	0.08	0.11	−0.23	0.24
Betaproteobacteria_Nitrosomonadaceae_Nitrosospira sp. PJA1	**0.29***	**0.34****	−0.11	**0.84*****
Betaproteobacteria_Nitrosomonadaceae_Nitrosospira sp. TCH711	0.259	0.26	−0.25	**0.66*****
Betaproteobacteria_Nitrosomonadaceae_Nitrosovibrio sp. RY3C	**0.28***	**0.30***	−0.04	**0.81*****
Betaproteobacteria_Nitrosomonadaceae_uncultured.Nitrosospira sp.	−0.05	−0.22	0.06	−0.26
Betaproteobacteria_unclassified	−0.06	−0.19	−0.16	**−0.72*****
Unclassified	−0.22	−0.26	−0.19	−0.16

*The amoA-AOB OTUs were assigned to their taxonomic affiliations of ammonia-oxidizing bacteria (AOB) by comparison to sequences in the amoA database from FunGene. [a] Significant difference: *$p \leq 0.10$, **$p \leq 0.05$, and ***$p \leq 0.01$; [b] (mg N m^{-2} d^{-1}). Bold values means significant correlation.*

including intense oxygen consumption (Renault et al., 2009) and it creates microoxic or anoxic conditions, resulting in anaerobic microsites (Torbert and Wood, 1992). Both conditions could favor denitrification, including nitrifier denitrification; however, the anaerobic conditions may prevail only for a short time, since the soil drains well and dries in a few hours. This then favors N_2O emission by nitrification. Here, the high N_2O emissions from treatments with inorganic N plus vinasse application (CV and V) might arise from the fertilizer N in combination with organic N and the organic carbon of vinasse.

In our study the addition of inorganic N plus vinasse application (CV and V) increased the N_2O emissions. The high emissions were related with only AOB abundances rather than AOA or heterotrophic denitrifiers abundances. The correlation values between N_2O and abundance of AOB is not a strong correlation, however, it is an indication that the AOB community is responsible for the N_2O emissions. We have to emphasize that the experiment was in field conditions where the spatial variation is expected to be higher than in laboratory conditions. The AOB are considered aerobic microorganisms, which obtain energy by the oxidation of inorganic N compounds, allowing for N_2O emissions from the soil during aerobic conditions. While nitrification by AOB is usually associated with aerobic conditions, N_2O production by AOB is also possible via nitrification under suboxic or anoxic conditions, although these situations are still relatively unstudied in soil field conditions (Caranto et al., 2016). Furthermore, nitrifier denitrification by AOB could also play a role in N_2O emissions in treatments with organic vinasse, under low oxygen and high concentration of nitrite (Joo et al., 2005; Spott et al., 2011; Zhao et al., 2012; Zhu et al., 2013; Bakken and Frostegård, 2017). The positive correlation between *amo*A abundance and WFPS due to rain events and vinasse application suggested that nitrification and nitrifier-denitrification processes were occurring during anaerobic conditions (Di et al., 2014). Further research is needed to explore the contribution of nitrifier nitrification versus nitrifier denitrification to N_2O emissions under these conditions and the relevant time scales.

The application of different vinasses and inorganic N did not change the AOB community compositions, nor diversity, but did increase the abundance of AOB in the soil. Thus, it is fair to conclude that, in the short time of the experiment, the AOB community structure was resistant to the organic and inorganic fertilization, with no changes in the alpha and beta diversity. Contrasting results were found in the literature, where studies have reported changes in AOB community composition in response to N fertilizers (Glaser et al., 2010; Ouyang et al., 2016; Xiang et al., 2017). Other studies have also reported changes in AOB abundance without a corresponding change in composition with N additions (Phillips et al., 2000; He et al., 2007). Verhamme et al. (2011) found that the abundance and community structure of AOB changed only in the soil treatment with the highest ammonia concentration (200 mg N g^{-1}). In our experiment, we used the N rate recommended for sugarcane fields in Brazil, which is a relatively small input rate of 0.75 mg N g^{-1}. Therefore, we suggest that the community structure of AOB in soils with sugarcane was found to be unchanged after N fertilization due to the low application rate. Moreover, the AOB community in these fields may have already been adapted to the straw and annual application of inorganic fertilizer since sugarcane has been cultivated in this area for more the 20 years. Interestingly, the AOB community is composed globally of only a few species of bacteria in soils. The AOB found in soils generally belong to the β-Proteobacteria Phylum and the *Nitrosomonas* and mainly *Nitrosospira* genera (Prosser et al., 2014). There is no reported evidence of γ- Proteobacteria ammonia oxidizers (*Nitrosococcus* sp.) in soil.

Here, the AOB phylogenetic tree revealed that *Nitrosospira* was the dominant genus (99.5% of the total AOB community) in the soils under sugarcane. Recently, 16S rRNA and *amo*A gene sequencing studies have provided evidence that *Nitrosospira* spp. dominate most natural soil populations (Stephen et al., 1996; Pommerening-Röser and Koops, 2005). Surprisingly, we found only two OTUs with low abundance of *Nitrosomonas* spp. in this soil. Usually, they are prevalent in soils that have received high inputs of inorganic N (Hastings et al., 1997; Oved et al., 2001) and

organic residues (Oved et al., 2001; Taylor and Bottomley, 2006; Habteselassie et al., 2013). Oved et al. (2001) and Habteselassie et al. (2013) showed that *Nitrosomonas* were not detected in soils that received inorganic fertilizer but were in soils that received liquid dairy waste and wastewater effluent. The low abundance of *Nitrosomonas* spp. in our study suggested that soil with sugarcane select for *Nitrosospira*. Even in treatments with the organic vinasse application, *Nitrosomonas* OTU abundances did not increase. On the other hand, this was the first time that vinasse was applied in the field experiment area.

The dominance of *Nitrosospira* sp. could be explained by specific conditions such as soil pH, which may have been consistent over the long period of over 20 years that this soil had been for sugarcane production. It has been postulated that pH may select for the presence of *Nitrosospira* group in acid soil (Pommerening-Röser and Koops, 2005) whereas strains of *Nitrosomonas* are not common in acidic environments (pH 4–5). The AOB isolated from acidic soils are generally *Nitrosospira* with ureolytic characteristics. For instance, some of these AOB produced urease enzymes catalyzing the breakdown of urea to ammonia (De Boer and Kowalchuk, 2001). This advantage allows the ureolytic AOB to grow at low pH with urea source (Pommerening-Röser and Koops, 2005; Ma et al., 2008). Our results showed that inorganic N application decrease soil pH over time. Therefore, the continual application of inorganic fertilizers could select the *Nitrosospira* population by lowering the soil pH.

Contrary to our hypothesis, the AOB community structure did not change with vinasse and inorganic N fertilization. The long-time inorganic N fertilization may have resulted in an AOB community that is adapted to fluctuations in mineral N in the soil, thus resulting in a diminished response of the soil AOB community structure to changes in available mineral N, affecting only the growth of the whole AOB community. Furthermore, soils with sugarcane seem to be enriched in *Nitrosospira* over *Nitrosomonas*, and the former was responsible for the N_2O emissions from soils fertilized with organic vinasse (CV and V) and inorganic N fertilizer. This study therefore expands the information available about the microbes responsible for the N_2O emission to define better strategies for mitigating the N_2O emissions in sugarcane agriculture.

AUTHOR CONTRIBUTIONS

KL, HC, and EK designed the research. KL conducted the experiments and performed the statistical analyses. KL and AP conducted the qPCR and PCR analyses. NC performed the bioinformatic steps. KL, JvV, HC, and EK wrote the paper. All authors reviewed the manuscript.

FUNDING

This research was supported by FAPESP and The Netherlands Organization for Scientific Research (NWO) Grant Nos. 2013/50365-5 and 729.004.003, FAPESP 2014/24141-5, FAPESP 2013/12716-0, and CNPq 311.197/2013-2. Publication 6506 of the Netherlands Institute of Ecology (NIOO-KNAW).

ACKNOWLEDGMENTS

The authors thank Dr. André C. Vitti (APTA), Dr. Raffaella Rossetto (APTA), MSc. Rafael M. Sousa, Dr. Zaqueu F. Montezano (IAC), and Dr. Mauricio R. Dimitrov for the technical assistance and MSc. Márcio F. A. Leite for the fitted generalized linear model applied to the data.

SUPPLEMENTARY MATERIAL

The Supplementary Material for this article can be found online at: https://www.frontiersin.org/articles/10.3389/fmicb.2018.00674/full#supplementary-material

REFERENCES

Bakken, L. R., and Frostegård, Å., (2017). Sources and sinks for N2O, can microbiologist help to mitigate N2O emissions? *Environ. Microbiol.* 19, 4801–4805. doi: 10.1111/1462-2920.13978

Bolker, B. M., Brooks, M. E., Clark, C. J., Geange, S. W., Poulsen, J. R., Stevens, M. H. H., et al. (2009). Generalized linear mixed models: a practical guide for ecology and evolution. *Trends Ecol. Evol. (Amst.)* 24, 127–135. doi: 10.1016/j.tree.2008.10.008

Breiman, L., Friedman, J. H., Olshen, R. A., and Stone, C. J. (1984). *Classification and Regression Trees*. Belmont, CA: Wadsworth international group.

Buchfink, B., Xie, C., and Huson, D. H. (2015). Fast and sensitive protein alignment using DIAMOND. *Nat. Methods* 12, 59–60. doi: 10.1038/nmeth.3176

Canfield, D. E., Glazer, A. N., and Falkowski, P. G. (2010). The evolution and future of earth's nitrogen cycle. *Science* 330, 192–196. doi: 10.1126/science.1186120

Caranto, J. D., Vilbert, A. C., and Lancaster, K. M. (2016). *Nitrosomonas europaea* cytochrome P460 is a direct link between nitrification and nitrous oxide emission. *Proc. Natl. Acad. Sci. U.S.A.* 113, 14704–14709. doi: 10.1073/pnas.1611051113

Carmo, J. B. D., Filoso, S., Zotelli, L. C., De Sousa Neto, E. R., Pitombo, L. M., Duarte-Neto, P. J., et al. (2013). Infield greenhouse gas emissions from sugarcane soils in Brazil: effects from synthetic and organic fertilizer application and crop trash accumulation. *GCB Bioenergy* 5, 267–280. doi: 10.1111/j.1757-1707.2012.01199.x

Christofoletti, C. A., Escher, J. P., Correia, J. E., Marinho, J. F. U., and Fontanetti, C. S. (2013). Sugarcane vinasse: environmental implications of its use. *Waste Manag.* 33, 2752–2761. doi: 10.1016/j.wasman.2013.09.005

CONAB (2017). *Acompanhamento da Safra Brasileira de Cana-de-Açúcar: V. 3 - SAFRA 2016/17 N. 3*. Available at: http://www.conab.gov.br [accessed October 15, 2017].

Daims, H., Lebedeva, E. V., Pjevac, P., Han, P., Herbold, C., Albertsen, M., et al. (2015). Complete nitrification by *Nitrospira* bacteria. *Nature* 528, 504–509. doi: 10.1038/nature16461

De Boer, W., and Kowalchuk, G. A. (2001). Nitrification in acid soils: micro-organisms and mechanisms. *Soil Biol. Biochem.* 33, 853–866. doi: 10.1016/S0038-0717(00)00247-9

De Figueiredo, E. B., and La Scala, N. Jr. (2011). Greenhouse gas balance due to the conversion of sugarcane areas from burned to green harvest in Brazil. *Agric. Ecosyst. Environ.* 141, 77–85. doi: 10.1016/j.agee.2011.02.014

De'ath, G. (2002). Multivariate regression trees: a new technique for modeling species–environment relationships. *Ecology* 83, 1105–1117. doi: 10.2307/3071917

De'ath, G. (2007). *mvpart: Multivariate Partitioning, R Package Version 1.6–2*. Available at: http://CRAN.R-project.org/package=mvpart

Di, H. J., Cameron, K. C., Podolyan, A., and Robinson, A. (2014). Effect of soil moisture status and a nitrification inhibitor, dicyandiamide, on ammonia oxidizer and denitrifier growth and nitrous oxide emissions in a grassland soil. *Soil Biol. Biochem.* 73, 59–68. doi: 10.1016/j.soilbio.2014.02.011

Dray, S., and Dufour, A. B. (2007). The ade4 package: implementing the duality diagram for ecologists. *J. Stat. Softw.* 22, 1–20. doi: 10.18637/jss.v022.i04

Edgar, R. C. (2010). Search and clustering orders of magnitude faster than BLAST. *Bioinformatics* 26, 2460–2461. doi: 10.1093/bioinformatics/btq461

Elia-Neto, A., and Nakahodo, T. (1995). *Caracterização Físico-Química da Vinhaça Projeto - 9500278. Relatório Técnico da Seção de Tecnologia de Tratamento de Águas do Centro de Tecnologia*. Piracicaba: Copersucar, 26.

FAO (2015). *World Reference Base for Soil Resources 2014, update 2015. International Soil Classification System for Naming Soils and Creating Legends for Soil Maps. World Soil Resources Reports No.* 106. Rome: Food and Agriculture Organization of the United Nations, 203.

Felsenstein, J. (1985). Confidence limits on phylogenies: an approach using the bootstrap. *Evolution* 39, 783–791. doi: 10.1111/j.1558-5646.1985.tb00420.x

Fierer, N., Jackson, J. A., Vilgalys, R., and Jackson, R. B. (2005). Assessment of soil microbial community structure by use of taxon-specific quantitative PCR assays. *Appl. Environ. Microbiol.* 71, 4117–4120. doi: 10.1128/aem.71.7.4117-4120.2005

Fish, J. A., Chai, B., Wang, Q., Sun, Y., Brown, C. T., Tiedje, J. M., et al. (2013). FunGene: the functional gene pipeline and repository. *Front. Microbiol.* 4:291. doi: 10.3389/fmicb.2013.00291

Fuess, L. T., and Garcia, M. L. (2014). Implications of stillage land disposal: a critical review on the impacts of fertigation. *J. Environ. Manage.* 145, 210–229. doi: 10.1016/j.jenvman.2014.07.003

Galdos, M. V., Cerri, C. C., Lal, R., Bernoux, M., Feigl, B., and Cerri, C. E. P. (2010). Net greenhouse gas fluxes in Brazilian ethanol production systems. *GCB Bioenergy* 2, 37–44. doi: 10.1111/j.1757-1707.2010.01037.x

Glaser, K., Hackl, E., Inselsbacher, E., Strauss, J., Wanek, W., Zechmeister-Boltenstern, S., et al. (2010). Dynamics of ammonia-oxidizing communities in barley-planted bulk soil and rhizosphere following nitrate and ammonium fertilizer amendment. *FEMS Microbiol. Ecol.* 74, 575–591. doi: 10.1111/j.1574-6941.2010.00970.x

Goreau, T. J., Kaplan, W. A., Wofsy, S. C., Mcelroy, M. B., Valois, F. W., and Watson, S. W. (1980). Production of NO2- and N2O by nitrifying bacteria at reduced concentrations of oxygen. *Appl. Environ. Microbiol.* 40, 526–532.

Habteselassie, M., Xu, L., and Norton, J. (2013). Ammonia-oxidizer communities in an agricultural soil treated with contrasting nitrogen sources. *Front. Microbiol.* 4:326. doi: 10.3389/fmicb.2013.00326

Hastings, R. C., Ceccherini, M. T., Miclaus, N., Saunders, J. R., Bazzicalupo, M., and Mccarthy, A. J. (1997). Direct molecular biological analysis of ammonia oxidising bacteria populations in cultivated soil plots treated with swine manure. *FEMS Microbiol. Ecol.* 23, 45–54. doi: 10.1111/j.1574-6941.1997.tb00390.x

He, J.-Z., Shen, J.-P., Zhang, L.-M., Zhu, Y.-G., Zheng, Y.-M., Xu, M.-G., et al. (2007). Quantitative analyses of the abundance and composition of ammonia-oxidizing bacteria and ammonia-oxidizing archaea of a Chinese upland red soil under long-term fertilization practices. *Environ. Microbiol.* 9, 2364–2374. doi: 10.1111/j.1462-2920.2007.01358.x

Hothorn, T. H., Hornik, K., Van De Wiel, M. A., and Zeileis, A. (2008). Implementing a class of permutation tests: the coin package. *J. Stat. Softw.* 28, 1–23. doi: 10.18637/jss.v028.i08

Hu, H.-W., Chen, D., and He, J.-Z. (2015). Microbial regulation of terrestrial nitrous oxide formation: understanding the biological pathways for prediction of emission rates. *FEMS Microbiol. Rev.* 39, 729–749. doi: 10.1093/femsre/fuv021

Huson, D. H., and Weber, N. (2013). "Chapter twenty-one - microbial community analysis using MEGAN," in *Methods in Enzymology*, ed. E. F. Delong (Amsterdam: Elsevier), 465–485.

IPCC (2013). *Anthropogenic and Natural Radiative Forcing. In: Climate Change 2013: The Physical Science Basis. Contribution of Working Group I to the Fifth Assessment Report of the Intergovernmental Panel on Climate Change [Online]*. Available at: https://www.ipcc.ch/pdf/assessment-report/ar5/wg1/WG1AR5_Chapter08_FINAL.pdf

Jones, C. M., Graf, D. R. H., Bru, D., Philippot, L., and Hallin, S. (2013). The unaccounted yet abundant nitrous oxide-reducing microbial community: a potential nitrous oxide sink. *ISME J.* 7, 417–426. doi: 10.1038/ismej.2012.125

Joo, H.-S., Hirai, M., and Shoda, M. (2005). Characteristics of ammonium removal by heterotrophic nitrification-aerobic denitrification by *Alcaligenes faecalis* No. 4. *J. Biosci. Bioeng.* 100, 184–191. doi: 10.1263/jbb.100.184

Kamphake, L. J., Hannah, S. A., and Cohen, J. M. (1967). Automated analysis for nitrate by hydrazine reduction. *Water Res.* 1, 205–216. doi: 10.1016/0043-1354(67)90011-5

Kindt, R., and Kindt, M. R. (2015). *Package 'BiodiversityR'*. Available at: https://CRAN.R-project.org/package=BiodiversityR.

Krom, M. D. (1980). Spectrophotometric determination of ammonia: a study of a modified Berthelot reaction using salicylate and dichloroisocyanurate. *Analyst* 105, 305–316. doi: 10.1039/AN9800500305

Kumar, S., Stecher, G., and Tamura, K. (2016). MEGA7: Molecular evolutionary genetics analysis version 7.0 for bigger datasets. *Mol. Biol. Evol.* 33, 1870–1874. doi: 10.1093/molbev/msw054

Letunic, I., and Bork, P. (2016). Interactive tree of life (iTOL) v3: an online tool for the display and annotation of phylogenetic and other trees. *Nucleic Acids Res.* 44, W242–W245. doi: 10.1093/nar/gkw290

Ma, W. K., Bedard-Haughn, A., Siciliano, S. D., and Farrell, R. E. (2008). Relationship between nitrifier and denitrifier community composition and abundance in predicting nitrous oxide emissions from ephemeral wetland soils. *Soil Biol. Biochem.* 40, 1114–1123. doi: 10.1016/j.soilbio.2007.12.004

Macedo, I. C., Seabra, J. E. A., and Silva, J. E. A. R. (2008). Greenhouse gases emissions in the production and use of ethanol from sugarcane in Brazil: the 2005/2006 averages and a prediction for 2020. *Biomass Bioenergy* 32, 582–595. doi: 10.1016/j.biombioe.2007.12.006

Mathieu, O., Hénault, C., Lévêque, J., Baujard, E., Milloux, M. J., and Andreux, F. (2006). Quantifying the contribution of nitrification and denitrification to the nitrous oxide flux using 15N tracers. *Environ. Pollut.* 144, 933–940. doi: 10.1016/j.envpol.2006.02.005

McMurdie, P. J., and Holmes, S. (2013). phyloseq: an R package for reproducible interactive analysis and graphics of microbiome census data. *PLoS One* 8:e61217. doi: 10.1371/journal.pone.0061217

Meinicke, P. (2015). UProC: tools for ultra-fast protein domain classification. *Bioinformatics* 31, 1382–1388. doi: 10.1093/bioinformatics/btu843

Nelson, M. B., Martiny, A. C., and Martiny, J. B. H. (2016). Global biogeography of microbial nitrogen-cycling traits in soil. *Proc. Natl. Acad. Sci. U.S.A.* 113, 8033–8040. doi: 10.1073/pnas.1601070113

Norton, J. M., Alzerreca, J. J., Suwa, Y., and Klotz, M. G. (2002). Diversity of ammonia monooxygenase operon in autotrophic ammonia-oxidizing bacteria. *Arch. Microbiol.* 177, 139–149. doi: 10.1007/s00203-001-0369-z

Oksanen, J., Blanchet, F. G., Kindt, R., Legendre, P., Minchin, P. R., O'hara, R., et al. (2015). *Package 'vegan'. Community Ecology Package, Version*, 2.2–1. Available at: https://github.com/vegandevs/vegan

Ouellette, M.-H., Legendre, P., and Borcard, D. (2012). Cascade multivariate regression tree: a novel approach for modelling nested explanatory sets. *Methods Ecol. Evol.* 3, 234–244. doi: 10.1111/j.2041-210X.2011.00171.x

Ouyang, Y., Norton, J. M., Stark, J. M., Reeve, J. R., and Habteselassie, M. Y. (2016). Ammonia-oxidizing bacteria are more responsive than archaea to nitrogen source in an agricultural soil. *Soil Biol. Biochem.* 96, 4–15. doi: 10.1016/j.soilbio.2016.01.012

Oved, T., Shaviv, A., Goldrath, T., Mandelbaum, R. T., and Minz, D. (2001). Influence of effluent irrigation on community composition and function of ammonia-oxidizing bacteria in soil. *Appl. Environ. Microbiol.* 67, 3426–3433. doi: 10.1128/AEM.67.8.3426-3433.2001

Paredes, D. S., Alves, B. J. R., Dos Santos, M. A., Bolonhezi, D., Sant'Anna, S. A., Urquiaga, S., et al. (2015). Nitrous oxide and methane fluxes following ammonium sulfate and vinasse application on sugar cane soil. *Environ. Sci. Technol.* 49, 11209–11217. doi: 10.1021/acs.est.5b01504

Paredes, D. S., Lessa, A. C. R., de Sant'Anna, S. A. C., Boddey, R. M., Urquiaga, S., and Alves, B. J. R. (2014). Nitrous oxide emission and ammonia volatilization induced by vinasse and N fertilizer application in a sugarcane crop at Rio de

Janeiro, Brazil. *Nutr. Cycling Agroecosyst.* 98, 41–55. doi: 10.1007/s10705-013-9594-5

Philippot, L., Hallin, S., and Schloter, M. (2007). Ecology of denitrifying prokaryotes in agricultural soil. *Adv. Agron.* 96, 249–305. doi: 10.1016/S0065-2113(07)96003-4

Phillips, C. J., Harris, D., Dollhopf, S. L., Gross, K. L., Prosser, J. I., and Paul, E. A. (2000). Effects of agronomic treatments on structure and function of ammonia-oxidizing communities. *Appl. Environ. Microbiol.* 66, 5410–5418. doi: 10.1128/AEM.66.12.5410-5418.2000

Pitombo, L. M., Do Carmo, J. B., De Hollander, M., Rossetto, R., López, M. V., Cantarella, H., et al. (2015). Exploring soil microbial 16S rRNA sequence data to increase carbon yield and nitrogen efficiency of a bioenergy crop. *GCB Bioenergy* 8, 867–879. doi: 10.1111/gcbb.12284

Pommerening-Röser, A., and Koops, H.-P. (2005). Environmental pH as an important factor for the distribution of urease positive ammonia-oxidizing bacteria. *Microbiol. Res.* 160, 27–35. doi: 10.1016/j.micres.2004.09.006

Prosser, J. I., Head, I. M., and Stein, L. Y. (2014). "The family Nitrosomonadaceae," in *The prokaryotes: Alphaproteobacteria and Betaproteobacteria*, eds E. Rosenberg, E. F. Delong, S. Lory, E. Stackebrandt, and F. Thompson (Berlin: Springer), 901–918.

Ravishankara, A. R., Daniel, J. S., and Portmann, R. W. (2009). Nitrous Oxide (N2O): The dominant ozone-depleting substance emitted in the 21st century. *Science* 326, 123–125. doi: 10.1126/science.1176985

Renault, P., Cazevieille, P., Verdier, J., Lahlah, J., Clara, C., and Favre, F. (2009). Variations in the cation exchange capacity of a ferralsol supplied with vinasse, under changing aeration conditions. *Geoderma* 154, 101–110. doi: 10.1016/j.geoderma.2009.10.003

Ritchie, G. A. F., and Nicholas, D. J. D. (1972). Identification of the sources of nitrous oxide produced by oxidative and reductive processes in *Nitrosomonas europaea*. *Biochem. J.* 126, 1181–1191. doi: 10.1042/bj1261181

Rodrigues Reis, C. E., and Hu, B. (2017). Vinasse from sugarcane ethanol production: better treatment or better utilization? *Front. Energy Res.* 5:7. doi: 10.3389/fenrg.2017.00007

Rotthauwe, J. H., Witzel, K. P., and Liesack, W. (1997). The ammonia monooxygenase structural gene amoA as a functional marker: molecular fine-scale analysis of natural ammonia-oxidizing populations. *Appl. Environ. Microbiol.* 63, 4704–4712.

Saitou, N., and Nei, M. (1987). The neighbor-joining method: a new method for reconstructing phylogenetic trees. *Mol. Biol. Evol.* 4, 406–425. doi: 10.1093/oxfordjournals.molbev.a040454

Schloss, P. D., Westcott, S. L., Ryabin, T., Hall, J. R., Hartmann, M., Hollister, E. B., et al. (2009). Introducing mothur: open-source, platform-independent, community-supported software for describing and comparing microbial communities. *Appl. Environ. Microbiol.* 75, 7537–7541. doi: 10.1128/aem.01541-09

Seabra, J. E. A., Macedo, I. C., Chum, H. L., Faroni, C. E., and Sarto, C. A. (2011). Life cycle assessment of Brazilian sugarcane products: GHG emissions and energy use. *Biofuels Bioproducts Biorefining* 5, 519–532. doi: 10.1002/bbb.289

Shaw, L. J., Nicol, G. W., Smith, Z., Fear, J., Prosser, J. I., and Baggs, E. M. (2006). Nitrosospira spp. can produce nitrous oxide via a nitrifier denitrification pathway. *Environ. Microbiol.* 8, 214–222. doi: 10.1111/j.1462-2920.2005.00882.x

Shi, X., Hu, H.-W., Zhu-Barker, X., Hayden, H., Wang, J., Suter, H., et al. (2017). Nitrifier-induced denitrification is an important source of soil nitrous oxide and can be inhibited by a nitrification inhibitor 3,4-dimethylpyrazole phosphate. *Environ. Microbiol.* 19, 4851–4865. doi: 10.1111/1462-2920.13872

Simpson, E. H. (1949). Measurement of diversity. *Nature* 163:688. doi: 10.1038/163688a0

Siqueira Neto, M., Galdos, M. V., Feigl, B. J., Cerri, C. E. P., and Cerri, C. C. (2016). Direct N2O emission factors for synthetic N-fertilizer and organic residues applied on sugarcane for bioethanol production in Central-Southern Brazil. *GCB Bioenergy* 8, 269–280. doi: 10.1111/gcbb.12251

Smith, P. S., and Hein, G. E. (1960). The alleged role of nitroxyl in certain reactions of aldehydes and alkyl halides1. *J. Am. Chem. Soc.* 82, 5731–5740. doi: 10.1021/ja01506a043

Soares, J. R., Cassman, N. A., Kielak, A. M., Pijl, A., Carmo, J. B., Lourenço, K. S., et al. (2016). Nitrous oxide emission related to ammonia-oxidizing bacteria and mitigation options from N fertilization in a tropical soil. *Sci. Rep.* 6:30349. doi: 10.1038/srep30349

Spott, O., Russow, R., and Stange, C. F. (2011). Formation of hybrid N2O and hybrid N2 due to codenitrification: first review of a barely considered process of microbially mediated N-nitrosation. *Soil Biol. Biochem.* 43, 1995–2011. doi: 10.1016/j.soilbio.2011.06.014

Stephen, J. R., Mccaig, A. E., Smith, Z., Prosser, J. I., and Embley, T. M. (1996). Molecular diversity of soil and marine 16S rRNA gene sequences related to beta-subgroup ammonia-oxidizing bacteria. *Appl. Environ. Microbiol.* 62, 4147–4154.

Systatsoftware (2014). *SSI. Sigmaplot for Windows, version* 13.0. San Jose, CA: Systat Software.

Taylor, A. E., and Bottomley, P. J. (2006). Nitrite production by *Nitrosomonas europaea* and *Nitrosospira* sp. AV in soils at different solution concentrations of ammonium. *Soil Biol. Biochem.* 38, 828–836. doi: 10.1016/j.soilbio.2005.08.001

Therneau, T. M., and Atkinson, E. J. (1997). *An Introduction to Recursive Partitioning using the RPART Routines. Technical Report*. Rochester, MN: Mayo foundation.

Torbert, H. A., and Wood, C. W. (1992). Effects of soil compaction and water-filled pore space on soil microbial activity and N losses. *Commun. Soil Sci. Plant Anal.* 23, 1321–1331. doi: 10.1080/00103629209368668

van Kessel, M. A. H. J., Speth, D. R., Albertsen, M., Nielsen, P. H., Op den Camp, H. J. M., Kartal, B., et al. (2015). Complete nitrification by a single microorganism. *Nature* 528, 555–559. doi: 10.1038/nature16459

Verhamme, D. T., Prosser, J. I., and Nicol, G. W. (2011). Ammonia concentration determines differential growth of ammonia-oxidising archaea and bacteria in soil microcosms. *ISME J.* 5, 1067–1071. doi: 10.1038/ismej.2010.191

Wrage, N., Velthof, G. L., Van Beusichem, M. L., and Oenema, O. (2001). Role of nitrifier denitrification in the production of nitrous oxide. *Soil Biol. Biochem.* 33, 1723–1732. doi: 10.1016/S0038-0717(01)00096-7

Xiang, X., He, D., He, J.-S., Myrold, D. D., and Chu, H. (2017). Ammonia-oxidizing bacteria rather than archaea respond to short-term urea amendment in an alpine grassland. *Soil Biol. Biochem.* 107, 218–225. doi: 10.1016/j.soilbio.2017.01.012

Zhao, B., An, Q., He, Y. L., and Guo, J. S. (2012). N2O and N2 production during heterotrophic nitrification by *Alcaligenes faecalis* strain NR. *Bioresour. Technol.* 116, 379–385. doi: 10.1016/j.biortech.2012.03.113

Zhu, X., Burger, M., Doane, T. A., and Horwath, W. R. (2013). Ammonia oxidation pathways and nitrifier denitrification are significant sources of N2O and NO under low oxygen availability. *Proc. Natl. Acad. Sci. U.S.A.* 110, 6328–6333. doi: 10.1073/pnas.1219993110

Conflict of Interest Statement: The authors declare that the research was conducted in the absence of any commercial or financial relationships that could be construed as a potential conflict of interest.

frontiers in Microbiology

ORIGINAL RESEARCH
published: 29 May 2018
doi: 10.3389/fmicb.2018.01137

Exploring the Denitrification Proteome of *Paracoccus denitrificans* PD1222

*Alfonso Olaya-Abril[1], Jesús Hidalgo-Carrillo[2], Víctor M. Luque-Almagro[1], Carlos Fuentes-Almagro[3], Francisco J. Urbano[2], Conrado Moreno-Vivián[1], David J. Richardson[4] and María D. Roldán[1]**

[1] Departamento de Bioquímica y Biología Molecular, Universidad de Córdoba, Córdoba, Spain, [2] Departamento de Química Orgánica, Universidad de Córdoba, Córdoba, Spain, [3] Servicio Central de Apoyo a la Investigación, Unidad de Proteómica, Córdoba, Spain, [4] School of Biological Sciences, University of East Anglia, Norwich, United Kingdom

Denitrification is a respiratory process that produces nitrous oxide as an intermediate, which may escape to the atmosphere before its reduction to dinitrogen through the nitrous oxide reductase NosZ. In this work, the denitrification process carried out by *Paracoccus denitrificans* PD1222 has been explored through a quantitative proteomic analysis. Under anaerobic conditions, with nitrate as sole nitrogen source, the synthesis of all the enzymes involved in denitrification, the respiratory nitrate, nitrite, nitric oxide, and nitrous oxide reductases, was increased. However, the periplasmic and assimilatory nitrate reductases decreased. Synthesis of transporters for alcohols, D-methionine, sulfate and copper, most of the enzymes involved in the tricarboxylic acid cycle, and proteins involved in other metabolic processes like lysine catabolism, fatty acids degradation and acetyl-CoA synthesis, was increased during denitrification in *P. denitrificans* PD1222. As consequence, an enhanced production of the central metabolite acetyl-CoA was observed. After establishing the key features of the denitrification proteome, its changes by the influence of a competitive electron acceptor, oxygen, or competitive nitrogen source, ammonium, were evaluated.

Keywords: acetyl-CoA, denitrification, liquid chromatography-mass spectrometry, nitrate reductase, nitrous oxide, nitrous oxide reductase, *Paracoccus*, proteomics

OPEN ACCESS

Edited by:
Lourdes Girard, Universidad Nacional Autónoma de México, Mexico

Reviewed by:
Stephen Spiro, The University of Texas at Dallas, United States
Rosa María Martínez-Espinosa, University of Alicante, Spain

***Correspondence:**
María D. Roldán
bb2rorum@uco.es

Specialty section:
This article was submitted to Terrestrial Microbiology, a section of the journal Frontiers in Microbiology

Received: *17 April 2018*
Accepted: *14 May 2018*
Published: *29 May 2018*

Citation:
Olaya-Abril A, Hidalgo-Carrillo J, Luque-Almagro VM, Fuentes-Almagro C, Urbano FJ, Moreno-Vivián C, Richardson DJ and Roldán MD (2018) Exploring the Denitrification Proteome of Paracoccus denitrificans PD1222. Front. Microbiol. 9:1137. doi: 10.3389/fmicb.2018.01137

INTRODUCTION

Denitrification is the respiratory reduction of the water soluble nitrogen oxyanions, nitrate (NO_3^-) and nitrite (NO_2^-), to the gaseous products nitric oxide (NO), nitrous oxide (N_2O) and molecular nitrogen (N_2) under oxygen-limited conditions through four reactions whereby 10 electrons are consumed in converting two nitrate ions to dinitrogen molecule (Zumft, 1997; Richardson, 2000; Philippot et al., 2007; van Spanning et al., 2007; Bakken et al., 2012; Hu et al., 2015). The complete process involves the enzymes nitrate reductase (Nar), nitrite reductase (Nir), nitric oxide reductase (Nor) and nitrous oxide reductase (Nos). The functioning of these enzymes is conditioned by both the need to regulate the process avoiding accumulation of toxic intermediates, mainly nitric oxide, and to maximize energy conservation when oxygen is fluctuating (Bergaust et al., 2008, 2010; Sullivan et al., 2013). The reduction of nitrite to nitric oxide by the nitrite reductase defines the denitrification process since it represents the conversion of a non-gaseous water-soluble nitrogen oxyanion to a nitrogen oxide gas.

Biological denitrification is a major biological process for producing the potent greenhouse gas N_2O and it accounts globally for about 60% of total N_2O emissions to the atmosphere. The denitrification pathway has been extensively studied, and several key factors have been described for controlling nitrous oxide/molecular nitrogen ratio in soils, such as oxygen levels, pH, temperature, water content and nitrate or carbon substrate availability (Bergaust et al., 2010). Copper concentration in the media has been also described to be essential to achieve an adequate synthesis of the nitrous oxide reductase (NosZ) of *P. denitrificans* PD1222 because this enzyme contains a Cu_z active center, which is a multi-copper-sulfide [Cu_4S] cluster (Richardson et al., 2009; Sullivan et al., 2013). The highest denitrification activity is observed under oxygen-limitation or anaerobic conditions, although aerobic denitrification has also been described in some bacteria isolated from soils and sediments (Patureau et al., 2000; Hu et al., 2015). Field experiments with bacterial denitrifiers have revealed that low pH increases nitrous oxide emissions (Richardson et al., 2009; Shcherbak et al., 2014; Hu et al., 2015). It has been demonstrated that nitrous oxide reduction is severely reduced under acidic pH, suggesting an effect of pH on nitrous oxide reductase at transcriptional or posttranscriptional level (Wrage et al., 2001; Bakken et al., 2012; Hu et al., 2015).

The α-proteobacteria *Paracoccus denitrificans* PD1222 (Baker et al., 1998) is a model soil microorganism able to perform the complete denitrification pathway, in which nitrate reduction is molybdenum-dependent (membrane-bound and periplasmic nitrate reductases), nitrite and nitric oxide reduction are iron-dependent (cytochrome cd_1-type nitrite reductase or heme *c/b* nitric oxide reductase) and nitrous oxide reduction is copper-dependent (Cu_z-nitrous oxide reductase). All these reductases can be coupled to the core electron transport pathway at the level of the ubiquinol pool in the membrane and the periplasmic heme-containing cytochrome c_{550} or Cu-containing pseudoazurin pool (Richardson, 2000; Felgate et al., 2012; Giannopoulos et al., 2017). Denitrification is negatively controlled in response to oxygen by FnrP and positively regulated in response to nitric oxide by Nnr. Recently, it has been suggested that FnrP can also be negatively regulated by nitric oxide (Crack et al., 2016). In addition, NarR, NirI, and NosR specifically regulate expression of the *nar*, *nir,* and *nos* genes, respectively (Saunders et al., 1999; van Spanning et al., 1999; Wood et al., 2001; Bergaust et al., 2012; Spiro, 2012). A recent genomic analysis of steady-state chemostat cultures revealed that the transition from aerobic to anaerobic growth supported by denitrification resulted in the up- or down-regulation (≥2-fold) of just 4% of the genome, with 157 upregulated genes putatively involved in the synthesis or activity of the *P. denitrificans* respirome, including the terminal reductases (Giannopoulos et al., 2017). This represents a very efficient adaptation from aerobic to anaerobic metabolism.

To date, much of the experimental work addressing the regulation of denitrification has been focused on transcriptional studies. However, to understand regulation in more detail it is important to get a perspective on protein synthesis, and therefore differences in the proteome, rather than just in the transcriptome of the denitrification. This is important because a twofold change in gene expression (the threshold used for significance in transcriptomics), does not necessarily lead to an equivalent change in levels of the relevant proteins, and indeed transcriptional analyses supply no information at all on protein levels. Thus, for a full (holistic) picture of the denitrification process, a global overview of all the denitrification proteins, most of them complex metalloproteins, is required. Second-generation proteomics uses gel-free approaches, based on liquid chromatography-mass spectrometry/mass spectrometry (LC-MS/MS) analysis for the identification of thousands of species (generally peptides, after sample treatment with a protease) in a liquid sample. The wide array of combinations derived from these approaches makes it possible to overcome the limitations attributed to gel-based proteomics regarding membrane proteins, as well as a more accurate quantification through both labeling and non-labeling strategies (Speers and Wu, 2007). In this work, a proteomic study of *P. denitrificans* PD1222 has been carried out under nitrate-respiring denitrifying conditions and used as reference point from which to consider the impact of the additional nitrogen source ammonium, and the additional electron acceptor oxygen.

RESULTS AND DISCUSSION

Defining the Growth Physiology of *P. denitrificans* Prior to Proteomic Analyses

Prior to undertaking the proteomic study, the experimental growth conditions for culturing *P. denitrificans* under: (i) anaerobic denitrifying conditions with nitrate as electron acceptor and sole N-source (Den-N); (ii) anaerobic denitrifying conditions with nitrate as electron acceptor and with both ammonium and nitrate as potential N-sources (Den-NA); and (iii) aerobically with both oxygen and nitrate as potential electron acceptors and nitrate as a sole N-source (Aer-N) were established. N-oxyanion concentrations and N-gas emissions were determined in bacterial cultures in early exponential phase (A_{600} ∼0.3) and stationary phase (A_{600} ∼0.9) of the growth curves (**Table 1**). In Den-N cultures (30 mM nitrate, 30 mM succinate) at early growth phase (A_{600} ∼0.3), about 11 mM nitrate remained in the media, whereas at stationary growth phase (A_{600} ∼0.9) nitrate was completely exhausted and mainly transformed to N_2 (**Table 1**). In the Den-NA cultures at early logarithmic phase only a small amount of nitrate was converted into dinitrogen. However, at the stationary growth phase (A_{600} ∼0.9) ammonium was completely exhausted and almost all nitrate was denitrified to N_2 (**Table 1**). Nitrite accumulated was ∼6-fold higher (∼600 μM) under Den-N conditions than in Den-NA conditions (**Table 1**). This high level of extracellular nitrite accumulation was also observed under Aer-N conditions, suggesting a link between nitrite extrusion and the process of assimilating nitrogen from nitrate under both aerobic and anaerobic growth conditions. The gaseous intermediates nitric oxide and nitrous oxide were not detected (<1 μM) under either Den-N or DenNA growth conditions. This suggests that

TABLE 1 | Concentration of nitrate, nitrite, ammonium, and gasses of denitrification in *P. denitrificans* PD1222.

Sample*	A_{600}	Protein (μg ml^{-1})	NO_2^- accumulation (μM)	NO_3^- consumed (mM)	NH_4^+ consumed (mM)	N_2 produced (mM)
Den-N	0.30 ± 0.01	32.4 ± 2.8	35.6 ± 4.2	19.2 ± 0.4	–	7.3 ± 0.2
Den-N	0.91 ± 0.02	219.8 ± 4.3	641.6 ± 2.9	30 ± 0	–	14.2 ± 1.0
Den-NA	0.30 ± 0.01	28.6 ± 1.2	124.7 ± 4.1	2.7 ± 1.9	4.7 ± 0.8	1.4 ± 0.4
Den-NA	0.93 ± 0.02	226.9 ± 0.3	109.5 ± 11.3	26.6 ± 0.1	10 ± 0	16.7 ± 0.3
Aer-N	0.30 ± 0.01	30.5 ± 1.0	616.0 ± 22.4	1.2 ± 0.3	–	0 ± 0
Aer-N	0.91 ± 0.01	222.6 ± 0.9	646.04 ± 1.6	10 ± 0	–	0 ± 0

**Den-N, cells grown in anaerobiosis with 30 mM nitrate; Den-NA, cells grown in anaerobiosis with 30 mM nitrate plus 10 mM ammonium; Aer-N, cells grown in aerobiosis with 10 mM nitrate. Samples were taken at early (A_{600} ∼0.3) or late (A_{600} ∼0.9) exponential growth phase. Data are means ± DE of 2 independent biological samples, and from each of these, 2 methodological replicates (n = 4). N-ions and denitrification gasses were determined as indicated in experimental procedures. NO and N_2O were not detected.*

denitrification was proceeding all the way through to dinitrogen gas as the end-product. In Aer-N cultures, neither dinitrogen nor nitric oxide/nitrous oxide intermediates were detected at significant levels, indicating suppression of denitrification. This is consistent with the cultures being highly aerated, with all nitrate used therefore assignable to nitrogen assimilation (**Table 1**).

The Proteome of *P. denitrificans* PD1222 During Anaerobic Denitrification With Nitrate as Sole Nitrogen Source

To gain insight into the metabolism of *P. denitrificans* when using nitrate as both electron acceptor and nitrogen source, the strain PD1222 was grown under anaerobic conditions with 30 mM succinate as carbon source and 30 mM nitrate as N-source, in the absence of ammonium (Den-N cultures). When cultures reached an absorbance at 600 nm of approximately 0.3, cells were harvested and processed to perform a LC-MS/MS analysis of the global proteome in response to denitrifying conditions. Two independent cultures were set up, and from each one two independent samples were prepared from each culture for a full proteome analysis. A total of 1293 proteins were reproducibly identified from ∼5100 putative structural genes present in the whole genome of the PD1222 strain (Supplementary Table S1), giving a ∼25% representation of the genome in the detectable proteome. Breaking down the proteome into gene ontology (GO) groups can give some insight into functional categories of proteins that are either enriched (highly represented) or suppressed (poorly represented) under denitrifying and nitrate assimilating conditions (**Figure 1A**). Highly represented GO groups included 'carbohydrate biosynthesis,' 'malate and pyruvate metabolism,' 'regulation of nitrogen utilization,' 'nitrate metabolic process,' 'electron transport chain,' 'protein folding,' 'RNA modification,' 'transcription anti-termination and translation.' Poorly represented GO groups (**Figure 1B**) included 'cobalamin biosynthesis,' 'nitrogen compound metabolism,' 'cytochrome complex assembly,' 'phosphorelay signal transduction,' 'DNA recombination' and 'regulation of transcription and translation.' Some of these proteins, encoded by genes located in several notable gene clusters, merit specific mention (**Figure 2**).

Firstly, most of the structural proteins required for denitrification were detected, including the respiratory nitrate reductase system NarKGHJI (A1B9V7-A1B9V3), the periplasmic nitrate reductase NapA (A1BB88), the cd_1-type nitrite reductase NirS (Q51700), the nitric oxide reductase NorBC (A1B4X6 and A1B4X7), the nitrous oxide reductase NosZ (A1B9T9), and the Cu-protein pseudoazurin (Q71RW5). Regarding regulatory proteins, the general transcriptional regulators of denitrification involved in the *P. denitrificans* NO-response Nnr (A1B353), the O_2-responsive FnrP (A1B9U4) and the system-specific regulatory proteins of the nitrite, nitric oxide and nitrous oxide reductases NirI (Q51699) and NosR (A1B9U0) were also detected (Supplementary Table S1).

Secondly, several proteins involved in assimilatory nitrate reduction were identified, including the structural NasABGHC proteins (A1BAH3-A1BAH0, A1BAG9) and the regulatory protein NasS (A1BAH4) that acts as a nitrate sensor (Gates et al., 2011; Luque-Almagro et al., 2013), along with proteins functionally associated with the nitrogen starvation response, such as the global regulatory proteins NtrBC (A1B9K0, A1B9J9), NtrYX (A1B9J8, A1B9J7) and PII-GlnB (A1BAI1), glutamine synthetase GlnA (A1BAI2), glutamate synthase large and small subunits (A1AZA6 and A1AZA8), urease structural and accessory proteins (A1B1B6, A1B1B8, A1B1B9, and A1B1C2), and the transporters of ammonium and some amino acids (A1B3N0, A1B061, A1B064, and A1B066) (Supplementary Table S1). Under denitrifying conditions in the presence of nitrate as the sole nitrogen source, the main fate of nitrate is to serve as end-electron acceptor, but some also needs to be assimilated *via* ammonium. NasH (A1BAUD) is a putative nitrite extrusion protein that may play a role in nitrite homeostasis during nitrate assimilation and, therefore could contribute to the high levels of extracellular nitrite observed in Den-N cultures (**Table 1**).

Thirdly, regarding central metabolic pathways, many enzymes of the Krebs and glyoxylate cycles could be detected in this proteomic study during denitrification, including malate dehydrogenase (A1B0K8), fumarate hydratase (A1B3A9), succinate and isocitrate dehydrogenases (A1AZI5, A1B6A1), aconitase (A1BAT6) and malate synthase (A1B9C3). Also, different components of the respiratory electron transport chain like proteins belonging to complex I-NADH-quinone oxidoreductase (A1B481, A1B486, A1B489, A1B491, A1B495, A1B496), complex II-succinate dehydrogenase (A1AZJ0, A1AZI7) and the cytochrome cbb_3-type cytochrome *c* oxidase (A1B348 and A1B350) were detected under denitrifying conditions (Supplementary Table S1).

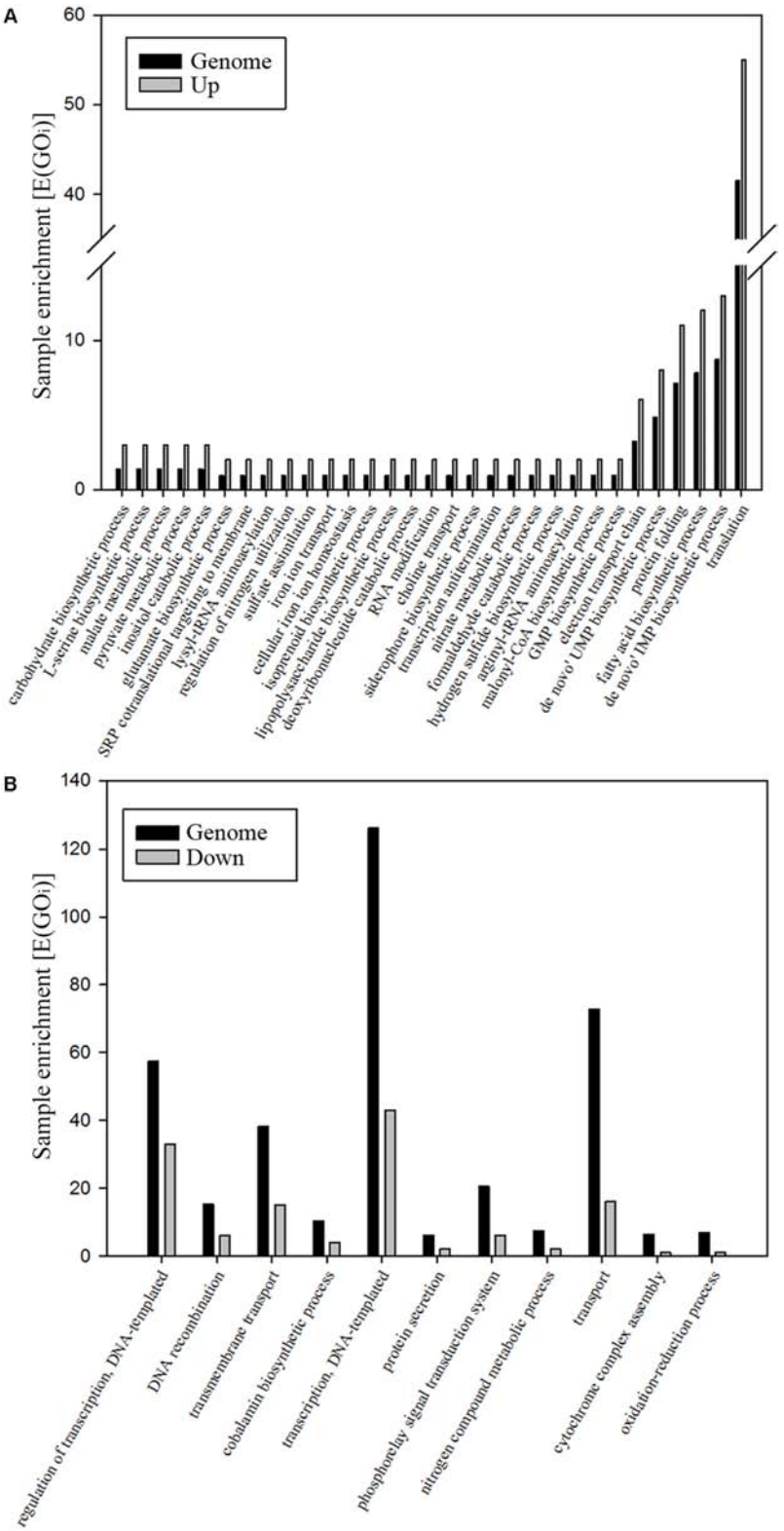

FIGURE 1 | Analysis of the denitrification proteome of *P. denitrificans* PD1222. Significative changes in GO groups. Only those changes with a p-value < 0.05 are shown. The whole genome of *P. denitrificans* PD1222 was used as reference (black bars) and over-represented **(A)** and down-represented **(B)** GO groups are shown (gray bars). Hyper-geometric distribution [E(GOi)] of GO (ComparativeGO), biological function, third level of proteins identified under denitrifying conditions. The parameter E(GOi) is calculated by using the formula: [E(GOi)] = sample size/genome size × GOi.

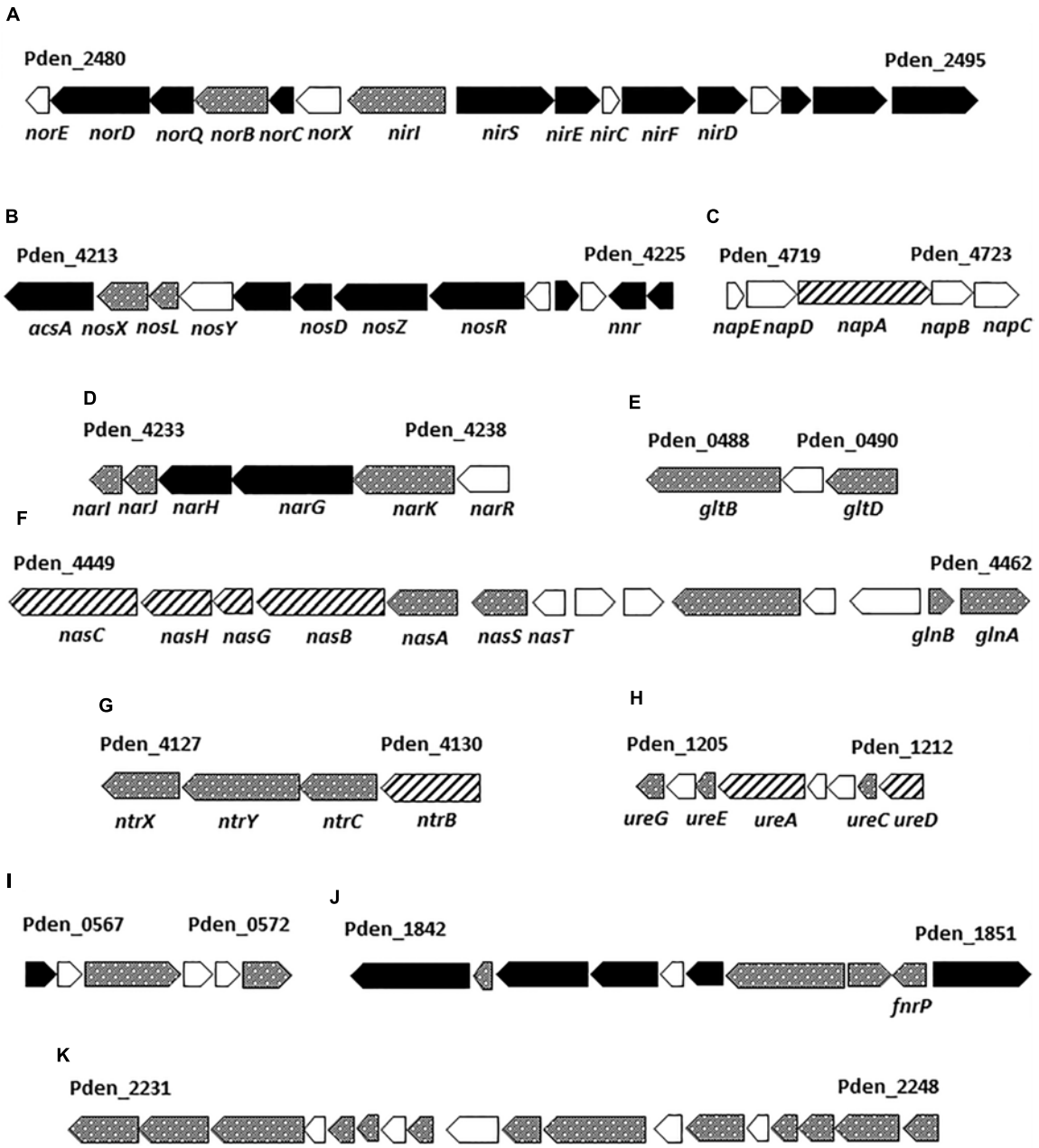

FIGURE 2 | *Paracoccus denitrificans* PD1222 genes encoding several proteins detected by LC-MS/MS under denitrifying conditions. The reference codes correspond to the first and the last gene of each gene cluster according with UniProt (UP000000361). Gene-filling: black, genes encoding proteins found in abundance under anaerobic denitrifying conditions when compared to aerobic cultures; dotted, genes that code for proteins of unchanged levels in the presence or absence of oxygen; dashed, genes encoding proteins displaying low abundance under anaerobic conditions. Gene cluster descriptions are provided in Supplementary Figure S2.

Fourthly, several membrane-bound transporters were highly represented under anaerobic denitrifying conditions, including those specific for carbon compounds (e.g., the C4-dicarboxylate transporter A1BBD2 and the ribose/galactose/methylgalactoside import ATP-binding protein A1B2N6) and, also for D-methionine (A1BA28). Microorganisms able to synthesize *de novo* methionine may require vitamin B_{12} as cofactor. Thus, a B_{12}-dependent methionine synthase catalyzes the conversion of 5-methyltetrahydrofolate and L-homocysteine to tetrahydrofolate and L-methionine. In *P. denitrificans* PD1222 it has been recently demonstrated that cytotoxic N_2O emissions modulate expression of genes controlled by vitamin B_{12} riboswitches, because N_2O binds to and inactivates vitamin B_{12}. Cytotoxicity of N_2O was relieved by the addition

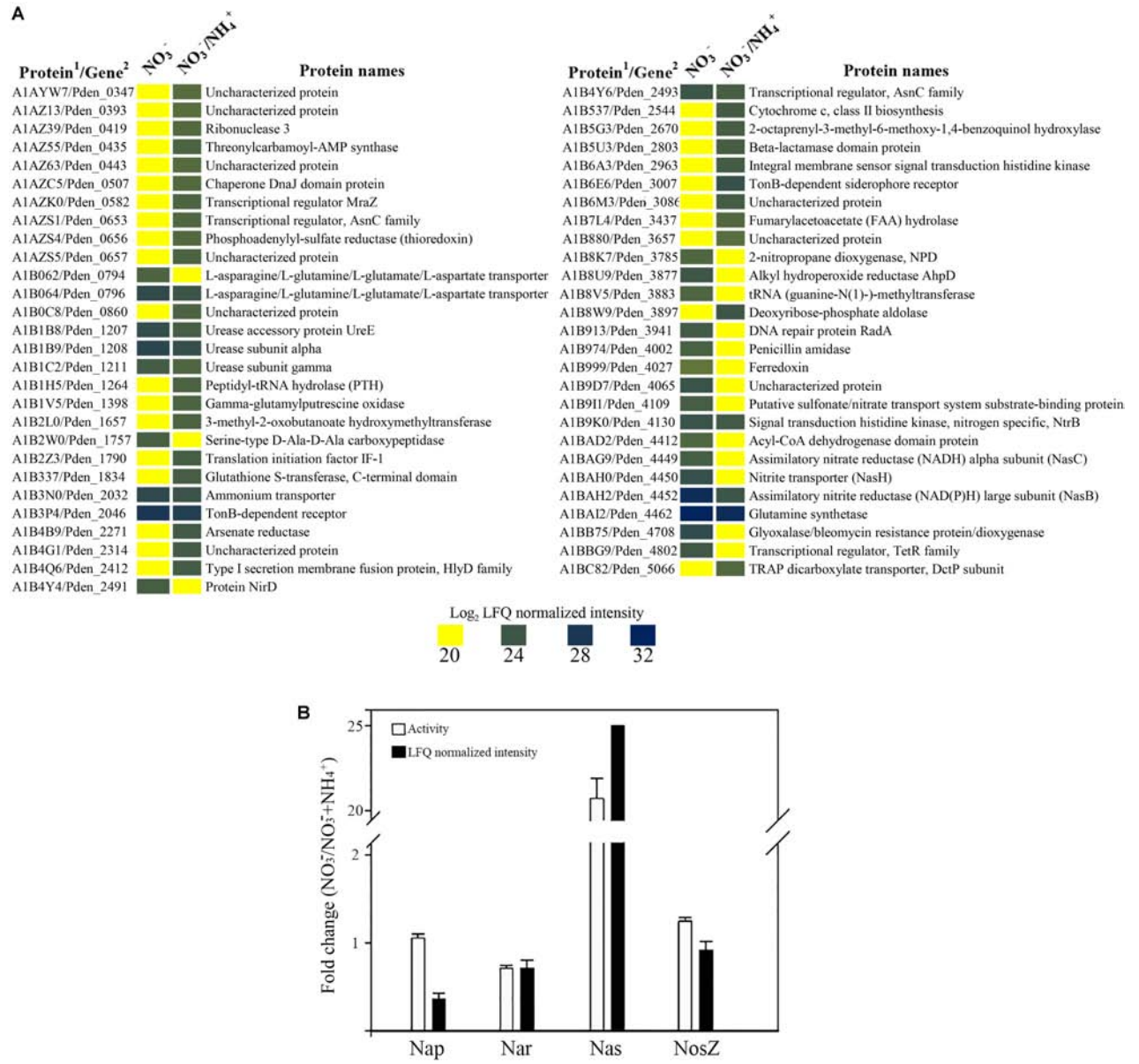

FIGURE 3 | Effect of ammonium on the denitrification proteome of *P. denitrificans* PD1222. Heatmap of over-represented (blue) or down-represented (yellow) proteins (log_2 normalized expression) of *P. denitrificans* PD1222 in the presence or absence of ammonium during denitrification. Proteomic data from cells grown with 30 mM nitrate were compared to data from cells grown with 30 mM nitrate plus 10 mM ammonium. ([1]) Protein code according to Uniprot database under the accession number UP000000361. (2) Gene code according to Genebank under the accession number CP000489.1 **(A)**. Fold change of Nar, Nap, Nas, and NosZ proteins. White bars represent enzymic activity and black bars show normalized peptide intensities. Fold changes were shown using the enzymic activity or peptide intensity ratio ($NO_3^-/NO_3^- + NH_4^+$) **(B)**, error bars correspond to data from at least 3 independent replicates.

of vitamin B_{12} to the media (Sullivan et al., 2013). Therefore, the import of methionine by the A1BA28 transporter could be a mechanism to bypass the cobalamin dependence of *de novo* biosynthetic process. Copper-limitation has a negative effect on the expression of the *nos* genes, leading to accumulation of N_2O and inhibition of vitamin B_{12} dependent-enzymes (Sullivan et al., 2013). The copper-binding periplasmic (A1B97T8) and the membrane (A1B97T7) components of an ABC transporter involved in NosZ maturation (Saunders et al., 2000) were found highly induced under denitrifying conditions in the strain PD1222. Although copper is a trace element essential for all aerobic organisms, it could exert toxicity to the cell when its homeostasis is not maintained. In this sense, a P-type copper extrusion system (A1B375) was highly induced under anaerobic growth in *P. denitrificans* PD1222, suggesting that copper needs to be transported inside the cell to favor its incorporation to metalloproteins, including NosZ, and therefore this metal extrusion system is induced under denitrifying conditions to

allow copper homeostasis in the cell. It is notable that the Pden_1842 gene coding for this metal extrusion component is located near the genes encoding the copper-containing cbb_3-type cytochrome oxidase (Pden_1845-Pden_1848) and the Pden-1850 gene that codes for the transcription regulator FnrP involved in the aerobic-anaerobic transition (**Figure 2**).

Changes in the Denitrification Proteome of *P. denitrificans* PD1222 in Response to Ammonium as Additional N-source

Paracoccus denitrificans was grown under anaerobic conditions with 30 mM succinate as carbon source and 30 mM nitrate as nitrogen source and electron acceptor, plus 10 mM ammonium as additional nitrogen source (Den-NA), and the global proteome was analyzed by LC-MS/MS as described above. Two independent cultures were set up and from each one two independent samples were prepared (Supplementary Figure S2). Variability within samples was assessed by heat maps and volcano plots (Supplementary Figure S1A). Then, a differential proteomic study was performed by comparison of data from cells grown with nitrate as sole nitrogen and electron acceptor (Den-N) with data from cells grown with nitrate plus ammonium (Den-NA). One thousand three hundred and eighty four proteins were detected from the Den-NA cultures, representing 27% of the total potential proteome (Supplementary Table S2). Of these, only 55 proteins (4% of the detectable proteome) significantly changed their intensities (26 proteins with increased expression and 29 with decreased expression) compared to in the absence of ammonium (**Figure 3A**). This reflects a very efficient adaptation to utilization of ammonium, rather than nitrate, as the primary nitrogen source.

Among the 29 proteins with decreased intensities under Den-NA conditions were peptides of the assimilatory nitrate (NasC, A1BAG9) and nitrite (NasB, A1BAH2) reductases, the nitrite transporter (NasH, A1BAH0) and the transcriptional regulators NtrB (A1B9K0) and NirD (A1B4Y4). NirD is involved in the biosynthesis of the heme d_1 from precorrin 2. The heme d_1 is required for the active site of NirS. Precorrin 2 is also an intermediate in siroheme biosynthesis, the active site cofactor for the large subunit of the assimilatory nitrite reductase NasB. It is likely therefore that NirS and NasB biosynthesis competes for precorrin 2. Levels of NirD may play an important role in the routing of precorrin 2 to siroheme or heme d_1 biosynthesis (Bali et al., 2011), which may impact in the apparent suppression by ammonium of onset of denitrification in the early stages of the growth cultures as illustrated in **Table 1**.

NtrB is a sensor kinase that autophosphorylates a histidine residue under low nitrogen conditions and, in turn, transfers a phosphoryl group on a specific aspartate residue to the response regulator NtrC. Phosphorylated NtrC acts as σ^{54}-dependent transcriptional activator of different genes related with nitrogen metabolism (Sanders et al., 1992; Luque-Almagro et al., 2011). In *P. denitrificans* it has been recently demonstrated that the NtrBC system controls, in response to ammonium, the glutamine synthetase *glnA* gene, the ammonium transporter *amtB* gene, the urease *ure* genes and the nitrate/nitrite assimilation *nas* genes, among others (Luque-Almagro et al., 2017). Although the regulation exerted by ammonium through the NtrBC system occurs at the post-transcriptional level, *P. denitrificans* PD1222 NtrB was found at a lower peptide intensity in the presence of ammonium than in its absence (**Figure 3A**), and this could also contribute to reduce the expression of genes with a predicted NtrC-binding site. A putative nitrate/sulfonate transporter (A1B9I1) was also decreased in representation, which may suggest a role for this protein in nitrate or nitrite uptake (**Figure 3A**).

The 26 proteins with increased intensities included a transcriptional regulator belonging to the AsnC family (A1AZS1) encoded by the Pden_0653 gene that clusters together with a putative heme-containing nitrite/sulfite reductase gene (Pden_0655) and a thioredoxin (A1AZS4) encoded by Pden_0656. A protein involved in cytochrome *c* class II biosynthesis, which is encoded by the Pden_2544 gene that clusters together with cobyrinate *a,c*-diamide synthase (Pden_2541) and precorrin-6A synthesis (Pden_2542) genes also displayed increased peptide intensity.

When the ratios of normalized peptide intensities of the three nitrate reductases (respiratory Nar, periplasmic Nap and assimilatory Nas), and the nitrous oxide reductase NosZ were calculated for the Den-N versus Den-NA cultures, it was clear that the synthesis of assimilatory nitrate reductase was negatively affected by the presence of ammonium in the media (Den-NA cultures), with an increase of ∼25-fold observed in lysates from Den-N cultures compared to Den-NA conditions. This data was also supported by determination of the assimilatory nitrate reductase activity in cytoplasmic fractions using NADH as electron donor in the enzymic assay (**Figure 3B**).

Gas emissions were measured during denitrification (**Table 1**). In the absence of ammonium, almost all nitrate reduced was converted into dinitrogen without accumulation of intermediate gasses, and only a low amount of nitrate was used for assimilative purposes. However, when ammonium was present in the media, the production of N_2 was very low at early exponential growth phase, and only when ammonium was consumed was denitrification maximal (**Table 1**). This finding may have an ecophysiological impact on microbial communities of nitrifiers *versus* denitrifiers and in denitrification itself that could be performed with both nitrate and ammonium coexisting in agricultural soils when they are used as crop fertilizers.

Effect of Oxygen on the Denitrification Proteome of *P. denitrificans* PD1222

A proteomic study of *P. denitrificans* cells grown in aerobic conditions with nitrate as sole N-source (Aer-N) was also performed (Supplementary Table S3). Variability within samples was shown by heatmap and volcano plots (Supplementary Figure S1B). Hundred and ninety one proteins were identified with significant changed levels in the comparative proteomic analysis carried out from cells cultured with nitrate as the nitrogen source and electron acceptor in the absence (Den-N) or presence (Aer-N) of oxygen (**Figures 4**, **5**). Of these 87 proteins were only found under anaerobic conditions (as defined here by

FIGURE 4 | Exclusive and over-represented proteins of *P. denitrificans* PD1222 under anaerobic-denitrifying conditions with nitrate as the sole nitrogen source. Data were obtained from a comparative analysis from cells cultured with or without oxygen in the presence of nitrate as the sole nitrogen source. Results are shown in a scale color from dark blue to yellow as $\log_2$ normalized expression. ([1]) Protein code according to Uniprot database under the accession number UP000000361.

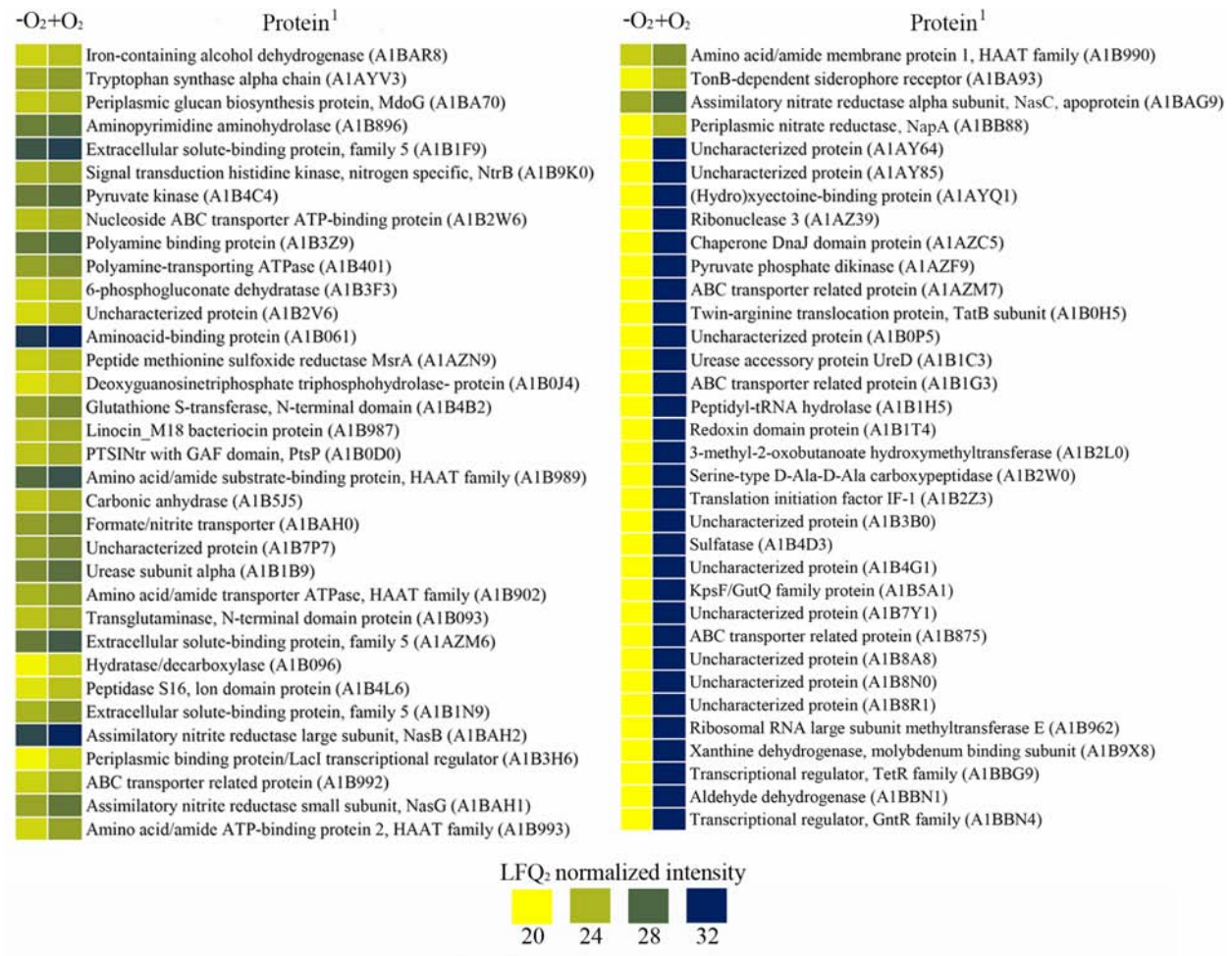

FIGURE 5 | Exclusive and over-represented proteins of *P. denitrificans* PD1222 under aerobiosis when nitrate was used as the sole nitrogen source. Data were obtained from a comparative analysis from cells grown with or without oxygen. Results are shown in a scale color from dark blue to yellow as log_2 normalized expression. ([1]) Protein code according to Uniprot database under the accession number UP000000361.

fold change > 552 in anaerobiosis compared to aerobiosis), and 36 proteins were up-represented in anaerobiosis (**Figure 4**). In addition, 38 proteins were down-represented under anaerobiosis and 30 proteins were exclusive to aerobic conditions as defined by a fold change > 13 in aerobiosis compared to anaerobiosis (**Figure 5**).

Peptides exclusively detected in anaerobic cultures (**Figure 4**) corresponded to the respiratory nitrate reductase NarGH (A1B9V6, A1B9V5), the cd_1-type nitrite reductase NirS (A1B4Y0), the nitric oxide reductase subunit NorC (A1BAX7), and the proteins NorQ (A1B4X5), NirD (A1B4Y4) and pseudoazurin (Q71RW5). Other peptides only found in anaerobiosis were the periplasmic components of several alcohol transporters (A1B9R0, A1BAA7, A1B2N6, and A1B2N7), the cytoplasmic ATPase component of a sulfate transporter (A1B300), a copper ABC transporter component (A1B9T7), a heavy metal (copper) translocating P-type ATPase component (A1B345) and the enzymes malate dehydrogenase (A1B0K8) and succinate dehydrogenase (A1AZI5). Highly represented in anaerobiosis, but also detected at lower intensities under aerobic conditions (**Figure 4**), were the nitrous oxide reductase NosZ (A1B9T9), and a D-methionine transporter (A1BA28). High levels of synthesis under denitrifying conditions was also observed for several enzymes of the tricarboxylic acid (TCA) and glyoxylate cycles, such as aconitase (A1BAT6), isocitrate dehydrogenase (A1B6A1), fumarate hydratase class II (A1B3A9) and malate synthase (A1B9C3), and several enzymes that produce the key metabolite acetyl-CoA, including the acetyl-CoA synthetase (A1B9T3 and A1BAR9), the 3-hydroxyalcyl-CoA dehydrogenase (A1B611) and the butyryl-CoA:acetate CoA transferase (A1BB51).

A regulatory protein involved in denitrification up-regulated under nitrate-anaerobic conditions was NosR (A1B9U0), whereas the levels of the regulators FnrP (A1B9U4) and NirI (Q51699) remained unchanged independently of presence/absence of oxygen. On the other hand, proteins down-regulated under Den-N conditions, with higher levels during aerobiosis than in anaerobiosis, were the assimilatory

nitrate reductase NasC (A1BAG9), the assimilatory nitrite reductase small (NasG) and large (NasB) subunits (A1BAH1, A1BAH2), the periplasmic nitrate reductase NapA (A1BB88), and the urease (A1B1B9) and the urease transporter (A1B989, A1B990, A1B992, A1B993), among others (**Figure 5**).

The high affinity cbb_3 terminal oxidase was negatively affected by the presence of oxygen as revealed by the decreased level of two of its cytoplasmic components quantified in the proteomic analysis (**Figure 4**). However, none of the cytochrome aa_3 oxidase components, which were expected to be expressed under aerobic conditions, could be detected in this study probably due to their large transmembrane regions.

In contrast to ammonium, oxygen showed a strong effect on the representation of reductases and other proteins involved in denitrification (**Figure 6**). Thus, the respiratory nitrate reductase Nar decreased in the presence of oxygen to half of the activity and protein intensity found in anaerobiosis. On the contrary, the assimilatory and periplasmic nitrate reductases, Nas and Nap, increased significantly under aerobic conditions (**Figure 6**). These results indicate that under anaerobic conditions the nitrate fate is mainly the denitrification pathway, whereas in aerobiosis nitrate assimilation is the major nitrate reduction pathway, although the periplasmic nitrate reductase may function as a redox balancing enzyme contributing to the production of extracellular nitrite through aerobic nitrate reduction (Richardson et al., 2001). The levels of gene expression, protein intensity and activity of the nitrous oxide reductase NosZ were much lower with oxygen than in anoxic conditions (**Figure 6**). Expression of *P. denitrificans* nitrous oxide reductase has been demonstrated to be regulated by oxygen and nitric oxide through FnrP and Nnr transcription regulators (Bergaust et al., 2012).

Focusing on the denitrification and nitrate assimilation proteins, analysis of the peptide quantification (normalized peptide intensities) revealed that in Den-N conditions the cytochrome cd_1-type nitrite reductase NirS was the most abundant enzyme, followed by the nitrous oxide reductase NosZ. The high abundance of NirS could be explained considering that nitrite is the most toxic soluble oxyanion described, or it may reflect the need to increase the amount of this enzyme compared to other denitrification enzymes to compensate for its reported catalytic inefficiency (Richter et al., 2002). Regarding the three nitrate reductases, the membrane-bound respiratory nitrate reductase (NarG) was the most abundant, whereas periplasmic (NapA) and assimilatory (NasC) nitrate reductases were detected at much lower levels (**Figure 7**). It was notable that NorC peptides were only detected at low levels, which may indicate some recalcitrance of this specific protein to LC-MS/MS analysis. Ammonium did not have a drastic effect on the peptide intensities of the main oxide-reductases involved in denitrification under anaerobic conditions (**Figure 7**). However, at early stages of growth it has been demonstrated that when ammonium is used as alternative N-source in the presence of nitrate (Den-NA), it exerts a negative effect on the denitrification process (**Table 1**). Normalized peptide intensities from cells grown aerobically with nitrate (Aer-N) revealed that the most abundant reductase was the assimilatory nitrate reductase Nas, whereas

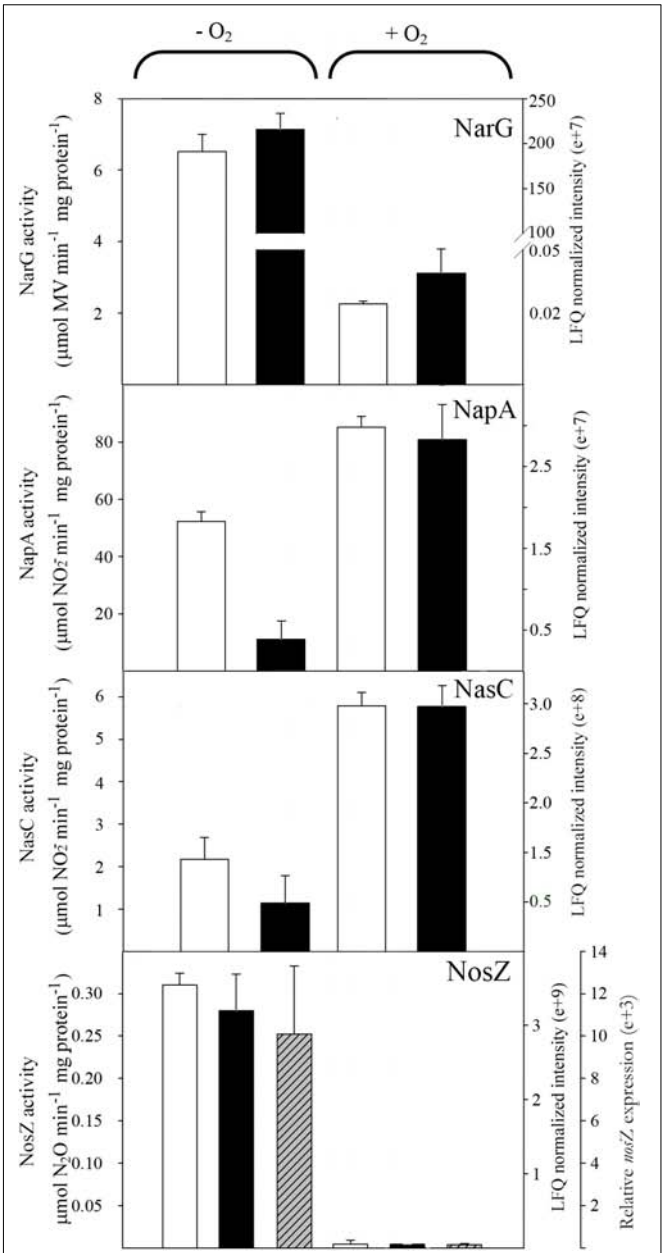

FIGURE 6 | Effect of oxygen on nitrate and nitrous oxide reductases in *P. denitrificans* PD1222. Cells were cultured under anaerobic or aerobic conditions with nitrate as the sole nitrogen source. Normalized peptide abundance (black bars) and enzymatic activity (white bars) of membrane-bound respiratory (Nar), periplasmic (Nap) and assimilatory (Nas) nitrate reductases and nitrous oxide reductase (NosZ) are shown in cells grown with nitrate under anaerobic or aerobic conditions. The relative *nosZ* gene expression (dashed bars) has been also determined (n = 3, error bars correspond to data from 3 independent replicates).

other reductases that are considered essential for denitrification decreased drastically (**Figures 6**, **7**). Accordingly, gasses involved in denitrification were not detected in cell cultures grown aerobically with nitrate, demonstrating that most of the nitrate is incorporated to organic nitrogen *via* the assimilatory pathway

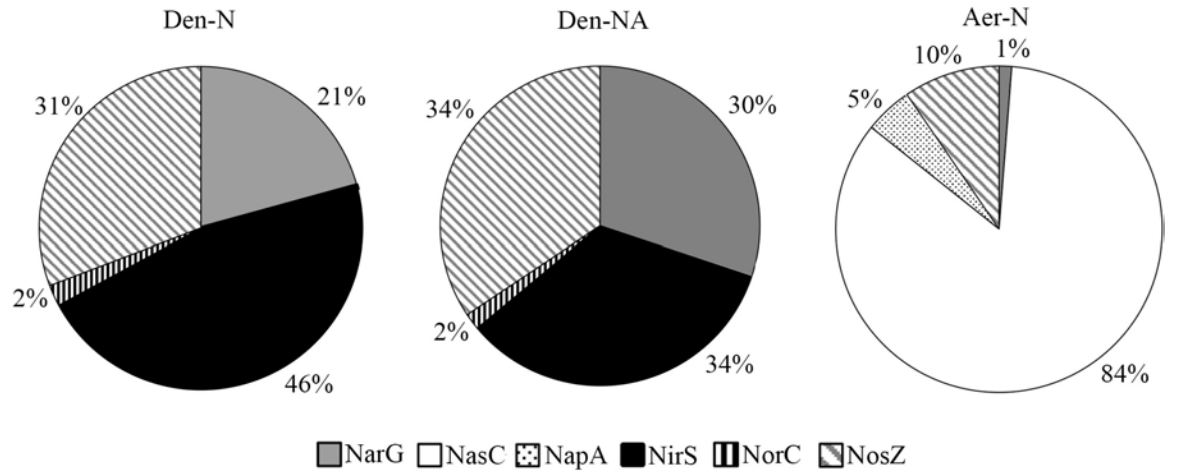

FIGURE 7 | Effect of ammonium and oxygen on the normalized protein intensity of the denitrification enzymes. Data are shown as percentages in each growth condition. The sum of the peptide intensities of the represented proteins was considered the 100% and this value was used as reference to calculate specific % for each protein. Den-N, cells cultured with nitrate in anaerobiosis; Den-NA, cells cultured with nitrate plus ammonium in anaerobiosis; Aer-N, cells cultured with nitrate in aerobiosis.

(**Table 1**). This result was also supported by the determination of the assimilatory nitrate reductase activity assayed in cytoplasmic fractions with NADH as electron donor (**Figure 6**). Also, the normalized intensities obtained in the proteomic study for the nitrous oxide reductase were the highest during denitrification, and this result was validated by determining NosZ enzymatic activity and also correlated with *nosZ* gene expression by qRT-PCR (**Figure 6**). This will contribute to maintaining low N_2O emissions during denitrification under the experimental conditions tested here.

To complement the proteomic analyses, several intracellular metabolites were examined (**Table 2**). Concentrations of acetyl-CoA and oxaloacetate were higher in anaerobiosis (Den-N and Den-NA) than in aerobiosis (Aer-N), whereas intracellular ammonium concentration was slightly higher under nitrate-aerobic (Aer-N) than in nitrate-respiring anaerobic conditions (Den-N). Accumulation of acetyl-CoA and oxaloacetate under anaerobic conditions could be related to the increased intensities found in anaerobiosis, when compared to aerobiosis, of several enzymes like the acetyl-CoA synthetase (A1B9T3, A1BAR9), the 3-hydroxyalcyl-CoA dehydrogenase (A1B611) and the butyryl-CoA:acetate CoA transferase (A1BB51). Levels of oxaloacetate were also higher in anaerobiosis than in aerobiosis because peptide intensities of TCA enzymes like aconitase (A1BAT6), isocitrate dehydrogenase (A1B6A1) and fumarate hydratase (A1B3A9) were increased under anaerobic conditions (**Figure 4**).

TABLE 2 | Intracellular metabolite determinations in *P. denitrificans* PD1222.

Sample*	Acetyl-CoA (pM)	Oxaloacetate (μM)	Ammonium (mM)
Den-N	3.72 ± 0.43	27.33 ± 1.15	2.66 ± 0.34
Den-NA	3.57 ± 0.31	20.90 ± 0.93	11.37 ± 1.20
Aer-N	0.51 ± 0.02	9.64 ± 0.20	3.54 ± .052

**Den-N, cells grown in anaerobiosis with 30 mM nitrate; Den-NA, cells grown in anaerobiosis with 30 mM nitrate plus 10 mM ammonium; Aer-N, cells grown in aerobiosis with 10 mM nitrate. Samples were taken at early exponential (A_{600} ~0.3) growth phase. Data are means ± DE of 2 independent biological replicates, and from each of these, 2 methodological samples (n = 4). Acetyl-CoA was determined by fluorescence, oxaloacetate was measured enzymatically with malate dehydrogenase and ammonium was determined spectrophotometrically as indicated in experimental procedures.*

CONCLUSION

This is the first study in which a global overview of the denitrification process has been described at a comprehensive quantitative proteome level, by using the soil denitrifier *P. denitrificans* PD1222 as a model organism. The proteomic approach by LC-MS/MS not only allowed identification and quantification of large number of proteins involved in denitrification, but also provided a holistic view of the effect of oxygen (an alternative electron acceptor) and ammonium (an alternative nitrogen source) on the denitrification process (**Figure 8**). Insights into the inter-relation of carbon and nitrogen metabolism were also forthcoming. In this sense, the low energetic yield obtained from the anaerobic reduction of nitrate to dinitrogen compared to the energy produced in aerobic respiration is compensated by the induction of enzymes that synthesize acetyl-CoA or belonging to the central metabolic carbon pathways like the TCA and the glyoxylate cycles.

EXPERIMENTAL PROCEDURES

Bacterial Strain, Media and Growth Conditions

Paracoccus denitrificans PD1222 was routinely cultured under aerobic or anaerobic conditions at 30°C in a defined mineral

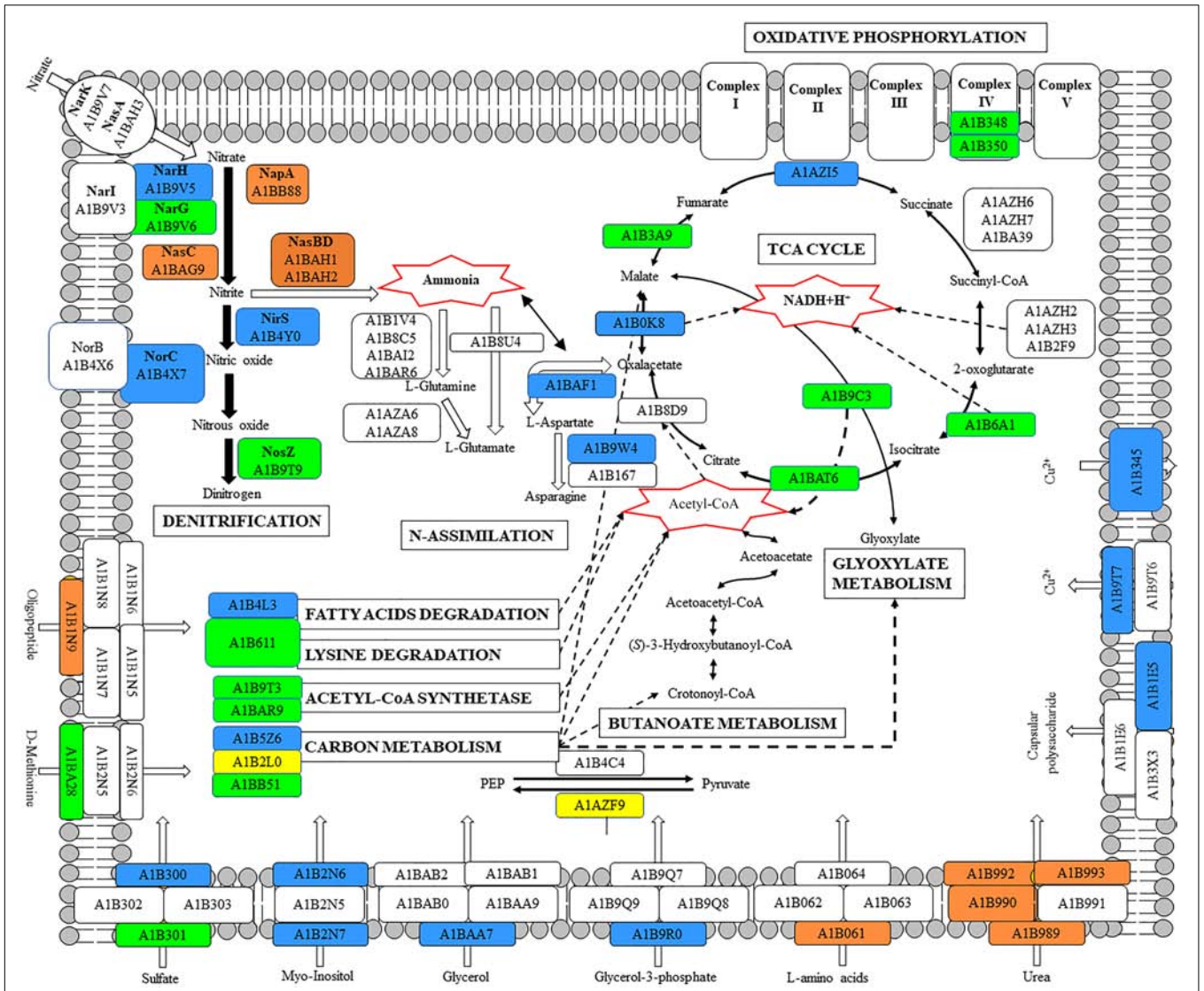

FIGURE 8 | Global scheme of *P. denitrificans* PD1222 whole proteome under denitrifying conditions. Color code: blue, exclusive of denitrifying conditions; green, over-represented in denitrification; orange, down-represented in denitrification; yellow, exclusive of aerobiosis; white, not detected or without change when comparing different growth conditions.

salt medium (Harms et al., 1985). Under aerobic conditions, potassium nitrate (10 mM) was used as nitrogen source, and sodium succinate (30 mM) was the sole carbon source in media adjusted to pH 7.2. Aerobic cultures (25 ml) were shaken at 225 rpm. Under anaerobic conditions, 30 mM potassium nitrate was used as nitrogen source and electron acceptor in the presence or absence of 10 mM ammonium chloride as additional nitrogen source, and 30 mM succinate was used as carbon source in media at pH 7.2. In all cases, an aerobic overnight culture, prepared from a frozen stock in mineral salt medium supplemented with 10 mM ammonium chloride, was centrifuged and used as inoculum. Cell growth was followed by measuring the absorbance of cultures at 600 nm (A_{600}) and cells were harvested at A_{600} ~0.3 or A_{600} ~0.9 as specified in the experiment. Spectinomycin was used as antibiotic at 25 μg ml^{-1} final concentration.

Nitrate and Nitrous Oxide Reductase Assays

To determine periplasmic nitrate reductase (Nap), respiratory nitrate reductase (Nar) and assimilatory nitrate reductase (Nas) activities, *P. denitrificans* cells (35 ml culture) were harvested by centrifugation at 6,000 rpm at 4°C for 15 min and washed twice with 10 mM Tris-HCl buffer at pH 7.5. Cells were resuspended in 5 ml STE buffer (10 mM Tris-HCl pH 8.3, 3 mM EDTA and 171 g l^{-1} sucrose) and incubated with 2 mg lysozyme at 30°C for 20 min. After centrifugation at 10,000 rpm and 4°C for 15 min, the supernatant corresponding to the periplasmic fraction was

stored on ice until used to determine Nap activity. The pellet with the spheroplasts was resuspended in 1 ml 100 mM Tris-HCl (pH 8) supplemented with DNase. Spheroplasts were sonicated (3 cycles of 20 s on/off pulsing) and unbroken spheroplasts were removed by centrifugation at 6,000 rpm at 4°C for 15 min. The membrane and cytoplasmic fractions were collected by ultracentrifugation at 45,000 rpm at 4°C for 45 min. Supernatant corresponding to cytoplasmic fraction was used to determine Nas activity and the membrane fraction was homogenized in 50 mM Tris-HCl (pH 8.0) to measure Nar activity.

Periplasmic nitrate reductase assay was performed with subcellular periplasmic fraction in 500 μl total volume of reaction mixture containing 50 μl sodium dithionite (prepared in 46 mM Tris-HCl, pH 7.5), 80 μM methyl viologen as non-physiological electron donor, 5 mM Tris-HCl (pH 7.5), 10 mM KNO_3 and 200 μl of periplasmic extract. After 15 min of incubation at 30°C, reactions were stopped by vigorous shaking and 500 μl distilled water was added. Finally, nitrite production was measured as previously described (Snell and Snell, 1949). As negative controls, reaction mixtures were prepared as indicated above, but an initial vigorous shaking was applied to reoxidize methyl-viologen.

Respiratory nitrate reductase (Nar) was measured following the microtiter protocol previously described (Ridley et al., 2006a,b). In a 200 μl final volume, 170 μl of a mixture with 80 μM methyl viologen, 10 mM KNO_3 and 5 mM Tris-HCl (pH 7.5) were incubated with 10 μl membrane fractions and 20 μl of a solution containing 46 mM sodium dithionite prepared in 0.5 M Tris-HCl, pH 7.5. Each biological replicate was measured in quadrupled, as well as two controls with an initial vigorous shaking. Other controls lacking either membrane fractions or KNO_3 were also used. Absorbance at 600 nm was recorded at 1-min intervals over a 10-min periods incubating at 30°C throughout to measure the disappearance of electrons from methyl viologen. A best-fit slope of each curve was used to calculate the activity.

Assimilatory nitrate reductase (Nas) was assayed in cytoplasmic fractions by using NADH as electron donor as previously described (Gates et al., 2011). The assay was performed in 1 ml total volume containing 200 μl cytoplasmic fraction, 1 mM NADH, 100 mM Tris-HCl (pH 8.0), 10 mM KNO_3 and distilled water. After 10 min incubation at 30°C, nitrite production was measured as described above. Negative controls were carried out in absence of the electron donor NADH.

N_2O-reducing NosZ activity was measured *in vivo* by using 35 ml cell cultures that were washed twice in 10 mM Tris-HCl (pH 7.5) and resuspended in 3 ml 50 mM Tris-HCl (pH 7.5). Then were sealed in a 10-ml serum vial under helium atmosphere. The reaction was started after 10 min of adaptation at 30°C by adding 500 μl N_2O. Samples from the headspace (100 μl) were analyzed by gas chromatography at 10 min intervals (Frunzke and Zumft, 1984) with a column SUPELCO CarboxenTM 1010. The concentration of NO, N_2O and N_2 was estimated by using a calibration plot previously elaborated.

Enzymic activities were assayed in three separated independent cultures. Protein concentration was estimated either in subcellular fractions (Bradford, 1976) or in whole cells by a modified method of the Lowry procedure (Shakir et al., 1994).

In Vivo Gas Emissions and Extracellular Nitrate and Nitrite Determinations

Paracoccus denitrificans PD1222 was cultured (30 ml total volume) in sealed tubes with 15 ml of anaerobic atmosphere. When cells reached an absorbance at 600 nm (A_{600}) of about 0.3 (early exponential growth phase) or about 0.9 (stationary growth phase), 1 ml from the headspace was analyzed by GC as described above. NO and N_2O gasses were not detected (<1 μM). The concentration of nitrate was measured in the extracellular media (supernatants) by using a previously described method with sulfamic and perchloric acids (Cawse, 1967). Nitrite and ammonium in the extracellular media were measured by using the Snell and Snell (1949) and the Solorzano (1969) methods, respectively.

Intracellular Metabolite Determinations

Total extracts were deproteinized by using 10% trichloroacetic acid. After 5 min of incubation on ice, samples were centrifuged at 14,000 rpm and supernatants were recovered for further analysis. Intracellular ammonium was determined by using a method previously described (Solorzano, 1969). Acetyl-CoA was measured from deproteinized total extracts by using the Acetyl-Coenzyme A Assay Kit (Sigma) according with the instructions of the manufacturer. Oxaloacetate measurement was enzymatically assayed with malate dehydrogenase in a spectrophotometer following the disappearance of NADH at 340 nm. The concentration of analytes was estimated by using calibration plots previously elaborated with stock solutions of the analytes detected.

Quantification of *nosZ* Gene Expression

Paracoccus denitrificans PD1222 cells were harvested at the early exponential growth (A_{600} ~0.3) and then washed in TEG buffer containing 25 mM Tris-HCl (pH 8.0) with 1% glucose and 10 mM EDTA. RNA isolations were performed following the Qiagen RNA extraction kit (RNeasy midi kit). DNase incubation was carried out in the column with RNase-free DNase set (Qiagen) and an additional post-column treatment was required with DNase I (Ambion). The concentration and purity of the RNA samples were measured by using a ND1000 spectrophotometer (Nanodrop Technologies). Synthesis of total cDNA was achieved in 20 μl final volume containing 500 ng RNA, 0.7 mM dNTPs, 200 U SuperScript II Reverse Transcriptase (Invitrogen), and 3.75 mM random hexamers (Applied Biosystems). Samples were initially heated at 65°C for 5 min and then incubated at 42°C for 50 min, followed by incubation at 70°C for 15 min. The cDNA was purified using Favorprep Gel/PCR purification kit (Favorgen) and the concentration was measured using a Nanodrop. The iQ5 Multicolor Real-Time PCR Detection System (Bio-Rad) was used in a 25 μl reaction (final volume), containing 2 μl of diluted cDNA (12.5, 2.5, and 0.5 ng), 0.2 μM of each primer nosZQ1: 5′-TCTTCTGCAATGGCGAGGACGAGAC-3′ and nosZQ2: 5′-CGAGCACCTGCCAGGCGACC-3′ and 12.5 μl of iQ SYBR

Green Supermix (Bio-Rad). Target cDNAs and reference samples were amplified three times in separate PCR reactions. Samples were initially denatured by heating at 95°C for 3 min, followed by 40 cycles of amplification (95°C, 30 s; test annealing temperature, 60°C, 30 s; elongation and signal acquisition, 72°C, 30 s). For relative quantification of the fluorescence values, a calibration curve was made using dilution series from 80 to 0.008 ng of *P. denitrificans* PD1222 genomic DNA sample. Data were normalized by using the *dnaN* gene as housekeeping with dnaN-1F′: 5′-CATGTCGTGGGTCAGCATAC-3′ and dnaN-1R′: 5′-CTCGCGACCATGCATATAGA-3′ primers.

Proteomic Analysis

Paracoccus denitrificans cells were grown both under anaerobic or aerobic conditions with different nitrogen sources as described above. When cultures reached A_{600} ∼0.3, cells were harvested by centrifugation at 12,000 rpm for 15 min and kept at −80°C until use. Samples for LC-MS/MS proteomic analysis were prepared by resuspension of frozen cells in 50 mM Tris-HCl buffer (pH 8.0) containing 4% CHAPS and 8 M urea, then cells were broken by cavitation with ultrasound (3 pulses of 90 W, for 5 min each pulse). Proteins were cleaned with the 2-D Clean-UP Kit (GE Healthcare, Little Chalfont, United Kingdom) and after precipitation were resuspended in a solution containing 6 M urea. Protein concentration was estimated as described previously (Bradford, 1976) and sample concentration ranged from 2 to 4 $\mu g\ \mu l^{-1}$. Samples were digested with trypsin overnight at 37°C without agitation. All analyses were performed at the Research Support Central Service (SCAI), University of Cordoba, with a Dionex Ultimate 3000 nano UHPLC system (Thermo Fisher Scientific, San Jose, CA, United States) connected to a mass spectrometer Orbitrap Fusion (Thermo Fisher Scientific, San Jose, CA, United States) equipped with nanoelectrospray ionization interface. The separation column was Acclaim Pepmap C18, 500 mm × 0.075 mm, 2 μm pore size (Thermo Fisher Scientific, San Jose, CA, United States). For trapping of the digest, it was used a 5 mm × 0.3 mm precolumn Acclaim Pepmap C18 (Thermo Fisher Scientific, San Jose, CA, United States). The samples, containing 0.2 $\mu g\ \mu l^{-1}$, were trapped at 10 $\mu l\ min^{-1}$ flow rate, for 5 min, with 2% acetonitrile/0.05% trifluoroacetic acid. After the trapping column was switched on-line with the separation column and the gradient was started. Peptides were eluted with a 60-min gradient 5–40% acetonitrile/0.1% formic acid solution at a flow rate of 300 nl min^{-1}. Survey scans of peptide precursors from 400 to 1500 m/z were performed at 120 K resolution (at 200 m/z) with a 5×10^5 ion count target. Tandem MS was performed by isolation at 1.6 Da with the quadrupole, CID fragmentation with normalized collision energy of 35, and rapid scan MS analysis in the ion trap. The AGC ion count target was set to 2×10^3 and the max injection time was 75 ms. Only those precursors with charge state 2–5 were sampled for MS2. The dynamic exclusion duration was set to 15 s with 10 ppm tolerance around the selected precursor and its isotopes. Monoisotopic precursor selection was turned on. The instrument was run in top speed mode with 3 s cycles, meaning the instrument would continuously perform MS2 events until the list of non-excluded precursors diminishes to zero or 3 s, whichever is shorter. Charge state deconvolution and deisotoping were not performed. MS2 spectra were searched using MaxQuant software v. 1.5.7.4 (Cox and Mann, 2008). MS2 spectra were searched with Andromeda engines, respectively, against a database of *P. denitrificans* PD1222 (deposited in the Uniprot database under the accession number UP000000361). Peptides generated from a tryptic digestion were searched by using the following parameters: up to one missed cleavages, carbamidomethylation of cysteines as fixed modifications, and oxidation of methionine as variable modifications. Precursor mass tolerance was 10 ppm and product ions were searched at 0.6 Da tolerances. Peptides were validated by filtering according with 1% FDR *q*-value. A target-decoy search strategy was applied, which integrates multiple peptide parameters such as length, charge, number of modifications and the identification score into a single quality that acts as the statistical evidence on the quality of each single peptide spectrum match. Peptide identifications were carried out by using MaxQuant software, in a MaxLFQ label-free quantification method (Cox and Mann, 2008; Cox et al., 2014). In the MaxLFQ label-free quantification method a retention time alignment and identification transfer protocol ("match-between-runs" feature in MaxQuant) was applied. Proteins identified from only one peptide were not considered in this analysis.

Identified peptides were grouped into proteins according with the law of parsimony and filtered to 1% FDR. Differentially expressed proteins analysis was carried out with the freely available software Perseus (version 1.5.6.0)[1]. Peak intensities across the whole set of quantitative data for all the peptides in the samples were imported from the LFQ intensities of proteins from the MaxQuant analysis and normalized according with the median. LFQ normalized intensity values were transformed to logarithmic scale with base two. Proteins identified in only one replicate were discarded. Proteins identified in at least three replicates per condition were used after replacing missing values (imputated) with the value of the lowest intensity. The protein quantification and calculation of statistical significance were carried out using two-way Student-*t* test and error correction (p-value < 0.05) with the Benjamini–Hochberg method. For further visualization, and to obtain p-value, a heat-map and a Principle Component Analysis (PCA) were performed. Relative protein quantification after LC-MS/MS procedure was performed by using the MaxQuant software (Cox and Mann, 2008). Results were then filtered, and a p-value ≤ 0.05 and a fold change ≥ 2 were considered. The mass spectrometry data have been deposited to the ProteomeXchange Consortium[2] via the PRIDE partner repository (Vizcaino et al., 2013) with the dataset identifier PDX006821.

BLAST2GO bioinformatics platform (Conesa et al., 2005) was used to assign GO terms to proteins identified by MS/MS. BLASTP search was conducted against the Bacteria protein database at Uniprot site and the recovery of up to 20 hits (e-value $< 10^{-5}$) was allowed. Interpro search, PSORTb subcellular prediction search, and subsequent mapping and annotation (e-value hit filter $< 10^{-6}$) steps were conducted using

[1]http://www.coxdocs.org/doku.php?id=perseus:start

[2]http://proteomecentral.proteomexchange.org

default parameters. Protein distribution within GO terms was retrieved from GO level 3. GO analysis were performed using the web application ComparativeGO (Fruzangohar et al., 2013). Integration of final proteomic data were performed by using the tool KEGG Mapper. Interaction maps were assembled by using STRING and functionally grouped network with ClueGO from Cytoscape, respectively.

AUTHOR CONTRIBUTIONS

Proteomic analysis was performed by AO-A and CF-A. qRT-PCR analysis was performed by VL-A. Gases determination and enzymic activities were carried out by JH-C, AO-A, and FU. Conceptualization, administration, and funding of the project were supplied by MR, CM-V, and DR. The manuscript was written by MR.

FUNDING

This work was supported by Ministerio de Economía y Competitividad, Spain (Grant BIO2015-64311-R, also supported by FEDER, UE), and Junta de Andalucía (Grant CVI-7560), Spain. DR was a Royal Society and Wolfson Foundation for Merit Award Fellow and thanks the Biotechnology and Biological Sciences Research Council (Grants BBEO219991 and BBD5230191).

SUPPLEMENTARY MATERIAL

The Supplementary Material for this article can be found online at: https://www.frontiersin.org/articles/10.3389/fmicb.2018.01137/full#supplementary-material

REFERENCES

Baker, S. C., Ferguson, S. J., Ludwig, B., Page, M. D., Richter, O. M. H., and van Spanning, R. J. M. (1998). Molecular genetics of the genus *Paracoccus*: metabolically versatile bacteria with bioenergetic flexibility. *Microbiol. Mol. Biol. Rev.* 62, 1046–1078.

Bakken, L., Bergaust, L., Liu, B., and Frostegård, Å. (2012). Regulation of denitrification at the cellular level: a clue to the understanding of N_2O emissions from soils. *Philos. Trans. R. Soc. Lond. B Biol. Sci.* 367, 1226–1234. doi: 10.1098/rstb.2011.0321

Bali, S., Lawrence, A. D., Lobo, S. A., Saraiva, L. M., Golding, B. T., Palmer, D. J., et al. (2011). Molecular hijacking of siroheme for the synthesis of heme and d1 heme. *Proc. Natl. Acad. Sci. U.S.A.* 108, 18260–18265. doi: 10.1073/pnas.1108228108

Bergaust, L., Mao, Y., Bakken, L., and Frostegård, A. (2010). Denitrification response patterns during the transition to anoxic respiration and posttranscriptional effects of suboptimal pH on nitrogen oxide reductase in *Paracoccus denitrificans*. *Appl. Environ. Microbiol.* 76, 6387–6396. doi: 10.1128/AEM.00608-10

Bergaust, L., Shapleigh, J., Frostegård, Å, and Bakken, L. (2008). Transcription and activities of NOx reductases in *Agrobacterium tumefaciens*: the influence of nitrate, nitrite and oxygen availability. *Environ. Microbiol.* 10, 3070–3081. doi: 10.1111/j.1462-2920.2007.01557.x

Bergaust, L., van Spanning, R., Frostegård, Å., and Bakken, L. (2012). Expression of nitrous oxide reductase in *Paracoccus denitrificans* is regulated by oxygen and nitric oxide through FnrP and NNR. *Microbiology* 158, 826–834. doi: 10.1099/mic.0.054148-0

Bradford, M. M. (1976). A rapid and sensitive method for the quantification of microgram quantities of protein utilizing the principle of protein dye binding. *Anal. Biochem.* 72, 248–256. doi: 10.1016/0003-2697(76)90527-3

Cawse, P. A. (1967). The determination of nitrate in soil solutions by ultraviolet spectrophotometry. *Analyst* 92, 311–315. doi: 10.1016/j.saa.2013.01.049

Conesa, A., Götz, S., García-Gómez, J. M., Terol, J., Talón, M., and Robles, M. (2005). Blast2GO: a universal tool for annotation, visualization and analysis in functional genomics research. *Bioinformatics* 21, 3674–3676. doi: 10.1093/bioinformatics/bti610

Cox, J., Hein, M. Y., Luber, C. A., Paron, I., Nagaraj, N., and Mann, M. (2014). Accurate proteome-wide label-free quantification by delayed normalization and maximal peptide ratio extraction, termed MaxLFQ. *Mol. Cell. Proteomics* 13, 2513–2526. doi: 10.1074/mcp.M113.031591

Cox, J., and Mann, M. (2008). MaxQuant enables high peptide identification rates, individualized ppb-range mass accuracies and proteome-wide protein quantification. *Nat. Biotechnol.* 26, 1367–1372. doi: 10.1038/nbt.1511

Crack, J. C., Hutchings, M. I., Thomson, A. J., and Le Brun, N. E. (2016). Biochemical properties of *Paracoccus denitrificans* FnrP: reactions with molecular oxygen and nitric oxide. *J. Biol. Inorg. Chem.* 21, 71–82. doi: 10.1007/s00775-015-1326-7

Felgate, H., Giannopoulos, G., Sullivan, M. J., Gates, A. J., Clarke, T. A., Baggs, E., et al. (2012). The impact of copper, nitrate and carbon status on the emission of nitrous oxide by two species of bacteria with biochemically distinct denitrification pathways. *Environ. Microbiol.* 14, 1788–1800. doi: 10.1111/j.1462-2920.2012.02789.x

Frunzke, K., and Zumft, W. G. (1984). Rapid, single sample analysis of H_2, O_2, N_2, NO, CO, N_2O and CO_2 by isothermal gas chromatography: applications to the study of bacterial denitrification. *J. Chromatogr.* 299, 477–483. doi: 10.1016/S0021-9673(01)97868-9

Fruzangohar, M., Ebrahimie, E., Ogunniyi, A. D., Mahdi, L. K., Paton, J. C., and Adelson, D. L. (2013). Comparative GO: a web application for comparative gene ontology and gene ontology-based gene selection in bacteria. *PLoS One* 8:e58759. doi: 10.1371/journal.pone.0058759

Gates, A. J., Luque-Almagro, V. M., Goddard, A. D., Ferguson, S. J., Roldán, M. D., and Richardson, D. J. (2011). A composite biochemical system for bacterial nitrate and nitrite assimilation as exemplified by *Paracoccus denitrificans*. *Biochem. J.* 435, 743–753. doi: 10.1042/BJ20101920

Giannopoulos, G., Sullivan, M. J., Hartop, K. R., Rowley, G., Gates, A. J., Watmough, N. J., et al. (2017). Tuning the modular *Paracoccus denitrificans* respirome to adapt from aerobic respiration to anaerobic denitrification. *Environ. Microbiol.* 19, 4953–4964. doi: 10.1111/1462-2920.13974

Harms, N., de Vries, G. E., Maurer, K., Veltkamp, E., and Stouthamer, A. H. (1985). Isolation and characterization of *Paracoccus denitrificans* mutants with defects in the metabolism of one-carbon compounds. *J. Bacteriol.* 164, 1064–1070.

Hu, W., Chen, D., and He, J.-Z. (2015). Microbial regulation of terrestrial nitrous oxide formation: understanding the biological pathways for prediction of emission rates. *FEMS Microbiol. Rev.* 39, 729–749. doi: 10.1093/femsre/fuv021

Luque-Almagro, V. M., Gates, A. J., Moreno-Vivián, C., Ferguson, S. J., Richardson, D. J., and Roldán, M. D. (2011). Bacterial nitrate assimilation; gene distribution and regulation. *Biochem. Soc. Trans.* 39, 1838–1843. doi: 10.1042/BST20110688

Luque-Almagro, V. M., Lyall, V. J., Ferguson, S. J., Roldán, M. D., Richardson, D. J., and Gates, A. J. (2013). Nitrogen oxyanion-dependent dissociation of a two-component complex that regulates bacterial nitrate assimilation. *J. Biol. Chem.* 288, 29692–29702. doi: 10.1074/jbc.M113.459032

Luque-Almagro, V. M., Manso, I., Sullivan, M. J., Rowley, G., Ferguson, S. J., Moreno-Vivián, C., et al. (2017). Transcriptional and translational adaptation to aerobic nitrate anabolism in the denitrifier *Paracoccus denitrificans*. *Biochem. J.* 474, 1769–1787. doi: 10.1042/BCJ20170115

Patureau, D., Zumstein, E., Delgenes, J. P., and Moletta, R. (2000). Aerobic denitrifiers isolated from diverse natural and managed ecosystems. *Microb. Ecol.* 39, 145–152. doi: 10.1007/s002480000009

Philippot, L., Hallin, S., and Schloter, M. (2007). Ecology of denitrifying prokaryotes in agricultural soil. *Adv. Agron.* 96, 249–305. doi: 10.1016/S0065-2113(07)96003-4

Richardson, D. J. (2000). Bacterial respiration: a flexible process for a changing environment. *Microbiology* 146, 551–571. doi: 10.1099/00221287-146-3-551

Richardson, D. J., Berks, B. C., Russell, D. A., Spiro, S., and Taylor, C. J. (2001). Functional, biochemical and genetic diversity of prokaryotic nitrate reductases. *Cell. Mol. Life Sci.* 58, 165–178. doi: 10.1007/PL00000845

Richardson, D. J., Felgate, H., Watmough, N., Thomson, A., and Baggs, E. (2009). Mitigating release of the potent greenhouse gas N_2O from the nitrogen cycle – could enzymic regulation hold the key? *Trends Biotechnol.* 27, 388–397. doi: 10.1016/j.tibtech.2009.03.009

Richter, C. D., Allen, J. W. A., Higham, C. W., Koppenhöfer, A., Watmough, N. J., and Ferguson, S. J. (2002). Cytochrome cd1, reductive activation and kinetic analysis of a multifunctional respiratory enzyme. *J. Biol. Chem.* 277, 3093–3100. doi: 10.1074/jbc.M108944200

Ridley, H., Watts, C. A., Richardson, D. J., and Butler, C. S. (2006a). Development of a viologen-based microtiter plate assay for the analysis of oxyanion activity: application to the membrane-bound selenate reductase from *Enterobacter cloacae* SLD1a-1. *Anal. Biochem.* 358, 289–294.

Ridley, H., Watts, C. A., Richardson, D. J., and Butler, C. S. (2006b). Resolution of distinct membrane-bound enzymes from *Enterobacter cloacae* SLD1a-1 that are responsible for selective reduction of nitrate and selenate oxyanions. *Appl. Envirom. Microbiol.* 72, 5173–5180.

Sanders, D. A., Gillece-Castro, B. L., Burlingame, A. L., and Koshland, D. E. Jr. (1992). Phosphorylation site of NtrC, a protein phosphatase whose covalent intermediate activates transcription. *J. Bacteriol.* 174, 5117–5122. doi: 10.1128/jb.174.15.5117-5122.1992

Saunders, N. F. W., Hornberg, J. J., Reijnders, W. N., Westerhoff, H. V., de Vries, S., and van Spanning, R. J. (2000). The NosX and NirX proteins of *Paracoccus denitrificans* are functional homologues: their role in maturation of nitrous oxide reductase. *J. Bacteriol.* 182, 5211–5217. doi: 10.1128/JB.182.18.5211-5217.2000

Saunders, N. F. W., Houben, E. N., Koefoed, S., de Weert, S., Reijnders, W. N., Westerhoff, H. V., et al. (1999). Transcription regulation of the nir gene cluster encoding nitrite reductase of *Paracoccus denitrificans* involves NNR and NirI, a novel type of membrane protein. *Mol. Microbiol.* 34, 24–36. doi: 10.1046/j.1365-2958.1999.01563.x

Shakir, F. K., Audilet, D., Drake, A. J., and Shakir, K. M. (1994). A rapid protein determination by modification of the Lowry procedure. *Anal. Biochem.* 216, 232–233. doi: 10.1006/abio.1994.1031

Shcherbak, I., Millara, N., and Robertson, G. P. (2014). Global metaanalysis of the nonlinear response of soil nitrous oxide (N_2O) emissions to fertilizer nitrogen. *Proc. Nat. Acad. Sci. U.S.A.* 111, 9199–9204. doi: 10.1073/pnas.1322434111

Snell, F. D., and Snell, C. T. (1949). *Colorimetric Methods of Analysis*. New York, NY: Van Nostrand, 802–807.

Solorzano, L. (1969). Determination of ammonia in natural waters by the phenol hypochlorite method. *Limnol. Oceanogr.* 14, 799–801.

Speers, A. E., and Wu, C. C. (2007). Proteomics of integral membrane proteins-theory and application. *Chem. Rev.* 107, 3687–3714. doi: 10.1021/cr068286z

Spiro, S. (2012). Nitrous oxide production and consumption: regulation of gene expression by gas-sensitive transcription factors. *Philos. Trans. R. Soc. Lond. B. Biol. Sci.* 367, 1213–1225. doi: 10.1098/rstb.2011.0309

Sullivan, M. J., Gates, A. J., Appia-Ayme, C., Rowley, G., and Richardson, D. J. (2013). Copper control of bacterial nitrous oxide emission and its impact on vitamin B12-dependent metabolism. *Proc. Nat. Acad. Sci. U.S.A.* 110, 19926–19931. doi: 10.1073/pnas.1314529110

van Spanning, R. J., Houben, E., Reijnders, W. N., Spiro, S., Westerhoff, H. V., and Saunders, N. (1999). Nitric oxide is a signal for NNR-mediated transcription activation in *Paracoccus denitrificans*. *J. Bacteriol.* 181, 4129–4132.

van Spanning, R. J., Richardson, D. J., and Ferguson, S. J. (2007). "Introduction to the biochemistry and molecular biology of denitrification," in *The Biology of the Nitrogen Cycle*, eds H. Bothe, S. J. Ferguson, and W. E. Newton (Amsterdam: Elselvier), 3–21.

Vizcaino, J. A., Cote, R. G., Csordas, A., Dianes, J. A., Fabregat, A., Foster, J. M., et al. (2013). The proteomics identifications (PRIDE) database and associated tools: status in 2013. *Nucleic Acids Res.* 41(Database issue), D1063–D1069. doi: 10.1093/nar/gks1262

Wood, N., Alizadeh, T., Bennett, S., Pearce, J., Ferguson, S. J., Richardson, D. J., et al. (2001). Maximal expression of membrane-bound nitrate reductase in *Paracoccus* is induced by nitrate via a third FNR-like regulator named NarR. *J. Bacteriol.* 183, 3606–3613. doi: 10.1128/JB.183.12.3606-3613.2001

Wrage, N., Velthoft, G. L., van Beisichem, M. L., and Oenema, O. (2001). Role of nitrifier denitrification in the production of nitrous oxide. *Soil Biol. Biochem.* 33, 1723–1732. doi: 10.1016/S0038-0717(01)00096-7

Zumft, W. G. (1997). Cell biology and molecular basis of denitrification. *Microbiol. Mol. Biol. Rev.* 61, 533–616.

Conflict of Interest Statement: The authors declare that the research was conducted in the absence of any commercial or financial relationships that could be construed as a potential conflict of interest.

frontiers in Microbiology

ORIGINAL RESEARCH
published: 04 September 2018
doi: 10.3389/fmicb.2018.02061

The Genomic Potentials of NOB and Comammox *Nitrospira* in River Sediment Are Impacted by Native Freshwater Mussels

*Ellen M. Black and Craig L. Just**

Department of Civil and Environmental Engineering, University of Iowa, Iowa City, IA, United States

Freshwater mussel assemblages of the Upper Mississippi River (UMR) sequester tons of ammonia- and urea-based biodeposits each day and aerate sediment through burrowing activities, thus creating a unique niche for nitrogen (N) cycling microorganisms. This study explored how mussels impact the abundance of N-cycling species with an emphasis on *Candidatus* Nitrospira inopinata, the first microorganism known to completely oxidize ammonia (comammox) to nitrate. This study used metagenomic shotgun sequencing of genomic DNA to compare nitrogen cycling species in sediment under a well-established mussel assemblage and in nearby sediment without mussels. Metagenomic reads were aligned to the prokaryotic RefSeq non-redundant protein database using BLASTx, taxonomic binning was performed using the weighted lowest common ancestor algorithm, and protein-coding genes were categorized by metabolic function using the SEED subsystem. Linear discriminant analysis (LDA) effect sizes were used to determine which metagenomes and metabolic features explained the most differences between the mussel habitat sediment and sediment without mussels. Of the N-cycling species deemed differentially abundant, *Nitrospira moscoviensis* and "*Candidatus* Nitrospira inopinata" were responsible for creating a distinctive N-cycling microbiome in the mussel habitat sediment. Further investigation revealed that comammox *Nitrospira* had a large metabolic potential to degrade mussel biodeposits, as evidenced the top ten percent of protein-coding genes including the cytochrome c-type biogenesis protein required for hydroxylamine oxidation, ammonia monooxygenase, and urea decomposition SEED subsystems. Genetic marker analysis of these two *Nitrospira* taxons suggested that *N. moscoviensis* was most impacted by diverse carbon metabolic processes while "*Candidatus* Nitrospira inopinata" was most distinguished by multidrug efflux proteins (AcrB), NiFe hydrogenase (HypF) used in hydrogen oxidation and sulfur reduction coupled reactions, and a heme chaperone (CcmE). Furthermore, our research suggests that comammox and NOB *Nitrospira* likely coexisted by utilizing mixotrophic metabolisms. For example, "*Candidatus* Nitrospira inopinata" had the

OPEN ACCESS

Edited by:
Lourdes Girard, Universidad Nacional Autónoma de México, Mexico

Reviewed by:
Rosa María Martínez-Espinosa, University of Alicante, Spain
Xuesong Luo, Huazhong Agricultural University, China

***Correspondence:**
Craig L. Just
craig-just@uiowa.edu

Specialty section:
This article was submitted to Terrestrial Microbiology, a section of the journal Frontiers in Microbiology

Received: *14 February 2018*
Accepted: *13 August 2018*
Published: *04 September 2018*

Citation:
Black EM and Just CL (2018) The Genomic Potentials of NOB and Comammox Nitrospira in River Sediment Are Impacted by Native Freshwater Mussels. Front. Microbiol. 9:2061. doi: 10.3389/fmicb.2018.02061

largest potentials for ammonia oxidation, nitrite reduction with NirK, and hydrogen oxidation, while NOB *Nitrospira* had the greatest potential for nitrite oxidation, and nitrate reduction possibly coupled with formate oxidation. Overall, our results suggest that this mussel habitat sediment harbors a niche for NOB and comammox *Nitrospira*, and ultimately impacts N-cycling in backwaters of the UMR.

Keywords: Upper Mississippi River, freshwater mussels, *Nitrospira,* comammox, nitrification, ammonia oxidizing bacteria, nitrite oxidizing bacteria

INTRODUCTION

Water quality of the Upper Mississippi River (UMR) has been documented for decades (Lerch et al., 2015), yet the UMR basin contributes over 50,000 metric tons of bioactive nitrogen (N) to the Gulf of Mexico each year (Donner and Kucharik, 2008). Research has shown that microbial communities are impacted by the addition of bioactive N (Hallin et al., 2009), and subsequently alter N-biogeochemical cycling in the UMR through nitrification and denitrification processes (Mulholland et al., 2008; Shange et al., 2012). Enhancing the vertical exchange between overlying water and groundwater (i.e., water-sediment interface) of UMR backwater channels has been proposed to significantly enhance N removal (Strauss et al., 2006; Gomez-Velez et al., 2015), particularly because biotic removal of N reaches a maximum efficiency of 40% as N loads increase in large streams (Mulholland et al., 2008) and denitrification rates plateau as nitrate (NO_3-N) reaches 5 mg/L in backwater channels (Kreiling et al., 2011). Taken together, these findings emphasize the large N-cycling potential of benthic organisms, by enhancing the flux of nutrients into sediment for microbial transformations (Vaughn and Hakenkamp, 2001; Atkinson et al., 2013).

Freshwater mussels (order Unionidae) native to the UMR live in assemblages of 3–5 mussels m^{-2}, collectively filter billions of gallons of water, and remove tons of N-containing biomass from overlying water each day (Newton et al., 2011). In addition to the ecosystem services of water filtration and enhancing nutrient exchange rates across the water-sediment interface (Atkinson et al., 2014), mussel excretion of feces and pseudofeces (biodeposition products) sequesters ammonia (NH_3) and carbon (C) into sediment porewater (Newton et al., 2011; Bril et al., 2014, 2017). As a result, mussel assemblages are attributed with creating "hotspots" of N and C in surrounding sediment (Atkinson and Vaughn, 2015), and create a microbial niche ripe for nitrification at the interface of oxic and anoxic conditions (Black et al., 2017).

Nitrifying organisms capable of mixotrophy may pose an advantage in a mussel-influenced habitat, owing to the adaptation of switching metabolic functions when conditions change from oxic to anoxic (Matantseva and Skarlato, 2013; Daebeler et al., 2014). It was previously thought that nitrite (NO_2^-) oxidizing bacteria (NOB) were restricted to oxic environments where ammonia (NH_3) oxidizing bacteria (AOB) produce NO_2^-, but recent genomic analyses have expanded the known metabolic functions of conventional NOB *Nitrospira*. For example, the NO_2^- oxidizing species *Nitrospira moscoviensis* is genetically capable of cyanate degradation (Palatinszky et al., 2015), aerobic hydrogen oxidation (Koch et al., 2014), and formate oxidation coupled with nitrate (NO_3^-) reduction (Koch et al., 2015). Nitrification was further expanded after discovering that *Nitrospira moscoviensis* can produce NH_3 and CO_2 by way of urea hydrolysis, and can reciprocally feed NH_3 to urease-lacking AOB and receive NO_2^- in return (Koch et al., 2015). Furthermore, the N-cycle was transformed after the discovery of a single organism capable of complete NH_3 oxidation (comammox) (van Kessel et al., 2015) and confirmation of genes required for complete nitrification encoded by "*Candidatus* Nitrospira inopinata" (Daims et al., 2015), and potentially even sulfur reduction (Camejo et al., 2017).

In a previous study, we showed that sediment of a well-established mussel habitat in UMR backwaters contained an enhanced niche for Nitrospirae in addition to a greater abundance of microorganisms indicative of an oxic-anoxic niche, like anaerobic ammonium oxidizers (anammox). This presumed oxic-anoxic niche was detected closer to the water-sediment interface in the mussel habitat, since the relative abundance of anammox bacteria peaked at shallow (3 cm) sediment depths with mussels, but were more abundant in deeper (5 cm) sediments in the no-mussel treatment (Black et al., 2017). Furthermore, the 16S rRNA amplicon survey showed fewer differences among N-cycling phylotypes in shallow sediment with mussels and deeper sediment without mussels (i.e., intrasample differences), and the fewest differences when comparing the shallow mussel sediment against the deeper no-mussel sediment (inter-sample differences). In response, this study used the deeper no-mussel sediment as the most stringent baseline to assess mussel influences on the N-cycling community with mussels. We employed metagenomic shotgun sequencing of total DNA corresponding with the aforementioned oxic-anoxic niche sediment components, with the goal of identifying the N-cycling species most impacted by mussels. We hypothesized that sediment from the mussel habitat would contain an increased abundance of nitrifying taxons, presumably due to an enhanced genomic potential for ammonia oxidation.

MATERIALS AND METHODS

Sediment Collection and DNA Isolation

Our study sites were located in the backwaters of the UMR navigation pool 16, where a consistently populated mussel assemblage has been studied for decades (USACE, 1981,

1984; Young et al., 2005; Morales et al., 2006). Sediment cores were obtained from the mussel habitat (41.452804, −90.763299) and upstream sediment (41.451540, −90.753275) lacking mussels (Black et al., 2017); both sites had similar hydraulics and sediment composition (Young et al., 2005), and will be considered as treatments "with-mussels" and with "no-mussels" according to previous studies (Mirto et al., 2000; Danovaro et al., 2004). Cores were removed from each site using a 2-in diameter, post-driver with a polypropylene liner (Multi-State Sediment Sampler, Art's Manufacturing and Supply, Inc.; American Falls, ID, United States), and an ethanol flame-sterilized 3/8-in diameter drill bit was used to penetrate the cores at depths of 3 and 5 cm. For each core, samples (0.25 g sediment) were removed in quadruplicate (n = 4, 3 cm depth with mussels; n = 4, 5 cm depth without mussels) and stored in sterile bead beating tubes overnight at -20°C. Genomic DNA was isolated (PowerSoil DNA Isolation Kit; MoBio Laboratories, Inc., Carlsbad, CA, United States) and stored at −20°C. Following verification of DNA quality and quantity (NanoDrop 1000; Thermo Fisher Scientific, Waltham, MA, United States), genomic DNA was sequenced at the University of Iowa Institute for Human Genetics (IIHG). As mentioned earlier, selection of these samples were informed by evidence suggesting oxic-anoxic interface niches were located at 5 cm sediment depth without mussels and 3 cm depth beneath mussels (Black et al., 2017). Samples chosen for this experiment correspond to the following 16S rRNA amplicon sequencing data at MG-RAST: without-mussels-mgm4705698.3, mgm4705704.3, mgm4705686.3, mgm4705697.3 with-mussels mgm4705708.3, mgm4705672.3, mgm4705699.3, mgm4705680.3.

Metagenomic Shotgun Sequencing

For each sample, 120 ng of genomic DNA in 60 μL of 10 mM Tris-HCl, pH 8.0 buffer, was placed into 1.5 mL RNase-/DNase-free, low binding microcentrifuge tubes. Library creation steps were performed by the IIHG Genomics Division, and included DNA shearing using the Covaris Adaptive Focused Acoustics™ process (Covaris E220 Focused-ultrasonicator; Covaris, Inc., Woburn, MA, United States), and DNA fragment purification and end polishing (KAPA Hyper prep kits; Kapa Biosystems, Inc., Wilmington, MA, United States) prior to ligation to indexed adaptors. The library size distribution was validated using the Agilent 2100 Bioanalyzer Instrument (Agilent Technologies, Santa Clara, CA, United States), and quantified using the q-PCR KAPA library amplification module following manufacturer instructions (Kapa Biosystems, Inc.). The indexed libraries were normalized, pooled, and clustered on a flow cell using the cBOT Cluster Generation System (Illumina, Inc., San Diego, CA, United States) and sequenced on the Illumina HiSeq 4000 System (Illumina, Inc.) in high output mode (1 lane, 2 × 150 bp). FASTQ files are accessible at ENA (Study Accession: PRJEB23134) and NCBI repositories (BioProject ID: PRJNA414922), and MG-RAST contains QA/QC and analyses of metagenomes (MG-RAST project mgp21252).

Bioinformatics Pipeline

FastQC (Andrews, 2010) was used for quality control and revealed an average sequence abundance of 42,606,252± 2,365,531 sequences, sequence lengths of 151 bp, and 60% (±0.84%) GC content for no-mussel samples, and 41,402,435 ± 3,444,191 sequences, with sequence lengths of 151 bp, and 60% (±1.31%) GC content for samples with mussels. For taxonomic and functional binning of reads, we employed the streamlined DIAMOND (Buchfink et al., 2015) and MEGAN (Huson et al., 2007) pipeline specialized for microbiome shotgun sequencing analyses (Huson et al., 2016). First, RefSeq (O'Leary et al., 2016) non-redundant (nr) archaeal and bacterial protein sequences (Release80) were concatenated to construct a database for BLASTx alignments in DIAMOND using the "make.db" command, and pairwise alignments were performed using the default BLASTx settings (BLOSUM62 matrix, γ = 0.267, K = 0.041, Penalties = 11/1). The aligned reads from DIAMOND were imported into MEGAN using *daa-meganizer* (Huson et al., 2016), keeping only the top 100 matches per read. The weighted lowest common ancestor (LCA) algorithm was used for taxonomic binning using default settings in MEGAN6 (Huson et al., 2016) (min score = 50.0, max expected = 0.01, top percent = 10.0%, min support percent = 0.05, min support = 1, 80% coverage for weighted LCA algorithm) and classified according to NCBI taxonomy IDs (Nov 2016 release). Furthermore, aligned reads were assigned functional roles using accession mapping files for SEED subsystems (Overbeek et al., 2005) (SEED May 2015 annotation). The resulting files contained all reads, alignments, taxonomic and functional classifications, and were normalized for sampling read depth (normalized to 12,726,950 reads per sample) and assigned metadata categories, "no-mussel" and "with-mussel." Reads aligned to N-cycling genomes were extracted from MEGAN for differential abundance analysis using LefSe (Segata et al., 2011). The most differentially abundant genomes belonged to "*Candidatus* Nitrospira inopinata" (GCF_001458695.1) and *Nitrospira moscoviensis* (GCF_001273775.1), and were further assembled and annotated in Unipro UGENE (Okonechnikov et al., 2012) and depicted using DNAPlotter (Carver et al., 2009). The UGENE workflow included mapping reads to indexed reference genomes using BWA MEM (Li and Durbin, 2009) with default settings, followed by filtering and sorting the BAM files using SAMtools (Li et al., 2009), and a final quality control step using FastQC (Andrews, 2010).

LDA Effect Size

A linear discriminant analysis (LDA) method was used to assess which genomes and genomic features were most discriminative of the freshwater mussel habitat. N-cycling taxonomies of interest were chosen based on previous research (Pfister et al., 2014) and included AOB and NOB phylotypes with the prefix "nitro," N-reducing phylotypes designated by "denitrificans" or "nitroreducens," and anammox candidate genera, *Brocadia* and *Jettenia*. The relative abundance of reads aligned to these N-cycling taxons were assessed for LDA effect size (LEfSe) (Segata et al., 2011) to determine which N-cycling taxonomic

features were most responsible for differences in the mussel habitat microbiomes. All samples were labeled by class ("mussel" and "no-mussel") and features were compared for differential distribution using the non-parametric factorial Kruskal–Wallis sum-rank test ($\alpha = 0.05$) and normalized to a total read count of 1 M. Features deemed differentially abundant were compared for significant effect size using the pairwise Wilcoxon rank-sum test ($\alpha = 0.05$; "all against all"), and ranked features according to greatest effect size. A minimum LDA score of 2.0 was chosen as a cutoff for significant features to limit analysis to the most distinctive metagenomic traits. "*Candidatus* Nitrospira inopinata" and *Nitrospira moscoviensis* were shown to be the most distinctive genomes with mussels, and follow-up genetic marker tests were performed for SEED assignments to address which metabolic functions may be responsible for this differentiation.

RESULTS

N-cycle Taxonomic Composition

The DIAMOND/MEGAN pipeline revealed metagenomic reads assigned to N-cycling organisms (**Figure 1**) were slightly more abundant with mussels (157,275 ± 17,503 reads) than without mussels (136,884 ± 20,982 reads), and the mussel habitat contained more reads belonging to N-cycling bacterial lineages (**Figure 1**) with Nitrospirae representing the most bacterial species. In both treatments, "*Candidatus* Methanoperdens nitroreducens" represented the largest number of archaeal metagenomic reads but was not differentially abundant between treatments. NO_2^- oxidizing organisms represented the largest N-cycling group, with *Nitrospira moscoviensis*, *Nitrospira defluvii*, and "*Candidatus* Nitrospira inopinata" comprising an average of 22, 15, and 11% of N-cycling metagenomic reads in the mussel habitat, respectively. *Steroidobacter denitrificans* was also a highly abundant component of the N-cycling community (12–14%) but was not differentially abundant between treatments.

Linear discriminant analysis effect size of the metagenomic reads assigned to N-cycle taxons further emphasized the major differences in the mussel habitat (**Figure 1**). Of the taxons considered, bacterial lineages experienced the most increases with mussels (LDA = 4.27, $P = 0.043$), and the most differentially abundant species were *Nitrospira moscoviensis* (LDA = 3.80, $P = 0.021$) and "*Candidatus* Nitrospira inopinata" (LDA = 3.63, $P = 0.021$). One other group of nitrifying taxons were differentially greater with mussels, and belonged to the *Nitrosococcus* genus (LDA = 2.20, $P = 0.021$). Multiple denitrifying taxons were greater with mussels, including *Methylomonas denitrificans*, *Denitrobacterium detoxificans*, *Competibacter denitrificans*, and a Gammaproteobacterial sulfur oxidizing symbiont, *Thiohalorhabdus denitrificans*. However, these denitrifying species were lower in abundance than *Nitrospira*, and thus were ranked lower as biomarker species. Protein functional assignments of "*Candidatus* Nitrospira inopinata" and *N. moscoviensis* were also assessed for distinctive features between the mussel and no-mussel treatments, with the goal of discovering niche differentiating functions responsible for the enhanced abundance of NOB and comammox *Nitrospira* genomes (McGill et al., 2007).

Nitrospira moscoviensis Genomic Potential

A total of 435,151 SEED protein functions were assigned to the genome of *N. moscoviensis* (normalized to 36,562 per sample) and was dominated by 5 SEED categories: carbohydrates, cofactors, vitamins, prosthetic groups, pigments, amino acids and derivatives, protein metabolism, and DNA metabolism (**Supplementary Table S1**). The 25% most abundant SEED subsystems included those indicative of metabolic activity and growth, such as peptidoglycan and cytoskeleton biosynthesis, respiration and carbon fixation, DNA replication and repair (**Supplementary Table S1**). Highly abundant SEED proteins unique to *N. moscoviensis* in the no-mussel treatment included those potentially functioned in motility, chemotaxis, biotin synthesis, and thiamin metabolism ("5-FCL-like protein"), while the mussel habitat treatment was dominated by genes encoding folate and cysteine biosynthesis, carbon cycling ("alpha carboxysome"), and the DNA regulatory proteins YebC and proteasomes (**Supplementary Table S1**).

Of the N-metabolism functional assignments (**Table 1**), formate hydrogenases were the most abundant N-cycling category for both treatments, and numerous enzymatic functions were relatively more abundant in the mussel habitat treatment. These included genes encoding an NH_4^+ permease, NO reductase proteins (NorD and NorQ), formate dehydrogenase subunits (beta and chain D), NO_2^-/NO_3^- transporters and sensors, periplasmic nitrate reductases (NapG and NapF), and urease proteins (UreA and ureF) (**Table 1**).

N. moscoviensis Genetic Markers

Genetic code processing was a major potential function of *N. moscoviensis* in the mussel habitat, as evidenced by increased functional proteins used in DNA, RNA, and protein metabolism (LDA up to 3.32). Two of the most distinct features were genes encoding YebC-like DNA-binding regulatory proteins, an ATP-dependent DNA helicase protein (PcrA), and ribonuclease H III (**Supplementary Table S2** and **Figure 2**), in addition to other proteins like DNA polymerase III and LSU ribosome. Unclassified hypothetical proteins (FIG039061) related to heme utilization was a highly ranked SEED subsystem (LDA = 3.33, $P = 0.043$) and likely was due to a large abundance a gene encoding a modular heme utilizing protein (NITMOv2_0147), with other iron-based genetic markers including Cytochrome C553 and an Fe-S cluster regulator (IscR). Other differentially abundant features were related to carbon cycling SEED subsystems (LDA = 2.99, $P = 0.021$) and included genes encoding ribulose phosphate-3 epimerase used for carbon fixation, and two glycogen synthesis enzymes, 4-alpha-glucanotransferase (MalQ), and 1,4-alpha glucan (glycogen) branching enzyme (GH-13 type) (GlgB).

Contrastingly, the *N. moscoviensis* potential protein functions without mussels were largely marked by genetic markers of stress response. The glutathione-regulated K^+ efflux system used in potassium metabolic processes (LDA = 3.28, $P = 0.043$)

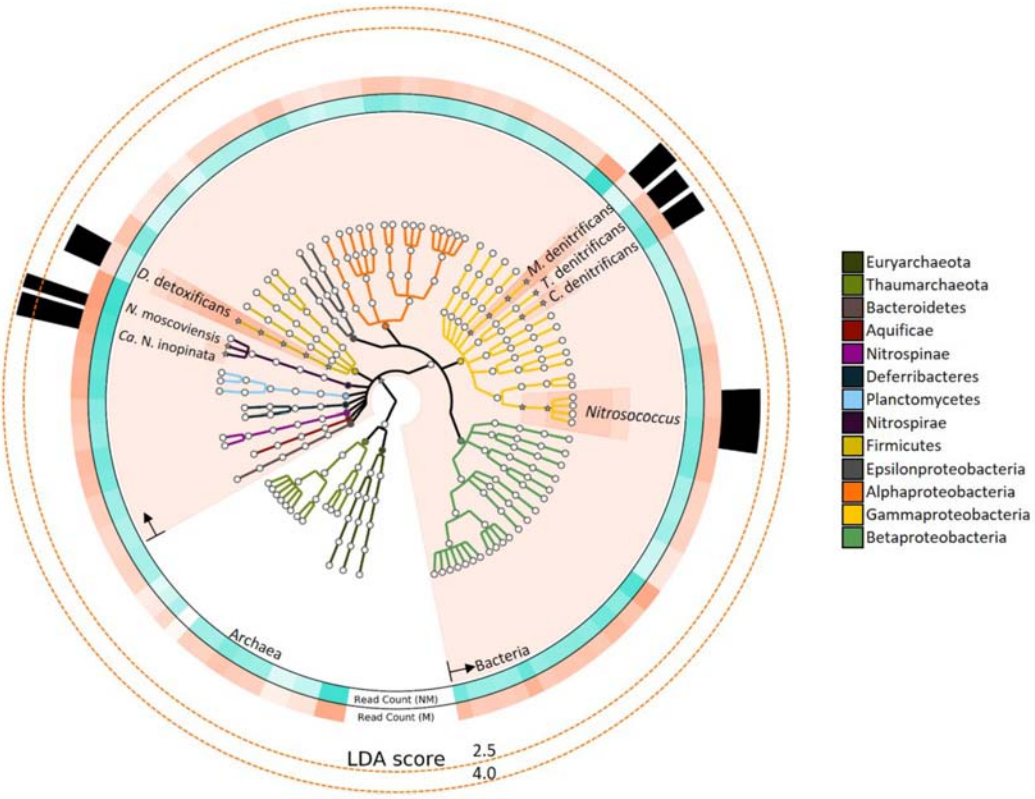

FIGURE 1 | Nitrogen-cycling taxonomies assessed for linear discriminant analysis (LDA) effect size are colored based on phylum, as specified in the legend. Taxons shown with a "*" icon and salmon-colored background had statistically significant LDA scores (LDA > 2, $P < 0.05$). Rings surrounding the phylogenetic tree depict the relative abundance of reads assigned to the respective species. Ring color intensity represents relative read count with mussels (salmon-colored; "M") and with no mussels (turquoise-colored; "NM"). The opacity of "Read count" ring-segments corresponds to the greatest taxonomic abundance. Several N-cycling taxons were differentially abundant with mussels and LDA effect sizes are represented by the height of black bars in the outer-most ring.

were the most definitive SEED subsystems of the no-mussel *N. moscoviensis* genome. Furthermore, the glutathione-regulated K^+ efflux system protein family (KefB) is activated in the presence of methylglyoxal (Ferguson et al., 1995), and the metabolism of methylglyoxal was also a genetic marker of the no-mussel treatment (LDA = 2.45, $P = 0.043$). These results may suggest a stress response genetic marker, as glutathione-regulated potassium efflux systems are often utilized to counteract electrophilic compounds during stress (Tötemeyer et al., 1998; Bott and Love, 2004). Additionally, superoxide dismutase was another highly ranked functional marker and may suggest an enhanced stress from reactive oxygen. Other stress genetic markers included the carbon starvation stress SEED subsystem (LDA = 2.85, $P = 0.021$) and an enhanced abundance of genes encoding carbon starvation protein A (CstA) (**Supplementary Table S2**). Other genetic markers suggest a potential metabolic ability to respond to diverse carbon compounds, including genes encoding gluconolactonase of the Entner Duodoroff pathway (LDA = 2.99, $P = 0.021$), acetoacetate metabolism with an enhanced regulatory protein, AtoC, and an acetyl-CoA biosynthesis enzyme, pyruvate decarboxylase (**Supplementary Table S2**). Differential features also included the potential metabolism of complex carbon sources, such as lactose (LDA = 2.40, $P = 0.021$) via 2-oxoglutarate decarboxylase, mannose by way of mannose-1-P guanylyltransferase, maltose and maltodextrin degradation via alpha amylase, and *N*-acetylglucosamine (LDA = 2.96, $P = 0.043$) with beta-hexosaminidase enzymes.

N metabolic genes were lowly abundant for *N. moscoviensis* genomes in both treatments, but a NO_3^-/NO_2^- sensor protein was a functional marker of the mussel habitat (LDA = 2.61, $P = 0.014$). This enhanced ability to transport NO_2^- and NO_3^- across the cell membrane could be linked to potential energy conservation processes or metabolic reactions beyond N-cycling. For example, the Nxr protein of *N. moscoviensis* is contained within the periplasm and does not require transportation of NO_2^- or NO_3^- into the cell (Spieck et al., 1998). Instead, *N. moscoviensis* likely transports NO_2^- and NO_3^- into the cell for assimilation and outside the cell to protect against excess NO_2^- (Lücker et al., 2010).

In comparison, the no-mussel treatment showed an enhance genetic ability to uptake and store N by way of encoding a cyanate ABC transporter (LDA = 2.40, $P = 0.043$) and asparagine synthetase (AsnB) (**Supplementary Table S2**), respectively. Differential abundance of cyanate transporters would indicate *N. moscoviensis* could have increased ability to obtain an

TABLE 1 | *Nitrospira moscoviensis* N-cycling protein functions from the mussel habitat in relative abundance (RPKM) and as a proportion of SEED enzymatic function.

SEED subsystems and protein functions	Average read abundance (RPKM)	Relative proportion of protein function
Ammonia assimilation		
Nitrogen regulatory protein P-II Gln	1409.04	0.34%
Nitrogen assimilation regulatory protein Ntr	395.687	
Ammonium transporter AmtB	300.22	
Glutamate-ammonia-ligase GlnEb	3267.89	
Denitrification		
Ferredoxin-type protein NapG (periplasmic nitrate reductase)	801.88	0.13%
Copper-containing nitrite reductase NirK (NO-forming)	ND	
Formate hydrogenase		
Formate hydrogenlyase, membrane subunit HyfB	95.37	0.71%
Putative formate hydrogenlyase, membrane subunit HyfC	ND	
Putative formate hydrogenlyase, membrane subunit HyfE	214.91	
Formate hydrogenlyase, membrane subunit HyfF	158.95	
Formate hydrogenlyase, large subunit HyfG	ND	
Putative formate hydrogenlyase, small subunit HyfI	94.81	
Formate dehydrogenase, alpha subunit FdsA	17.577	
Formate dehydrogenase, beta subunit FdsB	60.937	
Formate dehydrogenase, gamma subunit FdsG	ND	
Formate hydrogenlyase transcriptional activator FhlA	122.83	
Formate transporter FocA	ND	
Nitrate and nitrite ammonification		
Nitrate transporter NarK	80.79	0.15%
Nitrate ABC transporter Nrt	333.27	
Nitrite oxidoreductase, alpha subunit NxrA	1097.03	
Nitrite oxidoreductase, beta subunit NxrB	ND	
Nitrite oxidoreductase, membrane subunit NxrC	1695.47	
Nitrite reductase (NADH) small subunit NirD	474.06	
Nitrogen fixation		
Nitrogenase (molybdenum-iron)-specific transcriptional regulator NifA	63.33	0.15%
Nitrogenase (iron-iron) transcriptional regulator	ND	
Urea degradation		
Urease alpha subunit UreC	139.91	0.10%
Urease gamma subunit UreA	159.583	
Urea ABC transporter, urea binding protein UrtA	36.72	
Urease accessory protein UreD	ND	
Urease accessory protein UreF	70.38	
Urease accessory protein UreG	143.91	
Urease beta subunit UreB	ND	

SEED counts are shown as a percentage of the total classified protein function in the mussel habitat.

alternative source of N via the cyanase enzyme (Koch et al., 2015) or could be reciprocally fed to cyanase-lacking nitrifiers (Palatinszky et al., 2015). The co-increases of genes encoding AsnB and a cyanate transporter suggests that *N. moscoviensis* may have utilized alternative N sources in the sediment without mussels, perhaps due to inorganic N limitations in its environment.

Comammox *Nitrospira* Genomic Potential

A total of 163,253 SEED functionalities were assigned to the genome of "*Candidatus* Nitrospira inopinata" (normalized to 13,278 per sample) and the top 25% most prominent SEED subsystems did not differ substantially between treatments (**Supplementary Table S3** and **Figure 3**). The "restriction-modification system" represented the largest potential functional category for the no-mussel treatment, while the potential for thiamin metabolism ("5-FCL-like protein"), and stress response ("commensurate regulon activation") SEED assignments were the most abundant for the genome with mussels. The metabolic potential for "urea decomposition" was more abundant without mussels, while "biogenesis of c-type cytochromes" was greater in the mussel treatment. The "ammonia monooxygenase" potential function was the 4th most abundant SEED subsystem for both mussel and no-mussel treatments. Both treatments

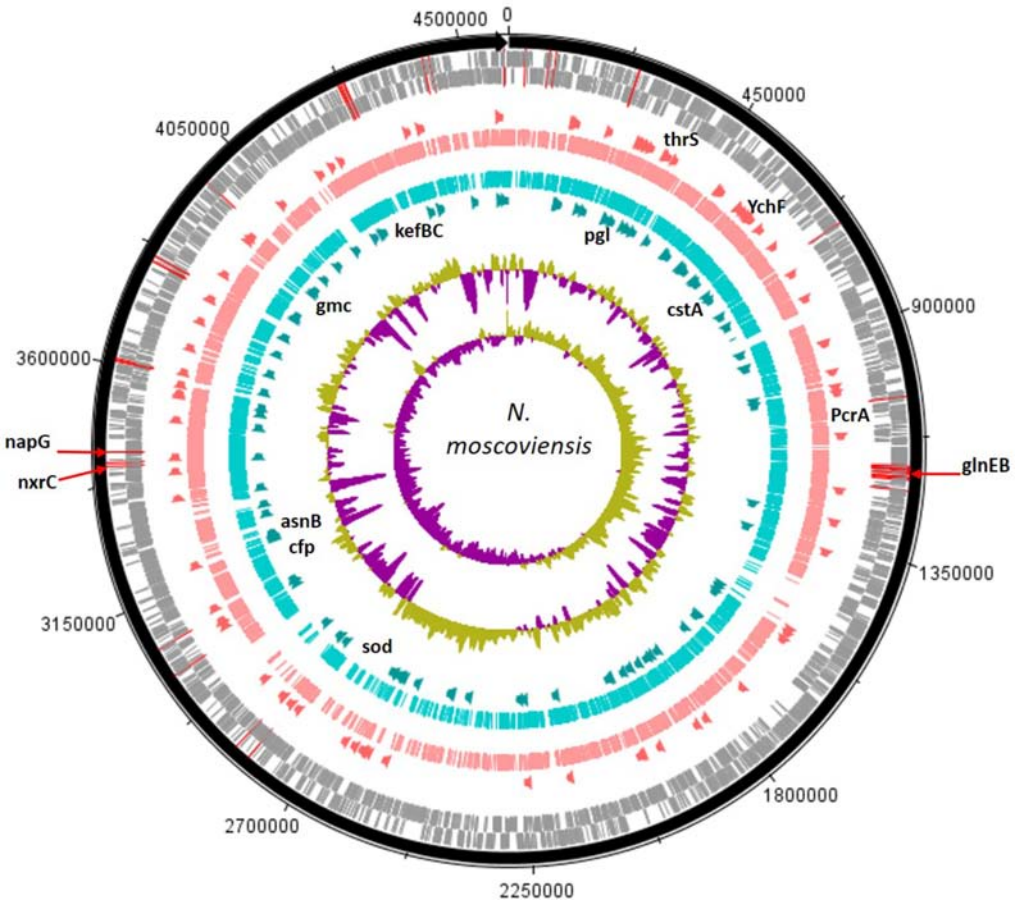

FIGURE 2 | The assembled *N. moscoviensis* genome is depicted with tick mark intervals of 225 kBp, and tracks are composed of the following components, starting with the outermost rings: Forward strand coding regions (gray), reverse strand coding regions (gray), the top 25% most abundant enzymes with mussels (dark orange), genomic read coverage from the mussel habitat (salmon colored), genomic coverage without mussels (turquoise colored), the top 25% most abundant enzymes with no mussels (dark green), GC coverage, and GC skew. The N-cycling genes with greatest abundance, GlnEB (NITMOv2_1289, NITMOv2_1290), nitrite oxidoreductase C (NITMOv2_3624), and periplasmic nitrate reductase (NITMOv2_3626) are marked with red lines over the outer rings. Gene names are shown for those with the largest LDA effect size (LDA > 3.0). For the mussel habitat, these include the YebC-like proteins, YchF and thrS, heme utilization protein, and DNA helicase (PcrA). Without mussels, these include the CPA2 protein families (kefBC in *N. moscoviensis*), 6-phosphogluconolactonase (pgl), a Fe-Mn superoxide dismutase (sod), asparagine synthetase (asnB), glucose methanol choline oxidoreductase (gmc), pyruvate decarboxylase (cfp), and carbon starvation protein (cstA).

shared numerous abundant SEED assignments (**Supplementary Table S3**), including genes encoding a resistance-nodulation-cell division (RND) efflux system inner membrane transporter, AmoC, alcohol dehydrogenase, and glycogen utilizing enzymes (**Supplementary Table S3**). Numerous N-cycling functions of "*Candidatus* Nitrospira inopinata" were highly abundant in the mussel habitat (**Table 2**), including genes encoding NO- and N_2O-forming enzymes, Amo, and NO_2^-/NO_3^- transforming enzymes (Nxr, NapG, and Nas). Although the total abundance of genes encoding Amo was slightly larger in the mussel treatment, this trend was most evident for AmoA and AmoB. Genes encoding urea transporters (UrtB and UrtC) and urease proteins (UreD, UreG, UreA, and UreF) were relatively more abundant in the mussel treatment, though the "urea decomposition" subsystem did not follow this overall trend.

Finally, N-cycling genes shared by *N. moscoviensis* and "*Candidatus* Nitrospira inopinata" were assessed for differential abundance to reveal if N-cycling genes could explain how both species were distinct to the mussel habitat, despite competing for similar N substrates. The protein functions present in both species include NH_4^+ transporters and permeases, copper-containing nitrite reductase (NirK), a "NnrS protein involved in response to NO," NO reductase, periplasmic NO_3^- reductase, NO_2^-/NO_3^- sensor and response regulator proteins, Nxr, urea transporters, and urease enzymes. A mean rank multiple comparison analysis (Kruskal–Wallis test with Dunn's multiple test correction) revealed that the sum of genes encoding urea transporters (Urt) (Mean rank difference = 53.8, P = 0.002) and copper-containing nitrite reductases (NO-forming) (NirK) (Mean rank difference = 54.0, P = 0.002) were more abundant from the "*Candidatus* Nitrospira inopinata" genome (mussel habitat) compared to *N. moscoviensis*. It should be noted that other studies have detected nirK in *Nitrospira* but we are not aware of studies detecting NO production (Camejo et al., 2017).

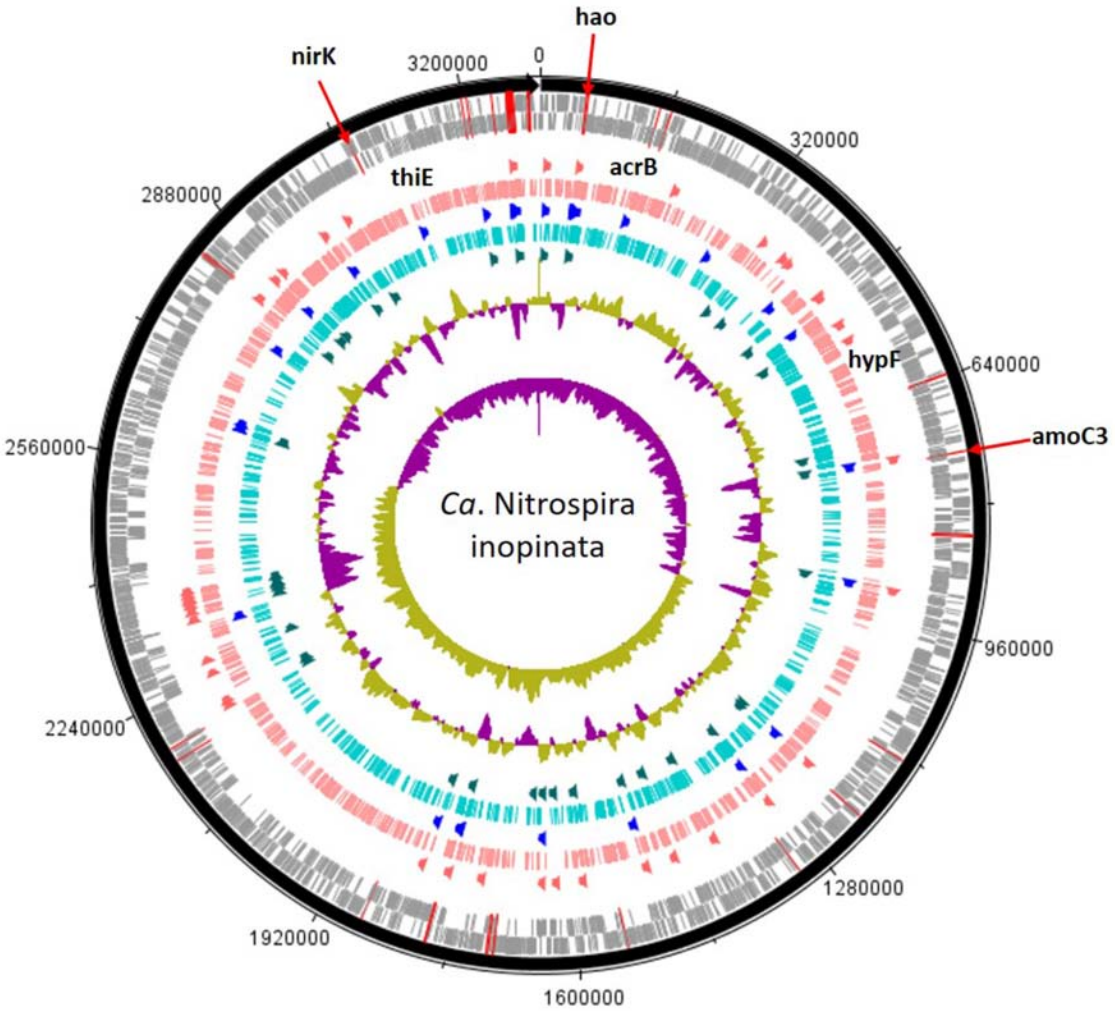

FIGURE 3 | *Candidatus* Nitrospira inopinata assembly shown with tick mark intervals of 160 kBp. Tracks within the genome are composed of the following, starting with the outermost rings: Forward strand coding regions, reverse strand coding regions, the top 25% most abundant enzymes with mussels (dark orange), genomic coverage with mussels (salmon colored), top 25% most abundant SEED subsystems in both treatments (royal blue), genomic coverage without mussels (turquoise colored), the top 25% most abundant enzymes with no mussels (dark green), GC coverage, and GC skew. N-cycling genes are designated with red lines across the CDS rings and the most abundant genes [amoC3 (NITINOP_0766), nirK (NITINOP_3146), hao (NITINOP_0065)] are designated with text. For simplicity, genes with LDA > 3 are named (acrB, hypF, and thiE), and therefore limits to the mussel habitat treatment (text shown above salmon-colored ring).

Additionally, it has been suggested that nirK from AOB could catalyze the oxidation of NO to NO_2^- (Kuypers et al., 2018), but we cannot make conclusions on enzymatic activity from metagenomic evidence alone.

Comammox *Nitrospira* Genetic Markers

The most discerning differences in the genome of "*Candidatus* Nitrospira inopinata" with mussels included a gene encoding the RND efflux system inner membrane transporter (AcrB) (**Supplementary Table S4** and **Figure 3**) as part of the SEED subclass "FOL commensurate regulon activation" (LDA = 3.71, P = 0.043). Numerous other potential stress response and virulence pathways were greater in the mussel treatment (**Supplementary Table S4**), such as genes encoding a RND efflux system membrane fusion protein (TtgA), a membrane protease with a mechanism for aminoglycoside resistance (HflK), an integral inner membrane protein type IV secretion complex (VirB), and "death on curing protein" (Doc) as part of the pathway of YdcE and YdcD toxin programmed cell death (LDA = 2.46, P = 0.014). Results also indicated a larger metabolic potential for metal tolerance in the mussel treatment, namely copper tolerance (LDA = 2.26, P = 0.047) by way of a gene encoding a periplasmic divalent cation tolerance protein (CutA).

Other genetic markers in the mussel habitat had indirect links to N metabolism through potential for urea cycling and cytochrome biosynthesis. A gene encoding a NiFe hydrogenase (HypF) assembly protein responsible for regulating the sulfur-reducing hydrogenase gene set (*hydBGDA* and *hybD*) was greater with mussels, and was recently suggested as giving comammox *Nitrospira* the potential function of hydrogen

TABLE 2 | "*Candidatus* Nitrospira inopinata" N-cycling protein functions from the mussel habitat as relative abundance (RPKM) and as a proportion of SEED enzymatic function.

SEED subsystems and protein functions	Average read abundance (RPKM)	Relative proportion of protein function
Ammonia monooxygenase		
Ammonia monooxygenase A-subunit AmoA	2955.70	3.79%
Ammonia monooxygenase B-subunit AmoB	1405.72	
Ammonia monooxygenase C-subunit AmoC	37945.15	
Urea decomposition		
Urea ABC transporter, ATPase protein UrtD	1634.33	3.52%
Urea ABC transporter, ATPase protein UrtE	1459.22	
Urea ABC transporter, permease protein UrtB	1713.41	
Urea ABC transporter, permease protein UrtC	735.02	
Urea ABC transporter, urea binding protein UrtA	1443.89	
Urea carboxylase-related amino acid permease UctT	201.53	
Urease accessory protein UreD	ND	
Urease accessory protein UreF	151.66	
Urease accessory protein UreG	303.31	
Urease alpha subunit UreC	724.79	
Urease beta subunit UreB	221.21	
Urease gamma subunit UreA	ND	
Denitrification		
Copper-containing nitrite reductase NirK	10156.73	0.50%
Nitric oxide reductase protein NorQ	127.68	
Nitrate and nitrite ammonification		
Hydroxylamine dehydrogenase (Hao)	3472.95	0.28%
Putative HaoB	107.52	
Nitrite/Nitrate oxidoreductase, alpha subunit (NxrA)	ND	
Nitrite/Nitrate oxidoreductase, beta subunit (NxrB)	ND	
putative Nitrite/Nitrate oxidoreductase, membrane subunit (NxrC)	522.64	
Ammonia assimilation		
Ammonium transporter Rh50	87.70	0.17%
Glutamate-ammonia-ligase (GlnEb)	271.58	

SEED counts are shown as a percentage of the total classified protein function in the mussel habitat.

oxidation coupled to sulfur reduction in anaerobic conditions (Camejo et al., 2017). Genes encoding a cytochrome c-type biogenesis protein (CcmF) were greater with mussels, and is a heme chaperone required for biogenesis of cytochrome c-type proteins located immediately downstream of hydroxylamine dehydrogenase (*hao*) (**Figure 3**). Another genetic functional marker greater with mussels encodes carbamoyl phosphate synthetase (CarB) and would effectively add urea-derived NH_3 into central metabolism.

SEED subsystems of "*Candidatus* Nitrospira inopinata" most indicative of the no-mussel treatment were those potentially functioned in potassium homeostasis (LDA = 3.53, $P = 0.043$), alpha carboxysome (LDA = 3.04, $P = 0.043$), and DNA metabolic CRISPR function (LDA = 3.04, $P = 0.043$). The only significantly different protein-coding gene classified in the "potassium homeostasis" subsystem encoded a potassium transporting ATPase (KdpC), and is a catalytic chaperone for high-affinity potassium uptake (Irzik et al., 2011). Greater function potential for rubrerythrin, a stress response protein used to combat oxidative stress (LDA = 2.45, $P = 0.021$) (Cardenas et al., 2016), was greater in the no-mussel treatment, and may be linked to greater abundances of genes encoding a recombination and repair protein (RecO) and excinuclease ABC genes in DNA repair pathways (LDA = 2.38, $P = 0.021$). N-cycling genes were not found to be a significant feature differentiating comammox *Nitrospira* genomes in the no-mussel treatment.

DISCUSSION

In support of our research goal, we provided metagenomic evidence of niche partitioning features to explain how two species of *Nitrospira* were greater in UMR sediment with mussels. This aligns with our previous 16S rRNA amplicon sequencing study which detected a 10% greater abundance of Nitrospirae in the mussel habitat (Black et al., 2017). Furthermore, this metagenomic research showed greater abundances of species capable of urea hydrolysis and clarifies our previous assumptions that an alternative source of N allowed co-increases in anammox, AOB, and NOB phylotypes. We found that *Nitrospira moscoviensis* and "*Candidatus* Nitrospira inopinata" were the most differentiating N-cycling taxons in this mussel habitat niche, and these organisms likely co-existed

because of metabolic flexibility beyond the conventional N-cycle.

Nitrospira moscoviensis Marked by Genetic Diversity and Potential for Carbon Metabolism

The most definitive genetic marker of *N. moscoviensis* from the mussel habitat encoded YebC (LDA = 3.49) and may suggest the potential for enhanced genetic diversity. For example, the YebC protein regulates genetic recombination and resolution of Holliday Junctions (Zhang et al., 2012), and enzymes classified within the YebC subsystem, YchF and ThrRS, function as translational control factors (Teplyakov et al., 2003; Zhou et al., 2016). These results suggest that *N. moscoviensis* in the mussel habitat had the genetic potential to synthesize proteins and respond to environmental variations (Hershey et al., 2012). Additionally, it makes sense that enhanced DNA repair using "UvrD-related helicases" and "two cell division clusters relating to chromosome partitioning" were also top differentiating features in the mussel habitat. Increased DNA repair and recombination genetic markers would also have permitted *N. moscoviensis* to respond to changing environments by way of genetic diversity. To this point, flexible metabolism and a mixotrophic lifestyle enables *N. moscoviensis* to be ecologically successful in numerous other environments (Koch et al., 2015).

We demonstrated that gene abundances associated with carbon metabolic processes of *N. moscoviensis* were impacted in the mussel habitat, as evidenced by increased Calvin cycle and glycogen metabolism genetic markers while the no-mussel treatments contained carbon stress protein genetic markers. CstA is a membrane protein predicted to be involved in peptide uptake when carbon availability is low (Rasmussen et al., 2013). Experimental evidence has also shown the *cstA* gene is upregulated during carbon starvation (Dubey et al., 2003) and allows for increased cellular growth by importing peptides as sources of C and N (Vastermark et al., 2014). Furthermore, it is possible that *N. moscoviensis* was genetically capable of responding to nutrient fluctuations in the no-mussel environment due to the glutathione-regulated potassium efflux gene (*kefC*) and methylglyoxal metabolism genetic markers. Evidence suggests that glutathione activates KefC potassium channels to protect against the toxic effects of methylglyoxal, and often occurs in response to limited phosphate or excessive carbon concentrations (Ferguson et al., 1998; Booth, 2005). It is possible that *N. moscoviensis* were C-stressed and nutrient-stressed in sediments without mussels, therefore the environment selected for the NOB *Nitrospira* possessing CstA and KefC proteins. Previous studies have shown that mussel biodeposits contain fairly consistent carbon and nutrient ratios (van Broekhoven et al., 2015) while others indicate biodeposit decomposition varies seasonally (Jansen et al., 2012), so future research should address if nutrient composition of mussel habitat sediments correspond to real-time metabolic activity of *N. moscoviensis*.

Furthermore, it is possible that mussel habitat sediments housed an enhanced niche for *N. moscoviensis* by containing a diverse source of carbon rather than nitrogen compounds. Contrary to our initial hypothesis, formate hydrogenase enzymes were a highly abundant N-cycling SEED category, while the gene families *nirK*, *ure* and *urt*, represented the lowest N-cycling genetic potential. These results suggest that *N. moscoviensis* had greater genetic potential to degrade to formate than from reciprocal feeding of mussel-derived urea. Taken together, these results signify *N. moscoviensis* in the mussel habitat had greatest potential for carbon degradation, NO_2^- oxidation, and likely thrived from fermentation products commonly found in sediments at the interface of oxic and anoxic conditions.

Comammox *Nitrospira* Marked by Potential for Multidrug Efflux Pumps and Diverse Metabolism

The comammox genome was marked with multidrug resistance efflux pumps (CmeB/AcrB), and metal resistance (Zn and Cu) in the mussel habitat, and suggests there may have been a selective pressure to use defense mechanisms. These multidrug resistance genes could be a response to one or more substrates and would enable resistance toward numerous antimicrobial substrates including antibiotics and heavy metals (Lin et al., 2002; Anes et al., 2015). Furthermore, our detected genetic markers for increased Phd-Doc toxin-antitoxin genes, are attributed with biochemical processes including antibiotic resistance (Liu et al., 2008). One explanation for these findings may be related to mussels hosting antibiotic resistant symbionts (Cooke, 1976; Liu et al., 2016), multidrug-resistant pathogens, (da Silveira et al., 2016), and enhanced horizontal gene transfer within their gut microbial community (Grevskott et al., 2017). Previous research has also shown that mussels bioaccumulate various metals (Naimo, 1995; Rzymski et al., 2014), including elements found in this genetic marker study, copper and zinc (Jorge et al., 2018). It is possible that horizontal gene transfer of multidrug resistance was facilitated by symbionts in mussel biodeposits, or from the decay of mussel tissue after death. However, this study was not designed to pinpoint antimicrobial stressors in the mussel habitat, so we cannot definitively say that commamox *Nitrospira* obtained these features as a direct result of their niche.

The genetic marker analysis also revealed that phosphorus metabolism was a distinctive feature of comammox *Nitrospira* in the mussel habitat. It is possible that phosphorus metabolic potential was influenced by mussel excretion products regenerating phosphate within the sediment, but would ultimately depend on the nutrient content and type of suspended food consumed by mussels (Jansen et al., 2012). Regeneration of phosphate in mussel habitat sediments would give comammox *Nitrospira* a selective advantage over AOA and AOB which do not encode an alkaline phosphatase (Palomo et al., 2018). Another genetic marker potentially explaining the success of comammox *Nitrospira* was the NiFe hydrogenase maturation protein (HypF) found in the mussel habitat. Recent studies have reported that comammox have the potential to oxidize H_2 and use sulfur as an electron acceptor in anaerobic conditions (Camejo et al., 2017), and this further emphasizes the importance of metabolic versatility in the UMR mussel habitat.

NOB and Comammox *Nitrospira* Coexisted in a Mussel Habitat Niche

Our results from the mussel habitat showed that "*Candidatus* Nitrospira inopinata" had the largest genomic potentials for ammonia oxidation, urea decomposition, and NO_2^- redox reactions. In comparison to *N. moscoviensis*, "*Candidatus* Nitrospira inopinata" was genetically equipped to obtain electrons from multiple N compounds. Furthermore, since the comammox genome contained large abundances of N-cycling genes compared to *N. moscoviensis*, this suggests that these two organisms were likely successful in the mussel habitat by utilizing different metabolic functions. In the mussel habitat, "*Candidatus* Nitrospira inopinata" had an order of magnitude greater capacity for urea decomposition than *Nitrospira moscoviensis*, with the most evident differences shown for urease proteins and urea transporters. It is likely that the comammox *Nitrospira* genome had greater metabolic potentials for urea decomposition since it contains the whole gene set encoding a urea ABC transporter (*urtABCDE*). This high affinity urea transporter is shared among most *Nitrospira* species (Ushiki et al., 2017) and likely enables an adaptation to environments with variable and micromolar concentrations of urea. In comparison, *N. moscoviensis* only has the potential to encode UrtA, and not accessory proteins UreD, UreE, UreF, and UreG (Koch et al., 2015).

Not only do these results suggest that *Ca.* N. inopinata had a greater genetic potential to degrade urea, but also may have outcompeted the potential for reciprocal feeding between *N. moscoviensis* and other ammonia oxidizers. Another explanation for this finding could be that *Ca.* N. inopinata has over an order of magnitude greater affinity for NH_3 than canonical AOB and is well suited for low NH_3 and variable environments (Kits et al., 2017*)*. The importance of scavenging urea and NH_3 is emphasized by the fact that "*Candidatus* Nitrospira inopinata" cannot survive on NO_2^- alone, since the organism lacks the ability to utilize NO_2^- as a source of N (Daims et al., 2015).

Although comammox *Nitrospira* would have the advantage over *N. moscovinesis* by scavenging NH_3 and urea, both organisms could occupy the same niche due to their unique metabolic flexibilities. NOB *Nitrospira* thrive in oxic-anoxic niches where formate is produced by fermentation, and would not be outcompeted by comammox *Nitrospira* clade A, which lack a formate dehydrogenase enzyme (Hu and He, 2017). Furthermore, *N. moscovinesis* can simultaneously produce and consume NO_2^-, by coupling formate oxidation to NO_3^- reduction while aerobically oxidizing NO_2^- (Koch et al., 2015). This may explain our findings that *Nitrospira moscoviensis* had high genomic potentials for NO_2^- oxidation (Nxr), NO_3^- reduction (NapG), and formate hydrogenation (Hyf, Fds).

Surprisingly, we detected an order of magnitude greater *nirK* compared to *nxr* in "*Candidatus* Nitrospira inopinata" and signifies that NO could be a major product of nitrification in this mussel habitat niche. Although previous studies have not documented gaseous NO_x production from nirK belonging to *Nitrospira*, comammox organisms do have the genetic capability for NO_3^- reduction to NO_2^- and NO (Camejo et al., 2017). Furthermore, *N. moscoviensis* showed genomic potential to respond to and degrade NO and N_2O, potentially removing the major gaseous products of nitrification.

Our findings agree with other comparative genomic studies showing that *Nitrospira* species are functionally diverse and provides new insights on the niche separation between comammox and NOB (Hu and He, 2017). Although many genomic features differed between *N. moscoviensis* and *Ca*. N. inopinata in this study, both had greater genetic potentials for type IV pili in the mussel habitat. This feature would enhance the ability of these organisms to respond to environmental changes and form protective flocs and biofilms (Hospenthal et al., 2017). Aggregation of these two species is feasible and consistent with their ecophysiological versatility (Kits et al., 2017). Ultimately, our results indicated that NOB- and comammox-*Nitrospira* were genetically capable of coexisting in the mussel habitat through niche differentiation features, but potentially also synergistically coupled their metabolic features.

CONCLUSION

This research used genomic markers to show that *Nitrospira moscoviensis* and "*Candidatus* Nitrospira inopinata" predominated an N-cycling oxic-anoxic niche in sediment of a mussel habitat. Our research showed that formate oxidation coupled to NO_3^- reduction by NOB *Nitrospira* may have enabled co-existence with comammox *Nitrospira* in this sediment niche. The mussel habitat harbored comammox *Nitrospira* with enhanced RND efflux transporters and metal resistance, phosphorus metabolism, and showed evidence of hydrogen oxidation, while decreasing the genomic potential for potassium homeostasis and oxidative stress. For *N. moscoviensis*, the mussel habitat contained greater abundances of translational control genes and heme utilization while the no-mussel treatment showed genomic evidence of carbon stress. Both NOB and comammox *Nitrospira* were marked by diverse metabolism in the mussel habitat and may have contributed toward the increased abundance of both organisms. More research is needed to determine the biogeochemical signatures of the mussel habitat that may be responsible for these various genetic markers. Ultimately, this study provided metagenomic evidence showing that niche partitioning and mixotrophic metabolism allowed NOB and commamox *Nitrospira* to coexist in mussel habitat sediment.

AUTHOR CONTRIBUTIONS

EB and CJ contributed conception and design of the study. EB performed the statistical analysis and bioinformatics. EB and CJ wrote sections of the manuscript. All the authors contributed to manuscript revision, read and approved the submitted version.

SUPPLEMENTARY MATERIAL

The Supplementary Material for this article can be found online at: https://www.frontiersin.org/articles/10.3389/fmicb.2018.02061/full#supplementary-material

REFERENCES

Andrews, S. (2010). *FastQC: A Quality Control tool for High Throughput Sequence Data*. Available at: http://www.bioinformatics.babraham.ac.uk/projects/fastqc

Anes, J., McCusker, M. P., Fanning, S., and Martins, M. (2015). The ins and outs of RND efflux pumps in *Escherichia coli*. *Front. Microbiol.* 6:587. doi: 10.3389/fmicb.2015.00587

Atkinson, C. L., Kelly, J., and Vaughn, C. C. (2014). Tracing consumer-derived nitrogen in riverine food webs. *Ecosystems* 17, 485–496. doi: 10.1007/s10021-013-9736-2

Atkinson, C. L., and Vaughn, C. C. (2015). Biogeochemical hotspots: temporal and spatial scaling of the impact of freshwater mussels on ecosystem function. *Freshw. Biol.* 60, 563–574. doi: 10.1111/fwb.12498

Atkinson, C. L., Vaughn, C. C., Forshay, J. K., and Cooper, J. T. (2013). Aggregated filter-feeding consumers alter nutrient limitation: consequences for ecosystem and community dynamics. *Ecology* 94, 1359–1369. doi: 10.1890/12-1531.1

Black, E. M., Chimenti, S. M., and Just, C. L. (2017). Effect of freshwater mussels on the vertical distribution of anaerobic ammonia oxidizers and other nitrogen-transforming microorganisms in upper Mississippi river sediment. *PeerJ* 5:e3536. doi: 10.7717/peerj.3536

Booth, I. R. (2005). Glycerol and methylglyoxal metabolism. *EcoSal Plus*. doi: 10.1128/ecosalplus.3.4.3

Bott, C. B., and Love, N. G. (2004). Implicating the Glutathione-Gated Potassium Efflux System as a Cause of Electrophile-Induced Activated Sludge Deflocculation. *Appl. Environ. Microbiol.* 70, 5569–5578. doi: 10.1128/AEM.70.9.5569-5578.2004

Bril, J. S., Durst, J. J., Hurley, B. M., Just, C. L., and Newton, T. J. (2014). Sensor data as a measure of native freshwater mussel impact on nitrate formation and food digestion in continuous-flow mesocosms. *Freshw. Sci.* 33, 417–424. doi: 10.1086/675448

Bril, J. S., Langenfeld, K., Just, C. L., Spak, N. S., and Newton, T. J. (2017). Simulated mussel mortality thresholds as a function of mussel biomass and nutrient loading. *PeerJ* 5:e2838. doi: 10.7717/peerj.2838

Buchfink, B., Xie, C., and Huson, H. D. (2015). Fast and sensitive protein alignment using DIAMOND. *Nat. Methods* 12, 59–60. doi: 10.1038/nmeth.3176

Camejo, P. Y., Santo, J., Domingo, D., McMahon, K. D., and Noguera, R. (2017). Genome-enabled insights into the ecophysiology of the comammox bacterium *Candidatus* Nitrospira nitrosa. *mSystems* 2, e00059-17. doi: 10.1128/mSystems.00059-17

Cardenas, J. P., Quatrini, R., and Holmes, D. S. (2016). Aerobic lineage of the oxidative stress response protein rubrerythrin emerged in an ancient microaerobic, (hyper)thermophilic environment. *Front. Microbiol.* 7:1822. doi: 10.3389/fmicb.2016.01822

Carver, T., Thomson, N., Bleasby, A., Berriman, M., and Parkhill, J. (2009). DNAPlotter: circular and linear interactive genome visualization. *Bioinformatics* 25, 119–120. doi: 10.1093/bioinformatics/btn578

Cooke, M. D. (1976). Antibiotic Resistance Among Coliform and Fecal Coliform Bacteria Isolated from the Freshwater Mussel Hydridella menziesii. *Antimicrob. Agents Chemother.* 9, 885–888. doi: 10.1128/AAC.9.6.885

da Silveira, C. S., de Sousa, O. V., and Evangelista-Barreto, N. S. (2016). Propagation of Antimicrobial Resistant *Salmonella* spp. *in* bivalve mollusks from estuary areas of bahia, brazil. *Rev. Caatinga* 29, 450–457. doi: 10.1590/1983-21252016v29n222rc

Daebeler, A., Bodelier, P. L. E., Yan, Z., Hefting, M. M., Jia, Z., and Laanbroek, H. J. (2014). Interactions between Thaumarchaea, *Nitrospira* and methanotrophs modulate autotrophic nitrification in volcanic grassland soil. *ISME J.* 8:2397. doi: 10.1038/ismej.2014.81

Daims, H., Lebedeva, E. V., Pjevac, P., Han, P., Herbold, C., and Albertsen, M. (2015). Complete nitrification by *Nitrospira* bacteria. *Nature* 528, 504–509. doi: 10.1038/nature16461

Danovaro, R., Gambi, C., Luna, G. M., and Mirto, S. (2004). "Sustainable impact of mussel farming in the Adriatic Sea (Mediterranean Sea): evidence from biochemical, microbial and meiofaunal indicators". *Mar. Pollut. Bull.* 49, 325–333. doi: 10.1016/j.marpolbul.2004.02.038

Donner, S. D., and Kucharik, C. J. (2008). "Corn-based ethanol production compromises goal of reducing nitrogen export by the Mississippi River".*Proc. Natl. Acad. Sci. U.S.A.* 105, 4513–4518. doi: 10.1073/pnas.0708300105

Dubey, A. K., Baker, C. S., Suzuki, K., Jones, A. D., Pandit, P., and Romeo, T. (2003). CsrA regulates translation of the *Escherichia coli* carbon starvation gene, cstA, by blocking ribosome access to the cstA transcript. *J. Bacteriol.* 185, 4450–4460. doi: 10.1128/JB.185.15.4450-4460.2003

Ferguson, G. P., McLaggan, D., and Booth, I. R. (1995). Potassium channel activation by glutathione-S-conjugates in *Escherichia coli*: protection against methylglyoxal is mediated by cytoplasmic acidification. *Mol. Microbiol.* 17, 1025–1033. doi: 10.1111/j.1365-2958.1995.mmi_17061025.x

Ferguson, G. P., Totemeyer, S., MacLean, M. J., and Booth, I. R. (1998). "Methylglyoxal production in bacteria: suicide or survival?" *Arch. Microbiol.* 170, 209–219. doi: 10.1007/s002030050635

Gomez-Velez, J. D., Harvey, J. W., Cardenas, M. B., and Kiel, B. (2015). Denitrification in the Mississippi River network controlled by flow through river bedforms. *Nat. Geosci.* 8:941. doi: 10.1038/ngeo2567

Grevskott, D. H., Svanevik, C. S., Sunde, M., Wester, A. L., and Lunestad, B. T. (2017). Marine bivalve mollusks as possible indicators of multidrug-resistant *Escherichia coli* and other species of the *Enterobacteriaceae* family. *Front. Microbiol.* 8:10. doi: 10.3389/fmicb.2017.00024

Hallin, S., Jones, C. M., Schloter, M., and Philippot, L. (2009). Relationship between N-cycling communities and ecosystem functioning in a 50-year-old fertilization experiment. *ISME J.* 3, 597–605. doi: 10.1038/ismej.2008.128

Hershey, J. W. B., Sonenberg, N., and Mathews, M. B. (2012). Principles of translational control: an overview. *Cold Spring Harb. Perspect. Biol.* 4:a011528. doi: 10.1101/cshperspect.a011528

Hospenthal, M. K., Costa, D. T. R., and Waksman, G. (2017). A comprehensive guide to pilus biogenesis in Gram-negative bacteria. *Nat. Rev. Microbiol.* 15, 365–379. doi: 10.1038/nrmicro.2017.40

Hu, H. W., and He, Z. J. (2017). Comammox—a newly discovered nitrification process in the terrestrial nitrogen cycle. *J. Soils Sediments* 17, 2709–2717. doi: 10.1007/s11368-017-1851-9

Huson, D. H., Auch, A. F., Qi, J., and Schuster, S. C. (2007). MEGAN analysis of metagenomic data. *Genome Res.* 17, 377–386. doi: 10.1101/gr.5969107

Huson, D. H., Beier, S., Flade, I., Gorska, A., El Hadidi, M., Mitra, S., et al. (2016). MEGAN community edition - interactive exploration and analysis of large-scale microbiome sequencing data. *PLoS Comput. Biol.* 12:e1004957. doi: 10.1371/journal.pcbi.1004957

Irzik, K., Pfrötzschner, J., Goss, T., Ahnert, F., Haupt, M., and Greie, C. J. (2011). The KdpC subunit of the *Escherichia coli* K+-transporting KdpB P-type ATPase acts as a catalytic chaperone. *FEBS J.* 278, 3041–3053. doi: 10.1111/j.1742-4658.2011.08224.x

Jansen, H. M., Verdegem, M. C. J., Strand, Ø, and Smaal, A. C. (2012). Seasonal variation in mineralization rates (C-N-P-Si) of mussel Mytilus edulis biodeposits. *Mar. Biol.* 159, 1567–1580. doi: 10.1007/s00227-012-1944-3

Jorge, M. B., Bianchini, A., Wood, M. C., and Gillis, P. L. (2018). Copper uptake, patterns of bioaccumulation, and effects in glochida (larvae) of the freshwater mussel (*Lampsilis cardium*). *Environ. Toxicol. Chem.* 37, 1092–1103. doi: 10.1002/etc.4041

Kits, K. D., Sedlacek, C. J., Lebedeva, E. V., Han, P., Bulaev, A., Pjevac, P., et al. (2017). Kinetic analysis of a complete nitrifier reveals an oligotrophic lifestyle. *Nature* 549, 269–272. doi: 10.1038/nature23679

Koch, H., Galushko, A., Albertsen, M., Schintlmeister, A., Gruber, C., and Dorninger, S. (2014). Growth of nitrite-oxidizing bacteria by aerobic hydrogen oxidation. *Science* 345, 1052–1054. doi: 10.1126/science.1256985

Koch, H., Lücker, S., Albertsen, M., Kitzinger, K., Herbold, C., and Spieck, E. (2015). Expanded metabolic versatility of ubiquitous nitrite-oxidizing bacteria from the genus *Nitrospira*. *Proc. Natl. Acad. Sci. U.S.A.* 112, 11371–11376. doi: 10.1073/pnas.1506533112

Kreiling, R. M., Richardson, W. B., Cavanaugh, J. C., and Bartsch, L. A. (2011). Summer nitrate uptake and denitrification in an upper Mississippi River backwater lake: the role of rooted aquatic vegetation. *Biogeochemistry* 104, 309–324. doi: 10.1007/s10533-010-9503-9

Kuypers, M. M. M., Marchant, K. H., and Kartal, B. (2018). The microbial nitrogen-cycling network. *Nat. Rev. Microbiol.* 16, 263–276. doi: 10.1038/nrmicro.2018.9

Lerch, R. N., Kitchen, N. R., Baffaut, C., and Vories, E. D. (2015). Long-term agroecosystem research in the central mississippi river basin: goodwater creek experimental watershed and regional nutrient water quality data. *J. Environ. Qual.* 44, 37–43. doi: 10.2134/jeq2013.12.0518

Li, H., and Durbin, R. (2009). Fast and accurate short read alignment with Burrows–Wheeler transform. *Bioinformatics* 25, 1754–1760. doi: 10.1093/bioinformatics/btp324

Li, H., Handsaker, B., Wysoker, A., Fennell, T., Ruan, J., and Homer, N. G. (2009). The sequence alignment/map format and SAMtools. *Bioinformatics* 25, 2078–2079. doi: 10.1093/bioinformatics/btp352

Lin, J., Michel, L. O., and Zhang, Q. (2002). CmeABC Functions as a Multidrug Efflux System in Campylobacter jejuni. *Antimicrob. Agents Chemother.* 46, 2124–2131. doi: 10.1128/AAC.46.7.2124-2131.2002

Liu, J., Jung, J. H., and Liu, Y. H. (2016). Antimicrobial compounds from marine invertebrates-derived microorganisms. *Curr. Med. Chem* 23, 2892–2905. doi: 10.2174/0929867323666160525113837

Liu, M., Zhang, Y., Inouye, M. N., and Woychik, A. (2008). Bacterial addiction module toxin Doc inhibits translation elongation through its association with the 30S ribosomal subunit. *Proc. Natl. Acad. Sci. U.S.A.* 105, 5885–5890. doi: 10.1073/pnas.0711949105

Lücker, S., Wagner, M., Maixner, F., Pelletier, E., Koch, H., and Vacherie, B. T. (2010). "A *Nitrospira* metagenome illuminates the physiology and evolution of globally important nitrite-oxidizing bacteria". *Proc. Natl. Acad. Sci. U.S.A.* 107, 13479–13484. doi: 10.1073/pnas.1003860107

Matantseva, O. V., and Skarlato, S. O. (2013). Mixotrophy in microorganisms: ecological and cytophysiological aspects. *J. Evol. Biochem. Physiol.* 49, 377–388. doi: 10.1134/S0022093013040014

McGill, B. J., Etienne, R. S., Gray, J. S., Alonso, D., Anderson, M. J., and Benecha, H. K. (2007). Species abundance distributions: moving beyond single prediction theories to integration within an ecological framework. *Ecol. Lett.* 10, 995–1015. doi: 10.1111/j.1461-0248.2007.01094.x

Mirto, S., La rosa, T., Danovaro, R., and Mazzola, A. (2000). Microbial and Meiofaunal Response to Intensive Mussel-Farm Biodeposition in Coastal Sediments of the Western Mediterranean. *Mar. Pollut. Bull.* 40, 244–252. doi: 10.1016/S0025-326X(99)00209-X

Morales, Y., Weber, L. J., Mynett, A. E., and Newton, T. J. (2006). Effects of substrate and hydrodynamic conditions on the formation of mussel beds in a large river. *J. North Am. Benthol. Soc.* 25, 664–676. doi: 10.1899/0887-3593(2006)25[664:EOSAHC]2.0.CO;2

Mulholland, P. J., Helton, A. M., Poole, G. C., Hall, R. O., Hamilton, S. K., and Peterson, B. J. (2008). Stream denitrification across biomes and its response to anthropogenic nitrate loading. *Nature* 452:202. doi: 10.1038/nature06686

Naimo, T. J. (1995). A review of the effects of heavy metals on freshwater mussels. *Ecotoxicology* 4, 341–362. doi: 10.1007/BF00118870

Newton, T. J., Zigler, S. J., Rogala, J. T., Gray, B. R., and Davis, M. (2011). Population assessment and potential functional roles of native mussels in the Upper Mississippi River. *Aquat. Cons.* 21, 122–131. doi: 10.1002/aqc.1170

Okonechnikov, K., Golosova, O., and Fursov, M. (2012). Unipro UGENE: a unified bioinformatics toolkit. *Bioinformatics* 28, 1166–1167. doi: 10.1093/bioinformatics/bts091

O'Leary, N. A., Wright, M. W., Brister, J. R., Ciufo, S., Haddad, D., McVeigh, R., et al. (2016). Reference sequence (RefSeq) database at NCBI: current status, taxonomic expansion, and functional annotation. *Nucleic Acids Res.* 44, D733–D745. doi: 10.1093/nar/gkv1189

Overbeek, R., Begley, T., Butler, R. M., Choudhuri, J. V., Chuang, Y. H., Cohoon, M., et al. (2005). The Subsystems Approach to Genome Annotation and its Use in the Project to Annotate 1000 Genomes. *Nucleic Acids Res.* 33, 5691–5702. doi: 10.1093/nar/gki866

Palatinszky, M., Herbold, C., Jehmlich, N., Pogoda, M., Han, P., von Bergen, M., et al. (2015). Cyanate as energy source for nitrifiers. *Nature* 524, 105–108. doi: 10.1038/nature14856

Palomo, A., Pedersen, A. G., Fowler, S. J., Dechesne, A., Sicheritz Pontén, T., and Smets, B. F. (2018). Comparative genomics sheds light on niche differentiation and the evolutionary history of comammox *Nitrospira*. *ISME J.* 12, 1779–1793. doi: 10.1038/s41396-018-0083-3

Pfister, C. A., Gilbert, J. A., and Gibbons, S. M. (2014). The role of macrobiota in structuring microbial communities along rocky shores. *PeerJ* 2:e631. doi: 10.7717/peerj.631

Rasmussen, J. J., Vegge, C. S., Frokiaer, H., Howlett, R. M., Krogfelt, K. A., and Kelly, D. J. (2013). Campylobacter jejuni carbon starvation protein A (CstA) is involved in peptide utilization, motility and agglutination, and has a role in stimulation of dendritic cells. *J. Med. Microbiol.* 62, 1135–1143. doi: 10.1099/jmm.0.059345-0

Rzymski, P., Niedzielski, P., Klimaszyk, P., and Poniedziałek, B. (2014). Bioaccumulation of selected metals in bivalves (Unionidae) and Phragmites australis inhabiting a municipal water reservoir. *Environ. Monit. Assess* 186, 3199–3212. doi: 10.1007/s10661-013-3610-8

Segata, N., Izard, J., Waldron, L., Gevers, D., Miropolsky, L., and Garrett, W. S. (2011). Metagenomic biomarker discovery and explanation. *Genome Biol.* 12:R60. doi: 10.1186/gb-2011-12-6-r60

Shange, R. S., Ankumah, R. O., Ibekwe, A. M., Zabawa, R., and Dowd, S. E. (2012). Distinct soil bacterial communities revealed under a diversely managed agroecosystem. *PLoS One* 7:11. doi: 10.1371/journal.pone.0040338

Spieck, E., Ehrich, S., Aamand, J., and Bock, E. (1998). Isolation and immunocytochemical location of the nitrite-oxidizing system in Nitrospira moscoviensis. *Arch. Microbiol.* 169, 225–230. doi: 10.1007/s002030050565

Strauss, E. A., Richardson, W. B., Cavanaugh, J. C., Bartsch, L. A., Kreiling, R. M., and Standorf, A. J. (2006). Variability and regulation of denitrification in an Upper Mississippi River backwater. *J. North Am. Benthol. Soc.* 25, 596–606. doi: 10.1899/0887-3593(2006)25[596:VARODI]2.0.CO;2

Teplyakov, A., Obmolova, G., Chu, S. Y., Toedt, J., Eisenstein, E., and Howard, A. J. (2003). Crystal Structure of the YchF Protein Reveals Binding Sites for GTP and Nucleic Acid. *J. Bacteriol.* 185, 4031–4037. doi: 10.1128/JB.185.14.4031-4037.2003

Tötemeyer, S., Booth, N. A., Nichols, W. W., Dunbar, B., and Booth, I. R. (1998). From famine to feast: the role of methylglyoxal production in *Escherichia coli*. *Mol. Microbiol.* 27, 553–562. doi: 10.1046/j.1365-2958.1998.00700.x

USACE (1981). *Survey of Freshwater Mussels (Pelecypoda: Unionidae) at Selected Sites in Pools 11 Through 24 of the Mississippi River*. Illinois, IL: EA Report 9031 Rock Island District.

USACE (1984). *Resources Inventory for the Upper Mississippi River Rock Island District*. Illinois, IL: US Army Corps of Engineers.

Ushiki, N., Fujitani, H., Shimada, Y., Morohoshi, T., Sekiguchi, Y., and Tsuneda, S. (2017). Genomic analysis of two phylogenetically distinct *Nitrospira* species reveals their genomic plasticity and functional diversity. *Front. Microbiol.* 8:2637. doi: 10.3389/fmicb.2017.02637

van Broekhoven, W., Jansen, H., Verdegem, M., Struyf, E., Troost, K., Lindeboom, H., et al. (2015). Nutrient regeneration from feces and pseudofeces of mussel *Mytilus edulis* spat. *Mar. Ecol. Prog. Ser.* 534, 107–120. doi: 10.3354/meps11402

van Kessel, M. A., Speth, D. R., Albertsen, M., Nielsen, P. H., Op den Camp, J. M., Kartal, B., et al. (2015). Complete nitrification by a single microorganism. *Nature* 528, 555. doi: 10.1038/nature16459

Vastermark, A., Wollwage, S., Houle, M. E., Rio, R., and Saier, M. H. (2014). Expansion of the APC superfamily of secondary carriers. *Prot.Struct. Funct. Bioinform.* 82, 2797–2811. doi: 10.1002/prot.24643

Vaughn, C. C., and Hakenkamp, C. C. (2001). The functional role of burrowing bivalves in freshwater ecosystems. *Freshw. Biol.* 46, 1431–1446. doi: 10.1046/j.1365-2427.2001.00771.x

Young, N., Andrew, M., and Weber, L. (2005). "Hydrodynamic Investigation of Upper Mississippi River Freshwater Mussel Habitats," in

Proceedings of the American Society of Civil Engineers World Water and Environmental Resources Congress, Anchorage, AL. doi: 10.1061/40792(173)585

Zhang, Y., Lin, J., and Gao, Y. (2012). In silico identification of a multi-functional regulatory protein involved in Holliday junction resolution in bacteria. *BMC Syst. Biol.* 6:S20. doi: 10.1186/1752-0509-6-S1-S20

Zhou, X. L., Chen, Y., Fang, Z. P., Ruan, Z. R., Wang, Y., and Liu, R. J. (2016). Translational quality control by bacterial threonyl-tRNA synthetases. *J. Biol. Chem.* 291, 21208–21221. doi: 10.1074/jbc.M116.740472

Conflict of Interest Statement: The authors declare that the research was conducted in the absence of any commercial or financial relationships that could be construed as a potential conflict of interest.

frontiers in Microbiology

ORIGINAL RESEARCH
published: 23 October 2018
doi: 10.3389/fmicb.2018.02529

Responses of Nitrogen-Cycling Microorganisms to Dazomet Fumigation

Wensheng Fang, Dongdong Yan, Xianli Wang, Bin Huang, Xiaoning Wang, Jie Liu, Xiaoman Liu, Yuan Li, Canbin Ouyang, Qiuxia Wang and Aocheng Cao**

Institute of Plant Protection, Chinese Academy of Agricultural Sciences, Beijing, China

The influence of soil fumigation on microorganisms involved in transforming nitrogen remains little understood, despite the use of fumigants for many decades to control soil-borne pathogens and plant-parasitic nematodes. We used real-time PCR (quantitative polymerase chain reaction) and 16S rRNA gene amplicon sequencing techniques to monitor changes in the diversity and community structure of microorganisms associated with nitrogen transfer after the soil was fumigated with dazomet (DZ). We also examined nitrous oxide (N_2O) emissions from these microorganisms present in fumigated fluvo-aquic soil and lateritic red soil. Fumigation with DZ significantly reduced the abundance of 16S rRNA and nitrogen cycling functional genes (*nifH,* AOA *amoA,* AOB *amoA, nxrB, narG, napA, nirK, nirS, cnorB, qnorB,* and *nosZ*). At the same time, N_2O production rates increased between 9.9 and 30 times after fumigation. N_2O emissions were significantly correlated with NH_4^+, dissolved amino acids and microbial biomass nitrogen, but uncorrelated with functional gene abundance. Diversity indices showed that DZ temporarily stimulated bacterial diversity as well as caused a significant change in bacterial community composition. For example, DZ significantly decreased populations of N_2-fixing bacteria *Mesorhizobium* and *Paenibacillus*, nitrifiers *Nitrosomonas,* and the denitrifiers *Bacillus*, *Pseudomonas,* and *Paracoccus.* The soil microbial community had the ability to recover to similar population levels recorded in unfumigated soils when the inhibitory effects of DZ fumigation were no longer evident. The microbial recovery rate, however, depended on the physicochemical properties of the soil. These results provided useful information for environmental safety assessments of DZ in China, for improving our understanding of the N-cycling pathways in fumigated soils, and for determining the potential responses of different N-cycling groups after fumigation.

Keywords: soil fumigation, dazomet, N_2O, nitrogen transfer, functional gene abundance, bacterial community composition

OPEN ACCESS

Edited by:
Maria J. Delgado, Consejo Superior de Investigaciones Científicas (CSIC), Spain

Reviewed by:
Antonio Castellano-Hinojosa, Universidad de Granada, Spain
J. P. Dundore-Arias, University of Minnesota Twin Cities, United States

****Correspondence:***
Qiuxia Wang
wqxcasy@163.com
Aocheng Cao
caoac@vip.sina.com

Specialty section:
This article was submitted to Terrestrial Microbiology, a section of the journal Frontiers in Microbiology

Received: *01 July 2018*
Accepted: *03 October 2018*
Published: *23 October 2018*

Citation:
Fang W, Yan D, Wang X, Huang B, Wang X, Liu J, Liu X, Li Y, Ouyang C, Wang Q and Cao A (2018) Responses of Nitrogen-Cycling Microorganisms to Dazomet Fumigation. Front. Microbiol. 9:2529. doi: 10.3389/fmicb.2018.02529

INTRODUCTION

Soil fumigation enables the production of crops of acceptable yield and quality by effectively controlling soil-borne pathogens, nematodes and weeds. Generally, root crops such as carrots, potato and ginger that have been grown in fumigated soil have fewer rejections for blemishes at harvest and better marketable yield than when they are grown in unfumigated soil

(Jonathan et al., 2005; Qiao et al., 2011, 2012; Mao et al., 2014). Dazomet (DZ) is a highly effective microbicide that kills pests by a carbonylation reaction with nucleophilic sites (such as amino, hydroxyl, thiol) that may be present in enzyme molecules (Lin et al., 2000). Fumigation of soil with DZ prior to planting provides effective control of soil-borne pathogens and weeds in the production of high-value crops. It has become a valuable replacement for methyl bromide, which was phased out globally because of its harmful contribution to stratospheric ozone (Martin, 2003).

Fumigants in general kill not only target pathogens but also off-target microorganisms that can be important in the soil microbial community. Microorganisms, and in particular bacteria, are reported to significantly influence the soil quality and crop yield by regulating several important soil processes, such as organic matter decomposition, organic pollutant degradation and nutrient transformation (Álvarez-Martín et al., 2016; Crouzet et al., 2016). Previous studies reported that the fumigants chloropicrin (CP), 1,3-dichloropropene and metam sodium (MS) significantly decreased soil bacterial diversity and significantly changed the predominance of bacterial phyla in microbial communities (Liu et al., 2015; Li et al., 2017a,b; Zhang et al., 2017). Recent studies also showed that CP and MS caused significant changes in the population size and community composition of bacteria involved in N-cycling (Li et al., 2017a,b). These changes significantly affected nitrogen transforming activities, including nitrogen mineralization (Shen et al., 1984) and nitrogen reduction (Yan et al., 2013, 2017). Furthermore, previous research reported that nitrous oxide (N_2O) production increased by 12.6 times following CP fumigation when these fumigants were combined with chemical inhibitors such as acetylene, antibacterial and antifungal agents and oxygen (Spokas et al., 2005, 2006). However, the microbial community's role of increasing N_2O emissions after soil fumigation was not fully investigated in these studies.

Our study examined the response of different groups of N-cycling microbes present in Jiangxi lateritic red and Beijing fluvo-aquic soils fumigated with DZ. Over a period of 59 days after fumigation, we quantified N_2O emissions, changes to the geochemical parameters NO_3^- and NH_4^+, as well as changes to the microbial biomass nitrogen (MBN) and dissolved amino acids (DAA). We also used real-time PCR to monitor the abundance of key functional marker genes (*nifH,* AOA *amoA,* AOB *amoA, nxrB, narG, napA, nirK, nirS, cnorB, qnorB,* and *nosZ*) involved in microbial N_2-fixation, nitrification and denitrification. At the same time, we used 16S rRNA gene amplicon sequencing techniques to determine the bacterial diversity and community structure of microorganisms involved in nitrogen transformation in Beijing soil fumigated with DZ. We hypothesized that (i) DZ fumigation would produce a significant change in the abundance and community composition of nitrogen-transforming bacteria; (ii) N_2O emissions would be significantly correlated with the abundance of N-cycling functional genes; and (iii) DZ fumigation would initially decrease N-cycling bacteria in the soil because of its unselective toxic effect, but this decrease would be followed shortly afterwards by an increase in these bacteria as the concentration of DZ in the soil reduced over time. The information obtained in this study will provide further insights into the N-cycling pathways in fumigated soils and into the potential responses of different N-cycling groups after fumigation.

MATERIALS AND METHODS

Soil Samples Collection

Soil samples were taken from the top 20 cm of two agricultural fields in Beijing Shunyi (40°03′17.62″ N, 116°56′23.71″ E) and Jiangxi Yudu (26°06′31.84″ N, 115°33′51.83″ E) districts. Specifically, spade-squares (10 cm × 10 cm to a depth of 20 cm) of soil were taken from five locations along a 'W' line. These two samples were typical alkaline fluvo-aquic soils ('Beijing soil') and acidic lateritic red soils ('Jiangxi soil'). The taxonomic names of the soils were determined according to PRC 1:1,000,000 scale soil map that was provided by the Data Center for Resources and Environmental Sciences, Chinese Academy of Sciences. Soil texture was determined using a Laser Particle Size Analyzer (Mastersizer 2000, China). Soil pH was measured when the soil: water ratio was 1:5. Salinity was measured by conductometric analysis. The physicochemical features of these soils are summarized in **Table 1**. The soils were pre-incubated for 7 days at room temperature (25 ± 5°C) in the dark and then adjusted to 45% water holding capacity (WHC) before fumigation.

Experimental Setup

The soils were sieved through a 2 mm screen before any treatments were applied. Microcosms were prepared with 220 g (dry weight) of sieved soil in 500 mL Duran® wide-neck glass bottles (Schott AG, Mainz, Germany). The fumigant DZ (98.5% purity) was obtained from Zhejiang Haizheng Chemical Co. Ltd., China. DZ was added at the typical field application rate of 58 mg kg^{-1} to both soil types, which were considered as treatment groups. The soil-fumigant mixture was homogenized using a spatula. The control group was treated without fumigant. Each treatment contained three replicates. Each microcosm bottle that contained soil was sealed with a butyl rubber stopper and an outlet port to allow sampling of the internal atmosphere using a syringe. The bottles were incubated at an ambient temperature of 28°C in daylight.

Soil Sampling and Geochemical Analyses

The N_2O emissions were measured using methods previously described (Harter et al., 2014). During the incubation stage, the soil samples in the bottles were thoroughly stirred for 10–15 min every day to create an aerobic incubation environment. At the designated time, a 10 mL gas sample was withdrawn from each bottle using a gas-tight syringe. The gas samples were transferred to a 21 mL headspace vial that was flushed with helium and evacuated (10 mL) before use. An Agilent 7890A gas chromatograph with an electron capture detector (^{63}Ni-ECD) that was connected to an Agilent 7694E headspace sampler (Agilent Technologies, United States) were used to quantify the N_2O concentrations. The gas chromatograph conditions and

TABLE 1 | Physical and chemical properties of Beijing and Jiangxi soils.

Soil name	Sand[a] %	Clay %	Silt %	Soil Type[b]	pH[c]	Salinity[d] μs/cm	OM[e] g/kg	NH_4^+-N[f] mg/kg	NO_3^--N[f] mg/kg
Beijing soil	72.9	2.7	24.3	Fluvo-aquic soil	7.2	899	30.7	9.4	58.9
Jiangxi soil	51.1	6.1	42.7	Lateritic red soil	4.3	136	24.5	30.4	28.1

[a]Soil texture was determined using a Laser Particle Size Analyzer; [b]soil taxonomic name was determined according to PRC 1:1,000,000 scale soil map. Data were provided by the Data Center for Resources and Environmental Sciences, Chinese Academy of Sciences; [c]Soil pH was measured when the soil: water ratio was 1:5; [d]salinity was measured by conductometric analysis; [e]organic matter was measured by the potassium dichromate method; [f]mineral nitrogen was extracted using 2 M KCl and measured with a continuous flow automated analyzer.

gas emission calculations used methods previously described (Loftfield et al., 1997; Wang and Wang, 2003). After each gas sample, the microcosm bottles were opened in a ventilation hood to vent any residual fumigant. At the designated time, 10 g soil sample was withdrawn from each bottle for geochemical and molecular biological analyses. After sampling, all bottles were pumped with fresh air and then returned to the incubator. During incubation the water content was controlled gravimetrically and adjusted each week to the initial WHC by adding deionized water from a spray bottle. Gas samples were collected every week (on days 10, 17, 24, 31, 38, 45, 52, and 59) and soil samples were collected on days 10, 24, 38, and 59. Soil samples were extracted for mineral nitrogen (NH_4^+-N and NO_3^--N) using 2 M KCl. The concentration of mineral nitrogen in each sample was determined using a continuous flow automated analyzer (Futura Continuous Flow Analytical System, Alliance Instruments, France). MBN was estimated using the chloroform fumigation method (Brookes et al., 1985). DAA was measured using the ninhydrin reaction method (Joergensen and Brookes, 1990).

Microbial DNA Extraction and Real-Time Quantitative PCR

Soil samples were stored at −80°C pending DNA extraction. Soil total genomic DNA was extracted from 0.25 g of each soil sample using a MoBio Powersoil® DNA Isolation Kit (Mo Bio Laboratories, United States) according to the manufacturer's protocol. The quality and concentration of extracted DNA were determined using gel electrophoresis (1% agarose) and a NanoDrop® 1000 spectrophotometer (Thermo Fisher Scientific, United States). The *nifH* gene copy number was used to quantify the abundance of bacteria capable of fixing nitrogen. The abundance of archaeal and bacterial ammonia monooxygenase and nitrite oxidases were assessed via the functional gene abundance of archaeal *amoA* (AOA *amoA*), bacterial amoA (AOB *amoA*) and *nxrB*, respectively. The abundance of bacteria capable of nitrate reduction, nitrite reduction, nitric oxide reduction and nitrous oxide reduction in denitrification were quantified by determining the copy numbers of *napA* and *narG, nirS* and *nirK, qnorB* and *cnorB,* and *nosZ* genes in the soil, respectively. Quantification of these functional marker genes as well as 16S rRNA (bacteria) was carried out using the SsoFast™ EvaGreen® Supermix (Bio-Rad Laboratories, United States) and gene-specific primers. Ten-fold serially diluted plasmids containing the target gene were constructed to generate a standard curve. Quantitative PCR was performed using CFX96 real-time PCR system (Bio-Rad, United States). Reactions mixtures of 20 μL contained 10 μL of 2 × SsoFast™ EvaGreen® Supermix, 20 ng of genomic DNA template and 0.5 μM of each primer. The details of gene-specific qPCR primers, reaction mixtures and thermal programs are listed in **Supplementary Tables S1–S3**. The MIQE guidelines (Bustin et al., 2009) were followed during the entire qPCR process for both evaluation and data analyses. These methods obtained a target genes amplification efficiency of 83–105%. The R^2 values ranged from 0.994 to 0.999. Special amplification of target genes was confirmed by melting curve analysis, which always resulted in a single peak.

High-Throughput Sequencing and Bioinformatics Analysis

MiSeq sequencing of the 16S rRNA genes in the V3–V4 regions using the total DNA extracted from Beijing soil microorganisms was conducted using the universal primer 338F [5′-ACTCCTACGGGAGGCAGCAG-3′] and 806R [5′-GGACTA CHVGGGTWTCTAAT-3′]. MiSeq sequencing was completed in equimolar and paired-end sequenced (2 × 300) on an Illumina® MiSeq sequencer (Illumina, United States) by Majorbio Biopharm Technology Co. Ltd. (Shanghai, China). The sequencing data, including reads merged and filtered, were carried out using the fast length adjustment of short reads (FLASh, Johns Hopkins University, United States) and Trimmomatic (AG Usadel, Germany). Sequences < 50 bp in length with an average quality score < 20 and those with ambiguous calls were discarded for the subsequent analyses. A total of 2,681,891 high-quality 16S rRNA reads was obtained. Sequences of the 16S rRNA gene were clustered into operational taxonomic units (OTUs) at the 97% similarity level using UPARSE (version 7.1[1]). The RDP Classifier Algorithm[2] was used to compare the taxonomy of each 16S rRNA gene sequence with the gene sequences stored in the Silva (SSU123) 16S rRNA database, based on a confidence threshold of 70%. The raw reads were deposited into the NCBI Sequence Read Archive (SRA) database (No. SRP124701). All the certified nitrogen cycle related functional microbes were collected from the NCBI database[3] (showed in **Supplementary Tables S4, S5**).

Statistical Analyses

A univariate analysis of variance (ANOVA) with the 'least significant difference (LSD)' test was applied using the SPSS

[1]http://drive5.com/uparse/

[2]http://rdp.cme.msu.edu/

[3]https://www.ncbi.nlm.nih.gov/

statistics software package, version 18.0 (IBM, United States) in order to identify the major effects of fumigation on the biochemical parameters and abundance of functional genes involved in N-cycling. The univariate ANOVA was used to reveal differences between the control and the fumigated soil microcosms. All concentration or gene copy number values from the control at each time point of sampling were individually compared with the fumigation soil microcosms. The α-diversity indices Chao1, Ace, Shannon and Simpson were calculated using the bioinformatics tool Mothur to determine the diversity of the bacterial communities in Beijing soil (Schloss et al., 2009).

Hierarchical clustering and a Heat Map analyses were used to determine changes in the relative abundance of genera of bacteria involved in N-cycling. The Bray–Curtis algorithm was used to show the relative abundance of these genera according to hierarchical clustering. A Heat Map figure and statistical correlations were generated to produce a visual display of the sequencing results using heatmap-package and vegan package in R, respectively (Version 2.15.3). Spearman's rank correlation coefficient was used to determine the relationship between N_2O emission rate, physicochemical parameters and microbial functional genes.

RESULTS

N_2O Production Rate

N_2O maximum production rates increased 9.9 times and 30 times within 10 days of DZ fumigation of Beijing soil and Jiangxi soil, respectively, compared with unfumigated soils (**Figure 1**). N_2O emission rates rapidly decreased after DZ fumigation. They returned to emission levels similar to the control by days 17 and 24 in fumigated Jiangxi soil and Beijing soil, respectively. However, significantly lower N_2O emissions in Jiangxi-fumigated soil were observed on days 38 (0.31 ± 0.12 vs. 0.73 ± 0.04 μg N kg^{-1} dry soil d^{-1}) and 52 (0.14 ± 0.03 vs. 0.48 ± 0.02 μg N kg^{-1} dry soil d^{-1}), compared with unfumigated soil.

Changes in Physiochemical Parameters

In general, compared with the unfumigated soils, fumigation with DZ significantly increased the concentration of NH_4^+-N and DAA in both soil types, whereas NO_3^--N and MBN were significantly decreased (**Table 2**). All these parameters recovered to levels similar to the control 38–59 days after fumigation (except NH_4^+-N and NO_3^--N in Jiangxi soil) (**Table 2**). However, compared to Beijing soil, DZ produced larger changes in NH_4^+-N and DAA concentrations that also persisted for longer in Jiangxi soil. For example, there were no significant differences in NH_4^+-N and NO_3^--N concentrations between the fumigated and unfumigated Beijing soil 24 days after DZ fumigation. In contrast, there was a significantly lower NO_3^--N concentration and significantly higher NH_4^+-N concentration in the fumigated Jiangxi soil compared to the unfumigated soil throughout the entire incubation period.

Changes in Abundance of 16S rRNA and N-Cycling Functional Marker Genes

Statistical analysis showed that DZ significantly decreased 16S rRNA gene copy number, but this inhibitory effect was most evident in fumigated Jiangxi soil than fumigated Beijing soil (**Figure 2**). In addition, total bacterial abundance following DZ fumigation of Beijing soil recovered to the control level 38 days after treatment. In contrast, DZ fumigation of Jiangxi soil inhibited total bacterial abundance for the entire incubation period. The copy number of the observed 11 N-cycling functional genes (*nifH,* AOA *amoA,* AOB *amoA, nxrB, napA, narG, nirK, nirS, cnorB, qnorB,* and *nosZ*) is summarized in **Figures 2–4**.

When the changes in gene abundance were examined by soil type, DZ fumigation of Beijing produced only a transient decrease in the abundance of the genes AOA *amoA, napA, narG, nirK, nirS,* and *qnorB*. Their abundance recovered to the control levels 38 days after fumigation. During this period, the genes AOB *amoA*, *cnorB,* and *nosZ* were relatively stable. DZ fumigation of Jiangxi soil, however, resulted in the long-term (observed at 59 days) reduction in the abundance of genes *nifH,* AOA

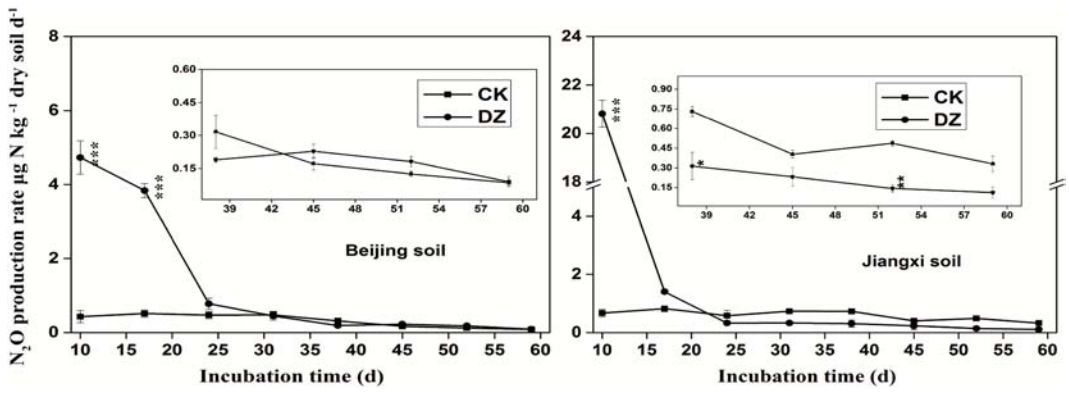

FIGURE 1 | Dynamics of N_2O production rate (μg N kg^{-1} dry soil d^{-1}) following Dazomet (DZ) fumigation of Beijing soil **(left)** and Jiangxi soil **(right)**. The small inserted graphs show a magnified view of the data for the last 23 days. Error bars represent standard errors of the means (n = 3). Statistically significant differences between the control (CK) and DZ fumigation treatments at specific time points are indicated by asterisks according to the level of significance (*$p < 0.05$, **$p < 0.01$, ***$p < 0.001$).

TABLE 2 | Values of selected biochemical parameters in fumigated and unfumigated soil over time.

Soil	Parameter	Treatment	Days after fumigation (*d*)				
			0	10	24	38	59
Beijing soil	NH_4^+-N	CK	8.22 ± 0.91	7.21 ± 0.44	6.41 ± 1.07	5.45 ± 0.54	4.97 ± 0.69
		DZ	8.51 ± 1.51	12.4 ± 2.51*	7.38 ± 0.56	5.72 ± 0.56	5.62 ± 0.23
	NO_3^--N	CK	47.4 ± 1.87	49.2 ± 1.67	50.3 ± 3.56	58.6 ± 1.05	68.2 ± 1.64
		DZ	50.8 ± 2.11	42.8 ± 1.58***	46.0 ± 0.55*	55.5 ± 2.55	67.4 ± 8.21
	MBN	CK	29.8 ± 1.77	27.2 ± 0.54	22.9 ± 1.07	20.4 ± 0.54	19.9 ± 0.69
		DZ	29.5 ± 2.11	12.4 ± 2.51***	10.3 ± 0.56***	16.7 ± 1.56	17.6 ± 0.23
	DAA	CK	6.22 ± 1.76	4.23 ± 0.67	5.32 ± 0.56	5.61 ± 0.65	6.21 ± 1.64
		DZ	5.34 ± 0.88	39.8 ± 1.58***	7.09 ± 0.85	6.56 ± 0.55	6.44 ± 1.21
Jiangxi soil	NH_4^+-N	CK	29.2 ± 0.71	28.9 ± 0.51	26.1 ± 0.76	25.1 ± 0.41	23.4 ± 0.24
		DZ	28.8 ± 1.22	39.2 ± 1.01***	42.3 ± 2.51***	43.7 ± 1.37***	43.4 ± 2.78***
	NO_3^--N	CK	22.4 ± 1.27	23.2 ± 0.61	24.5 ± 1.03	26.9 ± 0.72	31.6 ± 0.28
		DZ	23.8 ± 1.09	20.2 ± 0.35*	18.1 ± 0.03***	18.0 ± 0.29***	19.9 ± 0.15***
	MBN	CK	36.4 ± 2.45	37.2 ± 0.54	32.9 ± 1.07	32.4 ± 0.54	29.9 ± 0.69
		DZ	35.9 ± 3.12	9.45 ± 1.51***	12.3 ± 0.56***	24.7 ± 1.56	27.6 ± 0.23
	DAA	CK	3.93 ± 0.34	2.23 ± 0.47	3.32 ± 0.56	3.61 ± 0.65	4.21 ± 1.64
		DZ	5.01 ± 0.87	29.8 ± 1.38***	11.0 ± 0.45**	4.76 ± 0.75	6.54 ± 1.81

The data presented are the means and standard deviations of three separate experiments. NH_4^+-N (mg kg^{-1} soil), NO_3^--N (mg kg^{-1} soil), MBN (microbial biomass nitrogen, mg kg^{-1} soil), DAA (dissolved Amino Acids, mg kg^{-1} soil). The levels of statistical significance relative to the control are represented by asterisks ($p < 0.05$, **$p < 0.01$, ***$p < 0.001$).*

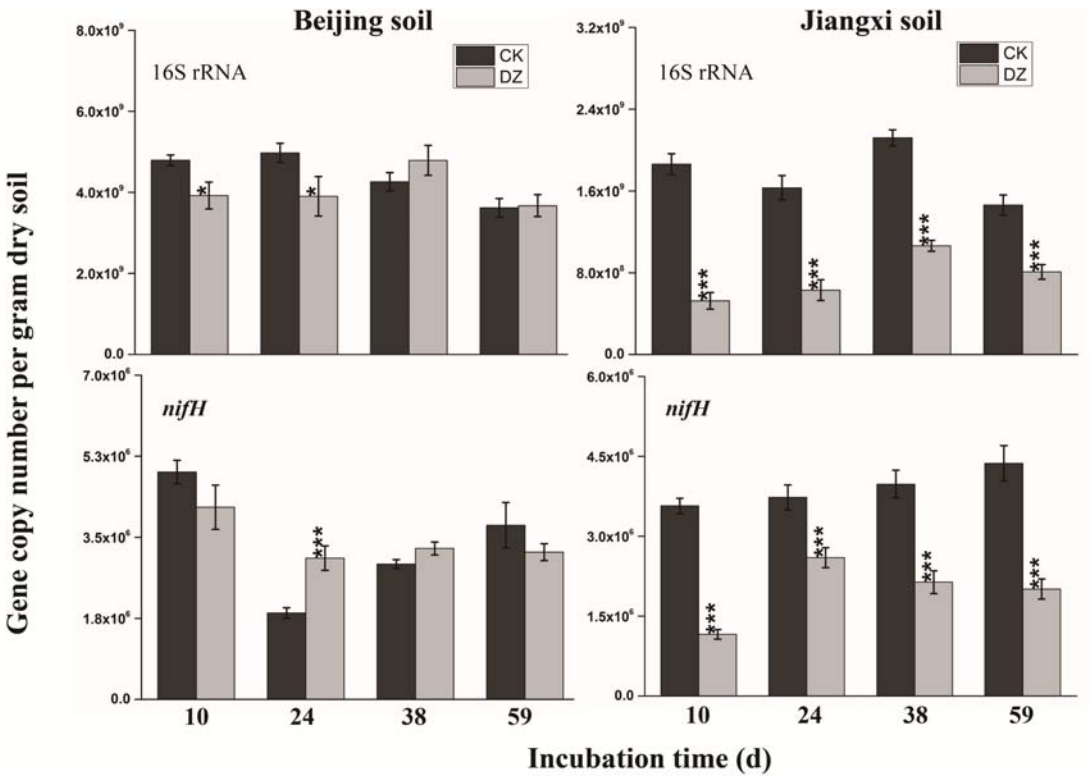

FIGURE 2 | Gene copy number per gram dry soil over time for the 16S rRNA gene and nitrogen-fixing gene (*nifH*) present in two types of soil fumigated with Dazomet (DZ) or unfumigated (CK). Error bars represent standard errors of the means ($n = 3$). Statistically significant differences between the control and fumigation treatments at a specific time points are shown by asterisks according to the level of significance (*$p < 0.05$, **$p < 0.01$, ***$p < 0.001$).

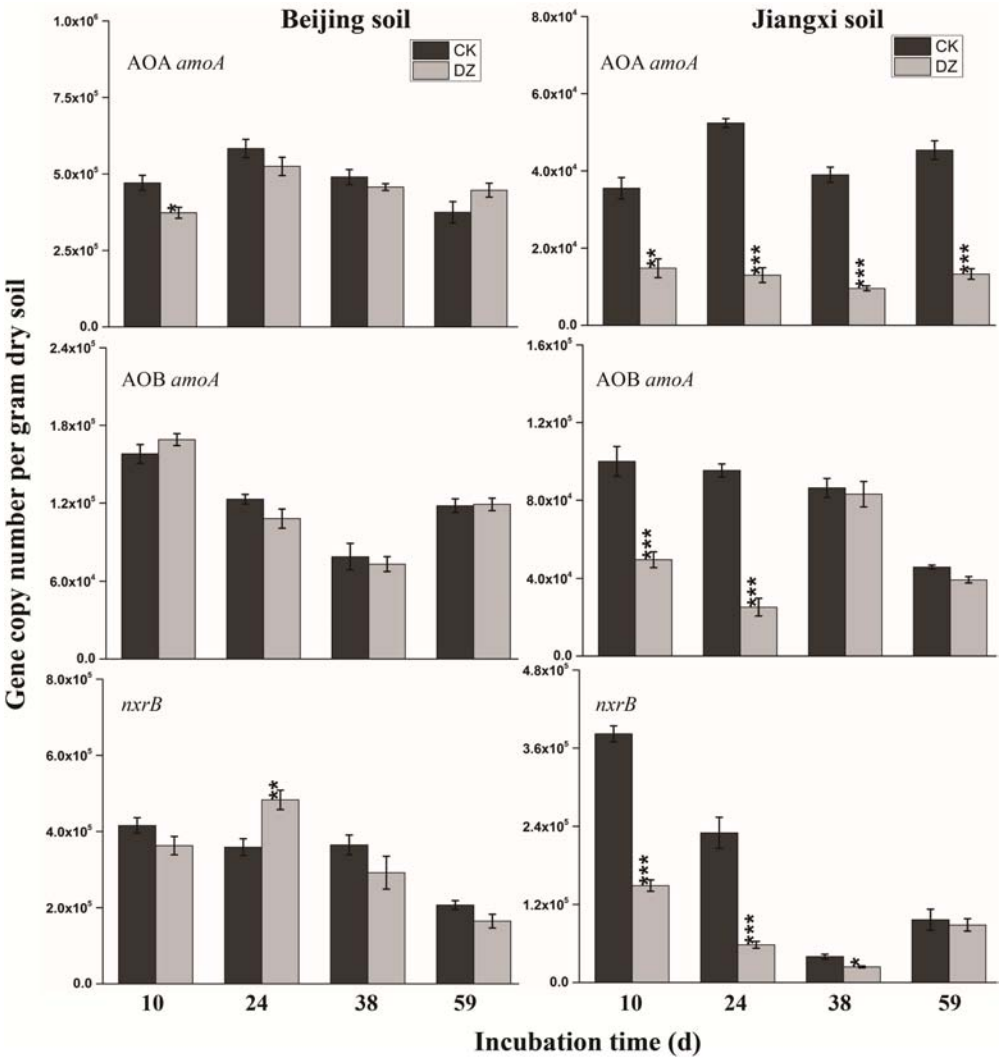

FIGURE 3 | Gene copy number per gram dry soil over time for three key genes (AOA *amoA*, AOB *amoA*, *nxrB*) involved in nitrification in two types of soil fumigated with Dazomet (DZ) or unfumigated (CK). Error bars represent standard errors of the means ($n = 3$). Statistically significant differences between the control and fumigation treatments at a specific time point are shown by asterisks (*$p < 0.05$, **$p < 0.01$, ***$p < 0.001$).

amoA, napA, narG, nirK, and *nosZ;* and fumigation triggered a short-term (∼24 days) depression in the abundance of genes AOB *amoA, cnorB, qnorB,* and *nirS*. However, the impact of DZ was not always inhibitory. The abundance of genes *nxrB* ($p = 0.007$), *nirK* ($p = 0.02$), *nirS* ($p = 0.001$), and *cnorB* ($p = 0.01$) on days 24 or 38 following DZ fumigation were significantly increased by fumigation, which suggested that DZ also has the ability to promote the growth of such N-cycling microorganisms.

Changes in Soil Bacterial Diversity and Community Composition

The 'Shannon,' 'ACE,' and 'Chao1' Diversity Indices increased significantly ($p < 0.01$) in Beijing soil fumigated with DZ and sampled 24 days after fumigation (**Table 3**) relative to those in the control group, but the Simpson Diversity Index was relatively stable. This suggested that DZ can increase the diversity of soil microbial communities, but this increase appeared to be temporary as it was eliminated by day 38.

Fumigation with DZ produced significant changes in the relative abundance of bacterial phyla as shown by changes in the abundance of the 16S rRNA gene (**Supplementary Figure S1**). This suggested that fumigation can have a significant impact on the structure of bacterial communities. For example, the abundance of predominant phyla such as *Acidobacteria* and *Chloroflexi* were significantly decreased 10 or 24 days after fumigation, whereas *Actinobacteria, Firmicutes, Gemmatimonadetes, Nitrospirae, Acidobacteria,* and *Chloroflexi* phyla increased in abundance 38–59 days after fumigation. *Proteobacteria*, however, the most frequently observed phylum involved in denitrification, increased initially and then significantly decreased by days 24 and 38.

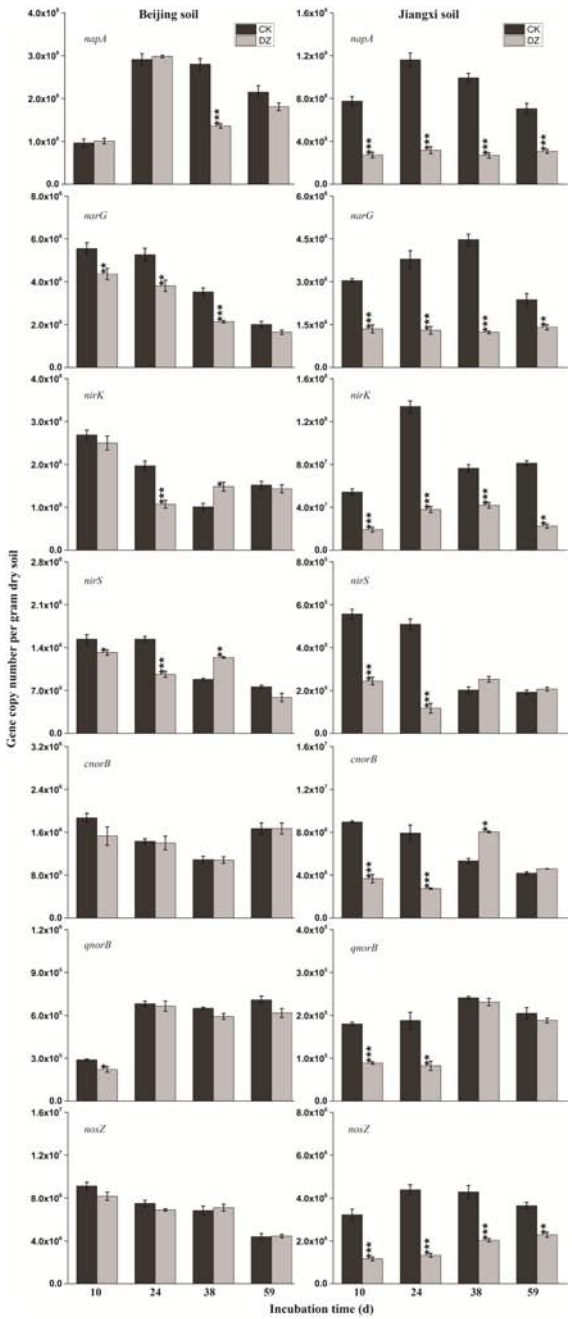

FIGURE 4 | Gene copy number per gram dry soil over time for the seven key genes (*napA, narG, nirK, nirS, cnorB, qnorB*, and *nosZ*) involved in bacterial denitrification process when present in two types of soil fumigated with Dazomet (DZ) or unfumigated (CK). Error bars represent the standard errors of the means ($n = 3$). Statistically significant differences between the control and fumigant treatments at a specific time point are shown by asterisks (*$p < 0.05$, **$p < 0.01$, ***$p < 0.001$).

Changes in Nitrogen Cycling Microorganisms

All 16S rRNA gene sequences that could be assigned to known functional genes involved in nitrogen transformation were selected to assess in more detail changes to populations of N-related bacteria in Beijing soil. The 28 genera of nitrogen cycling bacteria with the greatest abundance in our trials included 7 genera of N-fixation bacteria, 5 genera of nitrification bacteria and 16 genera of denitrification bacteria (**Figure 5**). Populations of N_2-fixing bacteria *Mesorhizobium, Azoarcus,* and *Paenibacillus* were initially reduced following DZ fumigation, while populations of *Bradyrhizobium* and *Rhizobium* were significantly increased by days 24 and 38. The abundance of ammonia-oxidizing bacteria *Nitrosospira* was increased initially by DZ fumigation, but *Nitrosomonas* abundance was significantly decreased by day 38. DZ fumigation caused a significant increase in the abundance of nitrite-oxidizing bacteria *Nitrospira* by day 59. DZ fumigation only initially increased denitrification bacteria *Anoxybacillus* and *Flavobacterium* but significantly increased *Streptomyces* populations for the entire incubation period of 59 days. However, many denitrification bacteria were decreased by DZ fumigation such as *Bacillus*, *Pseudomonas*, *Paracoccus, Cupriavidus, Sphingomonas,* and *Pseudomonas.* N_2-fixing bacteria *Azospirillum* and *Nostoc,* nitrifier bacteria *Nitrosococcus* and *Nitrolancea,* denitrifier bacteria *Ensifer*, *Mycobacterium, Thiobacillus,* and *Rhodococcus* all maintained relatively stable populations in the fumigated Beijing soil.

Linking N_2O Emission to Environmental Factors and Nitrogen Cycling Bacteria

The relationships between N_2O emissions rate, physicochemical parameters and microbial functional genes were investigated using Spearman's rank correlation coefficient (**Figure 6**). Both in fumigated Beijing soil and Jiangxi soil, the N_2O emission rates were positively correlated with NH_4^+ concentration (correlation coefficient $r > 0.43$, $p < 0.03$) and DAA ($r > 0.94$, $p < 0.00001$), but negatively correlated with MBN concentration ($r < -0.46$, $p < 0.02$). N_2O emission rates were also significantly negatively correlated with NO_3^- concentration in Beijing soil ($r = -0.57$, $p = 0.003$) but only weakly negatively correlated in Jiangxi soil ($r = -0.35$, $p = 0.08$).

However, N_2O emission rates in fumigated Beijing and Jiangxi soils showed no significant or consistent correlation with the abundance of microbial functional genes (**Figure 6**). Among the 11 genes, for example, only *qnorB* ($r = -0.65$, $p = 0.0006$) was negatively correlated with N_2O emission rate in DZ-fumigated Beijing soil, while in fumigated Jiangxi soil the negative correlation was weak ($r = -0.34$, $p = 0.1$). Furthermore, N_2O emission rates were positively correlated with *nosZ* ($r = 0.41$, $p = 0.04$) in DZ-fumigated Beijing soil, but negatively correlated ($r = -0.48$, $p = 0.01$) in DZ-fumigated Jiangxi soil.

DISCUSSION

Effects of DZ Fumigation on Bacteria Involved in the Transformation of Nitrogen

Microbial nitrogen-fixation is a primary source of new nitrogen for terrestrial ecosystems, but many environmental parameters

TABLE 3 | Diversity indices and estimated sample coverage of Beijing soil samples at the 97% sequence identity level.

Time	Treatments	Shannon	Simpson	ACE	Chao1
Day 10	CK	6.62 ± 0.07	0.0035 ± 0.0003	3773 ± 164	3744 ± 156
	DZ	6.73 ± 0.03	0.0029 ± 0.0001	3770 ± 27.4	3765 ± 14.1
Day 24	CK	6.58 ± 0.0007	0.0036 ± 0.0001	3453 ± 112	3474 ± 103
	DZ	6.74 ± 0.04**	0.0030 ± 0.0001	3958 ± 29.6**	4010 ± 63.4**
Day 38	CK	6.81 ± 0.01	0.0025 ± 0.000007	3794 ± 41.4	3769 ± 80.0
	DZ	6.70 ± 0.03	0.0029 ± 0.0001	3837 ± 93.6	3892 ± 85.2
Day 59	CK	6.76 ± 0.03	0.0028 ± 0.0001	3885 ± 125	3863 ± 157
	DZ	6.60 ± 0.04	0.0032 ± 0.0002	3487 ± 56.0	3462 ± 54.6*

*The data presented are the means and standard errors of three separate experiments. The levels of statistically significance relative to the control are represented by asterisks (*p < 0.05, **p < 0.01, ***p < 0.001).*

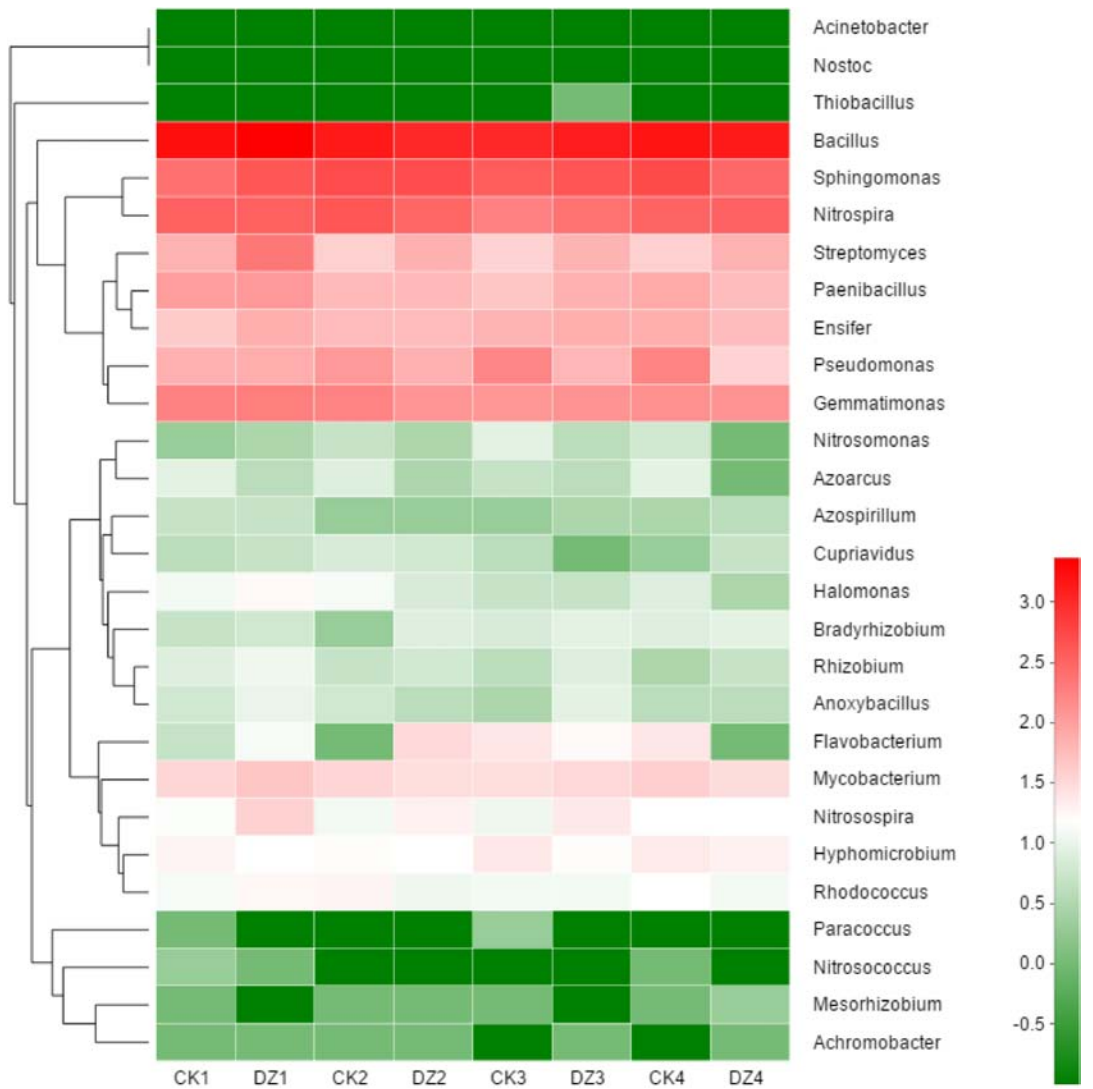

FIGURE 5 | Hierarchical clustering and a heat map show changes in the relative abundance of 28 genera of bacteria involved in nitrogen cycling after fumigation with DZ. The hierarchical clustering in the figure was based on the Bray–Curtis algorithm. It shows the relative abundance of 28 genera with the highest abundance in all the samples (dark green = rare; dark red = abundant). CK: Unfumigated control; 1, 2, 3, and 4 represent the four sampling time points of 10, 24, 38, and 59 days, respectively.

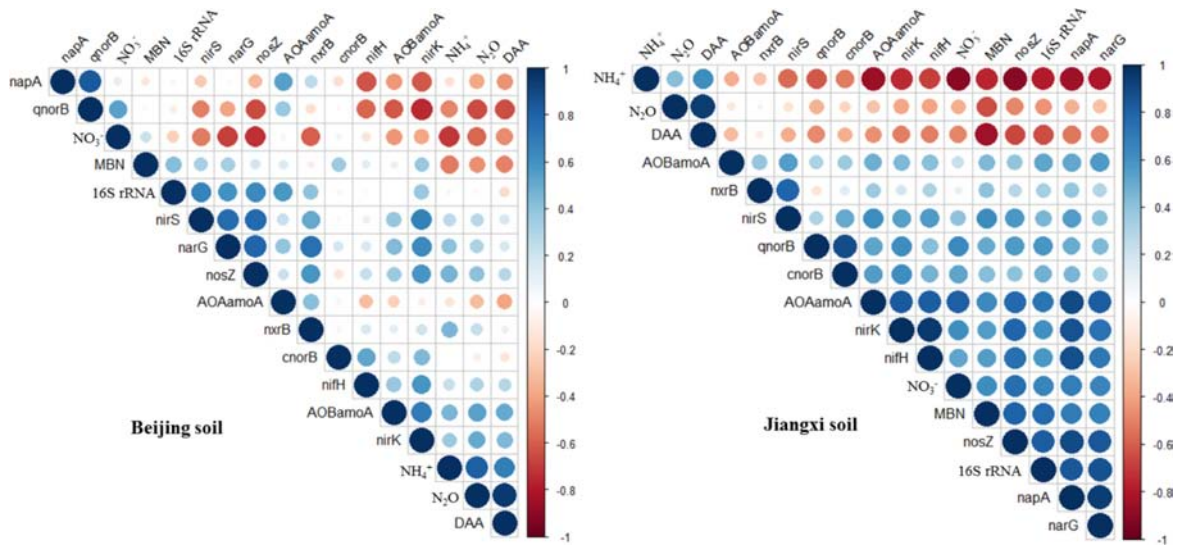

FIGURE 6 | Correlation matrices between N_2O emission rate, related functional genes and physicochemical parameters in dazomet-fumigated Beijing soil **(left)** and Jiangxi soil **(right)**. Smaller circles represent weaker Spearman's rank correlation coefficients than larger circles.

and farm operations such as fertilization and fumigation can moderate this biological process (Reed et al., 2010; Zheng et al., 2016). Previous research reported that fungicides (such as myclobutanil) and fumigants (such as metam sodium) can briefly inhibit the expression of the nitrogen-fixing functional gene *nifH* (Ju et al., 2016; Li et al., 2017a). We observed, however, that the abundance of *nifH* was increased in fumigated Beijing soil, suggesting that DZ can increase populations of nitrogen-fixing bacteria that contain *nifH*-encoding enzymes. Correlation analysis (**Supplementary Figure S2**) also showed that the abundance of *nifH* was positively correlated with the nitrogen-fixing genera *Paenibacillus* ($r = 0.49$, $p = 0.016$).

In general, the abundance of soil microorganisms is limited by nitrogen availability (Fisk and Fahey, 2001). The addition of nutrients to the soil increases the availability of nitrogen for microbes, which increases their populations (Fisk and Fahey, 2001; Fierer et al., 2003). Microorganisms are reported to adjust their efficiency of their use of carbon and nitrogen according to the environmental conditions (Mooshammer et al., 2014). Efficient use of carbon promotes microorganism abundance (Manzoni et al., 2012). The increase in the abundance of *nifH*–type bacteria 24 to 38 days after DZ fumigation in our trials might be due to the increased availability of nutrients such as NH_4^+-N, compared to unfumigated soils.

Mineral nitrogen content in soil can also increase as a result of the decomposition of microbes killed by fumigation. Microbial debris has been reported to increase nitrogen (Shen et al., 1984; De Neve et al., 2004). Our research showed there was a significant increase in NH_4^+-N concentration following DZ fumigation (**Table 2**). However, multiple NH_4^+-N consumption and production pathways, including ammonia oxidation, denitrification, and dissimilatory/assimilatory nitrate reduction to ammonium, can change the NH_4^+-N concentration in the soil. Our research suggested that a decrease in ammonia-oxidizing bacterial abundance might reduce ammonia oxidation, which in turn would prevent the utilization of NH_4^+. Although the abundance of the AOB *amoA* functional marker gene was relatively stable in fumigated Beijing soil over the entire incubation period of 59 days, the population of *Nitrosospira* was significantly decreased by DZ fumigation during this period (**Figure 5**). The inhibition of AOA and AOB functional marker genes (**Figure 3**) resulted in a larger concentration and a prolonged presence of NH_4^+-N in fumigated Jiangxi soil rather than in Beijing soil (**Table 2**). Microbial decomposition leads to increased microbial debris in the soil (Shen et al., 1984; De Neve et al., 2004; Yan et al., 2013, 2017). Therefore, our observation of decreased MBN and increased DAA concentrations in fumigated soil (**Table 2**) were most likely due to microorganism decomposition, suggesting that DZ promoted organic decomposition.

The decrease in NO_3^--N (**Table 2**) that we observed in fumigated soils could be attributed to microbes transforming nitrate, as reported previously (Sanders et al., 2013). The gene *nxrB* encodes nitrite oxidoreductase which converts NO_2^- to NO_3^-; and *napA*/*narG* encodes nitrate reductase which converts NO_3^- to NO_2^- (Canfield et al., 2010). We observed that the abundance of *nxrB* and *napA*/*narG* were significantly decreased while NO_3^--N was continuously utilized in DZ-fumigated Jiangxi soil, which disassociated nitrifier/denitrifier bacterial abundance with associated nitrogen metabolism. This is inconsistent with reports that considered the abundance of microbial genes associated with N-cycling being a good predictor of potential nitrification and denitrification rates (Petersen et al., 2012). However, researchers have also demonstrated that denitrifying bacterial abundance and diversity can be decoupled from N-recycling (Attard et al., 2011; Dandie et al., 2011). In theory, the abundance of a functional gene could be a better indicator of microbial activity than bacterial abundance and diversity

(Ka et al., 1997). Although *napA* and *narG* genes were reduced in abundance, DZ fumigation increased the relative population of denitrifying bacteria with *napA*- or *narG*-encoding enzymes, such as *Streptomyces, Anoxybacillus*, and *Flavobacterium* genera (**Figure 5**), which are known to have a role in NO_3^- metabolism.

Dazomet fumigation caused a significant decrease in populations of *Pseudomonas, Nitrosomonas,* and *Paracoccus* genera soon after fumigation, based on a reduction in *nirS* or *nirK*-encoding enzymes observed in our research. Previous studies reported *nirS* and *nirK* were also reduced by metam sodium fumigation. Chloropicrin fumigation, conversely, generated an increase in both *nirS* and *nirK* gene abundance (Li et al., 2017b). The diverse response of functional genes to fumigants may be due to (1) differences in the sensitivity of the functional genes; and (2) variations in the environmental performance of fumigants and their interaction with the physicochemical characteristics of different soils. DZ caused a significant increase in *nirS* and *nirK* abundance in Beijing soil that we observed on day 38, which suggested that DZ has the ability to promote the growth of *nirS* and *nirK*-type bacteria. The two different types of nitrite reductases that are responsible for nitrite reduction, either a cytochrome cd1 encoded by *nirS* or a Cu-containing enzyme encoded by *nirK*, are generally reported as the principal regulators in denitrification (Kandeler et al., 2006). In our study, we found a greater inhibition of *nirK* than *nirS* following DZ fumigation, suggesting that bacterial denitrifiers that possess copper nitrite reductase were more sensitive to DZ.

Although the abundance of *cnorB* and *qnorB* functional genes was relative stable in DZ-fumigated Beijing soil, populations of denitrifying bacteria containing these genes (such as the genera *Pseudomonas, Bacillus, Sphingomonas,* and *Cupriavidus*) were significantly reduced. We also observed that the abundance of denitrifying bacteria containing these genes was also reduced in DZ-fumigated Jiangxi soil. Two different nitric oxide reductases (Nor), which are encoded by the quinol-oxidizing single-subunit class (*qnorB*) and cytochrome bc-type complex (*cnorB*), are responsible for catalyzing the reduction of NO to N_2O (Braker and Tiedje, 2003). The poor stability of nitric oxide reductases, together with the cytotoxic effects of NO, results in the nitric oxide reduction process receiving less research attention. However, NO is unfavorable to many biological processes, such as biofilm formation, symbiosis and quorum sensing (Terasaka et al., 2017). Bacteria contain protective mechanisms to avoid the cytotoxic effects of NO during the process of denitrification. Nitric oxide reduction (NO to N_2O) is the most direct way to consume nitric oxide in soil. The decrease in the abundance of *cnorB* and *qnorB*-type denitrifiers, which would reduce NO consumption, results in less cytotoxic NO accumulation and emissions. Furthermore, nitric oxide reduction in the denitrification process is considered to be the primary source of N_2O produced in the soil (Ma et al., 2008). The inhibition of this process would theoretically cause the accumulation of large amounts of N_2O. We observed a significant increase in N_2O emissions in DZ-fumigated soil than unfumigated treatments (**Figure 1**). However, the abundance of denitrifying bacteria containing *nosZ*, such as the predominant genera *Pseudomonas*, as well as *Paracoccus, Cupriavidus,* and *Sphingomonas*, decreased following DZ fumigation, while at the same time we observed an increase in the abundance of *Streptomyces*. Multiple pathways are known to lead to N_2O production including nitrification, nitrifier-denitrification, heterotrophic nitrification and chemical denitrification. Further research is needed to fully understand the pathways of N_2O production or reduction by denitrifying bacteria in fumigated soil.

Effects of DZ Fumigation on N_2O Emissions

Increased N_2O production in soil has been attributed to the use of one or more pathways used by microbes involved in the nitrogen transformation processes (Ravishankara et al., 2009). We observed a significant correlation between N_2O emissions and increased concentrations of NH_4^+ and DAA. We surmise that the observed increase in N_2O emissions from fumigated soil was due the availability of alternative electron acceptors and donors that became available due to significant increases in NH_4^+-N and DAA. Conversely, the significant reduction in N_2O emissions after fumigation might be due to insufficient NH_4^+-N and DAA. Yan et al. (2015) observed similar correlations between increased N_2O emissions and increased DAA concentrations. As NH_4^+-N and DAA concentrations decreased, N_2O emissions reduced because electron donors and acceptors for microbial N_2O formation become scarce, which then limits N_2O emissions (Harter et al., 2014).

Previous studies identified ammonium as the main source for N_2O emissions, second only to N-based fertilizers (Bremner and Blackmer, 1979). Other research suggested that substrate availability (such as dissolved organic carbon, NO_3^- and NH_4^+) was a major factor limiting N_2O emissions in dry ecosystems (Liu et al., 2013). Assimilation of nitrogen from an exogenous source, such as dissolved organic nitrogen and inorganic nitrogen, was required for organism's growth and biosynthesis (Sanders et al., 2013). Soil amended with a source of carbon significantly stimulated nitrate reduction and denitrification activity (Henry et al., 2008; Miller et al., 2008), which increased both production and consumption of N_2O, respectively.

Production of N_2O can be mediated by microbial nitrification and denitrification functional gene groups. However, in many cases the abundance of these nitrification and denitrification genes may not be related to the N_2O emissions (Čuhel et al., 2010). Our research showed that the abundance of most nitrogen transformational genes (e.g., *nifH,* AOA *amoA,* AOB *amoA, nxrB* and *napA, narG, nirS, nirK, cnorB*) was not correlated with N_2O emissions, while *qnorB* and *nosZ* genes showed an inconsistent and unstable correlation with N_2O emissions in Beijing and Jiangxi soils (**Figure 6**). This suggested that the presence of these genes might not be the main factor governing N_2O emissions. The microbial community involved in nitrogen transformation is diverse, consisting of archaea, bacteria and fungi. Previous research reported a functional redundancy in this community that in effect decouples the relationship between functional gene abundance and

N_2O emissions (Wertz et al., 2007; Liu et al., 2013). In addition, changes in the rates of denitrification are a complex mix of the physiological activity of individual cells, denitrifier bacterial abundance and community microbe composition (Attard et al., 2011). Under specific environmental conditions, different strains of denitrifiers within a species were reported to generate different levels of denitrification and therefore community composition can influence community activity (Ka et al., 1997; Salles et al., 2009). Therefore, given this understanding based on previous research, it is reasonable to assume that functional gene abundance we observed might not necessarily be correlated with N_2O emissions in DZ-fumigated soil. On the other hand, our results showed that soil environmental factors (NH_4^+, DAA, MBN) were more significantly correlated to N_2O emissions than functional gene abundance (**Figure 6**), indicating that fumigant-induced shifts in nutrient availability and specific soil environmental factors have a significant impact on N_2O emissions. Our results agree with previous research reports of N_2O emission being more related to changes in soil environmental conditions than denitrifier microbial abundance (Attard et al., 2011; Liu et al., 2013). At the same time, other research reported that under conditions of limited carbon supply in soils, N_2O emissions were more closely related microbial respiration than to denitrifier abundance (Henry et al., 2008; Miller et al., 2008).

The Effect of Soil Physicochemical Parameters on N_2O Emission Rates

The different rates of N_2O emissions in Beijing and Jiangxi soil types (**Figure 1**) suggest that the soil's physicochemical parameters are important factors governing the rates of N_2O emissions from fumigated soil. Soil pH is one of the most important factors influencing both denitrification and N_2O production. In general, both denitrification rate and N_2O production increase with increasing pH values (up to the optimum pH) (Šimek and Cooper, 2002). However, higher N_2O emissions were observed in Jiangxi (acidic soil, pH = 4.3) than in Beijing (alkaline soil, pH = 7.2) following DZ fumigation (**Figure 1**). We deduce that fumigant-induced changes in N_2O production and reduction were more significant than could be attributed soil pH alone. The dissimilar physicochemical properties of the soils resulted in different responses when they were fumigated with DZ. We observed significantly higher NH_4^+ and lower NO_3^- concentrations in Beijing soil following DZ fumigation compared to the control on day 10 or day 24, but continuously higher NH_4^+ and lower NO_3^- in the Jiangxi soil throughout the entire incubation period of 59 days. This indicated that DZ-fumigated Jiangxi soil retained NH_4^+ at higher concentrations and NO_3^- at lower concentrations for a longer time than DZ-fumigated Beijing soil.

Considering the role of functional genes, we observed a greater reduction in Jiangxi soil than in Beijing soil in the abundance of the 11 nitrogen transfer genes and the 16S rRNA gene after DZ fumigation. Researchers reported that microbes in acidic soil were more sensitive to hexaconazole fungicide than those in alkaline soil (Ju et al., 2017). We observed a temporary inhibition of the functional genes in the Beijing soil and a fast recovery to levels similar to the control, probably because Beijing soils are alkaline and DZ is less persistent in such soils. The recovery of the functional genes is therefore closely linked with the persistence of DZ in the soil. Several studies reported that pesticides such as fosthiazate and hexaconazole were more persistent in acidic soils (Singh, 2002; Pantelelis et al., 2006). Furthermore, fumigants had a faster degradation rate in sandy loam soil compared to other soil types (Qin et al., 2016), which would account for the longer persistence of DZ in Jiangxi than in Beijing soil. The longer persistence of DZ or its metabolite acted to delay the recovery of the functional genes and the gene-encoded microbes in the Jiangxi soil. We deduce that microbes inhibited initially by DZ fumigation were able to recover faster in the alkaline Beijing soil than in the more acidic Jiangxi soil where DZ concentrations were able to persist for a longer period of time.

CONCLUSION

In summary, fumigation with DZ produced a significant decrease in the abundance of 16S rRNA and eleven functional genes present in microbes involved in N-cycling in a lateritic red soil (Jiangxi soil). This inhibition effect was also present in DZ-fumigated fluvo-aquic soil (Beijing soil) but weaker. DZ also temporarily stimulated bacterial diversity as well as caused a significant change in bacterial community composition. The N_2O emissions in fumigated soil were significantly correlated with key soil environmental factors (NH_4^+, DAA, MBN) and not functional gene abundance. However, when the concentrations of the fumigant declined and the inhibitory effects of DZ fumigation disappeared, the soil microbial community recovered to population levels observed in unfumigated soils. The microbial recovery rate, however, depended on the physicochemical properties of the soil. Laboratory research over a period of 3 months that examined changes in bacterial RNA levels can provides a useful and reliable method for examining the response of N-cycling microbes to soil fumigation with DZ. However, one needs to take into account that under non-destructive sampling how the nitrogen cycling microorganism response to DZ fumigation. In addition, field work using similar methods to monitor changes populations of N-cycling bacteria could usefully validate this laboratory work, particularly as it would take into account the natural microbial variability present in the soil prior to fumigation. However, our laboratory work that documents changes in the relative abundance of nitrogen transforming microbes provides (i) new mechanistic insights into the effect of soil fumigation on the structure and functioning of the N-cycling soil microbial community; and (ii) an explanation for the observed increase in N_2O emissions as a result of soil fumigation.

AUTHOR CONTRIBUTIONS

WF and AC designed the study and wrote the experimental protocol. WF, BH, and XLW measured the N_2O emissions. WF,

XNW, JL, and DY performed most of the experiments. WF, XL, YL, and CO carried out the literature search and analyses. WF and QW analyzed the data. WF, QW, and AC were responsible for the overall design and wrote the scientific paper.

FUNDING

This work was supported by the National Key Research and Development Program of China (2017YFD0201600).

ACKNOWLEDGMENTS

We thank Dr. Tom Batchelor for providing comments on the manuscript.

SUPPLEMENTARY MATERIAL

The Supplementary Material for this article can be found online at: https://www.frontiersin.org/articles/10.3389/fmicb.2018.02529/full#supplementary-material

REFERENCES

Álvarez-Martín, A., Hilton, S. L., Bending, G. D., Rodríguez-Cruz, M. S., and Sánchez-Martín, M. J. (2016). Changes in activity and structure of the soil microbial community after application of azoxystrobin or pirimicarb and an organic amendment to an agricultural soil. *Appl. Soil Ecol.* 106, 47–57. doi: 10.1016/j.apsoil.2016.05.005

Attard, E., Recous, S., Chabbi, A., De Berranger, C., Guillaumaud, N., Labreuche, J., et al. (2011). Soil environmental conditions rather than denitrifier abundance and diversity drive potential denitrification after changes in land uses. *Glob. Change Biol.* 17, 1975–1989. doi: 10.1111/j.1365-2486.2010.02340.x

Braker, G., and Tiedje, J. M. (2003). Nitric oxide reductase (norB) genes from pure cultures and environmental samples. *Appl. Environ. Microbiol.* 69, 3476–3483. doi: 10.1128/AEM.69.6.3476-3483.2003

Bremner, J., and Blackmer, A. (1979). Effects of acetylene and soil water content on emission of nitrous oxide from soils. *Nature* 280, 380–381. doi: 10.1038/280380a0

Brookes, P., Landman, A., Pruden, G., and Jenkinson, D. (1985). Chloroform fumigation and the release of soil nitrogen: a rapid direct extraction method to measure microbial biomass nitrogen in soil. *Soil Biol. Biochem.* 17, 837–842. doi: 10.1016/0038-0717(85)90144-0

Bustin, S. A., Benes, V., Garson, J. A., Hellemans, J., Huggett, J., Kubista, M., et al. (2009). The MIQE guidelines: minimum information for publication of quantitative real-time PCR experiments. *Clin. Chem.* 55, 611–622. doi: 10.1373/clinchem.2008.112797

Canfield, D. E., Glazer, A. N., and Falkowski, P. G. (2010). The evolution and future of Earth's Nitrogen cycle. *Science* 330, 192–196. doi: 10.1126/science.1186120

Crouzet, O., Poly, F., Bonnemoy, F., Bru, D., Batisson, I., Bohatier, J., et al. (2016). Functional and structural responses of soil N-cycling microbial communities to the herbicide mesotrione: a dose-effect microcosm approach. *Environ. Sci. Pollut. Res.* 23, 4207–4217. doi: 10.1007/s11356-015-4797-8

Čuhel, J., Šimek, M., Laughlin, R. J., Bru, D., Chèneby, D., Watson, C. J., et al. (2010). Insights into the effect of soil pH on N_2O and N_2 emissions and denitrifier community size and activity. *Appl. Environ. Microbiol.* 76, 1870–1878. doi: 10.1128/AEM.02484-09

Dandie, C. E., Wertz, S., Leclair, C. L., Goyer, C., Burton, D. L., Patten, C. L., et al. (2011). Abundance, diversity and functional gene expression of denitrifier communities in adjacent riparian and agricultural zones. *FEMS Microbiol. Ecol.* 77, 69–82. doi: 10.1111/j.1574-6941.2011.01084.x

De Neve, S., Csitári, G., Salomez, J., and Hofman, G. (2004). Quantification of the effect of fumigation on short-and long-term nitrogen mineralization and nitrification in different soils. *J. Environ. Qual.* 33, 1647–1652. doi: 10.2134/jeq2004.1647

Fierer, N., Allen, A. S., Schimel, J. P., and Holden, P. A. (2003). Controls on microbial CO_2 production: a comparison of surface and subsurface soil horizons. *Glob. Change Biol.* 9, 1322–1332. doi: 10.1046/j.1365-2486.2003.00663.x

Fisk, M. C., and Fahey, T. J. (2001). Microbial biomass and nitrogen cycling responses to fertilization and litter removal in young northern hardwood forests. *Biogeochemistry* 53, 201–223. doi: 10.1023/A:1010693614196

Harter, J., Krause, H. M., Schuettler, S., Ruser, R., Fromme, M., Scholten, T., et al. (2014). Linking N2O emissions from biochar-amended soil to the structure and function of the N-cycling microbial community. *ISME J. Multidiscip. J. Microb. Ecol.* 8, 660–674. doi: 10.1038/ismej.2013.160

Henry, S., Texier, S., Hallet, S., Bru, D., Dambreville, C., Cheneby, D., et al. (2008). Disentangling the rhizosphere effect on nitrate reducers and denitrifiers: insight into the role of root exudates. *Environ. Microbiol.* 10, 3082–3092. doi: 10.1111/j.1462-2920.2008.01599.x

Joergensen, R., and Brookes, P. (1990). Ninhydrin-reactive nitrogen measurements of microbial biomass in 0.5 M K2SO4 soil extracts. *Soil Biol. Biochem.* 22, 1023–1027. doi: 10.1016/0038-0717(90)90027-W

Jonathan, B., William, C., and Monisha, K. (2005). *Overview of the Use and Usage of Soil Fumigants*. Washington, DC: US EPA.

Ju, C., Xu, J., Wu, X., Dong, F., Liu, X., Tian, C., et al. (2017). Effects of hexaconazole application on soil microbes community and nitrogen transformations in paddy soils. *Sci. Total Environ.* 609, 655–663. doi: 10.1016/j.scitotenv.2017.07.146

Ju, C., Xu, J., Wu, X., Dong, F., Liu, X., and Zheng, Y. (2016). Effects of myclobutanil on soil microbial biomass, respiration, and soil nitrogen transformations. *Environ. Pollut.* 208(Pt B), 811–820. doi: 10.1016/j.envpol.2015.11.003

Ka, J.-O., Urbance, J., Ye, R. W., Ahn, T.-Y., and Tiedje, J. M. (1997). Diversity of oxygen and N-oxide regulation of nitrite reductases in denitrifying bacteria. *FEMS Microbiol. Lett.* 156, 55–60. doi: 10.1016/S0378-1097(97)00404-7

Kandeler, E., Deiglmayr, K., Tscherko, D., Bru, D., and Philippot, L. (2006). Abundance of narG, nirS, nirK, and nosZ Genes of denitrifying bacteria during primary successions of a glacier foreland. *Appl. Environ. Microbiol.* 72, 5957–5962. doi: 10.1128/AEM.00439-06

Li, J., Huang, B., Wang, Q., Li, Y., Fang, W., Han, D., et al. (2017a). Effects of fumigation with metam-sodium on soil microbial biomass, respiration, nitrogen transformation, bacterial community diversity and genes encoding key enzymes involved in nitrogen cycling. *Sci. Total Environ.* 598, 1027–1036. doi: 10.1016/j.scitotenv.2017.02.058

Li, J., Huang, B., Wang, Q., Li, Y., Fang, W., Yan, D., et al. (2017b). Effect of fumigation with chloropicrin on soil bacterial communities and genes encoding key enzymes involved in nitrogen cycling. *Environ. Pollut.* 227, 534–542. doi: 10.1016/j.envpol.2017.03.076

Lin, C.-M., Preston Iii, J. F., and Wei, C.-I. (2000). Antibacterial mechanism of allyl isothiocyanate. *J. Food Prot.* 63, 727–734. doi: 10.4315/0362-028X-63.6.727

Liu, X., Chen, C., Wang, W., Hughes, J., Lewis, T., Hou, E., et al. (2013). Soil environmental factors rather than denitrification gene abundance control N_2O fluxes in a wet sclerophyll forest with different burning frequency. *Soil Biol. Biochem.* 57, 292–300. doi: 10.1016/j.soilbio.2012.10.009

Liu, X., Cheng, X., Wang, H., Wang, K., and Kang, Q. (2015). Effect of fumigation with 1,3-dichloropropene on soil bacterial communities. *Chemosphere* 139, 379–385. doi: 10.1016/j.chemosphere.2015.07.034

Loftfield, N., Flessa, H., Augustin, J., and Beese, F. (1997). Automated gas chromatographic system for rapid analysis of the atmospheric trace gases methane, carbon dioxide, and nitrous oxide. *J. Environ. Qual.* 26, 560–564. doi: 10.2134/jeq1997.00472425002600020030x

Ma, W. K., Bedardhaughn, A., Siciliano, S. D., and Farrell, R. E. (2008). Relationship between nitrifier and denitrifier community composition and abundance in predicting nitrous oxide emissions from ephemeral wetland soils. *Soil Biol. Biochem.* 40, 1114–1123. doi: 10.1016/j.soilbio.2007.12.004

Manzoni, S., Taylor, P., Richter, A., Porporato, A., and Gren, G. I. (2012). Environmental and stoichiometric controls on microbial carbon-use efficiency in soils. *New Phytol.* 196, 79–91. doi: 10.1111/j.1469-8137.2012.04225.x

Mao, L., Wang, Q., Yan, D., Ma, T., Liu, P., Shen, J., et al. (2014). Evaluation of chloropicrin as a soil fumigant against *Ralstonia solanacearum* in ginger (*Zingiber officinale* Rosc.) production in China. *PLoS One* 9:e91767. doi: 10.1371/journal.pone.0091767

Martin, F. N. (2003). Development of alternative strategies for management of soilborne pathogens currently controlled with methyl bromide. *Annu. Rev. Phytopathol.* 41, 325–350. doi: 10.1146/annurev.phyto.41.052002.095514

Miller, M., Zebarth, B., Dandie, C., Burton, D., Goyer, C., and Trevors, J. (2008). Crop residue influence on denitrification, N_2O emissions and denitrifier community abundance in soil. *Soil Biol. Biochem.* 40, 2553–2562. doi: 10.1016/j.soilbio.2008.06.024

Mooshammer, M., Wanek, W., Hämmerle, I., Fuchslueger, L., Hofhansl, F., Knoltsch, A., et al. (2014). Adjustment of microbial nitrogen use efficiency to carbon: nitrogen imbalances regulates soil nitrogen cycling. *Nat. Commun.* 5:3694. doi: 10.1038/ncomms4694

Pantelelis, I., Karpouzas, D. G., Menkissoglu-Spiroudi, U., and Tsiropoulos, N. (2006). Influence of soil physicochemical and biological properties on the degradation and adsorption of the nematicide fosthiazate. *J. Agric. Food Chem.* 54, 6783–6789. doi: 10.1021/jf061098p

Petersen, D. G., Blazewicz, S. J., Firestone, M., Herman, D. J., Turetsky, M., and Waldrop, M. (2012). Abundance of microbial genes associated with nitrogen cycling as indices of biogeochemical process rates across a vegetation gradient in Alaska. *Environ. Microbiol.* 14, 993–1008. doi: 10.1111/j.1462-2920.2011.02679.x

Qiao, K., Shi, X., Wang, H., Ji, X., and Wang, K. (2011). Managing root-knot nematodes and weeds with 1,3-dichloropropene as an alternative to methyl bromide in cucumber crops in China. *J. Agric. Food Chem.* 59, 2362–2367. doi: 10.1021/jf104553f

Qiao, K., Zhu, Y., Wang, H., Ji, X., and Wang, K. (2012). Effects of 1,3-dichloropropene as a methyl bromide alternative for management of nematode, soil-borne disease, and weed in ginger (*Zingiber officinale*) crops in China. *Crop Prot.* 32, 71–75. doi: 10.1016/j.cropro.2011.08.017

Qin, R., Gao, S., Ajwa, H., and Hanson, B. D. (2016). Effect of application rate on fumigant degradation in five agricultural soils. *Sci. Total Environ.* 541, 528–534. doi: 10.1016/j.scitotenv.2015.09.062

Ravishankara, A. R., Daniel, J. S., and Portmann, R. W. (2009). Nitrous Oxide (N_2O): the dominant ozone-depleting substance emitted in the 21st century. *Science* 326, 123–125. doi: 10.1126/science.1176985

Reed, S. C., Cleveland, C. C., and Townsend, A. R. (2010). Controls over leaf litter and soil nitrogen fixation in two lowland tropical rain forests. *Biotropica* 39, 585–592. doi: 10.1111/j.1744-7429.2007.00310.x

Salles, J. F., Poly, F., Schmid, B., and Roux, X. L. (2009). Community niche predicts the functioning of denitrifying bacterial assemblages. *Ecology* 90, 3324–3332. doi: 10.1890/09-0188.1

Sanders, J., Beinart, R., Stewart, F., Delong, E., and Girguis, P. (2013). Metatranscriptomics reveal differences in in situ energy and nitrogen metabolism among hydrothermal vent snail symbionts. *ISME J.* 7, 1556–1567. doi: 10.1038/ismej.2013.45

Schloss, P. D., Westcott, S. L., Ryabin, T., Hall, J. R., Hartmann, M., Hollister, E. B., et al. (2009). Introducing mothur: open-source, platform-independent, community-supported software for describing and comparing microbial communities. *Appl. Environ. Microbiol.* 75, 7537–7541. doi: 10.1128/AEM.01541-09

Shen, S., Pruden, G., and Jenkinson, D. (1984). Mineralization and immobilization of nitrogen in fumigated soil and the measurement of microbial biomass nitrogen. *Soil Biol. Biochem.* 16, 437–444. doi: 10.1016/0038-0717(84)90049-X

Šimek, M., and Cooper, J. (2002). The influence of soil pH on denitrification: progress towards the understanding of this interaction over the last 50 years. *Eur. J. Soil Sci.* 53, 345–354. doi: 10.1046/j.1365-2389.2002.00461.x

Singh, N. (2002). Sorption behavior of triazole fungicides in Indian soils and its correlation with soil properties. *J. Agric. Food Chem.* 50, 6434–6439. doi: 10.1021/jf020501z

Spokas, K., Dong, W., and Venterea, R. (2005). Greenhouse gas production and emission from a forest nursery soil following fumigation with chloropicrin and methyl isothiocyanate. *Soil Biol. Biochem.* 37, 475–485. doi: 10.1016/j.soilbio.2004.08.010

Spokas, K., Wang, D., Venterea, R., and Sadowsky, M. (2006). Mechanisms of N_2O production following chloropicrin fumigation. *Appl. Soil Ecol.* 31, 101–109. doi: 10.1016/j.apsoil.2005.03.006

Terasaka, E., Yamada, K., Wang, P. H., Hosokawa, K., Yamagiwa, R., Matsumoto, K., et al. (2017). Dynamics of nitric oxide controlled by protein complex in bacterial system. *Proc. Natl. Acad. Sci. U.S.A.* 114, 9888–9893. doi: 10.1073/pnas.1621301114

Wang, Y., and Wang, Y. (2003). Quick measurement of CH4, CO2 and N2O emissions from a short-plant ecosystem. *Adv. Atmos. Sci.* 20, 842–844. doi: 10.1007/BF02915410

Wertz, S., Degrange, V., Prosser, J. I., Poly, F., Commeaux, C., Guillaumaud, N., et al. (2007). Decline of soil microbial diversity does not influence the resistance and resilience of key soil microbial functional groups following a model disturbance. *Environ. Microbiol.* 9, 2211–2219. doi: 10.1111/j.1462-2920.2007.01335.x

Yan, D., Wang, Q., Li, Y., Ouyang, C., Guo, M., and Cao, A. (2017). Analysis of the inhibitory effects of chloropicrin fumigation on nitrification in various soil types. *Chemosphere* 175, 459–464. doi: 10.1016/j.chemosphere.2017.02.075

Yan, D., Wang, Q., Mao, L., Ma, T., Li, Y., Guo, M., et al. (2015). Interaction between nitrification, denitrification and nitrous oxide production in fumigated soils. *Atmos. Environ.* 103, 82–86. doi: 10.1016/j.atmosenv.2014.09.079

Yan, D., Wang, Q., Mao, L., Ma, T., Li, Y., Guo, M., et al. (2013). Nitrification dynamics in a soil after addition of different fumigants. *Soil Sci. Plant Nutr.* 59, 142–148. doi: 10.1080/00380768.2012.754727

Zhang, S., Liu, X., Jiang, Q., Shen, G., and Ding, W. (2017). Legacy effects of continuous chloropicrin-fumigation for 3-years on soil microbial community composition and metabolic activity. *AMB Express* 7:178. doi: 10.1186/s13568-017-0475-1

Zheng, M., Chen, H., Li, D., Zhu, X., Zhang, W., Fu, S., et al. (2016). Biological nitrogen fixation and its response to nitrogen input in two mature tropical plantations with and without legume trees. *Biol. Fertil. Soils* 52, 665–674. doi: 10.1007/s00374-016-1109-5

Conflict of Interest Statement: The authors declare that the research was conducted in the absence of any commercial or financial relationships that could be construed as a potential conflict of interest.

frontiers in Microbiology

ORIGINAL RESEARCH
published: 21 November 2018
doi: 10.3389/fmicb.2018.02843

Sinorhizobium fredii Strains HH103 and NGR234 Form Nitrogen Fixing Nodules With Diverse Wild Soybeans (*Glycine soja*) From Central China but Are Ineffective on Northern China Accessions

*Francisco Temprano-Vera[1], Dulce Nombre Rodríguez-Navarro[1], Sebastian Acosta-Jurado[2], Xavier Perret[3], Romain K. Fossou[3], Pilar Navarro-Gómez[2], Tao Zhen[4], Deshui Yu[4], Qi An[4], Ana Maria Buendía-Clavería[2], Javier Moreno[5], Francisco Javier López-Baena[2], Jose Enrique Ruiz-Sainz[2] and Jose Maria Vinardell[2]**

[1] IFAPA, Centro Las Torres-Tomejil, Seville, Spain, [2] Departamento de Microbiología, Facultad de Biología, Universidad de Sevilla, Avenida Reina Mercedes, Seville, Spain, [3] Department of Botany and Plant Biology, University of Geneva, Geneva, Switzerland, [4] Institute of Microbiology, Heilongjiang Academy of Sciences, Harbin, China, [5] Departamento de Biología Celular, Facultad de Biología, Universidad de Sevilla, Seville, Spain

Sinorhizobium fredii indigenous populations are prevalent in provinces of Central China whereas *Bradyrhizobium* species (*Bradyrhizobium japonicum*, *B. diazoefficiens*, *B. elkanii*, and others) are more abundant in northern and southern provinces. The symbiotic properties of different soybean rhizobia have been investigated with 40 different wild soybean (*Glycine soja*) accessions from China, Japan, Russia, and South Korea. Bradyrhizobial strains nodulated all the wild soybeans tested, albeit efficiency of nitrogen fixation varied considerably among accessions. The symbiotic capacity of *S. fredii* HH103 with wild soybeans from Central China was clearly better than with the accessions found elsewhere. *S. fredii* NGR234, the rhizobial strain showing the broadest host range ever described, also formed nitrogen-fixing nodules with different *G. soja* accessions from Central China. To our knowledge, this is the first report describing an effective symbiosis between *S. fredii* NGR234 and *G. soja*. Mobilization of the *S. fredii* HH103 symbiotic plasmid to a NGR234 pSym-cured derivative (strain NGR234C) yielded transconjugants that formed ineffective nodules with *G. max* cv. Williams 82 and *G. soja* accession CH4. By contrast, transfer of the symbiotic plasmid pNGR234a to a pSym$^-$cured derivative of *S. fredii* USDA193 generated transconjugants that effectively nodulated *G. soja* accession CH4 but failed to nodulate with *G. max* cv. Williams 82. These results indicate that intra-specific transference of the *S. fredii* symbiotic plasmids generates new strains with unpredictable symbiotic properties, probably due to the occurrence of new combinations of symbiotic signals.

Keywords: ***Sinorhizobium*, *Bradyrhizobium*, *Glycine max*, *Glycine soja*, rhizobia-legume symbiosis**

OPEN ACCESS

Edited by:
Suhelen Egan, University of New South Wales, Australia

Reviewed by:
Euan James, James Hutton Institute, United Kingdom
Julie Ardley, Murdoch University, Australia

***Correspondence:**
Jose Maria Vinardell
jvinar@us.es

Specialty section:
This article was submitted to Microbial Symbioses, a section of the journal Frontiers in Microbiology

Received: *09 August 2018*
Accepted: *05 November 2018*
Published: *21 November 2018*

Citation:
Temprano-Vera F, Rodríguez-Navarro DN, Acosta-Jurado S, Perret X, Fossou RK, Navarro-Gómez P, Zhen T, Yu D, An Q, Buendía-Clavería AM, Moreno J, López-Baena FJ, Ruiz-Sainz JE and Vinardell JM (2018) Sinorhizobium fredii Strains HH103 and NGR234 Form Nitrogen Fixing Nodules With Diverse Wild Soybeans (Glycine soja) From Central China but Are Ineffective on Northern China Accessions. Front. Microbiol. 9:2843. doi: 10.3389/fmicb.2018.02843

INTRODUCTION

Rhizobia are α- and β-proteobacteria able to establish nitrogen-fixing symbioses with legumes (Sprent et al., 2017). The enormous ecological and economic importance of legume crops justifies the many extensive studies carried out these past four decades on rhizobia-legume symbioses. Different species belonging to the *Sinorhizobium* (=*Ensifer*) and *Bradyrhizobium* genera induce the formation of nitrogen-fixing nodules on soybean roots (Margaret et al., 2011; Yang et al., 2018). *Glycine max* [L.] Merr. (soybean) is the most important pulse legume in the world with its seeds as essential sources of proteins and oils. However, soybean is not only an important source of proteins and oils, but also a rich source of nutraceuticals compounds including bioflavonoids, lecithins, oligosaccharides, phytosterols, saponins, and tocopherols (Rosell et al., 2004; Hamilton-Reeves et al., 2007). *Glycine soja* (Siebold and Zucc.) is the wild ancestor of the domesticated soybean, *Glycine max* (recently reviewed by Kofsky et al., 2018). *G. soja* is native to East Asia and can be found in a broad geographic range that encompasses from East Russia to South China. Although wild and domesticated soybeans differ in many characteristics, the fact that they have the same number of chromosomes ($2n = 40$) and are cross-compatible make wild soybean very attractive as a potential genetic source of interesting traits that can have been partially or totally lost during domestication and improvement of *G. max* (Kofsky et al., 2018).

Soybeans are cropped on an estimated 6% of the world's arable land and, in the last 40 years, areas under soybean production increased more than any other major crop (Hartman et al., 2011). Such continuous increase in soybean production is to match a growing demand for soybean-based meals and oils. Total world soybean production has increased from 17 million metric tons (MMT) in 1960 to 320 MMT in 2015, according to the USDA data (Westcott and Hansen, 2016). Soybean production is still expected to raise with improved yields and development of additional production areas. The increase in soybean cropping is concomitant with a burgeoning inoculant industry. In fact, the development of effective rhizobial inoculants for this crop has been the key to its spread into non-native regions of the world (Alves et al., 2003).

China is the center of origin and diversification of soybean plants, where it has been cultivated for more than 5,000 years (Mammadov et al., 2018; Yang et al., 2018). According to ancient texts and mass spectrometry analyses of carbonized soybean seeds, the origin of soybean could be delimited from the North-eastern Hebei province to South-eastern areas of Northeast China. China should also be the center of origin of soybean rhizobia and the place where both symbionts coevolved. Apparently, the presence of root nodules was documented by Chinese writers from the very beginning of soybean cultivation, as illustrated by the ancient Chinese character "Shu" (soybean) that includes two dots below a horizontal stroke, which symbolizes root nodules belowground (Qiu and Chang, 2010). Slow-growing rhizobia isolated from either soybean or wild soybean nodules collected in Chinese soils belonged to diverse bradyrhizobia species including those currently classified as *Bradyrhizobium diazoefficiens*, *B. elkanii*, *B. japonicum*, *B. liaoningense*, and *B. yuanmingense*, while fast-growing soybean rhizobia belong to *Sinorhizobium fredii*, *S. sojae* or *Sinorhizobium* spp. (Tian et al., 2012; Zhao et al., 2014). The distribution of slow- versus fast-growing soybean rhizobia in Chinese provinces varies along a North–South axis (Tian et al., 2012), with fast-growers absent in Northern acidic soils (Heilongjiang, Jilin, and Liaoning provinces) that are mainly colonized by *Bradyrhizobium* species (Tian et al., 2012). Similarly, nodules of soybean plants grown in the acidic soils of Hubei, Anhui, and Jiangsu in Central China and all those provinces situated in the South mostly contain *Bradyrhizobium* strains (**Figure 1**) with few occurrences of *S. fredii* isolates (Tian et al., 2012). By contrast, the alkaline soil from Central China defined by the Huang-Huai-Hai rivers (Hebei, Shanxi, Henan, and Shandong provinces) mainly contains fast-growing soybean rhizobia, with *S. fredii* being the most abundant, as well as occasionally a few strains of *B. elkanii*, *B. liaoningense*, *B. yuanmingense*, and *Bradyrhizobium* spp. (Tian et al., 2012). Additional studies further highlighted the predominance of slow-growers in acidic soils while fast-growers dominated rhizobia populations in alkaline soils (Yang et al., 2018; Zhang et al., 2018). Thus, soil pH appears to be a decisive criterion in determining whether fast- or slow-growing soybean rhizobia communities will populate fields, including soils from alkaline spots of otherwise acidic soils of Honghu county (Hubei province) where *S. fredii* populations were found to be predominant (Camacho et al., 2002). In fact, sinorhizobial strains are often associated with legumes that are native to alkaline soils, not only in China but also in other countries such as India (Sankhla et al., 2017; Rathi et al., 2018).

The genetic differentiation and diversity from *Glycine soja* Sieb. & Zucc. to *G. max* [L.] Merr. has been studied at the DNA sequence level (Li et al., 2010, 2014; Zhou et al., 2015) and with proteomic analyses (Natarajan et al., 2007; Xu et al., 2007). Most of the reported results indicated that genetic diversity in *G. soja* was higher than in *G. max* (Qiu and Chang, 2010). The comparison of the genomes of seven *G. soja* accessions showed lineage-specific genes with variations in copy numbers and large-effect mutations, some of which may have contributed to the selection of important agronomic traits such as biotic resistance, composition of seeds, times of flowering and maturity, organ size and final biomass (Li et al., 2014).

Natural phenotypic changes affecting plant development, flowering time, seed size and color or dormancy have taken place during soybean domestication processes (Zhou et al., 2015; Mammadov et al., 2018). Wild soybeans (*G. soja*) can be a source of many elite traits, such as tolerance to salt (Luo et al., 2005), cold and dehydration stresses (Chen et al., 2006), or high lutein content (Kanamaru et al., 2006). Hence, wild soybeans can be used in breeding programs to obtain fertile hybrids of *G. max* and *G. soja* crosses (Singh, 2007; Li et al., 2010). In such *G. soja*/*G. max* hybrids, various important characteristics such as seed size, plant height and/or tolerance to waterlogging can be selected for, with some intermediate phenotypes occurring as well (Qiu and Chang, 2010).

In this work we compared the symbiotic capacity of 40 wild soybean accessions from Russia, South Korea, Japan, and China

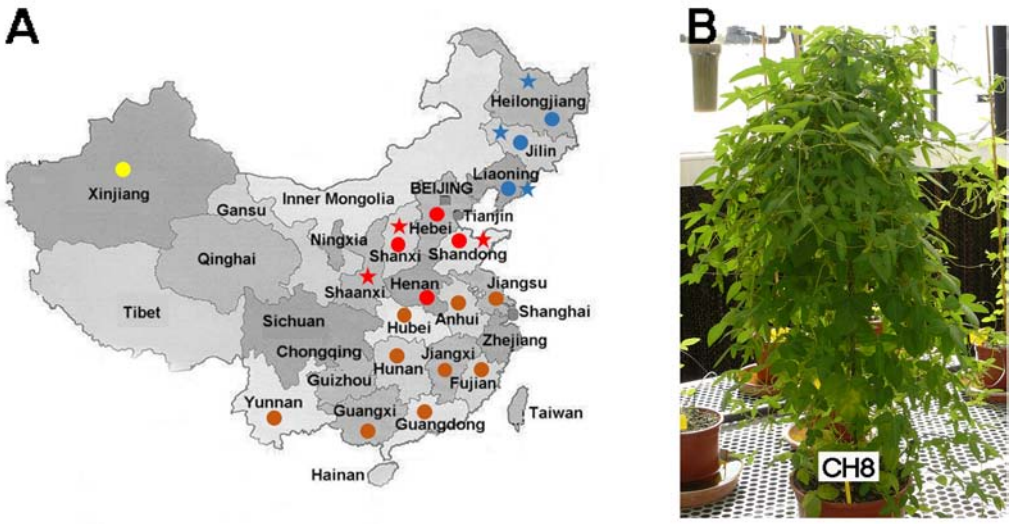

FIGURE 1 | (A) Biogeography of *Glycine soja* cultivars analyzed in this work (stars) and soybean-nodulating rhizobia (circles) studied by Tian et al. (2012). Blue and red stars indicate Northern and Central Chinese provinces, respectively. Blue, red, brown, and yellow circles indicate Northern, Central, Southern, and Western Chinese provinces respectively. According to Tian et al. (2012), *Sinorhizobium* species are predominant in Central China whereas *Bradyrhizobium* species predominate in Northern and Southern China. In Xinjiang (Western China), the proportions of *Sinorhizobium* and *Bradyrhizobium* species are similar. **(B)** A wild *G. soja* cultivar (CH8, from Heilongjiang, Northern China) grown in greenhouse conditions in Seville, Spain.

to associate with three different well-known soybean rhizobia strains: *B. diazoefficiens* USDA110^T, *B. elkanii* USDA76^T, and *S. fredii* HH103. Wild soybeans from North or Central China showed lower symbiotic efficiency with *S. fredii* HH103 than with bradyrhizobia strains USDA110^T and USDA76^T. By contrast, in association with *G. soja* accessions from Central China, strain HH103 was equally or more efficient than USDA110^T and USDA76^T strains.

In addition, several *G. soja* accessions from Central China inoculated with *S. fredii* NGR234 were found to form nitrogen-fixing nodules. Out of 30 rhizobia isolated from nodules of *Lablab purpureus* collected in a slightly alkaline soil (pH 8.5) of Papua New Guinea, NGR234 was the only fast-growing strain (soil pH 8.5) (Trinick, 1980). Because of its unsurpassed host-range (Pueppke and Broughton, 1999), NGR234 became a model to study the molecular basis of symbiotic promiscuity (Broughton et al., 2000; Perret et al., 2000), although this strain failed to nodulate all *G. max* or *G. soja* varieties tested so far (Pueppke and Broughton, 1999). Thus, to our knowledge, this is the first report of NGR234 forming proficient nitrogen-fixing nodules with *G. soja* accessions.

MATERIALS AND METHODS

Bacterial Strains, Plasmids, Culture Conditions, and Media

Bacterial strains and plasmids used in this study are listed in **Supplementary Table S1**. *S. fredii* strains were cultivated at 28°C in/on TY (Beringer, 1974), RMS (Broughton et al., 1986), or YMA (Vincent, 1970) media. *B. diazoefficiens* USDA110^T and *B. elkanii* USDA76^T were grown in/on YMA medium. *Escherichia coli* strains were cultivated on LB medium (Sambrook and Russell, 2001) at 37°C. When necessary, TY or YMA media were supplemented with streptomycin (50 μg/ml), rifampicin (50 μg/mL), chloramphenicol (5 μg/ml), kanamycin (25 μg/ml), neomycin (50 μg/ml) tetracycline (10 μg/ml), or spectinomycin (50 μg/ml). The isoflavone genistein was dissolved in ethanol and used at a final concentration of 1 μg/ml (3.7 μM). Plasmids were transferred from *E. coli* to rhizobia by conjugation as described by Simon (1984). Plasmid pMUS262 was used to detect conjugational transfer of symbiotic plasmids as described by Vinardell et al. (1993).

Construction of *Sinorhizobium fredii* Hybrids by Intra-Specific Transfer of *S. fredii* Symbiotic Plasmids

To provide a selectable marker in the transfer of plasmids by conjugation, the *S. fredii* NGR234 symbiotic plasmid p*Sf*NGR234a was tagged with transposon Tn*5*-Mob, which confers neomycin resistance (Nm^R). Random Tn*5*-Mob mutagenesis was carried out by crossing *E. coli* strain S17-1 carrying the suicide plasmid pSUP5011 with NGR234. A Nm^R derivative of NGR234, called NGR234-M, was identified by its capacity to transfer the Nm^R marker via a triparental cross between NGR234-M (as donor), *E. coli* HB101 (pRK2013) (as helper) and *Agrobacterium tumefaciens* GMI9023 Cm^R (pMUS262) (as recipient). Plasmid pMUS262 carries the *tet* gene from pBR322 [coding for tetracycline efflux MFS transporter Tet(C) protein, WP_010891057] under the control of a *nodA* promoter (p*nodA*). This construct only confers resistance to tetracycline when recipient cells are grown in presence of a

flavonoid inducer, such as genistein, that activates the NodD1 transcriptional regulator for p*nodA::tet* expression (Vinardell et al., 1993). Thus, only the symbiotic plasmid p*Sf*NGR234a that carries a functional copy of *nodD1* could change the Nm^R *A. tumefaciens* strain GMI9023 Cm^R (pMUS262) into a transconjugant resistant to tetracycline when it was grown in the presence of genistein (Vinardell et al., 1993). Then, the symbiotic plasmid of NGR234-M carrying a Tn*5*-Mob insertion, now called p*Sf*NGR234a::Tn*5*-Mob or pSymNGR234M, was mobilized into the pSym cured derivative strain called *S. fredii* USDA193C (Buendía-Clavería et al., 1989). Using another tri-parental mating, the symbiotic plasmid of *S. fredii* HH103 marked with Tn*5*-Mob (called p*Sf*HH103d::Tn*5*-Mob or pSymHH103M; Romero, 1993) was transferred to ANU265 (here after called NGR234C), a derivative strain of NGR234 cured of pNGR234a (Morrison et al., 1983).

Plant Tests

Nodulation tests on *G. max* (L.) Merr. cultivar Williams 82 (American soybean cultivar) were carried out as previously described (Buendía-Clavería et al., 1989; Yang et al., 2001). Leonard jars were used to grow plants for 6 weeks in a plant-growth chamber with a 16 h photoperiod at 25°C in the light and 18°C in the dark. *G. max* [L] and *G. soja* Sieb. & Zucc. (wild soybean) accessions from Japan, Korea, Russia, and China (**Figure 1**, **Table 1**, and **Supplementary Table S2**) were tested in a plant-growth chamber or in a greenhouse using Leonard jars. Because many *G. soja* accessions have very hard seed coats, treatments with sulfuric acid for 20 min followed by three washing steps with sterilized water were carried out. After this scarification treatment, seeds were surface sterilized with sodium hypochlorite 5% (w/v) for 5 min followed by six washes with sterilized water. Surface sterilized seeds were germinated on 1% (w/v) agar-water at 28°C for 2–3 days. Three or four germinated seeds were transferred to each sterilized Leonard jar consisting of a lower vessel with 500 ml of a pH 7 N-free half-strength nutrient solution (Rigaud and Puppo, 1975) supplemented with trace elements (Turner and Gibson, 1980) and an upper vessel with 300 ml of a mixture of moistened 2/1 (v/v) vermiculite-perlite (Camacho et al., 2002). Each seed was inoculated with approximately 10^8 bacteria. Jars were placed in a greenhouse under natural light supplemented with light lamps to reach 14 h daylight with a daily minimum-maximum temperature of 18/32°C or in a plant-growth chamber with a photoperiod of 16 h light/day and a temperature range of 18–25°C (night–day). A week after emergence, seedlings were thinned to two per jar. Forty two or 60 days after inoculation, plant tops were dried at 80°C for 48 h and weighed. The relative efficiency index (REI), that measures the accumulation of N fixed in relation to the controls (Brockwell et al., 1966), was calculated for each inoculant/wild-soybean combination. REI was defined as (I-U/N-U) × 100, where (I), (U), and (N) correspond to dry-weight of shoots in each inoculation treatment (I) and in the corresponding uninoculated (U), and nitrogen-fertilized (N) controls. Each jar of the N-fertilized controls received 120 mg N, divided in three treatments of 30, 40, and 50 mg N that were applied at 15, 25, and 35 days of cultivation. Bacterial isolation from surface-sterilized nodules was carried out as previously described (Buendía-Clavería et al., 2003). These nodulation assays were carried out at IFAPA Research Center (Sevilla, Spain) and Harbin (China).

Additional nodulation tests on *G. soja* CH2 and CH4, and those on *Leucaena leucocephala*, *Tephrosia vogelii,* and *Vigna radiata* cv. King were carried out at the University of Geneva (Switzerland) using Magenta jars. Seeds were surface sterilized as previously described (Fumeaux et al., 2011) and incubated for 2 days, at 27°C and in the dark to germinate. Once germinated, seedlings were planted in Magenta jars (two seedlings per jar) containing sterile vermiculite (Lewin et al., 1990) and watered with nitrogen-free B&D nutritive solution (Broughton and Dilworth, 1971). After 2–4 days recovery, each seedling was inoculated with 2×10^8 freshly grown bacteria. Plants were grown in controlled conditions with a 12 h photoperiod, a day temperature of 27°C and a night temperature of 20°C. To confirm the identity of bacteria found inside nodules, the 5′-end of the 23S rRNA genes of nodule bacteria was amplified using total genomic DNA of nodules as templates (Fossou et al., 2016) together with the 23S-For1 (5′-ACGAACTAGTGTCAAAAGGGC-3′) and ITS-Rev2 (5′-TGGTCCGCGTTCGCTCGCC-3′) primers. The resulting amplicons of NGR234 (317 bp) and HH103 (380 bp) were clearly discriminated after migration on a 1% agarose gel.

Experiments of competition for nodulation using pairs of co-inoculants among *S. fredii* HH103 Rif^R, *B. diazoefficiens* $USDA110^T$ or *B. elkanii* $USDA76^T$, were carried out on *G. soja* accessions CH2, CH3, and CH4. In accession CH2, only the $USDA110^T$/$USDA76^T$ combination was used, since it does not nodulate with strain HH103 Rif^R. Bacteria were grown to mid-log phase and *G. soja* plants were inoculated with 1 ml of a mixture of bacterial competitors containing 10^8 (O.D. ∼ 0.1) bacteria at a 1:1 ratio. Plants were grown for 60 days under greenhouse conditions. Nodule occupancy was determined by the differential intrinsic antibiotic-resistance of the inoculants used: tetracycline (10 μg/ml) to positively differentiate bradyrhizobia (resistant) from HH103 Rif^R (sensitive) and streptomycin (50 μg/ml) to distinguish between $USDA110^T$ (sensitive) and $USDA76^T$ (resistant) bradyrhizobia strains. In addition, rifampicin (50 μg/ml) was also used to distinguish between $USDA110^T$ (sensitive) and HH103 (resistant). These wild soybean accessions were also used in competition experiments between HH103 and its mutant derivatives affected in the T3SS HH103-1 *rhcJ*::Tn*5*::*lacZ* (=SVQ288) and HH103 Rif^R *ttsI*::**Ω** (=SVQ533). Nodule occupancy by mutants SVQ288 or SVQ533 was determined by plating bacterial nodule-isolates on TY media supplemented with neomycin (50 μg/ml) or spectinomycin (100 μg/ml), respectively.

Microscopy Studies

Small fragments of nodules were fixed in 4% (v/v) glutaraldehyde prepared in 0.1 M cacodylate buffer, pH 7.2 for 1 h at 4°C. Samples were washed in 0.1 M cacodylate buffer, pH 7.2 for 12 h and post-fixed in 1% OsO_4 for 1 h at 4°C. Then, samples were dehydrated in ethanol at progressively higher concentrations and

TABLE 1 | Geographical origin and maturity group of *G. soja* accessions from China.

G. soja accession number in IFAPA collection	Other accession numbers[A,B]	Chinese Region or province	Locality	Maturity group	GPS coordinates	
					Latitude	Longitude
Wild soybeans from Northern China						
CH1	65549[A]	Heilongjiang	Sungari River	II	45° 49′	126° 41′
CH2	407288[A]	Jilin	Nan Wai Tse	II	43° 30′	124° 48′
CH3	549039[A]	Liaoning	Kuandian	III	40° 42′	125° 2′
CH6	ZYD00034[B]	Heilongjiang	Aihui	000	50° 22′	127° 53′
CH7	ZYD00093	Heilongjiang	Nenjiang	000	49° 17′	125° 20′
CH8	ZYD00173	Heilongjiang	Tongjiang	0	47° 67′	132° 50′
CH9	ZYD00527	Heilongjiang	Harbin	I	45° 75′	126° 63′
CH10	ZYD00728	Heilongjiang	Hailin	00	44° 57′	129° 35′
CH11	ZYD00792	Jilin	Qianguo	I	45° 17′	124° 83′
CH12	ZYD00893	Jilin	Jiutai	I	44° 15′	125° 83′
CH13	ZYD01060	Jilin	Wangqing	II	43° 32′	129° 75′
CH14	ZYD01164	Jilin	Lishu	II	43° 32′	124° 33′
CH15	ZYD01396	Jilin	Huinan	II	42° 68′	126° 03′
Wild soybeans from Central China						
CH4	597455[A]	Shanxi	Yuci	III	37° 40′	112° 51′
CH5	597458[A]	Shandong	Laixi	IV	36° 48′	120° 28′
CH16	ZYD03019	Shaanxi	Loufan	III	38° 05′	111° 78′
CH17	ZYD03101	Shaanxi	Wuxiang	III	36° 83′	112° 83′
CH18	ZYD03152	Shaanxi	Hejin	IV	35° 58′	110° 70′
CH19	ZYD03163	Shaanxi	Ruicheng	V	34° 71′	110° 68′
CH20	ZYD03183	Shaanxi	Linfen	IV	36° 08′	111° 50′
CH21	ZYD03721	Shanxi	Huanglong	IV	35° 60′	109° 86′
CH22	ZYD03735	Shanxi	Longxian	VI	34° 91′	106° 86′
CH23	ZYD03803	Shanxi	Yaoxian	IV	34° 91′	108° 98′
CH24	ZYD03830	Shanxi	Dali	V	34° 82′	109° 96′
CH25	ZYD03870	Shanxi	Tongguan	V	34° 56′	110° 25′

[A]*Plant introduction numbers given by the United States Department of Agriculture (USDA) collection.*
[B]*Accession numbers starting by ZYD are the plant introduction numbers given by the National Crop Genebank of China (NCGC).*

embedded in Epon (epoxy embedding medium). Toluidine blue-stained semi-thin sections (0.5 μm thick) used as controls were viewed in a Leitz (Aristoplan) light microscope.

Thin sections (60-80 nm thick) were cut on a Reichert-Jung Ultracut E ultramicrotome, stained with uranyl acetate and lead citrate, and examined in a Libra 120 Plus transmission electron microscope (TEM) from Carl Zeiss (Germany) at an accelerating voltage of 80 kV.

RESULTS

Symbiotic Efficacy of *B. diazoefficiens* USDA110^T, *B. elkanii* USDA76^T, and *S. fredii* HH103 Rif^R on Soybean Accessions From Russia, North Korea, Japan, and China

Twenty wild soybean (*G. soja*) accessions from Russia (R1 to R5), South Korea (K1 to K5), Japan (J1 to J5), and China (CH1 to CH5) from the USDA-Soybean Germplasm Collection were inoculated with three different soybean rhizobia strains: *B. diazoefficiens* USDA110T, *B. elkanii* USDA76^T, and *S. fredii* HH103 Rif^R. Two independent nodulation tests showed that USDA110^T and USDA76^T formed nitrogen fixing nodules with all accessions tested.

Some particular accessions, such as K3, K4, J2, R2, R5, CH1, CH2, CH3, and CH5 inoculated with USDA110^T produced REI values higher than 50%, and three accessions (K2, K5, and R3) gave REI values higher than 80% (**Table 2** and **Supplementary Table S3**). The highest REI value in *G. soja* plants inoculated with USDA76^T was obtained with accession R4 (57.7%). REI values higher than 40% were found with Korean (K2 and K3), Russian (R3), Northern (CH1 and CH2) and Central China (CH3, CH4, and CH5) accessions (**Table 2** and **Supplementary Table S4**). Wild-soybean accessions from Russia, Korea, Japan, and Northern China nodulated with HH103 Rif^R but REI values were lower than 5% (**Table 2** and **Supplementary Table S5**). Accession CH2 (Jilin province, Northern China) failed to nodulate with HH103 Rif^R. In contrast, one of the accessions tested from Central China (CH4, Shanxi province) gave a REI value of 54%, which was associated with healthy plant growth and absence of nitrogen deficiency symptoms (**Supplementary Table S5**).

TABLE 2 | Relative Efficiency Indexes (REI) of *Glycine soja* accessions from Korea, Japan, Russia, and China when grown in combination with *B. diazoefficiens* USDA110^T, *B. elkanii* USDA76^T or *S. fredii* HH103 Rif^R.

Country (Province)	*G. soja* accession	REI of *G. soja* accessions inoculated with		
		USDA110^T	USDA76^T	HH103 Rif^R
Korea	K1	26.0	15.1	0.2
	K2	98.3	43.8	1.4
	K3	51.9	46.5	1.0
	K4	59.8	28.4	3.9
	K5	86.6	23.7	0.5
Japan	J1	35.0	18.1	0.6
	J2	51.8	33.4	0.9
	J3	48.1	19.7	0.8
	J4	36.6	18.1	1.5
	J5	31.4	6.9	0.0
Russia	R1	32.1	38.0	2.1
	R2	51.0	18.3	2.9
	R3	96.7	53.0	0.8
	R4	38.9	57.7	2.3
	R5	55.1	41.9	2.7
North of China (Heilongjiang)	CH1	59.3	40.5	2.1
	CH6	89.9	19.2	4.7
	CH7	33.1	13.9	2.7
	CH8	31.7	18.4	2.7
	CH9	50.5	18.5	2.7
	CH10	29.9	26.9	9.2
North of China (Jilin)	CH2	59.9	47.7	0.0
	CH11	31.1	33.9	4.1
	CH12	48.2	16.2	0.2
	CH13	37.8	12.6	0.7
	CH14	30.2	8.5	0.2
	CH15	48.3	8.7	2.6
North of China (Liaoning)	CH3	55.1	44.3	4.4
East-Central coastal China (Shandong)	CH5	50.1	42.6	1.9
Central China (Shaanxi)	CH16	44.5	41.8	34.3
	CH17	37.9	17.5	56.3
	CH18	35.5	45.5	30.2
	CH19	29.6	46.3	44.1
	CH20	46.3	17.1	67.4
Central China (Shanxi)	CH4	31.7	48.8	54.0
	CH21	12.0	11.3	5.6
	CH22	23.7	10.8	2.1
	CH23	41.4	20.0	4.2
	CH24	33.8	37.4	43.5
	CH25	40.7	44.9	65.9

The Relative Efficiency Index (REI) for each inoculant/soybean-accession combination was calculated by comparisons among Shoot Dry Weight of inoculated treatments (I), N-fertilized (N) and Untreated (U) controls. REI values were obtained by using the relation (I − U/N − U) × 100.

Indigenous *S. fredii* populations are predominant in soils of Central China while *B. japonicum* and other slow-growing soybean-rhizobial strains are more abundant in soils of Northern and Southern China (**Figure 1**; Tian et al., 2012). To investigate whether the relative abundance of fast- and slow-growing populations of indigenous soybean rhizobia in particular areas correlates with symbiotic preferences of local *G. soja* accessions to nodulate with slow- or fast-growing soybean rhizobia, 10 accessions from Shanxi and Shaanxi provinces (Central China) and 10 wild soybeans from Heilongjiang and Jilin provinces (Northern China) were tested in combination with USDA110^T, USDA76^T, or HH103 Rif^R. USDA110^T formed nitrogen-fixing nodules with the 20 wild soybeans tested. REI values close or equal to 50% were found with accessions CH9, CH12, and CH15, all from Northern China (**Table 2** and **Supplementary Table S6**). One accession (CH6) from Heilongjiang province gave a

TABLE 3 | Nodule occupancy of *Glycine soja* accessions CH2, CH3, and CH4 inoculated with pairs of competitors formed among *B. diazoefficiens* (Bd) USDA110^T, *B. elkanii* (Be) USDA76^T or *S. fredii* (Sf) HH103 Rif^R.

G. soja accession	Pairs of inoculants (A/B)	TNN	% of nodule occupancy		
			A	B	A + B
CH2	BdUSDA110^T/BeUSDA76^T	191	46.6	23.0	30.4
CH3	BdUSDA110^T/SfHH103 Rif^R	186	93.5	0	6.5
	BeUSDA76^T/SfHH103 Rif^R	192	100	0	0
	BdUSDA110^T/BeUSDA76^T	189	70.9	9.5	19.6
CH4	BdUSDA110^T/SfHH103 Rif^R	181	78.5	12.7	8.8
	BeUSDA76^T/SfHH103 Rif^R	190	75.8	12.1	12.1
	BdUSDA110^T/BeUSDA76^T	192	27.6	68.2	4.2

TNN, Total number of nodules tested in two independent experiments. In each experiment, 6 plants were inoculated per pair of competitors. Streptomycin (50 μg/ml) was used to distinguish between S. fredii HH103 Rif^R or B. diazoefficiens USDA110^T (sensitive) and B. elkanii USDA76^T (resistant). Rifampicin (50 μg/ml) and tetracycline (10 μg/ml) were used to distinguish between S. fredii HH103 Rif^R (rifampicin-resistant and tetracycline-sensitive) and B. diazoefficiens USDA110^T (rifampicin-sensitive and tetracycline-resistant).

remarkably high REI value of 89.9%. USDA76^T also nodulated all of the 20 accessions (**Supplementary Table S7**). None of the accessions from Northern or Central China gave REI values higher than 46.5%. Nine out of the 10 accessions from Northern China inoculated with HH103 Rif^R formed nodules, although REI values were below 9.5% (**Table 2** and **Supplementary Table S8**). In contrast, all of the 10 accessions from Central China were nodulated by HH103 Rif^R and 5 of them gave REI values in the range of 43–67%.

Competition Experiments Between *B. diazoefficiens* USDA110^T, *B. elkanii* USDA76^T and *S. fredii* HH103 Rif^R to Nodulate Different Wild Soybean Accessions

HH103 Rif^R formed nitrogen-fixing nodules with *G. soja* accessions CH3 (REI 4.4%) and CH4 (REI 54%). Competition experiments for nodulation of accessions CH3 and CH4 were carried out between HH103 Rif^R and USDA110^T or USDA76^T. Both bradyrhizobial strains outcompeted HH103 Rif^R to nodulate CH3 and CH4. HH103 Rif^r did not form nodules with accession CH3 when co-inoculated with both bradyrhizobial strains. On CH4, nodules occupied exclusively by HH103 Rif^R were less than 20% of the total number of nodules analyzed (**Table 3**). Similar experiments carried out between USDA110^T and USDA76^T showed that strain USDA110^T was always more competitive with accession CH2 and CH3 from Northern China, but less competitive with accession CH4 from Central China (**Table 3**).

S. fredii NGR234 Forms Nitrogen-Fixing Nodules With Wild Soybeans From Central China

Since the *G. soja* accession CH4 (Central China) formed proficient symbiosis with HH103 Rif^R, we tested whether NGR234 was also capable of inducing the formation of nitrogen-fixing nodules on CH4 roots. Accession CH2 (Northern China), which was unable to nodulate with HH103, was also included in the nodulations tests. CH4 plants inoculated

TABLE 4 | Symbiotic responses of *Glycine soja* accessions CH2, CH3, and CH4 to inoculation with diverse *S. fredii* HH103 and NGR234 mutants affected in the Type Three Secretion System (T3SS).

Treatments	Number of nodules	Dry weight of nodules (mg)	Shoot dry weight (mg)
***Glycine soja* CH2**			
HH103-1	0.0	0.0	15.7 ± 5.2b
SVQ288	7.1 ± 1.4a	13.0 ± 1.5a	49.1 ± 9.6b
SVQ533	7.0 ± 4.1a	16.6 ± 9.7a	96.8 ± 58.8a
Uninoculated	0.0	0.0	18.2 ± 9.0b
NGR234	16.2 ± 16.8	3.75 ± 4.6	105.6 ± 70.5a
NGRΩ*rhcN*	0.0	0.0	16.3 ± 13.4b
NGRΩ*ttsI*	0.0	0.0	23.3 ± 14.3b
Uninoculated	0.0	0.0	18.2 ± 9.0b
***Glycine soja* CH3**			
HH103-1	17.4 ± 6.4a	42.3 ± 11.1a	243.5 ± 61a
SVQ288	12.1 ± 6.3a	31.3 ± 6.1ab	213.5 ± 19ab
SVQ533	9.6 ± 7a	19.0 ± 8.8b	170.1 ± 55.6b
Uninoculated	0.0	0.0	14.5 ± 2.2c
NGR234	2.0 ± 3.3	4.9 ± 5.8	101.5 ± 88.8a
NGRΩ*rhcN*	0.0	0.0	27.8 ± 9b
NGRΩ*ttsI*	0.0	0.0	32.8 ± 14.1b
Uninoculated	0.0	0.0	14.5 ± 2.2b
***Glycine soja* CH4**			
HH103-1	26.1 ± 8.1a	59.4 ± 23.8a	858.0 ± 316.2a
SVQ288	12.6 ± 8.4b	52.9 ± 35.4a	762.8 ± 398.6a
SVQ533	14.9 ± 1.6b	60.8 ± 7a	774.5 ± 132.7a
Uninoculated	0.0	0.0	23.0 ± 5.8b
NGR234	6.6 ± 1.9a	19.0 ± 5.2a	269.8 ± 70.7a
NGRΩ*rhcN*	4.5 ± 3.6ab	13.6 ± 8.5a	262.9 ± 116a
NGRΩ*ttsI*	2.7 ± 2.3bc	3.8 ± 4.8b	61.7 ± 33.1b
Uninoculated	0.0	0.0	23.0 ± 5.8b

Numbers refer to mean values (±standard deviations) per plant of three Leonard jars, each containing two plants. Statistical comparisons among inoculations are shown using ANOVA. For each parameter, data followed by the same letter are not significantly different at α = 5%.

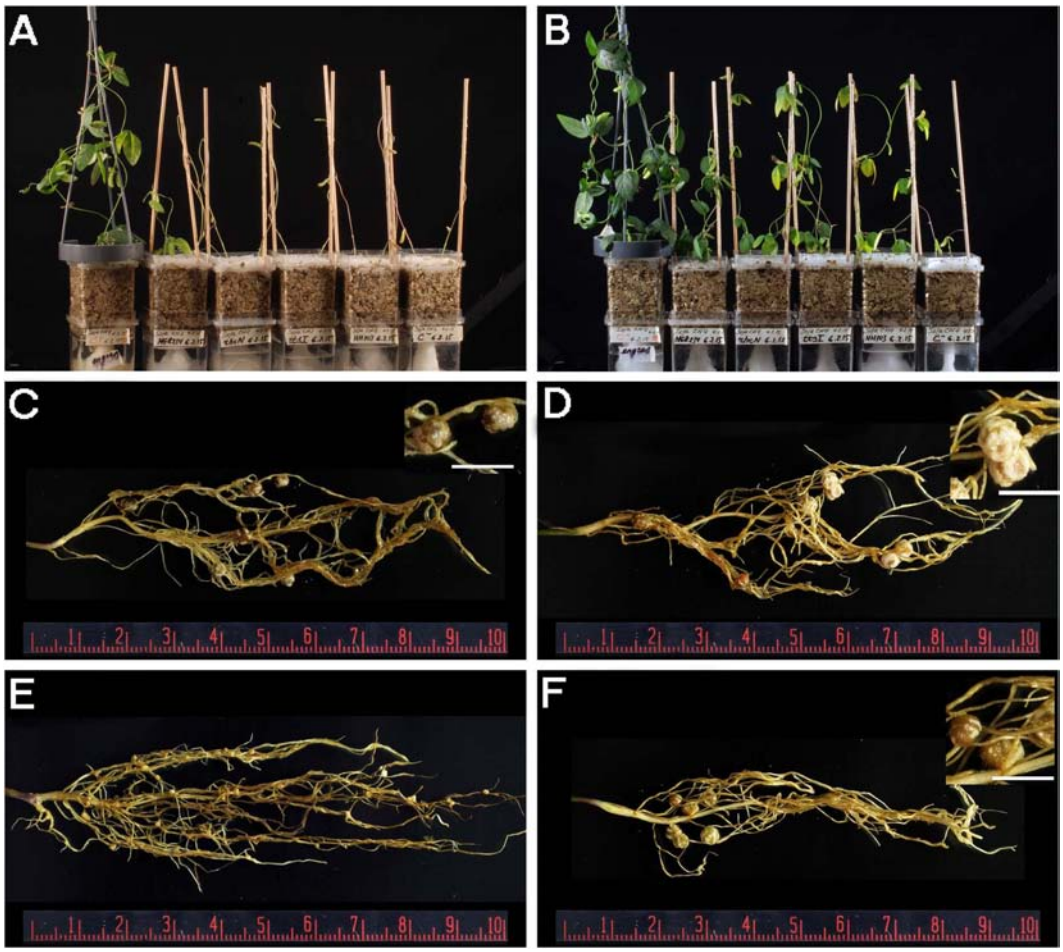

FIGURE 2 | (A,B) Plant responses of *G. soja* accessions CH2 **(A)** and CH4 **(B)** inoculated with different *S. fredii* strains. From left to right, Magenta jars were treated as follows: N-fertilizer, NGR234, NGRΩ*rhcN*, NGRΩ*ttsI*, HH103 Rif^R, and uninoculated control. **(C,D)** Nitrogen-fixing nodules induced by NGR234 on CH2 **(C)** and CH4 **(D)** roots. **(E)** Ineffective nodules induced by HH103 Rif^R on CH2 roots. **(F)** Nitrogen-fixing nodules induced by HH103 Rif^R on CH4 roots. White bars **(C,D,F)** correspond to 5 mm.

with NGR234 formed nitrogen-fixing nodules that effectively contributed to plant growth (**Table 4** and **Figure 2**), whereas on CH2 accession NGR234 induced the formation of more nodules than on CH4 but plants were poorly developed. To our knowledge, this is the first report showing that *S. fredii* NGR234 can form proficient symbiosis with *G. soja* plants. Then, bacteria from nodules formed on CH2 and CH4 plants were isolated and identified. Isolates from well-developed nodules of CH2 and CH4 plants inoculated with NGR234 were resistant to rifampicin, a chromosomal antibiotic-resistance maker for this strain. To further confirm the presence of NGR234, a pair of PCR primers that specifically amplifies the 5′ end of the 23S rRNA gene was used. These primers can also be used to distinguish between NGR234 and HH103 strains, since the size of the predicted amplicons are of 317 and 380 bp, respectively. PCR using bacteria isolated from nodules formed on CH2 plants inoculated with NGR234 only amplified the DNA fragment corresponding to this strain (**Figure 3**).

To investigate whether NGR234 was also able to effectively nodulate other wild soybean accessions from Central China, six accessions from Shanxi or Shaanxi provinces were inoculated with this strain. HH103 Rif^R was used as positive control in these experiments, which showed that NGR234 formed nitrogen-fixing nodules on all of the six accessions tested, albeit associations were clearly less proficient than those formed by HH103 Rif^R (**Table 5**).

Type Three Secretion Systems (T3SS) of *S. fredii* HH103 and NGR234 Determine Symbiotic Compatibility With Some *G. soja* Accessions

It has been established that secretion of nodulation outer proteins (Nop) through type three secretion systems (T3SS) modulates symbiotic compatibility of *S. fredii* strains with different *G. max* cultivars and other legume species (for a review see López-Baena et al., 2016). T3SS deliver effector proteins into the cytoplasm of animal and plant cells. In rhizobia, genes encoding structural

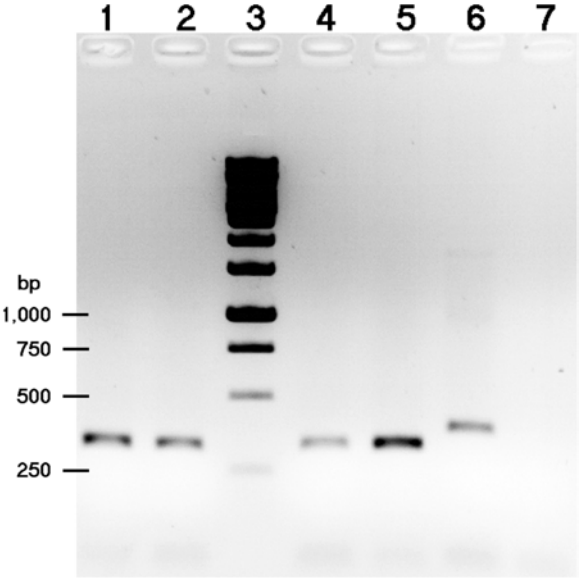

FIGURE 3 | Separation of 23S-For1+ITS-Rev2 PCR amplified products on 1% agarose gel. The templates used were as follows: lanes 1, 2, and 4, gDNA from bacteria isolated from different nodules of *G. soja* CH2 inoculated with NGR234; lane 5, NGR234 gDNA; lane 6, HH103 Rif^R gDNA; lane 7, no DNA. Lane 3, DNA molecular weight marker (bands corresponding to 1,000, 750, 500, and 250-bp are indicated on the left).

components of symbiotically active T3SS and effector proteins secreted by these systems are controlled by a transcriptional regulator called TtsI (for a recent review see Staehelin and Krishnan, 2015). Amongst the many proteins assembled into a functional secretion machinery, RhcJ (first annotated as NolT in *S. fredii* strain USDA257) is embedded in the protein ring that spans the inner membrane of bacteria. By contrast, the nodulation outer protein (Nop) NopJ is one of the several effectors that together contribute to define the host range of strain NGR234 (Kambara et al., 2009). To test whether Nop-secretion also contributed to symbioses with wild soybean accessions from different regions of China, the nodulation properties of parent (HH103 and NGR234) and T3SS-deficient (SVQ288, a mutant of HH103 in RhcJ, and NGRΩ*rhcN*) strains were compared.

Neither a streptomycin-resistant derivative (*S. fredii* HH103-1) nor a rifampicin resistant mutant (*S. fredii* HH103 Rif^R) of HH103 nodulated *G. soja* CH2, an accession from Northern China (**Table 4** and **Supplementary Table S5**). Interestingly, mutants of *S. fredii* HH103 in *ttsI* (strain SVQ533) or *rhcJ* (strain SVQ288), both of which cannot secrete Nops, induced the formation of nodules (**Table 4**). These nodules, however, poorly contributed to plant growth. Conversely, *S. fredii* NGR234 that induced the formation of nitrogen-fixing nodules with *G. soja* CH2, completely lost its nodulation capacity when T3SS was inactivated as in mutants NGRΩ*rhcN* or NGRΩ*ttsI* (**Table 4**). Both *S. fredii* strains HH103-1 and NGR234 induced the formation of nodules with *G. soja* accession CH3 (Northern China), with a shoot dry weight of inoculated plants significantly higher than that of uninoculated CH3 plants. While SVQ288 and

TABLE 5 | Symbiotic responses of some *Glycine soja* accessions from Central China with *S. fredii* HH103 and NGR234 strains.

Accessions	Number of nodules		Dry weight of nodules (mg)		Shoot dry weight (mg)		
	HH103	NGR234	HH103	NGR234	HH103	NGR234	Uninoculated
CH16	94.3 ± 13.2a	27.5 ± 13.5cde	110.3 ± 25.2abcd	63.5 ± 23.5bcde	1459 ± 337de	737 ± 66fg	118 ± 22gh
CH17	50.7 ± 3.4abcde	3.3 ± 1.9e	175.0 ± 16.4a	15.0 ± 4.9e	2340 ± 90ab	324 ± 12gh	79 ± 27h
CH19	86.7 ± 13.9ab	10.0 ± 0.6de	143.7 ± 19.7ab	55.7 ± 1.8cde	2040 ± 210abcd	1017 ± 112ef	124 ± 28gh
CH20	82.7 ± 25.1abc	88.7 ± 44.2ab	174.0 ± 57.4a	112.7 ± 51.2abc	2293 ± 408ab	1192 ± 561ef	122 ± 1gh
CH24	77.3 ± 30.8abc	59.3 ± 27.8abcde	136.0 ± 45.6abc	107.0 ± 28.4bcd	2177 ± 308abc	1552 ± 383cde	150 ± 19gh
CH25	47.3 ± 6.2abcde	35.3 ± 20.6bcde	194.3 ± 20.7a	60.0 ± 20.2bcde	2647 ± 421a	709 ± 287fgh	146 ± 18gh
CH4	62.0 ± 17.2abcd	13.3 ± 2.0de	167.3 ± 23.5a	23.7 ± 1.8de	1970 ± 257bcd	595 ± 47fgh	96 ± 1gh
LSD ($p < 0.05$)	58.6		86.8		646		

Numbers are mean values (±standard error of the mean, n = 3) of three Leonard jars, each containing two plants. Determinations were carried out 60 days after inoculation. For each parameter, data followed by the same lower-case letter are not significantly different at α = 5%, as determined by protected Fisher's LSD (Least Significant Difference).

TABLE 6 | Nodule occupancy of *Glycine soja* accessions CH3 and CH4 inoculated with *S. fredii* HH103 and its *ttsI* and *rhcJ* mutants.

G. soja accession	Pairs of inoculants	TNN	% of nodule occupancy by mutant SVQ533 or SVQ288
CH3	*S. fredii* HH103 Rif^R/SVQ533	127	10.2
	S. fredii HH103 Str^R/SVQ288	161	15.5
CH4	*S. fredii* HH103 Rif^R/SVQ533	156	10.9
	S. fredii HH103 Str^R/SVQ288	207	10.4

TNN, total number of nodules tested in two independent experiments.
In each experiment, 5 jars were inoculated per pair of competitors. Each jar contained 2 plants.
YMA supplemented with spectinomycin or neomycin (50 μg/ml) were used to detect the presence of SVQ533 or SVQ288, respectively.

SVQ533 mutants retained the ability to nodulate CH3 accession, the NGRΩ*rhcN* and NGRΩ*ttsI* could no longer induce the formation of nodules (**Table 4**). By contrast the less selective *G. soja* accession CH4 from Central China nodulated with all the HH103 and NGR234 mutants tested: plants inoculated with SVQ288 and SVQ533 strains formed fewer nodules but shoot dry weight was not significantly altered when compared to CH4 plants inoculated with HH103-1 at 60 days post-inoculation (dpi). *G. soja* CH4 responses to inoculation with NGRΩ*rhcN* or NGR234 were similar, while nodulation and nitrogen-fixation of NGRΩ*ttsI* was significantly reduced on CH4 (**Table 4**).

As previously described, *S. fredii* strains HH103 Rif^R and HH103-1 failed to nodulate *G. soja* CH2. As SVQ288 and SVQ533 mutants deficient in T3SS-dependent secretion gained nodulation, it seems likely that secretion of HH103 Nop complement triggers defensive responses in CH2 plants. Therefore, we tested whether presence of HH103 Rif^R would block nodulation of CH2 accession by the proficient symbiont $USDA110^T$. When co-inoculated at ratios of 1:1 and 1:10, $USDA110^T$ and HH103 Rif^R inocula formed at 25 dpi as many as 7.0 ± 1.8 and 7.1 ± 1.4 nodules/plant, respectively. Thus, the presence of HH103 Rif^R does not appear to block nodulation of CH2 accession by $USDA110^T$.

Competition experiments for nodulation of *G. soja* accessions CH3 and CH4 were carried out between HH103 Rif^R and its T3SS-mutant derivatives SVQ533 and SVQ288. On both accessions, SVQ533 and SVQ288 were clearly outcompeted by HH103 Rif^R with mutants only occupying 10–15% of the nodules (**Table 6**).

Host-Range of *S. fredii*-Symbiotic Plasmid Hybrids on *G. max*, *G. soja* and Other Legumes Normally Nodulated by NGR234

USDA193C and NGR234C transconjugants were tested in nodulation assays with *G. max* cv. Williams 82 and the *G. soja* accession CH4 (**Table 7** and **Figures 4**, **5**). Whereas strains NGR234, NGR234-M, and NGR234C (=ANU265) failed to nodulate *G. max* cv. Williams (**Table 7**), the NGR234C transconjugants carrying plasmid p*Sf*HH103d::Tn*5*-Mob (hereafter pSymHH103M) induced the formation of white ineffective nodules that did not contribute to plant growth. Similarly, USDA193C carrying the symbiotic plasmid p*Sf*NGR234a::Tn*5*-Mob (hereafter pSymNGR234M) only induced the formation of ineffective root outgrowths on *G. max* cv. Williams 82 (**Figure 5D**). By contrast, *G. soja* CH4 inoculated with USDA193C carrying the symbiotic plasmid pSymNGR234M induced the formation of nitrogen-fixing nodules (**Figures 4G,H**) and plants did not show symptoms of nitrogen starvation. On the same CH4 host, plants inoculated with the NGR234C pSymHH103M hybrid formed inefficient nodules, however (**Table 7**).

Nodules formed by *S. fredii* inoculants were sectioned, stained with methylene blue, and observed by light microscopy. As expected, *G. soja* CH4 nodules induced by NGR234 contained a high density of symbiosomes (**Figures 4C,D**), similarly to those induced by HH103 Rif^R (**Figures 4A,D**). By contrast, macroscopic root outgrowths (MRO) formed in *G. max* cv. Williams 82 inoculated with NGR234 were devoid of bacteria inside the cells and in the intercellular spaces. Clusters of plant cells showing thick walls were observed (**Figure 5A**). Ineffective nodules formed by *G. soja* CH4 and *G. max* cv. Williams 82 inoculated with NGR234C carrying pSymHH103M contained many but poorly infected cells as in senescent nodules (**Figures 4E**, **5E**). Electron micrographs confirmed that *G. soja* CH4 and *G. max* cv. Williams 82 nodules occupied by NGR234C carrying pSymHH103M were senescent, with nodule cells containing degraded bacteroids at 42 dpi (**Figures 4F**, **5F**). At this same time point, *G. soja* nodules infected with NGR234 (**Figures 4C,D**) and *G. max* nodules occupied by HH103 Rif^R (**Figures 5B,C**) did not show visible symptoms of senescence.

Further nodulation assays were carried out to investigate the capacity of the symbiotic plasmid donor *S. fredii* HH103-M and the resulting NGR234C pSymHH103M hybrid strain to nodulate with three different legumes that form indeterminate (*L. leucocephala* and *T. vogelii*) or determinate (*V. radiata*) nodules with NGR234. *V. radiata* cv. King and *T. vogelii* plants inoculated with HH103-M formed nodules (**Figures 6B,E**), although both symbioses were less effective than those established with NGR234 (**Table 8** and **Figures 6A,D**). *L. leucocephala* roots inoculated with HH103-M or NGR234C carrying pSymHH103M formed macroscopic root outgrowths (MRO) that did not contribute to plant growth (**Table 8** and **Figure 6K**). Although *V. radiata* plants inoculated with NGR234 or HH103-M formed nitrogen-fixing nodules, the hybrid strain NGR234C carrying pSymHH103M only formed ineffective nodules (**Figure 6C**) and the color and development of plants were similar to those of the uninoculated control (**Figure 6A**). Despite the number of nodules formed by *T. vogelii* roots inoculated with NGR234 or HH103-M being similar (**Table 8** and **Figures 6E,F**), the former was much more effective in supporting plant growth (**Figure 6D**). In contrast to the fully proficient indeterminate nodules induced by NGR234 on *T. vogelii*, (**Figure 6I**), those formed upon inoculation with HH103-M appeared mostly senescent with presence of leghemoglobin restricted to small sections of these

TABLE 7 | *Glycine max* cv. Williams 82 and *G. soja* CH4 responses to inoculation with *S. fredii* pSym-cured derivatives carrying different *S. fredii* pSym plasmids.

Legume	*S. fredii* inoculant	Symbiotic plasmid present	Number of nodules per plant[A,B,C]	Shoot dry-weight (mg)
G. max cv. Williams	HH103-M	p*Sf*HH103d::Tn*5*-Mob	79.5 ± 6.9[A] a	2612 ± 424 a
	NGR234	p*Sf*NGR234a	Nod^{-}[B]	645 ± 271 b
	NGR234-M	p*Sf*NGR234a::Tn*5*-Mob	Nod^{-}[B]	700 ± 205 b
	NGR234C	None	Nod^{-}[C]	545 ± 220 b
	NGR234C pSymHH103M	p*Sf*HH103d::Tn*5*-Mob	49.0 ± 16.3[D] b	480 ± 244 b
	USDA193C	None	Nod^{-}[C]	647 ± 122 b
	USDA193C pSymNGR234M	p*Sf*NGR234a::Tn*5*-Mob	Nod^{-}[B]	508 ± 77 b
	Uninoculated	–	–	507 ± 190 b
G. soja CH4	HH103-M	p*Sf*HH103d::Tn*5*-Mob	5.8 ± 2.4[A] b	239 ± 110 a
	NGR234	p*Sf*NGR234a	3.8 ± 1.1 bc	216 ± 83 ab
	NGR234-M	p*Sf*NGR234a::Tn*5*-Mob	3.2 ± 1.2[A] c	161 ± 47 c
	NGR234C	None	Nod^{-}[C]	55 ± 18 d
	NGR234C pSymHH103M	p*Sf*HH103d::Tn*5*-Mob	19.9 ± 5.6[D] a	66 ± 20 d
	USDA193C	None	Nod^{-}[C]	57 ± 13 d
	USDA193C pSymNGR234M	p*Sf*NGR234a::Tn*5*-Mob	3.7 ± 1.0[A] bc	181 ± 86 bc
	Uninoculated	–	–	64 ± 13 d

Three Leonard jars containing two (G. max) or four (G. soja) seedlings were inoculated with each bacterial strain. Numbers are mean values ± standard errors. Statistical comparisons among inoculants are shown using ANOVA. For each parameter, data followed by the same small letter are not significantly different at α = 5%.
Plants were analyzed 42 days after inoculation.
[A] Green plants with pink nodules of normal external morphology were formed.
[B] Yellow plants with macroscopic root outgrowths (MRO) were present.
[C] Yellow plants and absence of MRO.
[D] Yellow plants and small white ineffective nodules.
Uninoculated controls remained non-nodulated.

nodules (**Figure 6H**). Hybrid strain NGR234C pSymHH103M induced the formation of ineffective nodules on *T. vogelii* roots (**Table 8** and **Figures 6G,J**).

DISCUSSION

In the last two decades, different reports describing the geographical occurrence and distribution of slow- and fast-growing soybean rhizobia have been reported. A general conclusion from these studies is that soil pH appears to determine the prevalence of soybean bradyrhizobia (slow growers) or soybean sinorhizobia (fast growers). The most detailed report (Tian et al., 2012) confirmed that soybean bradyrhizobia populations are more abundant in acidic soils (Northern and Southern China), while soybean sinorhizobia are predominant in alkaline soils of Central China (Hebei, Shanxi, Henan, and Shandong provinces). The central province of Shaanxi was not included in this study. Recent work from India also suggests that *Bradyrhizobium* strains are very abundant as nodulators of a number of native legumes in acidic soils, whereas *Sinorhizobium* are more prevalent in neutral-alkaline soils (Ojha et al., 2017; Sankhla et al., 2017; Rathi et al., 2018).

In this work we have investigated the symbiotic capacity of wild soybeans from Northern and Central China to associate with *B. diazoefficiens* USDA110^{T}, *B. elkanii* USDA76^{T}, and *S. fredii* HH103 Rif^{R}, three well-known soybean-rhizobia strains whose genome have been fully sequenced and deposited in public databases. These soybean-rhizobia were also tested with wild soybeans from Russia, South Korea, and Japan, which are the only geographical areas outside China in which *G. soja* was so far reported.

Symbiotic nitrogen fixation of wild soybean accessions from Russia, South Korea, Japan, and Northern China inoculated with HH103 Rif^{R} was not effective enough to support appropriate plant growth in the absence of nitrogen fertilizers (**Table 2** and **Supplementary Tables S5, S8**). These results indicate that wild soybeans from geographical areas in which fast-growing soybean-rhizobia populations are absent, or at very low levels, appear to have a low symbiotic affinity for HH103 Rif^{R}. Moreover, two accessions from the Jilin province, CH2 and CH12, even failed to nodulate with this strain, indicating that in these two accessions, symbiotic incompatibility was triggered by yet unknown molecular determinants. All the *G. soja* accessions from Russia, South Korea, Japan, and Northern China formed nitrogen-fixing nodules with USDA110^{T} and USDA76^{T}, the former generally being more effective than the latter (**Table 2** and **Supplementary Tables S3, S4, S6, S7**). Interestingly, *B. japonicum* and *B. diazoefficiens* appear to be more abundant than *B. elkanii* in the Northern provinces of China (**Figure 1**; Tian et al., 2012). Nodules formed by HH103 Rif^{R} in six wild soybeans from the Shanxi province (Central China, alkaline soils) fixed enough nitrogen to support plant growth (**Supplementary Tables S5, S8**). All these results suggest that, at least in Northern and Central China, there is a correlation between symbiotic fitness of wild soybeans from a particular geographical area and the relative abundance of the different

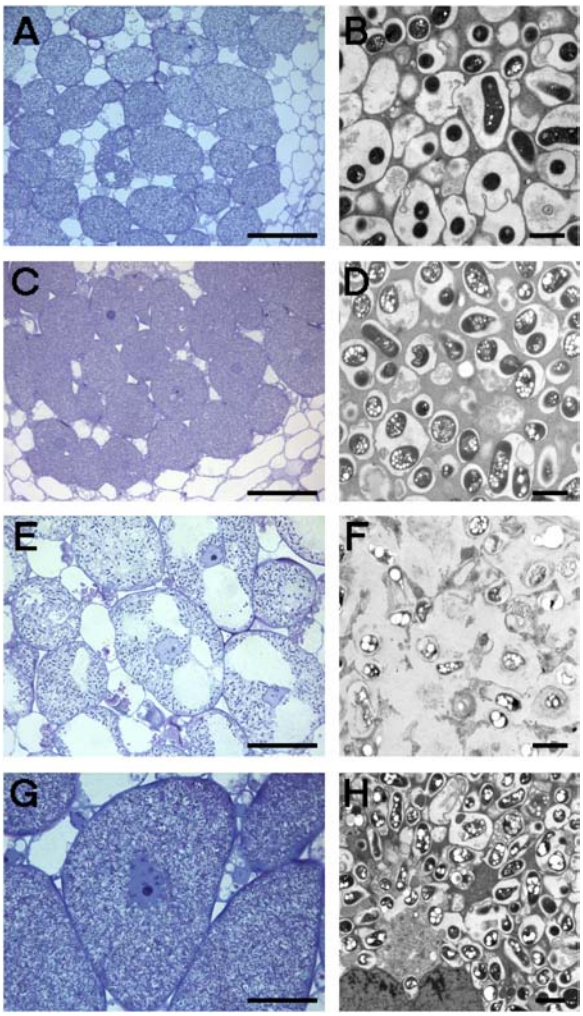

FIGURE 4 | Optical **(A,C,E,G)** and electronic **(B,D,F,H)** microscopy of nodules induced by different *S. fredii* strains in *G. soja* CH4. **(A,B)** HH103 Rif^R; **(C,D)** NGR234; **(E,F)** NGR234C pSymHH103M; **(G,H)** USDA193C pSymNGR234M. Bars correspond to 100 μm in **(A,C)**, 30 μm in **(E,G)**, and 2 μm in **(B,D,F,H)**.

soybean rhizobia genera and species dwelling in soils of that specific zone. Concomitantly, *G. soja* accessions from Northern China are generally more effective with USDA110^T than with USDA76^T.

In Central China *S. fredii* indigenous populations are more abundant than bradyrhizobia populations (Tian et al., 2012). Some *G. soja* accessions from Shanxi (CH4, CH24, and CH25) were found to be more effective with HH103 Rif^R than with USDA110^T, whereas the CH21 and CH23 accessions favored USDA110^T. Thus, the possible correlation between the relative abundance of specific soybean-rhizobia and symbiotic fitness with local *G. soja* accessions from Central China is not as clear as in the case of plant-rhizobia combinations from the Northern provinces. To our knowledge, there are no reports describing the soybean indigenous populations of soils from Shaanxi province. Some accessions (e.g., CH17 and CH20) were more effective with HH103 Rif^R but others showed higher REI values with USDA110^T and USDA76^T (such as CH16 and CH18). Together these results indicate that Shanxi and Shaanxi provinces are promising places for finding wild soybeans showing high nitrogen-fixation capacities with *S. fredii* strains. Central China also appears to be promising for finding wild soybeans showing good symbiotic capacities with slow- and fast-growing soybean rhizobia, which is in contrast with *G. soja* accessions from Northern China, that appear to be only effective with bradyrhizobia.

Competition studies showed that USDA110^T was more competitive than USDA76^T to nodulate accessions CH2 and CH3 (Northern China) but less competitive with accession CH4 (Central China). These results fit well with the fact that soils from Northern China contain *B. japonicum* and *B. diazoefficiens* strains but are apparently devoid of *B. elkanii* populations, whereas soils of Central China are rather populated by *B. elkanii* instead of *B. japonicum* or *B. diazoefficiens* strains (Tian et al., 2012).

Sinorhizobium fredii NGR234 shows the broadest nodulation host-range ever described (Pueppke and Broughton, 1999). Strikingly, and unlike most *S. fredii* strains known, NGR234 is unable to nodulate soybean (*G. max*). The fact that some wild soybeans from Central China formed effective symbioses with HH103 Rif^R prompted us to investigate whether NGR234 could also form nitrogen-fixing nodules with any of these *G. soja* accessions. In fact, NGR234 formed nitrogen-fixing nodules with at least 6 different wild soybean accessions form Shaanxi or Shanxi provinces. Plant tests carried out in Spain, Switzerland, and China proved that NGR234 consistently nodulated several *G. soja* accessions, regardless of experimental settings and plant growth conditions used. To our knowledge, this is the first report describing the formation of nitrogen-fixing nodules in *G. soja* plants inoculated with *S. fredii* NGR234. Such a robust symbiotic phenotype on *G. soja* make attractive further searches for finding amongst the *G. max* varieties grown by Chinese farmers in Central China those capable of forming nitrogen-fixing nodules with NGR234.

It is well known that formation of symbiotic root nodules in soybean is controlled by several host genes referred to as *Rj* (*rj*) genes and it has been repeatedly reported that *S. fredii* T3SS plays important roles in determining symbiotic compatibility with *G. max* cultivars and other legume species (Hayashi et al., 2012; Staehelin and Krishnan, 2015; López-Baena et al., 2016; Yasuda et al., 2016). Here, we also tested whether the T3SS of HH103 Rif^R and NGR234 strains influenced nodulation of wild soybeans. Results confirmed that mutations blocking Nop-secretion significantly impacted symbiosis with a number of *G. soja* accessions (**Table 4**). For example, CH2 accession from Northern China formed nodules with NGR234 but not with HH103 Rif^R. Conversely, while mutants of NGR234 with deficient T3SS (strains NGR**Ω***ttsI* and NGR**Ω***rhcN*) lost their capacity to nodulate CH2 the HH103 mutants in *ttsI* and *rhcJ* gained nodulation on this accession. These results indicate that one or more of the five Nop secreted by NGR234 promote(s) CH2 nodulation, while the combination of Nop secreted by HH103 Rif^R prevents CH2 nodulation. Although the sequences

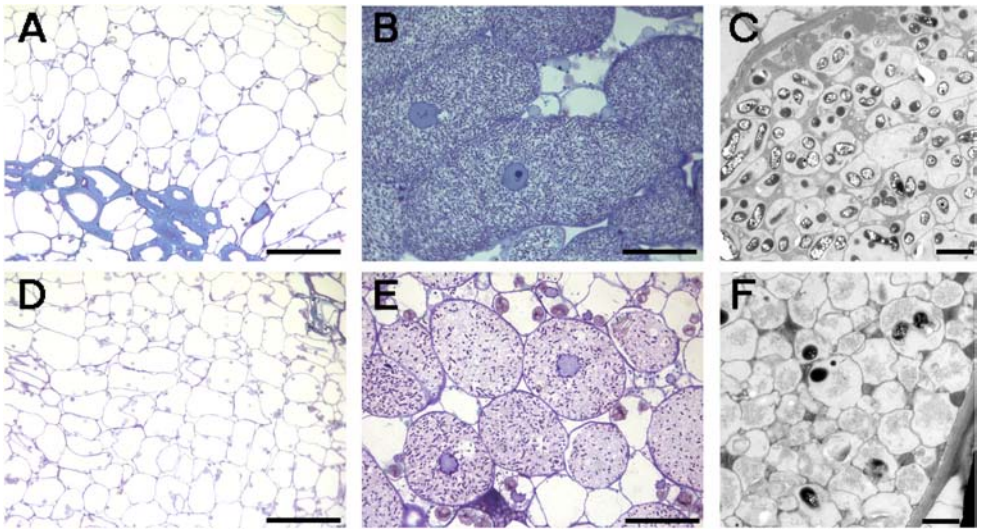

FIGURE 5 | Optical **(A,B,D,E)** and electronic **(C,F)** microscopy of nodules induced by different *S. fredii* strains in soybean cv. Williams 82. **(A)** NGR234; **(B,C)** HH103 Rif^R; **(D)** USDA193C pSymNGR234M; **(E,F)** NGR234C pSymHH103M. Bars correspond to 100 μm in **(A,D)**, 30 μm in **(B,E)**, and 2 μm in **(C,F)**.

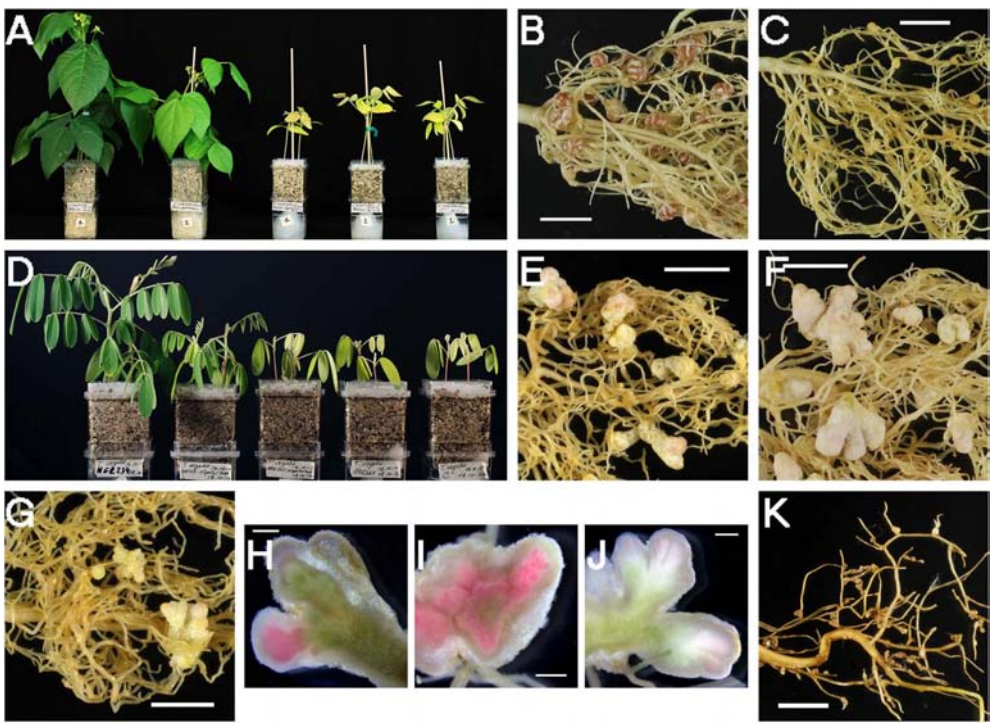

FIGURE 6 | Plant responses of three host legumes of *S. fredii* NGR234, *Vigna radiata* **(A–C)**, *Tephrosia vogelii* **(D–J)** and *Leucaena leucocephala* **(K)**, with different *S. fredii* strains. **(A)** Phenotypes of strains on mung bean (*V. radiata*) at 42 dpi. From left to right, plants inoculated with NGR234, HH103-M, NGR234C pSymHH103M, NGR234C, and uninoculated control. **(B)** Nodules induced by HH103-M in *V. radiata* roots (42 dpi). **(C)** Pseudonodules induced by NGR234C pSymHH103M in *V. radiata* roots (42 dpi). **(D)** Phenotypes of strains on *T. vogelii* at 58 dpi. From left to right, plants inoculated with NGR234, HH103-M, NGR234C pSymHH103M, NGR234C, and uninoculated controls. **(E–J)** Nodules induced by HH103-M **(E,H)**, NGR234 **(F,I)**, and NGR234C pSymHH103M **(G,J)** in *T. vogelii* roots (58 dpi). **(K)** Abnormal root outgrowths on *L. leucocephala* 81 dpi with NGR234C pSymHH103M. Bars correspond to 1 cm in **(B,C,E–G,K)**, and 1 mm in **(H–J)**.

of the Nop shared by HH103 Rif^R and NGR234 are nearly identical, there are some differences in the repertoire of T3SS effectors secreted by both strains (López-Baena et al., 2016). For example, HH103 Rif^R carries *nopI* and *nopD* genes, which are absent from the NGR234 genome. By contrast, NGR234 genome includes a copy of the *nopJ* gene that is absent from

TABLE 8 | *Leucaena leucocephala*, *T. vogelii*, and *V. radiata* responses to inoculation with a NGR234 pSym-cured derivative (ANU265) carrying the symbiotic plasmid of HH103 Rif^R tagged with Tn*5*-Mob.

Legume	Inoculant	Number of nodules	Shoot dry weight (mg)
L. leucocephala	Uninoculated	0.0	102 ± 8
	NGR234C	0.0	101 ± 40
	NGR234	36 ± 10	975 ± 259
	HH103-M	0.0	97 ± 27
	NGR234C pSymHH103M	0.0	120 ± 35
T. vogelii	Uninoculated	0.0	152 ± 24
	NGR234C	0.0	107 ± 26
	NGR234	18 ± 3	1171 ± 220
	HH103-M	13 ± 7	312 ± 106
	NGR234C pSymHH103M	5 ± 2	118 ± 37
V. radiata	Uninoculated	0.0	210 ± 47
	NGR234C	0.0	182 ± 40
	NGR234	162 ± 21	2919 ± 367
	HH103-M	57 ± 12	1564 ± 241
	NGR234C pSymHH103M	Only pseudonodules	175 ± 33

Numbers refer to mean values ± standard errors per plant of three Magenta jars containing two plants. Determinations were carried out 42 (V. radiata), 58 (T. vogelii), and 81 (L. leucocephala) days after inoculation.

HH103 Rif^R. These three genes are therefore good candidates for determining symbiotic specificity on CH2. On the CH3 (from Northern China) and CH4 (Central China) accessions, HH103 Rif^R and the *ttsI* (SVQ533) or *rhcJ* (SVQ288) derivative mutants retained nodulation. Shoot dry-weight of CH3 plants inoculated with SVQ533 was significantly lower than for plants inoculated with the parent strain (**Table 4**). Mutations in *ttsI* and *rhcN* of NGR234 totally abolished nodulation on both CH3 and CH2 accessions, however. These phenotypes suggest that NopJ (the only T3SS-effector not secreted by HH103 Rif^R) is a prime candidate for promoting nodulation of CH2 and CH3 by NGR234. Since CH4 plants responded in the same manner to inoculation with NGR234 or NGR**Ω***rhcN*, T3SS and its panel of effectors don't play a significant role during nodulation of this accession. That a significant reduction in all phenotypic parameters monitored occurred when CH4 plants were inoculated with NGR**Ω***ttsI*, indicate that a TtsI-regulated function other than T3SS plays an important role during the NGR234-CH4 interaction, however. Together these results confirm that T3SS play important roles (either positively or negatively) during symbioses between *S. fredii* strains and wild soybean accessions. Also, the different effect that the studied T3SS mutations have in the symbiotic behavior with the different *G. soja* accessions tested suggests that these *G. soja* accessions might have different *Rj* (*rj*) genotypes, although further research is necessary for clarifying this issue.

There is a theoretically alternative way to carry out screenings aimed to isolate new *S. fredii* strains showing altered symbiotic capacities with soybean and other legumes: the construction of *S. fredii* hybrid strains (chimeras) by intraspecific transfer of symbiotic plasmids. The simplest way for constructing such chimeras is by transferring *S. fredii* symbiotic plasmids to pSym-cured derivatives of other *S. fredii* strains. If the symbiotic properties of some of these combinations (*S. fredii* genome background/*S. fredii* pSym) appear to be interesting, the analysis of the hybrids will be easier if the genome sequences of the donor and recipient strains are already known. This would be the situation for hybrids constructed between *S. fredii* strains NGR234 and HH103 Rif^R. Following this approach, we transferred the symbiotic plasmid of HH103 Rif^R to strain NGR234C, a pSym-cured derivative of NGR234. The symbiotic plasmid of NGR234 was marked with transposon Tn*5*-Mob and transferred to *S. fredii* USDA193C, a pSym-cured derivative of *S. fredii* USDA193 (unfortunately, a pSym-cured derivative of HH103 Rif^R is not available). USDA193 forms nitrogen-fixing nodules with Asiatic soybean cultivars but root-swellings and/or ineffective nodules with American soybeans (Keyser et al., 1982).

NGR234 does not effectively nodulate the American soybean cultivar Williams 82. Although Trinick (1980) reported that NGR234 induce Fix$^+$ nodules on *G. max*, the cultivar employed in that study was not specified. Balatti et al. (1995) showed that NGR234 only induces the formation of small, irregular swellings on the roots of 89 different varieties of soybean, including McCall (restriction genotype *Rfg1*) and Dunfield (restriction genotype *Rj4*). Pueppke and Broughton (1999) also found that NGR234 was ineffective with one Asiatic (Peking) and two American (McCall and Preston) varieties of soybean. So, it can be concluded that NGR234 is ineffective with the vast majority of soybean cultivars tested so far.

The *Rj* genotype of soybean Williams 82 is *Rfg1*, which restricts nodulation by *S. fredii* USDA257 (reviewed by Hayashi et al., 2012). This *Rj* genotype is shared by other American varieties such as McCall. This restriction is most probably due to the type three associated effectors secreted by USDA257, since mutants of this strain in this secretion system gain the ability to nodulate American soybeans (reviewed by Staehelin and Krishnan, 2015; López-Baena et al., 2016). Most probably, this is also the reason why other *S. fredii* strains such as USDA192 or USDA193 also fail in nodulating American soybeans. However, the story appears to be more complex since strain HH103, which also possesses a functional symbiotic type three secretion system (T3SS), naturally nodulates American soybeans (including Williams 82) and mutants negatively affected in its T3SS undergo a partial impairment in their interactions with these soybeans (de Lyra et al., 2006).

The chimeric strain NGR234C pSymHH103M formed nodules that did not fix nitrogen with soybean Williams 82, so that the shoot dry-weight of plants inoculated with the hybrid strain was equal to that of the uninoculated control (**Table 7**). Thus, the presence of the pSymHH103M, which is the symbiotic plasmid of a strain (HH103-M) that effectively nodulates Williams 82, is not enough to enable NGR234C to form nitrogen-fixing nodules with this *G. max* cultivar. Three possible explanations can be formulated: (i) some genes essential for effective soybean nodulation are neither present in NGR234C nor provided by pSymHH103M; (ii) some of the NGR234C

genes block nodule development; and (iii) the combination of symbiotic signals produced by the resulting chimeric strain is not suitable for effective nodulation of *G. max* cultivar Williams 82. Although the NGR234C pSymHH103M transconjugant nodulated *G. soja* CH4, nodules that were formed did not contribute to plant growth (**Table 7**). Microscopy studies showed that peribacteroid membranes were disrupted or missing, as is often the case when nodules senesce (**Figure 4F**). This result, that was unexpected as both NGR234 and HH103 Rif^R strains were capable to form proficient nodules on this accession, suggest the combination of symbiotic signals produced by the hybrid strain might not be suitable for making nitrogen-fixing nodules on CH4 accession. For instance, the hybrid must produce the HH103 Rif^R complement of nodulation factors and secreted Nop since genes involved in these symbiotic functions are carried by the symbiotic plasmid. The hybrid, however, should produce the KPS synthesized by NGR234 because *rkp* genes are carried by pNGR234b (Schmeisser et al., 2009). Possibly, LPS of the NGR234C pSymHH103M hybrid should differ from those of NGR234 and HH103 Rif^R as most genes involved in LPS biosynthesis are chromosome born. However, some genes required for the biosynthesis of the flavonoid-inducible rhamnan modification of the NGR234 LPS (Marie et al., 2004) are encoded by p*Sf*NGR234a and thus neither present in NGR234 nor provided by plasmid pSymHH103M (Vinardell et al., 2015).

The *S. fredii* strains NGR234 and HH103-M nodulated *T. vogelii*, the former being more effective (**Table 8**). *T. vogelii* plants inoculated with the hybrid NGR234C pSymHH103M showed reduced nodulation in comparison to the parental strains and the nodules formed did not support plant growth (**Table 8**). These results suggest again that the combination of symbiotic signals produced by the hybrid is less appropriate than that produced by each parental strains. The failure of hybrid NGR234C pSymHH103M to nodulate *L. leucocephala* (**Table 8**) could be due to the absence of a functional *nodS* gene, which is required for nodulation of this legume (Lewin et al., 1990). The *nodS* gene is located in the symbiotic plasmid of NGR234 (missing in NGR234C) and the *nodS* present in pSymHH103 is not functional (Vinardell et al., 2015).

The hybrid USDA193C carrying the symbiotic plasmid of NGR234 (USDA193C pSymNGR234M) failed to nodulate *G. max* cv. Williams 82 but formed nitrogen-fixing nodules with *G. soja* CH4. Thus, the symbiotic properties of the two hybrids studied (NGR234C pSymHH103M and USDA193C pSymNGR234M) are different. We could expect that new combinations would produce "new" *S. fredii* strains in which the symbiotic interaction with a particular legume could be positive or negatively affected or without any noticeable change. The genetic information already available about *S. fredii* HH103 Rif^R and NGR234 strains, together with the structural information of their Nodulation factors, surface polysaccharides and nodulation outer proteins, might allow the prediction of the symbiotic signals produced by the hybrid strains. Taking the advantage that *S. fredii* strains nodulate many different legumes, the study of *S. fredii* hybrids could provide valuable information about the relative importance of particular symbiotic signals, or combination of signals, for the bacterial interaction with a wide range of legumes.

AUTHOR CONTRIBUTIONS

FT-V, XP, JR-S, and JV conceived and designed the experiments. All authors performed the experiments. FT-V, SA-J, XP, JR-S, FL-B, and JV analyzed the data. FT-V, XP, JR-S, and JV contributed with reagents, materials, and analysis tools. FT-V, XP, FL-B, JR-S, and JV wrote the paper. All authors read and approved the final manuscript.

FUNDING

This work was funded by grants P11-CVI-7500 from the Andalusian Government and BIO2016-78409-R from the Ministry of Economy and Competitiveness (Spanish Government). XP acknowledges the generous financial supports of the University of Geneva and the Swiss National Science Foundation (Grants 31003A-146548 and 31003A-173191).

ACKNOWLEDGMENTS

XP would like to thank Natalia Giot for her help in many aspects of this work. SA-J is the recipient of a Ph.D. grant from the VPPI of the University of Seville. They also thank the Centro de Investigación, Tecnología e Innovación (CITIUS) of the University of Seville for light and electronic microscopy facilities.

SUPPLEMENTARY MATERIAL

The Supplementary Material for this article can be found online at: https://www.frontiersin.org/articles/10.3389/fmicb.2018.02843/full#supplementary-material

REFERENCES

Alves, B. J. R., Boddey, R. M., and Urquiaga, S. (2003). The success of BNF in soybean in Brazil. *Plant Soil* 252, 1–9. doi: 10.1023/a:1024191913296

Balatti, P. A., Kovacs, L. G., Krishnan, H. B., and Pueppke, S. G. (1995). *Rhizobium* sp. NGR234 contains a functional copy of the soybean cultivar specificity locus, nolXWBTUV. *Mol. Plant Microbe Interact.* 8, 693–699. doi: 10.1094/MPMI-8-0693

Beringer, J. E. (1974). R factor transfer in *Rhizobium leguminosarum*. *J. Gen. Microbiol.* 84, 188–198. doi: 10.1099/00221287-84-1-188

Brockwell, J., Hely, F. W., and Neal-Smith, C. A. (1966). Some symbiotic characteristics of rhizobia responsible for spontaneous, effective field nodulation of *Lotus hispidus*. *Austr. J. Exp. Agric. Anim. Husband.* 6, 365–370. doi: 10.1071/EA9660365

Broughton, W. J., and Dilworth, M. J. (1971). Control of leghaemoglobin synthesis in snake beans. *Biochem. J.* 125, 1075–1080. doi: 10.1042/bj1251075

Broughton, W. J., Jabbouri, S., and Perret, X. (2000). Keys to symbiotic harmony. *J. Bacteriol.* 182, 5641–5652. doi: 10.1128/JB.182.20.5641-5652.2000

Broughton, W. J., Wong, C.-H., Lewin, A., Samrey, U., Myint, H., Meyer, H. z. A., et al. (1986). Identification of *Rhizobium* plasmid sequences involved in recognition of *Psophocarpus*, *Vigna*, and other legumes. *J. Cell Biol.* 102, 1173–1182. doi: 10.1083/jcb.102.4.1173

Buendía-Clavería, A. M., Moussaid, A., Ollero, F. J., Vinardell, J. M., Torres, A., Moreno, J., et al. (2003). A *purL* mutant of *Sinorhizobium fredii* HH103 is symbiotically defective and altered in its lipopolysaccharide. *Microbiology* 149, 1807–1818. doi: 10.1099/mic.0.26099-0

Buendía-Clavería, A. M., Romero, F., Cubo, T., Perez-Silva, J., and Ruiz-Sainz, J. E. (1989). Inter and intraspecific transfer of a *Rhizobium fredii* symbiotic plasmid: expression and incompatibility of symbiotic plasmids. *Syst. Appl. Microbiol.* 12, 210–215. doi: 10.1016/S0723-2020(89)80016-5

Camacho, M., Santamaría, C., Temprano, F., Rodriguez-Navarro, D. N., Daza, A., Espuny, R., et al. (2002). Soils of the Chinese Hubei province show a very high diversity of *S. fredii* strains. *Syst.. Appl. Microbiol.* 25, 592–602. doi: 10.1078/07233202602605177 33

Chen, Y., Chen, P., and de los Reyes, B. G. (2006). Differential responses of the cultivated and wild species of soybean to dehydration stress. *Crop Sci.* 46, 2041–2046. doi: 10.2135/cropsci2005.12.0466

de Lyra, M. C. C. P., Lopez-Baena, F. J., Madinabeitia, N., Vinardell, J. M., Espuny, M. R., Cubo, M. T., et al. (2006). Inactivation of the *Sinorhizobium fredii* HH103 *rhcJ* gene abolishes nodulation outer proteins (Nops) secretion and decreases the symbiotic capacity with soybean. *Int. Microbiol.* 9, 125–133.

Fossou, R. K., Ziegler, D., Zézé, A., Barja, F., and Perret, X. (2016). Two major clades of bradyrhizobia dominate symbiotic interactions with pigeonpea in fields of Côte d'Ivoire. *Front. Microbiol.* 7:1793. doi: 10.3389/fmicb.2016.01793

Fumeaux, C., Bakkou, N., Kopcińska, J., Golinowski, W., Westenberg, D. J., Müller, P., et al. (2011). Functional analysis of the *nifQdctA1*y4vGHIJ operon of *Sinorhizobium fredii* strain NGR234 using a transposon with a NifA-dependent read-out promoter. *Microbiology* 157, 2745–2758. doi: 10.1099/mic.0.049999-0

Hamilton-Reeves, J. M., Rebello, S. A., Thomas, W., Slaton, J. W., and Kurzer, M. S. (2007). Soy protein isolate increases urinary estrogens and the ratio of 2:16 α-hydroxyestrone in men at high risk of prostate cancer. *J. Nutr.* 137, 2258–2263. doi: 10.1093/jn/137.10.2258

Hartman, G. L., West, E. D., and Herman, T. K. (2011). Crops that feed the World 2. Soybean-worldwide production, use, and constraints caused by pathogens and pests. *Food Sec.* 3, 5–17. doi: 10.1007/s12571-010-0108-x

Hayashi, M., Saeki, Y., Haga, M., Harada, K., Kouchi, H., and Umehara, Y. (2012). Rj (rj) genes involved in nitrogen-fixing root nodule formation in soybean. *Breed. Sci.* 61, 544–553. doi: 10.1270/jsbbs.61.544

Kambara, K., Ardissone, S., Kobayashi, H., Saad, M. M., Schumpp, O., Broughton, W. J., et al. (2009). Rhizobia utilize pathogen-like effector proteins during symbiosis. *Mol. Microbiol.* 71, 92–106. doi: 10.1111/j.1365-2958.2008.06507.x

Kanamaru, K., Wang, S. D., and Abe, J. (2006). Identification and characterization of wild soybean (*Glycine soja* sieb. et Zucc.) strains with high lutein content. *Breed. Sci.* 56, 3231–3234. doi: 10.1270/jsbbs.56.231

Keyser, H. H., Bohlool, B. B., Hu, T. S., and Weber, D. F. (1982). Fast-growing rhizobia isolated from root nodules of soybean. *Science* 215, 1631–1632. doi: 10.1126/science.215.4540.1631

Kofsky, J., Zhang, H., and Song, B. H. (2018). The untapped genetic reservoir: the past, current, and future applications of the wild soybean (Glycine soja). *Front. Plant Sci.* 9:949. doi: 10.3389/fpls.2018.00949

Lewin, A., Cervantes, E., Wong, C.-H., and Broughton, W. J. (1990). *nodSU*, two new *nod* genes of the broad host range *Rhizobium* strain NGR234 encode host-specific nodulation of the tropical tree *Leucaena leucocephala*. *Mol. Plant Microbe Interact.* 3, 317–326. doi: 10.1094/MPMI-3-317

Li, Y., Zhou, G., Ma, J., Jiang, W., Jin, L., Zhang, Z., et al. (2014). De novo assembly of soybean wild relatives for pan-genome analysis of diversity and agronomic traits. *Nat. Biotechnol.* 32, 1045–1052. doi: 10.1038/nbt.2979

Li, Y.-H., Li, W., Zhang, C. H., Yang, L., Chang, R.-Z., Gaut, B. S., et al. (2010). Genetic diversity in domesticated soybean (*Glycine max*) and its wild progenitor (*Glycine soja*) for simple sequence repeat and single-nucleotide polymorphism loci. *New Phytol.* 188, 242–253. doi: 10.1111/j.1469-8137.2010.03344.x

López-Baena, F. J., Ruiz-Sainz, J. E., Rodríguez-Carvajal, M. A., and Vinardell, J. M. (2016). Bacterial molecular signals in the *Sinorhizobium fredii*-soybean symbiosis. *Int. J. Mol. Sci.* 17:E755. doi: 10.3390/ijms17050755

Luo, Q., Yu, B., and Liu, Y. (2005). Differential, sensitivity to chloride and sodium ions in seedlings of *Glycine max* and *G. soja* under NaCl stress. *J. Plant Physiol.* 162, 1003–1012. doi: 10.1016/j.jplph.2004.11.008

Mammadov, J., Buyyarapu, R., Guttikonda, S. K., Parliament, K., Abdurakhmonov, I. Y., and Kumpatla, S. P. (2018). Wild relatives of maize, rice, cotton, and soybean: treasure troves for tolerance to biotic and abiotic stresses. *Front. Plant Sci.* 9:886. doi: 10.3389/fpls.2018.00886

Margaret, I., Becker, A., Blom, J., Bonilla, I., Goesmann, A., Göttfert, M., et al. (2011). Symbiotic properties and first analyses of the genomic sequence of the fast growing model strain *Sinorhizobium fredii* HH103 nodulating soybean. *J. Biotechnol.* 155, 11–19. doi: 10.1016/j.jbiotec.2011.03.016

Marie, C., Deakin, W. J., Ojanen-Reuhs, T., Diallo, E., Reuhs, B., Broughton, W. J., et al. (2004). TtsI, a key regulator of *Rhizobium* species NGR234 is required for Type III-dependent protein secretion and synthesis of rhamnose-rich polysaccharides. *Mol. Plant Microbe Interact.* 17, 958–966. doi: 10.1094/MPMI.2004.17.9.958

Morrison, N. A., Hau, C. Y., Trinick, M. J., Shine, J., and Rolfe, B. G. (1983). Heat curing of a Sym plasmid in a fast-growing *Rhizobium* sp. that is able to nodulate legumes and the nonlegume *Parasponia* sp. *J. Bacteriol.* 153, 527–531.

Natarajan, S., Xu, C. P., and Bae, H. (2007). Proteomic and genomic characterization of *Kunitz trypsin* inhibitors in wild and cultivated soybean genotypes. *J. Plant Physiol.* 164, 756–763. doi: 10.1016/j.jplph.2006.05.014

Ojha, A., Tak, N., Rathi, S., Chouhan, B., Rao, S. R., Barik, S. K., et al. (2017). Molecular characterization of novel *Bradyrhizobium* strains nodulating *Eriosema chinense* and *Flemingia vestita*, important unexplored native legumes of the sub-Himalayan region (Meghalaya) of India. *Syst. Appl. Microbiol.* 40, 334–344. doi: 10.1016/j.syapm.2017.06.003

Perret, X., Staehelin, C., and Broughton, W. J. (2000). Molecular basis of symbiotic promiscuity. *Microbiol. Mol. Biol. Rev.* 64, 180–201. doi: 10.1128/MMBR.64.1.180-201.2000

Pueppke, S. G., and Broughton, W. J. (1999). *Rhizobium* sp. strain NGR234 and *R. fredii* USDA257 share exceptionally broad, nested host ranges. *Mol. Plant Microbe Interact.* 12, 293–318. doi: 10.1094/MPMI.1999.12.4.293

Qiu, L. J., and Chang, R. Z. (2010). "The origin and history of soybean," in *The Soybean. Botany, Production and Uses*, ed. G. Singh (Wallingford: CAB International), 4.

Rathi, S., Tak, N., Bissa, G., Chouhan, B., Ojha, A., Adhikari, D., et al. (2018). Selection of *Bradyrhizobium* or *Ensifer symbionts* by the native Indian caesalpinioid legume *Chamaecrista pumila* depends on soil pH and other edaphic and climatic factors. *FEMS Microbiol. Ecol.* 94:fiy180. doi: 10.1093/femsec/fiy180

Rigaud, J., and Puppo, A. (1975). Indole-3-acetic acid catabolism by soybean bacteroids. *J. Gen. Microbiol.* 88, 223–228. doi: 10.1099/00221287-88-2-223

Romero, F. (1993). *Estudio Genetico de la Nodulacion de Rhizobium fredii*. Ph.D. thesis, University of Seville, Seville.

Rosell, M. S., Appleby, P. N., Spencer, E. A., and Key, T. J. (2004). Soy intake and blood cholesterol considerations: a cross-sectional study of 1033 pre- and post-menopausal women in the Oxford arm of the European prospective investigation into cancer and nutrition. *Am. J. Clin. Nutr.* 80, 1391–1396. doi: 10.1093/ajcn/80.5.1391

Sambrook, J., and Russell, D. (2001). *Molecular Cloning: A Laboratory Manual*, 3rd Edn. Cold Spring Harbor, NY: Cold Spring Harbor Laboratory.

Sankhla, I. S., Tak, N., Meghwal, R. R., Choudhary, S., Tak, A., Rathi, S., et al. (2017). Molecular characterization of nitrogen fixing microsymbionts from root nodules of *Vachellia* (*Acacia*) *jacquemontii*, a native legume from the Thar Desert of India. *Plant Soil* 410, 21–40. doi: 10.1007/s11104-016-2838-9

Schmeisser, C., Liesegang, H., Krysciak, D., Bakkou, N., Le Quéré, A., Wollherr, A., et al. (2009). *Rhizobium* sp. NGR234 possesses a remarkable number of secretion systems. *Appl. Environ. Microbiol.* 75, 4035–4045. doi: 10.1128/AEM.00515-09

Simon, R. (1984). High frequency mobilization of gram-negative bacterial replicons by the in vivo constructed Tn5-Mob transposon. *Mol. Gen. Genet.* 196, 413–420. doi: 10.1007/BF00436188

Singh, R. J. (2007). Methods for Producing Fertile Crosses Between Wild and Domestic Soybean Species. US Patent. Application number 11/417,369. Washington, DC: U.S. Patent and Trademark Office.

Sprent, J. I., Ardley, J., and James, E. K. (2017). Biogeography of nodulated legumes and their nitrogen-fixing symbionts. *New Phytol.* 215, 40–56. doi: 10.1111/nph.14474

Staehelin, C., and Krishnan, H. B. (2015). Nodulation outer proteins: double-edged swords of symbiotic rhizobia. *Biochem. J.* 470, 263–274. doi: 10.1042/BJ20150518

Tian, C. F., Zhou, Y. J., Zhang, Y. M., Li, Q. Q., Zhang, Y. Z., and Li, D. F. (2012). Comparative genomics of rhizobia nodulating soybean suggest extensive recruitment of lineage specific genes in adaptations. *Proc. Natl. Acad. Sci. U.S.A.* 109, 8629–8634. doi: 10.1073/pnas.1120436109

Trinick, M. J. (1980). Relationships amongst the fast-growing *Rhizobium* of *Lablab purpureus*, *Leucarena leucocephala*, *Mimosa* sp., *Acacia farnesiana*, and *Sesbania grandiflora* and their affinities with other *Rhizobium* groups. *J. Appl. Bacteriol.* 49, 39–53. doi: 10.1111/j.1365-2672.1980.tb01042.x

Turner, G. L., and Gibson, A. H. (1980). "Measurement of nitrogen fixation by indirect means," in *Methods for Evaluating Biological Nitrogen Fixation*, ed. F. J. Bergersen (New York, NY: Wiley), 111–138.

Vinardell, J. M., Acosta-Jurado, S., Zehner, S., Göttfert, M., Becker, A., Baena, I., et al. (2015). The *Sinorhizobium fredii* HH103 genome: a comparative analysis with *S. fredii* strains differing in their symbiotic behavior with soybean. *Mol. Plant Microbe Interact.* 28, 811–824. doi: 10.1094/MPMI-12-14-0397-FI

Vinardell, J. M., Buendía-Clavería, A. M., and Ruiz-Sainz, J. E. (1993). A method for the positive selection of spontaneous *Rhizobium* mutants showing transcriptional activation of nodulation genes in the absence of nod-inducers. *Mol. Plant Microbe Interact.* 6, 782–785. doi: 10.1094/MPMI-6-782

Vincent, J. M. (1970). *A Manual for the Practical Study of Root-Nodule Bacteria*. Oxford: Blackwell Scientific Publications.

Westcott, P., and Hansen, J. (2016). *USDA Agricultural Projections to 2025. No. (OCE-2016-1). Office of the Chief Economist, World Agricultural Outlook Board, U.S. Department of Agriculture*. Available at: https://www.ers.usda.gov/publications/pub-details/?pubid=37818

Xu, C. P., Capena, T. J., and Garret, W. M. (2007). Proteomic analysis of the distribution of the major seed allergens in wild, landrace, ancestral, and modern soybean genotypes. *J. Sci. Food Agric.* 87, 2511–2518. doi: 10.1002/jsfa.3017

Yang, S. H., Chen, W. H., Wang, E. T., Chen, W. F., Yan, J., Han, X. Z., et al. (2018). Rhizobial biogeography and inoculation application to soybean in four regions across China. *J. Appl. Microbiol.* 125, 853–866. doi: 10.1111/jam.13897

Yang, S. S., Bellogin, R. A., Buendía, A., Camacho, M., Chen, M., Cubo, T., et al. (2001). Effect of pH and soybean cultivars on the quantitative analyses of soybean rhizobia populations. *J. Biotechnol.* 91, 243–255. doi: 10.1016/S0168-1656(01)00340-6

Yasuda, M., Miwa, H., Masuda, S., Takebayashi, Y., Sakakibara, H., and Okazaki, S. (2016). Effector-triggered immunity determines host genotype-specific incompatibility in Legume–Rhizobium symbiosis. *Plant Cell Physiol.* 57, 1791–1800. doi: 10.1093/pcp/pcw104

Zhang, B., Du, N., Li, Y., Shi, P., and Wei, G. (2018). Distinct biogeographic patterns of rhizobia and non-rhizobial endophytes associated with soybean nodules across China. *Sci. Total Environ.* 643, 569–578. doi: 10.1016/j.scitotenv.2018.06.240

Zhao, L., Fan, M., Zhang, D., Yang, R., Zhang, F., Xu, L., et al. (2014). Distribution and diversity of rhizobia associated with wild soybean (*Glycine soja* Sieb. & Zucc.) in Northwest China. *Syst. Appl. Microbiol.* 37, 449–456. doi: 10.1016/j.syapm.2014.05.011

Zhou, Z., Jiang, Y., Wang, Z., Gou, Z., Lyu, J., Li, W., et al. (2015). Resequencing 302 wild and cultivated accessions identifies genes related to domestication and improvement in soybean. *Nat. Biotechnol.* 33, 408–414. doi: 10.1038/nbt.3096

Conflict of Interest Statement: The authors declare that the research was conducted in the absence of any commercial or financial relationships that could be construed as a potential conflict of interest.

frontiers in Microbiology

ORIGINAL RESEARCH
published: 08 January 2019
doi: 10.3389/fmicb.2018.03208

Rapid Succession of Actively Transcribing Denitrifier Populations in Agricultural Soil During an Anoxic Spell

Binbin Liu[1]†, Xiaojun Zhang[2], Lars R. Bakken[1], Lars Snipen[1] and Åsa Frostegård[1]*

[1] Faculty of Chemistry, Biotechnology and Food Science, Norwegian University of Life Sciences, Ås, Norway, [2] State Key Laboratory of Microbial Metabolism and School of Life Sciences and Biotechnology, Shanghai Jiao Tong University, Shanghai, China

OPEN ACCESS

Edited by:
Maria J. Delgado, Spanish National Research Council (CSIC), Spain

Reviewed by:
Kristof Brenzinger, Netherlands Institute of Ecology (NIOO-KNAW), Netherlands
Katharina Kujala, University of Oulu, Finland

***Correspondence:**
Binbin Liu
binbinliu@sjziam.ac.cn

†Present address:
Binbin Liu, Center for Agricultural Resources Research, Institute of Genetics and Developmental Biology, Chinese Academy of Sciences, Shijiazhuang, China

Specialty section:
This article was submitted to Terrestrial Microbiology, a section of the journal Frontiers in Microbiology

Received: *16 September 2018*
Accepted: *11 December 2018*
Published: *08 January 2019*

Citation:
Liu B, Zhang X, Bakken LR, Snipen L and Frostegård Å (2019) Rapid Succession of Actively Transcribing Denitrifier Populations in Agricultural Soil During an Anoxic Spell. Front. Microbiol. 9:3208. doi: 10.3389/fmicb.2018.03208

Denitrification allows sustained respiratory metabolism during periods of anoxia, an advantage in soils with frequent anoxic spells. However, the gains may be more than evened out by the energy cost of producing the denitrification machinery, particularly if the anoxic spell is short. This dilemma could explain the evolution of different regulatory phenotypes observed in model strains, such as sequential expression of the four denitrification genes needed for a complete reduction of nitrate to N_2, or a "bet hedging" strategy where all four genes are expressed only in a fraction of the cells. In complex environments such strategies would translate into progressive onset of transcription by the members of the denitrifying community. We exposed soil microcosms to anoxia, sampled for amplicon sequencing of *napA/narG*, *nirK/nirS,* and *nosZ* genes and transcripts after 1, 2 and 4 h, and monitored the kinetics of NO, N_2O, and N_2. The cDNA libraries revealed a succession of transcribed genes from active denitrifier populations, which probably reflects various regulatory phenotypes in combination with cross-talks via intermediates (NO_2^-, NO) produced by the "early onset" denitrifying populations. This suggests that the regulatory strategies observed in individual isolates are also displayed in complex communities, and pinpoint the importance for successive sampling when identifying active key player organisms.

Keywords: denitrification, transcription, denitrifying genes, amplicon sequencing, OTU clustering

INTRODUCTION

Denitrification in agricultural soils is recognized as a major source of nitric and nitrous oxide emissions to the atmosphere (Opdyke et al., 2009; Syakila and Kroeze, 2011; Butterbach-Bahl et al., 2013; Gerber et al., 2016). The process is a dissimilatory metabolism that enables facultative anaerobic microorganisms to respire nitrogen oxides during periods of anoxia. Complete denitrification is the reduction of nitrate (NO_3^-) to dinitrogen (N_2) via nitrite (NO_2^-), nitric oxide (NO) and nitrous oxide (N_2O). These four consecutive steps are catalyzed by the complex metalloenzymes Nar, Nir, Nor, and N2OR (NO_3^--, NO_2^--, NO-, and N_2O reductase, encoded by *nar, nir, nor,* and *nos*, respectively). Nar reductases encompass the membrane bond NarG and the periplasmic NapA; Nir the copper containing NirK and the cytochrome cd_1 NirS; and Nor the

cytochrome c dependent cNor, the quinol dependent qNor and the less common copper-containing qCuANor (Shapleigh, 2013). The N2OR enzymes are separated into two main clades (I and II), both with two copper-containing redox centers (Hallin et al., 2017). Except for the two types of Nir, bacteria very seldom contain more than one type of the respective reductases (Graf et al., 2014). A complete denitrification pathway, comprising all four reduction steps of denitrification, is found among a wide range of taxonomically diverse bacteria, as well as in some Archaea (Shapleigh, 2013). In addition, there are many prokaryotes, and also some fungi, that have a truncated denitrification pathway where one or more of the steps are missing. This may be due either to a lack of the functional gene itself or another essential gene in the operon (Bergaust et al., 2008; Liu et al., 2013; Roco et al., 2017), or because transcriptional regulation or post-transcriptional mechanisms prevent or delay the expression of functional enzymes (Bergaust et al., 2010, 2012; Bueno et al., 2015). In a study by Chèneby et al. (2000) the numbers of denitrifiers (with or without N_2O reduction), isolated from a range of soils, was 0.9–4.7% of all the aerobic/facultative anaerobic bacterial isolates. More recently, Lycus et al. (2017) developed an improved isolation protocol and found that 6.7% of the bacteria isolated under aerobic conditions from agricultural peat soil could perform all four denitrification steps, and 16% were able to carry out NO_2^- reduction to NO, which is considered as the defining step of denitrification (Zumft, 1997; Shapleigh, 2013).

Oxygen gives a higher energy yield from respiration than nitrogen oxides, and is the preferred electron acceptor for denitrifiers. This requires strict genetic regulation, allowing the organisms to respire oxygen during oxic conditions, but to sense decreasing oxygen concentrations in time to initiate the denitrification apparatus, thus avoiding being entrapped in anoxia without the possibility to conserve energy (Højberg et al., 1997). In addition, the transition to anaerobic respiration should be balanced in order to avoid accumulation of the toxic intermediates NO_2^- and NO. The genetic regulation of denitrification is complex and involves over 50 genes, encoding not only the reductases but also transcription factors and assembly pathways (Zumft, 1997). The regulatory networks of denitrification are diverse, and may differ even between closely related organisms (Spiro, 2012), resulting in a range of regulatory phenotypes (Liu et al., 2013; Lycus et al., 2017). So far, this knowledge is based on detailed studies of a limited number of model organisms. Common to these is that their transcriptional regulation of denitrification genes involves proteins belonging to the bacterial superfamily of Crp/Fnr (cAMP receptor protein/fumarate and nitrate reduction regulatory protein). They include, among others, oxygen sensing proteins that act as transcriptional activators of *nar/nap* and *nos*, such as FnrP (in *Paracoccus denitrificans*), ANR (in *Pseudomonas aeruginosa*) and $FixK_2$ in *Bradyrhizobium diazoefficiens*; NO_3^-/NO_2^- sensing proteins such as DNR, DnrD, and NarR (in *Pseudomonas aeruginosa*, *P. stutzeri,* and *P. denitrificans*, respectively) as well as the two-component regulatory systems NarXL; NarQP and FixLJ; and NO-sensing regulators such as NNR (*P. denitrificans*) and DNR (*P. stutzeri*), which control the transcription of genes encoding Nir, Nor, and N2OR (Rodionov et al., 2005; Spiro, 2012; Gaimster et al., 2018).

A consequence of the large variation in genetic potential and in transcriptional regulation found in denitrifiers is that they differ substantially, not only in their denitrification end products (NO_2^-, NO, or N_2O), but also in their transient accumulation of intermediate products (Lycus et al., 2017). The differences may be large even between closely related organisms. For example, some strains of the genus *Thauera* showed a rapid, complete onset of all four denitrification genes in response to anoxia with little or no accumulation of denitrification intermediates (Liu et al., 2013). Other strains in the same genus instead showed a progressive onset where they first transcribed Nar while inhibiting the transcriptional activation of *nir* until all provided NO_3^- was consumed, resulting in mM accumulation of NO_2^-. The control of NO accumulation also varies, and batch incubations report values from nM to μM in different organisms (Bergaust et al., 2008, 2010; Lycus et al., 2017). Accumulation of N_2O by bacteria carrying N2OR can also vary by 2–3 orders of magnitude even between closely related strains (Liu et al., 2013).

In complex microbial communities such as soils, which harbor a large diversity of organisms with different denitrification regulatory phenotypes (Lycus et al., 2017), it can be expected that some populations induce the entire set of denitrification reductases in response to an anoxic spell, while others only initiate part of the pathway either in all cells, or only in a fraction of the population. This would mean that different denitrifier populations (and subpopulations) are active at different times after oxygen depletion, and that organisms with an "early onset" may trigger the onset of other denitrifiers through the production of intermediates such as the signaling molecule NO, which initiates transcription of genes encoding Nir and Nor via NNR-like regulators (Zumft, 2002; Spiro, 2017). In an earlier study of the same soil as the one used here, we observed a major peak in *nir* and *nos* transcription activity during the first ca. 5 h of anoxia (Liu et al., 2010). The main goal of the present investigation was to (1) identify the active groups of denitrifiers in a soil and compare this to the total bacterial denitrifier community in the same soil and (2) to investigate whether there was a shift in the composition of actively transcribing populations during the initial phase of an anoxic spell. We incubated intact soil in microcosms as described by Liu et al. (2010), and sequenced the DNA and cDNA amplicons of the *narG, napA, nirS, nirK,* and *nosZ clade I* genes in samples taken during the first 4 h after oxygen depletion. Since the same primer pairs were used for DNA and cDNA, we could identify the active organisms in the targeted groups at different time points. Our approach allowed us to identify shifts in the composition of active groups of denitrifiers during a transcription peak, in response to anoxia.

A specific, methodological problem that we address is the lack of consensus regarding the choice of similarity threshold values for the clustering of functional gene sequences into OTUs (operational taxonomic units). There is currently no "golden standard threshold" to define a taxon (Konstantinidis et al., 2017), although values between 97 and 99.5% similarity are often used for OTUs based on the 16S rRNA gene (Clarridge, 2004). These thresholds are, however, controversial, especially

when applying high throughput sequencing providing orders of magnitudes higher sequence coverage (Konstantinidis et al., 2006; Schloss and Westcott, 2011). Threshold values have also been developed for OTU classification of the denitrification genes (Palmer et al., 2009; Depkat-Jakob et al., 2013), by relating sequence divergence of the functional gene to that of the 16S rRNA gene. This could bias the results since the functional genes in strains that share 97% 16S rRNA sequence identity may have much lower sequence similarity (Gaby and Buckley, 2014) and, moreover, since highly homologous sequences for functional genes may originate from distantly related taxa. In the present study we developed a new strategy to define the sequence similarity threshold of OTUs based on the sequence variation of the targeted region of the functional gene and the number of taxa identified through taxonomy classification. Although the OTU thresholds obtained in this way are sample dependent, the method developed to generate these thresholds can potentially become a general strategy and be applied in any amplicon sequencing studies.

MATERIALS AND METHODS

Preparation of Soil Samples, Anaerobic Incubation, and Gas Kinetics

Peat soil was collected from a hay meadow field in a long-term liming experiment established at Fjaler in western Norway in 1976. The soil, classified as a Sapric Histosol (FAO/ISRIC/ISS), contained on average 45% organic C and 2% organic N. Soil pH had been raised to different levels by addition of shell sand (Sognnes et al., 2006; Mørkved et al., 2007). A plot limed to pH 8.0 (800 m^3 shell sand ha^{-1}) was sampled for the present study. The soil was sieved (4 mm mesh) and subjected to a flooding/drainage treatment with a solution containing 2 mM NO_3^- (equivalent to ca. 36 μmol N) and 10 mM glutamic acid, as described previously (Liu et al., 2010). Glutamate was added since this soil showed near-constant denitrification rates (no growth) and no detectable transcripts of denitrification genes if no C-source was added, suggesting severe nutrient limitation (Liu et al., 2010). Soil samples (20 g fresh weight) were transferred to 125 ml vials, which were sealed with aluminum caps. The headspace was made near anoxic (∼50 ppmv O_2 in headspace) by repeated evacuation/filling with He for six times and the vials were then placed in a robotized incubation system which monitored O_2, NO, N_2O, and N_2 continuously (Molstad et al., 2007). Samples were taken 1, 2, and 4 h after O_2 depletion, in line with earlier studies where transcription of the denitrification genes was observed primarily during the first 5 h (Liu et al., 2010). Destructive sampling was performed by snapshot freezing the soil from each vial in liquid nitrogen. Triplicate vials were sampled at each time point. The samples were then stored at −80°C until further analysis (no longer than 1 week before the mRNA extraction). Three replicate vials were left undisturbed and monitored for gas kinetics for 90 h (sampled for gas concentrations every 3 h) using the robotized incubation system described above, during which all available nitrate was reduced to N_2 (seen as N_2 reaching a stable plateau after ∼70 h).

Nucleic Acid Extraction, Barcoded PCR Amplification, and Pyrosequencing

Extraction of nucleic acids was done using phenol/chloroform, followed by nucleic acid purification using commercial kits, as described previously (Liu et al., 2010). Reverse transcription was performed with random hexamer primers using the Masterscript RT-PCR System (5 Prime GmbH, Hamburg, Germany). Triplicate samples were taken for DNA extraction at the start of the experiment, and for RNA extraction after 1, 2, and 4 h of incubation. DNA and RNA extracts of good quality and quantity were obtained from all samples. The ratios of $A_{260\ nm}$: $A_{280\ nm}$ measured using Nanodrop spectrophotometer were >1.7 for all the samples. The yield of genomic DNA and total RNA were 19.2–24.6 and 7.9–12.4 μg g^{-1} wet weight soil, respectively. The control samples, which were RNA treated with DNase (without performing reverse transcription), were amplified with the universal 16S rRNA gene primers 27f/1492r (Lane, 1991). No bands were visible on the agarose gels, indicating successful removal of genomic DNA. This was further confirmed by qPCR using the DNase treated RNA as template and cDNA with primer pair 27f/518r (targeting 16S rRNA gene sequences). No signal was detected for the RNA (Ct > 34), confirming that the genomic DNA was successfully digested.

A number of primers were tested, which were used in previous studies for amplification of *napA*, *narG*, *nirS*, *nirK*, *cnorB,* and *nosZ* clades I and II. Primer combinations which resulted in successful amplification are listed in **Supplementary Table S1**. For *nosZ*, amplicons were only obtained for clade I, from here on referred to as "*nosZ*". A barcode sequence was added to one primer in order to identify the source of the sample. PCR was performed using a total volume of 25 μl containing 0.5 unit GoTaq polymerase, 1× GoTaq buffer (Promega), 160 μM (each) dNTP, 0.4 μM (each) primer, and 50 ng of DNA/cDNA. All PCR reactions were carried out using the following conditions: an initial denaturation step at 95°C for 5 min, 11 cycles of denaturation at 95°C for 30 s, annealing with a gradient temperature from 52 to 56°C for 40 s, increased by 0.5°C each cycle, and extension at 72°C for 40 s, followed by 24 more cycles consisting of 95°C for 30 s, 54°C for 40 s, 72°C for 40 s, and a final extension step at 72°C for 10 min. The amplification products were examined on a 1% agarose gel in 1× Tris-acetate-EDTA (TAE), and the targeted bands were cut and purified using PCR product purification columns (Promega). Amplicons were obtained for all the genes from all the DNA samples. From the cDNA, amplicons were obtained for the *napA*, *narG*, *nirS,* and *nosZ* genes from all samples, except for the *narG* and *nosZ* genes in the cDNA from the 1 h sampling occasion. No amplicons were obtained for the *nirK* and *cnorB* genes from any of the cDNA samples. The concentrations of the different amplicons, after gel-purification, ranged between 8.5∼121.4 ng/μl. Molar concentrations were calculated based on an average base pair

molecular weight of 649 g/mol. The amplicons of similar sizes were pooled in equal numbers (measured as moles) and were sent to the W. M. Keck Center for Comparative and Functional Genomics at the University of Illinois at Urbana-Champaign (United States). A shotgun genomic DNA library was prepared from each pooled PCR sample using the Roche GS Rapid Library Prep Kit following the Roche Rapid Library Preparation Manual instructions (Roche Applied Sciences, Indianapolis, IN, United States). Sequencing was performed on a 454 Genome Sequencer beta FLX+ system (350 flow cycles) according to the manufacturer's instructions (454 Life Sciences, Branford, CT, United States).

Sequence Filtering and Analysis

The original sequences in FASTA format and the corresponding quality files were extracted from the raw sequence files by using the "sffinfo" tool from the Mothur pipeline (Schloss et al., 2009). Errors from pyrosequencing and PCR amplification, which can dramatically inflate the detected microbial diversity, were removed using the PyroNoise and SeqNoise algorithms from the AmpliconNoise pipeline (Quince et al., 2009, 2011). Chimera sequences were removed using the software Perseus from the same software package.

Reference Sequences

An on-the-fly database was constructed for each gene by standalone BLAST (Altschul et al., 1990) with pooled sequences from all samples of the same gene against the nucleotide database from GenBank[1]. The retrieved top 20 hits of each query sequences were pooled together, and the duplicated sequences removed. Detailed taxonomic information was retrieved for each GI number with a Perl script using Entrez Programming Utilities (NCBI E-utilities[2]), the sequences identified as unknown organisms were removed from the database. The resulting file, including an "id-to-taxonomy" file and a sequence file, were used for taxonomy assignment in QIIME (Caporaso et al., 2010).

Operational Taxonomic Units (OTU)

Denoised reads were clustered into OTUs using the UCLUST (Edgar, 2010) software implemented in QIIME pipeline (Caporaso et al., 2010). Representative sequences from each OTU were selected and taxonomy was assigned using the BLAST method with the default settings (Altschul et al., 1990; Camacho et al., 2009). The UCLUST method relies on a sequence identity threshold set by the user. A cluster is defined by a highly abundant sequence variant, and all its neighboring sequences within the set identity threshold are assigned to the same cluster. For clustering of the 16S rRNA genes a threshold of 0.97 (or 0.95 for genus) is common, but for other, less conserved genes, this is most likely too high. To find an appropriate threshold for the genes in this analysis, we used the approach sketched in **Figure 2**, where the cutoff value (x-axis) is identity threshold value. We changed the cutoff gradually between 0.6 and 1, determined the number of OTUs and assigned each OTU to a genus each time. The number of discovered genera (blue curve) and OTUs (green curve) shows that the number of taxa reaches saturation when the cutoff value increases above a certain value (illustrated by the red line), while the OTU number above this value increases sharply. Choosing a higher cutoff value will generate more OTUs without discovering more taxonomic groups, indicating we are just splitting genera by a finer resolution. Thus, the red vertical line indicates the threshold we used to cluster OTUs (**Figure 2**).

Statistical Analysis

The relative abundances of OTUs (% of total number) were subjected to principal component analysis (PCA) to elucidate major variation and covariation patterns in the cDNA and DNA libraries, and to evaluate the reproducibility of the techniques used by comparing the variation among replicate samples. Significant differences in the cDNA and DNA libraries were investigated by permutational analysis of variance (PERMANOVA, Anderson, 2001). Rarefaction analysis was performed to assess the richness of each library and to evaluate the sampling effort. The data matrix showing the relative abundances of each genus was achieved from QIIME pipeline. The relative abundances were standardized and used for PCA analysis. PCA and rarefaction analysis were performed with the software "R"[3], using package "FactoMineR"[4] and package "vegan" [5], respectively.

Nucleotide Sequence Accession Numbers

The sequences obtained in the study were deposited in GenBank with the Accession NOs. MH737773–MH740873.

RESULTS

Oxygen Availability During Incubation

We used the same soil and the same anaerobic incubation procedure as Liu et al. (2010), and obtained essentially identical N gas kinetics throughout the anaerobic incubation (**Figure 1**): early onset of N_2 production, transient accumulation of N_2O peaking after 24 h (2.7 μmol N_2O-N vial^{-1}) declining to zero after 40 h, while the transient NO accumulation (maximum 200 nmol vial^{-1}) lasted until nitrogen oxyanions were depleted after 70 h. The cumulated N_2 reached a plateau at approximately 36 μmol N_2-N, equivalent to the amount of NO_3^-N in the soil at the start of the incubation (2 mM NO_3^- added to 20 g soil, and assuming 90% soil moisture). The initial oxygen concentration in the headspace after He washing was 20–50 ppmv (90–220 nmol O_2 vial^{-1}), and fluctuated within this range throughout the entire incubation, despite the input of 50 nmol O_2 at each gas sampling (16 nmol h^{-1}) through leakage during the sampling. Thus, active oxygen consumption took place throughout, although denitrification was the dominant respiratory pathway. For the time increment when the soils were extracted for DNA and RNA (1–4 h after He washing), the electron flow to terminal oxidases accounted for ∼5% of

[1] ftp://ftp.ncbi.nlm.nih.gov/blast/db/

[2] http://www.ncbi.nlm.nih.gov/books/NBK25500/

[3] http://www.r-project.org

[4] http://factominer.free.fr

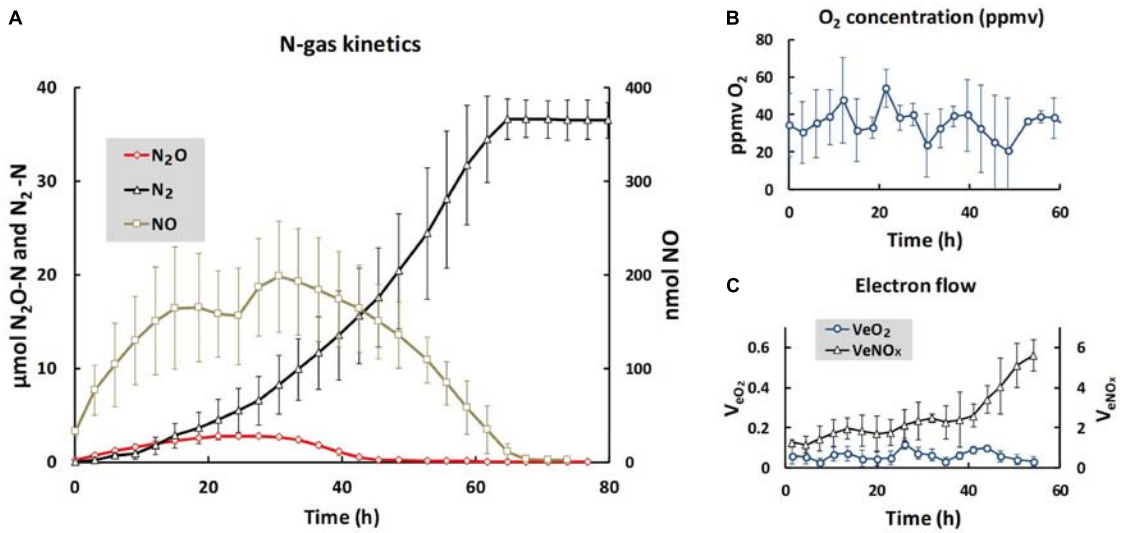

FIGURE 1 | Gas kinetics and electron flow throughout the entire incubation. **(A)** Shows the average amounts of N-gasses per vial: nmol NO (right axis), μmol N_2O- and N_2-N (left axis). **(B)** Shows the average O_2 concentrations (ppmv = uL O_2 L^{-1}), and **(C)** shows the electron flow to terminal oxidases (V_eO_2) and to denitrification (V_{eNOx}), both as μmol e- $vial^{-1}$ h^{-1}. Bars indicate standard deviation (n = 3). For N_2O **(A)**, the standard deviations are too low to be visible. The low and near constant electron flow to terminal oxidases was sustained by the O_2 leakage through the injection system, which was 50 nmol O_2 per sampling (= 16 nmol h^{-1}, since the vials were sampled every 3 h). Note that the scale for V_eO_2 is one 10th of the scale for V_{eNO_X}, thus V_eO_2 was approximately 5% of V_{eNOx} during the first 10 h of incubation. Given the fluctuation of oxygen concentrations between 20 and 50 ppmv, the equilibrium concentration of O_2 in the soil moisture fluctuated between 30 and 75 nM [solubility of oxygen at the incubation temperature (15°C) is 0.0015 mol L^{-1} atm^{-1}].

the total respiratory electron flow (**Figure 1C**). The evidence that the organisms had access to a minimum of oxygen is important, because cells without intact denitrification enzymes need a minimum of aerobic respiration to provide the energy to transcribe denitrification genes and synthesize the enzymes (Hassan et al., 2016).

OTU Classification

Noise removal processes eliminated 35–82% of the bad quality reads. The numbers of sequences before and after noise removal are shown in **Table 1**. The cutoff values to classify the OTUs for different genes were obtained using the principle described in the M&M section and illustrated in **Figure 2**. For each gene investigated, a series of sequence similarity threshold values (0.6–1) was selected and the thresholds were generated (shown in **Supplementary Figures S1–S6** and listed in **Table 1**).

Comparison of DNA and cDNA Libraries

Principal component analysis and PERMANOVA analyses were performed for each of the genes *napA*, *narG*, *nirS* and *nosZ*, which were the genes for which amplicons were obtained in both the DNA and cDNA samples. For PCA, the relative abundances (in %; standardized values) of OTUs in the respective libraries were used as variables, and the libraries of DNA and cDNA1-3 (sampled at 1, 2, and 4 h) were used as cases. The reproducibility was generally good as seen from the positions of the samples in the PCA plots (**Figures 3A–D**). For all four genes the DNA libraries were clearly separated from the cDNA libraries along the first principal component (PC1), which explained 51.9–73.7% of the total variation. This reflects the differences in community composition between the total denitrifier community (the DNA library) and the subset of the community that

TABLE 1 | Numbers of amplified sequences, OTUs and assigned genera for the different denitrification genes.

Gene	Total sequence numbers before noise removal	Total sequence numbers after noise removal	OTU threshold (%)	No. of OTUs	No. of assigned genera
napA	19140	12358	93	436	34
narG	13684	6786	96	1025	70
nirS	13286	2389	95	369	30
nirK	7665	4178	95	642	23
qnorB	10508	4683	83	465	31
nosZ	11213	4439	89	164	26

The OTU thresholds were defined based on the taxonomic assignment, for detailed information see ***Supplementary Figures S1–S6****.*

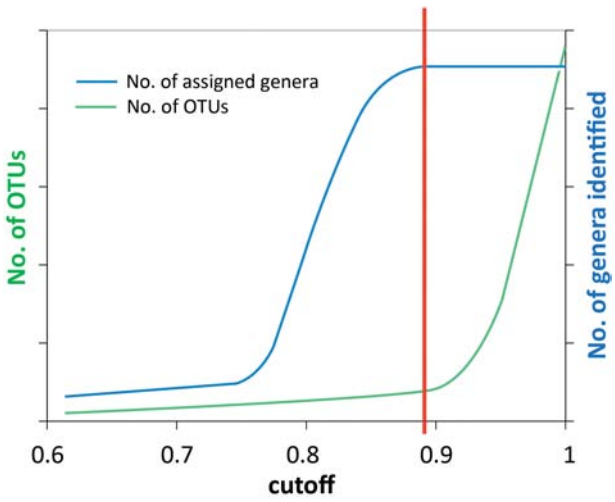

FIGURE 2 | Schematic illustration of how the similarity threshold value for defining OTUs was chosen. The reads were clustered into OTUs at a number of cutoff values ranging from 0.6 to 1. Taxonomy assignment was also performed at each cutoff value. By plotting the number of assigned genera (blue curve) and the number of OTUs (green curve) against the cutoff values, the point where the number of genera is saturated (red line) was chosen as the threshold value to define OTUs. This method was used for all genes analyzed in this study, and the results are shown in **Supplementary Figures S1–S6**.

transcribed the same gene (the cDNA library). This was further confirmed by PERMANOVA analysis, which showed that the differences between the DNA and the cDNA for the genes investigated were significant in most cases (**Supplementary Table S2**). Replicate samples from the cDNA were clustered according to sampling time in the PCA plots (**Figures 3A–D**), demonstrating a change in the composition of the active part of the microbial community over time, with the 4 h samples clearly separating from the earlier sampling times for all four genes.

Composition of Total and Active Denitrifier Communities

Taxonomy was assigned at the genus level and the phylogenetic composition of the seven largest genera for each gene is shown in **Figures 4**, **5**. The minor groups are listed in the **Supplementary File S2**. For the *narG* gene, which encodes the membrane-bound nitrate reductase NarG (Philippot and Højberg, 1999), amplification products were obtained from the DNA sample and from cDNA sampled at 2 and 4 h, while no amplicons were obtained from the 1 h sampling. A total of 1025 OTUs, assigned to 70 genera, were identified. The most dominant group in the DNA library for this gene was the genus *Pseudomonas*, which accounted for 30.9 ± 2.8% of the total number of sequences. In the cDNA samples, the proportion of this genus was only 9.1 ± 3.1% at 2 h, and increased to 13.2 ± 1.4% at 4 h. The second largest group carrying *narG* was *Acidovorax* (17.8 ± 2.7% in the DNA). This genus accounted for a similar proportion in the cDNA at the 2 h sampling occasion (17.3 ± 1.3%), but decreased to 11.5 ± 3.7% at 4 h. The genus *Delftia*, which only accounted for 3.8 ± 2.5% in the DNA, became the most dominant group in cDNA at 2 h, accounting for 31.6 ± 12.6% of the transcripts. A similar trend was observed for the genus *Halomonas,* which constituted 3.2 ± 2.0% of the DNA community but 38.0 ± 11.4% of the 4 h cDNA community (**Figure 4**).

Amplicons of *napA* were detected in the DNA as well as in the cDNA from all three sampling occasions. A total of 436 OTUs, assigned to 34 genera, were identified. A considerable portion of the *napA* sequences (25.1 ± 5.4% in the DNA, 20.9 ± 2.1% in the 2 h cDNA and 22.2 ± 3.3% in the 4 h cDNA) had no match in the database and were grouped as "unidentified." The most dominant group in both DNA and cDNA libraries for this gene was related to the genus *Pseudomonas*, which accounted for 52.3 ± 8.9% in the DNA, 32.4 ± 3.6% in the 1 h cDNA, 42.3 ± 5.1% in the 2 h cDNA and 34.4 ± 7.5% in the 4 h cDNA. A high *napA* gene expression level was observed for the genus *Dechloromonas*, which increased from 4.3 ± 2.4% in the DNA to 25.1 ± 4.7%, 11.5 ± 1.9 and 27.4 ± 2.4% in the 1, 2, and 4 h cDNA samples, respectively.

The *nirS* and *nirK* genes, encoding nitrite reductases, were both detected in the DNA, but only *nirS* was amplified from the cDNA. For the *nirS* gene, a total of 369 OTUs were identified and assigned to 30 genera. As for the other denitrification genes that were transcribed, there were substantial differences between the phylogenetic composition of the amplified genes (in the DNA) compared to that of the transcripts (cDNA) (**Figure 4**). Organisms belonging to the genus *Dechloromonas* comprised only 5.9 ± 2.1% of the *nirS* sequences in the DNA, but showed very high transcriptional activity of this gene that increased over time, from 48.5 ± 13.1 and 42.7 ± 14.7% of the total sequences in the cDNA at 1 and 2 h, to 61.2 ± 9.2% in the 4 h samples. Another, very active group belonged to the genus *Cupriavidus*, which comprised only 4.4 ± 5.2% of the *nirS* carrying community but 29.7 ± 10.3% of the *nirS* transcripts in the 1 h cDNA samples. In this case the gene transcription levels declined, however, to 23.7 ± 15.2% of the total transcripts at 2 h and to 8.3 ± 0.2% at 4 h. In contrast to the genera *Dechloromonas* and *Cupriavidus*, *Pseudomonas* was a major genus in the *nirS* carrying community, accounting for 19.3 ± 2.5% of the DNA sequences, but this group of organisms showed very low levels of gene expression, as indicated by the low proportion in the cDNA (<3.5%).

The *nirK* gene was only detected in the DNA samples. The majority of the organisms carrying this gene were different rhizobia, and the genera *Rhizobium, Bradyrhizobium, Mesorhizobium,* and *Sinorhizobium* constituted together more than 60% of all the sequences. Almost one third of the *nirK* sequences (30.3 ± 4.3%) did not match any known phylogenetic neighbors in GenBank (**Figure 5A**).

Several different primers were tested for the *nor* genes, both for the quinol-oxidizing single-subunit class (*qnorB*) and the cytochrome bc-type complex class (*cnorB*). Of these, successful amplification was only obtained for *qnorB* in DNA samples when using the 2F/7R primers (**Supplementary Table S1**). A total of 465 OTUs were identified and assigned to 31 genera. More than half of the sequences (56.3 ± 0.7%) were assigned to unidentified

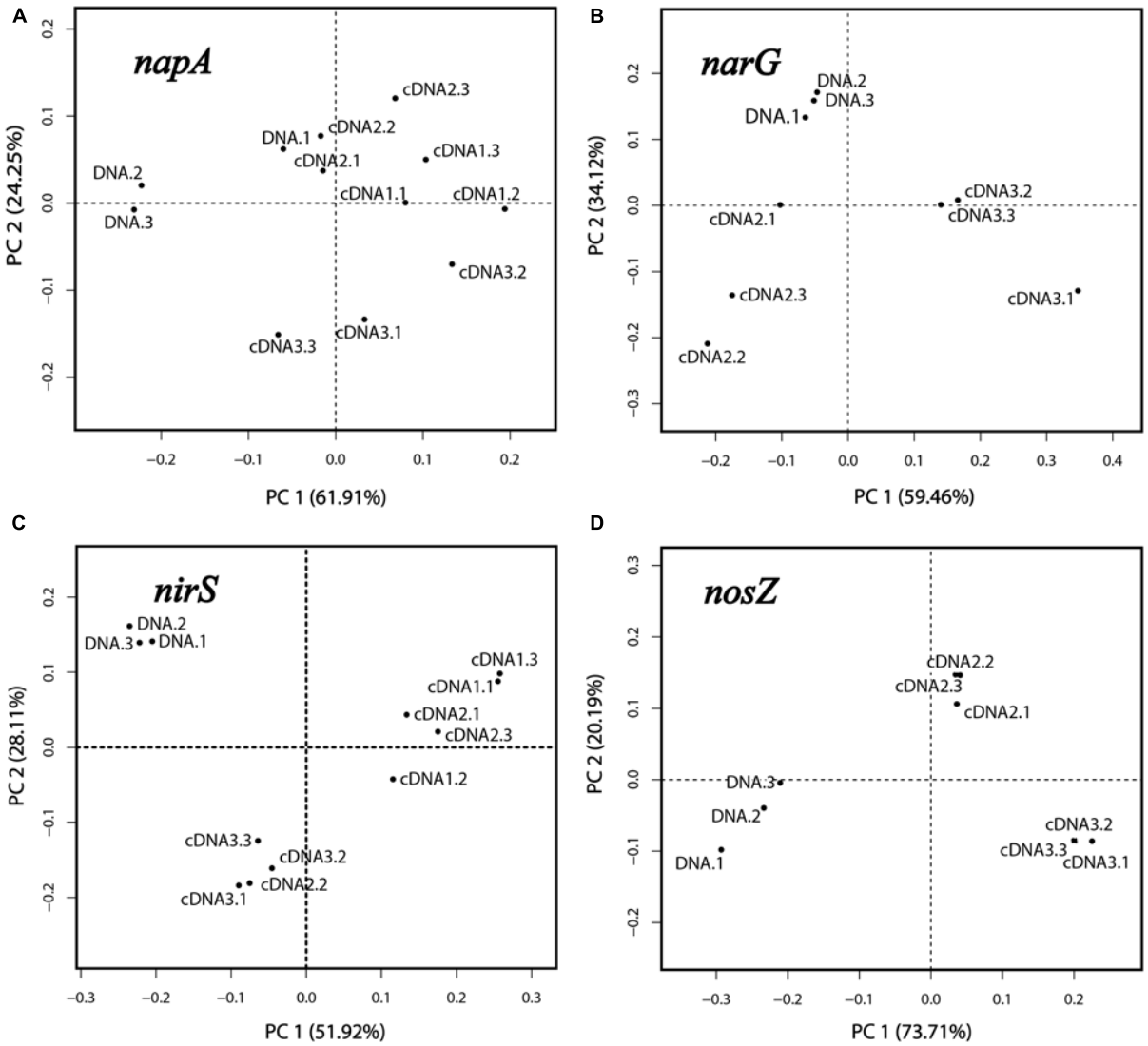

FIGURE 3 | Principal component analysis based on OTUs of the *napA*, *narG*, *nirS* and *nosZ* libraries **(A–D)**. Three replicate DNA libraries are shown (designated DNA.1, DNA.2 and DNA.3). For the cDNA, three libraries designated cDNA1, cDNA2, and cDNA3 were obtained, representing the three sampling times (after 1, 2, and 4 h of incubation). For each of these, three replicate samples were analyzed, designated "0.1," "0.2," and "0.3".

groups of organisms. The three most abundant groups were affiliated with the genera *Phenylobacterium, Cupriavidus* and *Pseudomonas,* which comprised 7.7 ± 2.0, 6.9 ± 1.1, and 4.7 ± 0.8% of the total number of sequences, respectively (**Figure 5B**).

Amplicons of *nosZ* were detected in the DNA and in the 2 and 4 h cDNA samples, but not in the 1 h cDNA samples. In total, 164 OTUs were defined from 4439 sequences, and assigned to 26 genera. The predominant (58.3 ± 4.4%) group in the DNA library belonged to *Herbaspirillum*. This genus comprised a substantial but yet smaller fraction of the cDNA (30.1 ± 0.8 and 22.0 ± 5.5% at 2 and 4 h, respectively). In contrast, the genus *Pseudomonas*, which was a relatively minor fraction of the *nosZ* carrying community with only 14.5 ± 2.6% of the total sequences in the DNA, showed dramatically higher abundance in the cDNA, with 28.3 ± 1.3 and 39.0 ± 5.1% of the total sequences at 2 and 4 h, respectively (**Figure 4**).

DISCUSSION

While there is a plethora of studies quantifying denitrification genes in soils, comparably few have determined the transcriptional activities of these genes, and only a few have sequenced the transcripts (Coyotzi et al., 2017; Harter et al., 2017). The present work follows up our earlier studies of the same agricultural peat soil, which demonstrated, both for intact soil and extracted soil microbial communities, that transcription of the *nirS* and *nosZ* genes was initiated as an immediate response to oxygen depletion (Liu et al., 2010). This was seen as a sharp

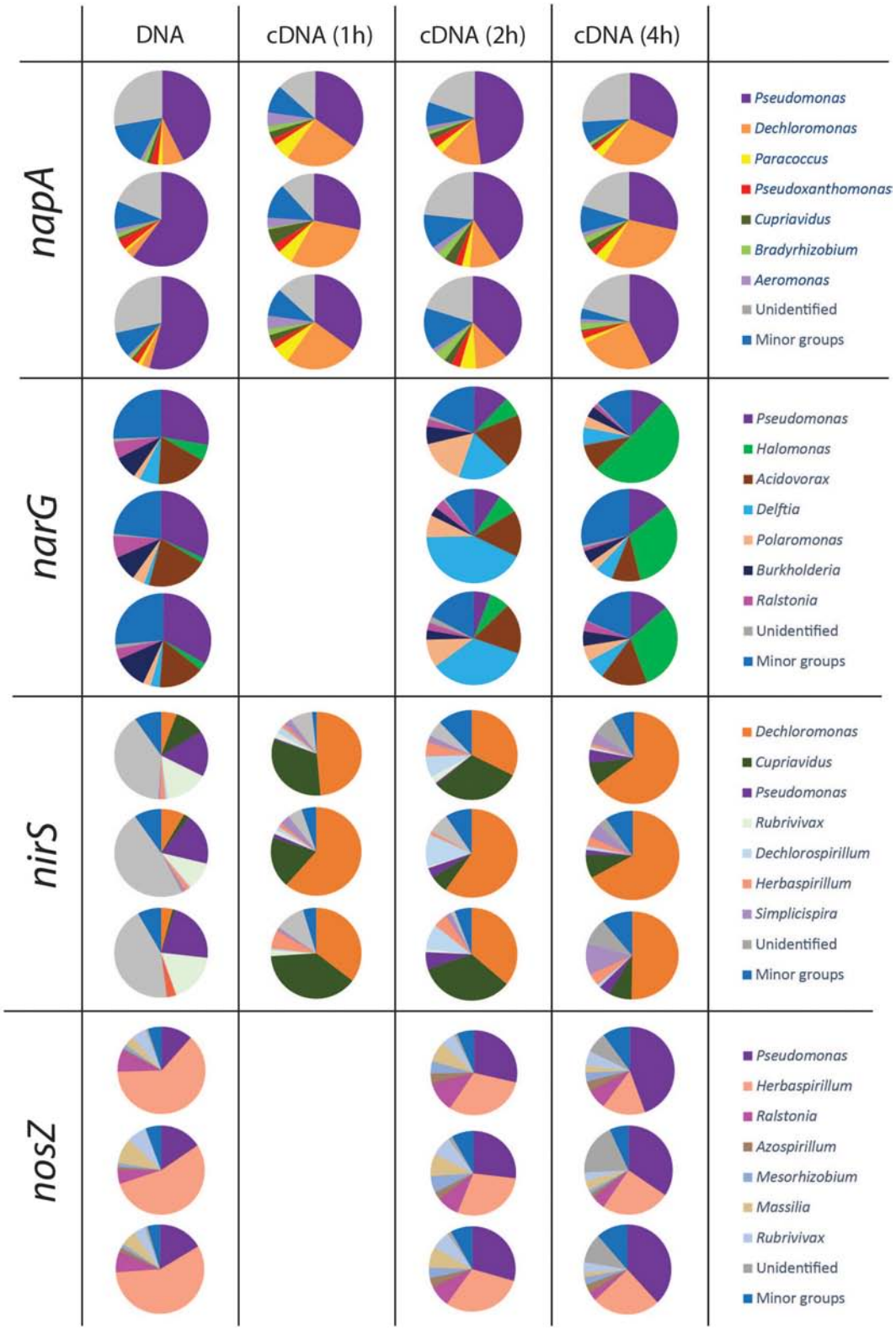

FIGURE 4 | Microbial community structure and shifts in the actively denitrifying populations, revealed by phylogenetic composition analysis of the DNA and cDNA of *narG napA nirS* and *nosZ* genes. The three pie charts in the same box are three replicates. No gene transcription was detected at 1 h for *nosZ* and *narG* genes. The phylogenetic composition of the minor groups is shown in **Supplementary File S2**.

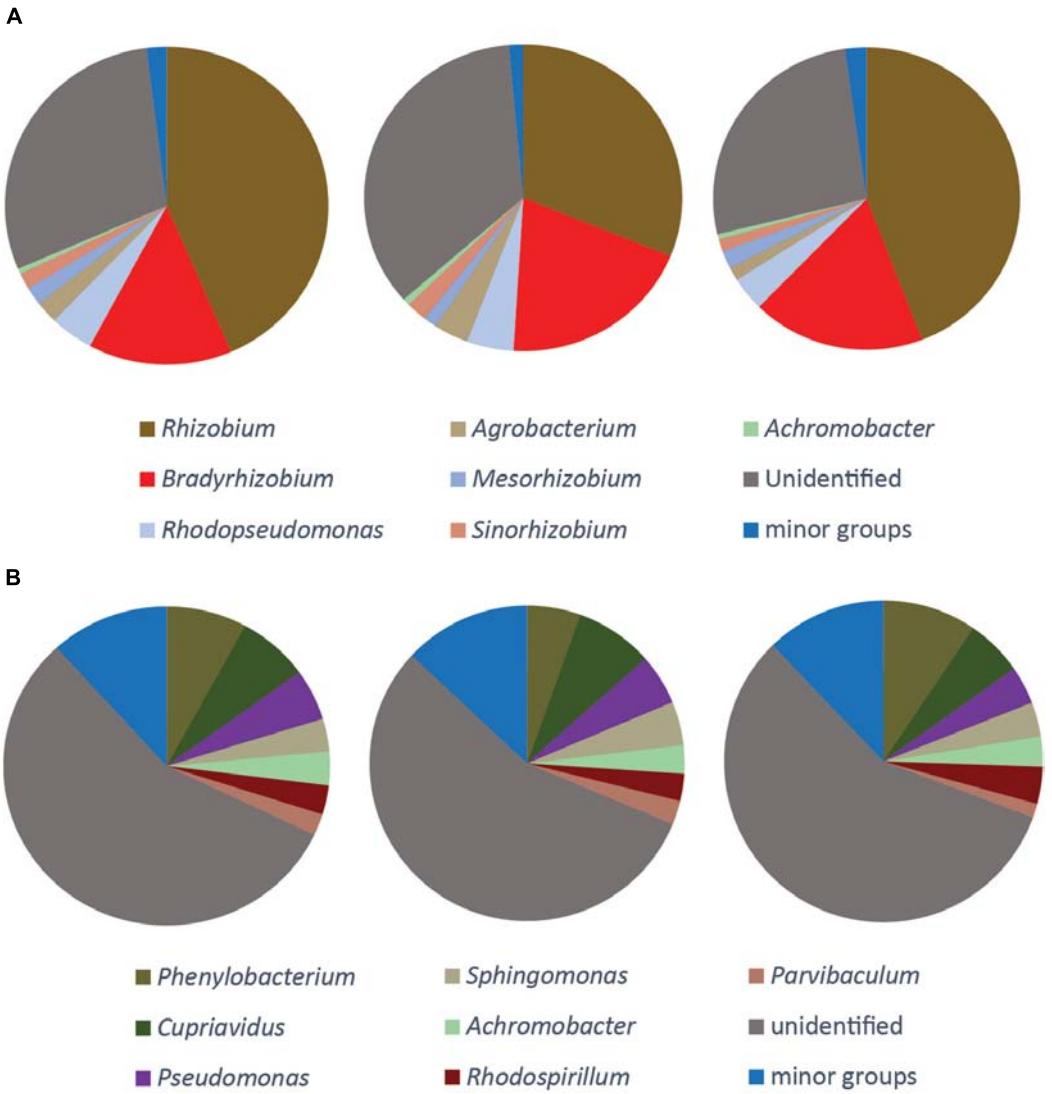

FIGURE 5 | Phylogenetic composition of the DNA of *nirK* gene **(A)**, *qnorB* gene **(B)**. The three pie charts show three replicate samples. No gene transcription was detected for these genes. The seven largest genera are shown and the composition of the minor groups is listed in **Supplementary File S2**.

peak in transcript numbers during the first 5 h of incubation, after which transcription dropped below detection limit or stayed at a low level for the rest of the incubation. In the present investigation, we found the same overall pattern and focused on analyzing transcripts in soil samples taken during the first hours of incubation when the peak in transcriptional activity was observed.

The knowledge gathered during the past decades shows substantial similarities in the main elements of the regulatory networks involved in denitrification (Spiro, 2012; Gaimster et al., 2018). Yet, detailed studies of an increasing number of denitrifying organisms have revealed that their regulatory phenotypes are profoundly different (Lycus et al., 2017). Some handle oxygen depletion by a complete onset of all denitrification genes (Liu et al., 2013), which gives rapid access to all available electron acceptors. This is probably an advantage if the anoxia persists, but the production of the entire denitrification machinery comes with a substantial energy investment. It is therefore not surprising to find organisms which express only some of their denitrification genes as a first response to anoxia. This is the case for some *Thauera* strains where the presence of nitrate appears to completely inhibit the transcription of *nirS* (Liu et al., 2013), or in *P. denitrificans* in which only a fraction of the cells in an isogenic population express *nirS* while all cells express *nosZ* and most of them also *narG* (Bergaust et al., 2010; Hassan et al., 2016; Lycus et al., 2018). Such regulatory strategies would translate into a succession of active denitrifiers during the course of an anoxic spell.

Analysis of the DNA showed that, among the dominant genera identified based on the method developed in this study, *Pseudomonas* was the only genus that was detected in all the four gene libraries (**Figure 4** and **Supplementary File S2**).

The apparent lack of one or more of the genes in the other genera could be taken to suggest that they have a truncated denitrification pathway (Shapleigh, 2013; Graf et al., 2014), but could just as well-reflect that some of their denitrification genes are not amplified by the primers used. It is well-known that no primers for denitrification genes are universal, and therefore a substantial part of the community remains undetected (Bonilla-Rosso et al., 2016; Decleyre et al., 2016).

Despite the limitations caused by primer biases, the results we obtained from sequencing both DNA and cDNA allowed a direct comparison between the genetic potential and the transcriptional activity of the individual genes. The results show that some groups that dominated in the DNA samples were equally or less abundant in the cDNA, such as *Pseudomonas* (*napA*, *narG,* and *nirS*), *Acidovorax* (*narG*) and *Herbaspirillum* (*nosZ*). Other groups showed a comparatively high activity with larger relative abundance in the cDNA than in the DNA. These included, e.g., *Dechloromonas* (*napA*, *nirS*), *Delftia* and *Polaromonas* (*narG*), *Cupriavidus* (*nirS*), and *Pseudomonas* (*nosZ*).

Our approach also allowed a time-resolved dissection of the denitrifying community during the transcription peaks for the individual genes. In accordance with our hypothesis, this revealed shifts in the composition of active groups of denitrifiers (**Figure 4**). For the genes targeted by the primers used, transcription of *nosZ* was not detected at the first sampling (1 h; **Figure 4**). Being the last step of denitrification, late transcription of *nosZ* is in itself not surprising. However, since transcription of *nosZ* before other denitrification genes has been shown in *P. denitrificans* (Bergaust et al., 2010), a more likely interpretation is that the *nosZ* gene of such organisms were not targeted by the primers used. Similarly, the lack of early *narG* transcription (**Figure 4**) only applies to the genes targeted by the present primers. Nitrate reduction most likely took place already after 1 h, providing nitrite for the already active nitrite reductases resulting from *narG* activity in other, non-targeted organisms and/or from *napA* activity. Thus, the results should be interpreted with care; lack of transcripts at a specific time point only reflects lack of transcription of the gene targeted by the primer pairs used. Yet, our approach revealed that the composition of the actively denitrifying community varied over time within the time frame of the 4 h transcription peak for all the genes (**Figure 3**). Some groups showed an "early onset" of the gene in question (i.e., their transcription started at a higher O_2 concentration, during O_2 depletion, compared to groups with a "later onset") and stayed active throughout, such as *Pseudomonas* (*napA*), *Dechloromonas* (*napA* and *nirS*), and *Cupriavidus* (*nirS*) (**Figure 4**). The nitrite and NO produced by "early onset" groups will likely act as triggers for the onset of denitrification in other organisms (Zumft, 2002; Spiro, 2017). All groups targeted by the *narG* and *nosZ* primers instead had a later onset. The reason for this is not clear, since transcription of both these genes is controlled by transcriptional regulators belonging to the FNR/CRP family which sense oxygen depletion (Zumft, 1997). The regulation of denitrification is, however, not well-understood and several aspects are probably yet to be unraveled. Recently, it was discovered that in an isogenic population of *Paracoccus denitrificans* only some cells initiated denitrification in response to decreasing oxygen (Lycus et al., 2018), a phenomenon that could explain the observation of late transcription in the present study. For the gene *nirS*, responsible for the defining step of denitrification (reduction of nitrite to a gaseous N-oxide), the genera *Dechlomonas* and *Cupriavidus* comprised a major part of the active community, although transcripts from *Cupriavidu*s became less abundant with time. For *nosZ, Pseudomonas* and *Herbaspirillum* comprised more than half of the detected transcripts, indicating that they play an important role for the reduction of the greenhouse gas N_2O in this soil.

For the genes *nirK* and *qnor* we could only detect sequences in the DNA, but not in the cDNA samples (**Figure 5**). The failure to detect *nirK* transcription is consistent with our previous study of the same soil (Liu et al., 2010). Since the gas kinetics (**Figure 1**) showed complete conversion of NO_3^- to N_2, meaning that Nir activity did take place, the NO_2^- reduction must be attributed to *nirS*-carrying organisms and possibly also to other *nirK* carrying organisms than those targeted by the primers used. In a similar way we did not detect transcription of *qnorB* even though we observed NO reduction, seen as N_2O production (**Figure 1**). We tested different published primers and only found one primer pair that successfully amplified *qnor*, but only in the DNA samples. Thus, the observed NO reduction could be from other *qnor* genes, and possibly also from *cnor* genes, from which we could not obtain any amplicons neither from the DNA nor from the cDNA samples. Most studies targeting denitrification genes in complex systems have focused on *nir* and *nos* genes, and it is therefore likely that *nor* genes are less well-represented in the gene databases. This could explain the large portion (56.3%) of unidentified sequences in *qnorB* library in the present study.

A database was constructed for each functional gene based on a blast search of all sets of sequences from the same gene against the NCBI nucleotide database. These databases are dramatically smaller in size than NCBI nucleotide database and therefore facilitated the downstream OTU clustering and taxonomy assignment by reducing the database searching time. The databases were produced based on the sequences generated in the present study, and may not be suitable for analysis of other sequence data sets. Yet, the principle of this strategy could be applied in other studies. Making databases useful for a wider user community would need further optimization, including a general purpose database and related OTU classification tools. A pipeline for this purpose named GENTAX is under development by our group.

To conclude, exposing a soil to near-anoxia induced a sequential transcription of the denitrifying genes, which reflect the presence of a variety of regulatory phenotypes, and an interaction between these via early production of intermediate products (NO_2^- and NO) triggering the transcription in other denitrifiers. The genera *Pseudomonas*, *Dechloromonas,* and *Herbaspirillum* were identified as dominant, active denitrifiers in this soil, under the given conditions. The results underscore the necessity to perform successive

samplings from a number of time points during a short anoxic spell, in order to detect key denitrifiers.

AUTHOR CONTRIBUTIONS

ÅF, LB, and BL conceived and designed the experiments. BL and LS developed the OTU clustering strategy. BL and XZ performed the experiments. All authors participated in the writing and improving of the paper.

FUNDING

This work was financially supported by Research Council of Norway (Project No. 193601) and State Key Laboratory of Microbial Metabolism, Shanghai Jiao Tong University (Project No. MMLKF18-04).

ACKNOWLEDGMENTS

We thank Chris Wright from University of Illinois at Urbana-Champaign (United States) for kindly providing useful advices for preparing the amplicon samples for sequencing.

SUPPLEMENTARY MATERIAL

The Supplementary Material for this article can be found online at: https://www.frontiersin.org/articles/10.3389/fmicb.2018.03208/full#supplementary-material

REFERENCES

Altschul, S. F., Gish, W., Miller, W., Myers, E. W., and Lipman, D. J. (1990). Basic local alignment search tool. *J. Mol. Biol.* 215, 403–410. doi: 10.1016/S0022-2836(05)80360-2

Anderson, M. J. (2001). A new method for non-parametric multivariate analysis of variance. *Austral. Ecol.* 26, 32–46. doi: 10.1111/j.1442-9993.2001.01070.pp.x

Bergaust, L., Mao, Y. J., Bakken, L. R., and Frostegård, Å (2010). Denitrification response patterns during the transition to anoxic respiration and posttranscriptional effects of suboptimal pH on nitrogen oxide reductase in *Paracoccus denitrificans*. *Appl. Environ. Microbiol.* 6387–6396. doi: 10.1128/AEM.00608-10

Bergaust, L., Shapleigh, J., Frostegård, Å, and Bakken, L. (2008). Transcription and activities of NOx reductases in *Agrobacterium tumefaciens*: the influence of nitrate, nitrite and oxygen availability. *Environ. Microbiol.* 10, 3070–3081. doi: 10.1111/j.1462-2920.2007.01557.x

Bergaust, L., Van Spanning, R. J., Frostegård, Å, and Bakken, L. R. (2012). Expression of nitrous oxide reductase in *Paracoccus denitrificans* is regulated by oxygen and nitric oxide through FnrP and NNR. *Microbiology* 158, 826–834. doi: 10.1099/mic.0.054148-0

Bonilla-Rosso, G., Wittorf, L., Jones, C. M., and Hallin, S. (2016). Design and evaluation of primers targeting genes encoding NO-forming nitrite reductases: implications for ecological inference of denitrifying communities. *Sci. Rep.* 6:39208. doi: 10.1038/srep39208

Bueno, E., Mania, D., Frostegård, Å, Bedmar, E. J., Bakken, L. R., and Delgado, M. J. (2015). Anoxic growth of Ensifer meliloti 1021 by N2O-reduction, a potential mitigation strategy. *Front. Microbiol.* 6:537. doi: 10.3389/fmicb.2015.00537

Butterbach-Bahl, K., Baggs, E. M., Dannenmann, M., Kiese, R., and Zechmeister-Boltenstern, S. (2013). Nitrous oxide emissions from soils: how well do we understand the processes and their controls? *Philos. Trans. R. Soc. Lond. B Biol. Sci.* 368:20130122. doi: 10.1098/rstb.2013.0122

Camacho, C., Coulouris, G., Avagyan, V., Ma, N., Papadopoulos, J., Bealer, K., et al. (2009). BLAST+: architecture and applications. *BMC Bioinformatics* 10:421. doi: 10.1186/1471-2105-10-421

Caporaso, J. G., Kuczynski, J., Stombaugh, J., Bittinger, K., Bushman, F. D., Costello, E. K., et al. (2010). QIIME allows analysis of high-throughput community sequencing data. *Nat. Methods* 7, 335–336. doi: 10.1038/nmeth.f.303

Chèneby, D., Philippot, L., Hartmann, A., Henault, C., and Germon, J. C. (2000). 16S rDNA analysis for characterization of denitrifying bacteria isolated from three agricultural soils. *FEMS Microbiol. Ecol.* 34, 121–128. doi: 10.1016/S0168-6496(00)00080-5

Clarridge, J. E. (2004). Impact of 16S rRNA gene sequence analysis for identification of bacteria on clinical microbiology and infectious diseases. *Clin. Microbiol. Rev.* 17, 840–862. doi: 10.1128/CMR.17.4.840-862.2004

Coyotzi, S., Doxey, A. C., Clark, I. D., Lapen, D. R., Van Cappellen, P., and Neufeld, J. D. (2017). Agricultural soil denitrifiers possess extensive nitrite reductase gene diversity. *Environ. Microbiol.* 19, 1189–1208. doi: 10.1111/1462-2920.13643

Decleyre, H., Heylen, K., Tytgat, B., and Willems, A. (2016). Highly diverse nirK genes comprise two major clades that harbour ammonium-producing denitrifiers. *BMC Genomics* 17:155. doi: 10.1186/s12864-016-2465-0

Depkat-Jakob, P. S., Brown, G. G., Tsai, S. M., Horn, M. A., and Drake, H. L. (2013). Emission of nitrous oxide and dinitrogen by diverse earthworm families from Brazil and resolution of associated denitrifying and nitrate-dissimilating taxa. *FEMS Microbiol. Ecol.* 83, 375–391. doi: 10.1111/j.1574-6941.2012.01476.x

Edgar, R. C. (2010). Search and clustering orders of magnitude faster than BLAST. *Bioinformatics* 26, 2460–2461. doi: 10.1093/bioinformatics/btq461

Gaby, J. C., and Buckley, D. H. (2014). A comprehensive aligned nifH gene database: a multipurpose tool for studies of nitrogen-fixing bacteria. *Database* 2014:bau001. doi: 10.1093/database/bau001

Gaimster, H., Alston, M., Richardson, D. J., Gates, A. J., and Rowley, G. (2018). Transcriptional and environmental control of bacterial denitrification and N2O emissions. *FEMS Microbiol. Lett.* 365:fnx277. doi: 10.1093/femsle/fnx277

Gerber, J. S., Carlson, K. M., Makowski, D., Mueller, N. D., De Cortazar-Atauri, I. G., Havlik, P., et al. (2016). Spatially explicit estimates of N2O emissions from croplands suggest climate mitigation opportunities from improved fertilizer management. *Glob. Change Biol.* 22, 3383–3394. doi: 10.1111/gcb.13341

Graf, D. R., Jones, C. M., and Hallin, S. (2014). Intergenomic comparisons highlight modularity of the denitrification pathway and underpin the importance of community structure for N2O emissions. *PLoS One* 9:e114118. doi: 10.1371/journal.pone.0114118

Hallin, S., Philippot, L., Löffler, F. E., Sanford, R. A., and Jones, C. M. (2017). Genomics and ecology of novel N2O-reducing microorganisms. *Trends Microbiol.* 26, 43–55. doi: 10.1016/j.tim.2017.07.003

Harter, J., El-Hadidi, M., Huson, D. H., Kappler, A., and Behrens, S. (2017). Soil biochar amendment affects the diversity of nosZ transcripts: implications for N_2O formation. *Sci. Rep.* 7:3338. doi: 10.1038/s41598-017-03282-y

Hassan, J., Qu, Z., Bergaust, L. L., and Bakken, L. R. (2016). Transient Accumulation of NO_2- and N_2O during denitrification explained by assuming cell diversification by stochastic transcription of denitrification genes. *PLoS Comput. Biol.* 12:e1004621. doi: 10.1371/journal.pcbi.1004621

Højberg, O., Binnerup, S. J., and Sørensen, J. (1997). Growth of silicone-immobilized bacteria on polycarbonate membrane filters, a technique to study microcolony formation under anaerobic conditions. *Appl. Environ. Microbiol.* 63, 2920–2924. doi: 10.1016/S0027-5107(97)00087-0

Konstantinidis, K. T., Ramette, A., and Tiedje, J. M. (2006). The bacterial species definition in the genomic era. *Philos. Trans. R. Soc. Lond. B Biol. Sci.* 361, 1929–1940. doi: 10.1098/rstb.2006.1920

Konstantinidis, K. T., Rossello-Mora, R., and Amann, R. (2017). Uncultivated microbes in need of their own taxonomy. *ISME J.* 11, 2399–2406. doi: 10.1038/ismej.2017.113

Lane, D. (1991). "16S/23S rRNA sequencing," in *Nucleic Acid Techniques in Bacterial Systematics*, eds E. Strackebrandt and M. Goodfellow (New York, NY: John Wiley & Sons), 131–175.

Liu, B., Mao, Y., Bergaust, L., Bakken, L. R., and Frostegård, A. (2013). Strains in the genus Thauera exhibit remarkably different denitrification regulatory phenotypes. *Environ. Microbiol.* 15, 2816–2828. doi: 10.1111/1462-2920.12142

Liu, B., Mørkved, P. T., Frostegård, Å, and Bakken, L. R. (2010). Denitrification gene pools, transcription and kinetics of NO, N2O and N2 production as affected by soil pH. *FEMS Microbiol. Ecol.* 72, 407–417. doi: 10.1111/j.1574-6941.2010.00856.x

Lycus, P., Bøthun, K. L., Bergaust, L., Shapleigh, J. P., Bakken, L. R., and Frostegård, Å (2017). Phenotypic and genotypic richness of denitrifiers revealed by a novel isolation strategy. *ISME J.* 11, 2219–2232. doi: 10.1038/ismej.2017.82

Lycus, P., Soriano-Laguna, M. J., Kjos, M., Richardson, D. J., Gates, A. J., Milligan, D. A., et al. (2018). A bet-hedging strategy for denitrifying bacteria curtails their release of N2O. *Proc. Natl. Acad. Sci. U.S.A.* 115, 11820–11825. doi: 10.1073/pnas.1805000115

Molstad, L., Dörsch, P., and Bakken, L. R. (2007). Robotized incubation system for monitoring gases (O_2, NO, N_2O,N_2) in denitrifying cultures. *J. Microbiol. Methods* 71, 202–211. doi: 10.1016/j.mimet.2007.08.011

Mørkved, P. T., Dörsch, P., and Bakken, L. R. (2007). The N_2O product ratio of nitrification and its dependence on long-term changes in soil pH. *Soil Biol. Biochem.* 39, 2048–2057. doi: 10.1016/j.soilbio.2007.03.006

Opdyke, M. R., Ostrom, N. E., and Ostrom, P. H. (2009). Evidence for the predominance of denitrification as a source of N_2O in temperate agricultural soils based on isotopologue measurements. *Glob. Biogeochem. Cycles* 23:GB4018. doi: 10.1029/2009GB003523

Palmer, K., Drake, H. L., and Horn, M. A. (2009). Genome-derived criteria for assigning environmental narG and nosZ sequences to operational taxonomic units of nitrate reducers. *Appl. Environ. Microbiol.* 75, 5170–5174. doi: 10.1128/AEM.00254-09

Philippot, L., and Højberg, O. (1999). Dissimilatory nitrate reductases in bacteria. *Biochim. Biophys. Acta* 1446, 1–23. doi: 10.1016/S0167-4781(99)00072-X

Quince, C., Lanzen, A., Curtis, T. P., Davenport, R. J., Hall, N., Head, I. M., et al. (2009). Accurate determination of microbial diversity from 454 pyrosequencing data. *Nat. Methods* 6, 639–641. doi: 10.1038/nmeth.1361

Quince, C., Lanzen, A., Davenport, R. J., and Turnbaugh, P. J. (2011). Removing noise from pyrosequenced amplicons. *BMC Bioinformatics* 12:38. doi: 10.1186/1471-2105-12-38

Roco, C. A., Bergaust, L. L., Bakken, L. R., Yavitt, J. B., and Shapleigh, J. P. (2017). Modularity of nitrogen-oxide reducing soil bacteria: linking phenotype to genotype. *Environ. Microbiol.* 19, 2507–2519. doi: 10.1111/1462-2920.13250

Rodionov, D. A., Dubchak, I. L., Arkin, A. P., Alm, E. J., and Gelfand, M. S. (2005). Dissimilatory metabolism of nitrogen oxides in bacteria: comparative reconstruction of transcriptional networks. *PLoS Comput. Biol.* 1:415–431. doi: 10.1371/journal.pcbi.0010055

Schloss, P. D., and Westcott, S. L. (2011). Assessing and improving methods used in operational taxonomic unit-based approaches for 16S rRNA gene sequence analysis. *Appl. Environ. Microbiol.* 77, 3219–3226. doi: 10.1128/AEM.02810-10

Schloss, P. D., Westcott, S. L., Ryabin, T., Hall, J. R., Hartmann, M., Hollister, E. B., et al. (2009). Introducing mothur: open-source, platform-independent, community-supported software for describing and comparing microbial communities. *Appl. Environ. Microbiol.* 75, 7537–7541. doi: 10.1128/AEM.01541-09

Shapleigh, J. (2013). *Denitrifying Prokaryotes in the Prokaryotes*, ed. E. Rosenberg (Berlin: Springer), 405–425. doi: 10.1007/978-3-642-30141-4_71

Sognnes, L. S., Fystro, G., Opstad, S. L., Arstein, A., and Borresen, T. (2006). Effects of adding moraine soil or shell sand into peat soil on physical properties and grass yield in western Norway. *Acta Agric. Scand. B* 56, 161–170. doi: 10.1080/09064710500218845

Spiro, S. (2012). Nitrous oxide production and consumption: regulation of gene expression by gas-sensitive transcription factors. *Philos. Trans. R. Soc. Lond. B Biol. Sci.* 367, 1213–1225. doi: 10.1098/rstb.2011.0309

Spiro, S. (2017). "Regulation of denitrification," in *Metalloenzymes in Denitrification: Applications and Environmental Impacts*, eds M. Isabel, J. J. G. Moura, S. R. Pauleta, and L. B. Maia (London: Royal Society of Chemistry), 312–330.

Syakila, A., and Kroeze, C. (2011). The global nitrogen budget revisited. *Greenhouse Gas Meas. Manage.* 1, 17–26. doi: 10.3763/ghgmm.2010.0007

Zumft, W. G. (1997). Cell biology and molecular basis of denitrification. *Microbiol. Mol. Biol. Rev.* 61, 533–616. doi: 10.1016/j.ccr.2004.08.030

Zumft, W. G. (2002). Nitric oxide signaling and NO dependent transcriptional control in bacterial denitrification by members of the FNR-CRP regulator family. *J. Mol. Microbiol. Biotech.* 4, 277–286. doi: 10.1016/j.pscychresns.2005.10.002

Conflict of Interest Statement: The authors declare that the research was conducted in the absence of any commercial or financial relationships that could be construed as a potential conflict of interest.

frontiers in Microbiology

ORIGINAL RESEARCH
published: 15 March 2019
doi: 10.3389/fmicb.2019.00495

Accessory Proteins of the Nitrogenase Assembly, NifW, NifX/NafY, and NifZ, Are Essential for Diazotrophic Growth in the Nonheterocystous Cyanobacterium *Leptolyngbya boryana*

*Aoi Nonaka[1], Haruki Yamamoto[2], Narumi Kamiya[1], Hiroya Kotani[2], Hisanori Yamakawa[2], Ryoma Tsujimoto[2] and Yuichi Fujita[1,2]**

[1] School of Agricultural Sciences, Nagoya University, Nagoya, Japan, [2] Graduate School of Bioagricultural Sciences, Nagoya University, Nagoya, Japan

OPEN ACCESS

Edited by:
Maria J. Delgado, Spanish National Research Council (CSIC), Spain

Reviewed by:
Luis M. Rubio, Polytechnic University of Madrid, Spain
Annegret Wilde, University of Freiburg, Germany
Shigeki Ehira, Tokyo Metropolitan University, Japan

***Correspondence:**
Yuichi Fujita
fujita@agr.nagoya-u.ac.jp

Specialty section:
This article was submitted to Terrestrial Microbiology, a section of the journal Frontiers in Microbiology

Received: *10 October 2018*
Accepted: *26 February 2019*
Published: *15 March 2019*

Citation:
Nonaka A, Yamamoto H, Kamiya N, Kotani H, Yamakawa H, Tsujimoto R and Fujita Y (2019) Accessory Proteins of the Nitrogenase Assembly, NifW, NifX/NafY, and NifZ, Are Essential for Diazotrophic Growth in the Nonheterocystous Cyanobacterium Leptolyngbya boryana. Front. Microbiol. 10:495. doi: 10.3389/fmicb.2019.00495

Since nitrogenase is extremely vulnerable to oxygen, aerobic or micro-aerobic nitrogen-fixing organisms need to create anaerobic microenvironments in the cells for diazotrophic growth, which would be one of the major barriers to express active nitrogenase in plants in efforts to create nitrogen-fixing plants. Numerous cyanobacteria are able to fix nitrogen with nitrogenase by coping with the endogenous oxygen production by photosynthesis. Understanding of the molecular mechanisms enabling to the coexistence of nitrogen fixation and photosynthesis in nonheterocystous cyanobacteria could offer valuable insights for the transfer of nitrogen fixation capacity into plants. We previously identified the *cnfR* gene encoding the master regulator for the nitrogen fixation (*nif*) gene cluster in the genome of a nonheterocystous cyanobacterium *Leptolyngbya boryana*, in addition to initial characterization of the *nif* gene cluster. Here we isolated nine mutants, in which the *nif* and *nif*-related genes were individually knocked out in *L. boryana* to investigate the individual functions of (1) accessory proteins (NifW, NifX/NafY, and NifZ) in the biosynthesis of nitrogenase metallocenters, (2) serine acetyltransferase (NifP) in cysteine supply for iron-sulfur clusters, (3) pyruvate formate lyase in anaerobic metabolism, and (4) NifT and HesAB proteins. Δ*nifW*, Δ*nifXnafY*, and Δ*nifZ* exhibited the most severe phenotype characterized by low nitrogenase activity (<10%) and loss of diazotrophic growth ability. The phenotypes of Δ*nifX*, Δ*nafY*, and Δ*nifXnafY* suggested that the functions of the homologous proteins NifX and NafY partially overlap. Δ*nifP* exhibited significantly slower diazotrophic growth than the wild type, with lower nitrogenase activity (22%). The other four mutants (Δ*pflB*, Δ*nifT*, Δ*hesA*, and Δ*hesB*) grew diazotrophically similar to the wild type. Western blot analysis revealed a high correlation between nitrogenase activity and NifD contents, suggesting that NifD is more susceptible to proteolytic degradation than NifK in *L. boryana*. The phenotype of the mutants lacking the accessory proteins was more severe than that

observed in heterotrophic bacteria such as *Azotobacter vinelandii*, which suggests that the functions of NifW, NifX/NafY, and NifZ are critical for diazotrophic growth of oxygenic photosynthetic cells. *L. boryana* provides a promising model for studying the molecular mechanisms that produce active nitrogenase, to facilitate the creation of nitrogen-fixing plants.

Keywords: cyanobacteria, nitrogen fixation, nitrogenase, MoFe protein, NifZ, NifW, NifX/NafY

INTRODUCTION

Nitrogen is an essential nutrient for all organisms, and its availability often limits plant productivity, for example, in cereals (Rosenblueth et al., 2018). Nitrogen fixation is a process by which atmospheric nitrogen (N_2) is converted into ammonia (NH_3), which is used by many organisms as a source of nitrogen.

The enzyme responsible for catalyzing the biological nitrogen fixation reaction is nitrogenase, which consists of two separable components: the Fe protein and the MoFe protein (Seefeldt et al., 2018). The Fe protein (a NifH dimer) catalyzes the ATP-dependent electron transfer reaction via a [4Fe-4S] cluster held in the interface between NifH protomers. The MoFe protein, serving as the catalytic component, has two metallocenters: the P-cluster (a [8Fe-7S] cluster) and the iron-molybdenum cofactor (FeMo-co; a [7Fe-9S-C-Mo-homocitrate] cluster). The electrons from the Fe protein are transferred to the P-cluster and, eventually, to FeMo-co, in which a nitrogen molecule is converted to two ammonia molecules. All three metallocenters are extremely vulnerable to oxygen. For example, upon exposure to air, the half-life of Fe protein holding the [4Fe-4S] cluster is only 30 s (Robson, 1979). In addition, FeMo-co is synthesized by a series of complex enzymatic reactions (Curatti and Rubio, 2014; Hu and Ribbe, 2016). In the first stage, a sulfur atom is released from Cys by Cys desulfurase (NifS), and a precursor cluster is assembled on NifU (Johnson et al., 2005). In the second stage, the NifB-cofactor (NifB-co) is formed by the action of NifB (Shah et al., 1994; Hernandez et al., 2007). In the third stage, the mature FeMo-co is assembled on the NifEN complex, and finally, the FeMo-co is transferred to the apo-form of the MoFe protein (Curatti et al., 2007; Kaiser et al., 2011; Fay et al., 2016). The intermediate clusters in the biosynthetic process of FeMo-co are also vulnerable to oxygen. Therefore, aerobic and micro-aerobic nitrogen-fixing organisms need to create strict anaerobic microenvironments in the cell to facilitate active nitrogenase functions.

Crop yields in current agriculture are heavily dependent on nitrogen fertilizer produced by industrial nitrogen fixation based on the Harbor-Bosch process. However, industrial nitrogen fixation consumes a lot of fossil fuel resulting in massive amounts of CO_2 emissions, which contribute to global warming, and the application of nitrogen fertilizer in excess in crop fields causes serious environmental pollution. To alleviate the negative impacts of industrial nitrogen fixation without reducing the crop yield, novel technological innovations are awaited. One of the most promising innovations is the creation of nitrogen-fixing crops by transferring nitrogen fixation genes into plants (Curatti and Rubio, 2014; Burén and Rubio, 2018; Good, 2018). However, it is a challenging undertaking. A key obstacle is that nitrogenase should be protected not only from environmental oxygen but also from the endogenous oxygen produced by photosynthesis in crops. In addition, a number of genes, including the genes for nitrogenase cofactor biosynthesis, should be transferred into the plant genome and their expression should be appropriately regulated, which is a major additional obstacle.

The [4Fe-4S] cluster of Fe protein can be produced by the iron-sulfur cluster biosynthesis systems (ISC and SUF) of non-diazotrophic cells (Lopez-Torrejon et al., 2016). In contrast, special enzymes/proteins are required for the biosynthesis of P-cluster and FeMo-co in the MoFe protein. The special enzymes/proteins have been identified through molecular genetics and biochemical analyses in a limited number of heterotrophic bacteria such as *Azotobacter vinelandii* and *Klebsiella pneumoniae*. According to the current model of nitrogenase biosynthesis in the diazotrophs, other than the essential six proteins (NifHDKBEN), some accessory proteins are involved in the efficient biosynthesis of the metallocenters and their introduction to apo-forms of the MoFe protein (Curatti and Rubio, 2014; Burén and Rubio, 2018). NifZ is involved in the maturation of the P-cluster, which is formed by the reductive coupling of a pair of precursor [4Fe-4S] clusters. NifW was found to bind to an apo-form of the MoFe protein without FeMo-co, while its biochemical function is still unknown. The NifX and NafY proteins are involved in efficient transfer processes of NifB-co and FeMo-co to the NifEN and NifDK proteins, respectively. These are homologous proteins since the amino acid sequence of the C-terminal half of NafY exhibits high similarity to that of the entire NifX protein. While the *nifT*, *hesA*, and *hesB* genes are largely conserved in diazotrophic organisms, the functions of the proteins remain unknown.

Cyanobacteria are prokaryotes that perform oxygenic photosynthesis similar to plants. About half of cyanobacterial species can fix nitrogen (Stal and Zehr, 2008). Therefore, nitrogen-fixing cyanobacteria are a unique group of organisms in which oxygen-sensitive nitrogen fixation coexists with oxygen-producing photosynthesis. Some filamentous cyanobacteria such as *Anabaena* sp. PCC 7120 develop heterocysts, which are special nitrogen fixation cells, to spatially separate nitrogenase from photosynthesis (Herrero et al., 2016). However, some nonheterocystous nitrogen-fixing cyanobacteria exhibit nitrogenase activity in light conditions (Evans et al., 2000; Rabouille et al., 2006). Such cyanobacteria potentially have some unique systems for the biosynthesis and use of nitrogenase to cope with the endogenously produced oxygen. Elucidation of

the molecular mechanisms could provide clues crucial to the mechanisms of functional expression of nitrogenase in plants.

The nonheterocystous cyanobacterium *Leptolyngbya boryana* offers a promising system for the investigation of the molecular mechanisms of functional expression of nitrogenase since a gene targeting technique has been established (Fujita et al., 1992; Tsujimoto et al., 2015) and the genome sequence is available (Hiraide et al., 2015). We have previously identified the nitrogen fixation (*nif*) gene cluster in *L. boryana*, wherein 50 *nif* and *nif*-related genes are clustered at the 50-kb chromosomal region. In the region, in addition to the structural genes of nitrogenase (*nifHDK*), there are numerous genes encoding proteins essential for the biosynthesis of FeMo-co (*nifBEN*) and iron-sulfur clusters (*nifSU*), accessory proteins (*nifWXZ*), ferredoxins (*fdx*), cytochrome *c* oxidase (*coxB2A2C2*), molybdenum transporter (*modABC*), transcriptional regulators (*cnfR* and *chlR*), and proteins with unknown functions (such as *nifT*, *hesAB*, and other open reading frames). Based on the phenotype of a mutant NK4 (Δ*cnfR*), in which *cnfR* was knocked out, we discovered that *cnfR* encodes the master transcriptional activator for the expression of *nif* genes in the *nif* gene cluster (Tsujimoto et al., 2014). In addition, we observed that four mutants, NK8, NK2, NK7, and NK9, in which chromosomal fragments carrying *nifX*, *nifZ-nifT*, *nifP-orf84-dpsA-orf99*, and *hesA-hesB-fdxH-feoA-fedB-mop*, respectively, were deleted, exhibited low nitrogenase activity and considerable growth defects under nitrogen fixation conditions. The phenotype of NK8 (Δ*nifX*) indicated that NifX is critical for nitrogenase activity and nitrogen-fixing growth. However, it remains unknown which gene is responsible for the phenotype in the three mutants.

L. boryana cells exhibit nitrogenase activity only under microoxic conditions. There are at least four genes (*pflA*, *pflB*, *adhE*, and *acs*) for anaerobic metabolism in the leftmost region of the *nif* gene cluster. *pflB* and *pflA* encode pyruvate formate lyase (PFL) and PFL activating enzyme (PFL-AE), respectively. PFL activated by PFL-AE catalyzes the conversion of pyruvate and CoA to acetyl-CoA and formate, playing a key role in anaerobic metabolism in *Escherichia coli*. However, it remains unknown whether PFL is critical in facilitating the nitrogenase activity and nitrogen fixation in cyanobacteria.

Here, we isolated eight *L. boryana* mutants, in which a single gene was deleted (*nifZ*, *nifT*, *nifP*, *nifW*, *hesA*, *hesB*, *pflB*, and *nafY*), and one *L. boryana* mutant, in which two homologous genes *nifX* and *nafY* were deleted. We evaluated them based on diazotrophic growth and nitrogenase activity, and classified them into four groups (Group 1 to 4). Particularly, the mutants of Group 1 (Δ*nifW*, Δ*nifX/nafY*, and Δ*nifZ*) exhibited much severer phenotype (no diazotrophic growth and low nitrogenase activity at less than 10%) than those of the relevant mutants in *A. vinelandii* and *K. pneumoniae*. The results suggest that the functions of NifW, NifX/NafY, and NifZ are critical for diazotrophic growth in oxygenic photosynthetic cells. The cyanobacterium *L. boryana* is a promising model photosynthetic organism for studying the molecular mechanisms that produce the active nitrogenase that facilitates diazotrophic growth and could facilitate efforts to create nitrogen-fixing plants.

MATERIALS AND METHODS

Strains and Culture Conditions

The cyanobacterium *L. boryana* strain *dg5* (Fujita et al., 1996; Hiraide et al., 2015) was used as the wild type. NK1 (Δ*nifDK*), NK2 (Δ*nifZT*), and NK8 (Δ*nifX*) isolated previously (Tsujimoto et al., 2014) were used as the control strains. For growth or induction of the *nif* genes under microoxic conditions, agar plates were incubated in an anaerobic jar (BBL GasPak anaerobic systems; BD Biosciences) with a sachet to create anaerobic conditions (Gas Generating Kit Anaerobic System, Oxoid, Basingstoke, Hants, United Kingdom or AnaeroPack-Anaero; Mitsubishi Gas Chemical; Tokyo, Japan). As described previously (Tsujimoto et al., 2018), dry anaerobic indicator strips (Dry Anaerobic Indicator Strips, BD Biosciences) were used to confirm anaerobic conditions in the jar.

Plasmid Construction

DNA fragments from *L. boryana* genomic DNA were amplified by PCR, using KOD FX Neo polymerase (Toyobo, Osaka, Japan), and separated by agarose electrophoresis to purify them from the excised agarose gel slice (Wizard SV Gel and PCR Clean-Up System, Sigma). After digestion with the appropriate restriction enzymes, the DNA fragments were ligated with an appropriate vector to construct a recombinant plasmid (DNA Ligation Kit, Mighty Mix, Takara, Kusatsu, Japan). To construct pNK75, we used the In-Fusion HD Cloning Kit (Takara). Detailed information on plasmid construction is provided in **Supplementary Table 1**.

Transformation of *L. boryana*

To prevent single recombination between the plasmid and the chromosome in *L. boryana* cells, the plasmid was linearized by digestion with the appropriate restriction enzyme(s). The digested plasmid was introduced into *L. boryana* cells by electroporation, and the transformants were selected by kanamycin resistance (or chloramphenicol resistance for Δ*nafY*) on BG-11 agar plates containing kanamycin or chloramphenicol (Tsujimoto et al., 2015). Gene disruption in the isolated transformants was confirmed using colony PCR (**Supplementary Figure 7** and **Supplementary Table 2**).

Growth Comparison

Cells were grown under nitrate-replete (BG-11) and aerobic conditions for 2 days (50 μmol m^{-2} s^{-1}) as pre-culture. The cells were subsequently suspended in sterile water to adjust the OD value to 1.0. An aliquot (6.0 μl) was spotted on new agar plates, BG-11 or $BG\text{-}11_0$ (BG-11 without combined nitrogen), and incubated under microoxic conditions in the light (40 μmol m^{-2} s^{-1}) for 5 days (Tsujimoto et al., 2014).

Acetylene Reduction Assay

Nitrogenase activity was assayed as described previously (Tsujimoto et al., 2014). The cells grown on BG-11 under aerobic conditions for 2 days were suspended in water. Aliquots (300 μl with OD_{730} of 7.7) of the cell suspensions were spread uniformly

to form a 4-cm diameter circle on a BG-11_0 agar plate, which was then incubated in an anaerobic jar under continuous light (50 μmol m^{-2} s^{-1}) conditions at 30°C for 16 h to induce the *nif* genes. After induction, the cells were harvested in liquid BG-11_0 medium (1.5 ml with OD_{730} of 3). An aliquot (1.0 ml) of the suspension was transferred into a 5-ml glass vial (V-5A, Nichiden-rika glass, Kobe, Japan) and sealed tightly using a butyl rubber septum, and covered with an aluminum seal in the anaerobic chamber. The glass vials were purged with a gas mixture of 10% (vol/vol) acetylene in argon as the standard gas (Japan Fine Products, Kawasaki, Japan) for 45 s. The glass vials were incubated for 10 min under illumination (50 μmol m^{-2} s^{-1}) at 30°C with stirring. The upper gas phase (500 μl) was analyzed using a gas chromatograph (GC-2014AF, Shimadzu, Kyoto, Japan) equipped with a Porapak N column (0.3 m × 3 mm, Shinwa Chemical Industries, Kyoto, Japan) using N_2 as the carrier gas under isothermal conditions at 40°C. Ethylene was detected using a flame ionization detector. After the ethylene formation assay, the cells were collected to estimate optical density at 730 nm (OD_{730}) using a V-550 spectrophotometer (JASCO, Hachioji, Japan).

Preparation of RNA, RT-PCR, and Real-Time PCR

Total RNA samples were prepared as described (Tsujimoto et al., 2014). To synthesize cDNA, extracted RNA was converted to cDNA using ReverTra Ace (Toyobo) and oligo-dT primer. The synthesized cDNAs were amplified using SYBR Premix Ex Taq II (Takara) with primer sets for each target gene (**Supplementary Table 2**). qPCR reaction was performed using the StepOne™ Plus Real-Time PCR System (Life technologies). As an internal control, the housekeeping gene, *rnpB*, which encodes the RNA subunit of RNase P, was used. Based on the comparative CT values, relative expression levels were calculated.

Western Blot Analysis

The induced cells were harvested in 1.5 ml protein extraction buffer (50 mM HEPES-KOH; pH 7.5, 10 mM $MgCl_2$) and the suspension's cell density was adjusted to OD_{730} of 20. An aliquot (500 μl) of the suspension was subjected to cell disruption in a beads-beater-type homogenizer (BugCrusher GM-01, Taitec, Koshigaya, Japan) with glass beads (100 mg glass beads, 150–212 microns, Sigma) at 4°C. The resultant homogenates were centrifuged at 1,360 × *g* for 3 min at 4°C to obtain the supernatant fraction. Protein concentration was determined using the Bradford assay (Protein Assay, Bio-Rad) with bovine serum albumin as the standard. Western blot analysis was carried out as described previously (Aoki et al., 2014). The NifH, NifD, and NifK proteins were detected using three antisera against NifH, NifD and NifK from *L. boryana*, respectively (Tsujimoto et al., 2018).

RESULTS

In the present study, we investigate the functional significance of the following proteins; (1) accessory proteins (NifW, NifX/NafY, and NifZ) for the biosynthesis of nitrogenase metallocenters, (2) Ser acetyltransferase (NifP) for Cys supply to the biosynthesis of iron-sulfur clusters of nitrogenase, (3) PFL (PflB) for anaerobic metabolism, and (4) proteins with unknown functions (NifT, HesA, and HesB). First, we confirmed the assignment of the eight genes by multiple alignments with amino acid sequences of *A. vinelandii* and other diazotrophic cyanobacteria (**Supplementary Figures 1–5**). In addition, we found another *nif*-related gene, LBDG_23680, outside the *nif* gene cluster that exhibited significant similarity to *nifY* and *nafY* (**Supplementary Figure 2**). LBDG_23680's amino acid sequence is more similar to that of NafY (48.9%) than that of NifY (41.2%) in *A. vinelandii*. In addition, His134 and Cys138 are conserved in LBDG_23680. The conserved His (His121 of NafY in *A. vinelandii*) is critical for FeMo-co binding in NafY of *A. vinelandii* (Rubio et al., 2004). Therefore, we tentatively identified the gene as *nafY*. Semi-quantification of mRNA using RT-PCR revealed that constitutive expression of *nafY* was largely different from the *nifHDK* genes whose expression was observed only under nitrogen-fixing conditions (**Supplementary Figure 6**).

We isolated eight mutants in which each gene was individually knocked out (**Figure 1**). Since NifX exhibits considerably similarity with that of the C-terminal half of NafY (**Supplementary Figure 2**). We also isolated another mutant, in which both *nifX* and *nafY* genes were disrupted, to examine the functional redundancy of the homologous genes. Complete segregation of the knock-out copies from the wild type copies in the mutants was confirmed using colony PCR (**Supplementary Figure 7**).

The isolated nine mutants were cultured on BG-11 and BG-11_0 agar plates under microoxic conditions with the other three mutants, Δ*nifDK*, Δ*nifZT*, and Δ*nifX*, as controls (**Figures 2A,B**). Acetylene reduction activity of the cells was also assayed in three independent experimental sets. We classified the mutants into four groups (Group 1 to 4) based on diazotrophic growth and nitrogenase activity.

Three Group 1 mutants, Δ*nifZ*, Δ*nifW*, and Δ*nifXnafY*, did not exhibit substantially growth under nitrogen-fixing conditions (Nif^- phenotype). Δ*nifDK* and Δ*nifZT*, which were previously isolated, were contained in Group 1 (Tsujimoto et al., 2014). The Nif^- phenotype appears to be correlated with very low nitrogenase activity (less than 10% of the wild type level). Group 2 contained Δ*nifP* and Δ*nifX* (Tsujimoto et al., 2014), which exhibited a phenotype with slow growth (Nif^S). Growth in Δ*nifP* was slightly better than that in Δ*nifX*, which is consistent with the higher nitrogenase activity in Δ*nifP* (22%) than that in Δ*nifX* (14%). Two Group 3 mutants, Δ*hesA* and Δ*hesB*, exhibited significantly lower nitrogenase activity (34 and 55 %, respectively) in the acetylene reduction assay, but they grew as well as the wild type. Three Group 4 mutants, Δ*nifT*, Δ*pflB*, and Δ*nafY*, did not exhibit diazotrophic growth defects under the experimental conditions, and they exhibited acetylene reduction activity comparable to that of the wild type or even higher than that of wild type.

The double mutant of *nifX* and *nafY* (Δ*nifXnafY*, Group 1) exhibited a Nif^- phenotype with low activity (4%). Considering that the relevant single mutants, Δ*nifX* and Δ*nafY*, exhibited

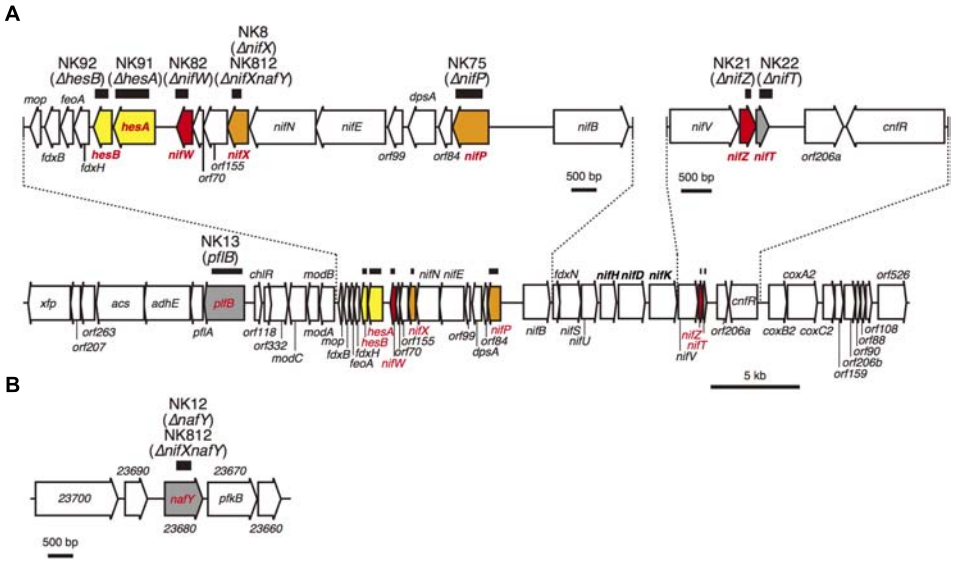

FIGURE 1 | (A) Gene organization of the 50 kb nitrogen fixation gene cluster. **(B)** A chromosomal 6 kb region containing the *nafY* gene. The thick horizontal bars above the genes indicate the region that was removed and replaced with a kanamycin cartridge in the NK mutants. To illustrate the details, two chromosomal parts, from *nifB* to *mop* and from *nifV* to *cnfR* in the *nif* gene cluster, are enlarged. Based on the phenotype, the nine genes are color-coded as follows: red, genes essential for nitrogen fixing growth (Nif$^-$ phenotype; Group 1); orange, genes critical for nitrogen fixing growth (Nif^S phenotype; Group 2); yellow, genes not essential for nitrogen fixing growth (Nif$^+$) but lower nitrogenase activity (Group 3); and gray, genes not critical for nitrogen fixing growth (Nif $^+$) and normal nitrogenase activity (Group 4).

a Nif^S (Group 2) and a wild-type (Group 4) phenotype, respectively, the slow diazotrophic growth with low nitrogenase activity (14%) in Δ*nifX* could be facilitated by NafY action while the chromosomal location is outside of *nif* gene cluster. The *nafY* transcript levels were almost constant in the four examined conditions, and the transcript level was slightly higher in nitrogen-deficient conditions than in nitrate-replete conditions irrespective of microoxic and aerobic conditions (**Supplementary Figure 6**).

Notably, Δ*nifT*'s acetylene reduction activity was significantly higher than that of the wild type (**Figure 2**). The stimulatory effect was also observed in the double mutant Δ*nifZT* compared to the single mutant Δ*nifZ*.

PFL converts pyruvate to acetyl-CoA and formate, which may support nitrogen fixation under anaerobic conditions. However, the Δ*pflB* mutant exhibited normal diazotrophic growth with similar nitrogenase activity levels (Group 4), suggesting that the *pflB* gene is not essential for nitrogen fixation under the present conditions. In addition, Δ*pflB* and the wild type grew heterotrophically with nitrate as the N source under aerobic and dark conditions, while Δ*pflB*'s anaerobic heterotrophic growth in the dark was slightly lower than that of the wild type (**Supplementary Figure 8**).

To assess the effect of gene disruption on the amounts of nitrogenase subunits in the mutants, Western blot analysis was performed using specific antisera against individual nitrogenase subunits including NifH, NifD, and NifK (**Figure 3**). The NifH protein did not exhibit considerable change except in Δ*nifW*, in which it decreased marginally. NifD contents were the most drastically affected by mutations among the three subunits. They were markedly reduced in Δ*nifZ*, Δ*nifW*, Δ*nifX*, Δ*nifXnafY*, and Δ*nifP*, which showed good correlation with the nitrogenase activity levels (**Figure 2**). The NifK contents were also affected similar to NifD contents. However, the degree of decrease of NifK contents was less apparent compared to those of NifD. Although NifD and NifK's signal intensities were almost similar to those in the wild type, NifD signals were much lower than those of NifK in Δ*nifZ*, Δ*nifW*, Δ*nifX*, Δ*nifXnafY*, and Δ*nifP*. The result suggests that NifD is more susceptible to proteolytic degradation than NifK in cyanobacterial cells when the MoFe protein is immature due to the absence of key accessory proteins.

DISCUSSION

In the present study, we isolated nine mutants in the nonheterocystous cyanobacterium *L. boryana* to investigate the targeted proteins′ physiological functions, particularly the role of nitrogenase assembly accessory proteins in cyanobacterial nitrogen fixation.

The kanamycin resistance (Km^R) cartridge was used for target mutagenesis in *L. boryana* (Fujita et al., 1992, 1996, 1998; Okuhara et al., 1999; Kimata-Ariga et al., 2000; Tsujimoto et al., 2014; Hiraide et al., 2015). We observed that inserting the Km^R cartridge into a target gene forming an operon in the same direction as the transcription of the operon does not have a significant polar effect on the downstream genes. For example, the mutant YFD1, in which the Km^R cartridge was inserted in the intergenic region between the *chlL* and *chlN* genes forming an operon, there was no apparent phenotype (Kada et al., 2003),

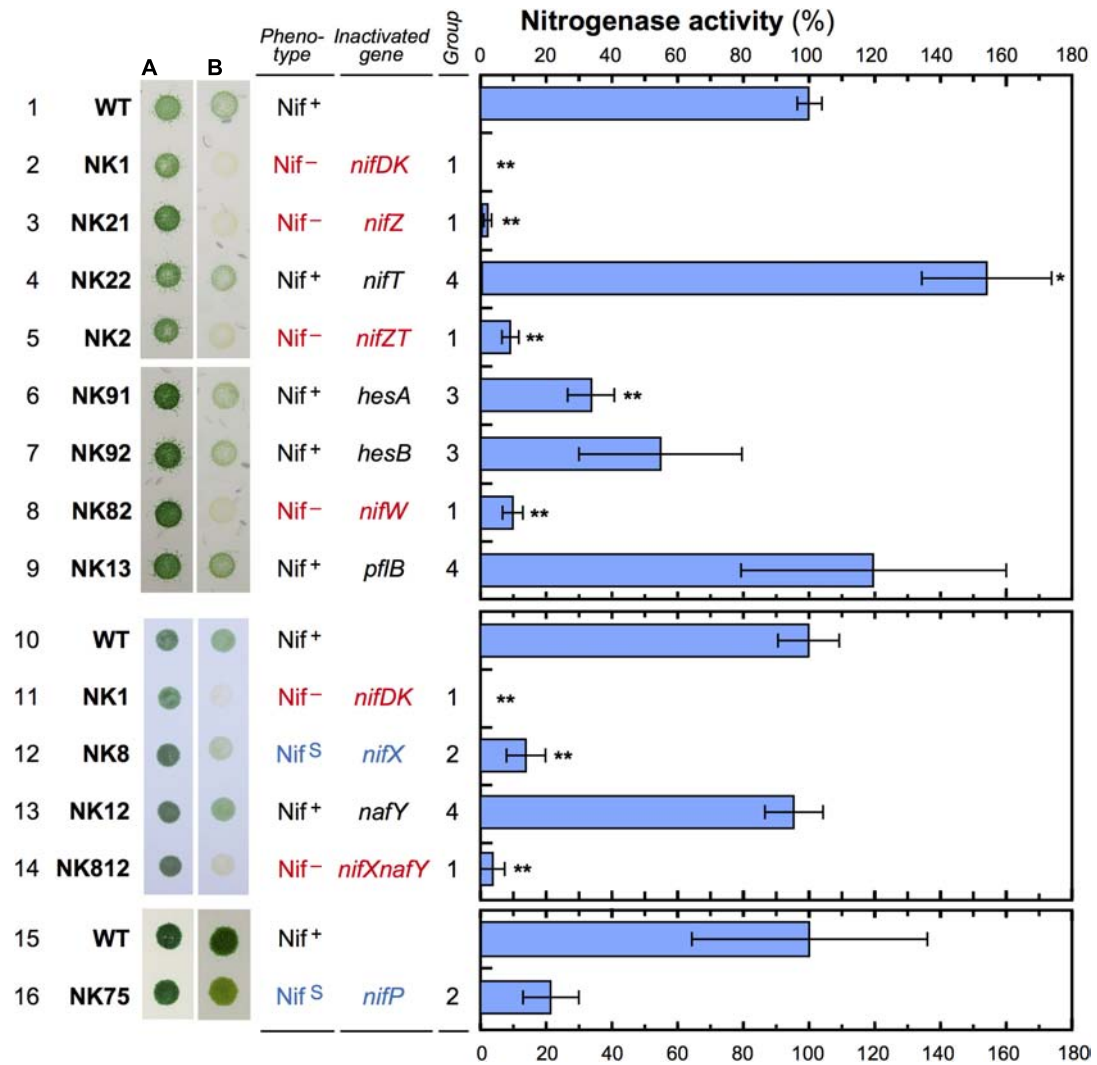

FIGURE 2 | Comparison of growth and nitrogenase activity among the mutants. *L. boryana* cells were grown on BG-11 agar plates containing nitrate **(A)** or BG-11_0 without combined nitrogen **(B)** under microoxic conditions for 5 days (light intensity, 40 μmol m^{-2} s^{-1}). To determine nitrogenase activity, cells grown in nitrate-replete conditions were incubated under nitrogen fixation conditions for 16 h to induce the *nif* genes, and used for an acetylene reduction assay. Bars indicate standard deviation (n = 3). Nitrogenase activity was measured in three independent experimental sets. Nitrogenase activity in wild type was 80.5 (first set, lanes 1–9; Δ*nifZ*, Δ*nifT*, Δ*hesA*, Δ*hesB*, Δ*nifW*, and Δ*pflB*), 80.8 (second set, lanes 10–14; Δ*nifX*, Δ*nafY,* and Δ*nifXnafY*), and 28.6 (third set, lanes 15 and 16; Δ*nifP*) nmol ml^{-1} h^{-1} $OD_{730}{}^{-1}$. Asterisks indicate statistically significant differences (*$p < 0.05$; **$p < 0.01$), compared with values of the wild type in the respective experiments. In Δ*hesB* (lane 7) and Δ*nifP* (lane 16), p-values were 0.086 and 0.07681 compared with the wild type, respectively. p-value of Δ*nifP* is less than 0.05 when compared with the two other wild-type (lanes 1 and 10).

and we have been used YFD1 as a wild type showing Km^R (Kada et al., 2003; Yamazaki et al., 2006).

Considering numerous genes are closely clustered in the *nif* gene cluster, we investigated how the Km^R cartridge insertion influences downstream gene expression. In the Δ*nifP* mutant, the transcript level of *nifE*, which was located downstream of *nifP*, was quantified using real-time PCR and compared with that in the control strain YFD1 (**Supplementary Figure 9**). As a control, *nifH* transcript level, which is not affected by the Km^R cartridge insertion, was also quantified. The *nifE* transcript level in Δ*nifP* was approximately 75% of that in YFD1, and the transcript level of *nifH* in Δ*nifP* was also slightly lower than that in YFD1 (80%). The ratio of *nifE* to *nifH* was almost similar between Δ*nifP* (0.91) and YFD1 (1.0). The result suggests that the transcript level in *nifE* was marginally decreased by the insertion of the Km^R cartridge into the *nifP* coding region in Δ*nifP*, but the polar effect was not adequately strong to suppress the transcript level of a downstream gene, *nifE*, significantly. Therefore, we considered the polar effect of the Km^R cartridge insertion almost negligible in the *nif* gene cluster, although it was somewhat apparent.

The contents of MoFe protein, particularly NifD, decreased substantially, in Group 1 and 2 mutants, suggesting that the proteins, namely NifZ, NifW, NifX/NafY, NifP, are mainly involved in the maturation processes of the MoFe protein

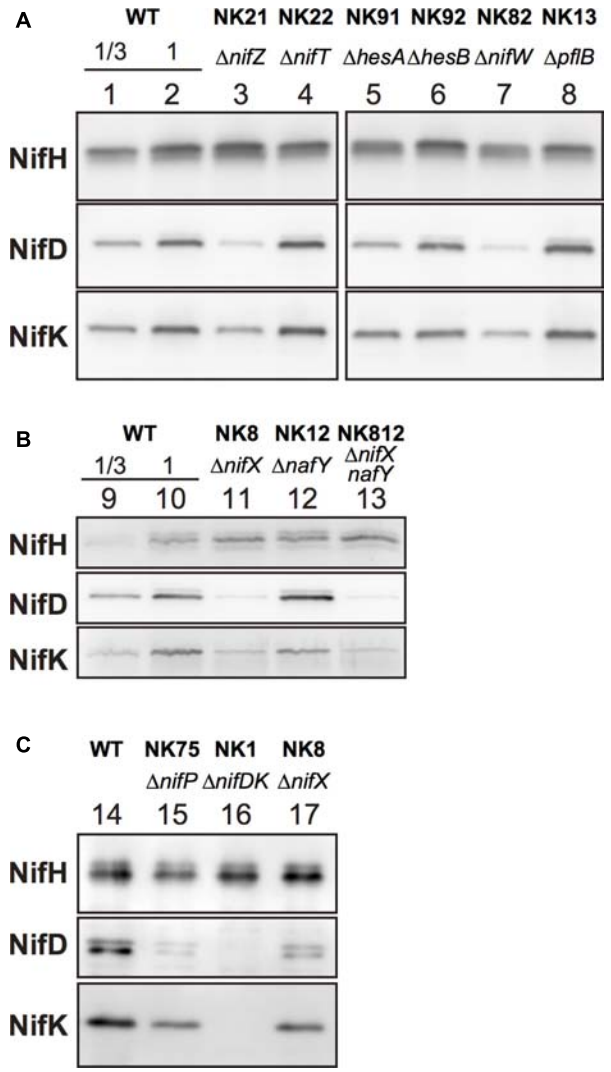

FIGURE 3 | Western blot analysis of extracts of the mutants. Aliquots [**(A,C)**, 0.5 μg; and **(B)**, 1.5 μg] of total extracts from cells that induced the expression of the *nif* genes by incubation on BG-11_0 under microoxic conditions for 16 h (24 h in **C**). For rough quantification, one-third of the protein amounts from the total extracts from the wild type cells were analyzed (lanes 1 and 9). The blotting membranes were the same in **(A)** (lanes 1–8). NifH, NifD, and NifK were detected by specific antisera (Tsujimoto et al., 2018).

including the biosynthesis of FeMo-co and the formation of the P-clusters. Nitrogenase biosynthesis, including the MoFe protein, has been studied mostly in heterotrophic bacteria such as *A. vinelandii* and *K. pneumonia*. NifZ is involved in P-cluster maturation (Hu et al., 2007). While NifW's biochemical function remains largely unknown, NifW is associated with an apo-form of the MoFe protein which carries immature P-clusters without FeMo-co (Jimenez-Vicente et al., 2018). Interactions between NifW and NifZ have previously been reported (Lee et al., 1998). NifX is involved in the transfer of the NifB-co, produced by NifB, to the scaffold protein NifEN (Hernandez et al., 2007). NafY is associated with another apo-form of the MoFe protein that has the P-cluster but not FeMo-co (Jimenez-Vicente et al., 2018), suggesting that NafY is involved in the efficient transfer and insertion of the FeMo-co in the MoFe protein.

Despite the potentially critical biochemical functions of accessory proteins during the maturation processes of MoFe protein, mutants that lacked the genes exhibited only weak or no phenotypes in *A. vinelandii* and *A. chroococcum* (Jacobson et al., 1989b; Paul and Merrick, 1989), which suggests that NifZ, NifW, NifX, and NafY are not essential for the production of active MoFe protein, and they may be required for efficient active MoFe protein production. The conditions under which the accessory proteins are required are unknown. However, NafY is thought to play important roles under molybdenum-deficient conditions (Rubio et al., 2002). In contrast, relevant cyanobacterial mutants showed much more severe phenotypes than heterotrophic bacteria, suggesting that NifZ, NifW, and NifX/NafY proteins play critical roles in production of active MoFe protein in cyanobacteria, which produce oxygen by photosynthesis. The accessory proteins may be critical in solving the oxygen paradox between nitrogen fixation and photosynthesis.

Cyanobacteria performing oxygenic photosynthesis may have some unique features during the nitrogenase biosynthesis. For example, *nifM* and *nifQ* are missing from diazotrophic cyanobacteria genomes, suggesting that the active Fe protein is assembled without NifM and that molybdenum is incorporated into the FeMo-co without NifQ in cyanobacteria (Tsujimoto et al., 2018). In addition, while the NafH protein is associated with the apo-form of MoFe protein in *A. vinelandii* (Jimenez-Vicente et al., 2018), the corresponding gene, *nafH*, has not been found in most diazotrophic cyanobacterial genomes including that of *L. boryana*.

We found the *nafY* gene outside the *nif* gene cluster in the *L. boryana* genome, and its transcription was largely constitutive (**Supplementary Figure 6**). Such features of the *nafY* gene are similar to those in *A. vinelandii*, in which the *nafY* mRNA was detected in cells grown with ammonia as well as in cells derepressed for nitrogen fixation (Rubio et al., 2002). While the single *nafY* mutant Δ*nafY* grew well, exhibiting normal nitrogenase activity, and Δ*nifX* retained diazotrophic growth capacity with very low nitrogenase activity (14%), the double mutant Δ*nifXnafY* lost all diazotrophic growth ability, exhibiting only 4% activity in *L. boryana*. Such phenotypic features suggest that the function(s) of the two homologous proteins, NifX and NafY, partially overlap and NafY slightly complements NifX's function in cyanobacteria. The result seems to be consistent with the observation in *A. vinelandii*, in which Δ*nafYnifX* mutant showed poor diazotrophic growth and very low nitrogenase activity under stress conditions where molybdate was not supplemented (Rubio et al., 2002). It may imply that the standard cyanobacterial diazotrophic condition corresponds to the stress condition in *A. vinelandii*. A biochemical analysis is required to reveal further insights on the Nif-related accessory proteins in *L. boryana*.

The *nifP* gene [or *cysE* or *nafG* (Jimenez-Vicente et al., 2018)] encodes Ser acetyltransferase (SAT), which catalyzes the conversion of Ser to *O*-acetylserine, the direct precursor

of Cys. CysM/CysK (*O*-acetylserine sulfhydrylase) converts *O*-acetylserine to Cys, and NifS liberates the sulfur atom of Cys for the iron-sulfur cluster assembly. The *nif*-specific SAT is dispensable during diazotrophic growth in *A. vinelandii* (Jacobson et al., 1989a). In contrast, the severe Δ*nifP* phenotype in *L. boryana* suggests that NifP contributes to Cys production under nitrogen fixation conditions, to produce nitrogenase carrying many iron-sulfur clusters. To satisfy sulfur atoms' high demand for Fe protein and for MoFe protein biosynthesis, the additional Cys production by NifP could be important, in addition to the CysE (encoded by LBDG_53060), which is constitutively expressed as a housekeeping enzyme (**Supplementary Figure 3**). It is notable that 32 Cys molecules are required to produce one [4Fe-4S] cluster (the Fe protein) and pairs of P-clusters and FeMo-co (the MoFe protein), which are slightly more than what are required by Cys molecules (30 molecules) for the polypeptide parts of the Fe protein $(NifH)_2$ and the MoFe protein $(NifD\text{-}NifK)_2$ (5, 6, and 4 Cys residues in NifH, NifD, and NifK, respectively). Considering the rapid turnover (with a half-life of 5 min) of the [4Fe-4S] cluster of the Fe protein in *A. vinelandii* (Curatti et al., 2005), the Cys demand would be much greater than such a static estimation.

The *hesA* and *hesB* genes are conserved in diazotrophic cyanobacteria genomes, but their functions remain unknown. *E. coli* transformants exhibiting nitrogenase activity were isolated by the overexpression of the *nif* and *nif*-related genes from a gram-positive soil bacterium, *Paenibacillus* sp. WLY78 (Wang et al., 2013). The *hesA* gene is contained in the *nif* gene cluster of *Paenibacillus* sp. An *E. coli* transformant, harboring the *nif* gene cluster without *hesA*, showed approximately 60% of the nitrogenase activity of the transformant harboring the intact *nif* gene cluster. In *L. boryana*, nitrogenase activity was reduced to 34% in Δ*hesA*, and the decreased nitrogenase activity was well correlated with the decrease in NifDK proteins. The result suggests that HesA is involved in the efficient production of the MoFe protein but is not essential in cyanobacteria.

Deletion of *nifT* does not affect diazotrophic growth in *K. pneumonia* and *A. vinelandii* (Jacobson et al., 1989a; Simon et al., 1996). However, notably, the *L. boryana* Δ*nifT* mutant had nitrogenase activity that was significantly higher than that of the wild type. The trend was also observed in Δ*nifZT*. The NifT protein may have some suppressive effects on nitrogenase. More biochemical studies are required to determine the functions of NifT in cyanobacteria.

The *pflB* gene encodes PFL, which is involved in anaerobic carbon metabolism along with CoA-linked acetaldehyde dehydrogenase-alcohol dehydrogenase (encoded in *adhE*) and acetyl-CoA synthase (encoded by *acs*). In the unicellular cyanobacterium *Synechococcus* OS-B' growing in the microbial mat of the Octopus Spring in Yellowstone National Park, the *pflB* gene was mainly expressed in the night time along with *nifHDK* genes, suggesting that the anaerobic metabolism supports energy production to facilitate nitrogenase activity in the dark (Steunou et al., 2006). However, the Δ*pflB* mutant did not show any phenotype under the nitrogen fixation conditions, although its heterotrophic growth under anaerobic conditions in the dark was slightly slower than that of the wild type (**Supplementary Figure 8**). To clarify the physiological functions of the enzyme during cyanobacterial nitrogen fixation, growth of Δ*pflB* under various diazotrophic conditions, such as low light, complete darkness, or the presence of glucose should be examined.

In addition to the target gene disruption technique, we recently developed an *in vivo* transposon tagging system to isolate random mutants in *L. boryana* (Tomatsu et al., 2018). The technique may facilitate the identification of novel genes that are not in the *nif* gene cluster of *L. boryana* or in the genomes of heterotrophic bacteria such as *A. vinelandii*. Further studies focusing on the molecular mechanisms underlying nitrogen fixation coexistence with photosynthesis are underway in our laboratory. Such studies using diazotrophic cyanobacteria may provide a molecular basis that could facilitate the creation of nitrogen-fixing plants in the future (Tsujimoto et al., 2018).

DATA AVAILABILITY

All datasets generated for this study are included in the manuscript and/or the **Supplementary Files**.

AUTHOR CONTRIBUTIONS

YF and RT conceived the study and designed the experiments. NK performed RT-PCR of *nifX* and *nafY*, and isolated Δ*nifX* and Δ*nafY* to perform initial characterization. AN, HK, and RT isolated all other mutants and characterized them except for Δ*nifP*. HaY isolated Δ*nifP* and characterized it. YF, AN, RT, and HiY wrote the manuscript. All authors reviewed the manuscript.

FUNDING

This work was supported by JSPS KAKENHI Grant Numbers 26660084, 15H04387, 15H01397, and 17H05525, and the Japan Science and Technology Agency (Advanced Low Carbon Technology Research and Development Program; JST-Mirai R&D Program).

ACKNOWLEDGMENTS

We thank Tatsuo Omata for use of the cultivation room and some facilities in Laboratory of Photosynthesis Research. We thank Takafumi Yamashino, members of Laboratory of Molecular and Functional Genomics and Laboratory of Photosynthesis Research and Kazuki Terauchi for valuable discussion.

SUPPLEMENTARY MATERIAL

The Supplementary Material for this article can be found online at: https://www.frontiersin.org/articles/10.3389/fmicb.2019.00495/full#supplementary-material

REFERENCES

Aoki, R., Hiraide, Y., Yamakawa, H., and Fujita, Y. (2014). A novel "oxygen-induced" greening process in a cyanobacterial mutant lacking the transcriptional activator ChlR involved in low-oxygen adaptation of tetrapyrrole biosynthesis. *J. Biol. Chem.* 289, 1841–1851. doi: 10.1074/jbc.M113.495358

Burén, S., and Rubio, L. M. (2018). State of the art in eukaryotic nitrogenase engineering. *FEMS Microbiol. Lett.* 365:fnx274. doi: 10.1093/femsle/fnx274

Curatti, L., Brown, C. S., Ludden, P. W., and Rubio, L. M. (2005). Genes required for rapid expression of nitrogenase activity in *Azotobacter vinelandii*. *Proc. Natl. Acad. Sci. U.S.A.* 102, 6291–6296. doi: 10.1073/pnas.0501216102

Curatti, L., Hernandez, J. A., Igarashi, R. Y., Soboh, B., Zhao, D., and Rubio, L. M. (2007). *In vitro* synthesis of the iron-molybdenum cofactor of nitrogenase from iron, sulfur, molybdenum, and homocitrate using purified proteins. *Proc. Natl. Acad. Sci. U.S.A.* 104, 17626–17631. doi: 10.1073/pnas.0703050104

Curatti, L., and Rubio, L. M. (2014). Challenges to develop nitrogen-fixing cereals by direct *nif*-gene transfer. *Plant Sci.* 225, 130–137. doi: 10.1016/j.plantsci.2014.06.003

Evans, A. M., Gallon, J. R., Jones, A., Staal, M., Stal, L. J., Villbrandt, M., et al. (2000). Nitrogen fixation by baltic cyanobacteria is adapted to the prevailing photon flux density. *New Phytol.* 147, 285–297. doi: 10.1046/j.1469-8137.2000.00696.x

Fay, A. W., Blank, M. A., Rebelein, J. G., Lee, C. C., Ribbe, M. W., Hedman, B., et al. (2016). Assembly scaffold nifen: a structural and functional homolog of the nitrogenase catalytic component. *Proc. Natl. Acad. Sci. U.S.A.* 113, 9504–9508. doi: 10.1073/pnas.1609574113

Fujita, Y., Takagi, H., and Hase, T. (1996). Identification of the *chlB* gene and the gene product essential for the light-independent chlorophyll biosynthesis in the cyanobacterium *Plectonema boryanum*. *Plant Cell Physiol.* 37, 313–323. doi: 10.1093/oxfordjournals.pcp.a028948

Fujita, Y., Takagi, H., and Hase, T. (1998). Cloning of the gene encoding a protochlorophyllide reductase: the physiological significance of the co-existence of light-dependent and -independent protochlorophyllide reduction systems in the cyanobacterium *Plectonema boryanum*. *Plant Cell Physiol.* 39, 177–185. doi: 10.1093/oxfordjournals.pcp.a029355

Fujita, Y., Takahashi, Y., Chuganji, M., and Matsubara, H. (1992). The *nifH*-like (*frxC*) gene is involved in the biosynthesis of chlorophyll in the filamentous cyanobacterium *Plectonema boryanum*. *Plant Cell Physiol.* 33, 81–92.

Good, A. (2018). Toward nitrogen-fixing plants. *Science* 359, 869–870. doi: 10.1126/science.aas8737

Hernandez, J. A., Igarashi, R. Y., Soboh, B., Curatti, L., Dean, D. R., Ludden, P. W., et al. (2007). NifX and NifEN exchange NifB cofactor and the VK-cluster, a newly isolated intermediate of the iron-molybdenum cofactor biosynthetic pathway. *Mol. Microbiol.* 63, 177–192. doi: 10.1111/j.1365-2958.2006.05514.x

Herrero, A., Stavans, J., and Flores, E. (2016). The multicellular nature of filamentous heterocyst-forming cyanobacteria. *FEMS Microbiol. Rev.* 40, 831–854. doi: 10.1093/femsre/fuw029

Hiraide, Y., Oshima, K., Fujisawa, T., Uesaka, K., Hirose, Y., Tsujimoto, R., et al. (2015). Loss of cytochrome c_M stimulates cyanobacterial heterotrophic growth in the dark. *Plant Cell Physiol.* 56, 334–345. doi: 10.1093/pcp/pcu165

Hu, Y., Fay, A. W., Lee, C. C., and Ribbe, M. W. (2007). P-cluster maturation on nitrogenase MoFe protein. *Proc. Natl. Acad. Sci. U.S.A.* 104, 10424–10429. doi: 10.1073/pnas.0704297104

Hu, Y., and Ribbe, M. W. (2016). Biosynthesis of the metalloclusters of nitrogenases. *Annu. Rev. Biochem.* 85, 455–483. doi: 10.1146/annurev-biochem-060614-034108

Jacobson, M. R., Brigle, K. E., Bennett, L. T., Setterquist, R. A., Wilson, M. S., Cash, V. L., et al. (1989a). Physical and genetic map of the major *nif* gene cluster from *Azotobacter vinelandii*. *J. Bacteriol.* 171, 1017–1027. doi: 10.1128/jb.171.2.1017-1027.1989

Jacobson, M. R., Cash, V. L., Weiss, M. C., Laird, N. F., Newton, W. E., and Dean, D. R. (1989b). Biochemical and genetic analysis of the *nifUSVWZM* cluster from *Azotobacter vinelandii*. *Mol. Gen. Genet.* 219, 49–57. doi: 10.1007/BF00261156

Jimenez-Vicente, E., Yang, Z. Y., Ray, W. K., Echavarri-Erasun, C., Cash, V. L., Rubio, L. M., et al. (2018). Sequential and differential interaction of assembly factors during nitrogenase MoFe protein maturation. *J. Biol. Chem.* 293, 9812–9823. doi: 10.1074/jbc.RA118.002994

Johnson, D. C., Dean, D. R., Smith, A. D., and Johnson, M. K. (2005). Structure, function, and formation of biological iron-sulfur clusters. *Annu. Rev. Biochem.* 74, 247–281. doi: 10.1146/annurev.biochem.74.082803.133518

Kada, S., Koike, H., Satoh, K., Hase, T., and Fujita, Y. (2003). Arrest of chlorophyll synthesis and differential decrease of Photosystems I and II in a cyanobacterial mutant lacking light-independent protochlorophyllide reductase. *Plant Mol. Biol.* 51, 225–235. doi: 10.1023/A:1021195226978

Kaiser, J. T., Hu, Y., Wiig, J. A., Rees, D. C., and Ribbe, M. W. (2011). Structure of precursor-bound NifEN: a nitrogenase FeMo cofactor maturase/insertase. *Science* 331, 91–94. doi: 10.1126/science.1196954

Kimata-Ariga, Y., Matsumura, T., Kada, S., Fujimoto, H., Fujita, Y., Endo, T., et al. (2000). Differential electron flow around photosystem I by two C4-photosynthetic-cell-specific ferredoxins. *EMBO J.* 19, 5041–5050. doi: 10.1038/sj.emboj.7593319

Lee, S. H., Pulakat, L., Parker, K. C., and Gavini, N. (1998). Genetic analysis on the NifW by utilizing the yeast two-hybrid system revealed that the NifW of *Azotobacter vinelandii* interacts with the NifZ to form higher-order complexes. *Biochem. Biophys. Res. Commun.* 244, 498–504. doi: 10.1006/bbrc.1998.8119

Lopez-Torrejon, G., Jimenez-Vicente, E., Buesa, J. M., Hernandez, J. A., Verma, H. K., and Rubio, L. M. (2016). Expression of a functional oxygen-labile nitrogenase component in the mitochondrial matrix of aerobically grown yeast. *Nat. Commun.* 7:11426. doi: 10.1038/ncomms11426

Okuhara, H., Matsumura, T., Fujita, Y., and Hase, T. (1999). Cloning and inactivation of genes encoding ferredoxin- and NADH-dependent glutamate synthases in the cyanobacterium *Plectonema boryanum*. Imbalances in nitrogen and carbon assimilations caused by deficiency of the ferredoxin-dependent enzyme. *Plant Physiol.* 120, 33–42. doi: 10.1104/pp.120.1.33

Paul, W., and Merrick, M. (1989). The roles of the *nifW*, *nifZ* and *nifM* genes of *Klebsiella pneumoniae* in nitrogenase biosynthesis. *Eur. J. Biochem.* 178, 675–682. doi: 10.1111/j.1432-1033.1989.tb14497.x

Rabouille, S., Staal, M., Stal, L. J., and Soetaert, K. (2006). Modeling the dynamic regulation of nitrogen fixation in the cyanobacterium *Trichodesmium* sp. *Appl. Environ. Microbiol.* 72, 3217–3227. doi: 10.1128/AEM.72.5.3217-3227.2006

Robson, R. L. (1979). Characterization of an oxygen-stable nitrogenase complex isolated from *Azotobacter chroococcum*. *Biochem. J.* 181, 569–575. doi: 10.1042/bj1810569

Rosenblueth, M., Ormeño-Orrillo, E., López-López, A., Rogel, M. A., Reyes-Hernández, B. J., Martínez-Romero, J. C., et al. (2018). Nitrogen fixation in cereals. *Front. Microbiol.* 9:1794. doi: 10.3389/fmicb.2018.01794

Rubio, L. M., Rangaraj, P., Homer, M. J., Roberts, G. P., and Ludden, P. W. (2002). Cloning and mutational analysis of the gamma gene from *Azotobacter vinelandii* defines a new family of proteins capable of metallocluster binding and protein stabilization. *J. Biol. Chem.* 277, 14299–14305. doi: 10.1074/jbc.M107289200

Rubio, L. M., Singer, S. W., and Ludden, P. W. (2004). Purification and characterization of NafY (Apodinitrogenase subunit) from *Azotobacter vinelandii*. *J. Biol. Chem.* 279, 19739–19746. doi: 10.1074/jbc.M400965200

Seefeldt, L. C., Hoffman, B. M., Peters, J. W., Raugei, S., Beratan, D. N., Antony, E., et al. (2018). Energy transduction in nitrogenase. *Acc. Chem. Res.* 51, 2179–2186. doi: 10.1021/acs.accounts8b00112

Shah, V. K., Allen, J. R., Spangler, N. J. and Ludden, P. W. (1994). *In vitro* synthesis of the iron-molybdenum cofactor of nitrogenase. Purification and characterization of NifB cofactor, the product of NIFB protein. *J. Biol. Chem.* 269, 1154–1158.

Simon, H. M., Homer, M. J., and Roberts, G. P. (1996). Perturbation of *nifT* expression in *Klebsiella pneumoniae* has limited effect on nitrogen fixation. *J. Bacteriol.* 178, 2975–2977. doi: 10.1128/jb.178.10.2975-2977.1996

Stal, L. J., and Zehr, J. P. (2008). "Cyanobacterial nitrogen fixation in the ocean: diversity, regulation, and ecology," in *The Cyanobacteria: Molecular Biology, Genomics and Evolution*. eds A. Herrero and E. Flores (Norfolk: Caister Academic Press), 423–446.

Steunou, A. S., Bhaya, D., Bateson, M. M., Melendrez, M. C., Ward, D. M., Brecht, E., et al. (2006). *In situ* analysis of nitrogen fixation and metabolic switching in unicellular thermophilic cyanobacteria inhabiting hot spring microbial mats. *Proc. Natl. Acad. Sci. U.S.A.* 103, 2398–2403. doi: 10.1073/pnas.0507513103

Tomatsu, C., Uesaka, K., Yamakawa, H., Tsuchiya, T., Ihara, K., and Fujita, Y. (2018). *In vivo* transposon tagging in the nonheterocystous nitrogen-fixing

cyanobacterium *Leptolyngbya boryana*. *FEBS Lett.* 592, 1634–1642. doi: 10.1002/1873-3468.13079

Tsujimoto, R., Kamiya, N., and Fujita, Y. (2014). Transcriptional regulators ChlR and CnfR are essential for diazotrophic growth in nonheterocystous cyanobacteria. *Proc. Natl. Acad. Sci. U.S.A.* 111, 6762–6767. doi: 10.1073/pnas.1323570111

Tsujimoto, R., Kotani, H., Nonaka, A., Miyahara, Y., Hiraide, Y., and Fujita, Y. (2015). Transformation of the cyanobacterium *Leptolyngbya boryana* by electroporation. *Bio Protoc.* 5:e1690. doi: 10.21769/BioProtoc.1690

Tsujimoto, R., Kotani, H., Yokomizo, K., Yamakawa, H., Nonaka, A., and Fujita, Y. (2018). Functional expression of an oxygen-labile nitrogenase in an oxygenic photosynthetic organism. *Sci. Rep.* 8:7380. doi: 10.1038/s41598-018-25396-7

Wang, L., Zhang, L., Liu, Z., Zhao, D., Liu, X., Zhang, B., et al. (2013). A minimal nitrogen fixation gene cluster from *Paenibacillus* sp. WLY78 enables expression of active nitrogenase in *Escherichia coli*. *PLoS Genet.* 9:e1003865. doi: 10.1371/journal.pgen.1003865

Yamazaki, S., Nomata, J., and Fujita, Y. (2006). Differential operation of dual protochlorophyllide reductases for chlorophyll biosynthesis in response to environmental oxygen levels in the cyanobacterium *Leptolyngbya boryana*. *Plant Physiol.* 142, 911–922. doi: 10.1104/pp.106.086090

Conflict of Interest Statement: The authors declare that the research was conducted in the absence of any commercial or financial relationships that could be construed as a potential conflict of interest.

frontiers in Microbiology

ORIGINAL RESEARCH
published: 21 March 2019
doi: 10.3389/fmicb.2019.00579

Genetic and Biochemical Analysis of the *Azotobacter vinelandii* Molybdenum Storage Protein

*Mónica Navarro-Rodríguez, José María Buesa and Luis M. Rubio**

Centro de Biotecnología y Genómica de Plantas (CBGP), Universidad Politécnica de Madrid (UPM), Instituto Nacional de Investigación y Tecnología Agraria y Alimentaria (INIA), Madrid, Spain

The N_2 fixing bacterium *Azotobacter vinelandii* carries a molybdenum storage protein, referred to as MoSto, able to bind 25-fold more Mo than needed for maximum activity of its Mo nitrogenase. Here we have investigated a plausible role of MoSto as obligate intermediate in the pathway that provides Mo for the biosynthesis of nitrogenase iron–molybdenum cofactor (FeMo-co). The *in vitro* FeMo-co synthesis and insertion assay demonstrated that purified MoSto functions as Mo donor and that direct interaction with FeMo-co biosynthetic proteins stimulated Mo donation. The phenotype of an *A. vinelandii* strain lacking the MoSto subunit genes (Δ*mosAB*) was analyzed. Consistent with its role as storage protein, the Δ*mosAB* strain showed severe impairment to accumulate intracellular Mo and lower resilience than wild type to Mo starvation as demonstrated by decreased *in vivo* nitrogenase activity and competitive growth index. In addition, it was more sensitive than the wild type to diazotrophic growth inhibition by W. The Δ*mosAB* strain was found to readily derepress *vnfDGK* upon Mo step down, in contrast to the wild type that derepressed Vnf proteins only after prolonged Mo starvation. The Δ*mosAB* mutation was then introduced in a strain lacking V and Fe-only nitrogenase structural genes (Δ*vnf* Δ*anf*) to investigate possible compensations from these alternative systems. When grown in Mo-depleted medium, the Δ*mosAB* and *mosAB*$^+$ strains showed low but similar nitrogenase activities regardless of the presence of Vnf proteins. This study highlights the selective advantage that MoSto confers to *A. vinelandii* in situations of metal limitation as those found in many soil ecosystems. Such a favorable trait should be included in the gene complement of future nitrogen fixing plants.

Keywords: nitrogenase, iron–molybdenum cofactor, nitrogen fixation, metal homeostasis, MoSto

OPEN ACCESS

Edited by:
Maria J. Delgado, Estación Experimental del Zaidín (CSIC), Spain

Reviewed by:
Emilio Fernandez, Universidad de Córdoba, Spain
Patricia Coutinho Dos Santos, Wake Forest University, United States

****Correspondence:***
Luis M. Rubio
lm.rubio@upm.es

Specialty section:
This article was submitted to Terrestrial Microbiology, a section of the journal Frontiers in Microbiology

Received: *14 January 2019*
Accepted: *06 March 2019*
Published: *21 March 2019*

Citation:
Navarro-Rodríguez M, Buesa JM and Rubio LM (2019) Genetic and Biochemical Analysis of the Azotobacter vinelandii Molybdenum Storage Protein. Front. Microbiol. 10:579. doi: 10.3389/fmicb.2019.00579

INTRODUCTION

Nitrogenase, the enzyme complex that catalyzes the fixation of N_2 into NH_3, is one of the most relevant enzymes in the nitrogen cycle since it converts inert N into a biologically usable form. In its most prevalent type nitrogenase is an iron–sulfur molybdoenzyme (Boyd and Peters, 2013), although other phylogenetically related nitrogenases exist that carry iron-sulfur-vanadium or iron–sulfur only cofactors (Bishop and Joerger, 1990; Eady, 1996). The Mo-nitrogenase consists of a dinitrogenase component, a NifDK heterotetramer containing two pairs of metalloclusters named

P-cluster (8Fe-7S) and FeMo-co (7Fe-9S-C-Mo-*R*-homocitrate) (Kim and Rees, 1992; Einsle et al., 2002; Rubio and Ludden, 2008; Spatzal et al., 2011), and a dinitrogenase reductase component formed by two NifH homodimers each one carrying a [4Fe-4S] cluster (Georgiadis et al., 1992). *Azotobacter vinelandii* has the peculiarity of having genes to encode the Mo-nitrogenase (*nif*) and the alternative V (*vnf*) and Fe-only (*anf*) nitrogenases (Bishop and Joerger, 1990). The dinitrogenase components of the alternative nitrogenases contain additional subunits (VnfG or AnfG) essential for N_2 reduction (Chatterjee et al., 1997; Krahn et al., 2002) and present subtle differences in cofactor structure (Sippel and Einsle, 2017). However, amino acid sequence comparisons of NifD/VnfD/AnfD and NifK/VnfK/AnfK indicate that residues that serve as ligands to the metal cofactors are conserved in all three nitrogenases (Joerger et al., 1990).

Azotobacter vinelandii nif, *vnf,* and *anf* genes are differentially expressed depending on the metal availability in the environment following a hierarchical *nif* > *vnf* > *anf* sequence. The presence of as low as 50 nM molybdate in the medium represses *vnf* and *anf* genes while vanadium represses the *anf* but not the *nif* genes (Jacobson et al., 1986; Luque and Pau, 1991; Jacobitz and Bishop, 1992). As consequence V-nitrogenase is active in the absence of Mo when V is available and Fe-only nitrogenase is active when neither Mo nor V is available in the medium.

Molybdenum is an essential transition metal for most organisms, which typically carry a number of enzymes and proteins involved in its uptake, storage, homeostasis, regulation, and Mo cofactor biosynthesis (Hernandez et al., 2009; Hille et al., 2014). This metal, and its biological antagonist tungsten (W), can exist in several oxidation states ranging from −II to +VI, with MoO_4^{2-} being the main source of Mo at neutral and basic pH. However, Mo availability in soil ecosystems depends on pH, reactive oxides and water drainage and it is often a limiting factor for nitrogen fixation (Reddy et al., 1997).

Bacteria have developed high-affinity chelation and uptake mechanisms to scavenge molybdate from the environment, including metallophores, ABC-type transporters, and Mo storage proteins (Mouncey et al., 1995; Kraepiel et al., 2009). *A. vinelandii* carries an unusual Mo-binding protein called molybdenum-storage protein (MoSto) (Pienkos and Brill, 1981; Fenske et al., 2005), a $(\alpha\beta)_3$ hexameric complex encoded by the homologous *mosA* and *mosB* genes that is capable of binding more than 100 Mo atoms in the form of polyoxomolybdate clusters (Schemberg et al., 2007; Kowalewski et al., 2012; Poppe et al., 2014). MoSto can also accumulate W (Schemberg et al., 2007). Metal binding to MoSto requires ATP hydrolysis while metal release is ATP-independent but pH-dependent occurring stepwise above pH 6.8 (Schemberg et al., 2008). No amino acid sequence to other Mo-containing enzymes has yet been described. MoSto structure has been related to nucleoside monophosphate kinases, particularly with the UMP kinase from bacteria and archaea, which uses ATP to phosphorylate UMP (Ramon-Maiques et al., 2002; Poppe et al., 2014).

Azotobacter vinelandii is known to accumulate 25-fold more Mo than required for maximum nitrogenase activity (Shah et al., 1984) probably due to the presence of MoSto. However, the effect on nitrogenase of eliminating MoSto has never been determined. The aims of this study are the phenotypical characterization of a MoSto deficient strain and the elucidation of MoSto involvement in FeMo-co biosynthesis.

RESULTS

MoSto Serves as Mo Donor for *in vitro* FeMo-co Biosynthesis

Two versions of MoSto were purified to test their capacity to serve as Mo donor in the *in vitro* FeMo-co synthesis assay. A non-tagged version was partially purified from cells of *A. vinelandii* DJ (**Figure 1A**) whereas a histidine-tagged version (hereinafter named rMoSto) was cloned, overexpressed, and purified from recombinant *Escherichia coli* cells (**Figure 1B**). As purified from *A. vinelandii*, MoSto carried 25-fold more Mo than rMoSto purified from *E. coli* cells grown in medium supplemented with 1 mM molybdate (**Table 1**). When purified from cells grown in not supplemented medium, rMoSto contained very little Mo, consistent with BL21 deficiency in high-affinity molybdate transport (Pinske et al., 2011). Both MoSto and rMoSto functioned as sole Mo source for *in vitro* FeMo-co synthesis, with both versions being equally efficient when normalized by Mo content (**Table 1**). Nitrogenase reconstitution levels correlated with Mo contents in all MoSto preparations. Direct interaction with FeMo-co biosynthetic proteins stimulated Mo donation by MoSto (**Figure 1C**). When MoSto (or rMoSto) was separated from the Nif proteins by a dialysis membrane threefold lower nitrogenase reconstitution levels were obtained (**Figure 1D**). These basal levels of reconstitution were probably due to Mo release from MoSto at pH 7.5 of the reaction mixture (Schemberg et al., 2008). Interestingly, reconstitution due to unspecific Mo release did not increase over time. These biochemical assays established a role for MoSto as direct Mo donor for FeMo-co synthesis.

The Absence of MoSto Impairs Molybdenum Accumulation and *in vivo* Nitrogenase Activity

An *A. vinelandii* strain with an in-frame deletion of MoSto-encoding genes (Δ*mosAB)* was generated to investigate cellular molybdenum levels and nitrogenase activity dependence on MoSto. Four culture conditions reflecting different levels and lengths of Mo starvation were tested. On one hand, precultures obtained by subculturing at least three times in Mo-limited Burk's modified medium (hereinafter called Mo Starved) were inoculated into N-free Mo-limited medium (−Mo) or into N-free Mo-standard medium (+Mo) (**Figure 2A**). On the other hand, precultures grown in Burk's modified medium (hereinafter called Mo Standard) were inoculated into N-free Mo-limited medium (−Mo) or into N-free Mo-standard medium (+Mo) (**Figure 2B**). To minimize nitrogen stress all testing growth media contained 1 μM vanadate to allow V-nitrogenase synthesis at low Mo concentrations.

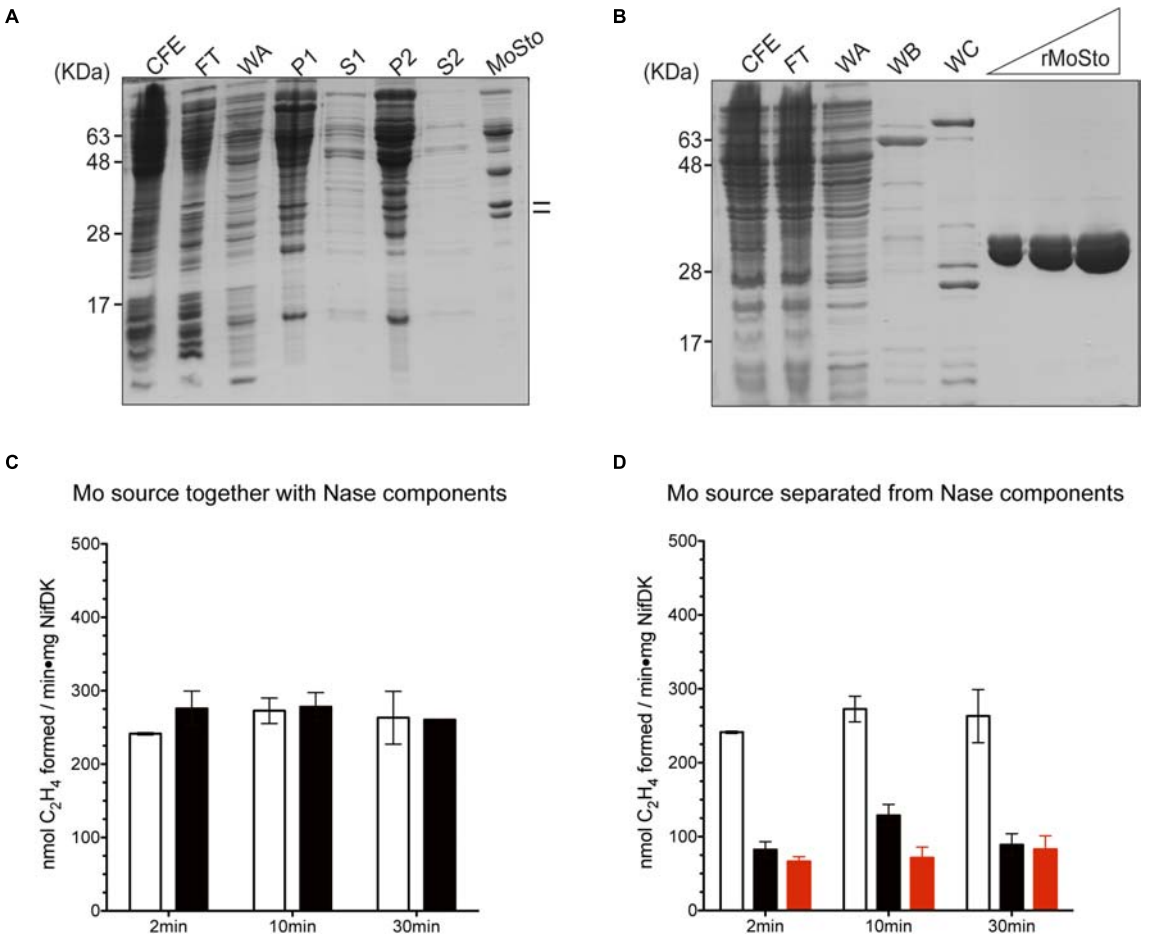

FIGURE 1 | *In vitro* FeMo-co synthesis and nitrogenase reconstitution time-course assays using MoSto as source of Mo. **(A)** Partial purification of MoSto from *Azotobacter vinelandii* cells. Lines indicate migration of MoSto subunits. **(B)** Purification of rMoSto from *Escherichia coli* cells. CFE, cell-free extract; FT, first column flow through; WA, WB, and WC column washes with increasing imidazole; P and S, pellet and supernatant of ammonium sulfate fractionations. **(C)** Reactions in which the molybdenum source (molybdate or MoSto) is mixed with the FeMo-co biosynthetic proteins. Molybdenum sources used were: 7.5 μM molybdate (white bars) or MoSto protein equivalent to 4.5 μM Mo (black bars). **(D)** Reaction mixtures in which the molybdenum source: molybdate (white bars), MoSto (black bars), or rMoSto (red bars) is separated from FeMo-co biosynthetic proteins by a dialysis membrane. Molybdenum sources used were: 7.5 μM molybdate, 22.8 μg MoSto (4.5 μM Mo), or 229 μg rMoSto (11 μM Mo). Data represent mean ± standard deviation of three independent experiments.

TABLE 1 | Activity of nitrogenase reconstituted with MoSto as Mo donor in the *in vitro* FeMo-co synthesis assay.

MoSto type	Mo in growth medium (mM)[a]	Mo atoms in MoSto[b]	μg MoSto used (μM Mo in reaction)	% Activity[c]
rMoSto	–	0.05 ± 0.00	10 (<0.01)	2.3 ± 0.8
			40 (0.02)	4.5 ± 0.3
rMoSto	1	4.12 ± 1.18	10 (0.48)	34.3 ± 3.2
			40 (1.94)	78.7 ± 4.6
MoSto	0.01	104.14 ± 19.8	0.5 (0.99)	55.3 ± 4.9
			1.0 (1.98)	63.1 ± 6.3

[a]*Cells used to purify MoSto were grown in media containing the indicated amount of molybdate.* [b]*Per purified MoSto hexamer.* [c]*Percentage of activity compared to control reactions containing 7.5 μM molybdate as Mo source. Molybdate containing reactions formed 475 nmol of C_2H_4 per minute per mg of MoFe protein. Data represent mean and standard deviations of three independent experiments.*

The following observations could be made: (*i*) In the presence of MoSto, Mo uptake by Mo-starved cells occurred much faster and maximum Mo accumulation was 100-fold higher; (*ii*) Mo content in cells lacking MoSto did not always correlate with nitrogenase levels (**Figures 2A,B**) suggesting the presence of alternative Mo sinks or reservoirs; (*iii*) MoSto was not

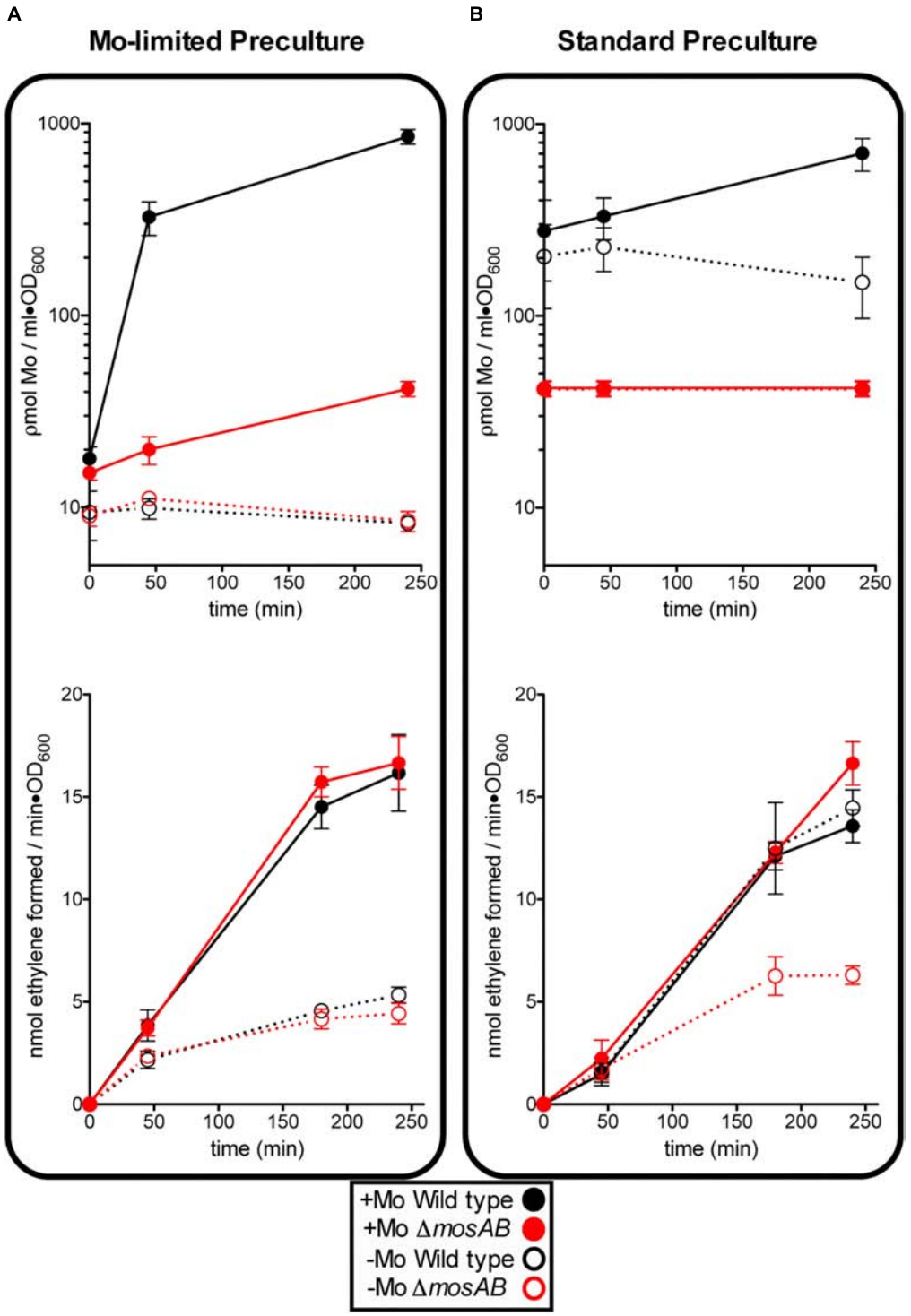

FIGURE 2 | Effect of MoSto on molybdenum accumulation and *in vivo* nitrogenase activity in *A. vinelandii*. Mo-Starved **(A)** or Standard grown **(B)** cells of *A. vinelandii* DJ (wild type; black symbols) or UW394 (Δ*mosAB*, red symbols) were inoculated into Burk's modified N-limited medium containing (close symbols) or lacking (open symbols) 1 μM molybdate. All media contained 1 μM vanadate. Data represent mean ± standard deviation of three independent experiments.

required for maximum nitrogenase activity as long as Mo was provided in the growth medium indicating that its role in Mo-nitrogenase is not essential; (*iv*) However, under transient Mo starvation, tested by derepressing standard precultures in Mo-limited medium, the MoSto mutant was impaired in nitrogenase activity while the wild type was not (compare

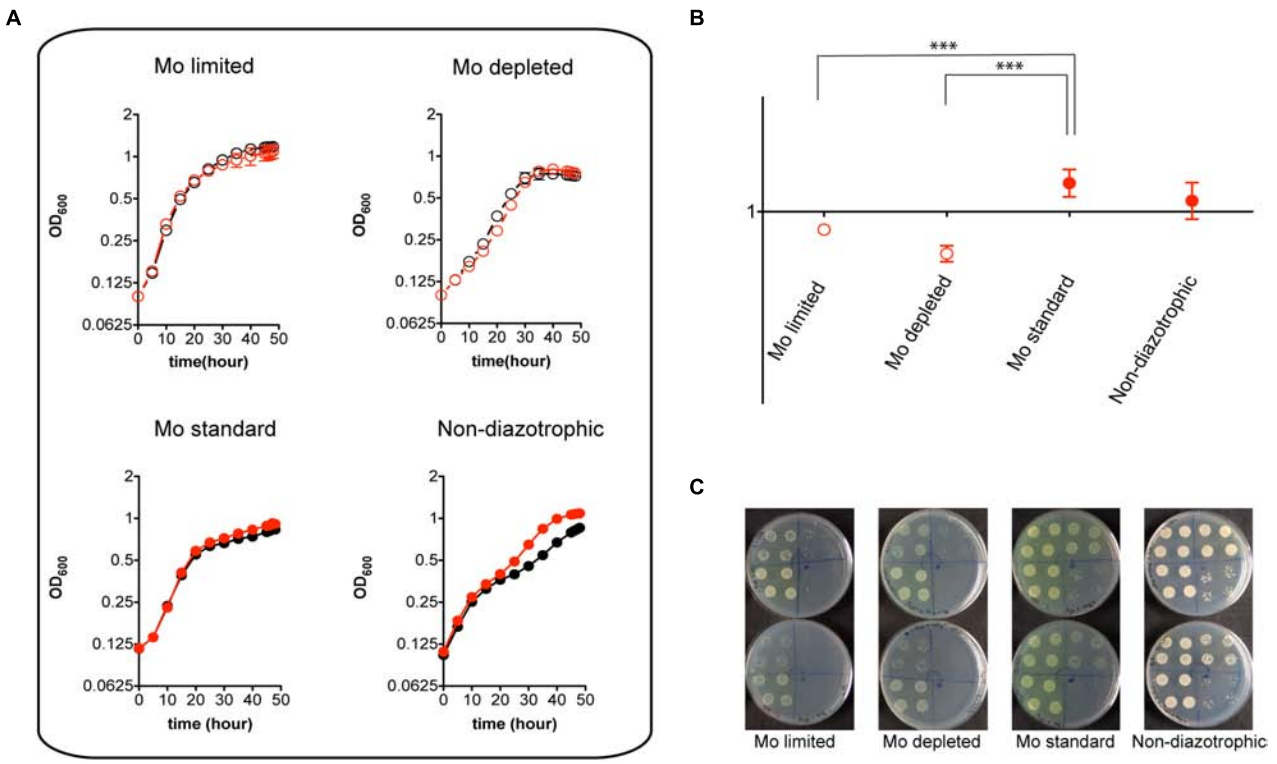

FIGURE 3 | Diazotrophic growth and CI analysis of the MoSto mutant. **(A)** *A. vinelandii* DJ (wild type; black symbols) and UW394 (Δ*mosAB*, red symbols) were cultured in Burk's modified N-free medium supplemented (close symbols) or not supplemented (open symbols) with 1 μM molybdate. Mo-limited (4 nM), Mo-depleted and Mo standard (1 μM) conditions were tested. All N-free media contained 1 μM vanadate. Growth in Burk's modified medium containing ammonium acetate (non-diazotrophic) was carried out as control. **(B)** CI values were obtained from mixed cultures (1:1 inoculum ratio) of DJ and UW394 strains. Data represent the mean and standard deviation of three or four independent experiments. *** Indicates unpaired *t*-test *P*-value < 0.001. **(C)** Plates showing growth on solid media of mixed cultures that were pre-grown in liquid medium for 22 h. Four 20-μl drops with different dilutions (10^3, 10^4, 10^5, and 10^6) of the mixed culture were plated on each quarter of the plate. Arrows show the direction of the dilutions. Upper plates contain media lacking spectinomycin (to allow DJ and UW394 growth) whereas lower plates contain media supplemented with spectinomycin (to only allow UW394 growth).

activity open circles of **Figures 2A,B**). This indicates that metal accumulated at MoSto is readily accessible for FeMo-co synthesis allowing maximum nitrogenase levels under transient Mo-limiting conditions. (*v*) Prolonged Mo starvation equally affected Mo content and nitrogenase activity in wild type and MoSto mutant; (*vi*) 30% nitrogenase activity remained in both strains after prolonged Mo starvation (**Figure 2A**) suggesting V-nitrogenase was being expressed.

Despite its pronounced impairment in Mo accumulation and nitrogenase activity, the MoSto mutant was only mildly affected in diazotrophic growth in Mo-limited conditions. This is consistent with the Mo requirements for maximum nitrogenase activity being much lower than the capacity of *A. vinelandii* to scavenge and accumulate Mo (Shah et al., 1984). In contrast, the MoSto mutant showed slightly better growth than wild type in the presence of 1 μM molybdate both under diazotrophic and non-diazotrophic conditions (**Figure 3A**). Competitive index (CI) assays were carried out to analyze the Δ*mosAB* phenotype in situations of competition for limiting Mo that are of environmental importance. In these assays growth interference takes place between the wild type and mutant strains. A CI > 1 indicates that the mutant is more competitive than wild type whereas a CI < 1 indicates the mutant is less competitive. **Figures 3B,C** shows that the MoSto mutant is less competitive than wild type in diazotrophic growth under Mo starvation. CI was lowest under severe Mo starvation imposed by continuous growing in Mo-depleted medium consistent with a MoSto role as Mo reservoir. Interestingly the MoSto mutant was more competitive than wild type in the presence of 1 μM molybdate in the medium. Because MoSto is present at similar levels in both conditions (see below) this result suggests that the energy burden of loading Mo into MoSto is not negligible.

MoSto Protects *A. vinelandii* Nitrogenase From W Toxicity

W is a well-known competitive inhibitor of Mo functions having negative effect on *A. vinelandii* growth (Keeler and Varner, 1957; Shah et al., 1984). Importantly, binding of W to MoSto has been shown to occur *in vivo* (Pienkos and Brill, 1981) and *in vitro* (Schemberg et al., 2007). The possible role of MoSto in protection against W toxicity was investigated by comparing Δ*mosAB* diazotrophic growth to that of the

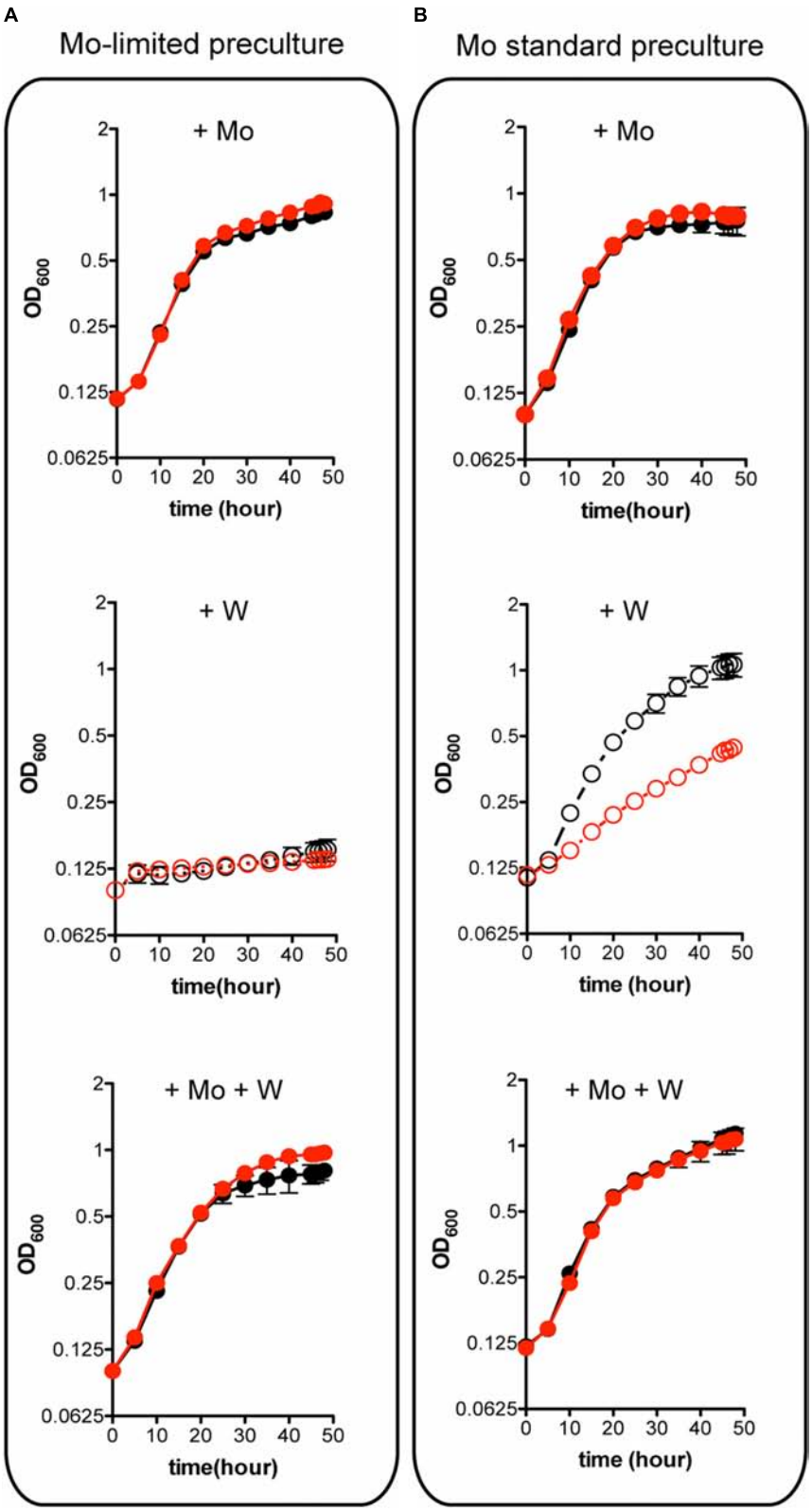

FIGURE 4 | Effect of W on the diazotrophic growth of an *A. vinelandii* Δ*mosAB* strain. Mo-starved **(A)** or Mo standard **(B)** precultures of *A. vinelandii* DJ (wild type; black symbols) or UW394 (Δ*mosAB*, red symbols) were inoculated into Burk's modified N-free medium containing 1 μM molybdate (close symbols) or 4 nM molybdate (open symbols). One μM tungstate was included when indicated and all media contained 1 μM vanadate. Data represent mean ± standard deviation of three independent experiments.

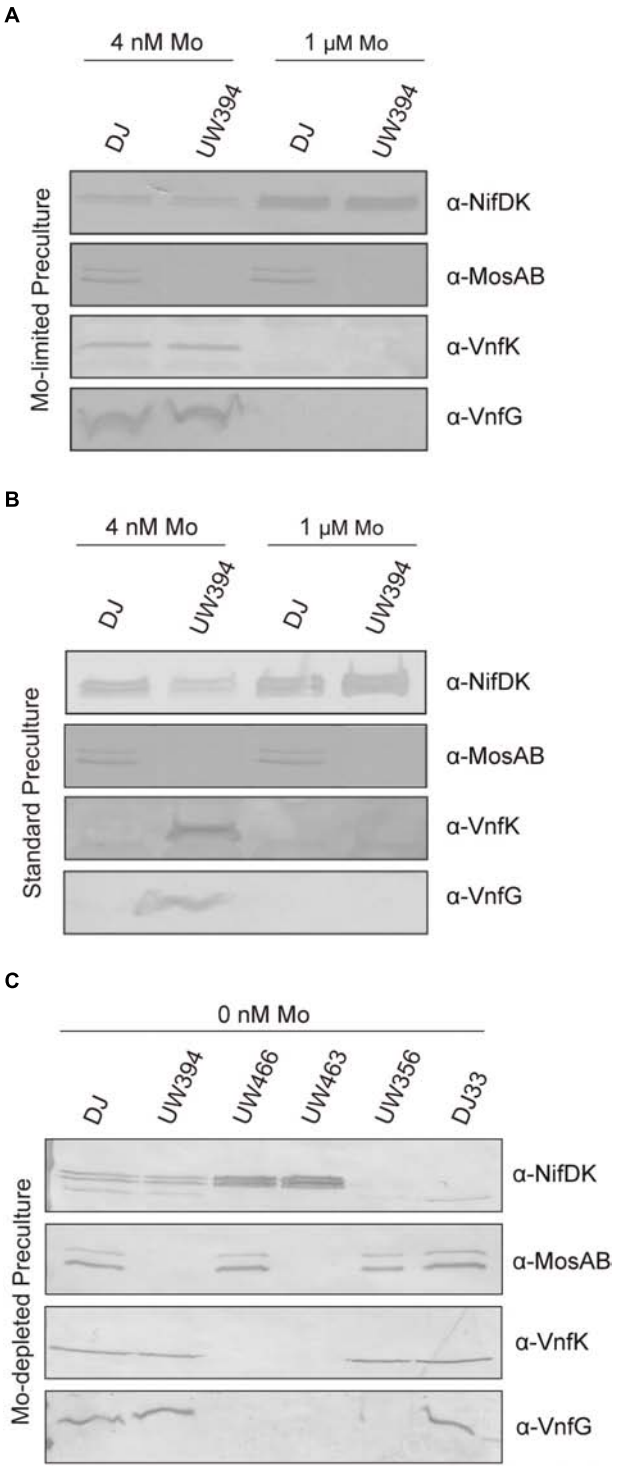

FIGURE 5 | Detection of Mo-nitrogenase and V-nitrogenase structural polypeptides in *A. vinelandii*. Mo-starved **(A,C)** or Mo standard **(B)** precultures of *A. vinelandii* DJ (wild type), UW394 (Δ*mosAB*), UW466 (Δ*vnf* Δ*anf*), UW463 (Δ*vnf* Δ*anf* Δ*mosAB*), UW356 (Δ*nifA*), or DJ33 (Δ*nifDK*) were inoculated into Burk's modified N-free medium containing either 0, 4 nM or 1 μM molybdate to allow nitrogenase derepression. NifDK, VnfK, VnfG, and MosAB polypeptides accumulated in the cells were detected by Western blot analysis against specific antibodies.

wild type at environmentally relevant metal concentrations (**Figure 4**). Mo starved precultures of both wild type and MoSto mutant were highly sensitive to inhibition by 1 μM W (a W/Mo ratio of 250) (**Figure 4A**) an amount that could exceed the W trapping capacity of MoSto. In contrast, when cells grown in Mo standard conditions were transferred to Mo-limited conditions in the presence of W the wild type strain grew normally while the MoSto mutant was clearly inhibited (**Figure 4B**). The differential behavior of wild type and the Δ*mosAB* mutant under transient Mo starving conditions can be rationalized considering MoSto as reservoir that continuously provides Mo for FeMo-co synthesis thus avoiding W toxicity. In all cases, co-presence of 1 μM molybdate in the medium protected from 1 μM tungstate inhibition whereas 1 μM vanadate did not.

Deletion of *mosAB* Genes Affects V-Nitrogenase Accumulation Under Mo Deficiency

Mo tightly represses expression of V-nitrogenase (Bishop and Joerger, 1990). However, V-nitrogenase and Mo-nitrogenase transcripts coexist when molybdate levels in the medium are in the range of 10–50 nM (Jacobson et al., 1986). Because the presence or absence of MoSto largely determines intracellular Mo concentration, the effect of Δ*mosAB* mutation on the accumulation of Mo-nitrogenase and V-nitrogenase structural components in relation to changes in Mo availability was investigated. On one hand, Mo starved cells were transferred to the same Mo-limiting conditions (4 nM Mo) or to medium with standard molybdate (1 μM Mo). Standard medium allowed maximum NifDK accumulation and repressed VnfDGK synthesis, as expected (**Figure 5A**). Under Mo-limiting conditions, Nif polypeptides were present at much lower levels and coexisted with Vnf polypeptides, both in the wild type and in the Δ*mosAB* strain. On the other hand, transferring Mo sufficient cells to Mo-limited medium (Mo step down) readily derepressed *vnfDGK* expression in the Δ*mosAB* strain but not in the wild type, which in contrast accumulated more NifDK than the mutant (**Figure 5B**). Importantly, MoSto was accumulated to similar levels under all Mo concentrations tested in this study, in agreement with previous observations (Pienkos and Brill, 1981; Fenske et al., 2005). These results indicates that the buffering effect that MoSto has in Mo homeostasis (**Figure 2B**) softens the regulatory response to transient Mo limitation repressing early *vnf* expression and maintaining higher Nif-dependent nitrogenase activity.

The *mosAB* Deletion Has No Effect on the Activity of Alternative Nitrogenases

The Δ*mosAB* mutation was also introduced into a Δ*vnfDGK* Δ*anfDGK* strain, lacking the V and Fe-only nitrogenase structural components, to investigate a possible role in these alternative systems. Cells cultured in Mo-depleted medium were derepressed for nitrogenase in either Mo-depleted or Mo-standard media supplemented with 1 μM vanadate. *In vivo*

TABLE 2 | Ratio of ethane to ethylene production in MoSto deficient strains derepressed in media with different metal availability.

Strain[a]	Metal	C_2H_4[b]	C_2H_6/C_2H_4 (%)[c]
DJ	V	1.58 ± 0.07	0.63
	Mo, V	13.65 ± 0.55	0
UW394	V	1.57 ± 0.01	0.71
	Mo, V	15.24 ± 1.04	0
UW466	V	1.83 ± 0.28	0.65
	Mo, V	13.94 ± 1.03	0
UW463	V	1.92 ± 0.18	0.60
	Mo, V	14.95 ± 1.04	0
UW356	V	0.47 ± 0.01	1.00
	Mo, V	0	0
DJ33	V	1.64 ± 0.59	1.22
	Mo, V	0	0

[a]*Precultures grown in NH_4^+-containing Mo-depleted medium were transferred to N-free medium supplemented with 1 μM of the indicated metal.* [b]*Activities are in nmol ethylene per min per ml at an OD_{600} of 1. Data represent mean and standard deviations of three independent experiments.* [c]*C_2H_6 production shown as % of C_2H_4.*

nitrogenase activities were estimated by measuring acetylene reduction into ethylene and ethane (**Table 2**), an exclusive property of alternative nitrogenases (Dilworth et al., 1987) while the presence of Mo- or V-nitrogenase structural components under Mo-depleted conditions was determined by immunoblot analysis (**Figure 5C**). Importantly, all Mo-depleted strains contained less than 0.7 pmol Mo per ml of culture at OD_{600} of 1 at 8 h of derepression.

Strains with intact Mo-nitrogenase structural genes produced maximum levels of ethylene and repressed alternative nitrogenase structural proteins in media containing 1 μM Mo and 1 μM V, as expected. Under Mo-depleted conditions, the wild type strain as well as DJ33 (Δ*nifDK*) and UW356 (Δ*nifA*, encoding the *nif* gene transcriptional activator) exhibited concomitant production of ethylene and ethane diagnostic of alternative nitrogenase activity. Surprisingly, the Δ*vnfDGK* Δ*anfDGK* strains UW466 and UW463 exhibited similar ethylene and ethane production levels than vnf^+anf^+ strains (**Table 2**) despite the absence of Vnf proteins (**Figure 5C**). However, these strains accumulated high levels of NifDK. This observation suggests the plausible insertion of FeV-co into NifDK under Mo-depleted conditions, which would be responsible for the observed residual nitrogenase activities. No effect of the *mosAB* mutation on nitrogenase activity was detected in this condition in any of the tested genetic backgrounds.

DISCUSSION

The *A. vinelandii* MoSto protein is rather unique both in function and in amino acid sequence having no known homologs in protein databases. It has the capacity to accumulate massive amounts of Mo (over 100 atoms per MoSto), which would be a favorable trait to add to engineered nitrogen fixing plants expressing bacterial Mo-nitrogenase provided this Mo was directly available to nitrogenase FeMo-co biosynthesis. However, such a direct transfer had not yet been experimentally proven. Here we show that the Mo stored at MoSto is directly available for FeMo-co synthesis *in vitro* and that interaction of MoSto with FeMo-co biosynthetic proteins stimulates cofactor synthesis. The exact mechanism by which this interaction stimulates cofactor synthesis is unclear. Direct transfer of Mo from NifQ to the NifEN/NifH complex during FeMo-co biosyntesis *in vitro* has been reported (Hernandez et al., 2008). The similarities between the Mo-Fe-S clusters found in NifQ and in NifEN purified from a Δ*nifH* background (Soboh et al., 2006; George et al., 2007) support such direct connection. The expected primary path for molybdenum incorporation into FeMo-co would include molybdate transport, storage at MoSto, transfer to NifQ, and finally to the NifEN/NifH complex. However the results shown here indicate some degree of NifQ function replacement by MoSto in the *in vitro* system. Mo release from MoSto occurs spontaneously *in vitro* above pH 6.8 (Schemberg et al., 2008) and perhaps an interaction with NifEN

TABLE 3 | Bacterial strains and plasmids.

Strain or plasmid	Genotype	Resource
Escherichia coli		
DH5α	F– φ80ΔlacZM15 Δ(lacZYA-argF)U169 deoP recA1 endA1 hsdR17 (rK^-mK^-)	Sambrook and Russell, 2001
BL21(DE3)pLysS	F′- ompT gal[dcm][lon] hsdsB (rB^-mB^-; an *E. coli* B strain) with DE3 and pLysS	Studier and Moffatt, 1986
Azotobacter vinelandii		
DJ	Highly transformable variant of OP	Setubal et al., 2009
UW394	Δ*mosBA::spc*	This study
UW466	Δ*vnfDGK::tet*→ ; Δ*anfDGK::kan*→	This study
UW463	Δ*mosBA::spc;* Δ*vnfDGK::tet*→ ; Δ*anfDGK::kan*→	This study
UW356	Δ*nifA::spc*	Poza-Carrion et al., 2014
DJ33	Δ*nifDK*	Robinson et al., 1986
Plasmids		
pBluescript KS (+)	Cloning vector	Agilent
pGEMT-vector	Cloning vector	Promega
pET28a (+)	Expression vector	Novagen
pUC4K	Vector containing Kan resistance cassette	Pharmacia
pBBR1-MCS3	Vector containing Tet resistance cassette	Obranic et al., 2013
pHP45Ω	Vector containing Spc/Sm resistance cassette	Prentki and Krisch, 1984
pRHB268	pGEMT carrying *mosBA* flanking regions and spc cassette	This study
pN2MN14	pBSKS(+) carrying *anfDGK* flanking regions and kan cassette	This study
pN2MN18	pBSKS(+) carrying *vnfDGK* flanking regions and tet cassette	This study
pN2MN72	*mosBA* genes cloned into pET28a (+)	This study

facilitated Mo transfer. In this context, it is interesting to note that a NifH-independent pathway for Mo transfer into NifEN was previously postulated (Soboh et al., 2006). Thus, the ability of MoSto to donate Mo for FeMo-co synthesis might also be relevant *in vivo* and could underlie the phenotypic reversal of *nifQ*$^{-}$ by excess molybdate (Joerger and Bishop, 1988; Rodriguez-Quinones et al., 1993).

Mo release from MoSto and its utilization for *in vitro* for FeMo-co synthesis occurs at pH 7.5 in the presence of 1.23 mM ATP and an ATP regenerating enzyme in the reaction mixtures. It is known that MoSto catalyzed ATP-hydrolysis promotes formation of polyoxomolybdate clusters inside the MoSto cage while molybdate release from MoSto is favored at pH 7.5, but only after ATP is consumed (Poppe et al., 2018). Therefore, the buffer composition of the *in vitro* FeMo-co synthesis assay should preclude Mo release from MoSto. This discrepancy can be explained if FeMo-co biosynthesis and nitrogenase reconstitution alter the equilibrium of Mo binding/release by removing Mo from the available pool.

MoSto endows *A. vinelandii* with the ability to maintain high Mo-dependent diazotrophic growth rates under transient Mo limitation thus increasing strain competitiveness. It also confers certain degree of protection against W, a Mo antagonist that renders inactive molybdoenzymes. Normally W toxicity for nitrogen-fixing cells of *A. vinelandii* is evident when large excess of W over Mo (i.e., for W/Mo ratios > 150) is present in the culture medium (Keeler and Varner, 1957). This is not the case of the MoSto mutant, which exhibits high sensitivity to equimolar concentrations of M and W. Similar W sensitive phenotypes have been observed in mutants deficient in catechol siderophore production (Wichard et al., 2008). Both, Mo fluctuating conditions, including severe Mo limitation, and the presence of W at concentrations equal or higher than Mo, are environmentally relevant conditions. The average concentration of molybdate in terrestrial environments is 50 nM but its distribution is irregular (Hernandez et al., 2009). The advantage that MoSto might confer in the environment is however obscured under laboratory growth conditions in which large excess of molybdate is present in the medium.

Under Mo sufficient conditions more than 95% intracellular Mo is bound to MoSto. However, Mo-storage is not essential to achieve maximum nitrogenase activity as long as the growth medium contains excess molybdate (**Figure 2B**). This indicates that *A. vinelandii* ATP-dependent high affinity molybdate transport (Mouncey et al., 1995) is independent of the storage process and that molybdate uptake rates are enough to support maximum nitrogenase activity. Mo loading into MoSto is also an ATP-dependent process (Allen et al., 1999; Schemberg et al., 2008), which might impose an energy burden to the cell. This fact would explain why the mutant strain lacking MoSto is more competitive than the wild type under non-diazotrophic Mo-sufficient growth conditions. There are discrepancies in the literature as to whether or not MoSto expression is regulated by Mo. Pienkos reported constitutive MoSto expression (Pienkos and Brill, 1981) while Fenske found MoSto in cells grown at molybdate concentrations as low as 1 nM but not in Mo-free medium (Fenske et al., 2005). Our results are in line with constitutive expression since we were able to detect MoSto in cells grown in medium with Mo levels below an ICP-MS detection limit of 0.05 ppb. It is however possible that molybdate traces below our experimental detection limit are enough to induce MoSto expression.

We observed the co-existence of NifDK and VnfDGK polypeptides in cells grown under severe Mo-limiting or Mo-depleted conditions, although NifDK levels were much lower than those at standard Mo conditions (**Figure 5**). Transcripts of *nif* and *vnf* structural genes had been shown to co-exist at concentrations of Mo in the medium between 10 and 50 nM (Jacobson et al., 1986) but neither at 4 nM nor in Mo-depleted medium. It is likely that these discrepancies are due to the different sensitivity of Mo determination or product (either RNA or antigen) detection methods. Under Mo-deplete conditions the Δ*vnf* Δ*anf* mutants, lacking VnfDGK, appear to compensate with higher amounts of NifDK. It is know that the alternative nitrogenases can catalyze the reduction of acetylene by either two or four electrons to yield ethylene and ethane, respectively (Dilworth et al., 1988). Surprisingly, all strains exhibited activity with features typical of alternative nitrogenases under Mo-depleted conditions regardless of the presence of VnfDGK. Thus, simultaneous contributions from both systems cannot be ruled out. Hybrid Mo-nitrogenases carrying the cofactor of the V-nitrogenase (Moore et al., 1994) or even a biosynthetic precursor to FeMo-co (Soboh et al., 2010) have been generated *in vitro* and were shown to exhibit altered substrate specificities and product formation. Although in standard derepressing conditions the NafY protein seems to have a discriminating role in the insertion of Mo-nitrogenase active site metal cofactor (Rubio et al., 2004) the situation under extremely Mo-deficient conditions had not been tested.

In the absence of MoSto Vnf polypeptides are readily derepressed upon Mo step down, in contrast to the wild type that requires prolonged Mo starvation to initiate derepression (**Figure 5B**). Thus, the buffering effect of MoSto may also be important to maintain tight regulation of nitrogenase with different metal specificities.

CONCLUSION

Under transient Mo-limiting conditions MoSto mutants showed low Mo accumulation levels, lost the ability to repress expression of the V-dependent nitrogenase, exhibited high sensitivity to W inhibition, and were less competitive than wild type in diazotrophic growth. Importantly, the *in vitro* FeMo-co synthesis assay establishes the donation of Mo from MoSto to FeMo-co biosynthetic proteins via direct interaction. MoSto provides robust Mo-dependent nitrogen fixation under Mo-limiting conditions to its prokaryotic host. A corollary to these results is the need to incorporate the MoSto genes into the prokaryotic gene complement required to engineer nitrogen-fixing plants (Allen et al., 2017; Buren et al., 2017; Buren and Rubio, 2018).

MATERIALS AND METHODS

Generation of *A. vinelandii* Strains

Strains and plasmids used are listed in **Table 3**. *A. vinelandii* DJ (wild type) (Setubal et al., 2009), UW356 (Δ*nifA::spc*) (Poza-Carrion et al., 2014) and DJ33 (Δ*nifDK*) (Robinson et al., 1986) have been previously described. Strains UW394, UW466, and UW463 carrying in-frame deletions of the *mosAB*, *vnfDGK/anfDGK,* and *mosAB/vnfDGK/anfDGK* genes, respectively, were generated in this work. Deletions were incorporated into the *A. vinelandii* chromosome by transformation and gene replacement as described (Dos Santos, 2011).

Strain UW394 was generated by transforming *A. vinelandii* DJ with plasmid pRHB268 in which the *mosBA* genes had been replaced by an spectinomycin resistance cassette obtained from pHP45**Ω** (Prentki and Krisch, 1984). pRHB268 is a derivative of pRHB266, which contains the *mosBA* region amplified by PCR using oligonucleotides 5′-CGCTCGCCCAGCTCGGTCAGGCGCA-3′ and 5′-CAG AGACCTGCTCGCCAGCTGAAATCC-3′ and cloned into pGEM-T. pRHB266 was digested with *BspEI*/*Age*I restriction enzymes to eliminate the *mosBA* genes, followed by Klenow treatment and blunt end ligation for the insertion of the *Sma*I-digested spectinomycin resistance cassette.

In-frame deletions of alternative nitrogenases were generated by co-introducing plasmids pN2MN14 and pN2MN18 into *A. vinelandii* DJ and UW394 to generate strains UW466 and UW463, respectively. To generate pN2MN14, DNA regions flanking *anfDGK* were amplified by PCR using oligonucleotides 5′-GGTTTCTCGAGATGACTCGTAAAGTAGCCAT-3′ and 5′-GA TGGGATCCGACACATCTCCTTTAGAGTGA-3′ for the region upstream *anfD* and oligonucleotides 5′-ACCTGGATCCG GAAATGGACATCGAAGCCA-3′ and 5′-TACCTCTAGAT GAGGACCCATTCCTTGTTC-3′ for the region downstream *anfK*. PCR products were digested with *Xho*I/*BamH*I/*Xba*I and cloned into *Xho*I and *Xba*I sites of pBlueScript KS (+) in a quadruple ligation reaction together with *BamH*I-digested kanamycin resistance cassette obtained from plasmid pUC4K by amplifying a PCR product using oligonucleotides 5′-AATTGGATCCGGGAAAGCCACGTTGTGTCTC-3′ and 5′ -AATTGGATCCCTTTTGCTTTGCCACGGAACGG-3′. To generate pN2MN18, DNA regions flanking *vnfDGK* were amplified by PCR using oligonucleotides 5′-AGGC CTCGAGTGCATGACCGATGGGAC-3′ and 5′-CCATGGA TCCGATTGAAGTCTCCTCGGCTCT-3′ for the region upstream *vnfD* and oligonucleotides 5′-GTGGTGGATC CAGGTGCCGGAGCGGTTTCC′-3′ and 5′-GGGTTCTA GAAGTCCAGGCGGACATGGC-3′ for the region downstream *vnfK*. PCR products were digested with *Xho*I/*BamH*I/*Xba*I and cloned into *Xho*I and *Xba*I sites of pBluescript KS (+) in a quadruple ligation reaction together with *BamH*I-digested tetracycline resistance cassette obtained from plasmid pBBR1-MCS3 by amplifying a PCR product using oligonucleotides 5′-CCGGGATCCCTCATGTTTGACAGCTT ATCAT-3′ and 5′-CCGGGATCCGGAGTGGTGAATCCGTTA GC-3′ (Obranic et al., 2013).

Isolation of genomic DNA from *A. vinelandii* strains was performed by using DNAeasy^{TM} Tissue Kits (Qiagen). Generated *A. vinelandii* mutant strains were confirmed by PCR analysis and by immunoblot analysis with appropriate antibodies.

Escherichia coli DH5α was used for cloning procedures. Plasmid constructions, PCR DNA amplifications, and *E. coli* transformations were carried out by standard methods (Sambrook and Russell, 2001). Restriction analysis and DNA sequencing was used to confirm accuracy of all DNA constructs. To overexpress the *A. vinelandii mosBA* genes in *E. coli*, the *mosBA* genomic region of *A. vinelandii* was amplified by PCR using oligonucleotides 5′-GCGCGAATTCGCCAACTCGACAGCG-3′ and 5′-GCGC GCGGCCGCTCAGGCCGGACGCACA-3′, digested with *Eco*RI and *Not*I, and cloned into the *Eco*RI and *Not*I restriction sites of expression vector pET28a (+) to generate plasmid pN2MN72.

Bacterial Strains and Growth Conditions

Escherichia coli DH5α was cultivated in Luria–Bertani medium at 37°C with shaking (250 r.p.m.). Antibiotics were added at standard concentrations (Sambrook and Russell, 2001). For MoSto overexpression experiments, *E. coli* BL21(DE3) pLysS strain was transformed with plasmid pN2MN72 and cultivated in 4 L fermentors in Luria–Bertani (LB) medium supplemented with 0.3 mM ammonium ferric citrate, 0.3 mM cysteine and, when indicated, 1 mM Na_2MoO_4. Fermentor cultures started at a cell OD_{600} of 0.022 and proceeded for 18 h at 30°C with air sparging (2.5 l/min) and stirring (300 r.p.m.).

Azotobacter vinelandii strains were cultivated in Burk's modified medium (containing 28 mM ammonium acetate) or in Burk's modified N-free medium at 30°C (Strandberg and Wilson, 1968) with modifications of metal contents (Mo, Fe, V, and W), when indicated. Antibiotics were added at standard concentrations (Curatti et al., 2005). Regarding Mo, three types of culture medium were used here and are defined as Mo-limited, Mo-depleted and Mo-standard. Mo-limited medium was prepared without molybdate and contained chemical components of high purity. All glassware used was acid washed and rinsed with milliQ water (Chatterjee et al., 1994). Mo-limited medium contained 2.1–4.4 nM Mo as determined by ICP-MS. Depletion of Mo traces still remaining in Mo-limited medium was achieved by incubating Mo-starved *A. vinelandii* DJ cells in 4 L of Burk's modified N-free Mo-limited medium supplemented with 1 μM $NaVO_3$. After 1 h of incubation, 2 L were collected and cells removed by centrifugation followed by filtration of the supernatant. The remaining 2 L of culture were supplemented with 28 mM ammonium acetate, incubated for 1 additional hour, after which cells were removed by centrifugation followed by filtration of the supernatant. Polypropylene plastic was used to harvest Mo-depleted medium. Collected medium remained sterile for months on the shelf. Mo levels in Mo-depleted medium were below the detection limit of the ICP-MS. Mo-depleted medium was used for competitive index analysis and the analysis of Anf$^-$ Vnf$^-$ strains. Mo-standard medium contained 1 μM Na_2MoO_4 and was prepared by standard procedures.

For nitrogenase derepression experiments, inoculum cultures were previously grown in Mo-limited Burk's modified medium (Mo-starving conditions), in Mo-depleted Burk's modified medium (Mo-depleted conditions), or in Burk's modified medium (Standard conditions). Mo-starved inoculum cultures had been previously grown and transferred at least three times in Mo-limited Burk's modified medium. *A. vinelandii* cells were then collected by centrifugation, washed with N-free Mo-limited medium and resuspended in N-free medium supplemented with 1 μM $NaVO_3$ and lacking or containing Mo, as indicated in each experiment. Similar procedure using Mo-depleted medium was followed to obtain Mo-depleted inoculum cultures. Each derepression culture was inoculated at an optical density at 600 nm (OD_{600}) of 0.3 and further cultivated for at least 4 h (8 h for *anf vnf* mutants) at 30°C with shaking (200 r.p.m.). At different times during derepression, culture samples were collected and subjected to the following analyses: determination of *in vivo* acetylene reduction activity, determination of cellular-bound molybdenum, growth as estimated by OD_{600}, and detection of MoSto, NifDK, and VnfDGK proteins y immunoblot. Polypropylene filter tips were used for sample manipulation to prevent molybdenum traces.

For growth curves, *A. vinelandii* strains were cultured in NH_4^+-containing (nitrogenase repressing) solid Burk's modified medium under Mo-limited or Standard conditions for at least 3 days. When Mo-starved cells were required, *A. vinelandii* strains were inoculated into Mo-limited Burk's modified medium at least three times. Individual colonies were inoculated into liquid Burk's modified medium and cultures were grown overnight to an $OD_{600} \approx 2$. Inoculum cultures were then used to inoculate liquid N-free (nitrogenase derepressing) Burk's modified medium with different Mo, V, and W contents: 1 μM $NaVO_3$; 1 μM Na_2MoO_4 plus 1 μM $NaVO_3$; 1 μM $NaVO_3$ plus 1 μM Na_2WO_4; and 1 μM Na_2MoO_4 plus 1 μM $NaVO_3$ plus 1 μM Na_2WO_4. Addition of $NaVO_3$ permitted expression of V-nitrogenase under Mo-limited conditions. Non-diazotrophic growth conditions in Burk's modified medium were analyzed as controls. Three hundred μl cultures were incubated at 30°C in 96-well plates at intensive speed setting for 48 h in a Bioscreen C apparatus (Thermo Fisher).

Competitive Index Assay

Competitive index (CI) was defined as the mutant-to-wild-type ratio within the output sample, divided by the corresponding ratio in the inoculum (Macho et al., 2007). Precultures of wild type and UW394 were grown in Burk's modified medium to exponential phase, mixed to a final OD_{600} of 0.1, and used to inoculate the Burk's modified N-free medium as indicated in each experiment. Molybdenum and nitrogen regimes established in the precultures were maintained during co-growth in liquid medium. Twenty μl of serial dilutions of the mixed cultures were sampled at incubation times 0 and 22 h and plated onto solid Burk's modified N-free medium and solid Burk's modified N-free medium supplemented with spectinomycin (to inhibit growth of the wild type strain). Time 0 h determinations give input mutant to wild type ratios whereas time 22 h determinations give output CI values. Calculated CIs are the mean of three independent experiments with standard errors.

In vivo Nitrogenase Activity Assays

In vivo nitrogenase activity was determined by the acetylene reduction assay (Stewart et al., 1967) with ethylene and ethane formation being analyzed in a Shimadzu GC-2014 gas chromatograph. Five ml culture samples were transferred to 26 ml vials sealed with rubber stoppers. After injection of 1.5 ml acetylene to each vial, reactions proceeded for 30 min at 30°C with shaking. Reactions were then stopped by addition of 0.1 ml of 8 M NaOH. To detect ethylene, 50 μl samples of the gas phase of each reaction assay were injected in a PoraPak N 80-100 column. Gas chromatography temperature conditions were: 150°C at the injection port; 90°C at the column and N_2 carrier gas; and 150°C at the flame ionization detector (FID). To detect ethylene and ethane, 500 μl of the gas phase of each reaction assay were injected in a PoraPak N 50-80 column. Gas chromatography temperature conditions were: 180°C at the injection port; 60°C at the column and N_2 carrier gas; and 200°C at the FID.

Mo Determinations

Determination of Mo content in Mo-limited and Mo-depleted media was carried out by ICP-MS. Mo content of *A. vinelandii* cells was determined by Inductively Coupled Plasma Optical Emission Spectroscopy (ICP-OES) or by Inductively Coupled Plasma Mass Spectroscopy (ICP-MS). Cell culture samples (40 ml) were harvested by centrifugation at 5,000 r.p.m. for 5 min at 4°C, washed three times with Mo-limited or Mo-depleted medium, and collected under the same conditions. Pellets were dried at 100°C until ashes were formed and then resuspended in 5% nitric acid solution for ICP analysis. Culture samples were analyzed by ICP-OES at the ionomic service of the CEBAS-CSIC (Spain) or at ICP-MS at the Unit of Metal Analysis of the University of Barcelona Scientific and Technology Center (Spain) if Mo levels were too low to be detected by ICP-OES. Whole cell Mo contents are referred to as pmol Mo per cells contained in 1 ml of culture at an OD_{600} equal to 1 (2.2×10^8 cells).

Mo determinations in purified MoSto preparations were carried out by ICP-OES or ICP-MS. The colorimetric method of Cárdenas (Cárdenas and Mortenson, 1974) was used to follow Mo-containing fractions during purification of MoSto from *A. vinelandii* cells.

Protein Methods

Protein concentration was determined by the bicinchoninic acid method with BSA as the standard (Smith et al., 1985). Procedures for SDS-PAGE (Laemmli, 1970) and immunoblot analysis (Brandner et al., 1989) have been described. Protein samples for immunoblot analyses were prepared by mixing pelleted cells with 100 mM Tris-HCl at a final OD_{600} of 4, adding Laemmli buffer 4X supplemented with 0.1 M DTT, heating at 95°C for 3 min, and removing debris by centrifugation at 12000

r.p.m. for 2 min to obtain solubilized protein samples. Six μl samples were loaded per lane for NifDK and MosAB detection, 8 μl for VnfK detection and 15 μl for VnfG detection. After SDS-PAGE, proteins were transferred to nitrocellulose membranes and detected with specific antibodies against NifDK, MosAB, VnfK, or VnfG used at 1:2500 dilutions. MosAB polyclonal antibodies were produced in rabbit (CIB-CSIC). Secondary anti-rabbit Alkaline Phosphatase was used at 1:5000 dilution. NBT/BCIP (Nitroblue tetrazolium and 5-Bromo-4-chloro-3-indolyl phosphate) was used to develop immunodetection signal membranes. ImageJ software was used to quantify the protein levels in immunoblot membranes. The amount of MoSto protein in partially purified preparations from *A. vinelandii* cells was quantified against calibration curves generated with known amounts of pure MoSto obtained from recombinant *E. coli* cells.

Purification of MoSto From *A. vinelandii* and Recombinant *E. coli* Cells

Escherichia coli BL21(DE3) pLysS pN2MN72 cell-free extracts were prepared by mixing cells in binding buffer 50 mM Na_3PO_4 pH 7.2 buffer, 500 mM NaCl, 10 mM imidazole in a ratio 1:2 and passing twice through a French Press (1,500 psi) followed by ultracentrifugation at 24,000 r.p.m. for 30 min at 4°C. Cell free extract is loaded into HiTrap Ni^+ column (GE Healthcare) pre-equilibrated with binding buffer in a AKTA prime FPLC inside the glove box. The column was washed with binding buffer followed by two extra washes at 30 and 60 mM imidazole. Elution was carried out at 250 mM of imidazole. Eluted fractions containing purified MoSto were pooled, desalted and exchanged in 50 mM Na_3PO_4 pH 7.2 buffer, 500 mM NaCl, 10% glycerol. MoSto was stored in liquid nitrogen until used.

To purify MoSto from *A. vinelandii* cells, strain DJ was grown in 100-L fermentor with Burk's modified medium containing 10 μMNa_2MoO_4 and 12.8 mM urea at 30°C for 20 h maintaining 3% dissolved O_2. Cell-free extract preparations (French Press followed by cell debris removal by ultracentrifugation) and MoSto purification, including DEAE-Sephacel chromatography, ammonium sulfate fractionation, and Superdex-200 gel filtration were performed as described (Fenske et al., 2005). Fractions pooled and used for further chromatographic steps were selected according to their SDS-PAGE profiles and Mo determination results. MoSto was stored in liquid nitrogen until used.

In vitro FeMo-co Synthesis and Nitrogenase Activation Assays

In vitro FeMo-co synthesis assays were carried out as described (Curatti et al., 2007). Reactions were carried out in acid-treated 9-ml serum vials sealed with serum stoppers under argon/acetylene (93%/7%) atmosphere. When indicated, MoSto purified either from *E. coli* or from *A. vinelandii* was added to the *in vitro* FeMo-co synthesis reactions as sole source of Mo. Activity of reconstituted NifDK was analyzed by the acetylene reduction assay after addition of excess NifH as described (Curatti et al., 2007). Ethylene formation was measured in a Shimadzu GC-2014 gas chromatograph equipped with a PoraPak N 80-100 column. The specific activity of each protein is defined as nanomoles of ethylene formed per minute per mg of NifDK protein.

Protein–protein interaction requirement for Mo donation by MoSto was addressed by inserting a 3-kDa pore-size cut-off dialysis membrane between a MoSto solution on one side and the mixture of FeMo-co biosynthetic proteins and apo-NifDK on the other side. FeMo-co synthesis and nitrogenase activation reactions were carried out at 30°C. Samples to quantify reconstituted nitrogenase activity were taken at 2, 10, and 30 min and analyzed for acetylene reduction.

AUTHOR CONTRIBUTIONS

MN-R and JB carried out the experimental work. MN-R and LR performed experimental design, data analysis, and wrote the manuscript.

FUNDING

Funding for this research was provided by the Bill & Melinda Gates Foundation Grant OPP1143172 (to LR) and UPM grant RP160050022 (to LR). MN-R was supported by a contract of the Programa Operativo de Empleo Juvenil y la Iniciativa de Empleo Juvenil (YEI) with the participation of the Consejeriìa de Educacioìn, Juventud y Deporte de la Comunidad de Madrid and the European Social Fund.

ACKNOWLEDGMENTS

We thank Zinaida Perova for the construction of plasmid pRHB268.

REFERENCES

Allen, R. M., Roll, J. T., Rangaraj, P., Shah, V. K., Roberts, G. P., and Ludden, P. W. (1999). Incorporation of molybdenum into the iron-molybdenum cofactor of nitrogenase. *J. Biol. Chem.* 274, 15869–15874. doi: 10.1074/jbc.274.22.15869

Allen, R. S., Tilbrook, K., Warden, A. C., Campbell, P. C., Rolland, V., Singh, S. P., et al. (2017). Expression of 16 nitrogenase proteins within the plant mitochondrial matrix. *Front. Plant Sci.* 8:287. doi: 10.3389/fpls.2017.00287

Bishop, P. E., and Joerger, R. D. (1990). Genetics and molecular biology of alternative nitrogen fixation systems. *Annu. Rev. Plant Physiol. Plant Mol. Biol.* 41, 109–125. doi: 10.1146/annurev.pp.41.060190.000545

Boyd, E. S., and Peters, J. W. (2013). New insights into the evolutionary history of biological nitrogen fixation. *Front. Microbiol.* 4:201. doi: 10.3389/fmicb.2013.00201

Brandner, J. P., McEwan, A. G., Kaplan, S., and Donohue, T. J. (1989). Expression of the *Rhodobacter sphaeroides* cytochrome c2 structural gene. *J. Bacteriol.* 171, 360–368. doi: 10.1128/jb.171.1.360-368.1989

Buren, S., and Rubio, L. M. (2018). State of the art in eukaryotic nitrogenase engineering. *FEMS Microbiol. Lett.* 365:fnx274. doi: 10.1093/femsle/fnx274

Buren, S., Young, E. M., Sweeny, E. A., Lopez-Torrejon, G., Veldhuizen, M., Voigt, C. A., et al. (2017). Formation of nitrogenase NifDK tetramers in the mitochondria of *Saccharomyces cerevisiae*. *ACS Synth. Biol.* 6, 1043–1055. doi: 10.1021/acssynbio.6b00371

Cárdenas, J., and Mortenson, L. E. (1974). Determination of molybdenum and tungsten in biological materials. *Anal. Biochem.* 60, 372–381. doi: 10.1016/0003-2697(74)90244-9

Chatterjee, R., Allen, R. M., Shah, V. K., and Ludden, P. W. (1994). Nucleotide and divalent cation specificity of in vitro iron-molybdenum cofactor synthesis. *J. Bacteriol.* 176, 2747–2750. doi: 10.1128/jb.176.9.2747-2750.1994

Chatterjee, R., Ludden, P. W., and Shah, V. K. (1997). Characterization of VNFG, the delta subunit of the *vnf*-encoded apodinitrogenase from *Azotobacter vinelandii*. Implications for its role in the formation of functional dinitrogenase 2. *J. Biol. Chem.* 272, 3758–3765. doi: 10.1074/jbc.272.6.3758

Curatti, L., Brown, C. S., Ludden, P. W., and Rubio, L. M. (2005). Genes required for rapid expression of nitrogenase activity in *Azotobacter vinelandii*. *Proc. Natl. Acad. Sci. U.S.A.* 102, 6291–6296. doi: 10.1073/pnas.0501216102

Curatti, L., Hernandez, J. A., Igarashi, R. Y., Soboh, B., Zhao, D., and Rubio, L. M. (2007). In vitro synthesis of the iron-molybdenum cofactor of nitrogenase from iron, sulfur, molybdenum and homocitrate using purified proteins. *Proc. Natl. Acad. Sci. U.S.A.* 104, 17626–17631. doi: 10.1073/pnas.0703050104

Dilworth, M. J., Eady, R. R., and Eldridge, M. E. (1988). The vanadium nitrogenase of *Azotobacter chroococcum*: reduction of acetylene and ethylene to ethane. *Biochem. J.* 249, 745–751. doi: 10.1042/bj2490745

Dilworth, M. J., Eady, R. R., Robson, R. L., and Miller, R. W. (1987). Ethane formation from acetylene as a potential test for vanadium nitrogenase in vivo. *Nature* 327, 167–168. doi: 10.1038/327167a0

Dos Santos, P. C. (2011). Molecular biology and genetic engineering in nitrogen fixation. *Methods Mol. Biol.* 766, 81–92. doi: 10.1007/978-1-61779-194-9_6

Eady, R. R. (1996). Structure-function relationships of alternative nitrogenases. *Chem. Rev.* 96, 3013–3030. doi: 10.1021/cr950057h

Einsle, O., Tezcan, F. A., Andrade, S. L., Schmid, B., Yoshida, M., Howard, J. B., et al. (2002). Nitrogenase MoFe-protein at 1.16 A resolution: a central ligand in the FeMo-cofactor. *Science* 297, 1696–1700. doi: 10.1126/science.1073877

Fenske, D., Gnida, M., Schneider, K., Meyer-Klaucke, W., Schemberg, J., Henschel, V., et al. (2005). A new type of metalloprotein: the Mo storage protein from *Azotobacter vinelandii* contains a polynuclear molybdenum-oxide cluster. *Chembiochem* 6, 405–413. doi: 10.1002/cbic.200400263

George, S. J., Igarashi, R. Y., Piamonteze, C., Soboh, B., Cramer, S. P., and Rubio, L. M. (2007). Identification of a Mo-Fe-S cluster on NifEN by Mo K-edge extended X-ray absorption fine structure. *J. Am. Chem. Soc.* 129, 3060–3061. doi: 10.1021/ja0663428

Georgiadis, M. M., Komiya, H., Chakrabarti, P., Woo, D., Kornuc, J. J., and Rees, D. C. (1992). Crystallographic structure of the nitrogenase iron protein from *Azotobacter vinelandii*. *Science* 257, 1653–1659. doi: 10.1126/science.1529353

Hernandez, J. A., Curatti, L., Aznar, C. P., Perova, Z., Britt, R. D., and Rubio, L. M. (2008). Metal trafficking for nitrogen fixation: NifQ donates molybdenum to NifEN/NifH for the biosynthesis of the nitrogenase FeMo-cofactor. *Proc. Natl. Acad. Sci. U.S.A.* 105, 11679–11684. doi: 10.1073/pnas.0803576105

Hernandez, J. A., George, S. J., and Rubio, L. M. (2009). Molybdenum trafficking for nitrogen fixation. *Biochemistry* 48, 9711–9721. doi: 10.1021/bi901217p

Hille, R., Hall, J., and Basu, P. (2014). The mononuclear molybdenum enzymes. *Chem. Rev.* 114, 3963–4038. doi: 10.1021/cr400443z

Jacobitz, S., and Bishop, P. E. (1992). Regulation of nitrogenase-2 in *Azotobacter vinelandii* by ammonium, molybdenum, and vanadium. *J. Bacteriol.* 174, 3884–3888. doi: 10.1128/jb.174.12.3884-3888.1992

Jacobson, M. R., Premakumar, R., and Bishop, P. E. (1986). Transcriptional regulation of nitrogen fixation by molybdenum in *Azotobacter vinelandii*. *J. Bacteriol.* 167, 480–486. doi: 10.1128/jb.167.2.480-486.1986

Joerger, R. D., and Bishop, P. E. (1988). Nucleotide sequence and genetic analysis of the *nifB-nifQ* region from *Azotobacter vinelandii*. *J. Bacteriol.* 170, 1475–1487. doi: 10.1128/jb.170.4.1475-1487.1988

Joerger, R. D., Loveless, T. M., Pau, R. N., Mitchenall, L. A., Simon, B. H., and Bishop, P. E. (1990). Nucleotide sequences and mutational analysis of the structural genes for nitrogenase 2 of *Azotobacter vinelandii*. *J. Bacteriol.* 172, 3400–3408. doi: 10.1128/jb.172.6.3400-3408.1990

Keeler, R. F., and Varner, J. E. (1957). Tungstate as an antagonist of molybdate in *Azotobacter vinelandii*. *Arch. Biochem. Biophys.* 70, 585–590. doi: 10.1016/0003-9861(57)90146-7

Kim, J., and Rees, D. C. (1992). Crystallographic structure and functional implications of the nitrogenase molybdenum-iron protein from *Azotobacter vinelandii*. *Nature* 360, 553–560. doi: 10.1038/360553a0

Kowalewski, B., Poppe, J., Demmer, U., Warkentin, E., Dierks, T., Ermler, U., et al. (2012). Nature's polyoxometalate chemistry: X-ray structure of the Mo storage protein loaded with discrete polynuclear Mo-O clusters. *J. Am. Chem. Soc.* 134, 9768–9774. doi: 10.1021/ja303084n

Kraepiel, A. M., Bellenger, J. P., Wichard, T., and Morel, F. M. (2009). Multiple roles of siderophores in free-living nitrogen-fixing bacteria. *Biometals* 22, 573–581. doi: 10.1007/s10534-009-9222-7

Krahn, E., Weiss, R., Krockel, M., Groppe, J., Henkel, G., Cramer, P., et al. (2002). The Fe-only nitrogenase from *Rhodobacter capsulatus*: identification of the cofactor, an unusual, high-nuclearity iron-sulfur cluster, by Fe K-edge EXAFS and 57Fe Mossbauer spectroscopy. *J. Biol. Inorg. Chem.* 7, 37–45. doi: 10.1007/s007750100263

Laemmli, U. K. (1970). Cleavage of structural proteins during the assembly of the head of bacteriophage T4. *Nature* 227, 680–685. doi: 10.1038/227680a0

Luque, F., and Pau, R. N. (1991). Transcriptional regulation by metals of structural genes for *Azotobacter vinelandii* nitrogenases. *Mol. Gen. Genet.* 227, 481–487. doi: 10.1007/BF00273941

Macho, A. P., Zumaquero, A., Ortiz-Martin, I., and Beuzon, C. R. (2007). Competitive index in mixed infections: a sensitive and accurate assay for the genetic analysis of *Pseudomonas syringae*-plant interactions. *Mol. Plant Pathol.* 8, 437–450. doi: 10.1111/j.1364-3703.2007.00404.x

Moore, V. G., Tittsworth, R. C., and Hales, B. J. (1994). Construction and characterization of hybrid component 1 from V-nitrogenase containing FeMo cofactor. *J. Am. Chem. Soc.* 116, 12101–12102. doi: 10.1021/ja00105a080

Mouncey, N. J., Mitchenall, L. A., and Pau, R. N. (1995). Mutational analysis of genes of the *mod* locus involved in molybdenum transport, homeostasis, and processing in *Azotobacter vinelandii*. *J. Bacteriol.* 177, 5294–5302. doi: 10.1128/jb.177.18.5294-5302.1995

Obranic, S., Babic, F., and Maravic-Vlahovicek, G. (2013). Improvement of pBBR1MCS plasmids, a very useful series of broad-host-range cloning vectors. *Plasmid* 70, 263–267. doi: 10.1016/j.plasmid.2013.04.001

Pienkos, P. T., and Brill, W. J. (1981). Molybdenum accumulation and storage in *Klebsiella pneumoniae* and *Azotobacter vinelandii*. *J. Bacteriol.* 145, 743–751.

Pinske, C., Bonn, M., Kruger, S., Lindenstrauss, U., and Sawers, R. G. (2011). Metabolic deficiences revealed in the biotechnologically important model bacterium *Escherichia coli* BL21(DE3). *PLoS One* 6:e22830. doi: 10.1371/journal.pone.0022830

Poppe, J., Brunle, S., Hail, R., Wiesemann, K., Schneider, K., and Ermler, U. (2018). The molybdenum storage protein: a soluble ATP hydrolysis-dependent molybdate pump. *FEBS J.* 285, 4602–4616. doi: 10.1111/febs.14684

Poppe, J., Warkentin, E., Demmer, U., Kowalewski, B., Dierks, T., Schneider, K., et al. (2014). Structural diversity of polyoxomolybdate clusters along the three-fold axis of the molybdenum storage protein. *J. Inorg. Biochem.* 138, 122–128. doi: 10.1016/j.jinorgbio.2014.05.009

Poza-Carrion, C., Jimenez-Vicente, E., Navarro-Rodriguez, M., Echavarri-Erasun, C., and Rubio, L. M. (2014). Kinetics of *nif* gene expression in a nitrogen-fixing bacterium. *J. Bacteriol.* 196, 595–603. doi: 10.1128/jb.00942-13

Prentki, P., and Krisch, H. M. (1984). In vitro insertional mutagenesis with a selectable DNA fragment. *Gene* 29, 303–313. doi: 10.1016/0378-1119(84)90059-3

Ramon-Maiques, S., Marina, A., Gil-Ortiz, F., Fita, I., and Rubio, V. (2002). Structure of acetylglutamate kinase, a key enzyme for arginine biosynthesis and a prototype for the amino acid kinase enzyme family, during catalysis. *Structure* 10, 329–342. doi: 10.1016/S0969-2126(02)00721-9

Reddy, K. J., Munn, L. C., and Wang, L. (1997). "Chemistry and mineralogy of molybdenum in soils," in *Molybdenum in Agriculture*, ed. U. C. Gupta (Cambridge: Cambridge University Press).

Robinson, A. C., Burgess, B. K., and Dean, D. R. (1986). Activity, reconstitution, and accumulation of nitrogenase components in *Azotobacter vinelandii* mutant strains containing defined deletions within the nitrogenase structural

gene cluster. *J. Bacteriol.* 166, 180–186. doi: 10.1128/jb.166.1.180-186.1986

Rodriguez-Quinones, F., Bosch, R., and Imperial, J. (1993). Expression of the *nifBfdxNnifOQ* region of *Azotobacter vinelandii* and its role in nitrogenase activity. *J. Bacteriol.* 175, 2926–2935. doi: 10.1128/jb.175.10.2926-2935.1993

Rubio, L. M., and Ludden, P. W. (2008). Biosynthesis of the iron-molybdenum cofactor of nitrogenase. *Annu. Rev. Microbiol.* 62, 93–111. doi: 10.1146/annurev.micro.62.081307.162737

Rubio, L. M., Singer, S. W., and Ludden, P. W. (2004). Purification and characterization of NafY (apodinitrogenase gamma subunit) from *Azotobacter vinelandii*. *J. Biol. Chem.* 279, 19739–19746. doi: 10.1074/jbc.M400965200

Sambrook, J., and Russell, D. W. (2001). *Molecular Cloning. A Laboratory Manual*. Cold Spring Harbor, NY: Cold Spring Harbor Laboratory Press.

Schemberg, J., Schneider, K., Demmer, U., Warkentin, E., Muller, A., and Ermler, U. (2007). Towards biological supramolecular chemistry: a variety of pocket-templated, individual metal oxide cluster nucleations in the cavity of a Mo/W-storage protein. *Angew. Chem. Int. Ed. Engl.* 46, 2408–2413. doi: 10.1002/anie.200604858

Schemberg, J., Schneider, K., Fenske, D., and Muller, A. (2008). *Azotobacter vinelandii* metal storage protein: "classical" inorganic chemistry involved in Mo/W uptake and release processes. *Chembiochem* 9, 595–602. doi: 10.1002/cbic.200700446

Setubal, J. C., dos Santos, P., Goldman, B. S., Ertesvåg, H., Espin, G., Rubio, L. M., et al. (2009). Genome sequence of *Azotobacter vinelandii*, an obligate aerobe specialized to support diverse anaerobic metabolic processes. *J. Bacteriol.* 191, 4534–4545. doi: 10.1128/JB.00504-09

Shah, V. K., Ugalde, R. A., Imperial, J., and Brill, W. J. (1984). Molybdenum in nitrogenase. *Annu. Rev. Biochem.* 53, 231–257. doi: 10.1146/annurev.bi.53.070184.001311

Sippel, D., and Einsle, O. (2017). The structure of vanadium nitrogenase reveals an unusual bridging ligand. *Nat. Chem. Biol.* 13, 956–960. doi: 10.1038/nchembio.2428

Smith, P. K., Krohn, R. I., Hermanson, G. T., Mallia, A. K., Gartner, F. H., Provenzano, M. D., et al. (1985). Measurement of protein using bicinchoninic acid. *Anal. Biochem.* 150, 76–85. doi: 10.1016/0003-2697(85)90442-7

Soboh, B., Boyd, E. S., Zhao, D., Peters, J. W., and Rubio, L. M. (2010). Substrate specificity and evolutionary implications of a NifDK enzyme carrying NifB-co at its active site. *FEBS Lett.* 584, 1487–1492. doi: 10.1016/j.febslet.2010.02.064

Soboh, B., Igarashi, R. Y., Hernandez, J. A., and Rubio, L. M. (2006). Purification of a NifEN protein complex that contains bound molybdenum and a FeMo-Co precursor from *an Azotobacter vinelandii* DeltanifHDK strain. *J. Biol. Chem.* 281, 36701–36709. doi: 10.1074/jbc.M606820200

Spatzal, T., Aksoyoglu, M., Zhang, L., Andrade, S. L., Schleicher, E., Weber, S., et al. (2011). Evidence for interstitial carbon in nitrogenase FeMo cofactor. *Science* 334:940. doi: 10.1126/science.1214025

Stewart, W. P. D., Fitzgerald, G. P., and Burris, R. H. (1967). *In situ* studies on N2 fixation using the acetylene reduction technique. *Proc. Natl. Acad. Sci. U.S.A.* 58, 2071–2078. doi: 10.1073/pnas.58.5.2071

Strandberg, G. W., and Wilson, P. W. (1968). Formation of the nitrogen-fixing enzyme system in *Azotobacter vinelandii*. *Can. J. Microbiol.* 14, 25–31. doi: 10.1139/m68-005

Studier, F. W., and Moffatt, B. A. (1986). Use of bacteriophage T7 RNA polymerase to direct selective high-level expression of cloned genes. *J. Mol. Biol.* 189, 113–130. doi: 10.1016/0022-2836(86)90385-2

Wichard, T., Bellenger, J. P., Loison, A., and Kraepiel, A. M. (2008). Catechol siderophores control tungsten uptake and toxicity in the nitrogen-fixing bacterium *Azotobacter vinelandii*. *Environ. Sci. Technol.* 42, 2408–2413. doi: 10.1021/es702651f

Conflict of Interest Statement: The authors declare that the research was conducted in the absence of any commercial or financial relationships that could be construed as a potential conflict of interest.

frontiers in Microbiology

ORIGINAL RESEARCH
published: 24 April 2019
doi: 10.3389/fmicb.2019.00875

A Two-Step Strategy for the Rapid Enrichment of *Nitrosocosmicus*-Like Ammonia-Oxidizing Thaumarchaea

Liangting Liu, Surong Li, Jiamin Han, Weitie Lin and Jianfei Luo**

Guangdong Provincial Key Laboratory of Fermentation and Enzyme Engineering, School of Biology and Biological Engineering, South China University of Technology, Guangzhou, China

Ammonia-oxidizing archaea (AOA) are widely distributed on the earth and play a significant role in the global nitrogen cycle. Although dozens of AOA strains were obtained in the last 13 years, it is still necessary to obtain more AOA strains for the entire exploration of their ecology, physiology, and underlying biochemistry in different environments. In this study, we designed a two-step strategy for the rapid enrichment of *Nitrosocosmicus*–like AOA from soils. Firstly, combination of kanamycin and ampicillin was chosen as the selective stress for bacteria and quartz sands were used as the attachment of AOA cells during the first step cultivation; only after 40–75 days cultivation, AOA enrichments with abundance >20% were obtained. Secondly, combination of ciprofloxacin and azithromycin was chosen as the selective stress for the following cultivation; it is able to penetrate the biofilms and kill the bacterial cells inside the aggregate, contributing to the AOA enrichments reached high abundances (90%) only after one-time cultivation. Basing on this strategy, three AOA strains were obtained from agricultural soils only after 90–150 days cultivation. Phylogenetic analysis suggested these AOA belong to the soil group I.1b *Thaumarchaeota* and are closely related to the genus *Nitrosocosmicus*. In general, AOA enrichment or isolation is very difficult and time-consuming (an average of 2–3 years). Here, we provide a new strategy for the rapid enrichment of high abundance of *Nitrosocosmicus*-like AOA from soil, which gives a new solution to the AOA enrichment and cultivation in a short period.

Keywords: ammonia-oxidizing archaea, *Nitrosocosmicus*, biofilms, quartz sand, ciprofloxacin, azithromycin

OPEN ACCESS

Edited by:
Maria J. Delgado, Spanish National Research Council (CSIC), Spain

Reviewed by:
Lisa Y. Stein, University of Alberta, Canada
Zhe-Xue Quan, Fudan University, China
Hanna Koch, Radboud University Nijmegen, Netherlands

****Correspondence:***
Weitie Lin
lfwtlin@scut.edu.cn
Jianfei Luo
ljfjf2002@scut.edu.cn

Specialty section:
This article was submitted to Terrestrial Microbiology, a section of the journal Frontiers in Microbiology

Received: *26 September 2018*
Accepted: *04 April 2019*
Published: *24 April 2019*

Citation:
Liu L, Li S, Han J, Lin W and Luo J (2019) A Two-Step Strategy for the Rapid Enrichment of Nitrosocosmicus-Like Ammonia-Oxidizing Thaumarchaea. Front. Microbiol. 10:875. doi: 10.3389/fmicb.2019.00875

INTRODUCTION

Autotrophic aerobic ammonia oxidation is the primary step in oxidizing ammonia to nitrate and is therefore central to the global nitrogen cycle (Kowalchuk and Stephen, 2001). This biochemical reaction could be performed by ammonia-oxidizing bacteria (AOB), ammonia-oxidizing archaea (AOA), and comammox bacteria (Beeckman et al., 2018). However, for a long time, AOB were assumed to be the sole drivers of ammonia oxidation in the environment. It was not until 2005, when the first AOA strain, *Nitrosopumilus maritimus* SCM1, was successfully isolated, that the member of AOA was recognized as one of the contributors to ammonia oxidation (Könneke et al., 2005). From then on, detection, enrichment and cultivation of AOA belonging to the phylum Thaumarchaeota have been widely carried out (Francis et al., 2007; Lehtovirta-Morley, 2018). Autotrophic ammonia-oxidizing microorganisms all possess ammonia monooxygenase (AMO),

but the overall stoichiometry of it in AOA is indistinguishable from that of AOB and shows a higher affinity to ammonia (Martens-Habbena et al., 2009; Kits et al., 2017; Kuypers, 2017). AOA appear to be adapted to life under nutrient limitation (Horak et al., 2013; Shiozaki et al., 2016), which suggests that they have a significantly broader habitat range than the characterized AOB. They appear to be the dominant archaeal clade in soil (generally comprising 1–5% of all prokaryotes) (Ochsenreiter et al., 2003; Lehtovirta et al., 2009; Tago et al., 2015), the marine system (comprising 20–40% of all marine bacterioplankton) (Karner et al., 2001; Church et al., 2003), and geothermal habitats (Zhang et al., 2008; Dodsworth et al., 2011).

According to their performances on the ammonia oxidation in most natural systems, AOA have been believed to play a significant role in the global nitrogen cycle (Leininger et al., 2006; Pratscher et al., 2011; He et al., 2012). However, their roles have not been studied as extensively as AOB; it is still necessary to fully explore their ecology, physiology, and underlying biochemistry in environments (Stahl and de la Torre, 2012). Then, it is urgent to obtain more AOA isolates or enrichments. Up to now, 32 different AOA strains distributing in eight archaeal genera (*Nitrosopumilus, Nitrosocaldus*, *Nitrosopelagicus*, *Nitrososphaera*, *Nitrosotalea*, *Nitrosoarchaeum*, *Nitrosotenuis,* and *Nitrosocosmicus*) have been reported (**Supplementary Table S1**). Though dozens of AOA isolates and enrichments were obtained in the last 13 years, a time-saving strategy of AOA enrichment and isolation has rarely been reported in this field.

Due to the low maximum specific growth rate (0.011–0.033 h^{-1}) and inhibition by low concentrations of ammonia (2–100 mM) and nitrite (0.028–5.7 mM) (Lehtovirta-Morley et al., 2016), it usually takes a very long time to obtain AOA enrichment from natural samples. Although some organics (such as pyruvate, oxaloacetate, malate, etc.) were reported to be able to promote the growth of AOA (Tourna et al., 2011; Kim et al., 2016; Sauder et al., 2017), they were also consumed by the symbiotic heterotrophic bacteria in the enrichment cultures. More importantly, AOA members related to the *Nitrosocosmicus* clade can produce extracellular polymeric substances (EPS) to form cell aggregates or biofilms, which provides nutrition and protection for bacterial cells (Flemming et al., 2016; Jung et al., 2016; Kerou et al., 2016). Antibiotics (such as Streptomycin, Kanamycin, and Ampicillin) are often used as the selective stress for the AOA enrichment and purification (**Supplementary Table S1**). However, the application of antibiotics often stimulates the biofilm formation and the bacterial antibiotic resistance (Hoffman et al., 2005; Kaplan, 2011).

In this study, we designed a two-step strategy for the rapid enrichment of AOA from the environment (**Figure 1**). During the first step, soil samples were cultivated in the culture media containing no antibiotic; after the identification of nitrite in the culture, 10% of the initial enrichment was transferred into the subculture using kanamycin-Ampicillin as selective stress for the bacterial growth, and quartz sands as attachment for the AOA cells; in the following transfer, the quartz sands in each subculture were obtained and used as inoculums for the next subculture. During the second step, the quartz sands were collected when AOA abundance on the attachment reached 20% and were transferred into a new subculture using Ciprofloxacin-Azithromycin as selective stress; after 2 to 3 subcultures, high abundance of AOA enrichment could be obtained. Using this strategy, three AOA enrichments (abundance >90%) that closely related to the genus *Nitrosocosmicus* were obtained from agricultural soils, after only 90 to 150 days of cultivation.

MATERIALS AND METHODS

Characterization of Soil Sample

Soil samples were collected from paddy fields, garden and vegetable fields (**Supplementary Table S2**). The diversity of AOA distributed in these soils were studied using high-throughput sequencing archaeal 16S rRNA and *amoA* genes, which generated an average of 9,109 and 8,838 filtered reads, respectively (**Supplementary Table S3**). Bioinformatics analysis indicated that the AOA community in these soils mainly consisted of *Nitrosocosmicus*, *Nitrososphaera*, *Nitrosopumilus*, *Nitrosotenuis,* and *Nitrosotalea* (**Supplementary Figure S1**); the Shannon estimator from alpha diversity indices indicated that the SS (Suishi village) soil had the highest AOA diversity and abundance of AOA (**Supplementary Table S3**). Based on these results, the SS soil was used as an environmental sample for the AOA enrichment in this study.

Cultivation and Enrichment

Five grams of soil collected from the SS site were inoculated into 100 mL of the culture medium and initialized the AOA enrichment in accordance with the two-step strategy. Cultivation of ammonia oxidizer was carried out using an mineral salts medium containing NaCl (1 g L^{-1}), $MgCl_2{\cdot}6H_2O$ (0.4 g L^{-1}), $CaCl_2{\cdot}2H_2O$ (0.1 g L^{-1}), KH_2PO_4 (0.2 g L^{-1}), KCl (0.5 g L^{-1}), and filtration-sterilized solutions including 1 mL L^{-1} trace element solution (1.5 g L^{-1} $FeCl_2{\cdot}4H_2O$, 190 mg L^{-1} $CoCl_2{\cdot}6H_2O$, 100 mg L^{-1} $MnCl_2{\cdot}6H_2O$, 70 mg L^{-1} $ZnCl_2$, 62 mg L^{-1} HBO_3, 36 mg L^{-1} $Na_2MoO_4{\cdot}2H_2O$, 24 mg L^{-1} $NiCl_2{\cdot}6H_2O$, and 17 mg L^{-1} $CuCl_2{\cdot}2H_2O$), 1 mL L^{-1} Fe-EDTA solution (details are presented in the **Supplemental Materials**), 336 mg L^{-1} $NaHCO_3$, and 107 mg L^{-1} NH_4Cl; the pH value of medium was adjusted to 7.0. Each enrichment culture was incubated at 30°C in the dark without shaking and transferred into fresh media by the time the ammonium concentration was reduced to about 20% of the initial level. 50 mg L^{-1} of streptomycin, kanamycin, ampicillin, carbenicillin, and tetracycline in different combinations were supplied to the mineral salt medium. Based on the accumulation of nitrite, an effective antibiotic combination was chosen as the selective stress for subcultures. During the cultivation, the concentrations of nitrite and ammonium were determined by Griess-Ilosvay method and indophenol blue method, respectively (ISO/TS 14256–1:2003, 2003). In order to remove fungi contamination, 10 mg L^{-1} natamycin was added to the initial culture medium. During the

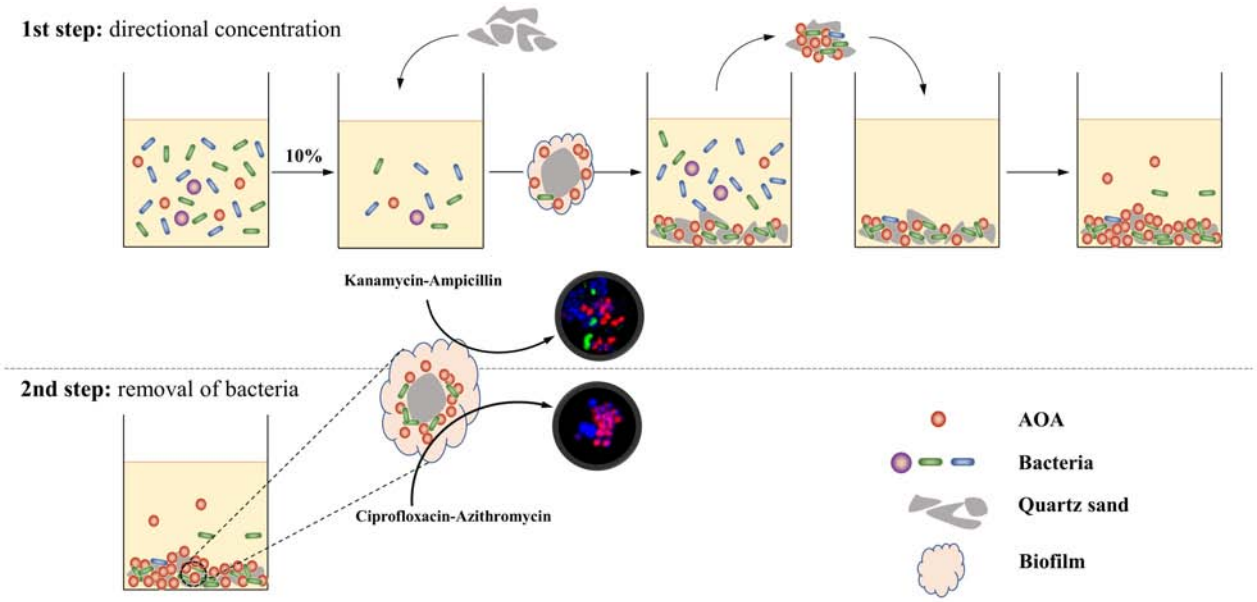

FIGURE 1 | Schematic process of a strategy for rapid enrichment of high abundance AOA. During the first step, the AOA cells were directly absorbed by quartz sands and concentrated on the surface of quartz sands; during the second step, the antibiotic combination ciprofloxacin-azithromycin penetrates biofilms and kills bacteria in the aggregate.

first transfer, the cultures were filtered through a 5 μm filter to remove soil debris and the bacterial cells embedded in the massive biofilms.

To assess the effect of quartz sands on the directional concentration of AOA, 10% (v/v) of enrichment cultures were transferred into the fresh liquid media containing 2, 5 or 10% (w/v) of quartz sands (∼ 1 mm diameter). After the ammonium was reduced to 20% of the initial level, the liquid cultures and quartz sands were collected and used for the AOA quantitative analysis, respectively. After the assessment, media containing 10% (w/v) of quartz sands were chosen for the following subcultures. During each transfer, all of the quartz sands in the culture were collected and transferred into fresh media for the next subculture. When the ammonia-oxidizing rate (nitrite-producing rate) and archaea abundance in subcultures reach a stable phase (the relative abundance of AOA in enrichment has no increase), antibiotics including kanamycin, ampicillin, tobramycin, ciprofloxacin, azithromycin, tetracycline, polymyxin, lincomycin, and spiramycin were used to evaluate the effect on the removal of bacterial cells in the biofilm that formed during the AOA enrichment.

Genomic DNA Extraction

To extract the total DNA in liquid culture, 20 mL enrichment culture was collected and filtered through a cellulose filter (0.22 μm, Thermo Fisher Scientific); the filter retaining with cells was collected and cut into pieces and placed in a 2 mL grinding tube containing 1 g quartz sand. To extract the total DNA from the quartz sand, 1 g quartz sand from the enrichment culture was collected and placed in a 2 mL grinding tube. 0.5 mL CTAB extraction buffer (10% CTAB, 0.7 M NaCl, 240 mM potassium phosphate buffer, pH 8.0) and 0.5 mL phenol-chloroform-isoamyl alcohol solution (25:24:1, pH 8.0) was added into the tube and mixed for 5 min using the Vortex Adapter (13000-V1-24, QIAGEN, Germany). After the pretreatment, genomic DNA was extracted according to a protocol that was previously reported by Griffiths (Griffiths et al., 2000). After the DNA extraction, 20 μg glycogen (Thermo Scientific, United States) was used as co-precipitant to deposit DNA from the DNA precipitated solution (30% polyethylene glycol 6000, 1.6 M NaCl). The DNA purity was determined using a UV spectrophotometer (NanoDrop 2000, Thermo Scientific, United States) and by agarose gel electrophoresis. The DNA samples were stored at −20°C for further PCR amplification.

Gene Clone, Identification and Phylogenetic Analysis

Nearly complete 16S rRNA gene and archaeal *amoA* gene of the AOA enrichments were PCR amplified using primer pairs A21f/1492r and CrenamoA23f/CrenamoA616r (**Supplementary Table S4**), respectively. PCR products were purified, ligated into pMD®19-T Vector (Takara, Dalian, China), and transformed into *Escherichia coli* DH5α. Recombinant clones were picked and sequenced with RV-M and M13-47 vector specific primers by IGE Biotechnology (Guangzhou, China).

Evolutionary histories of archaeal 16S rRNA gene nucleotide sequences and *amoA* gene translated protein sequences were inferred using the maximum likelihood method, based on the Tamura 3-parameter model. All alignments and

phylogenetic analyses were conducted by the software MEGA 7 (Kumar et al., 2016).

Quantitative PCR

Archaeal and bacterial 16S rRNA genes were PCR amplified using primer pairs SS16S-1F/SS16S-1R (a primer set specific for *Ca.* Nitrosocosmicus sp., designed with primer-blast tool in NCBI, according to the 16S rRNA gene sequences from genus *Nitrosocosmicus*) and 1369F/1492R (**Supplementary Table S4**), respectively. Agarose gel purified PCR products of archaeal or bacterial 16S rRNA genes were cloned using the TA-cloning kit (Takara, Dalian, China). Plasmids were extracted using the TIANpure Mini Plasmid Kit II (TIANGEN, Beijing, China) and digested using QuickCut^{TM} Hind III (Takara, Dalian, China). The linearized plasmid was used to construct the standard curves. Standard curves were prepared using six serial tenfold dilutions ranging from 10^2 to 10^7 gene copies/mL. The DNA was quantified by determining the copy number as well as the concentration and base pair composition of related genes. All quantitative PCR were performed in triplicate on an ABI 7500 Fast real-time PCR system (Applied Biosystems) using TransStart Tip Green qPCR SuperMix (Transgen, Beijing, China). The reaction condition was as follows: 2 min at 94°C; 40 cycles of 10 s at 94°C and 34 s at 60°C. The correlation coefficients (R^2) of the standard curves were 0.999. The amplification efficiencies (E) of archaeal and bacterial 16S rRNA gene were 85 to 93%.

Microscopy

To observe the biofilms formed on the surface of quartz sands, glass slides were used as the attachment and laid vertically in the enrichment cultures. After incubation, the slides were directly subjected to the Fluorescence *in situ* hybridization (FISH) analysis. FISH was performed by a modified method as previously described by Nielsen et al. (2009). In brief, samples were fixed with 50% ethanol (mixed with PBS) at 30°C for 48 h. After resuspending in PBS, samples were immobilized on Poly (L-lysine) slides and dehydrated by graded ethanol (50%, 80% and 98%, each gradient was treated for 3 min); cells were incubated with proteinase K (50 ug/mL) for 30 min at 37°C and washed three times using dH_2O. After permeabilized, cells were hybridized at 46°C for 3 h in hybridization buffer with 35% formamide using an Alexa Fluor 488 labeled probe Eub338 and an Alexa Fluor 546 labeled probe Arch915 (**Supplementary Table S4**). After hybridization, samples were covered with prewarmed washing buffer and incubated at 48 °C for 20 min, followed by covering with ProLong^{TM} Diamond Antifade Mountant with DAPI (Invitrogen, United States). Microscopic observation and documentation were accomplished using a scanning confocal microscope (LSM 710, Carl Zeiss, Germany) and the ZEN 2011 black software.

For scanning electron microscopy (SEM), the fixed cells were mounted on an aluminum stub and sputter-coated with platinum using a sputter coater EMS150T (EMS, United Kingdom), then imaged using a FEI Q25 scanning electron microscope (FEI, United States).

Nucleotide Sequence Accession Number

The nucleotide sequences accession number of the cultured AOA (16S rRNA and *amoA* gene sequence for phylogenetic analysis) and soil sample (amplicon raw data for community analysis) are summarized in **Supplementary Table S5**.

RESULTS

Cultivation and Enrichment of AOA

To find a suitable antibiotic for suppressing bacterial growth at the beginning of AOA enrichment, the nitrite that produced in ammonia oxidation was used as the evaluation index for antibiotic selection. As results show in **Supplementary Figure S2**, addition of kanamycin and ampicillin as the selective stress had 2.44 mg L^{-1} nitrite accumulation, which was higher than the other antibiotic combinations, indicating that they could be used for the AOA enrichment.

During the first subculture in the first step, the NH_4^+ consumption contributed to about 19.57 mg L^{-1} NO_2^--N production after 24 days cultivation (**Figure 2A**). The PCR detection performed using the bacterial *amoA* primers 1F/2R, suggested the absence of AOB in the first step enrichment. Since then, the period time of enrichment cultivation was shortened to 10 days in the third subculture, 8 days in the fifth subculture, and 6 days in the eighth subculture. From the eighth subculture, the ammonia-oxidizing rate and nitrite-producing rate always remained at stable levels, which indicated that the AOA enrichment cultivation reached a stable phase. This result was consistent with the result of a quantitative PCR analysis, that the archaea abundance in the cultures dynamically changed between 34 and 39% after the fourth subculture (**Figure 2B**). In fact, the archaea abundance had already reached 47% after the third subculture; however, the abundance no longer continuously increased after that time, while only archaeal and bacterial cells increased simultaneously at the same time (**Figure 2B**). This result suggests that the presences of some bacterial species in the enrichment culture obtained a tolerance or resistance to the activities of kanamycin and ampicillin and then survived under the antibiotic selective stress.

The resistance of bacteria to antibiotics might come from the protection by biofilms that formed by the AOA growing on the surface of quartz sands. Some AOA strains belonging to the *Nitrosocosmicus* clade have been reported to form aggregates and biofilms (Jung et al., 2016). Similarly, biofilms were also observed to form on the surface of quartz sands (**Supplementary Figures S3a,b**). Even though the biofilms were not as thick as the biofilms that were formed by many heterotrophic bacteria, they may still have the potential to decrease the activities of antibiotics. To inhibit the biofilm formation or suppress the bacterial growth in the biofilm, some new antibiotics were applied and assessed for their effects. As results shown in **Figure 3**, addition of tobramycin or polymyxin inhibited the ammonia oxidation of AOA enrichments, as well as the archaeal and bacterial growth in the enrichment cultures; the spiramycin not only inhibited the ammonia oxidation, but also resulted in a large increase of bacteria; tetracycline and lincomycin in some extent had no

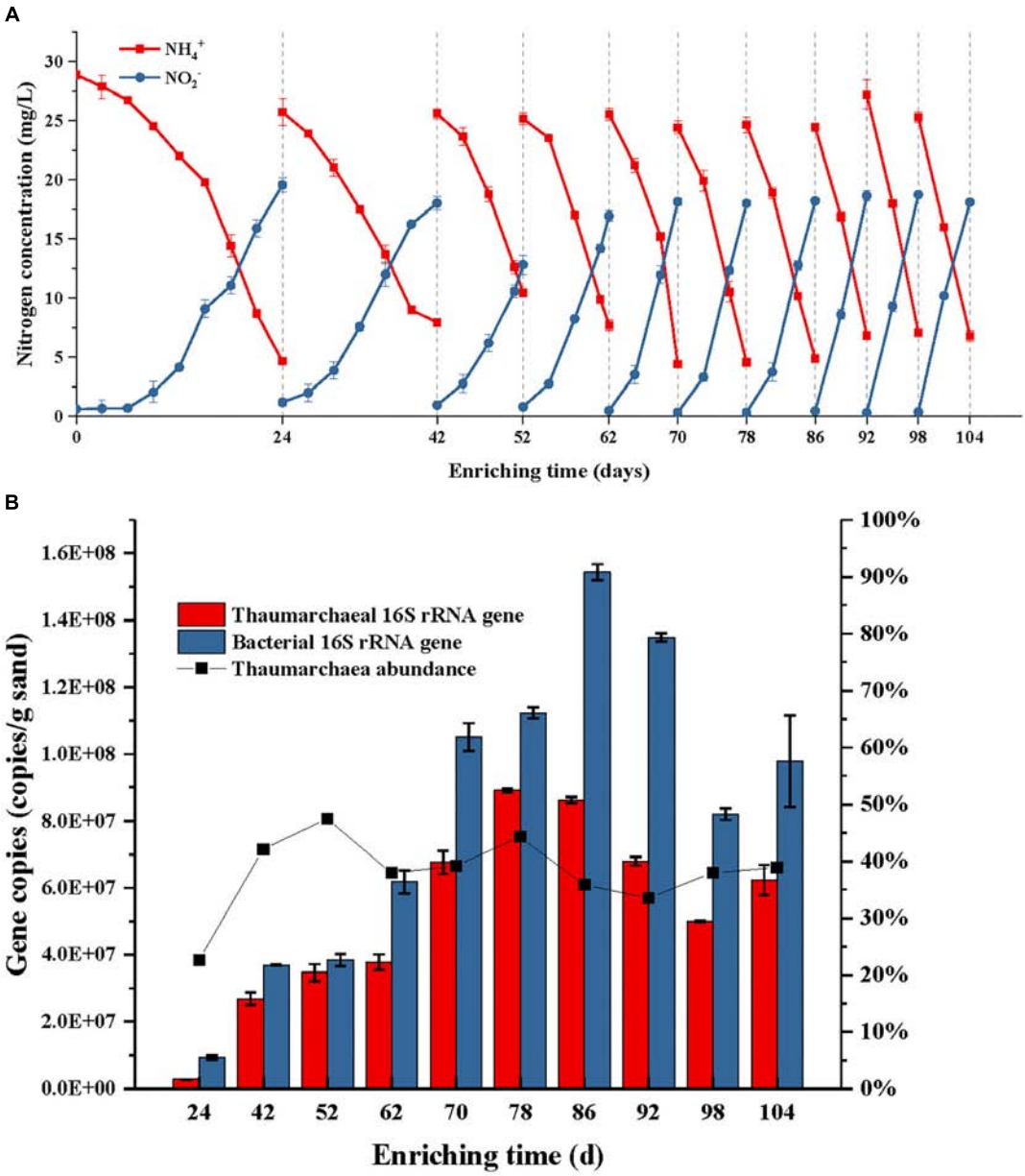

FIGURE 2 | Ammonia consumption and nitrite accumulation **(A)**, as well as thaumarchaeal and bacterial 16S rRNA gene copies **(B)** of the AOA enrichment during each subculture in use of kanamycin and ampicillin as selective stress; the ammonium with a concentration of 28 mg/L $NH4^+$-N was added into the initial culture medium and each subculture; when the concentration of $NH4^+$-N was reduced to about 20% of the initial level, the sands in the enrichment were obtained and transferred into a fresh medium for subculture. Error bars indicate the standard error of the mean for biological triplicates.

influence on the ammonia oxidation and showed positive effects on limiting the bacterial growth, which contributed to 61–72% of archaea abundance in the enrichment cultures. In comparison with other antibiotics, ciprofloxacin and azithromycin have no influence on the ammonia oxidation and contributed to the archaea abundances as high as 82% and 87%, respectively (**Figure 3B**). Moreover, the combination of ciprofloxacin and azithromycin resulted in 91% of the archaea abundance, which was about two times higher than that used in the combination of kanamycin and ampicillin. In the following, subcultures using ciprofloxacin-azithromycin, the archaea abundances remained steady at high levels ranging from 92 to 94% (**Figure 3C**).

During the AOA cultivation, the bacterial and archaeal cells would aggregate together and form biofilms in the absence of antibiotic (**Supplementary Figure S3c**). With the presence of kanamycin and ampicillin, thicker biofilms were formed, and more bacteria grew inside the biofilms (**Supplementary Figure S3d**). Differently, the combination of ciprofloxacin and azithromycin was able to limit the formation of thick biofilms (**Supplementary Figure S3e**). The comparison of FISH

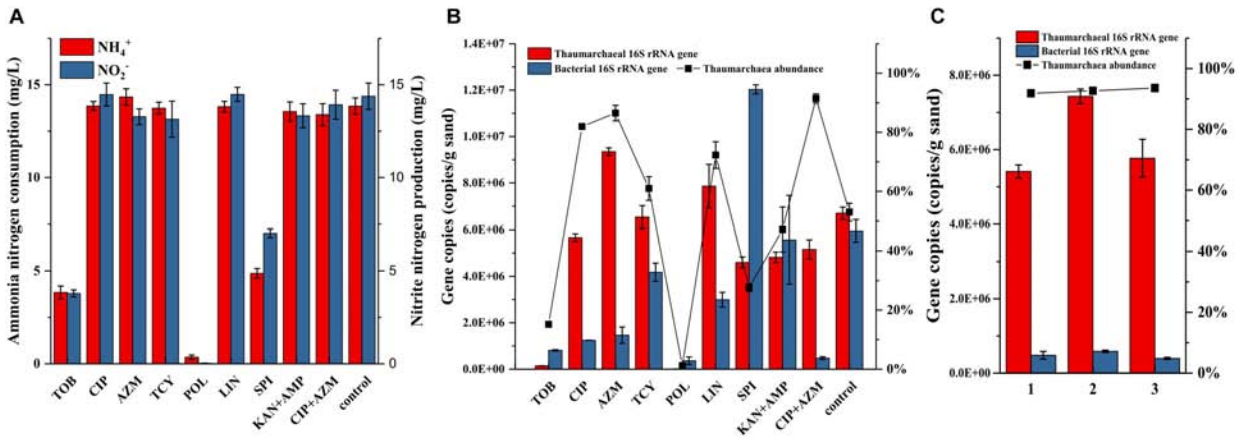

FIGURE 3 | Ammonia consumption and nitrite accumulation **(A)**, as well as thaumarchaeal and bacterial 16S rRNA gene copies **(B)** in the AOA enrichments using new antibiotics as selective stress; TOB: tobramycin, CIP: ciprofloxacin, AZM: azithromycin, TCY: tetracycline, POL: polymyxin, LIN: lincomycin, SPI: spiramycin, 50 mg/L of each antibiotic was added before inoculation. Thaumarchaeal and bacterial 16S rRNA gene copies, and archaea abundance in the AOA enrichments of three times repetition of the enrichment using ciprofloxacin and azithromycin as selective stress **(C)**. Error bars indicate the standard error of the mean for biological triplicates.

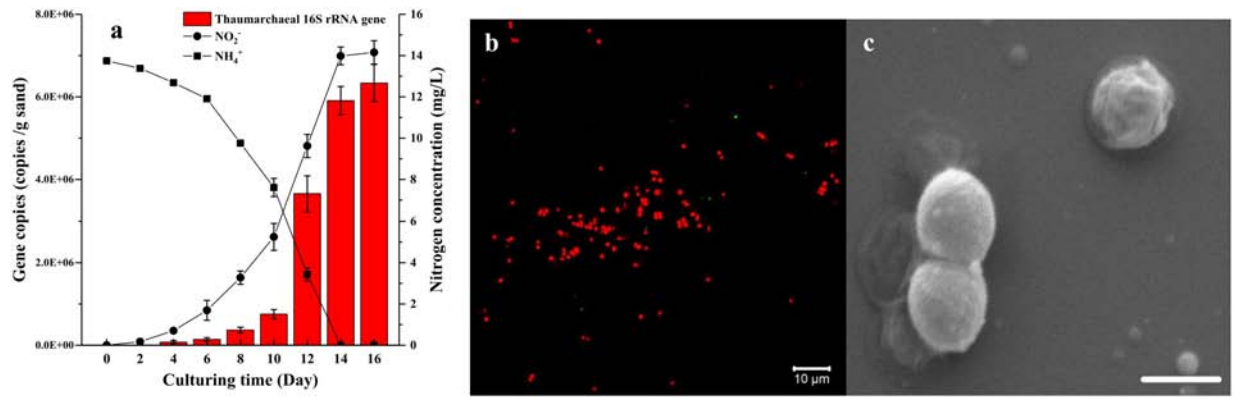

FIGURE 4 | Growth curve **(a)**, FISH profile **(b),** and SEM micrograph **(c)** of AOA enrichment culture (AOA abundance >95%) growing in the culture medium containing 14 mg/L $NH4^+$-N and using ciprofloxacin and azithromycin as selective stress. On the FISH profile, archaeal 16S rRNA was labeled with Alexa Fluor 546 Archaea-specific probe (Arc915, red) and bacterial 16S rRNA was labeled with Alexa Fluor 488 labeled Bacteria-specific probe (EUB338, green), objective: Plan-Apochromat 40×/1.3 Oil DIC M27; SEM condition was HV = 5.00 kV, mag = 40000×, scale bar = 1 μm. Error bars indicate the standard error of the mean for biological triplicates.

observation indicated that the combination was able to penetrate the biofilms and kill most of the bacterial cells (**Supplementary Figures S3c–e**). The stable high-abundance of AOA in the enrichment cultures indicated that the addition of ciprofloxacin combined with azithromycin as a selective stress is effective in the removal of bacteria in the aggregate, obtaining high abundance of AOA from the environment in a short-period.

Characterization of High Abundance AOA Enrichment

Based on the two-step strategy, one enrichment with high abundance of AOA was obtained after 150 days of cultivation. This AOA enrichment was able to consume 13.74 mg L^{-1} NH_4^+-N and reached a cell density of 6.34 × 10^6 cells g^{-1} sand in 14 days (**Figure 4a**). The FISH profile indicated that only a few bacterial cells was detected in the enrichment culture (**Figure 4b**), which is consistent with the result of quantitative PCR analysis. The SEM micrograph indicated that these archaeal cells are coccoid and 0.6–1.2 μm in diameter (**Figure 4c**). They often appeared in groups or aggregation, which may be covered in an extracellular matrix. On the basis of archaeal 16S rRNA and *amoA* gene sequences, the archaea strain in the enrichment culture belongs to the soil group I.1b *Thaumarchaeota*, specifically in the *Nitrosocosmicus* cluster, and is closely related to *Ca.* Nitrosocosmicus exaquare G61, showing 99.6% and 94.3% similarity, respectively. According to the phylogenetic analysis, the Thaumarchaea is named as *Ca.* Nitrosocosmicus sp. SS.

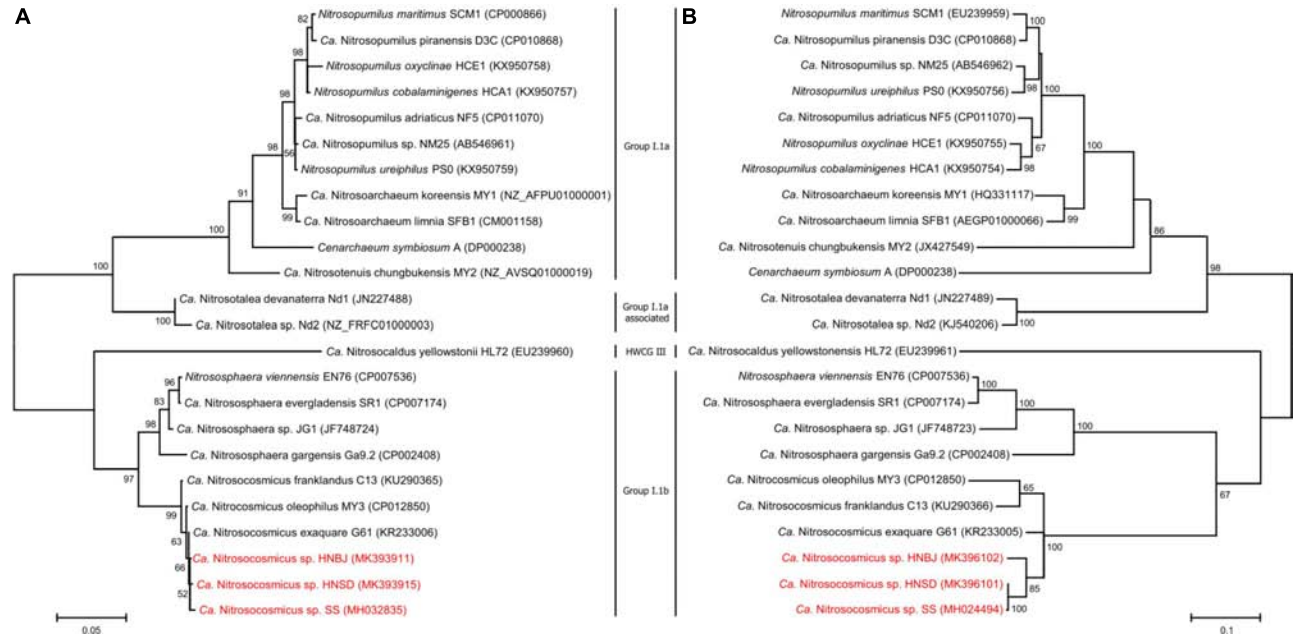

FIGURE 5 | Phylogenetic analyses of AOA 16S rRNA gene **(A)** and amoA gene **(B)** by using Maximum Likelihood method. Bootstrap values over 50% based on 1000 replicates are shown.

Application of the Two-Step Strategy to Other Soils

Soil samples that were collected from paddy fields (HN_SD) and banana fields (HN_BJ) were subjected to the AOA enrichment using the methods described above. The newly collected soils were checked for the presence of AOA species using PCR amplification of the *amoA* gene (**Supplementary Figure S4a**). During the first-step cultivation, the AOA abundance in the enrichments of HN_SD and HN_BJ soils reached 20% only after 75 days of cultivation (**Supplementary Figures S4b–d**), similar to the previous enrichment. During the second step, the AOA abundance in the enrichments of HN_SD and HN_BJ soils reached 91% and 89%, respectively, after only 12 days of cultivation (**Supplementary Figure S4d**). The FISH profiles also indicated that only a small number of bacterial cells were detected in the two enrichment cultures (**Supplementary Figures S4e,f**). Phylogenetic analysis, based on archaeal 16S rRNA and *amoA* gene sequences, suggested that the newly obtained archaea in the two enrichments are also affiliated with the genus *Nitrosocosmicus*, named *Ca.* Nitrosocosmicus sp. HNSD and *Ca.* Nitrosocosmicus sp. HNBJ, respectively (**Figure 5**).

DISCUSSION

In the last two decades, 32 AOA pure cultures and enrichments were obtained from different environments (**Supplementary Table S1**). However, the vast majority of AOA in natural ecosystems is uncultured and thus the ecology, physiology, and biochemistry of this vital N-cycling clade is still largely unknown, especially in soils. In this study, a two-step strategy was proposed and used for the rapid enrichment of AOA from soils. During the first step, the AOA cells were directly concentrated on the surface of quartz sands by the formation of biofilms. However, the bacterial cells were also embedded in the biofilms (**Supplementary Figure S3a**), which contributed to a low abundance of AOA in the enrichments. Then, in the second step, an antibiotic combination ciprofloxacin-azithromycin was applied to penetrate the biofilms and kill the bacterial cells inside the aggregate. Based on the strategy, high abundance AOA enrichments were obtained from agricultural soils after only 90 to 150 days of cultivation. This period is much shorter than other published AOA strains, like the hot spring groups *Ca.* Nitrosotenuis uzonensis N4 (7 years), *Ca.* Nitrososphaera gargensis (6 years) and *Ca.* Nitrosocaldus cavascurensis (4 years), the soil groups *Ca.* Nitrosotenuis chungbukensis MY2 (3 years), *Ca.* Nitrosotalea sp. Nd2 (3 years) and *Nitrososphaera viennensis* EN76 (2 years), and the manmade ecosystem groups *Ca.* Nitrosocosmicus exaquare G61 (3 years) and *Ca.* Nitrosotenuis cloacae SAT1 (1 year) (**Supplementary Table S1**).

In an oligotrophic environment, the CO_2 fixing activity of chemolithoautotrophic microorganisms often represents the primary organic source of complex microbial communities (Dattagupta et al., 2009; Denef et al., 2010). Similarly, during cultivation in inorganic media, AOA is the sole primary producers in the system and thus the sole source for organic carbon, which supports growth of heterotrophic bacteria and indirectly initiates the cells aggregate and biofilm formation on the surface of quartz sands. Notably, the member of the *Nitrosocosmicus* clade has usually been reported to form aggregates and biofilms by the secretion of EPS (Jung et al., 2016; Lehtovirta-Morley et al., 2016). It was reported that 77%

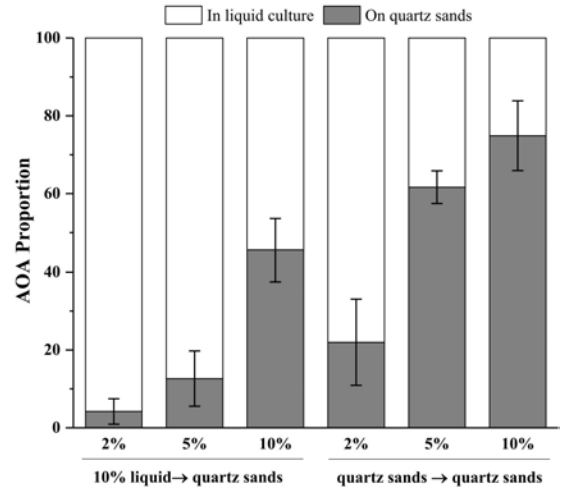

FIGURE 6 | Proportions of AOA in the liquid cultures and on the quartz sands. 10% liquid → quartz sands means 10% enrichment culture was transferred into the fresh media containing 2, 5, or 10% (w/v) quartz sands; quartz sands → quartz sands means all of the quartz sands in the enrichment cultures containing 2, 5, and 10% quartz sands were collected and transferred into the fresh media. Error bars indicate the standard error of the mean for biological triplicates.

and 73% of the cells of *Ca.* Nitrosocosmicus sp. MY3 were attached to hydrophobic bead and vermiculite, respectively; no significant attachment was observed for *Ca.* Nitrosotenuis chungbukensis (Jung et al., 2016). In addition, the genomic analysis indicated that members of Nitrososphaerales (such as *Nitrososphaera viennensis*) encode an extensive repertoire for biofilm formation including EPS production and cell surface modification (Kerou et al., 2016). Although the potential of biofilm formation has not been extensively studied in AOA, these results indicate that the presence of solid attachments (such as quartz sands) might benefit the rapid enrichment of AOA from environmental samples via the directional concentration of biofilms. As results show in **Figure 6**, the more quartz sands used the more the AOA attached on the quartz sands after 30 days of cultivation; with the addition of 10% (w/v) quartz sands, 46% of the AOA in enrichment culture attached on the surface of quartz sands when the culture inoculated with 10% of liquid seed, while 75% of the AOA attached on the quartz sands when the culture inoculated with quartz sands (attached with AOA cells). Moreover, the addition of kanamycin and ampicillin promoted the formation of biofilms, which might result in the concentration of AOA to the surface of quartz sands in a short time (**Figure 4b**).

During the enrichment cultivation, the AOA and bacterial cells formed a stable aggregate in biofilms, especially in the presence of antibiotics (**Supplementary Figures S3a,b,d**). Biofilm-induced antibiotic resistance has widely been reported in pathogenic bacteria (Hoffman et al., 2005); however, it is seldomly reported or discussed in AOA cultivation. Though it has become clear that archaeal biofilms are ubiquitous in a natural environment; we are still, however, far from comprehending the molecular mechanisms of interaction among the bacteria and the archaea in biofilm based antibiotic pressure (Orell et al., 2013). It is suggested that the presence of a bacterial partner in the biofilm stimulates AOA growth and enhances aggregate formation (Jung et al., 2016). The EPS synthesized by AOA could be used by heterotrophic bacteria as a substrate and embed the bacterial cells in the biofilm, which contributes to bacterial antibiotic resistance (Hallstoodley et al., 2004; Flemming et al., 2016). Moreover, the bacterial partners can reduce reactive oxygen stress of AOA by scavenging H_2O_2. This is beneficial for AOA, since they produce H_2O_2 during their growth, but many species lack a catalase for detoxification of the produced H_2O_2. Recently, it was shown that the absence of bacterial partners or H_2O_2 scavenging α-keto acids resulted in the inhibition of AOA growth (Kim et al., 2016). The H_2O_2 detoxification by bacterial partners harboring catalases is a key mechanism for supporting the AOA growth and would be a reason why it is difficult to remove the bacteria during the AOA enrichment. However, in this study, addition of different concentrations of pyruvate had no significant effect on improving the ammonia oxidation (**Supplementary Figure S5**). Catalase genes have been reported in the genomes of some soil AOA, such as *Nitrososphaera viennensis* EN76 (Stieglmeier et al., 2014), *Ca.* Nitrosocosmicus oleophilus MY3 (Jung et al., 2016) and *Ca.* Nitrosocosmicus exaquare (Sauder et al., 2017), the produced H_2O_2 could be scavenged by the catalases that produced by themselves, suggesting their growth independent of bacterial H_2O_2 scavengers. Overall, the detection of catalase genes in *Nitrosocosmicus* species and the unaffected ammonia oxidation with added pyruvate as H_2O_2 scavenger indicates that H_2O_2 detoxification might play only a minor role in the interaction of bacteria and *Nitrosocosmicus*-like AOA enrichments.

As discussed above, the interaction between AOA and bacterial partners in the enrichment culture allows them to better adapt to environmental stresses (such as antibiotic). To obtain highly enriched or even pure AOA cultures, this bacterial-archaeal interaction in the biofilm must be halted. In clinical therapy, some antibiotics (such as ciprofloxacin and azithromycin) have been proven to be available when killing pathogenic bacteria by destroying their biofilms (Saini et al., 2015). Azithromycin could slow biofilm formation down, penetrate the biofilms and reduce antibiotic resistance of bacterium as a quorum sensing inhibitor (Gillis and Iglewski, 2004 Persson et al., 2005; Yamamoto et al., 2015); Ciprofloxacin is a broad-spectrum fluoroquinolone antibiotic with good bactericidal activity and can prevent biofilm formation and reduce the preexisting biofilms (Reffuveille et al., 2014). Accordingly, we applied these antibiotics to the AOA enrichment. In comparison with the biofilms that formed in the cultures without addition of antibiotics and with addition of kanamycin and ampicillin, the biofilms in the culture with ciprofloxacin and azithromycin, appeared small and thin (**Supplementary Figures S3d,e**), which probably proves that the presence of these antibiotics can slow the formation of biofilms down. Higher hybridization rates of FISH also indicated that the presence of ciprofloxacin and azithromycin could increase the permeability of biofilms. Moreover, the dispersed cell that

grows without addition of quartz sand but with addition of antibiotics were applied to further explore the potential reason why the combination of ciprofloxacin and azithromycin has a positive effect on improving FISH hybridization. As results show in **Supplementary Figure S3**, the hybridization rate of *Ca*. Nitrosocosmicus sp. SS, that cultivated under ciprofloxacin and azithromycin (**Supplementary Figure S3f**), were higher than that under kanamycin and ampicillin (**Supplementary Figure S3g**). Ichimiya et al. (1996) had found that the azithromycin was able to inhibit the production of extracellular polysaccharides. It seemed that if fewer EPS coated on the cell surface, more fluorescent probes entered the cells. In summary, the addition of ciprofloxacin combined with azithromycin as selective stress in the cultivation effectively inhibited cell aggregation and biofilms formation, resulting in the removal of most cells and thus to high abundance of AOA in the cultures. Chen et al. (2017) have used ciprofloxacin and/or azithromycin in combination with streptomycin, kanamycin, ampicillin, and tetracycline to cultivate AOA enrichment. Unfortunately, the growth of AOA was significantly reduced or totally inhibited by using the antibiotic combinations. The presence of ciprofloxacin and azithromycin inhibit the cell aggregation and biofilm formation, which are believed to be essential for the AOA survival in the environment, suggesting that these antibiotics cannot be used in initial AOA enrichment. By contrast, in the second step of the AOA enrichment strategy in this study, biofilms with a relatively high abundance of AOA were formed after the first step of concentration by quartz sands; the addition of ciprofloxacin-azithromycin penetrated the biofilms and killed the bacterial cells inside the aggregate, but had no influence on the AOA growth.

It is tempting to speculate that biofilm-forming, terrestrial AOA species, such as members of genera *Nitrososphaera*, *Nitrosotenuis*, and *Nitrosotalea*, can also be enriched using this two-step enrichment strategy. Many AOA species had been detected in the soil samples; however, only the member of *Nitrosocosmicus* was obtained after the enrichment in this study. It is suggested that this member forms biofilms faster under antibiotic stress and attaches to quartz more easily or grows faster under ciprofloxacin and azithromycin.

CONCLUSION

In conclusion, the low specific growth rate, bacterial-archaeal interaction, and some other unknown features during the AOA enrichment leads to a lengthy of period time, before obtaining abundance of AOA from the environment. The two-step strategy discussed in this study, that addition of quartz sands to directly concentrate AOA cells and application of ciprofloxacin-azithromycin to effectively remove the bacterial cells inside biofilms, is an effective and timesaving method to obtain high abundance of *Nitrosocosmicus*–like AOA from the environment. To some extent, with appropriate adjustments, this strategy could be suitable for the enrichment of other AOA members in soils.

AUTHOR CONTRIBUTIONS

JL, LL, and WL conceived and designed the experiments. LL, JH, and SL performed the experiments and analyzed the data. LL, JL, and WL wrote the manuscript. All authors reviewed, edited, and approved the manuscript.

FUNDING

This work was supported by the National Natural Science Foundation of China (No. 41473072).

SUPPLEMENTARY MATERIAL

The Supplementary Material for this article can be found online at: https://www.frontiersin.org/articles/10.3389/fmicb.2019.00875/full#supplementary-material

REFERENCES

Beeckman, F., Motte, H., and Beeckman, T. (2018). Nitrification in agricultural soils : impact, actors and mitigation. *Curr. Opin. Biotechnol.* 50, 166–173. doi: 10.1016/j.copbio.2018.01.014

Chen, H., Yue, Y., Jin, W., Zhou, X., Wang, Q., Gao, S., et al. (2017). Enrichment and characteristics of ammonia-oxidizing archaea in wastewater treatment process. *Chem. Eng. J.* 323, 465–472. doi: 10.1016/j.cej.2017.04.130

Church, M. J., DeLong, E. F., Ducklow, H. W., Karner, M., Preston, C. M., and Karl, D. M. (2003). Abundance and distribution of planktonic archaea and bacteria in the waters west of the antarctic peninsula. *Limnol. Oceanogr.* 48, 1893–1902. doi: 10.4319/lo.2003.48.5.1893

Dattagupta, S., Schaperdoth, I., Montanari, A., Mariani, S., Kita, N. T., Valley, J. W., et al. (2009). A novel symbiosis between chemoautotrophic bacteria and a freshwater cave amphipod. *ISME J.* 3, 935–943. doi: 10.1038/ismej.2009.34

Denef, V. J., Mueller, R. S., and Banfield, J. F. (2010). AMD biofilms: using model communities to study microbial evolution and ecological complexity in nature. *ISME J.* 4, 599–610. doi: 10.1038/ismej.2009.158

Dodsworth, J. A., Hungate, B. A., and Hedlund, B. P. (2011). Ammonia oxidation, denitrification and dissimilatory nitrate reduction to ammonium in two US Great Basin hot springs with abundant ammonia-oxidizing archaea. *Environ. Microbiol.* 13, 2371–2386. doi: 10.1111/j.1462-2920.2011.02508.x

Flemming, H. C., Wingender, J., Szewzyk, U., Steinberg, P., Rice, S. A., and Kjelleberg, S. (2016). Biofilms: an emergent form of bacterial life. *Nat. Rev. Microbiol.* 14, 563–575. doi: 10.1038/nrmicro.2016.94

Francis, C. A., Beman, J. M., and Kuypers, M. M. (2007). New processes and players in the nitrogen cycle: the microbial ecology of anaerobic and archaeal ammonia oxidation. *ISME J.* 1, 19–27. doi: 10.1038/ismej.2007.8

Gillis, R. J., and Iglewski, B. H. (2004). Azithromycin Retards *Pseudomonas aeruginosa* Biofilm Formation. *J. Clin. Microbiol.* 42, 5842–5845. doi: 10.1128/jcm.42.12.5842-5845.2004

Griffiths, R. I., Whiteley, A. S., Anthony, G., Donnell, O., Bailey, M. J., and Donnell, A. G. O. (2000). Rapid method for coextraction of DNA and RNA from natural environments for analysis of ribosomal DNA- and rRNA-based microbial community composition. *Appl. Environ. Microbiol.* 66, 5488–5491. doi: 10.1128/aem.66.12.5488-5491.2000

Hallstoodley, L., Costerton, J. W., and Stoodley, P. (2004). Bacterial biofilms: from the natural environment to infectious diseases. *Nat. Rev. Microbiol.* 2, 95–108. doi: 10.1038/nrmicro821

He, J., Hu, H., and Zhang, L. (2012). Current insights into the autotrophic thaumarchaeal ammonia oxidation in acidic soils. *Soil Biol. Biochem.* 55, 146–154. doi: 10.1016/j.soilbio.2012.06.006

Hoffman, L. R., D'Argenio, D. A., MacCoss, M. A., Zhang, Z., Jones, R. A., and Miller, S. I. (2005). Aminoglycoside antibiotics induce bacterial biofilm formation. *Nature* 436, 1171–1175. doi: 10.1038/nature03912

Horak, R. E. A., Qin, W., Schauer, A. J., Armbrust, E. V., Ingalls, A. E., Moffett, J. W., et al. (2013). Ammonia oxidation kinetics and temperature sensitivity of a natural marine community dominated by Archaea. *ISME J.* 7, 2023–2033. doi: 10.1038/ismej.2013.75

Ichimiya, T., Takeoka, K., Hiramatsu, K., Hirai, K., Yamasaki, T., and Nasu, M. (1996). The Influence of Azithromycin on the Biofilm Formation of *Pseudomonas aeruginosa* in vitro. *Chemotherapy* 42, 186–191. doi: 10.1159/000239440

ISO/TS 14256–1:2003 (2003). *Soil Quality-Determination of Nitrate, Nitrite and Ammonium in Field Moist Soils by Extraction with Potassium Chloride Solution*. Geneva: International Organisation for Standardisation.

Jung, M. Y., Kim, J. G., Damsté, J. S. S., Rijpstra, W. I. C., Madsen, E. L., Kim, S. J., et al. (2016). A hydrophobic ammonia-oxidizing archaeon of the *Nitrosocosmicus* clade isolated from coal tar-contaminated sediment. *Environ. Microbiol. Rep.* 8, 983–992. doi: 10.1111/1758-2229.12477

Kaplan, J. B. (2011). Antibiotic-induced biofilm formation. *Int. J. Artif. Organ.* 34, 737–751. doi: 10.5301/ijao.5000027

Karner, M., DeLong, E. F., and Karl, D. M. (2001). Archaeal dominance in the mesopelagic zone of the Pacific Ocean. *Nature* 409, 507–510. doi: 10.1038/35054051

Kerou, M., Offre, P., Valledor, L., Abby, S. S., Melcher, M., Nagler, M., et al. (2016). Proteomics and comparative genomics of Nitrososphaera viennensis reveal the core genome and adaptations of archaeal ammonia oxidizers. *Proc. Natl. Acad. Sci. U.S.A.* 113, 7937–7946.

Kim, J. G., Park, S. J., Damsté, J. S. S., Schouten, S., Rijpstra, W. I. C., Jung, M. Y., et al. (2016). Hydrogen peroxide detoxification is a key mechanism for growth of ammonia-oxidizing archaea. *Proc. Natl. Acad. Sci. U.S.A.* 113, 7888–7893. doi: 10.1073/pnas.1605501113

Kits, K. D., Sedlacek, C. J., Lebedeva, E. V., Han, P., Bulaev, A., Pjevac, P., et al. (2017). Kinetic analysis of a complete nitrifier reveals an oligotrophic lifestyle. *Nature* 549, 269–272. doi: 10.1038/nature23679

Könneke, M., Bernhard, A. E., de la Torre, J., Walker, C. B., Waterbury, J. B., and Stahl, D. A. (2005). Isolation of an autotrophic ammonia oxidizing marine archaeon. *Nature* 437, 543–546. doi: 10.1038/nature03911

Kowalchuk, G. A., and Stephen, J. R. (2001). Ammonia-oxidizing bacteria: a model for molecular microbial ecology. *Annu. Rev. Microbiol.* 55, 485–529. doi: 10.1146/annurev.micro.55.1.485

Kumar, S., Stecher, G., and Tamura, K. (2016). MEGA7: molecular evolutionary genetics analysis version 7. 0 for bigger datasets. *Mol. Biol. Evol.* 33, 1–11. doi: 10.1093/molbev/msw054

Kuypers, M. M. M. (2017). Microbiology: a fight for scraps of ammonia. *Nature* 549, 162–163. doi: 10.1038/549162a

Lehtovirta, L. E., Prosser, J. I., and Nicol, G. W. (2009). Soil pH regulates the abundance and diversity of Group 1.1c *Crenarchaeota*. *FEMS Microbiol. Ecol.* 70, 367–376. doi: 10.1111/j.1574-6941.2009.00748.x

Lehtovirta-Morley, L. E. (2018). Ammonia oxidation: ecology, physiology, biochemistry and why they must all come together. *FEMS Microbiol. Lett.* 365:fny058. doi: 10.1093/femsle/fny058

Lehtovirta-Morley, L. E., Ross, J., Hink, L., Weber, E. B., Gubry-Rangin, C., Thion, C., et al. (2016). Isolation of "Candidatus Nitrosocosmicus franklandus", a novel ureolytic soil archaeal ammonia oxidiser with tolerance to high ammonia concentration. *FEMS Microbiol. Ecol.* 92, 1–10. doi: 10.1093/femsec/fiw057

Leininger, S., Urich, T., Schloter, M., Schwark, L., Qi, J., Nicol, G. W., et al. (2006). Archaea predominate among ammonia-oxidizing prokaryotes in soils. *Nature* 442, 806–809. doi: 10.1038/nature04983

Martens-Habbena, W., Berube, P. M., Urakawa, H., José, R., and Stahl, D. A. (2009). Ammonia oxidation kinetics determine niche separation of nitrifying Archaea and Bacteria. *Nature* 461, 976–979. doi: 10.1038/nature08465

Nielsen, P. H., Daims, H., Lemmer, H., Arslan-Alaton, I., and Olmez-Hanci, T. (2009). *FISH Handbook for Biological Wastewater Treatment*. London: IWA Publishing.

Ochsenreiter, T., Selezi, D., Quaiser, A., Bonchosmolovskaya, L., and Schleper, C. (2003). Diversity and abundance of Crenarchaeota in terrestrial habitats studied by 16S RNA surveys and real time PCR. *Environ. Microbiol.* 5, 787–797. doi: 10.1046/j.1462-2920.2003.00476.x

Orell, A., Fröls, S., and Albers, S. V. (2013). Archaeal biofilms: the great unexplored. *Annu. Rev. Microbiol.* 67, 337–354. doi: 10.1146/annurev-micro-092412-155616

Persson, T., Givskov, M., and Nielsen, J. (2005). Quorum sensing inhibition: targeting chemical communication in gramnegative bacteria. *Curr. Med. Chem.* 12, 3103–3115. doi: 10.2174/092986705774933425

Pratscher, J., Dumont, M. G., and Conrad, R. (2011). Ammonia oxidation coupled to CO2 fixation by archaea and bacteria in an agricultural soil. *Proc. Natl. Acad. Sci. U.S.A.* 108, 4170–4175. doi: 10.1073/pnas.1010981108

Reffuveille, F., de la Fuente-Núþnez, C., Mansour, S., and Hancock, R. E. W. (2014). A broad-spectrum antibiofilm peptide enhances antibiotic action against bacterial biofilms. *Antimicrob. Agents Chemother.* 58, 5363–5371. doi: 10.1128/AAC.03163-14

Saini, H., Chhibber, S., and Harjai, K. (2015). Azithromycin and ciprofloxacin: a possible synergistic combination against *Pseudomonas aeruginosa* biofilm-associated urinary tract infections. *Int. J. Antimicrob. Agents* 45, 359–367. doi: 10.1016/j.ijantimicag.2014.11.008

Sauder, L. A., Albertsen, M., Engel, K., Schwarz, J., Nielsen, P. H., Wagner, M., et al. (2017). Cultivation and characterization of *Candidatus* Nitrosocosmicus exaquare, an ammonia-oxidizing archaeon from a municipal wastewater treatment system. *ISME J.* 11, 1142–1157. doi: 10.1038/ismej.2016.192

Shiozaki, T., Ijichi, M., Isobe, K., Hashihama, F., Nakamura, K., Ehama, M., et al. (2016). Nitrification and its influence on biogeochemical cycles from the equatorial Pacific to the Arctic Ocean. *ISME J.* 10, 2184–2197. doi: 10.1038/ismej.2016.18

Stahl, D. A., and de la Torre, J. R. (2012). Physiology and diversity of ammonia-oxidizing archaea. *Annu. Rev. Microbiol.* 66, 83–101. doi: 10.1146/annurev-micro-092611-150128

Stieglmeier, M., Klingl, A., Alves, R. J. E., Rittmann, S. K. M. R., Melcher, M., Leisch, N., et al. (2014). *Nitrososphaera viennensis* gen. nov., sp. nov., an aerobic and mesophilic, ammonia-oxidizing archaeon from soil and a member of the archaeal phylum Thaumarchaeota. *Int. J. Syst. Evol. Microbiol.* 64, 2738–2752. doi: 10.1099/ijs.0.063172-0

Tago, K., Okubo, T., Shimomura, Y., Kikuchi, Y., Hori, T., Nagayama, A., et al. (2015). Environmental factors shaping the community structure of ammonia-oxidizing bacteria and archaea in sugarcane field soil. *Microbes Environ.* 30, 21–28. doi: 10.1264/jsme2.ME14137

Tourna, M., Stieglmeier, M., Spang, A., Konneke, M., Schintlmeister, A., Urich, T., et al. (2011). *Nitrososphaera viennensis*, an ammonia oxidizing archaeon from soil. *Proc. Natl. Acad. Sci. U.S.A.* 108, 8420–8425. doi: 10.1073/pnas.1013488108

Yamamoto, R., Noiri, Y., Yamaguchi, M., Asahi, Y., Maezono, H., Ebisu, S., et al. (2015). Inhibition of polysaccharide synthesis by the sinR orthologue PGN_0088 is indirectly associated with the penetration of *Porphyromonas gingivalis* biofilms by macrolide antibiotics. *Microbiology* 161, 422–429. doi: 10.1099/mic.0.000013

Zhang, C. L., Ye, Q., Huang, Z., Li, W., Chen, J., Song, Z., et al. (2008). Global occurrence of archaeal amoA genes in terrestrial hot springs. *Appl. Environ. Microbiol.* 74, 6417–6426. doi: 10.1128/AEM.00843-08

Conflict of Interest Statement: The authors declare that the research was conducted in the absence of any commercial or financial relationships that could be construed as a potential conflict of interest.

frontiers in Microbiology

ORIGINAL RESEARCH
published: 07 May 2019
doi: 10.3389/fmicb.2019.00980

Rhizobium etli Produces Nitrous Oxide by Coupling the Assimilatory and Denitrification Pathways

*Alba Hidalgo-García[1], María J. Torres[1], Ana Salas[1], Eulogio J. Bedmar[1], Lourdes Girard[2] and María J. Delgado[1]**

[1] Estación Experimental del Zaidín, Consejo Superior de Investigaciones Científicas, Granada, Spain, [2] Centro de Ciencias Genómicas, Universidad Nacional Autónoma de México, Cuernavaca, Mexico

More than two-thirds of the powerful greenhouse gas nitrous oxide (N_2O) emissions from soils can be attributed to microbial denitrification and nitrification processes. Bacterial denitrification reactions are catalyzed by the periplasmic (Nap) or membrane-bound (Nar) nitrate reductases, nitrite reductases (NirK/cd_1Nir), nitric oxide reductases (cNor, qNor/ Cu_ANor), and nitrous oxide reductase (Nos) encoded by *nap*/*nar*, *nir*, *nor* and *nos* genes, respectively. *Rhizobium etli* CFN42, the microsymbiont of common bean, is unable to respire nitrate under anoxic conditions and to perform a complete denitrification pathway. This bacterium lacks the *nap*, *nar* and *nos* genes but contains genes encoding NirK and cNor. In this work, we demonstrated that *R. etli* is able to grow with nitrate as the sole nitrogen source under aerobic and microoxic conditions. Genetic and functional characterization of a gene located in the *R. etli* chromosome and annotated as *narB* demonstrated that growth under aerobic or microoxic conditions with nitrate as nitrogen source as well as nitrate reductase activity requires NarB. In addition to be involved in nitrate assimilation, NarB is also required for NO and N_2O production by NirK and cNor, respectively, in cells grown microoxically with nitrate as the only N source. Furthermore, β-glucuronidase activity from *nirK::uidA* and *norC::uidA* fusions, as well as NorC expression and Nir and Nor activities revealed that expression of *nor* genes under microoxic conditions also depends on nitrate reduction by NarB. Our results suggest that nitrite produced by NarB from assimilatory nitrate reduction is detoxified by NirK and cNor denitrifying enzymes that convert nitrite into NO which in turn is reduced to N_2O, respectively.

Keywords: assimilatory nitrate reductase, denitrification, gene expression, soil bacteria, nitrous oxide

OPEN ACCESS

Edited by:
Marcus A. Horn,
Leibniz University Hannover, Germany

Reviewed by:
Stephen Spiro,
The University of Texas at Dallas, United States
Katharina Kujala,
University of Oulu, Finland

****Correspondence:***
Maria J. Delgado
mdelgado@eez.csic.es

Specialty section:
This article was submitted to Terrestrial Microbiology, a section of the journal Frontiers in Microbiology

Received: *30 November 2018*
Accepted: *18 April 2019*
Published: *07 May 2019*

Citation:
Hidalgo-García A, Torres MJ, Salas A, Bedmar EJ, Girard L and Delgado MJ (2019) Rhizobium etli Produces Nitrous Oxide by Coupling the Assimilatory and Denitrification Pathways. Front. Microbiol. 10:980. doi: 10.3389/fmicb.2019.00980

INTRODUCTION

Nitrous oxide (N_2O) is a powerful greenhouse gas (GHG) and a major cause of ozone layer depletion (Ravishankara et al., 2009) with an atmospheric lifetime of 114 years and an estimated 300-fold greater potential for global warming compared with that of carbon dioxide (CO_2), based on its radiative capacity (Intergovernmental Panel on Climate Change [IPCC], 2014). Human activities such as agriculture, fossil fuel combustion, wastewater management and industrial processes have provoked escalating emissions of N_2O which contribute to climate change.

More than 60% of N_2O emissions globally are emitted from agricultural soils (Smith et al., 2012). This contribution has been amplified through the so-called "green revolution," which has increased the presence of nitrogen (N) in soil through the application of synthetic nitrogen-based fertilizers mainly fabricated through the Haber-Bosch process. Many processes and microorganisms are sources of N_2O, being nitrifiers and denitrifiers the two most important groups of soil microorganisms involved (Pilegaard, 2013; Butterbach-Bahl et al., 2014). Denitrification consists in the respiratory reduction of the nitrate present in many terrestrial and aquatic ecosystems. This process is initiated by a periplasmic (Nap) or membrane-bound (Nar) nitrate reductase depending on the species. The nitrite produced from dissimilatory nitrate reduction is then transformed into nitric oxide (NO), a potent cytotoxic free radical and ozone-depleting gas, through the action of the respiratory Cu-containing (NirK) or the cd_1-type nitrite reductase (NirS). Then, NO is reduced to N_2O by cytochrome *cb*-type (cNor/Cu_ANor) or quinol-dependent (qNor) nitric oxide reductases. Finally, a nitrous oxide reductase (Nos) catalyzes the last step of denitrification by producing N_2 from N_2O (for recent reviews see de Vries et al., 2007; Zumft and Kroneck, 2007; Richardson, 2011; van Spanning, 2011; Simon and Klotz, 2013; Al-Attar and de Vries, 2015; Torres et al., 2016).

Strategies to mitigate N_2O emissions from agricultural soils have to be developed in order to decrease current levels of N_2O production in particular in the context of the continuing population growth (Thomson et al., 2012). One proposed strategy is to promote a sustainable agriculture reducing the dependence on chemical fertilizers and increasing biological nitrogen fixation (BNF) through the application of nitrogen-fixing bacteria to legume crops. However, legumes also contribute to N_2O emissions by providing N-rich residues into the soils or through the denitrification process that is performed by some rhizobia under free-living or symbiotic conditions (Inaba et al., 2009, 2012; Hirayama et al., 2011; Torres et al., 2016). In fact, many rhizobia species contain denitrification genes. Among them, *Bradyrhizobium diazoefficiens* is considered a model in the study of rhizobial denitrification given its capacity to grow with nitrate as respiratory substrate under anoxic conditions through denitrification, a process that has been extensively investigated in this bacterium (for reviews see Bedmar et al., 2005, 2013; Delgado et al., 2007; Sánchez et al., 2011; Torres et al., 2016). *B. diazoefficiens* denitrification reactions are catalyzed by Nap, NirK, cNor, and Nos enzymes encoded by *napEDABC*, *nirK*, *norCBQD,* and *nosRZDYFLX* genes, respectively. In addition to denitrify, *B. diazoefficiens* is also capable to grow under free-living conditions with nitrate as the sole N source. In this bacterium, the assimilatory nitrate reductase (NasC) constitutes an integrated biochemical system involved in nitrate assimilation and NO detoxification that has been demonstrated to be another source of NO and probably of N_2O (Cabrera et al., 2016).

Rhizobium etli CFN42, the endosymbiont of common bean (*Phaseolus vulgaris*) contains a chromosome and six large plasmids named from pCFN42a to pCFN42f (González et al., 2006). In this bacterium, genes encoding the NirK and cNor denitrification enzymes have been identified on plasmid pCFN42f (Gómez-Hernández et al., 2011). However, genes encoding either a respiratory nitrate reductase (Nar or Nap) or the nitrous oxide reductase enzyme (Nos) are not present in *R. etli* CFN42 genome. Consequently, this rhizobium species is unable to respire nitrate and to perform complete denitrification pathway. Genetic and functional characterization of the reductases encoded by *R. etli nirK* and *norC* suggest a detoxifying role for these enzymes. In fact, phenotypic characterization of *R. etli nirK* and *norC* mutants demonstrated that NirK is required for nitrite reduction to NO and that cNor is required to detoxify NO (Bueno et al., 2005; Gómez-Hernández et al., 2011). Under symbiotic conditions, recent analyses of the levels of nitrosylleghemoglobin complexes (LbNO) of the nodules from common bean plants exposed to nitrate clearly demonstrated the capacity of the nodules to produce NO from nitrate present in the nutrient solution (Gómez-Hernández et al., 2011; Calvo-Begueria et al., 2018). However, the capacity of *R. etli* to produce NO or N_2O from nitrate under free-living conditions has not been investigated so far. As mentioned before, *R. etli* lacks genes encoding the respiratory nitrate reductases (Nap or Nar). Sequence analysis revealed that an open reading frame in the *R. etli* chromosome (RHE_CHO1780) encodes a putative assimilatory nitrate reductase (NarB). RHE_CHO1780 resides within a cluster of other uncharacterized ORFs (RHE_CHO1781 and RHE_CHO1782) predicted to encode components (NirD and NirB) of an assimilatory nitrite reductase. This genomic context suggests a potential involvement of NarB in nitrate reduction to nitrite that would be further reduced to amonia by NirBD. However, the functional role of *R. etli* NarB has not been studied to date. Through the phenotypic characterization of a *R. etli narB* mutant, in this work we demonstrate the dual role of NarB in nitrate assimilation and in denitrification.

MATERIALS AND METHODS

Bacterial Strains, Plasmids, and Growth Conditions

The bacterial strains and plasmids used in this work are listed in **Table 1**. *Rhizobium etli* strains were grown at 30°C in TY rich medium (Tryptone Yeast, Beringer, 1974) or in Y minimal medium (MMY) with succinate (10 mM) and ammonium chloride (10 mM) as carbon and nitrogen sources, respectively (Bravo and Mora, 1988). For growth under microoxic or anoxic conditions, flasks containing cell cultures were sealed with rubber septa, and flushed at the starting point of the incubation with 2% (v/v) O_2 and 98% N_2 (v/v) or 100% (v/v) N_2, respectively. For growth with different nitrogen sources, cells were incubated in MMY with 10 mM $ClNH_4$, KNO_3 or $NaNO_2$ as sole N source. Antibiotics were added to *R. etli* CE3, and *narB*, *nirK*, and *norC* cultures (see **Table 1**) at the following concentrations ($\mu g\ ml^{-1}$): nalidixic acid (Nal) 20, kanamycin (Km) 30, spectinomycin (Sp) 100, streptomycin (Sm) 100. *Escherichia coli* DH5α used as receptor in cloning experiments and S17.1 used as donor in conjugation experiments were grown at 37°C in LB medium (Sambrook and Russell, 2001) and the antibiotics were added at the following concentrations

TABLE 1 | Bacterial strains and plasmids.

Strain or plasmid	Relevant characteristics	References
Bacteria		
Rhizobium etli		
CFN42	Nal^r (wild-type)	Quinto et al., 1982
CE3	Sm^r derivative of CFN42, Nal^{r}Sm^r (wild-type)	Noel et al., 1984
CFNX702	CE3 derivative, *nirK*::*lox*P, Nal^{r}Sm^r	Gómez-Hernández et al., 2011
CFNX701	CE3 derivative, *norC*::*lox*Sp, Nal^{r}Sm^r Sp^r	Gómez-Hernández et al., 2011
DR4000	CE3 derivative, Δ*narB*::ΩSpSm, Nal^{r}Sm^{r}Sp^r	This work
Escherichia coli		
DH5α	*supE*44Δ*lacU*169 (φ80*lacZ*ΔM15) *hsd*R17*rec*A1*end*A1*gyrA*96 *thi*-1*rel*A1	Sambrook et al., 1989
S17.1	*thi, pro*, recA,*hsdR, hsdM*, RP4Tc::Mu, Km::*Tn*7, Tp^{r}Sm^{r}Sp^r	Simon et al., 1983
Plasmids		
pBluescript KS	Cloning vector, Ap^r	Invitrogen
pK18*mobsacB*	Suicide cloning vector, Km^r	Schäfer et al., 1994
pBBR1MCS-2	Broad host range cloning vector, Km^r	Kovach et al., 1995
pHP45Ω	Vector carrying an ΩSpSm casette	Prentki and Krisch, 1984
pRK415	Broad host range plasmid, Tc^r	Keen et al., 1988
pNIC-01	pBBMCS53 derivative *norC*::*uid*A, Gm^r	Gómez-Hernández et al., 2011
pNIC-03	pBBMCS53 derivative *nirK*::*uid*A, Gm^r	Gómez-Hernández et al., 2011
pDR4000	pK18*mobsac*B carrying *narB* with 2287 bp delection and *narB*::Ω insertion, Sm^{r}Sp^{r}Km^r	This work
pDR4002	pBBR1MCS-2 derivative carrying *R. etli narB*, Km^r	This work
pLG4002	pRK415 derivative carrying *R. etli narB*, Tc^r	This work

(μg ml^{-1}): spectinomycin 25, streptomycin 25, kanamycin 20, and ampicillin 200.

For determination of growth rates and enzymatic activities, cells were firstly grown aerobically in TY medium for 24 h, harvested by centrifugation at 8000 *g* for 10 min and washed twice with MMY containing $ClNH_4$, KNO_3 or $NaNO_2$ as sole N source, depending on the treatment. Then, cells were incubated in the minimal medium for another 24 h under the desired oxygen conditions. Initial optical density at 600 nm of the cultures was around 0.05 for growth rates measurements or around 0.25 for enzymatic activity analyses.

For characterization of *narB* mutant growth, an additional step under starvation conditions was included before growing cells in the minimal medium. The starvation step consisted of a 24 h incubation of the cells in the minimal medium containing salts ($CaCl_2$ and $FeCl_3$), and lacking any nitrogen or carbon sources.

Construction and Complementation of *R. etli narB* Mutant

The oligonucleotide primers (Sigma) used in this work are listed in **Supplementary Table S1**. Genomic and plasmid DNA isolation were carried out using the REALPURE Genomic DNA purification Kit (Real) and Qiagen Plasmid Kit (Qiagen), respectively. PCR was performed using the High Fidelity DNA polymerase Phusion®enzyme (Thermo Fisher Scientific) and DNA digestions were carried out using Fast digest enzymes (Thermo Fisher Scientific).

To generate the *narB* mutant, the two regions flanking the *narB* gene (fragments F1 and F2), were amplified by PCR using narB_up_For/narB_up_Rev (in positions 1864715 to 1864732 and 1865293 to 1865310, respectively) and narB_down_For/narB_down_Rev (in positions 1867579 to 1867598 and 1868201 to 1868220, respectively) primer pairs. Then, fragments F1 and F2 were cloned into the pBlueScriptKS (pBSKS) vector (Invitrogen) as XbaI/BamHI and BamHI/EcoRI fragments, respectively, generating plasmid pBKS_F1F2. To construct a suicide plasmid useful for double recombination, the XbaI/EcoRI fragment from pBKS_F1F2 was cloned into the pK18*mobsacB* suicide vector (Schäfer et al., 1994) yielding plasmid pK18F1F2. This plasmid was further modified by inserting the ΩSp/Sm cassette (Prentki and Krisch, 1984) into the BamHI site of pK18F1F2 plasmid (between F1 and F2 fragments) obtaining plasmid pDR4000 that was analyzed by sequencing. Replacement of the *R. etli narB* wild type allele with the truncated mutant allele in plasmid pDR4000 was carried out by double recombination. With this purpose, plasmid pDR4000 was transferred via conjugation into *R. etli* CE3 using *E. coli* S17-1 as donor. Double recombination events were favored by growth on agar plates containing sucrose using the *sacB* marker present in plasmid pK18*mobsacB*. Double recombinants were selected as resistant to Sm and Sp and susceptible to Km. To verify that the gene replacement had occurred, the derivatives were analyzed by PCR using primers narB_EXT-For, narB_EXT-Rev, narB_IN-For, and narB_IN-Rev (**Supplementary Table S1**) and the *narB* mutant strain was named DR4000.

A plasmid carrying the *R. etli narB* gene constitutively expressed from the *lacZ* promoter was obtained by cloning the *narB* coding region in the broad-host range cloning vector pBBR1MCS-2 (Kovach et al., 1995). To that end, the *narB* gene was amplified by PCR using narB_compl_For/narB_compl_Rev

primers (**Supplementary Table S1**) and cloned as an XbaI/HindIII fragment into pBBR1MCS-2. The plasmid obtained (pDR4002) was sequenced and transferred to *R. etli* CE3 (WT) and DR4000 strains by conjugation using *E. coli* S17-1 as donor. The strain derivatives containing pDR4002 (WT/pDR4002 and DR4000/pDR4002, respectively) were checked by plasmid isolation and PCR. Concurrently, a WT strain containing pBBR1MCS-2 empty vector was obtained (WT/pBBR1MCS-2), as a control.

An additional plasmid carrying the *narB* gene constitutively expressed from the *lacZ* promoter was constructed by cloning the XbaI/HindIII fragment containing *narB* from pDR4002 into the pRK415 vector (Keen et al., 1988). The plasmid obtained (pLG4002) was introduced by conjugation into *R. etli* DR4000 strain harboring plasmids pNIC-03 and pNIC-01 that contain a *nirK*::*uidA* or *norC*::*uidA* transcriptional fusions, respectively. In addition, the pRK415 empty vector was introduced into WT-pNIC-03, WT- pNIC-01, DR4002- pNIC-03, and DR4002- pNIC-01 derivatives.

Extracelullar NO_2^- Determination

To measure the concentration of NO_2^- in the medium during growth with NO_3^- under aerobic or microoxic conditions, aliquots were taken from cultures at different time points. Culture samples were centrifuged at 8000 *g* for 10 min and nitrite concentration was estimated in the supernatant after diazotization by adding the sulphanilamide-naphthylethylenediamine dihydrochloride reagent (Nicholas and Nason, 1957).

Cell Extract Preparation and Determination of Nitrate and Nitrite Reductase Activities

To analyze nitrate reductase (NR) activity, cells at an initial OD_{600} of about 0.25 were incubated aerobically with KNO_3 as the sole nitrogen source for 24 h. After centrifugation at 8000 g for 10 min, cells were harvested and disrupted by using a French pressure cell (SLM Aminco, Jessup, MD, United States). Then, fractionated cells were centrifuged at 10000 *g* for 10 min and the supernatant containing the soluble cell extract was used for NR activity. To analyze nitrite reductase (Nir) activity, cells were grown microoxically with KNO_3 as the sole nitrogen source for 24 h. Then, cells were harvested by centrifugation, washed twice with 50 mM Tris–HCl pH 7.5 and resuspended in 1 ml of the same buffer.

Methyl-viologen dependent nitrate reductase (MV-NR) and nitrite reductase (MV-Nir) activities were determined by using 105 μl of the soluble cell extract (∼0.5 mg protein) or cell suspension (∼0.1 mg protein), respectively. The reaction mixture also contained 0.2 mM Methyl Viologen and 10 mM KNO_3 for NR activity or 0.01 mM $NaNO_2$ for Nir activity. The reaction was started by the addition of 15 μl of freshly prepared 144 mM sodium dithionite solution in 300 mM $NaHCO_3$. After incubation for 20 min at 30°C, the reaction was stopped by vigorous shaking until the samples had lost their blue color. Nitrite produced by NR or consumed by Nir enzymes was estimated after diazotization as described previously for extracellular NO_2^- determination.

NO Production and Consumption Activities

In order to investigate the capacity of the different mutants to produce or consume NO, cell cultures at an initial OD600 of about 0.25 were incubated microoxically with KNO_3 as the sole nitrogen source for 24 h, harvested by centrifugation, washed twice with 25 mM Na_2HPO_4/NaH_2PO4 buffer (pH 7.4), and resuspended in 1.5 ml of the same buffer. NO production and consumption activities were determined by using an ISONOP NO electrode APOLLO 4000®(World Precision Instruments). The reaction chamber (2 ml) was temperature-controlled, magnetically stirred and contained: 1410 μl of 25 mM Na_2HPO_4/NaH_2PO_4 buffer (pH 7.4) and 250 μl of cell suspension (0.4–0.7 mg protein) for NO production or 760 μl of 25 mM Na_2HPO_4/NaH_2PO_4 buffer (pH 7.4) and 900 μl of cell suspension (1.5–2.5 mg protein) for NO consumption. To generate an anoxic atmosphere, 100 μl of an enzymatic mix containing *Aspergillus niger* glucose oxidase (40 units·ml^{-1}), bovine liver catalase (250 units·ml^{-1}) (Sigma-Aldrich), 90 μl of 1 M sodium succinate and 100 μl of 320 mM glucose were added to the chamber. Once a steady base line was obtained, 50 μl of 50 mM $NaNO_2$ (NO production) or 50 μl of 2 mM NO (NO consumption) was added to the chamber to start the reaction.

N_2O Production

To measure N_2O accumulation, *R. etli* CE3 and the mutant strains were cultured as indicated above for NO experiments. After 24 h growth, 1 ml was taken from the headspace of cultures, using a Hamilton®Gastight syringe, and manually injected into an HP 4890D gas chromatography instrument equipped with an electron capture detector (ECD) as described by Torres et al. (2014).

Haem-Staining Analysis

To study the expression of the NorC component of cNor, we performed haem *c*-staining analyses of proteins from membranes of *R. etli* CE3 and the mutant strains cultured as indicated above for NO and N_2O experiments. After 24 h growth, cells were harvested by centrifugation, washed twice with 50 mM Na_2HPO_4/NaH_2PO_4 (pH 6.8) buffer containing 1 mM $MgCl_2$, 0.9% NaCl and 0.1 mM $CaCl_2$, and resuspended in 2.5 ml of the same buffer containing 0.1 mM 4-(2-aminoethyl) benzene-sulfonyl fluoride hydrochloride (ABSF), RNase (20 μg ml^{-1}), and DNase I (20 μg ml^{-1}). Cells were disrupted using a French pressure cell (SLM Aminco, Jessup, MD, United States) and the membrane fraction was prepared as described previously (Torres et al., 2013). Then, membrane proteins were separated by SDS-PAGE, transferred to a nitrocellulose membrane and stained for haem-dependent peroxidase activity as described previously (Vargas et al., 1993) using the chemiluminescence detection kit "SuperSignal" (Thermo Fisher Scientific, Pierce, IL, United States). Protein concentration was estimated using the Bio-Rad assay (Bio-Rad Laboratories).

Measurement of β-Glucuronidase Activity

To analyze the expression of *nirK* and *nor* genes, *R. etli* CE3 and the mutant cells containing a *nirK::uidA* or a *norC::uidA* transcriptional fusions were incubated microoxically (2% initial O_2 concentration) for 14 h in MMY medium containing $ClNH_4$ or KNO_3 as sole N source, with exception of the *narB* mutant that was grown for 21 h. Quantitative GUS activity was determined on 1.0-ml culture samples using 4-nitrophenyl β-D-glucuronide as substrate as described previously (Girard et al., 2000). Data were normalized to total cell protein concentration by the Lowry method over a second set of 1.0-ml samples.

RESULTS

R. etli narB Encodes the Assimilatory Nitrate Reductase

Figure 1 shows that *R. etli* (WT) is able to grow with NO_3^- as the sole nitrogen source under oxic or microoxic (2% initial O_2 concentration) conditions reaching values of optical densities (OD) at 600 nm of around 0.6 or 0.4, respectively. However, this bacterium was unable to use NO_3^- for respiration being incapable to grow under anoxic conditions with nitrate as the sole N source (**Figure 1**). These results suggest that *R. etli* uses nitrate through the assimilatory pathway under oxic or microoxic conditions where oxygen was used for respiration. However, it is unable to respire nitrate when oxygen is absent. Similar growth rates were reached when the wild-type (WT) cells were grown in minimal medium amended with 10 mM of $ClNH_4$ as the sole N source (**Figure 1**).

In order to determine the implication of RHE_CHO1780 encoding for a putative assimilatory nitrate reductase (NarB) in nitrate assimilation, a *R. etli* mutant strain lacking the *narB* gene was constructed. As shown in **Figure 2A**, aerobic growth of *R. etli narB* mutant was highly decreased compared to that reached by the WT strain (0.1 and 0.4 OD_{600}, respectively, after 35 h culture). However, when the *narB* mutant was complemented with plasmid pDR4002 that constitutively expresses *narB* (*narB* + $NarB^+$), similar growth rates as those from WT cells were observed (**Figure 2A**). No significant differences of growth rates were found when the WT strain was complemented with plasmid pDR4002 (WT + $NarB^+$) or with pBBR1MCS-2 (WT + vector) (**Figure 2A**). Moreover, NO_2^- was not detected in the culture medium of *narB* mutant grown oxicallly (**Figure 2B**). However, WT cells accumulated around 100 μM NO_2^- in the medium after 35 h growth (**Figure 2B**). Interestingly, both *narB* and WT strains containing pDR4002 (*narB* + $NarB^+$ or WT + $NarB^+$) accumulated about 180 μM NO_2^- in the medium. These results suggest that *R. etli* NarB is the enzyme responsible for nitrate reduction to nitrite, the first step of nitrate assimilation.

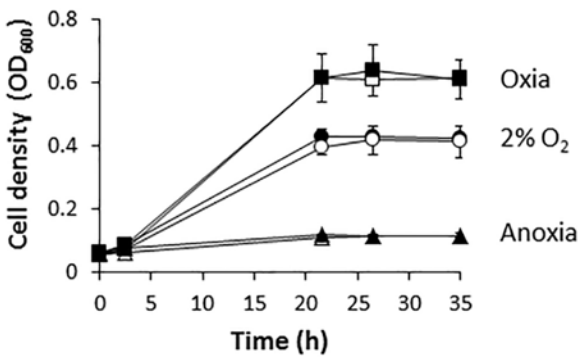

FIGURE 1 | Nitrate-dependent growth of *R. etli*. Cells were cultured under oxic (squares), microoxic (circles) or anoxic (triangles) conditions, with either NH_4^+ (white) or NO_3^- (black), as sole N source. Results are the mean values and error bars from at least two different cultures assayed in triplicate.

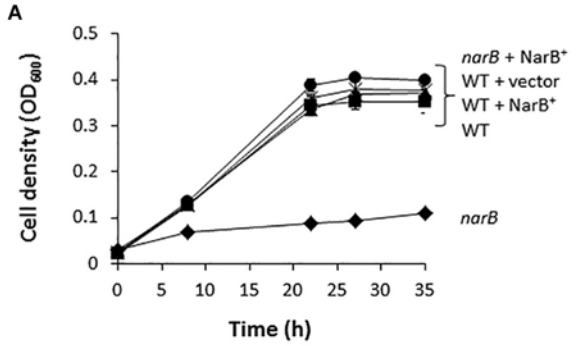

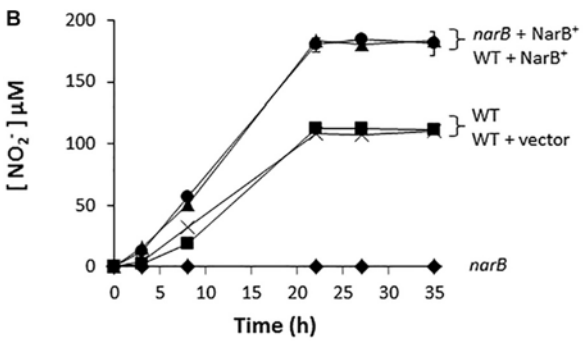

C

Strains	Relevant genotype	MV-NR activity
CE3	WT	9.3 ± 1.1
CE3-pBBR1MCS2	WT + vector	10 ± 0.9
DR4000	*narB*	0.9 ± 0.2
DR4000-pDR4002	*narB* + $NarB^+$	142 ± 24
CE3-pDR4002	WT + $NarB^+$	119 ± 18

FIGURE 2 | Nitrate-dependent aerobic growth and NR activity of a *R. etli narB* mutant. **(A)** Growth curves. **(B)** Extracellular nitrite concentration in the growth medium. **(C)** MV-NR activity expressed as nmol NO_2^- produced mg $protein^{-1}$ h^{-1}. *R. etli* WT (■), WT + vector (X), *narB* (♦), *narB* + $NarB^+$ (●), and WT + $NarB^+$ (▲) strains were incubated aerobically in minimal medium with NO_3^- as sole N-source. Data are expressed as the mean value ± SD from two different cultures assayed in triplicate.

To corroborate this observation, we also measured MV-NR activity of *R. etli* cells grown under oxic conditions with NO_3^- as sole N source. As shown in **Figure 2C**, MV-NR activity was around 10-fold lower in the *narB* mutant compared to that observed in the WT strain. The constitutive expression of *narB* in the *narB* mutant (*narB* + $NarB^+$), restored NR activity to levels significantly higher (about 15-fold) to those observed in WT cells. A similar increase of NR activity (about 13-fold) was observed in WT cells containing pDR4002 compared to NR levels of WT strain with or without the empty vector pBBR1MCS-2 (**Figure 2C**). The higher effect of the presence of pDR4002 on nitrite accumulation (**Figure 2B**) and MV-NR activity (**Figure 2C**) is due to the over-expression of *narB* gene by the constitutive *lacZ* promoter present in pDR4002. Taken together, these results confirm the participation of NarB in nitrate reduction to nitrite when cells are cultured under aerobic conditions with nitrate as the only N source.

R. etli narB, *nirK*, and *norC* Are Required for Denitrification

To investigate the implication of *R. etli narB*, *nirK* and *norC* genes in the denitrification process, we performed growth rate experiments of the *R. etli narB, nirK* and *norC* mutant cells cultured under microoxic conditions and in the presence of nitrate as sole nitrogen source. While *narB* was obtained in this work, the *nirK* or *norC* mutants were previously constructed by Gómez-Hernández et al. (2011). As observed when cells were incubated under oxic conditions (**Figure 1A**), the *narB* mutant showed a clear defect in its ability to grow when compare to the WT cells (**Figure 3A**). Complementation of *narB* mutant with plasmid pDR4002 expressing constitutively *narB* (*narB*+ $NarB^+$) restored the WT ability to grow under microoxic conditions (**Figure 3A**). The *norC* mutant was completely unable to grow microoxically with nitrate as unique nitrogen source. However, no differences in nitrate-dependent growth rates were detected between the *nirK* mutant and WT strain (**Figure 3A**). The capacity of the *nirK* mutant to grow with nitrate might be due to its ability to assimilate nitrate and nitrite through the activity of the NarB and NirBD assimilatory nitrate and nitrite reductase enzymes. As shown in **Figure 3B**, WT cells incubated microoxically with NO_3^- accumulated low levels of NO_2^- in the medium after 8 h incubation (5 μM NO_2^-) that was consumed after 45 h growth. Growth of the *R. etli nirK* mutant under the same growth conditions resulted in higher levels of NO_2^- concentration in the medium compared to those observed in WT cultures (20 μM *versus* 0 μM NO_2^- after 45 h incubation) (**Figure 3B**). Furthermore, levels of nitrite detected in the culture medium of *narB* or *norC* mutants cultivated under the same conditions were undetectable (**Figure 3B**). Interestingly, *narB* mutant containing plasmid pDR4002 (*narB* + $NarB^+$) accumulated about 11-times more NO_2^- in the medium compared to WT cells (56 μM *versus* 5 μM NO_2^- after 8 h incubation) (**Figure 3B**).

In order to investigate the denitrification capacity of the *narB*, *nirK* and *norC* mutants, we determined MV-Nir, NO consumption activity (Nor), NO production capacity and N_2O accumulation (**Figure 4** and **Table 2**). As shown in **Table 2**, MV-Nir activity was about 5-times lower in the *nirK* mutant compared to that observed in WT, *narB* or *narB* containing pDR4002 (*narB* + $NarB^+$) strains. The residual Nir activity observed in the *nirK* mutant could be due to the activity of an assimilatory Nir, enzyme that is also encoded in the *R. etli* CFN42 genome. Concerning Nor activity, it was significantly lower (around ninefold) in cells of the *norC* mutant compared to the values reached by WT cells (**Table 2**). These observations indicate that NirK and NorC are the main enzymes responsible of MV-Nir and Nor activities, respectively. Furthermore, a significant reduction (around twofold) of Nor activity was observed in the *narB* mutant. On the contrary, the constitutive expression of *narB* in the *narB* mutant background (*narB* + $NarB^+$) resulted in an increase of about 3.4-fold of Nor activity compared to that observed in the *narB* mutant (**Table 2**). Additionally, we measured NO production capacity of *nirK*, *norC*, and *narB*

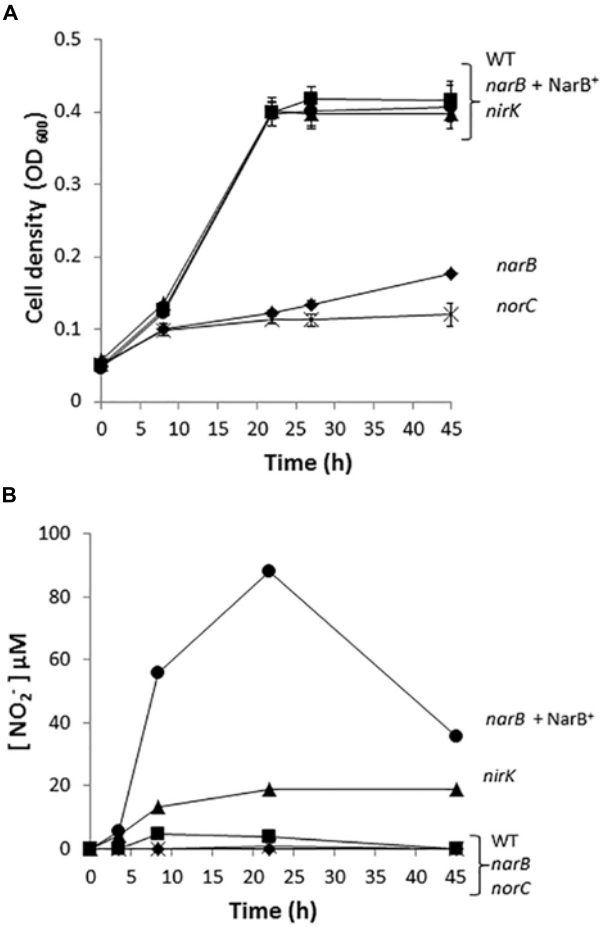

FIGURE 3 | Nitrate dependent micro-oxic growth of *R. etli narB*, *nirK,* and *norC* mutants. **(A)** Growth curves. **(B)** Extracellular nitrite concentration in the growth medium. *R. etli* WT (■), *narB* (♦), *narB*+ $NarB^+$ (●), *norC* (X), and *nirK* (▲) strains were cultured microoxically in minimal medium with NO_3^- as sole N-source. Data are expressed as the mean value and error bars from two different cultures assayed in triplicate.

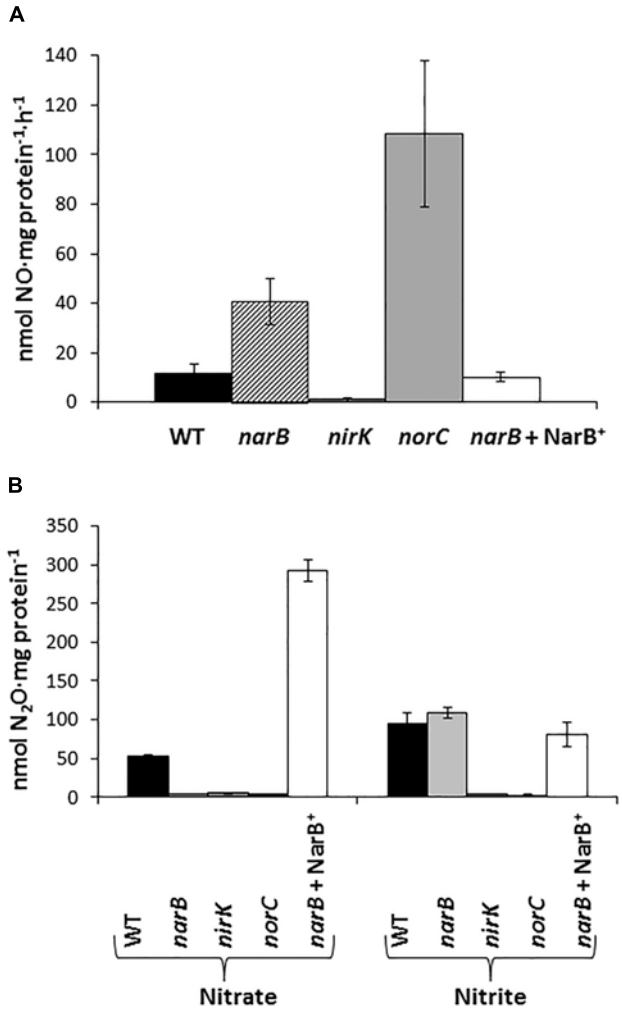

FIGURE 4 | Nitric oxide production capacity **(A)** and N_2O accumulation **(B)** by *R. etli narB*, *narB* + $NarB^+$, *nirK*, and *norC* mutants. In **(A)** cells incubated microoxically with NO_3^- were transferred to a reaction chamber with NO_2^-. In **(B)** cells were cultured microoxically with NO_3^- or NO_2^- as the sole N-source. Data are expressed as the mean value and error bars from two different cultures assayed in triplicate.

TABLE 2 | MV-Nir and Nor activities of *R. etli narB*, *nirK*, *norC*, or *narB* complemented with pDR4002 ($NarB^+$).

		Activities	
Strains	**Genotype**	**MV-Nir**	**Nor**
CE3	WT	195 ± 2.3	269 ± 58
DR4000	*narB*	182 ± 1.6	155 ± 43
CFNX702	*nirK*	40 ± 2.3	nd
CFNX701	*norC*	nd	31 ± 5.4
DR4000-pDR4002	*narB* + $NarB^+$	190 ± 4.5	532 ± 72

Cells were cultured microoxically with NO_3^- as the sole N-source. MV-NiR and Nor activities are expressed as nmol of NO_2^- or NO consumed·h^{-1}·mg $protein^{-1}$, respectively. Data are expressed as the mean value ± SD from at least two different cultures assayed in triplicate; nd, not determined.

mutants cultured microoxically with nitrate that were transferred to a reaction chamber with NO_2^- as substrate (**Figure 4A**). The *norC* mutant accumulated about 10-times more NO than the WT being the toxicity of NO the reason that might explain the inability of this mutant to grow under microoxic conditions (**Figures 3A**, **4A**). On the contrary, the *nirK* mutant did not produce NO. NO accumulation capacity by the *narB* mutant was 4-times higher than that observed in the WT strain (**Figure 4A**) probably due to the twofold reduction of NO consumption activity observed in the *narB* mutant (**Table 2**) compared to WT cells. Accordingly, NO produced by the *narB* mutant containing pDR4002 (*narB* + $NarB^+$) decreased to WT levels (**Figure 4A**). Interestingly, N_2O production was observed in the headspace of WT cultures grown under microoxic conditions with nitrate as the only N source (**Figure 4B**). By contrary, *narB*, *nirK* and *norC* mutants appeared to be unable to produce N_2O (**Figure 4B**). However, the *narB* mutant complemented with pDR4002 (*narB* + $NarB^+$) showed a significant accumulation (about sixfold) of N_2O compared to those levels produced by the WT strain in the presence of nitrate in the growth medium. These results clearly demonstrate the involvement of nitrate reduction by NarB on *R. etli* N_2O emission in cells grown with nitrate. However, when cells were grown in the presence of nitrite as the sole nitrogen source, the *narB* mutant as well as the *narB* + $NarB^+$ strain reached similar values of N_2O accumulation to the WT (**Figure 4B**). As observed in nitrate-cultured cells, *nirK* and *norC* mutants were defective in their capacity to produce N_2O in cells with NO_2^- as N source (**Figure 4B**). These results indicate that NirK and NorC but not NarB are required for N_2O production by *R. etli* cells cultured with nitrite as N source.

Involvement of Nitrate Reduction by NarB in *R. etli nirK* and *nor* Expression

Results from **Table 2** suggest the involvement of NarB in Nor activity, but not in Nir activity. Our next goal was to evaluate the participation of NarB in the expression of *nirK* and *nor* genes. To achieve this goal, a *nirK::uidA* and a *norC::uidA* transcriptional fusions present in plasmids pNIC-03 or pNIC-01, respectively (Gómez-Hernández et al., 2011) were used in this work. *R. etli* WT cells grown with NO_3^- showed a slight increase of about twofold of *nirK::uidA* expression compared to that from NH_4^+-grown cells (**Table 3**). However, about fourfold increase of *norC::uidA* was observed in NO_3^--grown cells compared to those grown with NH_4^+ as N source (**Table 3**). Interestingly, a differential dependence on NarB for expression of *nirK* and *norC* genes was observed when NO_3^- was present in the culture medium. While *nirK* showed only a marginal dependence of NarB for expression in this condition (2087 ± 106 in the WT vs. 1617 ± 131 in the *narB* mutant), the fourfold induction of *norC* expression by nitrate in the WT was not observed in the *narB* mutant (**Table 3**). As shown in **Table 3**, the expression of *norC* in the *narB* mutant strain was restored when it contained plasmid pLG4002 with a constitutive expression of *narB* (223 ± 8 to 1493 ± 108 activity values). By contrast, the presence of pLG4002 in the *narB* mutant slightly increased *nirK::uidA* expression in NO_3^--grown cells (1617 ± 131 to 2356 ± 122 activity units).

TABLE 3 | β-glucuronidase specific activity of *nirK*::*uidA* and *norC*::*uidA* transcriptional fusions in *R. etli* WT, *narB*, or *narB* complemented with pLG4002 (NarB$^+$).

		β-glucuronidase specific activity[1]	
Strains	**Genotype**	**NH_4^+**	**NO_3^-**
CE3-pRK415-pNIC-03	WT (*nirK*::*uidA*)	1115 ± 72	2087 ± 106
CE3-pRK415-pNIC-01	WT (*norC*::*uidA*)	352 ± 51	1451 ± 185
DR4000-pRK415-pNIC-03	*narB (nirK*::*uidA*)	912 ± 17	1617 ± 131
DR4000-pRK415-pNIC-01	*narB* (*norC*::*uidA*)	245 ± 6	223 ± 8
DR4000-pLG4002-pNIC-03	*narB*+NarB$^+$ (*nirK*::*uidA*)	1236 ± 75	2356 ± 122
DR4000-pLG4002-pNIC-01	*narB*+NarB$^+$ (*norC*::*uidA*)	453 ± 58	1493 ± 108
CFNX702- pNIC-01	*nirK (norC::uidA)*	91 ± 33	119 ± 23

Cells were cultured microoxically with NH_4^+ or NO_3^- as the sole N source.
[1]Values are expressed as nmol min^{-1} mg $protein^{-1}$. Data are the mean of three replicates from two independent experiments ± SD.

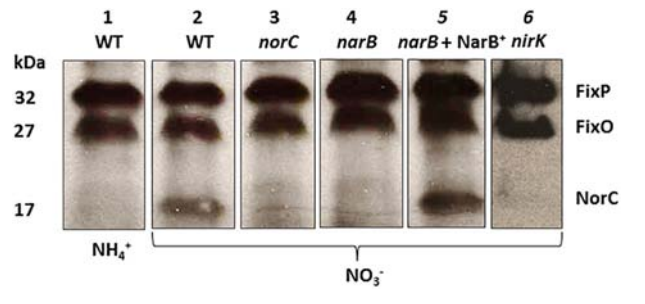

FIGURE 5 | Expression of NorC in *R. etli narB* mutant. Haem-stained proteins of membranes prepared from *R. etli* WT (lanes 1 and 2), *norC* (lane 3), *narB* (lane 4), *narB* + NarB$^+$ (lane 5), and *nirK* (lane 6) mutants cultured microoxically with NH_4^+ (lane 1) or NO_3^- (lanes 2, 3, 4, 5, and 6) as the sole N-source. Each lane contains 25 μg of membrane proteins. Haem-stained *c*-type cytochromes indentified previously (FixP and FixO) and in this work (NorC) are indicated. Apparent protein molecular masses (kDa) are also shown.

These results clearly show that the induction of the microoxic expression of *norC* by nitrate is dependent on NarB. We also observed that the induction of the *norC*::*uidA* expression in response to nitrate did not occur in a *nirK* mutant background (**Table 3**). These results suggest that NO produced from NO_3^- reduction to NO_2^- by NarB and from NO_2^- reduction by NirK is the nitrogen oxide (NOx) required for *nor* expression.

To confirm the participation of NarB in the induction of *nor* genes, we examined the expression of NorC by performing haem *c* staining analyses in proteins from membranes of a *narB* mutant cultured microoxically with nitrate as N source. To identify NorC protein, we also included in these experiments the *R. etli norC* mutant. As shown in **Figure 5**, a 32- and 27-kDa *c*-type cytochromes, identified previously as the FixP and FixO subunits of the terminal oxygen high-affinity cbb_3-type cytochrome oxidase (Soberon et al., 1999) were observed in all strains. A third band of about 17 kDa which was observed in WT cells grown with NO_3^- could not be detected in membranes from the *norC* mutant cultured under the same conditions (**Figure 5**, lanes 2 and 3). These results allowed us to identify by the first time in *R. etli* the NorC component of cNor. By contrary to WT nitrate-dependent cells, growth with NH_4^+ as N source did not allowed expression of NorC suggesting the requirement of nitrate in the medium to induce NorC in *R. etli* (**Figure 5**, lanes 1 and 2). Interestingly, NorC could not be detected in membranes from the *narB* mutant grown with nitrate indicating that nitrate reduction by NarB, is required to induce NorC expression in *R. etli* (**Figure 5**, lanes 2 and 4). In fact, constitutive expression of NarB in the *narB* mutant (*narB* + NarB$^+$) restored the expression of NorC in *R. etli narB* mutant cultured microoxically with nitrate (**Figure 5**, lanes 2, 4, and 5). These results clearly demonstrate the role of nitrate reduction by NarB in NorC expression in *R. etli*. In this bacterium, the reduction products of nitrate under microoxic conditions are NO_2^- or NO. In order to identify the NOx (NO_2^- or NO) required for expression of NorC, we included in the haem-staining experiments the *nirK* mutant which does not produce NO from nitrate (**Figure 4A**). As shown in **Figure 5** (lane 6), NorC was not detected in membranes from the *nirK* mutant in response to nitrate, suggesting that NO could be the signal molecule implicated in NorC expression.

DISCUSSION

R. etli NarB Is Required for Nitrate Assimilation and Denitrification

Rhizobium etli is a N_2-fixing soil bacterium able to establish endosymbiotic associations with common bean plants. Up to now, the capacity of this bacterium to perform other processes of the N-cycle was unknown. In this work, we have demonstrated for the first time the ability of *R. etli* to assimilate nitrate as well as to produce NO and N_2O from NO_3^- through denitrification. However, *R. etli* is unable to grow under anoxic conditions using NO_3^- as the final electron acceptor since it lacks the respiratory Nap or Nar nitrate reductases. The denitrification enzymes NirK and cNor are not proton pump or electrogenic. In this case, is the electron transfer from UQ pool to bc_1 complex that can be used to drive the translocation of protons across the mitochondrial membrane to generate a *trans*-membrane proton electrochemical gradient or proton motive force (Δp) that can drive the synthesis of ATP. However, in incomplete denitrifiers like *R. etli* CFN42 that lack Nar or Nap, ATP synthesis from electron transfer to NirK and cNor is limited and it does not allow cells to grow from nitrate respiration

anoxically. An inspection of the *R. etli* CFN42 genome[1], allowed us to identify a gene (RHE_CHO1780) annotated as *narB*, which encodes a putative NarB. Two classes of assimilatory nitrate reductases (Nas) have been described from microorganisms: the NADH-dependent Nas and the ferrodoxin- or flavodoxin-dependent Nas (Fd-Nas, Moreno-Vivian et al., 1999). NADH-Nas proteins are heterodimers consisting of a 45 kDa FAD-containing diaphoarase and the 95 kDa catalytic subunit with a molybdenum *bis*-molybdopterin dinucleotide (Mo-*bis*-MGD) cofactor and a N-terminal [4Fe-4S] center (Richardson et al., 2001). Fd-Nas usually present in cyanobacteria are monomers with a molecular weight between 75 and 85 kDa (Moreno-Vivián and Flores, 2007). The *in silico* analysis of the *R. etli* NarB sequence (web.expasy.org) found that it has 885 aa, a predicted molecular weight of approximately 94.5 kDa, as well as the typical Mo-*bis*-MGD binding domain and the consensus motifs for co-ordination of an N-terminal [4Fe-4S] cluster present in NADH-Nas.

In nitrate assimilation, NO_3^- is incorporated into the cells by its sequential reduction to NO_2^- and NH_4^+ by the assimilatory nitrate and nitrite reductases, respectively. The presence of NarB in *R. etli* led us to hypothesize that this bacterium could use this enzyme to assimilate nitrate together with the two additional ORFs located in the same gene cluster that are predicted to encode the NirB and NirD components of an assimilatory nitrite reductase. The NH_4^+ produced is further incorporated into carbon skeletons (reviewed by Luque-Almagro et al., 2011). In fact, a *R. etli narB* mutant was unable to grow aerobically with nitrate as the only N source and was impaired in nitrate reductase activity.

Rhizobium etli CFN42 only possesses in its genome the *nirK* and *nor* denitrification genes, encoding NirK and cNor, respectively. Previous results have demonstrated that NirK is required for nitrite reduction to NO and that cNor is needed to detoxify NO (Bueno et al., 2005; Gómez-Hernández et al., 2011). However, up to now, no evidence has been reported about the putative link between NarB and nitrite and NO detoxification in nitrate-dependent microoxically grown cells. In this work, we have demonstrated that NarB is required for N_2O formation in cells grown microoxically with nitrate as N source given the inability of the *R. etli narB* mutant to produce N_2O from nitrate. These observations led us to suggest that NO_2^- produced by NO_3^- reduction in the cytoplasm through NarB activity might be exported outside the cell where is detoxified by NirK and cNor to produce NO and N_2O, respectively, in the periplasmic space. In the same genomic region where NarB is located, there is an ORF (RHE_CHO1783) that is predicted to encode a major facilitator family NO_3^-/NO_2^- transporter (NarK) similar to that found in *B. diazoefficiens* that has been reported to be involved in NO_2^- extrussion (Cabrera et al., 2016). The implication of this NarK-like protein in transporting NO_2^- from the cytoplasm to the periplasm is under investigation. The involvement of NarB in nitrate assimilation and denitrification was also demonstrated by complementing the *narB* mutant with the constitutively expressed *narB* gene allowing the restoration of the ability to assimilate nitrate and to produce N_2O in the *narB* mutant. Interestingly, the constitutive expression of *narB* in the *narB* mutant resulted in a remarkable increase of NR activity, NO_2^- accumulation in the medium and Nor activity that resulted in higher levels of N_2O respect to WT cells under microoxic conditions. However, this increase in nitrate reduction and N_2O formation did not result in higher growth rates probably due to the fact that NarB, NirK, and cNor enzymes do not allow the cells to obtain energy through the assimilative NO_3^- reduction by NarB coupled to denitrification by NirK and cNor. In fact, constitutive expression of NarB in *R. etli* WT strain did not allow the cells to grow under anoxic conditions with nitrate (data not shown). On the contrary, it has been recently reported that constitutive expression of Nap allowed *Ensifer meliloti* to increase the production of NO_2^-, NO, and N_2O as well as its capacity to grow anoxically using nitrate as respiratory substrate (Torres et al., 2018). In spite of *R. etli narB*, *nirK*, and *norC* genes do not allow cell growth through denitrification, when cells are cultured microoxically through nitrate assimilation, *nirK*, and *norC* have a detoxifying role preventing the accumulation of the cytotoxic molecules nitrite and NO and contributing to the production of the GHG N_2O having an environmental impact to climate change. In this context, the role of *R. etli* NirK and cNor on nitrite and NO detoxification has been previously reported (Gómez-Hernández et al., 2011).

Nitrate-Dependent Induction of *R. etli nor* Expression Requires NarB

Bradyrhizobium diazoefficiens, the symbiont of soybeans, is considered a model for the study of denitrification in rhizobia given its capacity to grow anoxically from nitrate respiration. In this bacterium, where denitrification has been extensively studied, expression of *nap*, *nirK*, *nor*, and *nos* genes requires both oxygen limitation and the presence of a NOx (for a recent review see Torres et al., 2016). In *R. etli*, it has been reported that low-oxygen concentration (1%) induces expression of *nirK* and *norC* denitrification genes (Gómez-Hernández et al., 2011). In this work, we demonstrate that in addition to low oxygen conditions, nitrate or a product derived from its reduction generated by NarB activity is also required for induction of *nor* genes but not for *nirK*. In fact, Gómez-Hernández et al. (2011) found that *R. etli norC* and *nirK* genes display a different level of dependence for the transcriptional regulator NnrR. A null mutation in *nnrR* causes a drastic drop in the expression of *norC*, while *nirK* still exhibits significant expression. In *B. diazoefficiens*, NnrR is the direct transcriptional regulator of *nor* genes in response to NO but not of *nirK* that is controlled directly by $FixK_2$ in response to low oxygen (Bueno et al., 2017). These findings are in agreement with the different dependency on nitrate and NarB of the *R. etli nor* and *nirK* genes we show in this work.

In order to identify the NOx (NO_2^- or NO) derived from nitrate reduction required for induction of *R. etli nor* genes, we analyzed the expression of the *norC::uidA* transcriptional fusion as well as the haem *c* component of cNor (NorC) in a *R. etli nirK* mutant that is defective in nitrite reduction to NO as it has been

[1]http://genome.microbedb.jp/rhizobase

demonstrated in this work. The absence of NorC in membranes as well as the very basal levels of β-glucuronidase activity in the *nirK* mutant cultured with nitrate as sole N source indicates that the signal molecule required for induction of *nor* genes is NO. Similarly, it has been recently demonstrated in *B. diazoefficiens* that *norCBQD* expression requires, in addition to microoxia, the presence of NO (Bueno et al., 2017).

In this work, we propose for the first time a new pathway in bacteria to produce N_2O by coupling nitrate assimilation and denitrification under microoxic conditions. In this context, it has been recently identified in *B. diazoefficiens,* an integrated system for nitrate assimilation and nitric oxide detoxification which is connected to denitrification through the induction of *nor* genes when a single domain hemoglobin (Bjgb) encoded in this pathway is not functional (Cabrera et al., 2016).

AUTHOR CONTRIBUTIONS

AH-G and MD conceived and designed the study. AH-G, MT, AS, and LG performed the experiments. AH-G, MT, AS, LG, and MD analyzed the results and wrote the manuscript. EB critically revised the manuscript. All authors read and approved the final manuscript.

FUNDING

This work was supported by Fondo Europeo de Desarrollo Regional (FEDER)-co-financed grants (AGL2013-45087-R and AGL2017-85676-R) from the Ministerio de Economía y Competitividad (Spain). Grant P12-AGR-1968 from the Junta de Andalucía was also acknowledged.

ACKNOWLEDGMENTS

We are grateful to G. Tortosa (EEZ, CSIC, Granada, Spain), M. Rodríguez, and M. P. Salas (CCG, UNAM, Cuernavaca, México) for their excellent technical assistance. We thank D. Francis Lewis for the improvement of the written English. We acknowledge support of the publication fee by the CSIC Open Access Publication Support Initiative through its Unit of Information Resources for Research (URICI).

SUPPLEMENTARY MATERIAL

The Supplementary Material for this article can be found online at: https://www.frontiersin.org/articles/10.3389/fmicb.2019.00980/full#supplementary-material

REFERENCES

Al-Attar, S., and de Vries, S. (2015). An electrogenic nitric oxide reductase. *FEBS Lett.* 589, 2050–2057. doi: 10.1016/j.febslet.2015.06.033

Bedmar, E. J., Bueno, E., Correa, D., Torres, M. J., Delgado, M. J., and Mesa, S. (2013). "Ecology of denitrification in soils and plant-associated," in *Beneficial Plant-Microbial Interactions: Ecology and Applications*, eds B. Rodelas and J. Gonzalez-López (Boca Ratón, FL: CRC Press), 164–182.

Bedmar, E. J., Robles, E. F., and Delgado, M. J. (2005). The complete denitrification pathway of the symbiotic, nitrogen-fixing bacterium *Bradyrhizobium japonicum*. *Biochem. Soc. Trans.* 33, 141–144. doi: 10.1042/BST0330141

Beringer, J. E. (1974). R factor transfer in *Rhizobium leguminosarum*. *J. Gen. Microbiol.* 84, 188–198. doi: 10.1099/00221287-84-1-188

Bravo, A., and Mora, J. (1988). Ammonium assimilation in *Rhizobium phaseoli* by the glutamine synthetase-glutamate synthase pathway. *J. Bacteriol.* 170, 980–984. doi: 10.1128/jb.170.2.980-984.1988

Bueno, E., Gomez-Hernandez, N., Girard, L., Bedmar, E. J., and Delgado, M. J. (2005). Function of the *Rhizobium etli* CFN42 *nirK* gene in nitrite metabolism. *Biochem. Soc. Trans.* 33, 162–163. doi: 10.1042/BST0330162

Bueno, E., Robles, E. F., Torres, M. J., Krell, T., Bedmar, E. J., Delgado, M. J., et al. (2017). Disparate response to microoxia and nitrogen oxides of the *Bradyrhizobium japonicum napEDABC*, *nirK* and *norCBQD* denitrification genes. *Nitric. Oxide* 68, 137–149. doi: 10.1016/j.niox.2017.02.002

Butterbach-Bahl, K., Baggs, E. M., Dannenmann, M., Kiese, R., and Zechmeister-Boltenstern, S. (2014). Nitrous oxide emissions from soils: how well do we understand the processes and their controls? *Philos. Trans. R. Soc. B* 368:20130122. doi: 10.1098/rstb.2013.0122

Cabrera, J. J., Salas, A., Torres, M. J., Bedmar, E. J., Richardson, D. J., Gates, A. J., et al. (2016). An integrated biochemical system for nitrate assimilation and nitric oxide detoxification in *Bradyrhizobium japonicum*. *Biochem. J.* 473, 297–309. doi: 10.1042/BJ20150880

Calvo-Begueria, L., Rubio, M. C., Martinez, J. I., Perez-Rontome, C., Delgado, M. J., Bedmar, E. J., et al. (2018). Redefining nitric oxide production in legume nodules through complementary insights from electron paramagnetic resonance spectroscopy and specific fluorescent probes. *J. Exp. Bot.* 69, 3703–3714. doi: 10.1093/jxb/ery159

de Vries, S., Suharti, S., and Pouvreau, L. A. M. (2007). "Nitric oxide reductase: structural variations and catalytic mechanism," in *Biology of the Nitrogen Cycle*, ed. W. E. Newton (Amsterdam: Elservier Science), 57–67.

Delgado, M. J., Casella, S., and Bedmar, E. J. (2007). "Denitrification in rhizobia-legume symbiosis," in *Biology of the Nitrogen Cycle*, ed. W. E. Newton (Amsterdam: Elservier Science).

Girard, L., Brom, S., Davalos, A., Lopez, O., Soberon, M., and Romero, D. (2000). Differential regulation of *fixN*-reiterated genes in *Rhizobium etli* by a novel *fixL-fixK* cascade. *Mol. Plant Microbe Interact.* 13, 1283–1292. doi: 10.1094/MPMI.2000.13.12.1283

Gómez-Hernández, N., Reyes-Gonzalez, A., Sanchez, C., Mora, Y., Delgado, M. J., and Girard, L. (2011). Regulation and symbiotic role of *nirK* and *norC* expression in *Rhizobium etli*. *Mol. Plant Microbe Interact.* 24, 233–245. doi: 10.1094/MPMI-07-10-0173

González, V., Santamaria, R. I., Bustos, P., Hernandez-Gonzalez, I., Medrano-Soto, A., Moreno-Hagelsieb, G., et al. (2006). The partitioned *Rhizobium etli* genome: genetic and metabolic redundancy in seven interacting replicons. *Proc. Natl. Acad. Sci. U.S.A.* 103, 3834–3839. doi: 10.1073/pnas.0508502103

Hirayama, J., Eda, S., Mitsui, H., and Minamisawa, K. (2011). Nitrate-dependent N_2O emission from intact soybean nodules via denitrification by *Bradyrhizobium japonicum* bacteroids. *Appl. Environ. Microbiol.* 77, 8787–8790. doi: 10.1128/AEM.06262-11

Inaba, S., Ikenishi, F., Itakura, M., Kikuchi, M., Eda, S., Chiba, N., et al. (2012). N_2O emission from degraded soybean nodules depends on denitrification by *Bradyrhizobium japonicum* and other microbes in the rhizosphere. *Microbes Environ.* 27, 470–476. doi: 10.1264/jsme2.me12100

Inaba, S., Tanabe, K., Eda, S., Ikeda, S., Higashitani, A., Mitsui, H., et al. (2009). Nitrous oxide emission and microbial community in the rhizosphere of nodulated soybeans during the late growth period. *Microbes Environ.* 24, 64–67. doi: 10.1264/jsme2.me08544

Intergovernmental Panel on Climate Change [IPCC] (2014). *Climate Change 2014: Synthesis Report Contribution of Working Groups I, II and III to the Fifth Assessment Report of the Intergovernmental Panel on Climate Change*. Geneva: IPCC. doi: 10.1264/jsme2.me08544

Keen, N. T., Tamaki, S., Kobayashi, D., and Trollinger, D. (1988). Improved broad-host-range plasmids for DNA cloning in gram-negative bacteria. *Gene* 70, 191–197. doi: 10.1016/0378-1119(88)90117-5

Kovach, M. E., Elzer, P. H., Hill, D. S., Robertson, G. T., Farris, M. A., Roop, R. M., et al. (1995). Four new derivatives of the broad-host-range cloning vector pBBR1MCS, carrying different antibiotic-resistance cassettes. *Gene* 166, 175–176. doi: 10.1016/0378-1119(95)00584-1

Luque-Almagro, V. M., Gates, A. J., Moreno-Vivian, C., Ferguson, S. J., Richardson, D. J., and Roldan, M. D. (2011). Bacterial nitrate assimilation: gene distribution and regulation. *Biochem. Soc. Trans.* 39, 1838–1843. doi: 10.1042/BST20110688

Moreno-Vivian, C., Cabello, P., Martinez-Luque, M., Blasco, R., and Castillo, F. (1999). Prokaryotic nitrate reduction: molecular properties and functional distinction among bacterial nitrate reductases. *J. Bacteriol.* 181, 6573–6584.

Moreno-Vivián, C., and Flores, E. (2007). "Nitrate assimilation in bacteria," in *Biology of the Nitrogen Cycle*, eds H. Bothe, S. J. Ferguson, and W. E. Newton (Amsterdam: Elsevier), 263–282. doi: 10.1016/b978-044452857-5.50018-7

Nicholas, D. J. D., and Nason, A. (1957). "Determination of nitrate and nitrite," in *Methods in Enzymolog*, ed. N. O. Kaplan (London: Academic Press), 974–977.

Noel, K. D., Sanchez, A., Fernandez, L., Leemans, J., and Cevallos, M. A. (1984). *Rhizobium phaseoli* symbiotic mutants with transposon Tn5 insertions. *J. Bacteriol.* 158, 148–155.

Pilegaard, K. (2013). Processes regulating nitric oxide emissions from soils. *Philos. Trans. R. Soc. Lond. B Biol. Sci.* 368:20130126. doi: 10.1098/rstb.2013.0126

Prentki, P., and Krisch, H. M. (1984). In vitro insertional mutagenesis with a selectable DNA fragment. *Gene* 29, 303–313. doi: 10.1016/0378-1119(84)90059-3

Quinto, C., de la Vega, H., Flores, M., Fernández, L., Ballado, T., Soberón, G., et al. (1982). Reiteration of nitrogen fixation gene sequences in *Rhizobium phaseoli*. *Nature* 299, 724–726. doi: 10.1038/299724a0

Ravishankara, A. R., Daniel, J. S., and Portmann, R. W. (2009). Nitrous oxide (N_2O): the dominant ozone-depleting substance emitted in the 21st century. *Science* 326, 123–125. doi: 10.1126/science

Richardson, D. J. (2011). "Redox complexes of the nitrogen cycle," in *Nitrogen Cycling in Bacteria*, ed. J. W. B. Moir (Norkfolk: Caister Academic Press), 23–39.

Richardson, D. J., Berks, B. C., Russell, D. A., Spiro, S., and Taylor, C. J. (2001). Functional, biochemical and genetic diversity of prokaryotic nitrate reductases. *Cell. Mol. Life Sci.* 58, 165–178. doi: 10.1007/pl00000845

Sambrook, J., Fritsch, E. F., and Maniatics, T. (1989). *Molecular Cloning: A Laboratory Manual*. New York, NY: Cold Spring Harbor Laboratory Press. doi: 10.1007/pl00000845

Sambrook, J., and Russell, D. W. (2001). *Molecular Cloning : A Laboratory Manual*. New York, N.Y: Cold Spring Harbor Laboratory. doi: 10.1007/pl00000845

Sánchez, C., Bedmar, E. J., and Delgado, M. J. (2011). "Denitrification in legume-associated endosymbiotic Bacteria," in *Nitrogen Cycling in Bacteria*, ed. J. W. B. Moir, (Norfolk: Caister Academic Press), 197–210.

Schäfer, A., Tauch, A., Jager, W., Kalinowski, J., Thierbach, G., and Puhler, A. (1994). Small mobilizable multi-purpose cloning vectors derived from the *Escherichia coli* plasmids pK18 and pK19: selection of defined deletions in the chromosome of *Corynebacterium glutamicum*. *Gene* 145, 69–73. doi: 10.1016/0378-1119(94)90324-7

Simon, J., and Klotz, M. G. (2013). Diversity and evolution of bioenergetic systems involved in microbial nitrogen compound transformations. *Biochim. Biophys. Acta* 1827, 114–135. doi: 10.1016/j.bbabio.2012.07.005

Simon, R., Priefer, U., and Pühler, A. (1983). "Vector plasmids for in vivo and in vitro mainpulation of gram-negative bacteria," in *Molecular Genetics of the Bacteria-Plant Interaction*, ed. A. Pühler (Heidelberg: Springer-Verlag), 98–106. doi: 10.1007/978-3-642-69338-0_11

Smith, K. A., Mosier, A. R., Crutzen, P. J., and Winiwarter, W. (2012). The role of N_2O derived from crop-based biofuels, and from agriculture in general, in Earth's climate. *Philos. Trans. R. Soc. Lond. B Biol. Sci.* 367, 1169–1174. doi: 10.1098/rstb.2011.0313

Soberon, M., Lopez, O., Morera, C., Girard, M. L., Tabche, M. L., and Miranda, J. (1999). Enhanced nitrogen fixation in a *Rhizobium etli ntrC* mutant that overproduces the *Bradyrhizobium japonicum* symbiotic terminal oxidase cbb_3. *Appl. Environ. Microbiol.* 65, 2015–2019.

Thomson, A. J., Giannopoulos, G., Pretty, J., Baggs, E. M., and Richardson, D. J. (2012). Biological sources and sinks of nitrous oxide and strategies to mitigate emissions. *Philos. Trans. R. Soc. Lond. B Biol. Sci.* 367, 1157–1168. doi: 10.1098/rstb.2011.0415

Torres, M. J., Avila, S., Bedmar, E. J., and Delgado, M. J. (2018). Overexpression of the periplasmic nitrate reductase supports anaerobic growth by *Ensifer meliloti*. *FEMS Microbiol. Lett.* 365:fny041. doi: 10.1093/femsle/fny041

Torres, M. J., Hidalgo-Garcia, A., Bedmar, E. J., and Delgado, M. J. (2013). Functional analysis of the copy 1 of the *fixNOQP* operon of *Ensifer meliloti* under free-living micro-oxic and symbiotic conditions. *J. Appl. Microbiol.* 114, 1772–1781. doi: 10.1111/jam.12168

Torres, M. J., Rubia, I., de la Pena, T. C., Pueyo, J. J., Bedmar, E. J., and Delgado, M. J. (2014). Genetic basis for denitrification in *Ensifer meliloti*. *BMC Microbiol.* 14:142. doi: 10.1186/1471-2180-14-142

Torres, M. J., Simon, J., Rowley, G., Bedmar, E. J., Richardson, D. J., Gates, A. J., et al. (2016). Nitrous oxide metabolism in nitrate-reducing bacteria: physiology and regulatory mechanisms. *Adv. Microb. Physiol.* 68, 353–432. doi: 10.1016/bs.ampbs.2016.02.007

van Spanning, R. J. (2011). "Structure, function, regulation and evolution of the nitrite and nitrous oxide reductase: denitrification enzymes with a β-propeller fold," in *Nitrogen Cycling in Bacteria*, ed. J. W. B. Moir (Norkfolk: Caister Academic Press), 135–161.

Vargas, C., McEwan, A. G., and Downie, J. A. (1993). Detection of *c*-type cytochromes using enhanced chemiluminescence. *Anal. Biochem.* 209, 323–326. doi: 10.1006/abio.1993.1127

Zumft, W. G., and Kroneck, P. M. (2007). Respiratory transformation of nitrous oxide (N_2O) to dinitrogen by Bacteria and archaea. *Adv. Microb. Physiol.* 52, 107–227. doi: 10.1016/S0065-2911(06)52003-X

Conflict of Interest Statement: The authors declare that the research was conducted in the absence of any commercial or financial relationships that could be construed as a potential conflict of interest.

frontiers in Microbiology

ORIGINAL RESEARCH
published: 07 May 2019
doi: 10.3389/fmicb.2019.00924

An Integrated Systems Approach Unveils New Aspects of Microoxia-Mediated Regulation in *Bradyrhizobium diazoefficiens*

Noemí Fernández[1†], Juan J. Cabrera[1†], Adithi R. Varadarajan[2,3†], Stefanie Lutz[2], Raphael Ledermann[4], Bernd Roschitzki[5], Leo Eberl[6], Eulogio J. Bedmar[1], Hans-Martin Fischer[4], Gabriella Pessi[6], Christian H. Ahrens[2] and Socorro Mesa[1]**

[1] Department of Soil Microbiology and Symbiotic Systems, Estación Experimental del Zaidín, Consejo Superior de Investigaciones Científicas, Granada, Spain, [2] Agroscope, Research Group Molecular Diagnostics, Genomics and Bioinformatics and Swiss Institute of Bioinformatics, Wädenswil, Switzerland, [3] Department of Health Sciences and Technology, Institute of Molecular Systems Biology, ETH Zurich, Zurich, Switzerland, [4] Institute of Microbiology, ETH Zurich, Zurich, Switzerland, [5] Functional Genomics Center Zurich, ETH & UZH Zurich, Zurich, Switzerland, [6] Department of Plant and Microbial Biology, University of Zurich, Zurich, Switzerland

OPEN ACCESS

Edited by:
Xavier Perret,
Université de Genève, Switzerland

Reviewed by:
Anibal Roberto Lodeiro,
Instituto de Biotecnología y Biología Molecular (CONICET) and National University of La Plata, Argentina
Michael Göttfert,
Dresden University of Technology, Germany

***Correspondence:**
Christian H. Ahrens
christian.ahrens@agroscope.admin.ch
Socorro Mesa
socorro.mesa@eez.csic.es

[†]These authors share first authorship

Specialty section:
This article was submitted to Microbial Symbioses, a section of the journal Frontiers in Microbiology

Received: *15 February 2019*
Accepted: *11 April 2019*
Published: *07 May 2019*

Citation:
Fernández N, Cabrera JJ, Varadarajan AR, Lutz S, Ledermann R, Roschitzki B, Eberl L, Bedmar EJ, Fischer H-M, Pessi G, Ahrens CH and Mesa S (2019) An Integrated Systems Approach Unveils New Aspects of Microoxia-Mediated Regulation in Bradyrhizobium diazoefficiens. Front. Microbiol. 10:924. doi: 10.3389/fmicb.2019.00924

The adaptation of rhizobia from the free-living state in soil to the endosymbiotic state comprises several physiological changes in order to cope with the extremely low oxygen availability (microoxia) within nodules. To uncover cellular functions required for bacterial adaptation to microoxia directly at the protein level, we applied a systems biology approach on the key rhizobial model and soybean endosymbiont *Bradyrhizobium diazoefficiens* USDA 110 (formerly *B. japonicum* USDA 110). As a first step, the complete genome of *B. diazoefficiens* 110*spc*4, the model strain used in most prior functional genomics studies, was sequenced revealing a deletion of a ∼202 kb fragment harboring 223 genes and several additional differences, compared to strain USDA 110. Importantly, the deletion strain showed no significantly different phenotype during symbiosis with several host plants, reinforcing the value of previous OMICS studies. We next performed shotgun proteomics and detected 2,900 and 2,826 proteins in oxically and microoxically grown cells, respectively, largely expanding our knowledge about the inventory of rhizobial proteins expressed in microoxia. A set of 62 proteins was significantly induced under microoxic conditions, including the two nitrogenase subunits NifDK, the nitrogenase reductase NifH, and several subunits of the high-affinity terminal cbb_3 oxidase (FixNOQP) required for bacterial respiration inside nodules. Integration with the previously defined microoxia-induced transcriptome uncovered a set of 639 genes or proteins uniquely expressed in microoxia. Finally, besides providing proteogenomic evidence for novelties, we also identified proteins with a regulation similar to that of $FixK_2$: transcript levels of these protein-coding genes were significantly induced, while the corresponding protein abundance remained unchanged or was down-regulated. This suggested that, apart from $fixK_2$, additional *B. diazoefficiens* genes might be under microoxia-specific post-transcriptional control. This hypothesis was indeed confirmed for several targets (HemA, HemB, and ClpA) by immunoblot analysis.

Keywords: comparative genomics, FNR/CRP proteins, genome sequencing, proteogenomics, post-transcriptional control, rhizobia, symbiosis, transcriptomics

INTRODUCTION

Rhizobia are primary contributors to biological nitrogen fixation, a process that is highly relevant both for agronomy and, by reducing the need of chemical fertilizers, for the environment. Optimizing the efficiency of nitrogen fixation is of great interest for sustainable agriculture and to potentially exploit symbiotic plant-microbe interactions for additional crops in the future. Consequently, there is a pressing need to further advance our understanding of the regulatory mechanisms that control rhizobia-leguminous plant interactions.

Rhizobia comprise a large group of both alpha- and beta-proteobacteria (reviewed in Sprent et al., 2017) which can establish symbiotic relationships with legumes. They encode the enzyme nitrogenase, which catalyzes the conversion of atmospheric nitrogen gas to ammonium inside plant root (and occasionally stem) nodules (reviewed in Dixon and Kahn, 2004; Terpolilli et al., 2012). During the establishment of a rhizobia-legume symbiosis, bacteria need to adapt their physiology from the free-living state in soil to the highly specialized environment of a plant cell, the so called bacteroid state. This multi-step process is tightly controlled at different stages of the symbiotic interaction and includes various signals released and sensed by both the bacteria and the host plant. One of these signals is the extremely low partial pressure of free oxygen (microoxia) within nodules. Microoxia represents a critical signal both for the expression and activity of nitrogenase and the cbb_3-type high-affinity terminal oxidase required for bacterial respiration inside nodules (reviewed in Fischer, 1994, 1996; Dixon and Kahn, 2004; Terpolilli et al., 2012; Poole et al., 2018).

Bradyrhizobium diazoefficiens USDA 110 (formerly *B. japonicum* USDA 110; Delamuta et al., 2013) is one of the most important and best-studied rhizobial model species; it can form nodules on soybean (*Glycine max*) roots and a few other host plants like cowpea, mungbean, siratro, and others (reviewed in Sprent et al., 2017). Its molecular genetics, physiology, and ecology has been intensively investigated. The availability of several rhizobial genome sequences, including that of *B. diazoefficiens* USDA 110 (Kaneko et al., 2002; Davis-Richardson et al., 2016), has enabled functional genomics studies that have explored gene expression differences using either custom-made microarrays or RNA-Seq. Moreover, protein expression profiling studies using 2-D gels and later shotgun proteomics approaches provided further insights. The analysis of selected regulatory mutant strains, all grown under free-living microoxic conditions (Hauser et al., 2007; Lindemann et al., 2007; Pessi et al., 2007; Mesa et al., 2008), have greatly contributed to a better understanding of the regulatory mechanisms underlying the adaptation to the low oxygen tension encountered inside nodules. A complex regulatory network composed of two interlinked signaling cascades (FixLJ-$FixK_2$ and RegSR-NifA) controls the expression of genes in response to microoxia, both in free-living conditions and in symbiosis (Sciotti et al., 2003; Pessi et al., 2007; reviewed in Fernández et al., 2016). For the transcription factor $FixK_2$, which plays a key role in the microoxia-mediated regulation in *B. diazoefficiens* both in free-living conditions and in symbiosis, more than 300 regulated genes were identified including the *fixNOQP* operon, which encodes the cbb_3-type high-affinity terminal oxidase (Mesa et al., 2008). The expression of $fixK_2$ is induced by the superimposed two-component regulatory system FixLJ in response to microoxia, and is self-repressed by a yet unknown mechanism (reviewed in Fernández et al., 2016). $FixK_2$ is a peculiar member of the cyclic AMP (cAMP) receptor protein (CRP) and the fumarate and nitrate reductase (FNR) activator protein family of bacterial transcription factors (Körner et al., 2003). It is active *in vitro* without additional effector molecules and is regulated post-translationally by the oxidation of its singular cysteine residue and by proteolysis (Mesa et al., 2005, 2009; Bonnet et al., 2013; reviewed in Fernández et al., 2016).

Due to the often modest correlation between gene expression and protein levels in bacteria, a comprehensive differential protein expression profiling of cells grown under microoxic conditions would complement the existing transcriptomics data and potentially uncover further aspects of the rhizobial adaptation to the nodule environment. However, while several proteomics studies exist on various stages of the rhizobial symbiosis (Winzer et al., 1999; Natera et al., 2000; Panter et al., 2000; Morris and Djordjevic, 2001; Djordjevic et al., 2003; Djordjevic, 2004; Sarma and Emerich, 2005; Larrainzar et al., 2007; Delmotte et al., 2010, 2014; Koch et al., 2010; Tatsukami et al., 2013; Clarke et al., 2015; Nambu et al., 2015; Marx et al., 2016; reviewed in Larrainzar and Wienkoop, 2017), data on the importance of microoxia in the adaptation to a nodule environment are scarce for rhizobial species. Two 2-D gel-based studies exist where protein expression patterns in oxic and low oxygen conditions were compared (Regensburger et al., 1986; Dainese-Hatt et al., 1999). The latter study had identified 24 of 38 differentially expressed proteins in cells grown under low oxygen (2% O_2) or anaerobic conditions.

Notably, for *B. diazoefficiens*, most of the above functional genomics studies have in fact been performed with a spontaneous spectinomycin resistant derivative of *B. diazoefficiens* USDA 110 (*B. diazoefficiens* 110*spc*4; Regensburger and Hennecke, 1983). Since this strain was derived from the reference strain 36 years ago, it might well harbor genomic differences compared to the published USDA 110 NCBI reference genome sequence (NC_004463; Kaneko et al., 2002). In order to close this knowledge gap and to unravel new facets of the adaptation of *B. diazoefficiens* 110*spc*4 going from an oxic to a microoxic lifestyle, we applied an integrated systems approach. This included as first step a *de novo* genome assembly of the 110*spc*4 model strain, which revealed a deletion of 202 kb and several additional differences, that were not affecting symbiotic functions. We next performed a shotgun proteomics study using an adapted protocol of the gel-free, filter-aided sample preparation (FASP) methodology combined with liquid chromatography-tandem mass spectrometry (LC-MS/MS) and downstream bioinformatic data analysis, which included a detailed comparison of the genome of strain 110*spc*4 used in this study vs. that of the USDA 110 reference strain. Integration of protein expression data from oxic and microoxic conditions with those from previous transcriptomics experiments not only allowed us to identify proteins specifically induced under microoxic conditions, but

also to discover new genes that are probably subject to post-transcriptional control like it was previously demonstrated for $fixK_2$ (Mesa et al., 2009).

MATERIALS AND METHODS

Bacterial Strains and Growth Conditions

B. diazoefficiens 110*spc*4 (wild type, a spontaneous spectinomycin-resistant derivative of *B. diazoefficiens* USDA 110), formerly *B. japonicum* USDA 110 (3I1b110; U.S. Department of Agriculture, Beltsville, MD, USA) (8,373 genes, 8,317 CDS), was routinely grown at 30°C in a peptone-salts-yeast extract (PSY) medium (Regensburger and Hennecke, 1983) as modified in Mesa et al. (2008). Oxic (21% O_2) and microoxic cultures (0.5% O_2, 99.5% N_2) for shotgun proteomics, western blot analyses, and heme staining were grown to mid-exponential phase (optical density at 600 nm [OD_{600}] of 0.45–0.6). For these experiments, oxic cultures were grown in 1-l Erlenmeyer flasks containing 50 ml of medium with vigorous shaking (170 rpm), while microoxic cultures were grown in 500 ml rubber-stoppered serum bottles containing 25 ml of medium with moderate shaking (60 rpm). In the latter, the gas phase was exchanged every 8–16 h. Spectinomycin was added to solid media at 200 μg/ml and liquid media at 100 μg/ml.

Genome Sequencing, Assembly, and Annotation

B. diazoefficiens 110*spc*4 chromosomal DNA was isolated with a phenol/chloroform protocol as described previously (Hahn and Hennecke, 1984). PacBio SMRT sequencing was performed on an RSII machine using 1 SMRT cell. Size selection was performed using the BluePippin system which resulted in fragments with an average subread length of 13 kb. The PacBio reads were assembled using HGAP v.3, which was run on the SMRT Portal using the protocol "RS_HGAP_Assembly.3" (default parameters, except: minimum subread length of 1,000, estimated genome size of 9 Mb). The resulting contig was start-aligned with the RefSeq USDA 110 strain (NC_004463; Kaneko et al., 2002), and further polished with Quiver using the "RS_Resequencing.1" protocol (default parameters). To verify the circularity and completeness of the *de novo* assembly, the filtered PacBio subreads were mapped to the circular chromosome using graphmap (v.0.5.2) (Sović et al., 2016). The assembly was further improved using 2 × 300 bp paired end Illumina MiSeq reads and Freebayes (v.1.2.0; minimum alternate fraction: 0.5, minimum alternate count: 5) to correct small errors (e.g., homopolymer errors). Variants were manually inspected in the Integrated Genome Viewer (Thorvaldsdóttir et al., 2013) and subsequently corrected using bcftools (v.0.1.19) (Narasimhan et al., 2016). The genome was annotated with the prokaryotic genome annotation pipeline (Tatusova et al., 2016) used by the National Center of Biotechnology and Information (NCBI), which returned 8,407 genes, 8,348 CDS, and 248 pseudogenes. A functional classification of the genes in Clusters of Orthologous Groups (COG) categories was performed using eggNOG and the database "bactNOG," "proNOG," and "aproNOG" (Huerta-Cepas et al., 2016). Best hits with an e-value below 0.001 were used to assign the COG category. In addition, all protein-coding genes were also annotated using Interproscan v5.30-69.0 (Jones et al., 2014) to add information on protein domains, families, and patterns, PSORTb (Yu et al., 2010) to identify a predicted subcellular localization, and LipoP (Rahman et al., 2008) to identify lipoproteins. Further, proteins were classified as transmembrane (TM), secreted or membrane anchored using a combination of TM spanning helices and signal peptides predicted by TMHMM v2.0, SignalP v4.1, and Phobius v1.01 (predictions were extracted from Interproscan results), basically as described before (Delmotte et al., 2010) except that we considered a cutoff of 2 TM domains. We only considered cases where the predictions for TM helices and signal peptides of the two tools overlapped by at least 10 amino acids.

Comparative Genomics

The genome sequence of *B. diazoefficiens* 110*spc*4 was aligned to that of the USDA 110 RefSeq strain using the progressive Mauve algorithm (v.2.4.0) (Darling et al., 2010) in order to inspect for larger-scale structural variations. Furthermore, it was mapped to the RefSeq genome sequence using Minimap2 (v.2.10; preset parameters: asm5) (Li, 2018) and smaller variants were detected using Freebayes (v.1.2.0; minimum alternate fraction: 0.1, minimum alternate count: 1). SnpEff (v.4.3) (Cingolani et al., 2012) was used to annotate and predict potential effects of the detected variants in strain USDA 110. For this, a database of the RefSeq genome was built using the annotated GenBank file, which was subsequently used to interpret variants. Related data summarizing major genomic differences are shown in **Figure 1**; **Table 1** and **Supplementary Tables S1**, **S2**. Finally, we also compared the proteins encoded by the two genomes using blastp (Johnson et al., 2008). Only hits below an e-value of 1e-5 were considered. For proteins with multiple hits, we considered the hit with the highest amino acid identity and query coverage, respectively (**Supplementary Table 3**, **Data Sheet A**). All references cited in the Supplementary Material are listed in **Supplementary Data Sheet 1**.

Sample Preparation for Shotgun Proteomics

Three replicates of 100 ml of culture grown to mid-exponential phase under oxic and microoxic conditions were collected by centrifugation (11,139 × *g* for 5 min at 4°C), and pellets were kept at −80°C. Each pellet was resuspended in 1 ml of 125 mM Tris-HCl pH 8.2 buffer supplemented with a protease inhibitor cocktail (cOmplete, Roche Diagnostics) according to the manufacturer's recommendations, before the cell suspension was sonicated (1 min, cycle 5, 50% amplitude; Bandelin UW2070). The above procedure was followed by disruption through an ice-cold French pressure cell (SLM Aminco) at about 120 MPa, and another round of sonication (same settings). One-hundred μl lysate per sample were mixed with 4% sodium dodecyl sulfate (SDS) and 0.1 M dithiothreitol (DTT) and boiled at 95°C for 6 min with gentle shaking (at 700 rpm) in a thermomixer comfort (Vaudaux-Eppendorf AG). Samples were then processed with an ultrasonic cup horn (UTR200, Heilscher Ultrasonics GmbH) for 15 min at an amplitude of 65% for a 0.5 cycle and

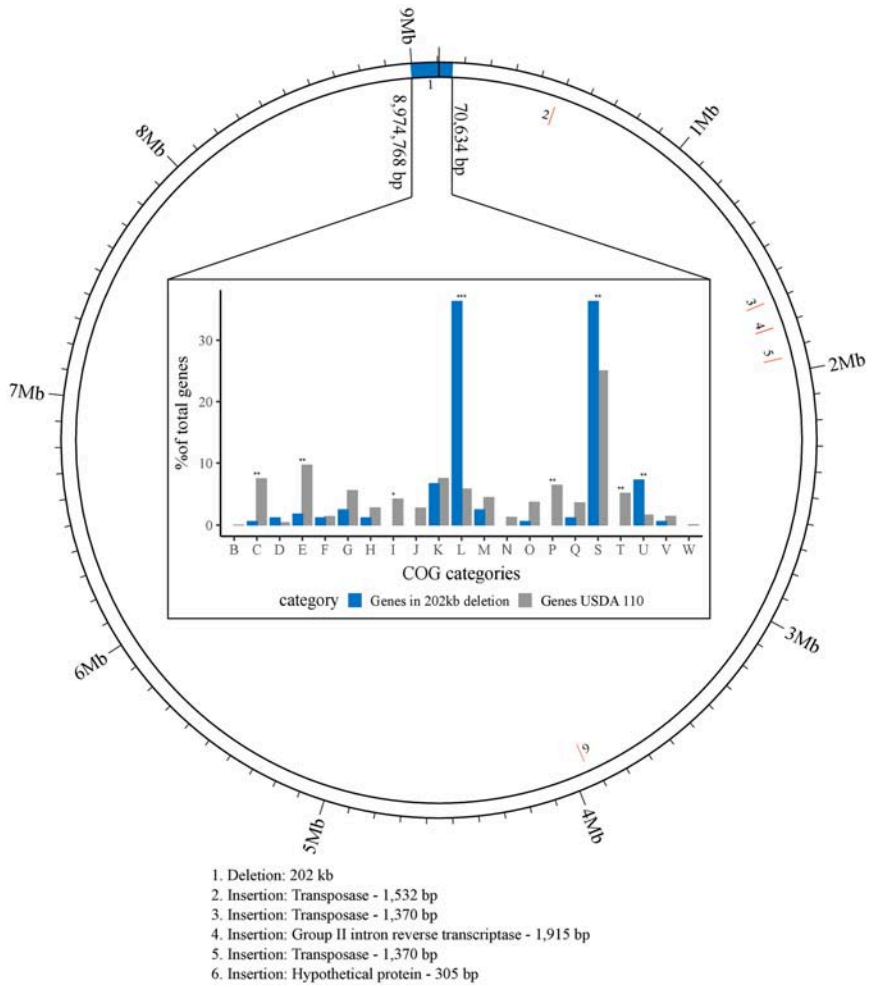

FIGURE 1 | Visualization of larger genomic changes in *B. diazoefficiens* strain 110*spc*4 (inner ring) compared to the USDA 110 NCBI reference genome (outer ring). Five insertions (2 through 6; red) and a large deletion region (1; blue) are shown (see **Table 1**). The bar chart shows the results of a Fisher's exact test for enrichment of COG categories annotated in 142 of 223 genes located in the 202 kb region of USDA 110 that is absent in strain 110*spc*4. Significant *p*-values are highlighted above each category (**p*-value < 0.01; ***p*-value < 0.001; ****p*-value < 0.00001). The percentages of genes (count of genes / total no. of genes) for each COG category (X-axis) from USDA 110 (gray) or from the 202 kb deletion region (blue) are shown on the Y-axis.

centrifuged for 10 min at 16,000 × *g*. Protein concentration was determined using the Qubit™ Protein Assay Kit (Invitrogen Life Technologies). Twenty microgram protein of each sample were used for on-filter digestion using a modified version of the FASP protocol (Wiśniewski et al., 2009a,b). Proteins were diluted in 200 µl of 100 mM Tris-HCl pH 8.2 buffer containing 8 M urea (UA buffer), loaded on Ultracel 30,000 MWCO centrifugal units (Amicon Ultra, Merck), and centrifuged at 14,000 × *g* for 20 min. The loaded filter was washed once with 200 µl UA buffer at 14,000 × *g* for 15 min. Alkylation of reduced proteins was carried out by adding 100 µl 0.05 M iodoacetamide in UA buffer shaking for 1 min at 600 rpm in a thermomixer, followed by 5 min incubation at room temperature and centrifugation at 14,000 × *g* for 20 min. Then, samples were washed with 100 µl UA buffer three times (centrifugation at 14,000 × *g* for 15 min), followed by two washing steps with 100 µl 0.5 M NaCl in water. On-filter protein digestion was carried out by adding 120 µl trypsin containing triethylammonium bicarbonate buffer (pH 8.5) (Promega) at a ratio of 1:50 (w/w) onto the filter, mixing for 1 min in a thermomixer at 600 rpm, and overnight incubation in a wet chamber at room temperature. The filter units were then centrifuged at 14,000 × *g* for 20 min and the peptide containing solution was acidified to a final concentration of 0.1% trifluoroacetic acid and 3% acetonitrile. Peptides were desalted using Finisterre C18 SPE cartridges (Teknokroma) following the manufacturer's protocol. Eluted peptides were dried in a centrifugal vacuum concentrator (Thermo Servant SPD 121P) and dissolved in 50 µl of 3% acetonitrile and 0.1% formic acid for mass spectrometry (MS) analysis.

Liquid Chromatography-Tandem Mass Spectrometry (LC-MS/MS) Analysis

Dissolved peptides were separated on a self-made reverse-phase column (75 µm × 150 mm) packed with C18 material (ReproSil-Pur, C18, 120 Å, AQ, 1.9 µm, Dr. Maisch GmbH). The column was equilibrated with 100% solvent A (0.1% formic acid in

TABLE 1 | Overview of larger genomic differences between strain *B. diazoefficiens* 110*spc*4 compared to the NCBI *B. diazoefficiens* USDA 110 reference genome (see also **Figure 1**).

Change in 110*spc*4	Start pos. in USDA 110 (RefSeq)	Start pos. in 110*spc*4	Length (bp)	Gene(s) affected or contained in inserted region	Gene, product interrupted (CDS in reference)
DEL	1	1	70,634	78 CDS	Together with the deletion below (next row), 223 CDS are affected. See **Supplementary Table S1**
DEL	8,974,768	8,910,608	131,060	145 CDS	Together with the deletion above (previous row), 223 CDS are affected. See **Supplementary Table S1**
INS	483,970	413,137	1,532	Transposase (Bdiaspc4_01920)	No CDS in USDA 110 reference
INS	1,699,880	1,630,578	1,370	Transposase (Bdiaspc4_07865)	No CDS in USDA 110 reference
INS	1,806,987	1,739,052	1,915	Group II intron reverse transcriptase (Bdiaspc4_08330)	No CDS in USDA 110 reference
INS	1,936,754	1,870,731	1,370	Transposase (Bdiaspc4_09015)	Bll1778[a], unknown protein (1,936,357–1,937,313)
INS	3,936,542	3,872,887	305	Hypothetical protein (Bdiaspc4_18405)	Bll3563[b], unknown protein (3,930,196–3,940,521)

[a] *Bll1778 is a hypothetical protein of 318 amino acids; it has no PFAM-A protein domains.*
[b] *Bll3563 is a large protein (3441 aa) with many VCBS domains (suggested role in adhesion).*
DEL, deletion; INS, insertion.

water). Peptides were eluted using the following gradient of solvent B (0.1% FA in acetonitrile): 0–50 min, 0–25% B; 50–60 min, 25–32% B; 60–70 min, 32–97% B at a flow rate of 0.3 µl/min. High accuracy mass spectra were acquired with an Orbitrap Fusion (Thermo Scientific) that was operated in data-dependent acquisition mode. All precursor signals were recorded in the Orbitrap using quadrupole transmission in the mass range of 300–1,500 m/z. Spectra were recorded with a resolution of 120,000 at 200 m/z, a target value of 4E5 and the maximum cycle time was set to 3 s. Data-dependent MS/MS were recorded in the linear ion trap using quadrupole isolation with a window of 1.6 Da and HCD fragmentation with 30% fragmentation energy. The ion trap was operated in rapid scan mode with a target value of 2E3 and a maximum injection time of 300 ms. Precursor signals were selected for fragmentation with a charge state from +2 to +7 and a signal intensity of at least 5E3. A dynamic exclusion list was used for 30 s and maximum parallelizing ion injections was activated.

Protein Identification, Differential Protein Expression Analyses, and Integration With Transcriptomics Data

Data from three LC MS/MS runs per condition were processed with an in-house data analysis pipeline (Omasits et al., 2013). Raw data were converted with msconvert (ProteoWizard release 3.09.9098) before extracting fragment-ion spectra. A search against a *B. diazoefficiens* USDA 110 (8,317 CDS) and a 110*spc*4 (8,348 CDS) protein search database (both also containing 256 common contaminants) was carried out with MS-GF+ (v2017.01.13) (Kim and Pevzner, 2014) using a precursor mass accuracy of 10 ppm (the fragment ion mass tolerance is determined by the algorithm). Cysteine carbamidomethylation as fixed, oxidation of methionine and deamidation of asparagine and glutamine as variable modifications were set. Using the target-decoy approach of MS-GF+, the false discovery rate (FDR) at the peptide-spectrum-matching (PSM) level was estimated and then set below 0.35%. For protein inference, we only considered unambiguous peptides (class 1a, class 3a) as identified by a PeptideClassifier analysis (Qeli and Ahrens, 2010). Requiring at least two peptides or three PSMs per condition per protein, i.e., the same thresholds as used previously (Delmotte et al., 2010; Koch et al., 2014), 3,188 proteins were identified overall for strain 110*spc*4 with a protein level FDR below 1%. To detect differentially expressed proteins, we used DESeq2 (Love et al., 2014) which returns a list of proteins ranked according to their statistical significance. A multiple testing corrected *p*-value threshold of ≤ 0.2 was applied as selection criterion for the identification of the top significantly expressed proteins. Since previous transcriptomics data were filtered based on a fold change (FC) expression difference level ($\log_2$ FC ≥ 1 or ≤ -1), we applied the same, less stringent filter for the further overlap analysis of genes and proteins upregulated in microoxia ($\log_2$ FC ≥ 1).

Western Blot Analyses

Steady-state levels of *B. diazoefficiens* NapA, and NosZ (microoxia-induced proteins) and ClpA, $FixK_2$, HemA, and HemB (the corresponding protein-encoding genes are subject to post-transcriptional control) were monitored in cells grown oxically and microoxically by immunoblot analysis. Proteins with constant accumulated levels in both oxic and microoxic conditions, i.e., ClpP, CoxA, CoxB, and ScoI were used as controls in the experiments. At least three biological replicates of two hundred milliliters of mid-exponential grown oxic and microoxic cultures were collected by centrifugation (9,000 × *g*, 7 min, 4°C), resuspended in 2 ml of lysis buffer (40 mM Tris-HCl pH 7.0, 150 mM KCl, 0.2 mM 4-[2-Aminoethyl] benzenesulfonyl fluoride hydrochloride [AEBSF]) and disrupted by four passages through an ice-cold French pressure cell (SLM Aminco) at about 120

MPa. Cell suspensions were centrifuged (21,000 × *g*, 30 min, 4°C) to obtain total cell-free extracts. For fractionation, cell-free extracts were then ultracentrifuged at 140,000 × *g* for 45 min at 4°C. Membrane pellets were resuspended in 100 µl of lysis buffer. Ten to forty micrograms of protein (crude extract, soluble fraction, or membranes) were then mixed with one sixth volume of SDS loading dye (280 mM Tris-HCl, pH 6.8, 20% glycerol, 8% SDS, 480 mM DTT, 0.02% bromophenol blue). For ClpA, CoxB, and HemB detection, protein samples were mixed with an equal volume of SDS loading dye containing mercaptoethanol (125 mM Tris-HCl, pH 6.8, 20% glycerol, 4% SDS, 10% mercaptoethanol, 0.02% bromophenol blue). Proteins were subsequently resolved in 14% sodium dodecyl sulfate polyacrylamide gel electrophoresis (SDS-PAGE), and analyzed by western blotting basically as previously described by Torres et al. (2017) (except for ClpA, CoxB, and HemB detection, 1% casein instead of 5% non-fat dry milk was added in the blocking buffer in our experiments). Samples were boiled prior to electrophoresis except for CoxA detection, where samples were equilibrated for 15 min in SDS loading dye. Polyclonal antibodies against $FixK_2$, HemA, and HemB of *B. diazoefficiens* (Chauhan and O'Brian, 1995; Jung et al., 2004; Mesa et al., 2009), ClpA of *Caulobacter crescentus* (Grünenfelder et al., 2004), NosZ of *Paracoccus denitrificans* (Felgate et al., 2012), and NapA of *P. pantotrophus* M6 (Gates et al., 2003) were available from previous work. A polyclonal antibody against *C. crescentus* ClpP (Jenal and Fuchs, 1998), peptide antibodies raised against *B. diazoefficiens* CoxA (Loferer et al., 1993) and *B. diazoefficiens* CoxB (Bühler et al., 2010), and a polyclonal antibody against the soluble part of *B. diazoefficiens* ScoI (Bühler et al., 2010) were used to monitor protein levels in extracts of oxic and microoxic cultures. Except for *C. crescentus* anti-ClpP (1:5,000 dilution), *B. diazoefficiens* anti-CoxB (1:10,000 dilution), and *B. diazoefficiens* anti-HemB (1:2,000 dilution) primary antibodies were diluted at 1:1,000 in blocking buffer. Horseradish peroxidase (HRP)-conjugated goat anti-rabbit IgG (for ClpA, ClpP, CoxA, CoxB, $FixK_2$, HemB, NapA, and ScoI; Bio-Rad), HRP-conjugated goat anti-mouse IgG (for HemA; Bio-Rad), and HRP-conjugated donkey anti-sheep (for NosZ; Sigma-Aldrich) were used as secondary antibodies at a 1:3,000 dilution. Chemiluminescent signals were detected using the ECL Select western-blotting detection reagent (GE Healthcare) in a Chemidoc XRS instrument (Universal Hood II, Bio-Rad). The Quantity One and Image Lab softwares (Bio-Rad) were used for image analyses.

Cytochrome *c* Detection by Heme Staining

Membrane-bound heme-*c* protein detection was performed as described elsewhere (Delgado et al., 2003; Mesa et al., 2008; Bueno et al., 2010). Two hundred milliliters of *B. diazoefficiens* cells grown oxically and microoxically were harvested at mid-exponential phase, washed with 50 mM Tris-HCl buffer (pH 7.5) (fractionation buffer) and resuspended in 2 ml of the same buffer containing 1 mM AEBSF, and 10 µg DNase I/ml. Cell fractionation was performed as described above. Membrane pellets were resuspended in 100 µl of fractionation buffer. Membrane fractions were mixed with one sixth volume of SDS loading dye with reduced DTT concentration (20 mM instead of 480 mM), incubated at room temperature for 15 min and loaded without boiling onto 12% SDS-PAGE. Proteins were then transferred to a nitrocellulose filter and stained for heme-dependent peroxidase activity by chemiluminescence (Vargas et al., 1993), which was detected and analyzed as described above for the western blot assays. Experiments were carried out with at least two biological replicates.

Determination of Protein Concentration

Protein concentration of samples for western blot and heme staining was estimated spectrophotometrically using the Bio-Rad assay (Bio-Rad Laboratories) with bovine serum albumin (BSA) as standard.

Plant Infection Test and Determination of Nitrogenase Activity

Seeds of soybean (*G. max* (L.) Merr.) cv. Williams 82 (kindly provided by D.-N. Rodríguez Navarro, CIFA, Las Torres-Tomejil, Seville, Spain), and cv. Black Jet, cowpea (*Vigna unguiculata* (L.) Walp.) cv. Iron and Clay, mung bean (*Vigna radiata* (L.) R. Wilczek) (all purchased from Johnny's Selected Seeds, Albion, ME, USA), and siratro (*Macroptilium atropurpureum* (DC.) Urb. provided by W. D. Broughton, University of Geneva, Switzerland) were surface-sterilized by immersion in 100% ethanol for 5 min and subsequently in 35% H_2O_2 for 15 min. After intense washing with sterile water, seeds were germinated for 48 h at 28°C. Sterilization and germination of *Aeschynomene afraspera* seeds was done as described (Renier et al., 2011). Plant growth conditions were described previously (Göttfert et al., 1990). *A. afraspera* plants were cultivated as all other plants, except that the substrate was kept water-logged.

Nitrogenase activity was determined by gas chromatographic detection of ethylene (C_2H_4) resulting from acetylene (C_2H_2) reduction by nitrogenase. To do so, whole roots of nodulated plants were incubated in 50-ml sealed vials and 1 ml acetylene (2% [v/v]) was added to the gas atmosphere. After incubation for 30 min at room temperature, 25 µl of the gas phase were analyzed on a GC6850 gas chromatograph (Agilent Technologies) equipped with a 30 m × 0.53 mm HP-PLOT/Q column. Enzyme activity (units; calculated by dividing the C_2H_4 peak area by the sum of the C_2H_4 + C_2H_2 peak area) was normalized to the total nodule dry weight of individual plants and 1 min incubation time.

RESULTS

Sequencing and *de novo* Genome Assembly of *B. diazoefficiens* Strain 110*spc*4

Many gene and protein expression profiling studies of *B. diazoefficiens* cells grown under free-living conditions or in symbiosis (Lardi and Pessi, 2018 and Discussion) have been performed with *B. diazoefficiens* 110*spc*4 (Regensburger and Hennecke, 1983). Given the split from the USDA 110 reference strain 36 years ago, strain 110*spc*4 might well harbor genomic differences compared to the 9,105,828 bp genome of the

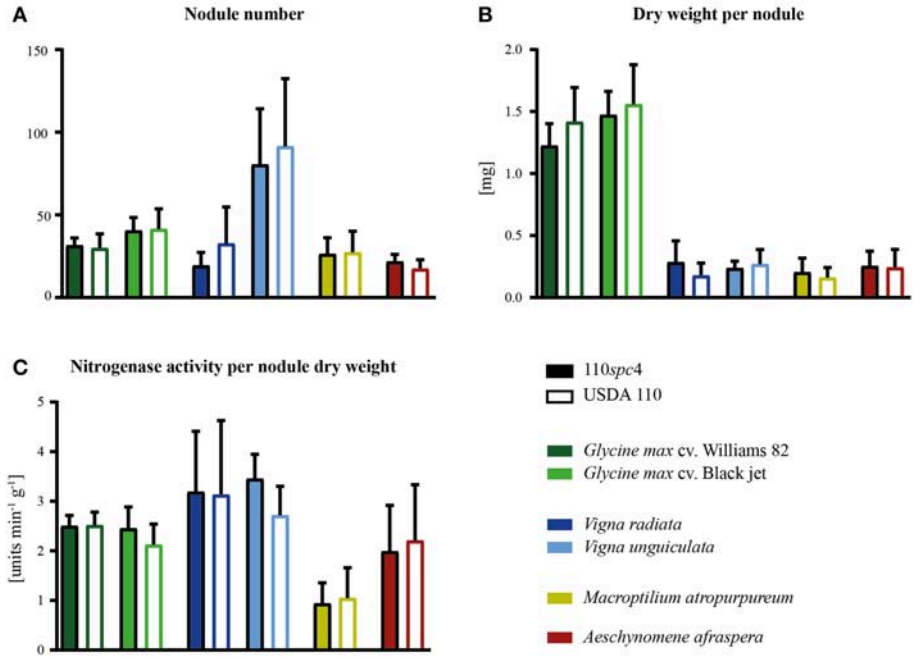

FIGURE 2 | Symbiotic properties of *B. diazoefficiens* strains 110*spc*4 and USDA 110 on different legume host plants. No significant difference was found between strains 110*spc*4 and USDA 110 with respect to nodule number **(A)**, dry weight per nodule **(B)**, or nitrogenase activity normalized to total nodule dry weight **(C)** on all six tested host plants, following a one way ANOVA with Holm-Šídáks correction (0.05 α). The two soybean (*Glycine max*) cultivars Williams 82 ($n = 9$ and 10 for 110*spc*4 and USDA 110, respectively) and Black jet ($n = 10$ and 10), mung bean (*Vigna radiata*; $n = 9$ and 7), cowpea (*Vigna unguiculata*, $n = 8$ and 8), and the crack-entry host *Aeschynomene afraspera* ($n = 10$ and 9) were analyzed 21 days post inoculation (dpi) whereas siratro plants (*Macroptilium atropurpureum*, $n = 8$ and 10) were analyzed 28 dpi. Error bars represent standard deviation of the mean.

reference strain (NC_004463; Kaneko et al., 2002). Aiming to provide an optimal basis for subsequent functional genomics and systems-wide analyses for strain 110*spc*4, we sequenced and *de novo* assembled its complete genome using a combination of long PacBio reads (average read length 13 kb) and short Illumina MiSeq reads (paired-end, 300 bp). The latter were used to correct any potentially remaining homopolymer errors in the PacBio assembly. The finished, high-quality genome sequence of *B. diazoefficiens* 110*spc*4 consisted of a single, circular chromosome of 8,910,608 bp. A genome comparison uncovered several differences compared to the USDA 110 reference genome (**Table 1**), most notably a 202 kb deletion of a genomic region corresponding to nucleotides 1–70,634 and 8,974,768–9,105,828 of the USDA 110 reference genome sequence (**Figure 1**). This 202 kb deletion, which harbors 223 CDS (**Supplementary Table S1**), was confirmed by a PCR analysis (**Supplementary Figure S1**). The genome alignment further revealed insertion of genes for three transposases, one group II intron transcriptase and one hypothetical protein in the 110*spc*4 genome (**Figure 1**). These insertions did either not affect a CDS or occurred in genes encoding proteins of unknown function (**Table 1**). Among additional changes based on smaller differences (insertion or deletion of one nucleotide, non-synonymous substitutions), 26 were predicted to lead to a frameshift in a CDS (**Supplementary Table S2**, see below).

Importantly, a test carried out with six major host plants of *B. diazoefficiens*, namely two soybean (*G. max*) cultivars (Williams 82, Black jet), mungbean (*Vigna radiata*), cowpea (*Vigna unguiculata*), siratro (*Macroptilium atropurpureum*), and the crack-entry host *Aeschynomene afraspera*, revealed that none of the four analyzed parameters relevant for symbiosis (nodule number, dry weight per nodule, nitrogenase activity, leaf color) were significantly affected by the genomic deletion in strain 110*spc*4 compared to the USDA 110 reference strain (**Figure 2**; **Supplementary Figure S2**). A Fisher's exact test of COG categories indicated a significant under-representation of several important functional categories among the 223 deleted genes compared to all genes. These included categories C (energy production and conversion), E (amino acid transport and metabolism), I (lipid transport and metabolism), P (inorganic ion transport and metabolism), and T (signal transduction mechanisms) (**Figure 1**). Conversely, genes in category U (intracellular trafficking, secretion, and vesicular transport), S (function unknown) and most prominently in category L (replication, recombination and repair), which includes many transposases, were significantly enriched. These genes apparently do not play an important role in symbiosis.

Determination of the Proteome Expressed Under Oxic and Microoxic Conditions

With the *de novo* assembled and annotated genome of our model strain *B. diazoefficiens* 110*spc*4 at hand, we next aimed to identify the set of proteins differentially expressed in microoxia,

which has been recognized as a key signal for the induction of symbiosis-related genes during different steps of bacteria-host plant interaction (Terpolilli et al., 2012; Poole et al., 2018). Therefore, we performed a shotgun proteomics approach based on the gel-free FASP technology (Wiśniewski et al., 2009a,b) of cells grown under microoxic and oxic conditions (three replicates each; **Supplementary Figure S3**). Using a stringent FDR at the PSM level (0.35%) and requiring two distinct peptides or three PSMs of unambiguous peptides (Qeli and Ahrens, 2010) per condition, i.e., the same thresholds as used in previous studies (Delmotte et al., 2010; Koch et al., 2014), we were able to detect 3,188 expressed proteins (including two cases of 3a protein groups; i.e., identical protein sequences encoded by different genetic loci; **Supplementary Table S3**, **Data Sheet B**). The overall estimated FDR at the protein level was below 1%. 2,900 and 2,826 proteins were identified in oxic and microoxic conditions, respectively (**Figure 3**; **Supplementary Table S3**, **Data Sheets C,D**), corresponding to roughly 34% each of the 8,348 proteins encoded by the *B. diazoefficiens* 110*spc*4 genome. A search against the USDA 110 reference genome database returned virtually identical results. As expected, none of the protein products of the 223 genes located in the deletion region of 110*spc*4 were detected by unambiguous peptide evidence. Among the 26 genes affected by a frameshift (single nucleotide insertion or deletion), 9 protein products were expressed (**Supplementary Table S2**). It has to be noted that the NCBI genome annotation pipeline annotated more CDS (8,348) in the smaller genome of strain 110*spc*4 compared to the USDA 110 reference strain (8,317 CDSs). To enable the *Bradyrhizobium* research community to carry out similar comparative analyses, we have included **Supplementary Table S3**, **Data Sheet A**, which lists for each of the 8,348 annotated *B. diazoefficiens* 110*spc*4 proteins the respective best Blast hit in the USDA 110 genome along with the locus tag information, additional functional annotations, and other metadata.

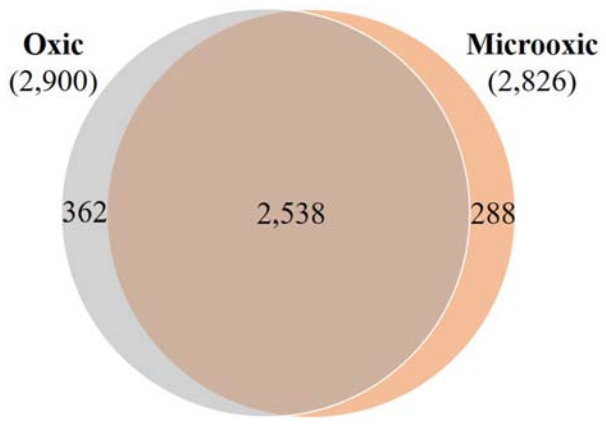

FIGURE 3 | Overlap of proteins whose expression was identified in oxic and microoxic conditions. Venn diagram representing the proteins identified in oxic (2,900) and microoxic (2,826) conditions, their overlap (2,538), as well as microoxia-specific (288) and oxia-specific (362) proteins.

Of the 2,826 proteins expressed under microoxic conditions, 2,538 proteins were also identified in cells cultured under oxic conditions (**Figure 3**). However, a group of 288 proteins was exclusively expressed under microoxic conditions. Previous transcriptomics experiments performed with a customized tiling-type GeneChip array designed based on the USDA 110 reference genome had revealed that 5,568 and 5,439 genes were transcribed in microoxically and oxically grown cells, respectively (Pessi et al., 2007), and that 506 genes were specifically transcribed under microoxic conditions. While minor genomic annotation differences might affect a few of these genes, we relied on **Supplementary Table S3** (**Data Sheet A**) and focused on matching all transcribed USDA 110 protein-coding genes to their respective counterpart in strain 110*spc*4 (via a best Blast hit analysis at the protein level). Following this approach, 72 proteins of 506 microoxia-specific genes were present among the 288 microoxia-specific proteins identified in this study (**Supplementary Figure S4**). Another 75 of the microoxia-specific genes were detected at the protein level under oxic conditions. Considering an additional eight annotation differences between the two strains (see **Supplementary Figure S4**), the remaining 639 genes/proteins represent the set of microoxia-specific expressed genes and proteins (**Supplementary Table S3**, **Data Sheet E**).

Comparison of Differential Protein and Gene Expression Under Microoxic Conditions

To identify proteins specifically induced in cells grown under microoxic conditions compared to oxic conditions, we used DESeq2 (Love et al., 2014). By applying a multiple testing corrected p-value threshold of ≤ 0.2, the comparison resulted in a list of top 66 significantly differentially expressed proteins (**Figure 4A**). These included 62 proteins that were induced under microoxic conditions ("core microoxic proteome") and four proteins whose expression was significantly downregulated under microoxic conditions, respectively (**Table 2**). Among the top upregulated proteins, we found many of the prominent targets characteristic for the microoxic lifestyle, e.g., the two subunits of the nitrogenase (NifD and NifK) and nitrogenase reductase (NifH), two subunits of the cbb_3 high-affinity terminal oxidase (FixO, FixP), the NifA transcription regulator, one of the five polyhydroxybutyrate polymerase paralogs (PhaC2), or the 1-aminocyclopropane-1-carboxylate (ACC) deaminase protein (AcdS) involved in degradation of the ethylene intermediate ACC (Ma et al., 2002; Murset et al., 2012). The overlap between the 62 proteins and the previously defined microoxia-induced transcriptome of 620 genes (17 of which are non-protein coding) (Pessi et al., 2007) led to the definition of 46 genes/proteins induced under microoxic conditions (**Table 2**). Further, by comparing the 62 upregulated proteins with the group of genes activated by two of the main regulatory proteins (NifA, $FixK_2$) that respond to microoxic conditions in *B. diazoefficiens*, we found that 18 protein-encoding genes overlap with the combined NifA + $RpoN_{1/2}$ regulon which consists of 65 genes (Hauser et al., 2007) (**Table 2**). RpoN is an alternative sigma factor

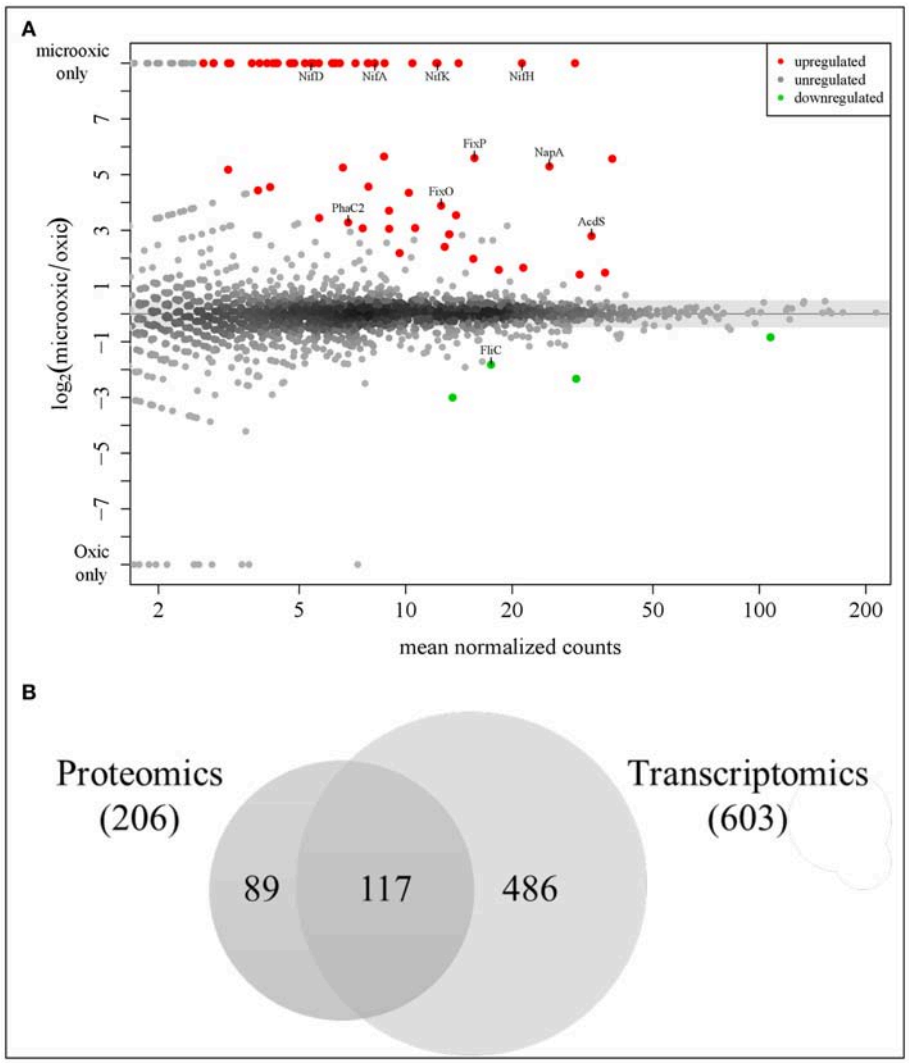

FIGURE 4 | Analysis of differential protein and gene expression in microoxia. **(A)** MA plot visualizing the differential protein expression data. Sixty-two proteins most significantly up-regulated in microoxia are shown in red, those most significantly down-regulated (four proteins) in green. The names of selected proteins are indicated. **(B)** Overlap of proteins upregulated in microoxic conditions with previous transcriptomics data (Pessi et al., 2007). Using a less stringent threshold ($\log_2$ FC $\geq$ 1) identical to that used in a prior transcriptome analysis, 206 proteins fulfilled the criterion, including the top 62 up-regulated proteins (p-value $\leq$ 0.2) shown in **(A)**. The overlap with 603 protein-coding genes among the 620 genes previously found to be induced at the transcript level (Pessi et al., 2007) is shown here: 117 genes/proteins are upregulated both at transcript and protein level (see **Table 2**).

that functions in concert with the regulatory protein NifA for the activation of the expression of nitrogen fixation-related genes (*nif*, *fix*) among others (reviewed in Dixon and Kahn, 2004). Interestingly, 13 protein-encoding genes are also part of the described putative direct targets for $FixK_2$ (Mesa et al., 2008) (**Table 2**). Notably, ∼89% of the genes coding for the 62 microoxia-induced proteins (i.e., 55 genes), were also shown to be upregulated in soybean nodules (Pessi et al., 2007) (**Table 2**).

To further explore the overlap of microoxically induced proteins with the microoxia-induced transcriptome of 603 protein-coding genes (fold change $\geq$ 2; i.e., $\log_2$ FC $\geq$ 1) (Pessi et al., 2007), we went beyond the top statistically differentially regulated proteins identified by DESeq2 and now also considered proteins upregulated by a $\log_2$ FC of more than 1 in microoxia. Applying this more lenient threshold returned 206 microoxia-induced proteins (**Supplementary Table S3**, **Data Sheet F**); their overlap with the 603 protein-coding genes amounted to 117 genes/proteins that form the "expanded microoxia-induced transcriptome/proteome" (i.e., 71 extra genes/proteins in addition to the group of 46 that overlap with the "core microoxic proteome"; **Figure 4B**; **Table 2**). This group of 71 genes/proteins includes four NifA+$RpoN_{1+2}$ targets, 14 $FixK_2$ direct targets, and 38 genes induced at transcriptional level in wild-type soybean bacteroids in comparison to oxic conditions (Pessi et al., 2007). Overall, the latter comparison showed an overlap of 66% (78 out of 117 microoxia-induced genes/proteins) (**Table 2**).

TABLE 2 | List of the top 66 significantly differentially expressed proteins in *B. diazoefficiens* cells grown under microoxic conditions (0.5% O_2) in comparison to oxic conditions (62 proteins upregulated that constitute the "core microoxic proteome," and four proteins downregulated; multiple testing corrected p-value ≤ 0.2).

Locus_tag[a]	Product[b]	Gene name[c]	Query[d]	log_2 FC (microoxic vs. oxic)[e]	FC (microoxic vs. oxic)[f]	FC (soybean bacteroids vs. oxic)[g]	NifA+RpoN$_1$ targets[h]	FixK$_2$ targets[i]
Sixty-two proteins showing increased expression in microoxic conditions in comparison to oxic conditions (p-value ≤ 0.2)								
Bdiaspc4_00855	Aminocyclopropane-1-carboxylate deaminase/D-cysteine desulfhydrase family protein	*acdS*	blr0241	2.8	4.8	20.1	–	–
Bdiaspc4_05275	Benzoyl-CoA-dihydrodiol lyase	–	blr1080	3.1	–	25.4	–	–
Bdiaspc4_06495	Propionyl-CoA synthetase	*acs*	blr1309	1.6	3.1	–	–	–
Bdiaspc4_06505	OmpW family protein	–	blr1311	6.0	44.9	23.3	–	+
Bdiaspc4_07020	ATP-dependent chaperone ClpB	*clpB*	blr1404	1.5	2.7	3.0	–	–
Bdiaspc4_08825	Nitrogenase molybdenum-iron protein alpha chain	*nifD*	blr1743	6.0	13.8	107.3	+	–
Bdiaspc4_08830	Nitrogenase molybdenum-iron protein subunit beta	*nifK*	blr1744	7.1	12.4	106.1	+	–
Bdiaspc4_08835	Nitrogenase iron-molybdenum cofactor biosynthesis protein NifE	*nifE*	blr1745	6.2	4.7	62.9	+	–
Bdiaspc4_08840	Nitrogenase iron-molybdenum cofactor biosynthesis protein NifN	*nifN*	blr1746	5.6	2.9	47.8	+	–
Bdiaspc4_08845	Nitrogen fixation protein NifX	*nifX*	blr1747	5.8	–	33.5	+	–
Bdiaspc4_08880	Hypothetical protein	–	bll1754	6.2	5.5	120.9	–	–
Bdiaspc4_08885	Iron-sulfur cluster assembly accessory protein	–	blr1755	5.0	7.0	138.7	+	–
Bdiaspc4_08890	Cysteine desulfurase NifS	*nifS*	blr1756	7.3	4.1	78.7	–	–
Bdiaspc4_08895	Putative nitrogen fixation protein NifT	*nifT*	bsr1757	5.6	4.8	105.4	–	–
Bdiaspc4_08905	Nitrogenase cofactor biosynthesis protein NifB	*nifB*	blr1759	5.8	2.9	74.1	+	–
Bdiaspc4_08945	OmpW family protein	–	bll1766	5.6	6.6	23.6	–	+
Bdiaspc4_08960	Nitrogenase iron protein	*nifH*	blr1769	7.9	7.0	96.2	+	–
Bdiaspc4_08975	Nitrogenase stabilizing/protective protein NifW	*nifW*	blr1771	5.4	2.2	95.2	–	–
Bdiaspc4_08985	Protein FixB	*fixB*	blr1773	6.0	2.2	47.6	–	–
Bdiaspc4_08990	Protein FixC	*fixC*	blr1774	5.8	–	38.1	–	–
Bdiaspc4_09875	Porin family protein	–	bll1944	8.4	3.8	89.7	+	–
Bdiaspc4_10340	SDR family oxidoreductase	*fixR*	blr2036	7.1	–	8.5	–	–
Bdiaspc4_10345	nif-specific transcriptional activator NifA	*nifA*	blr2037	6.6	–	3.2	–	–
Bdiaspc4_10350	Electron transfer flavoprotein subunit beta/FixAfamily protein	*fixA*	blr2038	5.9	–	31.9	+	–
Bdiaspc4_10455	Molecular chaperone GroEL	*groEL$_3$*	bll2059	5.6	2.9	47.4	+	–
Bdiaspc4_10460	Co-chaperone GroES	*groES$_3$*	bll2060	6.9	4.4	83.0	+	–
Bdiaspc4_10475	Flavin-dependent monooxygenase	*nrgC*	bll2063	5.2	4.4	105.0	+	–
Bdiaspc4_10495	Nodulate formation efficiency C protein	*nfeC*	bll2067	5.0	–	47.4	+	–
Bdiaspc4_10745	Non-ribosomal peptide synthetase	–	blr2108	6.5	–	39.0	+	–

(Continued)

TABLE 2 | Continued

Locus_tag[a]	Product[b]	Gene name[c]	Query[d]	log_2 FC (microoxic vs. oxic)[e]	FC (microoxic vs. oxic)[f]	FC (soybean bacteroids vs. oxic)[g]	NifA+$RpoN_1$ targets[h]	$FixK_2$ targets[i]
Bdiaspc4_10870	Oxygenase	–	blr2131	5.5	15.9	298.2	–	–
Bdiaspc4_10935	Cytochrome P450	*cyp*112	blr2144	6.2	7.6	107.0	+	–
Bdiaspc4_10940	Cytochrome P450 BJ-3	*cyp*114	blr2145	6.5	3.3	55.0	+	–
Bdiaspc4_10950	Short-chain type dehydrogenase/reductase	–	blr2146	6.6	–	243.3	–	–
Bdiaspc4_10955	Cytochrome P450 BJ-4	*cyp*117	blr2147	6.2	2.4	26.4	–	–
Bdiaspc4_12590	Isocitrate lyase	*aceA*	blr2455	3.5	2.0	–	–	–
Bdiaspc4_13350	Universal stress protein	–	bll2590	3.1	11.1	5.2	–	–
Bdiaspc4_14280	Universal stress protein	–	blr2761	3.1	14.8	3.8	–	+
Bdiaspc4_14295	Cytochrome-*c* oxidase cbb_3-type subunit II	*ccoO/fixO*	blr2764	3.9	47.0	26.8	–	+
Bdiaspc4_14305	cbb_3-type cytochrome c oxidase subunit FixP	*fixP*	blr2766	5.6	43.7	23.9	–	+
Bdiaspc4_14950	1,2-phenylacetyl-CoA epoxidase subunit A	*ppaA*	blr2891	4.6	9.8	6.1	–	–
Bdiaspc4_18960	NAD(P)-dependent alcohol dehydrogenase	–	blr3675	6.4	–	54.4	–	–
Bdiaspc4_21300	Cation acetate symporter	–	blr4115	4.9	21.9	12.3	–	+
Bdiaspc4_21600	Glutamine synthetase 2	*glnII*	blr4169	2.0	–	2.1	–	–
Bdiaspc4_24320	Universal stress protein	–	bll4644	3.4	19.3	–	–	–
Bdiaspc4_24375	J domain-containing protein	*dnaJ*	blr4653	4.4	14.3	–	–	–
Bdiaspc4_24405	1-phosphofructokinase family hexose kinase	–	blr4659	5.2	12.1	–	–	–
Bdiaspc4_28005	Host attachment protein	–	bll5315	2.9	15.0	5.9	–	+
Bdiaspc4_31965	MCE family protein	–	bll6063	2.2	10.5	–	–	–
Bdiaspc4_31990	GNAT family N-acetyltransferase	–	bll6068	4.3	5.4	2.3	–	–
Bdiaspc4_32015	Alpha/beta fold hydrolase	*phaC2*	bll6073	3.3	13.5	4.1	–	+
Bdiaspc4_35215	Bacterioferritin	*bfr*	bll6680	1.7	–	–	–	–
Bdiaspc4_36320	Porin	–	bll6888	1.4	–	19.2	–	–
Bdiaspc4_36645	ModD protein	*modD*	bll6950	5.6	–	36.3	–	–
Bdiaspc4_36650	Molybdate ABC transporter substrate-binding protein	*modA*	blr6951	6.6	18.7	128.0	+	–
Bdiaspc4_37130	Periplasmic nitrate reductase subunit alpha	*napA*	blr7038	5.3	22.0	8.5	–	+
Bdiaspc4_38745	Hypothetical protein	–	blr7345	2.9	19.9	3.7	–	+
Bdiaspc4_39840	Hypothetical protein	–	bll7551	5.5	23.4	5.8	–	–
Bdiaspc4_41200	Hypothetical protein	–	bll7787	5.3	12.2	14.1	–	+
Bdiaspc4_41905	ABC transporter substrate-binding protein	–	bll7921	2.4	–	6.5	–	–
Bdiaspc4_41910	ABC transporter substrate-binding protein	–	blr7922	6.2	–	23.1	–	–
Bdiaspc4_42205	Dehydrogenase	–	bll7981	4.6	7.6	2.1	–	+
Bdiaspc4_42210	Class I SAM-dependent methyltransferase	–	bll7982	3.7	10.5	3.6	–	+
Four proteins showing decreased expression in microoxic conditions in comparison to oxic conditions (p-value ≤ 0.2)								
Bdiaspc4_01330	PQQ-dependent dehydrogenase, methanol/ethanol family	–	bll0333	−0.8	–	–	–	–
Bdiaspc4_05515	Sugar ABC transporter substrate-binding protein	–	blr1123	−3.0	–	–	–	–

(Continued)

TABLE 2 | Continued

Locus_tag[a]	Product[b]	Gene name[c]	Query[d]	log_2 FC (microoxic vs. oxic)[e]	FC (microoxic vs. oxic)[f]	FC (soybean bacteroids vs. oxic)[g]	NifA+$RpoN_1$ targets[h]	$FixK_2$ targets[i]
Bdiaspc4_36200	Flagellin	*fliC/lafA2*	bll6865	−1.8	–	–	–	–
Bdiaspc4_39525	GMC Family oxidoreductase	–	blr7491	−2.3	–	–	–	–
Seventy-one genes/proteins showing increased expression in microoxic conditions in comparison to oxic conditions (log_2 FC ≥ 1) at both trancriptional and protein levels not included above								
Bdiaspc4_01235	TAT-dependent nitrous-oxide reductase	*nosZ*	blr0315	1.8	2.4	–	–	–
Bdiaspc4_02185	Hypothetical protein	–	blr0497	3.8	14.1	12.7	–	+
Bdiaspc4_02350	SDR family oxidoreductase	–	bll0527	1.1	2.9	–	–	–
Bdiaspc4_06385	Long-chain fatty acid-CoA ligase	–	blr1288	3.2	3.9	3.6	–	–
Bdiaspc4_06390	Oleate hydratase	–	blr1289	3.2	19.0	2.7	–	+
Bdiaspc4_06420	Aldo/keto reductase	–	bll1295	1.2	3.0	–	–	–
Bdiaspc4_06685	Hypothetical protein	–	bll1342	1.7	2.5	–	–	–
Bdiaspc4_06740	Amidohydrolase	–	blr1352	1.7	2.1	–	–	–
Bdiaspc4_07460	Sulfate ABC transporter substrate-binding protein	–	blr1482	1.2	3.2	–	–	–
Bdiaspc4_08965	Nitrogen fixation protein NifQ	*nifQ*	blr1770	4.6	3.2	85.0	–	–
Bdiaspc4_09000	Alkyl hydroperoxide reductase AhpD	*ahpD*	bll1776	4.7	4.1	78.6	+	–
Bdiaspc4_09005	Peroxiredoxin	*ahpC*	bll1777	4.5	7.8	169.8	+	–
Bdiaspc4_09500	Omptin family outer membrane protease	–	bll1872	4.7	4.2	115.4	+	–
Bdiaspc4_09550	RNA polymerase σ^{54} factor	$rpoN_1$	blr1883	4.4	3.9	7.8	–	+
Bdiaspc4_09680	GNAT family N-acetyltransferase	–	bll1906	4.3	8.3	120.0	+	–
Bdiaspc4_10185	Oxygen-independent coproporphyrinogen III oxidase	$hemN_1$	bll2007	4.5	17.3	29.1	–	+
Bdiaspc4_10960	Polyprenyl synthetase family protein	–	blr2148	4.6	4.2	25.4	–	–
Bdiaspc4_11365	Aspartate aminotransferase family protein	–	blr2221	1.5	2.9	–	–	–
Bdiaspc4_12935	Phosphoketolase family protein	–	bll2518	4.3	8.2	–	–	–
Bdiaspc4_14265	Response regulator	–	bll2758	4.8	5.5	2.4	–	–
Bdiaspc4_14285	CBS domain-containing protein	–	blr2762	4.8	13.2	3.1	–	–
Bdiaspc4_14310	Cytochrome c oxidase accessory protein CcoG	*ccoG/fixG*	blr2767	4.3	32.5	13.0	–	+
Bdiaspc4_14320	Copper-translocating P-type ATPase	*fixI*	blr2769	3.8	23.5	11.0	–	+
Bdiaspc4_14930	Phasin	–	blr2887	1.8	2.4	3.4	–	–
Bdiaspc4_14960	Phenylacetate-CoA oxygenase subunit PaaI	*paaI*	blr2893	2.1	9.3	5.6	–	–
Bdiaspc4_14970	Phenylacetate-CoA oxygenase/reductase subunit PaaK	*paaK*	blr2895	1.9	5.0	2.6	–	–
Bdiaspc4_14980	Phenylacetate-CoA ligase	*paaF*	blr2897	2.0	4.5	–	–	–
Bdiaspc4_16100	MBL fold metallo-hydrolase	–	bll3115	2.9	15.4	–	–	–
Bdiaspc4_16105	Ribose-phosphate pyrophosphokinase	–	bll3116	4.4	7.7	–	–	–
Bdiaspc4_16110	Thymidine phosphorylase family protein	–	bll3117	2.1	5.1	–	–	–
Bdiaspc4_19720	HAD family hydrolase	–	blr3815	3.7	5.8	–	–	–
Bdiaspc4_20685	NAD-dependent succinate-semialdehyde dehydrogenase	–	bll3998	2.6	28.1	8.4	–	+

(Continued)

TABLE 2 | Continued

Locus_tag[a]	Product[b]	Gene name[c]	Query[d]	log_2 FC (microoxic vs. oxic)[e]	FC (microoxic vs. oxic)[f]	FC (soybean bacteroids vs. oxic)[g]	NifA+$RpoN_1$ targets[h]	$FixK_2$ targets[i]
Bdiaspc4_21285	CusA/CzcA family heavy metal efflux RND transporter	–	blr4112	4.8	6.4	–	–	–
Bdiaspc4_21700	Hypothetical protein	–	bsl4187	4.5	2.3	–	–	–
Bdiaspc4_22005	Pyridoxamine 5'-phosphate oxidase family protein	–	blr4240	3.8	12.5	–	–	–
Bdiaspc4_22345	Amidase	–	bll4303	1.6	3.9	–	–	–
Bdiaspc4_22980	Translational machinery protein	–	bll4412	2.6	6.6	–	–	–
Bdiaspc4_24325	Host attachment protein	–	bll4645	3.2	21.8	–	–	–
Bdiaspc4_24330	CBS domain-containing protein	–	blr4646	3.2	28.1	–	–	–
Bdiaspc4_24365	Protein-L-isoaspartate(D-aspartate) O-methyltransferase	–	bll4651	4.6	28.7	9.7	–	+
Bdiaspc4_24370	Nitroreductase	–	blr4652	2.9	51.6	5.9	–	+
Bdiaspc4_24385	Phosphoenolpyruvate synthase	–	blr4655	4.3	11.2	2.0	–	–
Bdiaspc4_24400	Glucokinase	*glk*	blr4658	3.7	9.4	2.9	–	–
Bdiaspc4_27515	Co-chaperone GroES	$groES_1$	blr5226	3.4	2.1	–	–	–
Bdiaspc4_29305	CBS domain-containing protein	–	bll5551	1.1	2.0	–	–	–
Bdiaspc4_29865	Alcohol dehydrogenase AdhP	*adhP*	bll5655	2.8	18.0	3.9	–	+
Bdiaspc4_30480	Efflux RND transporter permease subunit	–	bll5771	3.8	2.6	–	–	–
Bdiaspc4_30485	Efflux RND transporter periplasmic adaptor subunit	–	bll5772	4.0	3.5	–	–	–
Bdiaspc4_30510	DUF302 domain-containing protein	–	blr5777	4.3	5.0	3.3	–	–
Bdiaspc4_30515	Cytochrome c oxidase accessory protein CcoG	*ccoG/fixG*	blr5778	3.4	4.6	4.1	–	–
Bdiaspc4_31945	Cyclase family protein	–	blr6059	1.5	2.6	–	–	–
Bdiaspc4_31950	CRP/FNR family transcriptional regulator	–	bll6060	1.3	2.3	2.2	–	–
Bdiaspc4_31970	ABC transporter ATP-binding protein	–	bll6064	2.8	4.6	2.1	–	–
Bdiaspc4_31975	MlaE family lipid ABC transporter permease subunit	–	bll6065	3.4	6.7	–	–	–
Bdiaspc4_31995	Universal stress protein	–	bll6069	2.7	18.5	7.5	–	+
Bdiaspc4_32020	CBS domain-containing protein	–	blr6074	2.6	35.6	4.7	–	+
Bdiaspc4_34005	Methyltransferase	–	bll6449	1.4	2.7	–	–	–
Bdiaspc4_34035	ABC transporter substrate-binding protein	–	bll6455	2.8	4.4	–	–	–
Bdiaspc4_34375	Aryl-sulfate sulfotransferase	–	bsr6521	2.6	3.4	–	–	–
Bdiaspc4_36795	Chaperonin GroEL	$groEL_2$	blr6979	1.6	3.9	2.0	–	–
Bdiaspc4_37135	Nitrate reductase cytochrome c-type subunit	*napB*	blr7039	2.8	47.4	22.6	–	–
Bdiaspc4_37380	CRP/FNR family transcriptional regulator	*nnrR*	blr7084	3.6	7.1	–	–	–
Bdiaspc4_37390	Oxygen-independent coproporphyrinogen III oxidase	$hemN_2$	bll7086	4.3	29.4	7.3	–	+
Bdiaspc4_37770	DUF2852 domain-containing protein	–	bll7160	2.5	2.1	4.9	–	–
Bdiaspc4_39110	Elongation factor G	–	bll7414	1.9	4.1	2.8	–	–
Bdiaspc4_40040	Indolepyruvate ferredoxin oxidoreductase family protein	–	blr7589	1.1	3.6	–	–	–

(Continued)

TABLE 2 | Continued

Locus_tag[a]	Product[b]	Gene name[c]	Query[d]	log_2 FC (microoxic vs. oxic)[e]	FC (microoxic vs. oxic)[f]	FC (soybean bacteroids vs. oxic)[g]	NifA+RpoN$_1$ targets[h]	FixK$_2$ targets[i]
Bdiaspc4_40955	Molecular chaperone	–	blr7740	3.2	2.1	4.5	–	–
Bdiaspc4_41165	Hypothetical protein	–	blr7780	4.5	8.6	17.0	–	–
Bdiaspc4_41645	HlyD family efflux transporter periplasmic adaptor subunit	–	blr7872	3.5	14.1	–	–	–
Bdiaspc4_42105	Hsp20/alpha crystallin family protein	–	blr7961	4.8	28.4	25.2	–	+
Bdiaspc4_43115	HugZ family protein	–	bll8143	3.2	2.2	–	–	–

Shown are also 71 genes/proteins; i.e., 117 genes/proteins comprising the "expanded microoxia-induced transcriptome/proteome" (log_2 fold change ≥ 1 at both transcriptional and protein level) minus 46 genes/proteins included in the "core microoxic proteome."

[a]Nomenclature of B. diazoefficiens 110spc4 genes according to the NCBI annotation (GenBank acc. # CP032617); this work.

[b]Protein/gene product according to the NCBI annotation (GenBank acc. # CP032617); this work.

[c]Gene name according to the NCBI annotation with modifications shaded in gray (GenBank acc. # CP032617); this work.

[d]Best blast hit in the B. diazoefficiens USDA 110 genome (Kaneko et al., 2002; GenBank acc. # NC_004463.1; RefSeq annotation as from January 2016).

[e]Log_2 fold change (FC) values from the comparison of wild-type cells grown microoxically (0.5% O_2) in comparison with those of cells grown oxically in proteomics experiments.

[f]FC values from the comparison of wild-type cells grown microoxically (0.5% O_2) in comparison with those of cells grown oxically in transcriptomics experiments (Pessi et al., 2007). – indicates the gene was not differentially expressed.

[g]FC values from the comparison of wild-type soybean bacteroids in comparison with those of wild-type cells grown oxically in transcriptomics experiments (Pessi et al., 2007). – indicates the gene was not differentially expressed.

[h]The gene belongs to the defined NifA + RpoN$_{1+2}$ regulon according to Hauser et al. (2007). +, yes; –, not.

[i]The gene is part of the direct FixK$_2$-dependent regulon as defined by Mesa et al. (2008). +, yes; –, not.

Microoxia-Mediated Post-transcriptional Regulation

The integration of our proteomics data with previous transcriptomics data revealed that for 486 protein-coding genes induced under microoxic conditions (603 minus 117; **Figure 4B**), there was only a more moderate or even no correlation between transcript and protein abundance. Indeed, in contrast to the induction of the respective genes under microoxia, a group of 91 proteins was even downregulated (log_2 FC $\leq$ 0.5 or p-value $\geq$ 0.9) under microoxic conditions compared to oxic conditions (**Supplementary Table S4**). Interestingly, such a profile was previously observed for the *fixK*$_2$ gene which encodes the transcription factor FixK$_2$ that plays a key role in microoxia-mediated regulation. Transcriptional induction of the *fixK*$_2$ gene in cells grown under microoxic conditions in comparison to oxic conditions (Nellen-Anthamatten et al., 1998; Pessi et al., 2007) did not correlate with increased steady-state levels of the FixK$_2$ protein (Mesa et al., 2009). To identify potential target genes with a regulation similar to that described for *fixK*$_2$, we applied the following selection criteria for the list of 91 genes/proteins: (i) Soluble proteins (using the combined prediction of potential protein localization, TM helices, and signal peptides as described in the Materials and Methods section). (ii) Genes that code for proteins with an assigned function according to the NCBI annotation (GenBank accession number CP032617). (iii) Availability of antibodies against the corresponding *B. diazoefficiens* protein or a cross-reacting protein ortholog. While 59 targets fulfilled criteria (i) and (ii), only three proteins also fulfilled criterion (iii) (**Supplementary Table S4**). These three targets were selected for validation by western blot analysis, along with the FixK$_2$ protein (Bdiaspc4_14260 gene) as positive control (**Figure 5A**): HemA (Bdiaspc4_05915 gene) coding for a 5-aminolevulinate (ALA) synthase (Page and Guerinot, 1995; Jung et al., 2004), HemB (Bdiaspc4_26465 gene) coding for a porphobilinogen synthase or ALA dehydratase (Chauhan and O'Brian, 1995), and ClpA (Bdiaspc4_27090) coding for the ATP-binding chaperone component of the ClpAP proteolytic system (Bonnet et al., 2013). As further controls, we also included four genes not induced in microoxia (Pessi et al., 2007), whose products were accumulated to constant levels (**Figure 5B**): ClpP (Bdiaspc4_25960 gene) categorized as a soluble protein, CoxA or CtaD (Bdiaspc4_05770 gene), CoxB (Bdiaspc4_05765 gene), and ScoI (Bdiaspc4_05560 gene) classified as membrane proteins. Crude extracts, soluble and membrane fractions were isolated from *B. diazoefficiens* cells cultivated oxically and microoxically, separated by SDS-PAGE, and immunoblotted against the corresponding antibody (a list of antibodies used in this work together with associated details of the immunoblot methodology are listed in **Supplementary Table S5**). Similar to the constant accumulated levels of ClpP$_1$, CoxA, CoxB, and ScoI, steady-state levels of ClpA, FixK$_2$, HemA, and HemB were comparable in cells of *B. diazoefficiens* cultivated oxically or microoxically (**Figure 5A**), despite of the induction of the respective genes in microoxic conditions (**Supplementary Table S4**; Pessi et al., 2007). Together, these data suggested that in addition to *fixK*$_2$ other genes might also be under microoxia-mediated post-transcriptional control in *B. diazoefficiens*.

We also validated the up-regulation of the membrane proteins FixO and FixP, and the periplasmic proteins NapA and NosZ, respectively, by heme-staining (**Figure 5C**) and immunoblotting (**Figure 5D**), using the same membrane and cytosolic samples employed in **Figures 5A,B**. The heme-staining technique allows detection of proteins covalently bound to heme (Vargas et al., 1993) such as cytochromes. In line with the differential protein abundance (see above), the protein bands corresponding to FixO, and FixP were more prominent in membrane preparations from the wild-type strain grown microoxically, while the accumulated levels of CycM, a cytochrome of about 19 kDa encoded by the Bdiaspc4_07150 gene, remained constant irrespective of the growth condition (**Figure 5C**). Similarly, we validated the upregulation of NapA and NosZ proteins by using heterologous antibodies (see Materials and Methods) (**Figure 5D**).

DISCUSSION

We applied an integrated systems biology approach to analyze the adaptation of a key rhizobial model species to microoxic conditions. We used *B. diazoefficiens* strain 110*spc*4 as a model, as a wealth of functional genomics data have been compiled for this strain. These comprise microarray-based gene expression and RNA-Seq studies, including experiments carried out under microoxia, a number of shotgun proteomics studies and efforts to integrate transcriptomics, proteomics and metabolomics datasets (Hauser et al., 2007; Lindemann et al., 2007; Pessi et al., 2007; Hacker et al., 2008; Lang et al., 2008; Mesa et al., 2008, 2009; Delmotte et al., 2010; Koch et al., 2010, 2014; Reutimann et al., 2010; Masloboeva et al., 2012; Serventi et al., 2012; Torres et al., 2014; Čuklina et al., 2016; Lardi et al., 2016; reviewed in Lardi and Pessi, 2018). Motivated by previous observations that the genome of this important strain might differ from that of the NCBI USDA 110 reference strain (Kaneko et al., 2002), we sequenced and *de novo* assembled the complete genome of *B. diazoefficiens* 110*spc*4 using long reads from PacBio's third generation sequencing technology. As predicted by a repeat complexity analysis of close to 10'000 prokaryotic genomes (Schmid et al., 2018), this approach was straightforward as *B. diazoefficiens* genomes do not harbor very long repeats that complicate genome assembly. Furthermore, a complete genome sequence is the basis to identify differences compared to a prior reference genome sequence using proteogenomics: such differences can affect annotated genes as shown in **Supplementary Figure S5A**, where proteogenomic evidence of a peptide directly confirms the protein sequence of a CDS in strain 110*spc*4 that is affected by a frameshift in USDA 110. Moreover, proteogenomics can also identify strain-specific and/or previously unannotated short protein-coding genes (Omasits et al., 2017), evidence for expressed pseudogenes (**Supplementary Figure S5B**), and even provide evidence for shorter proteins than annotated (Čuklina et al., 2016). Corroborating earlier hints (Mesa et al., 2001), we indeed identified a genomic deletion of roughly 202 kb in strain 110*spc*4, which however did not show any significantly different symbiotic phenotype compared to strain USDA 110. The extensive table with the genomic coordinates of all protein-coding genes of *B. diazoefficiens* 110*spc*4, the respective homolog of strain USDA 110, additional functional predictions and all experimental evidence (**Supplementary Table S3**, **Data Sheet A**) will facilitate researchers to readily compare datasets that were using the USDA 110 annotation.

The results of our proteomics analysis provide the first extensive protein expression dataset for microoxic growth of *B. diazoefficiens*. We deliberately selected the FASP method, which is known to achieve a higher coverage of membrane proteins (Wiśniewski et al., 2009a,b), that otherwise are typically significantly underrepresented in shotgun proteomics studies (Ahrens et al., 2010). Indeed, compared to the study of Delmotte et al. (2010), where ∼7.8% of the 2,315 experimentally identified root nodule proteins were classified as TM proteins, we identified close to 12% of TM proteins in our dataset. This percentage is still lower than that of the entire 110*spc*4 proteome (19.9%); however, we did not apply the costly and time-consuming iterative feedback loop strategy that was used in one of the only studies that accomplished a complete membrane proteome coverage to date (Omasits et al., 2013).

Applying an adjusted p-value ≤ 0.2 as first cut-off, 62 proteins were significantly upregulated (**Figure 4A**; **Table 2**), including many targets known to be important for the microoxic free-living and symbiotic lifestyles, including NifD, NifK, NifH, FixO, FixP, NifA, PhaC2, and AcdS. These results reinforced our previous findings, that the conditions in our experiments mimic the microoxic environment inside root nodules. Likewise, using this cut-off, four proteins were significantly downregulated in cells grown under microoxic conditions. Interestingly, one of those is FliC (Bdiaspc4_36200, bll6865 in USDA 110), a protein that plays a role in the lateral flagellar system in *B. diazoefficiens,* which was named LafA2 (Mongiardini et al., 2017). Bacterial motility is seemingly beneficial for a free-living organism in the environment, where the lateral system contributes to swimming in wet soil and competition for nodulation. For instance, a mutant lacking lateral flagellar filaments was found to be more competitive for nodulation than the wild type (Althabegoiti et al., 2011). Furthermore, expression of the *fliC*/*lafA2* gene was upregulated in oxic conditions (Pessi et al., 2007) and was shown to be under the positive control of the RegR regulatory protein (Lindemann et al., 2007).

Applying a more relaxed selection threshold ($\log_2$ FC ≥ 1; i.e., the same as used in the prior transcriptomics study) a total of 117 genes/proteins represented the "expanded microoxia-induced transcriptome/proteome" (**Table 2**). Among these proteins/genes upregulated in microoxia we found: (i) The denitrifying proteins NapA, NapB (subunits of the periplasmic nitrate reductase) and NosZ, the structural subunit of the nitrous oxide reductase (Delgado et al., 2003; Velasco et al., 2004). It is worth mentioning that microoxia has been addressed as the key signal for the expression of nitrate-, nitrite- and nitrous oxide reductase-encoding genes in the denitrification process in *B. diazoefficiens* (Bueno et al., 2017; Torres et al., 2017). (ii) Two copies of the oxygen-independent coproporphyrinogen III oxidase involved in heme biosynthesis under low-oxygen conditions (i.e., $HemN_1$

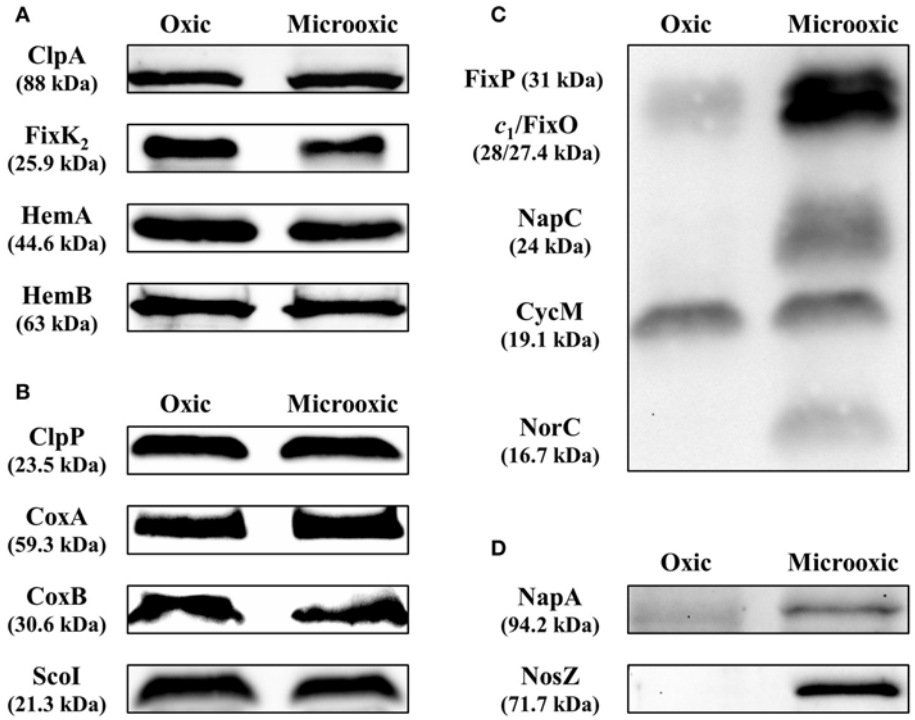

FIGURE 5 | Validation of protein abundance for genes subject to post-transcriptional regulation determined by heme-staining and western blot analyses. Steady-state levels of ClpA, $FixK_2$, HemA, and HemB **(A)**, targets subject to post-transcriptional control, were analyzed by western blot. ClpP, CoxA, CoxB, and ScoI, proteins with constant accumulated levels, were included as controls **(B)**. Up-regulation of the membrane-bound FixO and FixP proteins and the periplasmic, soluble NapA and NosZ proteins were monitored by heme-staining **(C)** or western blot **(D)**. The membrane-bound cytochrome CycM was used as reference in the heme-staining experiments in **(C)** as the protein levels remained constant in both oxic and microoxic conditions. Crude extracts, soluble and membrane fractions were isolated from *B. diazoefficiens* cells cultivated oxically and microoxically. 10–40 μg of cytosolic (ClpA, ClpP, HemA, HemB, NapA, NosZ), membrane (CoxB, ScoI), or crude extract (CoxA, $FixK_2$) fractions were loaded in the gel in the western blot experiments (identical amount of protein extracted from cells grown oxically and microoxically for each validated target). Twenty-five microgram membranes were loaded in the gel for the heme-staining analyses. Apparent molecular masses of the proteins are shown on the left. Note that as described previously (Loferer et al., 1993), the CoxA protein migrated at ≈45 kDa instead of the corresponding predicted mass of 59.3 kDa. Shown are representative results of different experiments carried out with at least three independent biological replicates. A detailed description of the methodology is described in **Supplementary Table S5**.

and $HemN_2$). Mutant strains with a defective *hemN*$_2$ gene failed to grow under denitrifying conditions and were also unable to fix nitrogen in symbiosis with soybeans (Fischer et al., 2001). (iii) Subunits of the FixGHIS complex, i.e., CcoG/FixG (Bdiaspc4_14310) and FixI (Bdiaspc4_14320) required for the functional assembly of the high affinity *cbb*$_3$ terminal oxidase FixNOQP (Preisig et al., 1996). (iv) The AhpD and AhpC proteins that form part of an alkylhydroperoxide reductase (Ahp), whose encoding genes were reported to be upregulated in soybean bacteroids and also belong to the NifA + $RpoN_{1+2}$ regulon (Hauser et al., 2007; Pessi et al., 2007). Although the Ahp reductase might play a role in the bacterial response against reactive oxygen species produced during rhizobia-legumes interaction (Pauly et al., 2006; Damiani et al., 2016), its exact role in the microoxic metabolism of this bacterium is under debate. (v) The product of the Bdiaspc4_20685 gene (bll3998 in USDA 110), a succinate-semialdehyde dehydrogenase that probably acts a tricarboxylic acid cycle bypass enzyme (Green et al., 2000). Expression of bll3998 was activated by $FixK_2$ and also found to be upregulated in soybean bacteroids (Pessi et al., 2007; Mesa et al., 2008). (vi) The glyoxylate shunt enzyme isocitrate lyase (AceA) which also plays a protective role in the response to several stresses (Jeon et al., 2015). (vii) The subunits ModA (Bdiaspc4_36650) and ModD (Bdiaspc4_36645) that form part of one of the predicted molybdenum transport systems (Kaneko et al., 2002; Delgado et al., 2006). Molybdenum is the cofactor of the oxygen-sensitive enzyme nitrogenase and the periplasmic nitrate oxide reductase. Expression of *modA* was highly induced in soybean bacteroids and it also belongs to the NifA + $RpoN_{1+2}$ regulon. (viii) Several regulatory proteins such as the CRP/FNR-type transcription factor NnrR involved in denitrification (Mesa et al., 2003) or the alternative sigma factor $RpoN_1$.

Among the microoxia-induced proteins that did not correlate with increased transcript levels of the corresponding gene we found two proteins involved in iron metabolism, i.e., a bacterioferritin (encoded by Bdiaspc4_35215, bll6680 in USDA 110; **Table 2**; **Supplementary Table S3**, **Data Sheet F**) and a rubrerythrin (encoded by Bdiaspc4_41765, blr7895 in USDA 110; **Supplementary Table S3**, **Data Sheet F**). The expression of these

two genes was induced in iron-replete media (Rudolph et al., 2006), in agreement with their assigned function to maintain proper levels of free iron in the cells. As they share oxygen-sensitive structural features (deMaré et al., 1996), they might be degraded in oxic conditions. Finally, we also identified a set of 639 genes/proteins that were only expressed in microoxia (**Supplementary Table S3**, **Data Sheet E**).

Our data set greatly increased the proteome coverage compared to previous 2-D gel-based studies (Regensburger et al., 1986; Dainese-Hatt et al., 1999). The more recent of the studies reported 38 differentially regulated proteins when comparing anoxic and low oxygen (2% O_2) conditions to oxic conditions, 34 of which were also controlled by either NifA or $FixK_2$. Fourteen of these proteins could not be identified by N-terminal sequencing, peptide mass fingerprinting and MS/MS analysis at the time. When searching the respective *N*-terminal protein sequences reported in the original paper (Dainese-Hatt et al., 1999) against our *de novo* assembled genome sequence, we could readily identify several of them. These included Bdiaspc4_24330 (blr4646 in USDA 110, CBS domain-containing protein; spot 17.1; **Table 2**; **Supplementary Table S3**, **Data Sheet F**) and Bdiasspc4_09275 (blr1830 in USDA 110, hypothetical protein; spot 5.1; **Supplementary Table S3**, **Data Sheet F**), both of which were also among the upregulated proteins under microoxic conditions in our study (0.5% O_2).

More recently, RNA-Seq studies performed in rhizobial species grown under low-oxygen conditions (Schlüter et al., 2013; Robledo et al., 2015; Čuklina et al., 2016) revealed a poorly characterized post-transcriptional control via ubiquitous small RNA-dependent regulation. Here we focus on post-transcriptional control of protein-encoding genes that are regulated in response to the cellular oxygen status. Differences between the patterns of accumulated transcripts and proteins could be due to condition-dependent differences in transcript and protein stabilities or stochastic effects of protein synthesis from scarce and unstable mRNA molecules (Taniguchi et al., 2010, and references therein). Our study identified a group of genes whose transcript and protein profile is similar to the one described for the $fixK_2$ gene, and therefore probably subject to microoxia-specific post-transcriptional control: Despite transcriptional induction in response to microoxic conditions there is no increase in the amount of the protein (Nellen-Anthamatten et al., 1998; Mesa et al., 2008). The $FixK_2$ protein is also post-translationally controlled by oxidation (Mesa et al., 2009) and by proteolysis mediated by the ClpAP proteolytic system (Bonnet et al., 2013). In order to validate other potential genes subjected to post-transcriptional regulation, we performed western blot analyses with antibodies available against the proteins encoded by three genes: *hemA*, *hemB*, and *clpA*.

The 5-aminolevulinate (ALA) synthase (EC:2.3.1.37) HemA and the ALA dehydratase (EC:4.2.1.24) HemB catalyze the first two steps of heme biosynthesis in *B. diazoefficiens*. In addition to iron control of *hemA* and *hemB* expression *via* two different regulatory mechanisms (Hamza et al., 2000; reviewed in O'Brian, 2015), Page and Guerinot (1995) reported that *hemA* expression is also under post-transcriptional regulation, as increased *hemA* mRNA levels in bacteroids compared to free-living cells were not accompanied by elevated ALA synthase activity. The third validated candidate under putative post-transcriptional control is *clpA* encoding the ATP-dependent chaperone component of the ClpAP proteolytic system involved in $FixK_2$ degradation (Bonnet et al., 2013). ClpA itself is also a specific substrate for the ClpAP system with the recognition signal located within the C-terminal 12 amino acids. Notably, the recognition sequence of *E. coli* ClpA is also C-terminally located since a protein variant lacking the last nine residues is protected from auto-degradation (Maglica et al., 2008). Furthermore, post-translational control of ClpA is not dependent on oxygen limitation. Here, we confirmed previous observations on the absence of other FixK paralogs in the nodule proteome determined by Delmotte et al. (2010). In fact, the other three predicted *B. diazoefficiens* FixK paralogs (i.e., Bll2109, [Bdiaspc4_10755 gene]; Bll3466, [Bdiaspc4_17910 gene]; Bll7696, [Bdiaspc4_40670 gene]; (Mesa et al., 2006) were not detected at the protein level under microoxic conditions despite the respective genes belong to the group of 603 protein-coding genes with significantly increased transcript levels in microoxia (Pessi et al., 2007).

Altogether our data suggest that additional genes beyond $fixK_2$ are subject to microoxia-mediated post-transcriptional control in *B. diazoefficiens*. A more detailed analysis of this type of regulation and elucidating its physiological relevance are interesting avenues for future investigations.

DATA AVAILABILITY

The genome sequence of *B. diazoefficiens* 110*spc*4 is available from Genbank under accession CP032617 (BioProject: PRJNA493766). In addition, the raw sequence data (and methylation analysis) has been submitted to the NCBI Sequence Read Archive (SRA) which can be accessed under study number: SRP162984. The mass spectrometry proteomics data have been deposited to the ProteomeXchange Consortium via the PRIDE (Perez-Riverol et al., 2019) partner repository with the dataset identifier PXD012491 and 10.6019/PXD012491. An integrated proteogenomics database (iPtgxDB) for *B. diazoefficiens* 110*spc*4 will be available (https://iptgxdb.expasy.org).

AUTHOR CONTRIBUTIONS

NF performed the proteomics experiments and contributed to data interpretation and manuscript writing. AV performed the genome comparison, proteogenomics analysis, analyzed proteomics data, contributed to the comparison with prior transcriptomics data and manuscript writing, and prepared figures and tables. JC performed the western blot and heme-staining experiments, contributed to data interpretation, and prepared figures and tables. SL performed the *de novo* genome assembly, genome comparison, and contributed to figures and tables. BR also performed proteomics experiments. RL and H-MF contributed genomic DNA of strain 110*spc*4, data interpretation, and compared the symbiotic phenotype of strains USDA 110 and 110*spc*4 in symbiosis with different plant hosts. LE and EB critically revised the manuscript. CA oversaw sequencing,

de novo genome assembly and comparison, data analysis and proteogenomics. GP devised the proteomics shotgun strategy, and contributed to the study design, and data interpretation. SM conceived and designed the study, contributed to the comparison with previous transcriptomics data, devised the strategy for selection of post-transcriptionally regulated targets, and interpreted data. CA, GP, and SM wrote the manuscript. All authors read and approved the final version of the manuscript.

FUNDING

This work was funded by FEDER-co-financed grants AGL2011-23383 and AGL2015-63651-P, (MINECO, Spain) to SM. NF was granted by the FPI Program (MINECO, Spain; grant BES-2011-049587). Support from the Junta de Andalucía to group BIO-275 is also acknowledged. CA acknowledges support from the Swiss National Science Foundation (grant 31003_156320) for AV.

ACKNOWLEDGMENTS

We thank the Functional Genomics Center (Zürich) for access to the infrastructure, Yilei Liu (University of Zurich, Zurich, Switzerland), Germán Tortosa (Estación Experimental del Zaidín, CSIC, Granada, Spain) for expert technical support, and Ulrich Omasits for expert bioinformatics support in the initial phase of the project. We are grateful to Mark O'Brian (University at Buffalo, Buffalo, USA), Kyoungwhan Back (Chonnam National University, Gwangju, Republic of Korea), David J. Richardson, Andrew J. Gates (University of East Anglia, Norwich, United Kingdom) and Urs Jenal (Biozentrum, Basel, Switzerland) for kindly providing antibodies for western blot validation experiments. The support of the publication fee by the CSIC Open Access Publication Support Initiative through its Unit of Information Resources for Research (URICI) is also acknowledged.

SUPPLEMENTARY MATERIAL

The Supplementary Material for this article can be found online at: https://www.frontiersin.org/articles/10.3389/fmicb.2019.00924/full#supplementary-material

Supplementary Figure S1 | PCR verification of the ∼202 kb deletion present in *Bradyrhizobium diazoefficiens* USDA 110 derivatives 110*spc*4 (Regensburger and Hennecke, 1983) and 110*rif*15 (Regensburger and Hennecke, 1984). **(A)** Schematic representation of the genomic region comprising the deletion between genome position no. 8,974,768 and 70,634 in the reference strain USDA 110 (acc. no. NC_004463.1). Primer binding sites and corresponding amplification products are indicated by horizontal arrows and thin solid lines, respectively. Not drawn to scale. **(B)** Analysis of PCR products obtained with indicated primer combinations and genomic template DNA from different *B. diazoefficiens* strains. No PCR products were obtained with strain 110*spc*4 when at least one primer binding site was located within the deleted region (primer combinations Del-1/2, 3/4, 5/6). By contrast, a 1,031 bp product spanning the deletion was obtained when primers Del-2/3 were used. No differences between the resequenced clone (a; preserved in 2018) and the oldest available clone (b; preserved in 1987) was observed. Identical PCR results were obtained with strain 110*rif*15, which was independently isolated from the same parental strain as 110*spc*4. Using genomic DNA of strain USDA 110 as template, amplification products spanning the ends of the 203 kb region (Del-1/2, 3/4) and an internal fragment thereof (Del-5/6) were obtained. The very weak band in the outermost right lane likely represents an off-target product amplified by primers Del-2/-3 from USDA 110 template DNA.

Supplementary Figure S2 | Leaf phenotype of different legume hosts inoculated with *Bradyrhizobium diazoefficiens* 110*spc*4 or USDA 110. All tested host plants [*Glycine max* cv. Williams 82 and cv. Black jet (soybeans), *Vigna radiata* (mung bean), *Vigna unguiculata* (cowpea), *Macroptillium atropurpureum* (siratro), and *Aeschynomene afraspera*] displayed dark-green leaves when inoculated with either 110*spc*4 (center) or USDA 110 (right) compared to the chlorotic, yellowish leaves of non-inoculated plants (left) typical for nitrogen-starved plants. No qualitative differences between 110*spc*4- and USDA 110-inoculated plants were visible. Shown are three leaves of three representative plants for each condition. The necrotic spots on *V. radiata* leaves regularly appear under the given growth conditions, independently of the inoculated strain and do not interfere with symbiosis.

Supplementary Figure S3 | Quality assessment of the shotgun proteomics samples (3 biological replicates each for growth under oxic and microoxic conditions) by a clustering analysis (heatmap based on semi-quantitative spectral count data).

Supplementary Figure S4 | Venn diagram showing the overlap of 110*spc*4 orthologs (see section Materials and Methods) of the 506 previously identified microoxia-specific transcribed genes (Pessi et al., 2007) with the 288 proteins uniquely expressed in microoxia (this study) and 2,900 proteins expressed in oxia (this study). The overlap revealed that 647 genes/proteins were only expressed in microoxia (506-75-72+288). Among these 647, six genes are not present (annotated) in the *B. diazoefficiens* 110*spc*4 genome, one is affected by a frameshift (blr6071) and one gene is encoded in the 202 kb deletion region (bsr0039; erroneously implicated to be transcribed likely due to cross-hybridization with cDNA originating from another gene) resulting in 639 microoxia-specific genes/proteins (**Supplementary Table S3**, **Data Sheet E**).

Supplementary Figure S5 | Example of proteogenomic evidence for novelties based on genome sequence differences. **(A)** The correct genomic sequence of strain 110*spc*4 is shown for a region of interest along with that of the USDA 110 reference strain and the respective annotations. Bdiaspc4_16655 is annotated as a sugar ABC transporter gene in strain 110*spc*4 (upper panel), predicted to encode a protein of 438 amino acids (blue arrow). A single nucleotide deletion in the genome sequence of strain USDA110 causes a frameshift. Accordingly, two shorter protein-coding genes are annotated (blr3220, blr3221; gray arrows) in the same reading frame. The peptide evidence underlines that our *de novo* genome assembly is correct: we observed a peptide (red peptide on the left) whose sequence directly confirmed the change compared to USDA 110 and another one traversing the incorrect stop codon (adjacent red peptide). **(B)** Additional examples can be uncovered using the publicly available iPtgxDB for strain 110*spc*4. Here, a genomic region of 110*spc*4 is shown where the NCBI annotation listed two CDSs (Bdiaspc4_31490, Bdiaspc4_31500; blue arrows) and one pseudogene (Bdiaspc4_31495; open arrow). We find proteogenomic evidence for this ORF (red peptides), which was predicted to represent a *bona fide* CDS by Prodigal (gray boxes; particular gene identifier highlighted in red), underlining the value of such iPtgxDBs to improve the genome annotation of prokaryotic genomes (Omasits et al., 2017).

Supplementary Data Sheet 1 | List of references included in the Supplementary Material.

Supplementary Table S1 | List of 223 CDS located in the ∼202 kb genomic region that is deleted in *B. diazoefficiens* 110*spc*4 compared to the USDA110 NCBI reference genome (corresponding to nucleotide positions 8,974,768–9,105,828 and 1–70,634). The respective COG classification was determined using the eggNOG database "bactNOG" (Huerta-Cepas et al., 2016) and is shown for 142 of the 223 CDSs.

Supplementary Table S2 | List of 26 USDA 110 genes affected by a frameshift caused by a single nucleotide insertion or deletion compared to strain 110*spc*4. We also list which of the encoded proteins (based on a search against the USDA 110 protein database) and their respective 110*spc*4 orthologs (based on a search against the 110*spc*4 protein database) were found to be expressed. An example of proteogenomics evidence for the protein sequence difference of an annotated CDS is shown in **Supplementary Figure S5**.

Supplementary Table S3 | Lookup "master" table containing 6 sheets with different lists of proteins (corresponding to the results section) from *B. diazoefficiens* 110*spc*4, their locustag identifiers, genomic coordinates, the respective equivalent protein-coding gene (with locustag and coordinates) in *B. diazoefficiens* USDA 110 as well as functional annotations. The "Overview" sheet provides explanations to the individual protein lists; the "Legend" sheet explains the headers of columns shown in individual sheets.

Supplementary Table S4 | List of the 91 *B. diazoefficiens* microoxia-induced genes (log_2 fold change ≥ 1; i.e., FC ≥ 2) whose corresponding protein product was not induced under microoxic conditions compared to oxic conditions (log_2 FC ≤ 0.5 or multiple testing corrected p-value ≥ 0.9).

Supplementary Table S5 | List of antibodies and conditions applied in western blot experiments performed in this study.

REFERENCES

Ahrens, C. H., Brunner, E., Qeli, E., Basler, K., and Aebersold, R. (2010). Generating and navigating proteome maps using mass spectrometry. *Nat. Rev. Mol. Cell. Biol.* 11, 789–801. doi: 10.1038/nrm2973

Althabegoiti, M. J., Covelli, J. M., Pérez-Giménez, J., Quelas, J. I., Mongiardini, E. J., López, M. F., et al. (2011). Analysis of the role of the two flagella of *Bradyrhizobium japonicum* in competition for nodulation of soybean. *FEMS Microbiol. Lett.* 319, 133–139. doi: 10.1111/j.1574-6968.2011.02280.x

Bonnet, M., Stegmann, M., Maglica, Z., Stiegeler, E., Weber-Ban, E., Hennecke, H., et al. (2013). $FixK_2$, a key regulator in *Bradyrhizobium japonicum*, is a substrate for the protease ClpAP *in vitro*. *FEBS Lett.* 587, 88–93. doi: 10.1016/j.febslet.2012.11.014

Bueno, E., Mesa, S., Sanchez, C., Bedmar, E. J., and Delgado, M. J. (2010). NifA is required for maximal expression of denitrification genes in *Bradyrhizobium japonicum*. *Environ. Microbiol.* 12, 393–400. doi: 10.1111/j.1462-2920.2009.02076.x

Bueno, E., Robles, E. F., Torres, M. J., Krell, T., Bedmar, E. J., Delgado, M. J., et al. (2017). Disparate response to microoxia and nitrogen oxides of the *Bradyrhizobium japonicum napEDABC*, *nirK* and *norCBQD* denitrification genes. *Nitric Oxide* 68, 137–149. doi: 10.1016/j.niox.2017.02.002

Bühler, D., Rossmann, R., Landolt, S., Balsiger, S., Fischer, H. M., and Hennecke, H. (2010). Disparate pathways for the biogenesis of cytochrome oxidases in *Bradyrhizobium japonicum*. *J. Biol. Chem.* 285, 15704–15713. doi: 10.1074/jbc.M109.085217

Chauhan, S., and O'Brian, M. R. (1995). A mutant *Bradyrhizobium japonicum* delta-aminolevulinic acid dehydratase with an altered metal requirement functions *in situ* for tetrapyrrole synthesis in soybean root nodules. *J. Biol. Chem.* 270, 19823–19827. doi: 10.1074/jbc.270.34.19823

Cingolani, P., Platts, A., Wang le, L., Coon, M., Nguyen, T., Wang, L., et al. (2012). A program for annotating and predicting the effects of single nucleotide polymorphisms, SnpEff: SNPs in the genome of *Drosophila melanogaster* strain w^{1118}; *iso*-2; *iso*-3. *Fly* 6, 80–92. doi: 10.4161/fly.19695

Clarke, V. C., Loughlin, P. C., Gavrin, A., Chen, C., Brear, E. M., Day, D. A., et al. (2015). Proteomic analysis of the soybean symbiosome identifies new symbiotic proteins. *Mol. Cell Proteomics* 14, 1301–1322. doi: 10.1074/mcp.M114.043166

Čuklina, J., Hahn, J., Imakaev, M., Omasits, U., Förstner, K. U., Ljubimov, N., et al. (2016). Genome-wide transcription start site mapping of *Bradyrhizobium japonicum* grown free-living or in symbiosis - a rich resource to identify new transcripts, proteins and to study gene regulation. *BMC Genomics* 17:302. doi: 10.1186/s12864-016-2602-9

Dainese-Hatt, P., Fischer, H. M., Hennecke, H., and James, P. (1999). Classifying symbiotic proteins from *Bradyrhizobium japonicum* into functional groups by proteome analysis of altered gene expression levels. *Electrophoresis* 20, 3514–3520. doi: 10.1002/(SICI)1522-2683(19991201)20:18<3514::AID-ELPS3514>3.0.CO;2-T

Damiani, I., Pauly, N., Puppo, A., Brouquisse, R., and Boscari, A. (2016). Reactive oxygen species and nitric oxide control early steps of the legume-*Rhizobium* symbiotic interaction. *Front. Plant Sci.* 7:454. doi: 10.3389/fpls.2016.00454

Darling, A. E., Mau, B., and Perna, N. T. (2010). Progressive Mauve: multiple genome alignment with gene gain, loss and rearrangement. *PLoS ONE* 5:e11147. doi: 10.1371/journal.pone.0011147

Davis-Richardson, A. G., Russell, J. T., Dias, R., McKinlay, A. J., Canepa, R., Fagen, J. R., et al. (2016). Integrating DNA methylation and gene expression data in the development of the soybean-*Bradyrhizobium* N_2-fixing symbiosis. *Front. Microbiol.* 7:518. doi: 10.3389/fmicb.2016.00518

Delamuta, J. R., Ribeiro, R. A., Ormeño-Orrillo, E., Melo, I. S., Martínez-Romero, E., and Hungría, M. (2013). Polyphasic evidence supporting the reclassification of *Bradyrhizobium japonicum* group Ia strains as *Bradyrhizobium diazoefficiens* sp. *nov. Int. J. Syst. Evol. Microbiol.* 63, 3342–3351. doi: 10.1099/ijs.0.049130-0

Delgado, M. J., Bonnard, N., Tresierra-Ayala, A., Bedmar, E. J., and Müller, P. (2003). The *Bradyrhizobium japonicum napEDABC* genes encoding the periplasmic nitrate reductase are essential for nitrate respiration. *Microbiology* 149, 3395–3403. doi: 10.1099/mic.0.26620-0

Delgado, M. J., Tresierra-Ayala, A., Talbi, C., and Bedmar, E. J. (2006). Functional characterization of the *Bradyrhizobium japonicum modA* and *modB* genes involved in molybdenum transport. *Microbiology* 152, 199–207. doi: 10.1099/mic.0.28347-0

Delmotte, N., Ahrens, C. H., Knief, C., Qeli, E., Koch, M., Fischer, H. M., et al. (2010). An integrated proteomics and transcriptomics reference data set provides new insights into the *Bradyrhizobium japonicum* bacteroid metabolism in soybean root nodules. *Proteomics* 10, 1391–1400. doi: 10.1002/pmic.200900710

Delmotte, N., Mondy, S., Alunni, B., Fardoux, J., Chaintreuil, C., Vorholt, J. A., et al. (2014). A proteomic approach of *Bradyrhizobium*/*Aeschynomene* root and stem symbioses reveals the importance of the *fixA* locus for symbiosis. *Int. J. Mol. Sci.* 15, 3660–3670. doi: 10.3390/ijms15033660

deMaré, F., Kurtz, D. M. Jr., and Nordlund, P. (1996). The structure of *Desulfovibrio vulgaris* rubrerythrin reveals a unique combination of rubredoxin-like FeS_4 and ferritin-like diiron domains. *Nat. Struct. Biol.* 3, 539–546. doi: 10.1038/nsb0696-539

Dixon, R., and Kahn, D. (2004). Genetic regulation of biological nitrogen fixation. *Nat. Rev. Microbiol.* 2, 621–631. doi: 10.1038/nrmicro954

Djordjevic, M. A. (2004). *Sinorhizobium meliloti* metabolism in the root nodule: a proteomic perspective. *Proteomics* 4, 1859–1872. doi: 10.1002/pmic.200300802

Djordjevic, M. A., Chen, H. C., Natera, S., Van Noorden, G., Menzel, C., Taylor, S., et al. (2003). A global analysis of protein expression profiles in *Sinorhizobium meliloti*: discovery of new genes for nodule occupancy and stress adaptation. *Mol. Plant Microbe Interact.* 16, 508–524. doi: 10.1094/MPMI.2003.16.6.508

Felgate, H., Giannopoulos, G., Sullivan, M. J., Gates, A. J., Clarke, T. A., Baggs, E., et al. (2012). The impact of copper, nitrate and carbon status on the emission of nitrous oxide by two species of bacteria with biochemically distinct denitrification pathways. *Environ. Microbiol.* 14, 1788–1800. doi: 10.1111/j.1462-2920.2012.02789.x

Fernández, N., Cabrera, J. J., Salazar, S., Parejo, S., Rodríguez, M. C., Lindemann, A., et al. (2016). "Molecular determinants of negative regulation of the *Bradyrhizobium diazoefficiens* transcription factor $FixK_2$," in *Biological Nitrogen Fixation and Beneficial Plant-Microbe Interactions,* eds F. González-Andrés and E. James (Cham: Springer International Publishing Switzerland), 57–72. doi: 10.1007/978-3-319-32528-6_6

Fischer, H. M. (1994). Genetic regulation of nitrogen fixation in rhizobia. *Microbiol. Rev.* 58, 352–386.

Fischer, H. M. (1996). Environmental regulation of rhizobial symbiotic nitrogen fixation genes. *Trends Microbiol.* 4, 317–320. doi: 10.1016/0966-842X(96)10049-4

Fischer, H. M., Velasco, L., Delgado, M. J., Bedmar, E. J., Schären, S., Zingg, D., et al. (2001). One of two *hemN* genes in *Bradyrhizobium japonicum* is functional during anaerobic growth and in symbiosis. *J. Bacteriol.* 183, 1300–1311. doi: 10.1128/JB.183.4.1300-1311.2001

Gates, A. J., Hughes, R. O., Sharp, S. R., Millington, P. D., Nilavongse, A., Cole, J. A., et al. (2003). Properties of the periplasmic nitrate reductases from *Paracoccus pantotrophus* and *Escherichia coli* after growth in tungsten-supplemented media. *FEMS Microbiol. Lett.* 220, 261–269. doi: 10.1016/S0378-1097(03)00122-8

Göttfert, M., Hitz, S., and Hennecke, H. (1990). Identification of *nodS* and *nodU*, two inducible genes inserted between the *Bradyrhizobium japonicum nodYABC* and *nodIJ* genes. *Mol. Plant Microbe Interact.* 3, 308–316. doi: 10.1094/MPMI-3-308

Green, L. S., Li, Y., Emerich, D. W., Bergersen, F. J., and Day, D. A. (2000). Catabolism of α-ketoglutarate by a *sucA* mutant of *Bradyrhizobium japonicum*: evidence for an alternative tricarboxylic acid cycle. *J. Bacteriol.* 182, 2838–2344. doi: 10.1128/JB.182.10.2838-2844.2000

Grünenfelder, B., Tawfilis, S., Gehrig, S., M, O.S., Eglin, D., and Jenal, U. (2004). Identification of the protease and the turnover signal responsible for cell cycle-dependent degradation of the *Caulobacter* FliF motor protein. *J. Bacteriol.* 186, 4960–4971. doi: 10.1128/JB.186.15.4960-4971.2004

Hacker, S., Gödeke, J., Lindemann, A., Mesa, S., Pessi, G., and Narberhaus, F. (2008). Global consequences of phosphatidylcholine reduction in *Bradyrhizobium japonicum*. *Mol. Genet. Genomics* 280, 59–72. doi: 10.1007/s00438-008-0345-2

Hahn, M., and Hennecke, H. (1984). Localized mutagenesis in *Rhizobium japonicum*. *Mol. Gen. Genet.* 193, 46–52. doi: 10.1007/BF00327412

Hamza, I., Qi, Z., King, N. D., and O'Brian, M. R. (2000). Fur-independent regulation of iron metabolism by Irr in *Bradyrhizobium japonicum*. *Microbiology* 146 669–676. doi: 10.1099/00221287-146-3-669

Hauser, F., Pessi, G., Friberg, M., Weber, C., Rusca, N., Lindemann, A., et al. (2007). Dissection of the *Bradyrhizobium japonicum* NifA+ σ^{54} regulon, and identification of a ferredoxin gene (*fdxN*) for symbiotic nitrogen fixation. *Mol. Genet. Genomics* 278, 255–271. doi: 10.1007/s00438-007-0246-9

Huerta-Cepas, J., Szklarczyk, D., Forslund, K., Cook, H., Heller, D., Walter, M. C., et al. (2016). eggNOG 4.5: a hierarchical orthology framework with improved functional annotations for eukaryotic, prokaryotic and viral sequences. *Nucleic Acids Res.* 44, D286–D293. doi: 10.1093/nar/gkv1248

Jenal, U., and Fuchs, T. (1998). An essential protease involved in bacterial cell-cycle control. *EMBO J.* 17, 5658–5669. doi: 10.1093/emboj/17.19.5658

Jeon, J. M., Lee, H. I., Sadowsky, M. J., Sugawara, M., and Chang, W. S. (2015). Characterization of a functional role of the *Bradyrhizobium japonicum* isocitrate lyase in desiccation tolerance. *Int. J. Mol. Sci.* 16, 16695–16709. doi: 10.3390/ijms160716695

Johnson, M., Zaretskaya, I., Raytselis, Y., Merezhuk, Y., McGinnis, S., and Madden, T. L. (2008). NCBI BLAST: a better web interface. *Nucleic Acids Res.* 36, W5–W9. doi: 10.1093/nar/gkn201

Jones, P., Binns, D., Chang, H. Y., Fraser, M., Li, W., McAnulla, C., et al. (2014). InterProScan 5: genome-scale protein function classification. *Bioinformatics* 30, 1236–1240. doi: 10.1093/bioinformatics/btu031

Jung, S., Yang, K., Lee, D.-E., and Back, K. (2004). Expression of *Bradyrhizobium japonicum* 5-aminolevulinic acid synthase induces severe photodynamic damage in transgenic rice. *Plant Sci.* 167, 789–795. doi: 10.1016/j.plantsci.2004.05.038

Kaneko, T., Nakamura, Y., Sato, S., Minamisawa, K., Uchiumi, T., Sasamoto, S., et al. (2002). Complete genomic sequence of nitrogen-fixing symbiotic bacterium *Bradyrhizobium japonicum* USDA110. *DNA Res.* 9, 189–197. doi: 10.1093/dnares/9.6.189

Kim, S., and Pevzner, P. A. (2014). MS-GF+ makes progress towards a universal database search tool for proteomics. *Nat. Commun.* 5:5277. doi: 10.1038/ncomms6277

Koch, M., Delmotte, N., Ahrens, C. H., Omasits, U., Schneider, K., Danza, F., et al. (2014). A link between arabinose utilization and oxalotrophy in *Bradyrhizobium japonicum*. *Appl. Environ. Microbiol.* 80, 2094–2101. doi: 10.1128/AEM.03314-13

Koch, M., Delmotte, N., Rehrauer, H., Vorholt, J. A., Pessi, G., and Hennecke, H. (2010). Rhizobial adaptation to hosts, a new facet in the legume root-nodule symbiosis. *Mol. Plant Microbe Interact.* 23, 784–790. doi: 10.1094/MPMI-23-6-0784

Körner, H., Sofia, H. J., and Zumft, W. G. (2003). Phylogeny of the bacterial superfamily of CRP-FNR transcription regulators: exploiting the metabolic spectrum by controlling alternative gene programs. *FEMS Microbiol. Rev.* 27, 559–592. doi: 10.1016/S0168-6445(03)00066-4

Lang, K., Lindemann, A., Hauser, F., and Göttfert, M. (2008). The genistein stimulon of *Bradyrhizobium japonicum*. *Mol. Genet. Genomics* 279, 203–211. doi: 10.1007/s00438-007-0280-7

Lardi, M., Murset, V., Fischer, H. M., Mesa, S., Ahrens, C. H., Zamboni, N., et al. (2016). Metabolomic profiling of *Bradyrhizobium diazoefficiens*-induced root nodules reveals both host plant-specific and developmental signatures. *Int. J. Mol. Sci.* 17:815. doi: 10.3390/ijms17060815

Lardi, M., and Pessi, G. (2018). Functional genomics approaches to studying symbioses between legumes and nitrogen-fixing rhizobia. *High Throughput* 7:15. doi: 10.3390/ht7020015

Larrainzar, E., and Wienkoop, S. (2017). A proteomic view on the role of legume symbiotic interactions. *Front. Plant. Sci.* 8:1267. doi: 10.3389/fpls.2017.01267

Larrainzar, E., Wienkoop, S., Weckwerth, W., Ladrera, R., Arrese-Igor, C., and González, E. M. (2007). *Medicago truncatula* root nodule proteome analysis reveals differential plant and bacteroid responses to drought stress. *Plant Physiol.* 144, 1495–1507. doi: 10.1104/pp.107.101618

Li, H. (2018). Minimap2: pairwise alignment for nucleotide sequences. *Bioinformatics* 34, 3094–3100. doi: 10.1093/bioinformatics/bty191

Lindemann, A., Moser, A., Pessi, G., Hauser, F., Friberg, M., Hennecke, H., et al. (2007). New target genes controlled by the *Bradyrhizobium japonicum* two-component regulatory system RegSR. *J. Bacteriol.* 189, 8928–8943. doi: 10.1128/JB.01088-07

Loferer, H., Bott, M., and Hennecke, H. (1993). *Bradyrhizobium japonicum* TlpA, a novel membrane-anchored thioredoxin-like protein involved in the biogenesis of cytochrome aa_3 and development of symbiosis. *EMBO J.* 12, 3373–3383. doi: 10.1002/j.1460-2075.1993.tb06011.x

Love, M. I., Huber, W., and Anders, S. (2014). Moderated estimation of fold change and dispersion for RNA-seq data with DESeq2. *Genome Biol.* 15:550. doi: 10.1186/s13059-014-0550-8

Ma, W., Penrose, D. M., and Glick, B. R. (2002). Strategies used by rhizobia to lower plant ethylene levels and increase nodulation. *Can. J. Microbiol.* 48, 947–954. doi: 10.1139/w02-100

Maglica, Z., Striebel, F., and Weber-Ban, E. (2008). An intrinsic degradation tag on the ClpA C-terminus regulates the balance of ClpAP complexes with different substrate specificity. *J. Mol. Biol.* 384, 503–511. doi: 10.1016/j.jmb.2008.09.046

Marx, H., Minogue, C. E., Jayaraman, D., Richards, A. L., Kwiecien, N. W., Siahpirani, A. F., et al. (2016). A proteomic atlas of the legume *Medicago truncatula* and its nitrogen-fixing endosymbiont *Sinorhizobium meliloti*. *Nat. Biotechnol.* 34, 1198–1205. doi: 10.1038/nbt.3681

Masloboeva, N., Reutimann, L., Stiefel, P., Follador, R., Leimer, N., Hennecke, H., et al. (2012). Reactive oxygen species-inducible ECF sigma factors of *Bradyrhizobium japonicum*. *PLoS ONE* 7:e43421. doi: 10.1371/journal.pone.0043421

Mesa, S., Bedmar, E. J., Chanfon, A., Hennecke, H., and Fischer, H. M. (2003). *Bradyrhizobium japonicum* NnrR, a denitrification regulator, expands the FixLJ-$FixK_2$ regulatory cascade. *J. Bacteriol.* 185, 3978–3982. doi: 10.1128/JB.185.13.3978-3982.2003

Mesa, S., Göttfert, M., and Bedmar, E. J. (2001). The *nir*, *nor*, and *nos* denitrification genes are dispersed over the *Bradyrhizobium japonicum* chromosome. *Arch. Microbiol.* 176, 136–142. doi: 10.1007/s002030100305

Mesa, S., Hauser, F., Friberg, M., Malaguti, E., Fischer, H. M., and Hennecke, H. (2008). Comprehensive assessment of the regulons controlled by the FixLJ-$FixK_2$-$FixK_1$ cascade in *Bradyrhizobium japonicum*. *J. Bacteriol.* 190, 6568–6579. doi: 10.1128/JB.00748-08

Mesa, S., Hennecke, H., and Fischer, H. M. (2006). A multitude of CRP/FNR-like transcription proteins in *Bradyrhizobium japonicum*. *Biochem. Soc. Trans.* 34, 156–159. doi: 10.1042/BST0340156

Mesa, S., Reutimann, L., Fischer, H. M., and Hennecke, H. (2009). Posttranslational control of transcription factor $FixK_2$, a key regulator for the *Bradyrhizobium japonicum*-soybean symbiosis. *Proc. Natl. Acad. Sci. U.S.A.* 106, 21860–21865. doi: 10.1073/pnas.0908097106

Mesa, S., Ucurum, Z., Hennecke, H., and Fischer, H. M. (2005). Transcription activation *in vitro* by the *Bradyrhizobium japonicum* regulatory protein $FixK_2$. *J. Bacteriol.* 187, 3329–3338. doi: 10.1128/JB.187.10.3329-3338.2005

Mongiardini, E. J., Quelas, J. I., Dardis, C., Althabegoiti, M. J., and Lodeiro, A. R. (2017). Transcriptional control of the lateral-flagellar genes of *Bradyrhizobium diazoefficiens*. *J. Bacteriol.* 199, e00253–e00217. doi: 10.1128/JB.00253-17

Morris, A. C., and Djordjevic, M. A. (2001). Proteome analysis of cultivar-specific interactions between *Rhizobium leguminosarum* biovar *trifolii* and

subterranean clover cultivar Woogenellup. *Electrophoresis* 22, 586–598. doi: 10.1002/1522-2683(200102)22:3<586::AID-ELPS586>3.0.CO;2-L

Murset, V., Hennecke, H., and Pessi, G. (2012). Disparate role of rhizobial ACC deaminase in root-nodule symbioses. *Symbiosis* 57, 45–50. doi: 10.1007/s13199-012-0177-z

Nambu, M., Tatsukami, Y., Morisaka, H., Kuroda, K., and Ueda, M. (2015). Quantitative time-course proteome analysis of *Mesorhizobium loti* during nodule maturation. *J. Proteomics* 125, 112–120. doi: 10.1016/j.jprot.2015.04.034

Narasimhan, V., Danecek, P., Scally, A., Xue, Y., Tyler-Smith, C., and Durbin, R. (2016). BCFtools/RoH: a hidden Markov model approach for detecting autozygosity from next-generation sequencing data. *Bioinformatics* 32, 1749–1751. doi: 10.1093/bioinformatics/btw044

Natera, S. H., Guerreiro, N., and Djordjevic, M. A. (2000). Proteome analysis of differentially displayed proteins as a tool for the investigation of symbiosis. *Mol. Plant Microbe Interact.* 13, 995–1009. doi: 10.1094/MPMI.2000.13.9.995

Nellen-Anthamatten, D., Rossi, P., Preisig, O., Kullik, I., Babst, M., Fischer, H. M., et al. (1998). *Bradyrhizobium japonicum* $FixK_2$, a crucial distributor in the FixLJ-dependent regulatory cascade for control of genes inducible by low oxygen levels. *J. Bacteriol.* 180, 5251–5255

O'Brian, M. R. (2015). Perception and homeostatic control of iron in the rhizobia and related bacteria. *Annu. Rev. Microbiol.* 69, 229–245. doi: 10.1146/annurev-micro-091014-104432

Omasits, U., Quebatte, M., Stekhoven, D. J., Fortes, C., Roschitzki, B., Robinson, M. D., et al. (2013). Directed shotgun proteomics guided by saturated RNA-seq identifies a complete expressed prokaryotic proteome. *Genome Res.* 23, 1916–1927. doi: 10.1101/gr.151035.112

Omasits, U., Varadarajan, A. R., Schmid, M., Goetze, S., Melidis, D., Bourqui, M., et al. (2017). An integrative strategy to identify the entire protein coding potential of prokaryotic genomes by proteogenomics. *Genome Res.* 27, 2083–2095. doi: 10.1101/gr.218255.116

Page, K. M., and Guerinot, M. L. (1995). Oxygen control of the *Bradyrhizobium japonicum hemA* gene. *J. Bacteriol.* 177, 3979–3984. doi: 10.1128/jb.177.14.3979-3984.1995

Panter, S., Thomson, R., de Bruxelles, G., Laver, D., Trevaskis, B., and Udvardi, M. (2000). Identification with proteomics of novel proteins associated with the peribacteroid membrane of soybean root nodules. *Mol. Plant Microbe Interact.* 13, 325–333. doi: 10.1094/MPMI.2000.13.3.325

Pauly, N., Pucciariello, C., Mandon, K., Innocenti, G., Jamet, A., Baudouin, E., et al. (2006). Reactive oxygen and nitrogen species and glutathione: key players in the legume-*Rhizobium* symbiosis. *J. Exp. Bot.* 57, 1769–1776. doi: 10.1093/jxb/erj184

Perez-Riverol, Y., Csordas, A., Bai, J., Bernal-Llinares, M., Hewapathirana, S., Kundu, D. J., et al. (2019). The PRIDE database and related tools and resources in 2019: improving support for quantification data. *Nucleic Acids Res.* 47, D442–D450. doi: 10.1093/nar/gky1106

Pessi, G., Ahrens, C. H., Rehrauer, H., Lindemann, A., Hauser, F., Fischer, H.-M., et al. (2007). Genome-wide transcript analysis of *Bradyrhizobium japonicum* bacteroids in soybean root nodules. *Mol. Plant Microbe Interact.* 20, 1353–1363. doi: 10.1094/MPMI-20-11-1353

Poole, P., Ramachandran, V., and Terpolilli, J. (2018). Rhizobia: from saprophytes to endosymbionts. *Nat. Rev. Microbiol.* 16, 291–303. doi: 10.1038/nrmicro.2017.171

Preisig, O., Zufferey, R., and Hennecke, H. (1996). The *Bradyrhizobium japonicum fixGHIS* genes are required for the formation of the high-affinity cbb_3-type cytochrome oxidase. *Arch. Microbiol.* 165, 297–305. doi: 10.1007/s002030050330

Qeli, E., and Ahrens, C. H. (2010). PeptideClassifier for protein inference and targeted quantitative proteomics. *Nat. Biotechnol.* 28, 647–650. doi: 10.1038/nbt0710-647

Rahman, O., Cummings, S. P., Harrington, D. J., and Sutcliffe, I. C. (2008). Methods for the bioinformatic identification of bacterial lipoproteins encoded in the genomes of Gram-positive bacteria. *World J. Microbiol. Biotechnol.* 24, 2377–2382. doi: 10.1007/s11274-008-9795-2

Regensburger, B., and Hennecke, H. (1983). RNA polymerase from *Rhizobium japonicum*. *Arch. Microbiol.* 135, 103–109. doi: 10.1007/BF00408017

Regensburger, B., and Hennecke, H. (1984). Free-living and symbiotic nitrogen-fixing ability of *Rhizobium japonicum* is unaffected by rifampicin resistance mutations. *FEMS Microbiol. Lett.* 21, 77–81. doi: 10.1111/j.1574-6968.1984.tb00189.x

Regensburger, B., Meyer, L., Filser, M., Weber, J., Studer, D., Lamb, J. W., et al. (1986). *Bradyrhizobium japonicum* mutants defective in root-nodule bacteroid development and nitrogen fixation. *Arch. Microbiol.* 144, 355–366. doi: 10.1007/BF00409885.

Renier, A., Maillet, F., Fardoux, J., Poinsot, V., Giraud, E., and Nouwen, N. (2011). Photosynthetic *Bradyrhizobium* sp. strain ORS285 synthesizes 2-O-methylfucosylated lipochitooligosaccharides for *nod* gene-dependent interaction with *Aeschynomene* plants. *Mol. Plant Microbe Interact.* 24, 1440–1447. doi: 10.1094/MPMI-05-11-0104

Reutimann, L., Mesa, S., and Hennecke, H. (2010). Autoregulation of $fixK_2$ gene expression in *Bradyrhizobium japonicum*. *Mol. Genet. Genomics* 284, 25–32. doi: 10.1007/s00438-010-0547-2

Robledo, M., Jiménez-Zurdo, J. I., and Becker, A. (2015). Antisense transcription of symbiotic genes in *Sinorhizobium meliloti*. *Symbiosis* 67, 55–67. doi: 10.1007/s13199-015-0358-7

Rudolph, G., Semini, G., Hauser, F., Lindemann, A., Friberg, M., Hennecke, H., et al. (2006). The iron control element, acting in positive and negative control of iron-regulated *Bradyrhizobium japonicum* genes, is a target for the Irr protein. *J. Bacteriol.* 188, 733–744. doi: 10.1128/JB.188.2.733-744.2006

Sarma, A. D., and Emerich, D. W. (2005). Global protein expression pattern of *Bradyrhizobium japonicum bacteroids*: a prelude to functional proteomics. *Proteomics* 5, 4170–4184. doi: 10.1002/pmic.200401296

Schlüter, J. P., Reinkensmeier, J., Barnett, M. J., Lang, C., Krol, E., Giegerich, R., et al. (2013). Global mapping of transcription start sites and promoter motifs in the symbiotic α-proteobacterium *Sinorhizobium meliloti* 1021. *BMC Genomics* 14:156. doi: 10.1186/1471-2164-14-156

Schmid, M., Frei, D., Patrignani, A., Schlapbach, R., Frey, J. E., Remus-Emsermann, M. N. P., et al. (2018). Pushing the limits of *de novo* genome assembly for complex prokaryotic genomes harboring very long, near identical repeats. *Nucleic Acids Res.* 46, 8953–8965. doi: 10.1093/nar/gky726

Sciotti, M. A., Chanfon, A., Hennecke, H., and Fischer, H. M. (2003). Disparate oxygen responsiveness of two regulatory cascades that control expression of symbiotic genes in *Bradyrhizobium japonicum*. *J. Bacteriol.* 185, 5639–5642. doi: 10.1128/JB.185.18.5639-5642.2003

Serventi, F., Youard, Z. A., Murset, V., Huwiler, S., Bühler, D., Richter, M., et al. (2012). Copper starvation-inducible protein for cytochrome oxidase biogenesis in *Bradyrhizobium japonicum*. *J. Biol. Chem.* 287, 38812–38823. doi: 10.1074/jbc.M112.406173

Sović, I., Šikić, M., Wilm, A., Fenlon, S. N., Chen, S., and Nagarajan, N. (2016). Fast and sensitive mapping of nanopore sequencing reads with GraphMap. *Nat. Commun.* 7:11307. doi: 10.1038/ncomms11307

Sprent, J. I., Ardley, J., and James, E. K. (2017). Biogeography of nodulated legumes and their nitrogen-fixing symbionts. *New Phytol.* 215, 40–56. doi: 10.1111/nph.14474

Taniguchi, Y., Choi, P. J., Li, G. W., Chen, H., Babu, M., Hearn, J., et al. (2010). Quantifying *E. coli* proteome and transcriptome with single-molecule sensitivity in single cells. *Science* 329, 533–538. doi: 10.1126/science.1188308

Tatsukami, Y., Nambu, M., Morisaka, H., Kuroda, K., and Ueda, M. (2013). Disclosure of the differences of *Mesorhizobium loti* under the free-living and symbiotic conditions by comparative proteome analysis without bacteroid isolation. *BMC Microbiol.* 13:180. doi: 10.1186/1471-2180-13-180.

Tatusova, T., DiCuccio, M., Badretdin, A., Chetvernin, V., Nawrocki, E. P., Zaslavsky, L., et al. (2016). NCBI prokaryotic genome annotation pipeline. *Nucleic Acids Res.* 44, 6614–6624. doi: 10.1093/nar/gkw569

Terpolilli, J. J., Hood, G. A., and Poole, P. S. (2012). What determines the efficiency of N_2-fixing *Rhizobium*-legume symbioses? *Adv. Microb. Physiol.* 60, 325–389. doi: 10.1016/B978-0-12-398264-3.00005-X

Thorvaldsdóttir, H., Robinson, J. T., and Mesirov, J. P. (2013). Integrative Genomics Viewer (IGV): high-performance genomics data visualization and exploration. *Brief Bioinform.* 14, 178–192. doi: 10.1093/bib/bbs017

Torres, M. J., Argandoña, M., Vargas, C., Bedmar, E. J., Fischer, H. M., Mesa, S., et al. (2014). The global response regulator RegR controls expression of denitrification genes in *Bradyrhizobium japonicum*. *PLoS ONE* 9:e99011. doi: 10.1371/journal.pone.0099011

Torres, M. J., Bueno, E., Jiménez-Leiva, A., Cabrera, J. J., Bedmar, E. J., Mesa, S., et al. (2017). $FixK_2$ Is the main transcriptional activator of *Bradyrhizobium diazoefficiens nosRZDYFLX* genes in response to low oxygen. *Front. Microbiol.* 8:1621. doi: 10.3389/fmicb.2017.01621

Vargas, C., McEwan, A. G., and Downie, J. A. (1993). Detection of *c*-type cytochromes using enhanced chemiluminescence. *Anal. Biochem.* 209, 323–326. doi: 10.1006/abio.1993.1127

Velasco, L., Mesa, S., Xu, C. A., Delgado, M. J., and Bedmar, E. J. (2004). Molecular characterization of *nosRZDFYLX* genes coding for denitrifying nitrous oxide reductase of *Bradyrhizobium japonicum*. *Antonie Van Leeuwenhoek* 85, 229–235. doi: 10.1023/B:ANTO.0000020156.42470.db

Winzer, T., Bairl, A., Linder, M., Linder, D., Werner, D., and Müller, P. (1999). A novel 53-kDa nodulin of the symbiosome membrane of soybean nodules, controlled by *Bradyrhizobium japonicum*. *Mol. Plant Microbe Interact.* 12, 218–226. doi: 10.1094/MPMI.1999.12.3.218

Wiśniewski, J. R., Zougman, A., and Mann, M. (2009a). Combination of FASP and StageTip-based fractionation allows in-depth analysis of the hippocampal membrane proteome. *J. Proteome Res.* 8, 5674–5678. doi: 10.1021/pr900748n

Wiśniewski, J. R., Zougman, A., Nagaraj, N., and Mann, M. (2009b). Universal sample preparation method for proteome analysis. *Nat. Methods* 6, 359–362. doi: 10.1038/nmeth.1322

Yu, N. Y., Wagner, J. R., Laird, M. R., Melli, G., Rey, S., Lo, R., et al. (2010). PSORTb 3.0: improved protein subcellular localization prediction with refined localization subcategories and predictive capabilities for all prokaryotes. *Bioinformatics* 26, 1608–1615. doi: 10.1093/bioinformatics/btq24

Conflict of Interest Statement: The authors declare that the research was conducted in the absence of any commercial or financial relationships that could be construed as a potential conflict of interest.

The handling editor declared a past supervisory role with one of the authors RL.

frontiers in Microbiology

ORIGINAL RESEARCH
published: 03 July 2019
doi: 10.3389/fmicb.2019.01526

The Nitrate Assimilatory Pathway in *Sinorhizobium meliloti*: Contribution to NO Production

*Bryan Ruiz, Alexandre Le Scornet, Laurent Sauviac, Antoine Rémy, Claude Bruand and Eliane Meilhoc**

Laboratoire des Interactions Plantes-Microorganismes (LIPM), INRA, CNRS, INSA, Université de Toulouse, Castanet-Tolosan, France

The interaction between rhizobia and their legume host plants culminates in the formation of specialized root organs called nodules in which differentiated endosymbiotic bacteria (bacteroids) fix atmospheric nitrogen to the benefit of the plant. Interestingly, nitric oxide (NO) has been detected at various steps of the rhizobium-legume symbiosis where it has been shown to play multifaceted roles. It is recognized that both bacterial and plant partners of the *Sinorhizobium meliloti–Medicago truncatula* symbiosis are involved in NO synthesis in nodules. *S. meliloti* can also produce NO from nitrate when living as free cells in the soil. *S. meliloti* does not possess any NO synthase gene in its genome. Instead, the denitrification pathway is often described as the main driver of NO production with nitrate as substrate. This pathway includes the periplasmic nitrate reductase (Nap) which reduces nitrate into nitrite, and the nitrite reductase (Nir) which reduces nitrite into NO. However, additional genes encoding putative nitrate and nitrite reductases (called *narB* and *nirB*, respectively) have been identified in the *S. meliloti* genome. Here we examined the conditions where these genes are expressed, investigated their involvement in nitrate assimilation and NO synthesis in culture and their potential role *in planta*. We found that *narB* and *nirB* are expressed under aerobic conditions in absence of ammonium in the medium and most likely belong to the nitrate assimilatory pathway. Even though these genes are clearly expressed in the fixation zone of legume root nodule, they do not play a crucial role in symbiosis. Our results support the hypothesis that in *S. meliloti,* denitrification remains the main enzymatic way to produce NO while the assimilatory pathway involving NarB and NirB participates indirectly to NO synthesis by cooperating with the denitrification pathway.

Keywords: nitric oxide, *Sinorhizobium meliloti*, denitrification, symbiosis, *Medicago truncatula*, nitrate assimilation

OPEN ACCESS

Edited by:
Maria J. Delgado, Spanish National Research Council (CSIC), Spain

Reviewed by:
Michael Kahn, Washington State University, United States
Nicholas James Watmough, University of East Anglia, United Kingdom

****Correspondence:***
Eliane Meilhoc
Eliane.Meilhoc@inra.fr

Specialty section:
This article was submitted to Microbial Symbioses, a section of the journal Frontiers in Microbiology

Received: *21 December 2018*
Accepted: *18 June 2019*
Published: *03 July 2019*

Citation:
Ruiz B, Le Scornet A, Sauviac L, Rémy A, Bruand C and Meilhoc E (2019) The Nitrate Assimilatory Pathway in Sinorhizobium meliloti: Contribution to NO Production. Front. Microbiol. 10:1526. doi: 10.3389/fmicb.2019.01526

INTRODUCTION

Rhizobia are Gram negative bacteria which are found as free-living organisms in the soil but also have the unique capacity to establish a nitrogen fixing endosymbiosis with legumes. Indeed rhizobia possess the capacity to reduce atmospheric nitrogen into ammonium to the benefit of their host plants thanks to their nitrogenase. As a consequence, in contrast to other plants, legumes can grow

without addition of exogenous nitrogen (i.e., fertilizers) which is compatible with the development of sustainable agriculture practices.

Due to their agronomical and environmental interest, legume-rhizobium symbioses have been studied for many years and molecular determinants governing the recognition step between the two partners, the infection and the bacteroid differentiation process including nitrogen fixation, have been identified. Among those, nitric oxide (NO) has been detected at every step of the symbiotic interaction (Hichri et al., 2016b). NO is a diffusible and reactive gaseous molecule that plays a major signaling role in various processes in mammals. The importance of NO in plants emerged recently but it is now well described that it participates in numerous plant signaling pathways such as those controlling seed germination, root growth, flowering and stomatal closure (Domingos et al., 2015). Interestingly, it has also been shown that NO is involved in the hypersensitive response (HR) during the plant defense response against pathogen attack (Boccara et al., 2005).

Although the role of NO during the symbiotic interaction is not fully understood, it has been shown that NO can have a positive role during the infection steps, while it can inhibit the bacterial nitrogenase responsible for nitrogen fixation, and the plant glutamine synthetase involved in nitrogen assimilation (Trinchant and Rigaud, 1982; del Giudice et al., 2011; Melo et al., 2011). NO has also been shown to be a signal for nodule senescence (Cam et al., 2012). Hence, to maintain efficient infection and nitrogen fixation, the level of NO inside legume root nodules must be finely tuned. The NO level results from a balance between NO synthesis and consumption, two processes which rely on both partners (Hichri et al., 2016a). Indeed, both plant and bacterial hemoglobins have been shown to be involved in NO transformation or detoxification (Berger et al., 2018). In addition, the bacterial NO reductase Nor, catalyzing the reduction of NO into nitrous oxide (N_2O) in the denitrification pathway is also involved in NO consumption in legume nodules.

Even though both plant and bacteroid participate in NO production, the relative contribution of each partner varies between different legume-rhizobium models (Sánchez et al., 2010; Horchani et al., 2011). In the symbiosis between *Bradyrhizobium japonicum* and soybean, bacteria account for about 90% of NO present in the nodules, while in the *S. meliloti*–*M. truncatula* symbiosis the bacteria produce about 35% of the amount of NO detected. Neither rhizobia nor legumes possess a gene that encodes a NO synthase of the type found in mammalian cells (Jeandroz et al., 2016). NO can originate from different routes in plants, the best characterized being the stepwise reduction of nitrate (Boscari et al., 2013; Astier et al., 2017). In *M. truncatula*, at least two out of the three nitrate reductase genes identified in the genome encode proteins that seem to be involved in NO synthesis (Berger et al., 2018). The second step of the reaction (i.e., production of NO from nitrite) could be catalyzed through the action of the mitochondrial electron transport chain in plants (Horchani et al., 2011).

On the bacteroid side, the denitrification pathway, which has been well characterized in *B. japonicum* and *S. meliloti* (**Figure 1**) is the most likely source of NO, not only during the symbiotic interaction with legumes but also in soils (Torres et al., 2011, 2014). The regulation of this pathway has been well described in both organisms. In *S. meliloti*, the expression of *nap* genes is regulated in response to oxygen levels by the transcriptional regulator FixK, itself under the control of the two-component system FixLJ. The expression of the *nir* and *nor* genes is mainly regulated by the NO specific regulator NnrR, present in many rhizobia and, as a consequence, their expression depends upon the presence of NO (Meilhoc et al., 2010).

Recent work has shown that in *B. japonicum*, the nitrate assimilation pathway which includes a nitrate reductase NasC and an assimilatory nitrite reductase NirA, could also produce NO by a yet unknown mechanism (Cabrera et al., 2016). Luque-Almagro et al. (2011) examined a number of available genomes and suggested that the nitrate assimilation pathway in *S. meliloti* might include four genes (i.e., *nirB nirD narB cysG*). Assimilatory nitrate and nitrite reductase enzymatic activities were detected in *S. meliloti* cultures grown in presence of nitrate and reduced in the presence of ammonium (Kumar Halder and Chakrabartty, 2015). Interestingly NarB displays 53% identity and shares four main protein domains with NasC. NirBD is anticipated to be a siroheme-dependent assimilatory nitrite reductase that catalyses reduction of nitrite to ammonia and as such, shares the same function with NirA from *B. japonicum*. However, there is no synteny between both organisms regarding these genes. Indeed while both genes are located next to each other in the *S. meliloti* genome, in *B. japonicum* the genes that encode NasC and NirA are located at different loci. *cysG* (SMb20987) encodes a putative uroporphyrin-III C-methyltransferase involved in the synthesis of sirohaem, the nitrite reductase cofactor.

In this work we analyzed the expression profiles of *narB* and *nirB* genes in free-living conditions and *in planta*, and addressed the question whether they belong to the nitrate assimilatory pathway and are involved in NO synthesis. Finally, we examined different phenotypes of *M. truncatula* plants inoculated with a *S. meliloti* strain mutated in *narB* or *nirBD narB*.

MATERIALS AND METHODS

Bacterial Strains and Growth Conditions

The bacterial strains and plasmids used are listed in **Table 1**.

Sinorhizobium meliloti strains were grown in Luria Bertani medium supplemented with 2.5 mM $CaCl_2$ and 2.5 mM $MgSO_4$ (LBMC). When necessary, antibiotics were added in the medium at the following concentrations: streptomycin (Sm) 100 or 300 μg/ml, neomycin (Neo) 100 μg/ml and gentamycin (Gm) 40 μg/ml. To test cell growth, gene expression or NO production, *S. meliloti* was grown in the exponential phase at an optical density at 600 nm of 0.2 (OD_{600} = 0.2) in Vincent Minimal Medium (VMM) with either NH_4Cl (18.7 mM) or glutamate (10 mM) as nitrogen source, at 28°C (del Giudice et al., 2011). When needed, KNO_3 (20 mM), or spermine NONOate (25 μM, from a 100 mM stock solution in NaOH 1 mM) were added to the culture. Microaerobic cultures were grown under a 2% oxygen atmosphere.

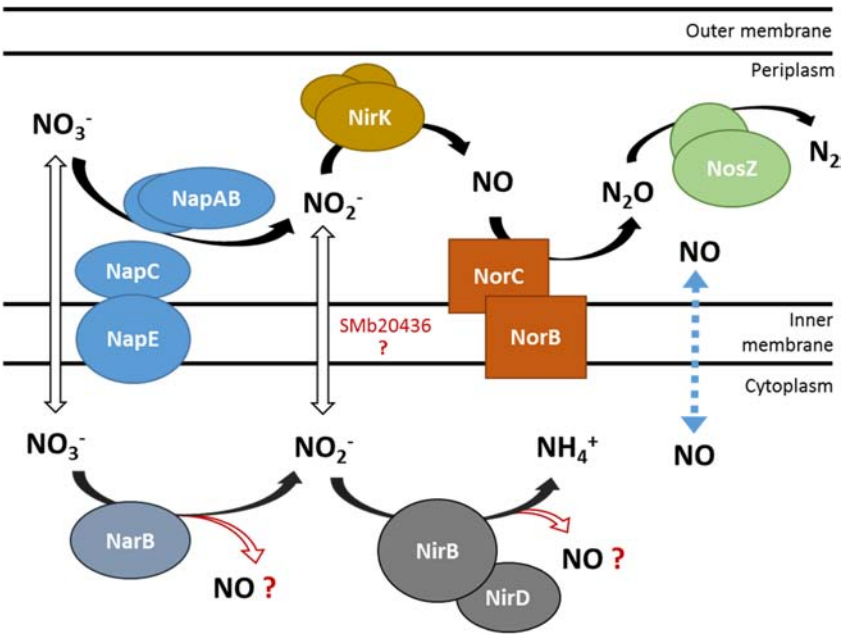

FIGURE 1 | Schematic representation of nitrate utilization and NO production by the denitrification and putative NarB NirB pathways. NO_3^- and NO_2^- transporters are not identified yet in *S. meliloti*. The dotted line represents NO diffusion across the cytoplasmic membrane. Enzymes involved in the denitrification pathway: Nap (nitrate reductase), Nir (nitrite reductase), Nor (NO reductase), Nos (nitrous oxide reductase). SMb20436: *B. japonicum* NarK homolog, putative nitrite transporter. NarB, putative assimilatory nitrate reductase; NirBD, putative assimilatory nitrite reductase.

Construction of *S. meliloti* Mutant Strains

All plasmid constructions were performed in *Escherichia coli* DH5α. The DNA sequences of oligonucleotide primers used for PCR amplification are shown in **Table 2**.

To construct the *narB* mutant, the 5′ and 3′ flanking regions of *narB* were amplified by PCR by using genomic DNA of the strain GMI11495 (CBT707) as template and the oligonucleotides OCB1567/OCB1568 to amplify the 5′ flanking region (413 bp) and OCB1569/OCB1570 to amplify the 3′ flanking region (413 bp). The PCR fragments were then ligated with pGEM-T yielding plasmids pGEM 5′UTR*narB* and pGEM 3′UTR*narB,* respectively. The cloned *S. meliloti* regions were verified by DNA sequencing. The plasmids were digested with either *Bam*HI/*Sal*I or BamHI/*Sac*I to isolate the 5′ and 3′ UTR, respectively. The UTRs were ligated with pJQ200mp19 digested with *Sal*I/*Sac*I yielding pJQ 5′3 ′UTR*narB*.

pJQ 5′3′UTR*narB* was introduced into *S. meliloti* GMI11495 (CBT707) by electroporation to yield the strain CBT2474 (Ferri et al., 2010; Dupuy et al., 2017). For this, first a single crossing over genomic integration was selected by Gm resistance. The resulting strain was then grown in the absence of antibiotics and cells having lost the plasmid following a second recombination event were selected by plating on LBMC medium supplemented with 5% sucrose as the plasmid carries the *sacB* gene which is lethal for *S. meliloti* in the presence of sucrose. A Gm sensitive clone that grew on sucrose containing medium was selected and the deletion was verified by PCR using the primers OCB1611/OCB1612 and by sequencing the product.

The whole *nirBD–narB* region was deleted by constructing a pJQ200mp19 plasmid containing the 5′*nirB* flanking region and the 3′*narB* flanking region. The 5′ flanking region of *nirB* was amplified by PCR by using genomic DNA of the

TABLE 1 | List of plasmids and strains used.

Plasmids and strains	Description	References
Plasmids		
pGEM-T	Cloning vector, Amp^r	Promega
pGEM 5′UTR*nirB*	5′UTR*nirB* ligated with pGEM-T	This work
pGEM 5′UTR*narB*	5′UTR*narB* ligated with pGEM-T	This work
pGEM 3′UTR*narB*	3′UTR*narB* ligated with pGEM-T	This work
pJQ200mp19	Gene replacement vector, Gm^r	Quandt and Hynes, 1993
pJQ 5′3′UTR*narB*	5′3′UTR*snarB* ligated with pJQ	This work
pJQ 5′UTR*nir*B3′UTR*narB*	5′UTR*nir*B3′UTR*narB* ligated with pJQ	This work
E. coli		
DH5α	F-Φ80 *lacZ*ΔM15 Δ(*lacZYα argF*) U169 *recA1 endA1 hsdR17* (rk−, mk+) *phoA supE44 thi-1 gyrA96 relA1* λ-	Invitrogen
S. meliloti		
GMI11495 (CBT707)	*S. meliloti* 2011 Sm^R	Pobigaylo et al., 2006
CBT612	CBT707 *napA*::Tn*5*, Sm^R, Neo^R	Pobigaylo et al., 2006
CBT614	CBT707 *nirK*::Tn*5*, Sm^R, Neo^R	Pobigaylo et al., 2006
CBT2473	CBT707 Δ*nirB nirD narB*, Sm^R	This work
CBT2474	CBT707 Δ*narB*, Sm^R	This work

TABLE 2 | List of oligonucleotides.

Oligonucleotides	Sequences 5′-3′	Description
OCB1557	GTCGACGCTGATCATTGCGA	fw *nirB5*′
OCB1558	GGATCCTTCAGTCATGTGGT	rev *nirB5*′
OCB1606	CGTCATCCTTGACCAGGGTC	fw *nirBDnarB* deletion screening
OCB1567	GTCGACGACAAGCACGAGTT	fw *narB5*′
OCB1568	GGATCCTCTTATTCCGCCGC	rev *narB5*′
OCB1569	GGATCCATCTGGCCCAAAAG	fw *narB3*′
OCB1570	GAGCTCCGATCCGAACTGGA	rev *narB3*′
OCB1611	CCTATTTCGACCGCTTCGTC	fw *narB* deletion screening
OCB1612	CGGATCGCCTGTGCCAGG	rev *narB* and *nirBDnarB* deletion screening
OCB1607	CTGCCGAAATTGGCGGGATG	*nirB* rev
OCB1587	TTCTTCCGGCTCTTCGAAAC	qRTPCR *narB* fw
OCB1588	CGAGATGGCAGTTGATGATG	qRTPCR *narB* rev
OCB1583	ATGTCATGCCGACACTGATG	qRTPCR *nirB* fw
OCB1584	CTTTGTGACGACCTTGATGC	qRTPCR *nirB* rev
OCB1638	GTCATCGACCTCACCCATTT	qRTPCR SMc01171 fw
OCB1639	TCTGCAGCAAGAACCACTTG	qRTPCR SMc01171 rev
OCB1914	TCGGCGTCAACCAGATCACTGC	qRTPCR *narB* fw
OCB1915	AATGCTTCTGCATCGGATTGCTCG	qRTPCR *cysG* rev

strain GMI11495 (CBT707) as template and the oligonucleotides OCB1557/OCB1558 as primers (fragment size 423 bp). The PCR fragment was then ligated with pGEM-T yielding plasmid pGEM 5′UTR*nirB*. The cloned *S. meliloti* region was verified by DNA sequencing. The plasmids pGEM 5′UTR*nirB* and pGEM 3′UTR*narB* were digested with either *Bam*HI/*SalI* or BamHI/*Sac*I to obtain the 5′ and 3′ UTR, respectively. The UTRs were ligated with pJQ200mp19 digested with *Sal*I/ *Sac*I yielding pJQ 5′UTR*nir*B3′UTR*narB*. The plasmid was introduced into *S. meliloti* GMI11495 (CBT707) by electroporation to give the strains CBT2473. The deletion was verified by PCR using the primers OCB1606/OCB1612 and by sequencing the product.

Measurement of NO Production in *S. meliloti* Cultures

Sinorhizobium meliloti strains were grown exponentially at 28°C in VMM containing either NH_4Cl or glutamate (OD_{600} = 0.2–0.3). To remove NH_4Cl or glutamate from the medium, cells were collected by centrifugation (8000 × *g*, 10 min), washed once with sterile water, resuspended in VMM without NH_4Cl or glutamate. When needed, KNO_3 (20 mM) was added to the cultures. Cultures were then either kept at 28°C under agitation (aerobic conditions) or left without agitation under 2% oxygen atmosphere (microaerobic conditions) for 1.5 h. The NO produced by bacteria and released in the culture medium was quantified using the fluorescent non-permeable probe DAF-2 (Sigma-Aldrich). To measure NO level, 1 ml of culture was transferred to a tube containing DAF-2 (1 µl of a 5 mM solution in DMSO). Tubes were then kept for 1 h at 20°C in the dark. 100 µl of the suspension were then transferred to a 96 well plate (Greiner, dark bottom). Fluorescence was measured using a microplate spectrofluorimeter (Fluostar Omega, BMG Labtech, Champigny sur Marne, France) (excitation wavelength 485 nm/emission wavelength 520 nm). NO produced is expressed as fluorescence/OD_{600} (measured just before incubation with DAF-2). Different concentrations of the NO donor, spermineNONOate, were tested under the same conditions to verify that the fluorescence obtained was proportional to the NO amount. In addition, two other controls were performed to test the method specificity (data not shown): (1) the fluorescence signal was drastically increased when using an *hmp S. meliloti* mutant strain affected in NO degradation, (2) the fluorescence was reduced when using an *S. meliloti* strain overexpressing *hmp* (Cam et al., 2012). The experiment was repeated four times, with two technical repeats for each biological repeat.

Nitrite Determination in the Culture Medium

Cultures were grown as described above. For every culture sample collected to measure NO production, a second 1 ml aliquot was withdrawn to assay nitrite concentration in the medium. For this, the sample was centrifuged (10000 *g*, 5 min) and 100 µl of supernatant were incubated for 30 min (room temperature) with the Griess reagent (Nicholas and Nason, 1957). Absorbance was measured at 540 nm. NO_2^- concentration was calculated from a calibration curve using $NaNO_2$ (from 0 to 50 µM). The experiment was repeated five times, with two technical repeats for each biological repeat.

RNA Extraction

Strains were grown exponentially at 28°C in VMM. At an OD_{600} between 0.2 and 0.3, Spermine NONOate (25 µM) or KNO_3 (20 mM) was added to the culture. Cultures were incubated at 28°C either under agitation in aerobic conditions or under 2% oxygen atmosphere without agitation. 1.5 and 3 h later, cells (20 ml) were collected by filtration, immediately frozen in liquid nitrogen and stored at −80°C until RNA extraction. When needed, NH_4Cl was removed as described before.

RNA was prepared from the collected samples by incubating filters for 20 min at 65°C in lysis buffer (SDS 1.4%, EDTA 4 mM, Proteinase K 40 µg/ml). Lysates were then incubated at 4°C (10 min) in presence of NaCl (1.7 M) and centrifuged. Nucleic acids were precipitated from the supernatant in the presence of isopropanol (4°C, 1 h), washed with ethanol 70%, dried and resuspended in DEPC-treated water (100 µg/µl). RNA was purified using the RNeasy kit (Qiagen) followed by DNAse treatment (TURBO DNA-free kit, Invitrogen) (37°C, 1 h). Sample concentration and purity were measured with a nanodrop (Nanodrop ND-1000, ThermoFisher Scientific).

qRT-PCR Analysis

Reverse transcription was performed using Superscript II (Invitrogen) and random hexamers as primers. RNA samples isolated from at least three independent cultures were tested for

each condition. Real time RT-PCR tests were run on a Light Cycler 480 (Roche) using the SYBR Green I Master kit (Roche) according to the manufacturer instructions. A calibration curve was established for each gene with known amounts of *S. meliloti* genomic DNA. The *S. meliloti* gene SMc01171 was used as a reference for normalization as its expression was constant in all conditions tested. Primers used for expression analyses of each gene are indicated in **Table 2**.

The cDNA generated were also used for amplification of putative intergenic regions between *nirBD* and *narB* using primers OCB1611/OCB1607 and between *narB* and *cysG* using primers OCB1914/OCB1915. In negative controls, reverse transcriptase was omitted while in positive controls PCR was performed with *S. meliloti* genomic DNA as template.

Plant Assays

Seeds of *M. truncatula* cv jemalong A17 were surface sterilized, germinated on agar plates and allowed to grow on nitrogen-free Fahreus medium in test tubes during 2 days (Garcia et al., 2006). Series of plants were inoculated with either the wild type or the mutant strains (100 µl per plant of a resuspension in sterile water at OD_{600} = 0.001) or with 100 µl water as a control. Plants were grown in a culture room (22°C) with day and night periods of 16 and 8 h, respectively. Dry weights of the plant shoots were measured 4 and 5 weeks post-inoculation.

Nodules were macroscopically estimated as senescent when a green color was visible on a significant part of the nodule volume. The proportion of senescent nodules for each plant was calculed by dividing the number of senescent nodules by the total number of nodules (expressed in %).

The average number of nodules per plant, the percentage of senescent nodules and the dry weight of shoots were calculated from 19 to 27 plants (total number of plants obtained from three independent series).

Nitrogenase activity was determined by the acetylene reduction assay (Hardy et al., 1968), using plants grown in test tubes fitted with rubber stoppers. 1 ml of acetylene was added to each tube. Plants were then incubated in the growth chamber for 3 h. One ml of gas was taken from each tube and analyzed for ethylene content, using a gas chromograph equipped with a hydrogen flame ionization detector (7820A Agilent). The amount of ethylene produced by each plant was assessed by measuring the ethylene peak area and comparing to a standard (ethylene). Nitrogenase activity was measured on 7–9 plants for each genotype and each time point.

RESULTS

Expression of *narB* and *nirB* Genes in *S. meliloti*

Even though *narB* and *nirB* are assumed to be part of the nitrate assimilation pathway in *S. meliloti* no experimental data were available (Luque-Almagro et al., 2011). Ferroni and colleagues measured nitrate reductase total activity in *S. meliloti* cultures grown under aerobic and microaerobic conditions in the presence of nitrite and/or nitrate (Ferroni et al., 2011). These authors suggested that nitrate reductase activity in aerobic conditions could be associated with assimilatory ammonification, in line with the work of (Sekiguchi and Maruyama, 1988). A more recent study in *S. meliloti* showed that a nitrate assimilatory enzyme activity, estimated through detection of nitrite in the medium, was observed when nitrate was in the medium and that the generation of nitrite was drastically reduced when ammonium was also present (Kumar Halder and Chakrabartty, 2015). No link has been made so far between assimilatory nitrate/nitrite reductase activities and the genes encoding these functions.

To gain insight into the conditions of expression of *narB* and *nirB* we analyzed gene expression in different culture conditions by using qRT-PCR.

First, to investigate the transcriptional architecture of the region, PCR experiments were performed on cDNA to detect whether a transcript spanned the intergenic regions shown in **Figure 2** between *nirBD* and *narB* (a) or between *narB* and *cysG* (b). PCR generated a 600 bp DNA fragment for the region labelled as (a) indicating that *narB*, *nirB, and nirD* could be in a single transcriptional unit. Similarly, a 473 bp fragment was obtained for region (b) showing that *cysG*, located downstream of *narB* could also be transcribed with it.

narB and *nirB* expression was first analyzed in conditions in which denitrification genes are known to be expressed. Expression was analyzed 1.5 and 3 h after addition of either nitrate or NO donor. A decrease in gene expression level was observed at 3 h (data not shown); hence, only the set of results obtained at 1.5 h is shown in **Figure 3A**. We first observed that the expression of both genes were at comparable levels, confirming that they share the same regulation, as expected if they were part of the same operon. The expression level was low whether cells were grown in aerobic (20% O_2) or microaerobic conditions (2% O_2). Expression was not significantly affected by addition of nitrate or a NO donor in the medium. These results are in agreement with previous microarray data which did not identify these genes as being regulated by low oxygen or NO (Bobik et al., 2006; Meilhoc et al., 2010). *napA* and *nirK* expression was assessed in the same set of experiments. *napA* expression level was low, with about the same order of magnitude as *narB* and *nirB*. *nirK* was found to be expressed at a much higher level, especially when NO was added to the medium (in either aerobic or microaerobic conditions) in agreement with previous results (Meilhoc et al., 2010) (data not shown). In a second set of experiments we removed NH_4Cl from the culture medium as ammonium is known to repress assimilatory nitrate reductase activity. The results obtained are shown in **Figure 3B**. Strikingly, the expression of *narB* and *nirB* was about 1000-fold higher when ammonium was removed from the medium, indicating that *narB* and *nirB* gene expression was indeed inhibited by ammonium. Both *narB* and *nirB* displayed similar expression patterns and their expression was comparable whether cells were incubated in aerobic or microaerobic conditions. NO did not influence significantly *narB* and *nirB* gene expression and nitrate only slightly induced the expression level of both genes. *napA* and *nirK* expression levels were not significantly modified when NH_4Cl was removed from the medium (data not shown).

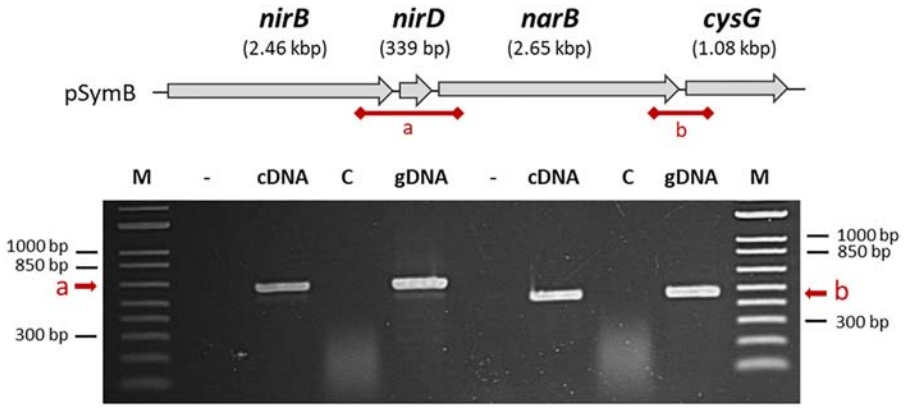

FIGURE 2 | Organization of *nirB*, *nirD,* and *narB* genes on the *S. meliloti* genome. *nirB, nirD*, *narB,* and *cysG* genes are located on the *S. meliloti* megaplasmid pSymB as indicated at the top of the figure. The putative intergenic regions which are tested by PCR in the bottom part of the Figure are called (a) and (b). Total RNA isolated from cells grown in aerobic conditions in VMM without NH_4Cl in the presence of nitrate served as template for cDNA synthesis in the presence (cDNA) or in absence of reverse transcriptase enzyme (control, C). Genomic DNA was used as a positive control for PCR amplifications. The first lane (–) is a negative control without DNA.

Growth of *S. meliloti* Strains in Presence of Nitrate

In order to test whether NarB and NirBD are involved in nitrate assimilation, we grew both the WT and *nirBDnarB* strains in aerobic conditions, in Vincent minimal medium (VMM) containing either nitrate as the sole nitrogen source or a combination NH_4Cl/nitrate or glutamate/nitrate. The results are shown in **Figure 4**. Growth of the WT strain was comparable whether the nitrogen source in the medium was NH_4Cl or glutamate. When glutamate was removed from the medium and replaced by nitrate the WT strain also displayed similar growth kinetics. Interestingly, when NH_4Cl was removed from the culture medium before adding nitrate as the sole nitrogen source, WT cells displayed a 6 h lag phase before resuming growth. This could be explained by a previous repression of *narB nirB* gene expression by NH_4Cl which could limit nitrate assimilation. The *narB nirBD* mutant growth was similar to that of the WT when glutamate or NH_4Cl was present in the medium. Remarkably, the strain lacking NarB and NirBD was barely able to grow when nitrate was the sole N source present in the medium. These results suggest that *narB nirBD* genes are involved in nitrate assimilation.

Production of NO From the NarB NirBD Pathway

The only enzymatic source of NO described so far in *S. meliloti* is the denitrification pathway. Indeed Horchani and colleagues used *napA* and *nirK* mutants to demonstrate that about 35% of NO inside *M. truncatula* root nodules was produced by the bacteria (Horchani et al., 2011). To confirm these results we tested the involvement of *napA* and *nirK* in the production of NO in *S. meliloti* cultures grown in microaerobic conditions (oxygen 2%). We first examined the production of NO in the presence of nitrate in a WT strain grown in Vincent minimal medium (VMM) containing NH_4Cl or glutamate (**Figure 5A**). NO was produced in both cases and to a higher extent (fivefold) when glutamate was used as a nitrogen source. NO was not detectable in absence of nitrate. We found that a *napA* mutant still produced about 39% of the amount of NO measured in the WT strain suggesting that either there might be an independent way of producing NO or an alternative way to produce nitrite.

To test the involvement of *narB* and *nirB* in NO synthesis, we constructed a *narB* deletion mutant and a mutant deleted for both *nirB* and *narB*. It has to be noted that this deletion also encompasses *nirD*, a gene located between *nirB* and *narB*. *nirD* is predicted to encode a small protein (112 amino acids) displaying homology with a nitrite reductase small subunit probably involved in the electron transfer to NirB. As *narB* and *nirB* expression is repressed in the presence of ammonium, we grew these strains in VMM medium containing glutamate and nitrate.

Under these conditions, the *narB* and *nirBDnarB* mutants produced only 21 and 17% of the NO produced by the WT strain, respectively. A similar decrease was observed when NH_4Cl was present in the culture medium, conditions where *narB* and *nirB* were poorly expressed. In these experiments, NO was measured with a different method (chemiluminescence, data not shown). These data show that NarB and NirB have a role to play in NO production. Strikingly, the amount of NO dropped to almost zero in a *nirK* mutant showing that NO is produced by reduction of nitrite and indicating that the NarB/NirB involvement is likely due to the generation of nitrite by NarB. In this context it is interesting to note that NO production in the WT grown in the minus ammonium conditions where *nirBDnarB* were fully expressed, was increased by a factor of about 4 compared to the condition where ammonium was present. This observation also supports the idea that NarB NirBD promote NO production by generating nitrite to be used by the denitrification pathway.

In order to test whether NarB NirBD are involved in NO synthesis independently from the denitrification pathway, we tested NO production from the same strains grown in the same media as described above in aerobic conditions (**Figure 5A**).

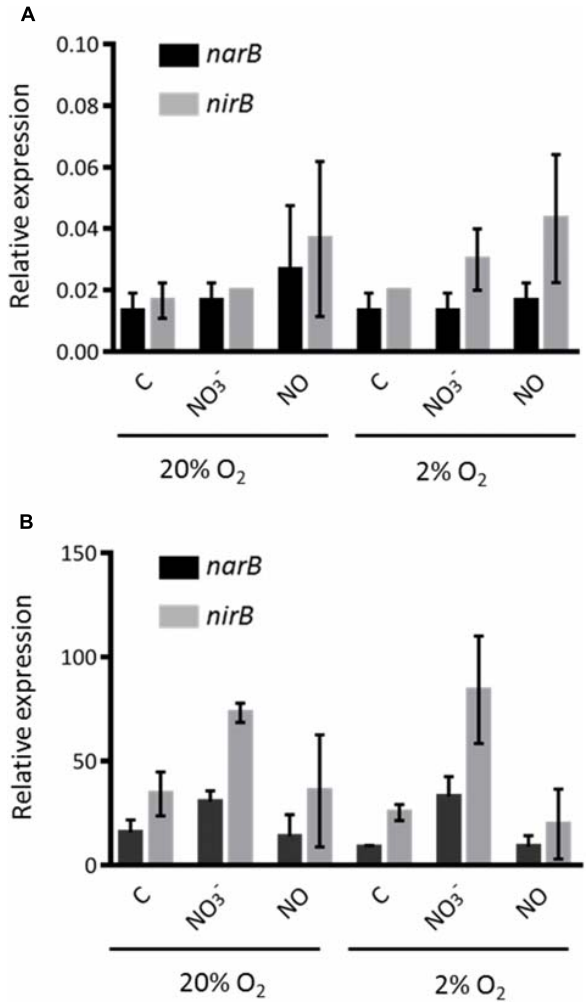

FIGURE 3 | Expression level of *nirB* and *narB* genes. **(A)** *S. meliloti* WT strain was grown to exponential phase in Vincent minimal medium (with NH_4Cl) (OD_{600} = 0.2–0.3). Cells were then exposed (1.5 h) to a NO donor (25 μM spermineNONOate) or nitrate (20 mM KNO_3) in aerobic (20% O_2) or microaerobic (2% O_2) conditions. Cells were recovered by filtration and frozen in liquid nitogen. RNA was extracted and transcript levels of *narB* (black bars) and *nirB* (gray bars) were determined by qRT-PCR. Transcript levels were normalized by using *SMc01171* as a reference gene. **(B)** *S. meliloti* WT strain was grown as in **(A)** except that NH_4Cl was removed from the medium by centrifugating cells and resuspending them in Vincent minimal medium without NH_4Cl before exposing cells to the different conditions tested. All values shown are the means and standard errors of the mean of data from three independent experiments (two technical repeats for each experiment).

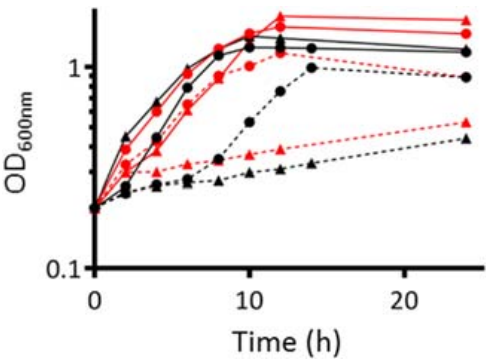

FIGURE 4 | Growth of WT and *nirBD narB S. meliloti* strains. WT (•) or *nirBD narB* (▲) strain were grown to exponential phase (OD_{600} = 0.2–0.3) in Vincent Minimal Medium (VMM) containing either glutamate (red lines) or NH_4Cl (black lines) as the sole nitrogen source. At time zero, cells grown in VMM with glutamate or NH_4Cl were collected, centrifuged, washed once by centrifugation, and resuspended at the same OD_{600} in VMM containing only KNO_3 (dotted line), or a combination of KNO_3 and glutamate (red solid line) or NH_4Cl (black solid line). OD_{600} was measured over a 24 h period. A representative experiment is shown on the figure.

Under these conditions, the denitrification pathway and especially the NirK nitrite reductase is not active. The results clearly show that NO was not produced in significant amount in the WT strain growing in aerobic conditions in VMM with glutamate and nitrate. These results strongly suggest that NarB NirBD only participates in NO production when denitrification is active. To verify whether NarB NirBD were active under aerobic conditions, we quantified the amount of nitrite produced by the different strains in the same conditions as for the NO production assay. The results are shown in **Figure 5B**. Interestingly, in aerobic conditions, in the presence of nitrate and ammonium, nitrite was barely detectable in the medium while in the presence of glutamate a much higher level (20-fold) of nitrite was measured, indicating that NarB was functional in these conditions. Nitrite production by the *napA* and *nirK* mutants was not significantly different from that of the WT strain. Nitrite production in the *narB* and *nirBD narB* strains was reduced by 60 and 95%, respectively as compared to the WT. These data show that the NarB- NirBD pathway was active in aerobic conditions even though no production of nitric oxide could be measured. When the same experiment was performed in microaerobic conditions (**Figure 5B**) the level of nitrite was much lower, perhaps due to nitrite reductase activity in the denitrification pathway.

Nitrite was only produced when nitrate was present in the medium. The amount of nitrite produced by the WT strain was higher when the strain was grown in presence of glutamate as compared to ammonium suggesting that NarB could participate to nitrite production in these conditions. Accordingly, the nitrite production was reduced by a factor of 2.5 and 3 in the *narB* or *nirBD narB* mutant strains, respectively. Altogether these results show that in conditions where only *narB* and *nirB* are expressed there is a production of nitrite but not NO.

Role of NarB and NirB *in planta*

To assess *narB* and *nirB* gene expression in symbiosis, we analyzed transcriptomic data generated by Roux and colleagues (Roux et al., 2014). *M. truncatula* forms indeterminate nodules in which all the developmental stages can be seen in a mature nodule. These different zones are: the meristem (Zone I), the infection zone (Zone II distal and proximal) where bacteria are released in the plant cells, the Interzone (IZ) between Zones II and III, and the nitrogen fixing zone (Zone III). Roux et al. (2014)

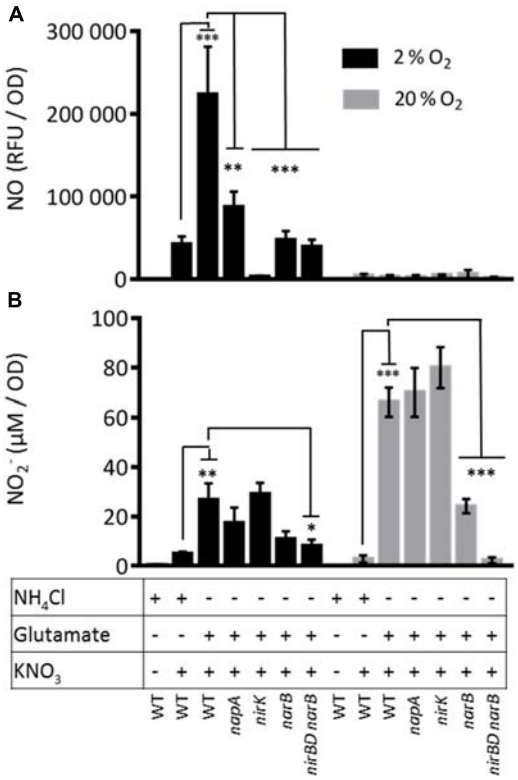

FIGURE 5 | Nitric oxide and nitrite production by *S. meliloti* WT and mutant strains. *S. meliloti* strains were grown exponentially at 28°C in VMM containing either NH_4Cl or glutamate (OD_{600} = 0.2–0.3). To remove NH_4Cl or glutamate from the medium, cells were collected by centrifugation and resuspended in VMM without NH_4Cl or glutamate. When needed, KNO_3 (20 mM) was added to the cultures. Cultures were either kept at 28°C under agitation (aerobic conditions, gray bars) or left without agitation under 2% oxygen atmosphere (microaerobic conditions, dark bars) for 1.5 h. Samples were collected to measure: **(A)** NO production : NO produced by the bacteria and released in the culture medium was quantified using the fluorescent non-permeable probe DAF-2. Fluorescence was measured using a microplate spectrofluorimeter (excitation wavelength 485 nm/emission wavelength 520 nm). NO produced is expressed as relative fluorescence unit $(RFU)/OD_{600\ nm}$. **(B)** Nitrite concentration in the medium: 100 µl of culture medium was incubated for 30 min with the Griess reagent. Absorbance was measured at 540 nm. NO_2^- concentration was calculated from a calibration curve using $NaNO_2$ (from 0 to 50 µM). The means and standard errors of the mean obtained from 4 (NO production) or 5 (Nitrite concentration) independent experiments are presented on the Figure. Statistical analysis was performed by means of a one-way ANOVA followed by a Bonferroni statistical test. *, **, and *** indicate significant difference ($P < 0.05$, $P < 0.01$, and $P < 0.001$, respectively) when compared with the wild type strain (WT).

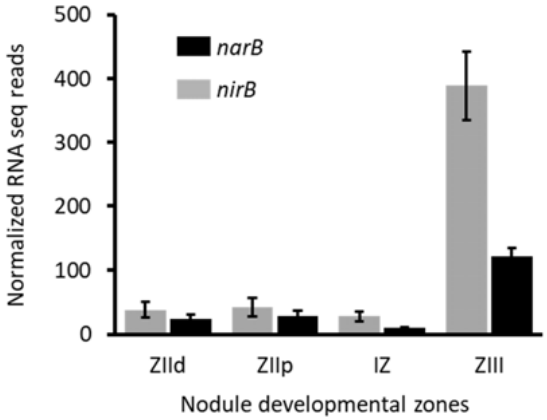

FIGURE 6 | Expression level of *nirB* and *narB* genes in nodules. Data shown on this figure are extracted from the work of Roux et al. (2014) (https://iant.toulouse.inra.fr/symbimics). They represent the RNA–seq analysis of bacterial transcripts of *narB* (black) and *nirB* (gray) obtained from laser–dissected *M. truncatula* nodules occupied by a WT *S. meliloti* strain. ZIId, infection zone, distal part; ZIIp, infection zone, proximal part; IZ, interzone; ZIII, nitrogen fixation zone.

isolated each zone by laser microdissection and the plant and bacterial RNA they contained were extracted and sequenced. The zone-specific expression of *narB* and *nirB* genes is reported in **Figure 6**. The strongest expression of *narB* and *nirB* was observed in the nitrogen fixing zone (ZIII). *nirK* was also expressed in ZIII but to a lesser extent than *nirB* (not shown). Therefore *narB* and *nirB* are expressed in bacteroids contained in plant nodules and particularly in the fixation zone.

As these genes are more highly and specifically expressed in the nitrogen fixation zone we hypothesized that they could have a role to play in the symbiotic interaction. To assess the role of these genes *in planta* we inoculated series of *M. truncatula* plantlets with the WT strain or with *narB* and *nirBD narB* mutants and analyzed different plant phenotypes such as the number of root nodules (**Figure 7A**), appearance of senescent nodules (**Figure 7B**), shoot dry weight (**Figure 7C**), and nitrogen fixation (**Figure 7D**). The average number of nodules per plant was identical when these plants were inoculated with the wild type or the mutant strains. Five weeks post-inoculation of the plants with the WT strain, 33% of the nodules were senescent. When plants were inoculated with the mutant and WT strains the proportion of senescent nodules was comparable though sligthly lower in the mutants. Nitrogen fixation measured 2, 4, or 5 weeks post-inoculation was more or less similar for all strains. Dry weight of shoots measured 5 weeks post-inoculation was also similar. Hence *narB* or *nirBD narB* deletions do not lead to substantial effects on various aspects of plant fitness during symbiosis.

DISCUSSION

NarB and NirB Are Part of the Nitrate Assimilatory Pathway in *Sinorhizobium meliloti*

The denitrification pathway including the nitrate reductase Nap and the nitrite reductase NirK has been described in different rhizobia and especially in *B. japonicum* and *S. meliloti* (**Figure 1**; Torres et al., 2011, 2014). Surprisingly the nitrate assimilation pathway in *S. meliloti* has received less attention. Eventhough *nirBD* and *narB* were suggested to be part of this pathway and biochemical data obtained from crude extracts of *S. meliloti* indicated the existence of two kinds of nitrate reductase activities (assimilatory and dissimilatory) (Sekiguchi and Maruyama, 1988;

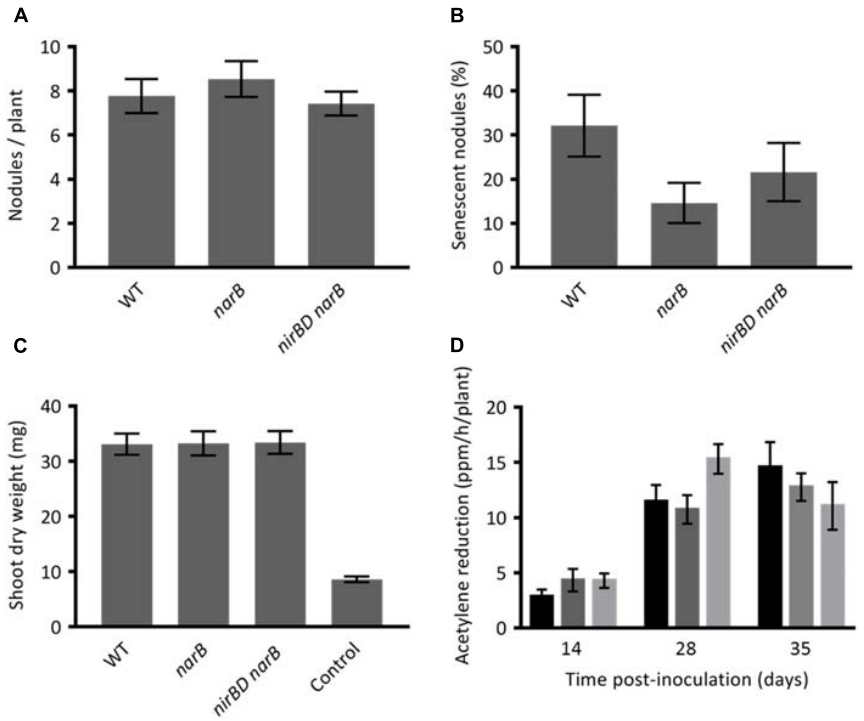

FIGURE 7 | Phenotypes of *Medicago truncatula* inoculated with *narB* or *nirBD narB* mutants. *M. truncatula* plantlets were inoculated with *S. meliloti* WT or mutant strains. **(A)** The number of nodules per plant (19 to 27 plants were tested). **(B)** Percentage of senescent nodules. A nodule was estimated senescent when a green color was visible on a significant surface of the nodule (19–27 plants were tested). **(C)** The dry weight of the aerial part of the plant (18–20 plants were tested). These three parameters were tested 5 weeks post-inoculation. **(D)** The nitrogen fixation activity was assessed by using the acetylene reduction assay (ARA). ARA was performed at 14, 28, and 35 dpi on whole plants inoculated with the WT strain (black bars), *narB* mutant (dark gray bars) or *nirBD narB* mutant (light gray bars). For each strain and time point 7–9 plants were tested. All values are the mean ± standard error of the mean (SEM).

Ferroni et al., 2011; Luque-Almagro et al., 2011; Kumar Halder and Chakrabartty, 2015), experimental data were really scarce on the whole. We initiated a study to determine whether NarB and NirB are part of the nitrate assimilatory pathway.

narB and *nirB* display an expression pattern different from that of denitrification genes. Indeed both genes are expressed under microaerobic and aerobic conditions, which is not the case for denitrification genes. Strikingly, although their expression level was measurable when cells were grown in the presence of NH_4Cl, it was highly induced (∼1000-fold) when NH_4Cl was removed from the medium. In previous work, assimilatory nitrate and nitrite reductase activities were observed only in bacteria grown with nitrate as sole nitrogen source and thus they were described to be inducible (Kumar Halder and Chakrabartty, 2015). In that work, nitrite levels were measured in the medium of cultures grown in presence of glutamate as nitrogen source and found to be inhibited by NH_4Cl. Our results show that this regulation occurs at the transcriptional level.

RT-PCR experiments demonstrated that *nirB, nirD*, *narB* and *cysG*, the gene located downstream of *narB,* constitute a single transcriptional unit. *cysG* encodes a putative uroporphyrin-III C-methyltransferase involved in the synthesis of sirohaem, the nitrite reductase cofactor (Luque-Almagro et al., 2011). In all conditions tested, *nirB* and *narB* displayed similar expression profiles confirming that they belong to a same operon.

It is interesting to note that synteny of these genes is maintained in about one third of the alpha-proteobacteria reference genomes (214) and in half of the 25 rhizobial reference genomes found in the Microbial Genome Annotation & Analysis Platform MAGE[1] database. This organization is not conserved in *B. japonicum* where the assimilatory nitrite reductase encoded by *nirA* is located at a locus distinct from *nasC* (**Figure 8**). *nirD* encodes a putative protein which displays homology with a nitrite reductase small subunit and is conserved among rhizobia (**Figure 8**) except most Bradyrhizobial reference genomes (MAGE).

The regulation mechanism of these genes is not known yet in *S. meliloti*. In *B. japonicum* NasT and NasS are involved in the regulation of the assimilatory nitrate reductase encoding gene *nasC* and *nirA*, NasS being a nitrate/nitrite sensor and NasT predicted to be a transcription anti-terminator (Luque-Almagro et al., 2011; Cabrera et al., 2016). *nasTS* are located close to *nirA* on the *B. japonicum* genome and this architecture is conserved in about 57% of reference bradyrhizobial genomes (MAGE) indicating that NasST could act at distance or that they might also be involved in the regulation of other genes or metabolic pathways. *S. meliloti* encodes homologs of NasS and NasT, SMb21114 (46.8% identity) and SMb21115

[1]http://www.genoscope.cns.fr

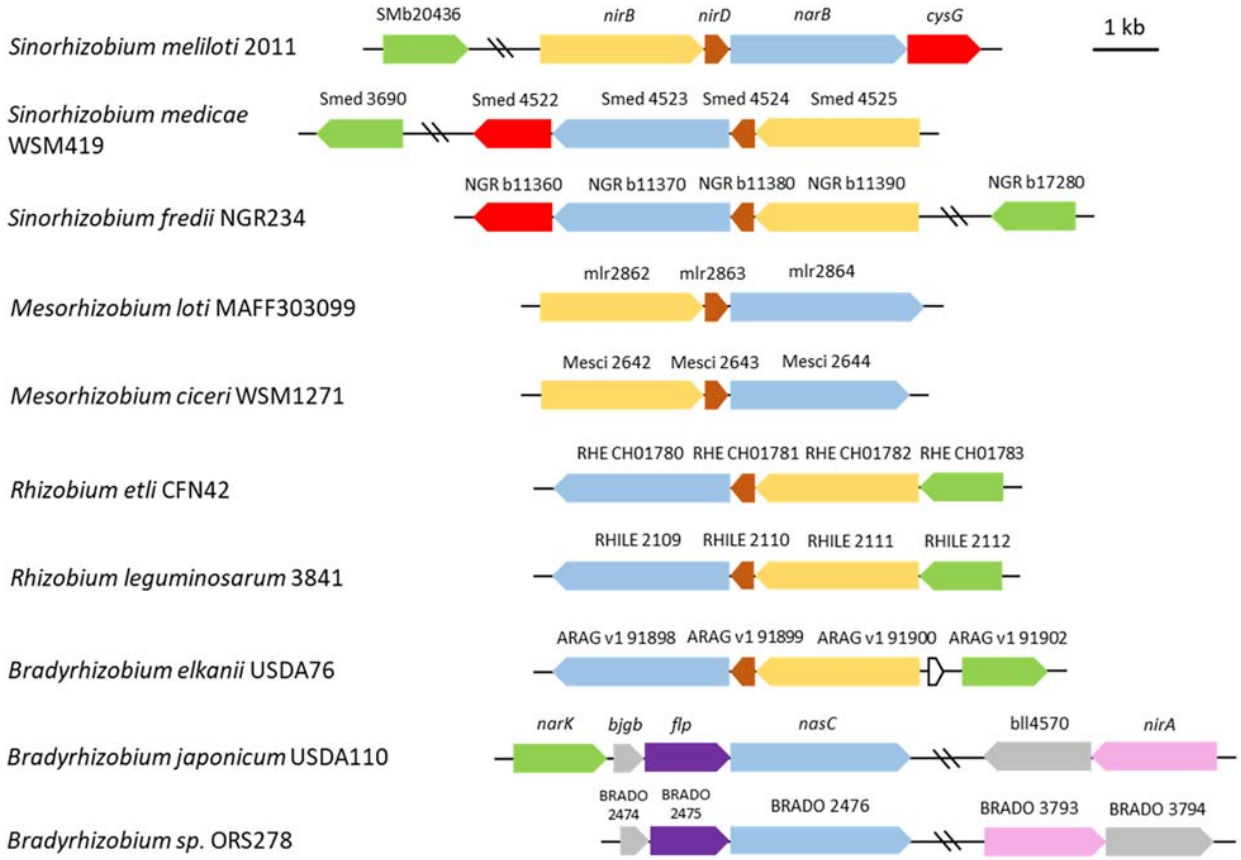

FIGURE 8 | Genomic arrangement of genes involved in nitrate assimilation in selected rhizobia. Genes encoding the assimilatory nitrate reductase (NarB) and nitrite reductase (NirB) in *Sinorhizobium meliloti* are colored in blue and yellow, respectively. Other genes are colored as follow: brown, *nirD* (encoding a small nitrite reductase subunit); green, SMb20436 (encoding the putative nitrite transporter); red, *cysG* (SMb20987) (encoding the putative protein involved in the synthesis of sirohaem, the nitrite reductase cofactor); purple, *flp*. Closest homologs (protein identity) found in other rhizobia are shown with the same color code. The assimilatory nitrite reductase NirA (pink) in *Bradyrhizobium japonicum* doesn't display significant identity with NirB. The scheme was constructed based on data from the Microbial Genome Annotation & Analysis Platform MAGE (http://www.genoscope.cns.fr) database. The strains are listed according to their phylogenetic proximity from *S. meliloti*.

(65.4% identity), respectively. It will be interesting to test whether these genes are involved in regulation of nitrate assimilation. Interestingly, microarray experiments analyzing the transcriptome of *S. meliloti* cells entering the stationary phase following a nitrogen deprivation showed that *narB* and *nirB* are induced about 15-fold together with SMb21114 and SMb21115 (12- and 65-fold, respectively) (Sauviac et al., 2007, LS and CB, unpublished). In addition, a small non-coding RNA (160 bp) has been annotated on the antisense strand of the *narB* genomic sequence (SMb23331). Interestingly we have observed that in the different zones of the nodule, the expression pattern of this ncRNA is inversely correlated to that of *narB* and *nirB* (Roux et al., 2014). Work is underway to determine the role of SMb21114/21115 and ncRNA SMb23331 on *narB nirB* expression.

Finally, a *S. meliloti* strain deleted for *narB* and *nirBD* failed to grow in a medium with nitrate as the sole nitrogen source. On the whole our results support the conclusion that NarB and NirBD are involved in the nitrate assimilatory pathway in *S. meliloti*.

NarB Contributes to the Production of NO via the Denitrification Pathway in Free-Living *S. meliloti* Cells

Nitric oxide is an important gas signaling molecule which has a role in diverse biological processes in eukaryotic as well as prokaryotic cells. NO is produced by mammalian cells in response to pathogen attack but surprisingly this molecule is also produced by the pathogen itself. Indeed some gram positive pathogens including *Bacillus* or *Staphylococcus* species were shown to possess bacterial analogs of mammalian NO synthases (Crane et al., 2010).

Surprisingly in the legume-rhizobium symbiotic interaction, NO is also produced by both partners (Sánchez et al., 2010; Horchani et al., 2011). The proportion of NO produced by the bacteria is variable depending upon the legume-rhizobium model considered. Indeed in soybean nodules about 90% of the NO detected is produced by the symbiont *B. japonicum* (Sánchez et al., 2010). These data were confirmed very recently by means of a fluorescent probe as well as electron paramagnetic

resonance spectroscopy to assess NO production in nodules (Calvo-Begueria et al., 2018). On the other hand 35% of the NO found in *M. truncatula* nodules is produced by *S. meliloti*. In both cases the role of NO produced by the bacterial partner is still puzzling in the symbiotic context. *S. meliloti* does not contain any NO synthase gene in its genome. Instead, NO synthesized by rhizobium species is thought to be an intermediate product of denitrification. In this process bacteria produce NO as an intermediate of nitrate reduction to N_2 with the purpose of acquiring energy ("nitrate respiration") or balancing the redox state during oxygen deprivation conditions. The fraction of NO produced by *S. meliloti* in *M. truncatula* nodules has been estimated by using bacterial strains affected in the denitrification genes *napA* and *nirK*. This amount could have been underestimated if other sources of NO exist in the bacteria. In *B. japonicum*, it was shown that NasC is involved in nitrate assimilation but also in NO production (Cabrera et al., 2016). In the present study we show that a *S. meliloti* mutant strain affected in the periplasmic nitrate reductase NapA still produces NO although at a lower level (39% of the WT), suggesting that there is another way to produce NO from nitrate in *S. meliloti* cells. Indeed our data indicate that NarB participates to NO synthesis as the production of NO was diminished by 80% as compared to the WT strain when *narB* was deleted. Interestingly, NO was barely detectable when measured in a WT strain under conditions where denitrification is not active. This confirms that the assimilatory nitrate reductase contributes to NO production indirectly via the denitrification pathway. NO_2^- produced in the cytoplasm by NarB could serve as substrate for NirK in the periplasm. To render this possible, nitrite must be exported to the cell periplasm. In *B. japonicum* NarK might insure this role and it is interesting to note that the closest NarK homolog in *S. meliloti* (26.5% identity) is encoded by SMb20436 which has not been characterized yet but was found to be highly induced under nitrogen deprivation conditions (LS and CB, unpublished). Its involvement in NO_2^- export remains, however, to be examined. Our results confirm that denitrification remains the main source of NO in *S. meliloti* as NO production was almost null when *nirK* was mutated indicating also that there is no other detectable source of NO in these conditions. NarB contributes to NO production via the denitrification pathway even in presence of ammonium (data not shown) and enhances greatly this production in condition where the *narB* gene is fully expressed. Whether this synergy has a role to play in *S. meliloti* metabolism is a question which remains to be addressed.

NarB and NirB Do Not Play a Major Role in the Symbiotic Interaction

NarB and NirB are part of the *S. meliloti* nitrate assimilatory pathway, and contribute to NO production in free living cells. Both genes are specifically expressed in the nitrogen fixing zone of *M. truncatula* nodules. This might seem in contradiction with the fact that ammonium produced from nitrogen fixation is present in nodules. However, the assimilation rate of ammonium by the plant might be high enough to avoid any accumulation of ammonium in nodules. Results which might appear contradictory have been published in the past concerning the link between nitrogen fixation and nitrate reduction: indeed a significant correlation between nitrate reductase and nitrogenase activities was suggested in *S. meliloti* (Kondorosi et al., 1973) while no correlation between nitrate reductase (including assimilatory nitrate reductase) and nitrogenase activities was found in a different study (Antoun et al., 1980). Recently Liu and colleagues have shown, by using three *Sinorhizobium* species, a lineage-dependent contribution of the *nap nir* gene cluster to the symbiosis efficiency with soybean (Liu et al., 2017). Here we found that inoculating *M. truncatula* with *S. meliloti* strains affected in *narB*, or *nirB-narB* region do not affect nodulation kinetics or plant shoot dry weight or nitrogen fixation efficiency suggesting that these genes do not play an essential role in symbiosis. The questions remain whether these genes participate to NO production in nodules and what their function in symbiosis could be.

AUTHOR CONTRIBUTIONS

BR carried out the experiments. ALS and AR constructed the *narB* and *nirBD narB* mutants. LS supervised BR, ALS, and AR works. CB and EM supervised the project and wrote the manuscript.

FUNDING

This work was supported by the French Laboratory of Excellence Project "TULIP" (ANR-10-LABX-41) and the "Agence Nationale de la Recherche" (STAYPINK-ANR-15-CE20-0005). EM was supported by the National Institute for Applied Sciences (INSA-Toulouse).

ACKNOWLEDGMENTS

We thank A. Becker and B. Happel (Philipps University of Marburg, Germany) for providing us some *S. meliloti* mutants. We thank C. Delon and D. Serça (Laboratoire Aérologie, CNRS, Université de Toulouse, France) for giving us access to their NO analyser. We also thank Frans de Bruijn and Anne-Claire Cazalé for critical reading of this manuscript.

REFERENCES

Antoun, H., Bordeleau, L. M., Prévost, D., and Lachance, R.-A. (1980). Absence of correlation between nitrate reductase and symbiotic nitrogen fixation efficiency in *Rhizobium meliloti*. *Can. J. Plant Sci.* 60, 209–212. doi: 10.4141/cjps80-028

Astier, J., Gross, I., and Durner, J. (2017). Nitric oxide production in plants: an update. *J. Exp. Bot.* 69, 3401–3411. doi: 10.1093/jxb/erx420

Berger, A., Brouquisse, R., Pathak, P. K., Hichri, I., Singh, I., Bhatia, S., et al. (2018). Pathways of nitric oxide metabolism and operation of phytoglobins in legume nodules: missing links and future directions. *Plant Cell Environ.* doi: 10.1111/pce.13151 [Epub ahead of print].

Bobik, C., Meilhoc, E., and Batut, J. (2006). FixJ: a major regulator of the oxygen limitation response and late symbiotic functions of *Sinorhizobium meliloti*. *J. Bacteriol.* 188, 4890–4902. doi: 10.1128/JB.00251-06

Boccara, M., Mills, C. E., Zeier, J., Anzi, C., Lamb, C., Poole, R. K., et al. (2005). Flavohaemoglobin HmpX from *Erwinia chrysanthemi* confers nitrosative stress tolerance and affects the plant hypersensitive reaction by intercepting nitric oxide produced by the host. *Plant J. Cell Mol. Biol.* 43, 226–237. doi: 10.1111/j.1365-313X.2005.02443.x

Boscari, A., Meilhoc, E., Castella, C., Bruand, C., Puppo, A., and Brouquisse, R. (2013). Which role for nitric oxide in symbiotic N2-fixing nodules: toxic by-product or useful signaling/metabolic intermediate? *Front. Plant Sci.* 4:384. doi: 10.3389/fpls.2013.00384

Cabrera, J. J., Salas, A., Torres, M. J., Bedmar, E. J., Richardson, D. J., Gates, A. J., et al. (2016). An integrated biochemical system for nitrate assimilation and nitric oxide detoxification in *Bradyrhizobium japonicum*. *Biochem. J.* 473, 297–309. doi: 10.1042/BJ20150880

Calvo-Begueria, L., Rubio, M. C., Martínez, J. I., Pérez-Rontomé, C., Delgado, M. J., Bedmar, E. J., et al. (2018). Redefining nitric oxide production in legume nodules through complementary insights from electron paramagnetic resonance spectroscopy and specific fluorescent probes. *J. Exp. Bot.* 69, 3703–3714. doi: 10.1093/jxb/ery159

Cam, Y., Pierre, O., Boncompagni, E., Hérouart, D., Meilhoc, E., and Bruand, C. (2012). Nitric oxide (NO): a key player in the senescence of *Medicago truncatula* root nodules. *New Phytol.* 196, 548–560. doi: 10.1111/j.1469-8137.2012.04282.x

Crane, B. R., Sudhamsu, J., and Patel, B. A. (2010). Bacterial nitric oxide synthases. *Annu. Rev. Biochem.* 79, 445–470. doi: 10.1146/annurev-biochem-062608-103436

del Giudice, J., Cam, Y., Damiani, I., Fung-Chat, F., Meilhoc, E., Bruand, C., et al. (2011). Nitric oxide is required for an optimal establishment of the *Medicago truncatula–Sinorhizobium meliloti* symbiosis. *New Phytol.* 191, 405–417. doi: 10.1111/j.1469-8137.2011.03693.x

Domingos, P., Prado, A. M., Wong, A., Gehring, C., and Feijo, J. A. (2015). Nitric oxide: a multitasked signaling gas in plants. *Mol. Plant* 8, 506–520. doi: 10.1016/j.molp.2014.12.010

Dupuy, P., Gourion, B., Sauviac, L., and Bruand, C. (2017). DNA double-strand break repair is involved in desiccation resistance of *Sinorhizobium meliloti*, but is not essential for its symbiotic interaction with *Medicago truncatula*. *Microbiol. Read. Engl.* 163, 333–342. doi: 10.1099/mic.0.000400

Ferri, L., Gori, A., Biondi, E. G., Mengoni, A., and Bazzicalupo, M. (2010). Plasmid electroporation of sinorhizobium strains: the role of the restriction gene *hsdR* in type strain Rm1021. *Plasmid* 63, 128–135. doi: 10.1016/j.plasmid.2010.01.001

Ferroni, F. M., Rivas, M. G., Rizzi, A. C., Lucca, M. E., Perotti, N. I., and Brondino, C. D. (2011). Nitrate reduction associated with respiration in *Sinorhizobium meliloti* 2011 is performed by a membrane-bound molybdoenzyme. *Biometals* 24, 891–902. doi: 10.1007/s10534-011-9442-5

Garcia, J., Barker, D. G., and Journet, E.-P. (2006). *Seed Storage and Germination*. Available at: https://www.noble.org/globalassets/docs/medicago-handbook/seed-storage-germination.pdf (accessed December 21, 2018).

Hardy, R. W. F., Holsten, R. D., Jackson, E. K., and Burns, R. C. (1968). The acetylene-ethylene assay for n2 fixation: laboratory and field evaluation. *Plant Physiol.* 43, 1185–1207. doi: 10.1104/pp.43.8.1185

Hichri, I., Boscari, A., Meilhoc, E., Catalá, M., Barreno, E., Bruand, C., et al. (2016a). "Nitric oxide: a multitask player in plant–microorganism symbioses," in *Gasotransmitters in Plants: The Rise of a New Paradigm in Cell Signaling Signaling and Communication in Plants*, eds L. Lamattina and C. García-Mata (New York, NY: Springer International Publishing), 239–268. doi: 10.1007/978-3-319-40713-5_12

Hichri, I., Meilhoc, E., Boscari, A., Bruand, C., Frendo, P., and Brouquisse, R. (2016b). "Chapter ten - nitric oxide: jack-of-all-trades of the nitrogen-fixing symbiosis?," in *Advances in Botanical Research Nitric Oxide and Signaling in Plants*, ed. D. Wendehenne (Cambridge, MA: Academic Press), 193–218.

Horchani, F., Prévot, M., Boscari, A., Evangelisti, E., Meilhoc, E., Bruand, C., et al. (2011). Both plant and bacterial nitrate reductases contribute to nitric oxide production in *Medicago truncatula* nitrogen-fixing nodules1[W][OA]. *Plant Physiol.* 155, 1023–1036. doi: 10.1104/pp.110.166140

Jeandroz, S., Wipf, D., Stuehr, D. J., Lamattina, L., Melkonian, M., Tian, Z., et al. (2016). Occurrence, structure, and evolution of nitric oxide synthase-like proteins in the plant kingdom. *Sci. Signal.* 9:re2. doi: 10.1126/scisignal.aad4403

Kondorosi, A., Barabas, I., Svab, Z., Orosz, L., Sik, T., and Hotchkiss, R. D. (1973). Evidence for common genetic determinants of nitrogenase and nitrate reductase in *Rhizobium meliloti*. *Nat. New Biol.* 246, 153–154.

Kumar Halder, A., and Chakrabartty, P. R. (2015). Expression of assimilatory nitrate and nitrite reductase of *Rhizobium meliloti*. *Indian J. Microbiol. Res.* 2:133. doi: 10.5958/2394-5478.2015.00001.1

Liu, L. X., Li, Q. Q., Zhang, Y. Z., Hu, Y., Jiao, J., Guo, H. J., et al. (2017). The nitrate-reduction gene cluster components exert lineage-dependent contributions to optimization of sinorhizobium symbiosis with soybeans. *Environ. Microbiol.* 19, 4926–4938. doi: 10.1111/1462-2920.13948

Luque-Almagro, V. M., Gates, A. J., Moreno-Vivián, C., Ferguson, S. J., Richardson, D. J., and Roldán, M. D. (2011). Bacterial nitrate assimilation: gene distribution and regulation. *Biochem. Soc. Trans.* 39, 1838–1843. doi: 10.1042/BST20110688

Meilhoc, E., Cam, Y., Skapski, A., and Bruand, C. (2010). The response to nitric oxide of the nitrogen-fixing symbiont *Sinorhizobium meliloti*. *Mol. Plant Microbe Interact.* 23, 748–759. doi: 10.1094/MPMI-23-6-0748

Melo, P. M., Silva, L. S., Ribeiro, I., Seabra, A. R., and Carvalho, H. G. (2011). Glutamine synthetase is a molecular target of nitric oxide in root nodules of *Medicago truncatula* and is regulated by tyrosine nitration. *Plant Physiol.* 157, 1505–1517. doi: 10.1104/pp.111.186056

Nicholas, D. J. D., and Nason, A. (1957). "Determination of nitrate and nitrite," in *Methods in Enzymology*, Vol. 3, eds S. P. Colowick and N. O. Kaplan (Cambridge, MA: Academic Press), 981–984.

Pobigaylo, N., Wetter, D., Szymczak, S., Schiller, U., Kurtz, S., Meyer, F., et al. (2006). Construction of a large signature-tagged mini-Tn5 transposon library and its application to mutagenesis of *Sinorhizobium meliloti*. *Appl. Environ. Microbiol.* 72, 4329–4337. doi: 10.1128/AEM.03072-05

Quandt, J., and Hynes, M. F. (1993). Versatile suicide vectors which allow direct selection for gene replacement in gram-negative bacteria. *Gene* 127, 15–21.

Roux, B., Rodde, N., Jardinaud, M.-F., Timmers, T., Sauviac, L., Cottret, L., et al. (2014). An integrated analysis of plant and bacterial gene expression in symbiotic root nodules using laser-capture microdissection coupled to RNA sequencing. *Plant J. Cell Mol. Biol.* 77, 817–837. doi: 10.1111/tpj.12442

Sánchez, C., Gates, A. J., Meakin, G. E., Uchiumi, T., Girard, L., Richardson, D. J., et al. (2010). Production of nitric oxide and nitrosylleghemoglobin complexes in soybean nodules in response to flooding. *Mol. Plant Microbe Interact.* 23, 702–711. doi: 10.1094/MPMI-23-5-0702

Sauviac, L., Philippe, H., Phok, K., and Bruand, C. (2007). An extracytoplasmic function sigma factor acts as a general stress response regulator in *Sinorhizobium meliloti*. *J. Bacteriol.* 189, 4204–4216. doi: 10.1128/JB.00175-07

Sekiguchi, S., and Maruyama, Y. (1988). Assimilatory reduction of nitrate in *Rhizobium meliloti*. *J. Basic Microbiol.* 28, 529–539. doi: 10.1002/jobm.3620280813

Torres, M. J., Bueno, E., Mesa, S., Bedmar, E. J., and Delgado, M. J. (2011). Emerging complexity in the denitrification regulatory network of *Bradyrhizobium japonicum*. *Biochem. Soc. Trans.* 39, 284–288. doi: 10.1042/BST0390284

Torres, M. J., Rubia, M. I., de la Peña, T. C., Pueyo, J. J., Bedmar, E. J., and Delgado, M. J. (2014). Genetic basis for denitrification in *Ensifer meliloti*. *BMC Microbiol.* 14:142. doi: 10.1186/1471-2180-14-142

Trinchant, J. C., and Rigaud, J. (1982). Nitrite and nitric oxide as inhibitors of nitrogenase from soybean bacteroids. *Appl. Environ. Microbiol.* 44, 1385–1388.

Conflict of Interest Statement: The authors declare that the research was conducted in the absence of any commercial or financial relationships that could be construed as a potential conflict of interest.

frontiers in Microbiology

ORIGINAL RESEARCH
published: 29 January 2020
doi: 10.3389/fmicb.2020.00015

Efficacy of a Plant-Microbe System: *Pisum sativum* (L.) Cadmium-Tolerant Mutant and *Rhizobium leguminosarum* Strains, Expressing Pea Metallothionein Genes *PsMT1* and *PsMT2*, for Cadmium Phytoremediation

Viktor E. Tsyganov[1,2], Anna V. Tsyganova[1], Artemii P. Gorshkov[1], Elena V. Seliverstova[1,3], Viktoria E. Kim[1], Elena P. Chizhevskaya[1], Andrey A. Belimov[1], Tatiana A. Serova[1], Kira A. Ivanova[1], Olga A. Kulaeva[1], Pyotr G. Kusakin[1], Anna B. Kitaeva[1] and Igor A. Tikhonovich[1,4]*

[1] All-Russian Research Institute for Agricultural Microbiology, Saint Petersburg, Russia, [2] Saint Petersburg Scientific Center (RAS), Saint Petersburg, Russia, [3] Sechenov Institute of Evolutionary Physiology and Biochemistry (RAS), Saint Petersburg, Russia, [4] Department of Genetics and Biotechnology, Saint Petersburg State University, Saint Petersburg, Russia

OPEN ACCESS

Edited by:
Juan Sanjuan, Experimental Station of Zaidín (EEZ), Spain

Reviewed by:
Eloisa Pajuelo, University of Seville, Spain
Raul Huertas, Noble Research Institute, LLC, United States

***Correspondence:**
Viktor E. Tsyganov
tsyganov@arriam.spb.ru

Specialty section:
This article was submitted to Microbial Symbioses, a section of the journal Frontiers in Microbiology

Received: 12 August 2019
Accepted: 06 January 2020
Published: 29 January 2020

Citation:
Tsyganov VE, Tsyganova AV, Gorshkov AP, Seliverstova EV, Kim VE, Chizhevskaya EP, Belimov AA, Serova TA, Ivanova KA, Kulaeva OA, Kusakin PG, Kitaeva AB and Tikhonovich IA (2020) Efficacy of a Plant-Microbe System: Pisum sativum (L.) Cadmium-Tolerant Mutant and Rhizobium leguminosarum Strains, Expressing Pea Metallothionein Genes PsMT1 and PsMT2, for Cadmium Phytoremediation. Front. Microbiol. 11:15. doi: 10.3389/fmicb.2020.00015

Two transgenic strains of *Rhizobium leguminosarum* bv. *viciae*, 3841-PsMT1 and 3841-PsMT2, were obtained. These strains contain the genetic constructions *nifH-PsMT1* and *nifH-PsMT2* coding for two pea (*Pisum sativum* L.) metallothionein genes, *PsMT1* and *PsMT2*, fused with the promoter region of the *nifH* gene. The ability of both transgenic strains to form nodules on roots of the pea wild-type SGE and the mutant SGECd^t, which is characterized by increased tolerance to and accumulation of cadmium (Cd) in plants, was analyzed. Without Cd treatment, the wild type and mutant SGECd^t inoculated with *R. leguminosarum* strains 3841, 3841-PsMT1, or 3841-PsMT2 were similar histologically and in their ultrastructural organization of nodules. Nodules of wild-type SGE inoculated with strain 3841 and exposed to 0.5 μM $CdCl_2$ were characterized by an enlarged senescence zone. It was in stark contrast to Cd-treated nodules of the mutant SGECd^t that maintained their proper organization. Cadmium treatment of either wild-type SGE or mutant SGECd^t did not cause significant alterations in histological organization of nodules formed by strains 3841-PsMT1 and 3841-PsMT2. Although some abnormalities were observed at the ultrastructural level, they were less pronounced in the nodules of strain 3841-PsMT1 than in those formed by 3841-PsMT2. Both transgenic strains also differed in their effects on pea plant growth and the Cd and nutrient contents in shoots. In our opinion, combination of Cd-tolerant mutant SGECd^t and the strains 3841-PsMT1 or 3841-PsMT2 may be used as an original model for study of Cd tolerance mechanisms in legume-rhizobial symbiosis and possibilities for its application in phytoremediation or phytostabilization technologies.

Keywords: symbiotic engineering, cadmium tolerance, nodulation, metallothionein, bacteroid, symbiosome, *Rhizobium*

INTRODUCTION

Plant-microbial systems formed by legumes and soil bacteria, called rhizobia, are widely used to enrich soils with nitrogen (Stagnari et al., 2017). Nitrogen fixation takes place in symbiotic nodules formed on plant roots (and in some cases on shoots), and this nodule formation creates a new ecological niche for rhizobia. For many legume plants, rhizobia use the infection thread to penetrate inside their roots (Tsyganova and Tsyganov, 2018). From these infection threads, rhizobia are released into host cells' cytoplasm where they differentiate into bacteroids and form symbiosomes, the main units fixing nitrogen. Simultaneously, infected plant cells may become differentiated during this process, thus enabling them to host numerous symbiosomes (Tsyganova et al., 2018).

The process of nitrogen fixation is sensitive to environmental cues, including the action of heavy metals (Angle et al., 1993; Neumann et al., 1998). Cadmium (Cd) is one of the most toxic elements and plants use different mechanisms to mitigate its toxic effects (Kulaeva and Tsyganov, 2011). The presence of Cd in the soil often reduces the formation of nodules and inhibits their functioning. For example, in *Lupinus albus* L., the biomass of nodules from plants treated with Cd reached just 57% of that attained by control plants, having an average nodule weight that decreased by 51% while their total nitrogen content decreased by 32% (Carpena et al., 2003). In *Medicago sativa* L. plants treated with Cd, nodule development was delayed (Ibekwe et al., 1996). Negative effects of Cd on nitrogen fixation were also demonstrated for nodules of *Pisum sativum* L. (Hernandez et al., 1995), *Glycine max* (L.) Merr. (Balestrasse et al., 2004), *L. albus* (Sánchez-Pardo et al., 2013), *M. sativa* L. (Shvaleva et al., 2010), *M. truncatula* Gaertn. (Marino et al., 2013), and in some other species too. Cd also affects nodule ultrastructure, leading to accumulated glycoproteins in the intercellular space, accumulation of insoluble Cd in the cell wall, and degradation of bacteroids (Carpena et al., 2003). In *P. sativum* nodules exposed to Cd, expansion of the peribacteroid space, destruction of the symbiosome membrane, fusion of symbiosomes, and the formation of symbiosomes containing several bacteroids were all observed (Tsyganova et al., 2019). Similar features of Cd's adverse influence on nodule ultrastructure were reported for nodules of *M. sativa* (Shvaleva et al., 2010).

Despite the high sensitivity of nodule development and functioning to Cd, legume-rhizobial systems have only recently been considered as a promising tool for soil phytoremediation, including Cd-contaminated soils (Safronova et al., 2011; Hao et al., 2014; Pajuelo et al., 2014; Gómez-Sagasti and Marino, 2015; Teng et al., 2015; Fagorzi et al., 2018). The advantages of rhizobia include their rapid growth and being isolated in a nodule, where Cd is accumulated and then transported to aboveground parts of the host plant. Legumes are also characterized by fast growth and the accumulation of large biomass. Yet, to take full advantage of legume-rhizobial systems for phytoremediation applications, it is crucial to select plant and bacterial genotypes with increased tolerance to Cd. In general, rhizobia are much more tolerant to Cd than are legumes (Belimov et al., 2015b). Thus, selecting appropriate plant genotypes tolerant to Cd is paramount for developing plant-microbial systems for Cd phytoremediation.

In pea, the mutant SGECd^t (*cdt*) displayed an increased tolerance of Cd and accumulated it in excess amounts (Tsyganov et al., 2007). The mutation was localized on its genetic map, but the gene has yet to be identified (Kulaeva and Tsyganov, 2013; Tsyganov et al., 2013). The mutation *cdt* increases the tolerance of nodulation of mutant plants to Cd in comparison with wild-type plants (Tsyganov et al., 2005). Recently, it was shown that nodules in the mutant SGECd^t demonstrate an increased tolerance of short exposure to high Cd concentrations (100 μM and 1 mM of $CdCl_2$) when compared with wild-type SGE nodules (Tsyganova et al., 2019).

Despite rhizobia having higher tolerance than legumes to Cd, their genetic modification allows the introduction of additional tolerance not observed in the original strain. The use of legumes and transgenic strains of rhizobia for phytoremediation, called "symbiotic engineering," was suggested just over 10 years ago (Sriprang and Murooka, 2007). Its first successful experiment was the construction of a transgenic—carrying the gene of human metallothionein *MTL4*—strain of *Mesorhizobium huakuii* subsp. *rengei*, which formed nodules with *Astragalus sinicus* L. (Sriprang et al., 2002). The *MTL4* gene was fused with the promoters of *nifH* and *nolB* genes of *M. huakuii*, which ensured its expression both in nodule bacteria cells and in symbiotic nodules. Using the obtained strain in symbiosis with *A. sinicus* led to a 6-fold increase in Cd accumulation in its nodules (Sriprang et al., 2002). Importantly, it was estimated that one nodule could accumulate 1.4 nM of Cd, which for 100 nodules per plant on average, this amounts to 140 nM captured per plant (Sriprang and Murooka, 2007). A transgenic strain carrying the *Arabidopsis thaliana PCS* gene, encoding phytochelatin synthase, has also been obtained, for which a 9–19-fold increase in the Cd content of free-living rhizobia was observed, accompanied by a 1.5-fold increase in symbiotic nodules (Sriprang et al., 2003). However, the construction of transgenic strains carrying both *MTL4* and *PCS* genes could enable further increases in the Cd content of nodules when compared with recombinant strains carrying only one of these genes. Moreover, such a strain has already been successfully applied for phytoremediation of rice fields, in that 9% of Cd was removed from the soil within 2 months of cultivation (Ike et al., 2007). In addition to transgenic strains resistant to Cd, a genetically modified *Ensifer medicae* strain MA11 expressing copper tolerance genes *copAB* was obtained (Delgadillo et al., 2015). More recently, a double genetically modified symbiotic system was created for the phytostabilization of copper in the roots of the legume plant *M. truncatula*. This system included composite plants of *M. truncatula*, in which the metallothionein gene *MT4a* from *A. thaliana* was expressed in transformed hairy roots and a transgenic strain *E. medicae* that expressed the *copAB* genes (Pérez-Palacios et al., 2017). This double symbiotic system enabled an increase in tolerance to copper and fostered elevated levels of copper in roots. However, the translocation of copper from roots to shoots was decreased in plants inoculated with the transgenic strain MA11-*copAB*; hence,

this double symbiotic system was deemed appropriate for copper phytostabilization (Pérez-Palacios et al., 2017).

Among the most used genes in "symbiotic engineering" are those of metallothioneins, small cysteine-rich proteins involved in metal detoxification processes and homeostasis (Joshi et al., 2016). Plant metallothioneins are also involved in responses to other different stresses including salt and oxidative stress, pathogen attacks, temperature, and others (Guo et al., 2003). According to the arrangement of cysteine residues, metallothioneins may be subdivided into four types (Cobbett and Goldsbrough, 2002), whose expression is known to display some organ specificity (Joshi et al., 2016). Activation of their expression by Cd has already been demonstrated for various plant species (Guo et al., 2003; Lee et al., 2004; Zhang et al., 2005; Zimeri et al., 2005; Pagani et al., 2012). Thus, metallothionenins clearly play a key role in the detoxification of Cd in plants, and this explains the growing interest in using them for "symbiotic engineering".

Thus, the aim of this work was to obtain two strains of *R. leguminosarum* bv. *viciae* expressing the pea metallothionein genes *PsMT1* and *PsMT2*, and to investigate formation of symbiotic nodules in the presence of toxic Cd concentrations using Cd-tolerant pea mutant SGECd^t. Due to the presence of the *nifA* promoter, their expression was activated only in nodules formed on pea plants. According to our knowledge, this is the first example of using genes that are not alien to the symbiotic system for the explicit purpose of "symbiotic engineering."

MATERIALS AND METHODS

Plant Material

The pea (*Pisum sativum* L.) laboratory line SGE (Kosterin and Rozov, 1993), and its corresponding mutant line SGECd^t characterized by an increased tolerance to Cd and higher levels of Cd accumulation (Tsyganov et al., 2007), were both used in this study.

Bacterial Strain Construction

Two plant genes, encoding metallothioneins of type 1 (AB176564.1) and type 2 (AB176565.1), respectively named *PsMT1* and *PsMT2*, were amplified from *P. sativum* cDNA with the use of these primer pairs: MT1-F/MT1-R (for *PsMT1*) and MT2-F/MT2-R (for *PsMT2*) (**Supplementary Table S1**). The primers MT1-F and MT2-F contained the first 21 and 22 nucleotide ORFs of *PsMT1* and *PsMT2*, respectively. The sequences for the MT1-R and MT2-R primers were located outside the ORFs of *PsMT1* and *PsMT2* (after the stop codons). Hence, using these primers permitted the PCR-amplification of 268-bp and 264-bp DNA fragments containing the complete ORF of *PsMT1* and *PsMT2*, starting strictly from the start-codons.

The promoter of *nifH* gene was amplified from genomic DNA of *R. leguminosarum* bv. *viciae* by using the primer pair nifH-F/nifH-R. Primer nifH-R consisted of the last 23 nucleotides before the start-codon of the *nifH* gene, while primer nifH-F contained an additionally introduced site for *Bam*HI restrictase. Using primers nifH-F and nifH-R thus enabled amplification of a 750-bp DNA fragment, located strictly in front of the *nifH* gene and containing a promoter.

PCR amplifications were performed using Pfu polymerase (Thermo Fisher Scientific, Waltham, MA, USA) according to standard protocol: initial denaturation at 95°C for 3 min, followed by 30 cycles at denaturation at 94°C for 30 s, primer annealing at 52°C for 30 s, extension at 72°C for 1 min, and a final extension lasting 4 min.

PCR fragments were extracted from agarose gel (Onishchuk et al., 2015), with each *PsMT*-gene ligated with a *nifH* promoter. The obtained ligase mixtures were then used as a matrix in the PCR with primers nifH-F and MT1-R (for fusion with *PsMT1*) or with primers nifH-F and MT2-R (for fusion with *PsMT2*). Each PCR was conducted following the standard technique and using Taq polymerase (Thermo Fisher Scientific). The respectively amplified 1018-bp and 1014-bp fragments were cloned into the pAL-TA vector (Evrogen, Moscow, Russia). The obtained *E. coli* clones were tested *via* PCR with M13-primers. PCR fragments of the corresponding size (approximately 1 kb) were isolated from the gel and sequenced. Sequencing was carried out using the ABI PRISM 3500xl (Applied Biosystems, Waltham, MA, USA) according to the manufacturer's instructions.

Cloned fragments containing the correct fusions of *PsMT1* and *PsMT2* genes with the *nifH* promoter were restricted by the enzymes *Bam*H1 (included in the nifH-F primer) and *Pst*I (contained in the pAL-TA polylinker) and recloned into the corresponding sites of the vector pCAMBIA 0390 (CAMBIA, Canberra, Australia), which is capable of replication in rhizobia.

In the final step, the obtained *nifH-PsMT1* and *nifH-PsMT2* fusions in the pCAMBIA 0390 plasmid were transferred to the strain 3841 *R. leguminosarum* bv. *viciae* (Wang et al., 1982), by using the method of conjugation (Chizhevskaya et al., 2011). The resulting Km^R transconjugants were tested *via* PCR with the primers nifH-F/MT1-R, followed by sequencing of the amplified fragments. The recombinant strains were called 3841-PsMT1 and 3841-PsMT2, respectively, and deposited in the Russian Collection of Agricultural Microorganisms (RCAM 01523 and RCAM 01558, respectively).

Inoculation and Plant Growth Conditions

Seeds were sterilized with concentrated sulfuric acid for 30 min and rinsed with sterile water 10 times. Seeds were germinated on Petri dishes with moisture filter paper at 24°C in an incubator (Memmert GmbH, Schwabach, Germany). Seven-day-old seedlings were inoculated (1 ml of bacterial suspension containing 10^7–10^8 cells per plant) with one of the *R. leguminosarum* bv. *viciae* strains: 3841, 3841-PsMT1, or 3841-PsMT2. Inoculated seedlings were left overnight at 24°C in the incubator. Next, the seedlings were placed on floating rafts in a plastic container (approximately 50 seeds per container) filled with 5 L of a hydroponic solution (μM): NaCl, 5; KH_2PO_4, 110; $Ca(NO_3)_2$, 50; $MgSO_4$, 400; KCl, 300; $CaCl_2$, 70; H_3BO_3, 1; $MnSO_4$, 1; $ZnSO_4$, 1; $CuSO_4$, 0.8; Na_2MoO_4, 0.03; Fe-tartrate 2.5. The root system was immersed in this solution while the shoots were on the raft's surface. Each container's hydroponic solution was supplemented with additional inoculum (bacterial lawn from one Petri dish was used for 5 L of hydroponic solution) and

the following day exposed to permanent bubbling. All seedlings were first grown for 3 days, at which point the nutrient solution was replaced and supplemented with 0.5 μM of $CdCl_2$, and this hydroponic solution then replaced every 3 days with 0.5 μM of $CdCl_2$. All plants were grown in a growth cabinet (a day/night cycle of 16/8 h, at 21°C, 60% relative humidity, and photon flux density during the light phase of 300 mmol quanta m^{-2} s^{-1}). Nodules were harvested at 28 day after inoculation.

Plasmid Stability and Strain Tolerance to Cadmium

Nodules, separated from the roots, were surface sterilized with 96% alcohol for 1 min and homogenized. Serial dilutions were planted on TY agar plates followed by incubation at 28°C for 3 days. The stability of plasmids was estimated by quantifying the number of colonies that maintained antibiotic resistance encoded by the plasmid pCAMBIA. Three independent experiments were performed. The ability of strains to grow under Cd stress was estimated on a liquid mannitol medium containing 5 μM and 10 μM of $CdCl_2$.

Nodule Phenotype Analysis

Photographs of pea nodules were taken with a SteREO Lumar. V12 stereomicroscope equipped with an AxioCam MRc 5 video camera (Zeiss, München, Germany). Object visualization was performed using AxioVision Rel. 4.8 software (Zeiss).

Expression Analysis

Pea nodules were harvested and ground in liquid nitrogen. Their total RNA extraction and cDNA synthesis were performed as previously described (Serova et al., 2018). The quantity of total RNA was determined using Qubit™ RNA Assay Kits on a Qubit® 2.0 Fluorometer (Invitrogen, Waltham, MA, USA).

For gene expression analysis, the primer pairs PsMT-1F/PsMT-1R and PsMT-2F/PsMT-2R were used (**Supplementary Table S1**). Gene-encoding glyceraldehyde-3-phosphate dehydrogenase (*PsGapC1*, L07500.1) served as the reference gene (Ivanova et al., 2015).

Relative real-time PCR was performed using a 10-μl PCR mix (SsoFast Eva Green Supermix (Bio-Rad, Hercules, CA, USA)) in a C1000™ Thermal Cycler combined with the optical module CFX96™ Real-Time System (Bio-Rad), according to the manufacturer's protocol. The reaction's results were processed with Bio-Rad CFX Manager software (Bio-Rad) and analyzed by the $2^{-\Delta\Delta CT}$ method. Statistical analysis of the experimental results was carried out in GraphPad Prism software.[1] Statistically significant differences were determined with two-way ANOVA ($p \leq 0.05$). The experiment was performed in three replicates. For each variant, nodules were collected from several (5–7) plants.

Light and Electron Microscopy

Nodules from Cd-treated and untreated plants of wild-type SGE and the mutant SGECd^t were harvested and placed directly into the fixative. The nodules were fixed in 3% paraformaldehyde and 0.1% glutaraldehyde (Sigma-Aldrich, St. Louis, MO, USA) in 0.01% PBS (2.48 g/L NaH_2PO_4, 21.36 g/L Na_2HPO_4, 87.66 g/L NaCl, pH 7.2). After fixation, the samples were post-fixed in 2% osmium tetroxide in a 0.1 M phosphate buffer for 2 h; each sample was then dehydrated, as described previously (Serova et al., 2018), and progressively infiltrated with Eponate 12 (Ted Pella Inc., Redding, CA, USA) at room temperature. Embedded samples were transferred to small plastic containers in fresh resin, following the manufacturer's instructions, and polymerized at 60°C for 48 h.

For light microscopy, semi-thin sections (1-μm-thick) were cut on a Leica EM UC7 ultramicrotome (Leica Microsystems, Wetzlar, Germany). Sections were placed on glass slides SuperFrost (Menzel-Gläser, Thermo Fisher Scientific, Waltham, MA USA) and stained with methylene blue-azure II for 20 min at 70°C (Humphrey and Pittman, 1974) for later examination under a microscope Axio Imager.Z1 (Zeiss). Photos were taken using a digital video camera Axiocam 506 (Zeiss). For transmission electron microscopy, 90–100-nm-thick ultrathin sections were cut and counterstained as described by Serova et al. (2018). The nodule tissues were examined and photographed under a Tecnai G2 Spirit electron microscope (FEI, Eindhoven, the Netherlands) at 80 kV. Digital micrographs were taken with a MegaView G2 CCD camera (Olympus-SIS, Münster, Germany).

Cadmium and Nutrient Contents in Plants

Dried plant shoots were ground into powder. To determine their Cd and nutrient—P, K, Ca, Mg, S, Fe, B, Mn, Co, Cu, Mo, Na, Ni, and Zn—contents, ground shoot samples were digested in a mixture of concentrated HNO_3 and 38% H_2O_2 at 70°C using the DigiBlock digester (LabTech, Sorisole, Italy), and the content of each element measured by an inductively coupled plasma emission spectrometer ICPE-9000 (Shimadzu, Tokyo, Japan). Total nitrogen in shoot samples was determined using a Kjeltec 8200 Auto distillation unit (FOSS Analytical, Hillerød, Denmark). Statistical analysis of the data was performed using the STATISTICA v10 (StatSoft Inc., Tulsa, OK, USA). ANOVA analysis and Fisher's least significant difference (LSD) test were used to evaluate differences between means.

RESULTS AND DISCUSSION

Bacterial Strain Construction, Plasmid Stability, and Strain Tolerance to Cadmium

To create a symbiotic system capable of accumulating Cd, transgenic strains of *R. leguminosarum* bv. *viciae* 3841-PsMT1 and 3841-PsMT2 were first obtained. These strains carried the genes of plant metallothioneins *PsMT1* and *PsMT2* fused with the *nifH* gene promoter of *R. leguminosarum* bv. *viciae*. Encoding a small subunit of nitrogenase, *nifH* has a strong promoter providing the stable transcription of a gene under its control in micro-aerophilic conditions, which characterize the symbiotic nodule.

At first, we tested plasmid stability in the transgenic strains of *R. leguminosarum* bv. *viciae* 3841-PsMT1 and 3841-PsMT2.

[1]https://www.graphpad.com/scientific-software/prism/

In the absence and presence of Cd, all the recovered clones of strains 3841-PsMT1 and 3841-PsMT2 were found to be resistant to kanamycin, indicating that the culturable nodule bacteria maintained 100% of pCAMBIA plasmids in nodules of the wild-type SGE and the mutant SGECd^t.

In addition, these strains grew similarly on a liquid medium without Cd, as well as in the presence of 5 and 10 μm of $CdCl_2$, indicating that treatment is not affecting bacteria viability.

In contrast to this study, in previous studies, rhizobial transgenic strains used in "symbiotic engineering" technology for phytoremediation of Cd-contaminated soils were created based on alien genes for the symbiotic system (Sriprang et al., 2002, 2003; Ike et al., 2007).

Nodule Phenotype Analysis

The formation of effective pink nodules was observed in the wild-type SGE inoculated with *R. leguminosarum* bv. *viciae* strains 3841, 3841-PsMT1, or 3841-PsMT2 (**Figures 1A,C,E**). Treatment with 0.5 μM $CdCl_2$ resulted in the formation of several small pale nodules on wild-type plants inoculated with 3841 (**Figure 1B**); however, pink nodules developed on wild-type plants inoculated with transgenic strains 3841-PsMT1 and 3841-PsMT2 treated with Cd (**Figures 1D,F**). The mutant SGECd^t pea plants also formed pink nodules after inoculation with 3841, 3841-PsMT1, or 3841-PsMT2 (**Figures 2A,C,E**). The SGECd^t plants inoculated with either 3841 or 3841-PsMT1 still formed pink nodules after treatment with 0.5 μM $CdCl_2$ (**Figures 2B,D**), while nodules that formed on 3841-PsMT2 were small and pale (**Figure 2F**).

The wild-type strain 3841 and transgenic strains 3841-PsMT1 and 3841-PsMT2 formed normal pink nodules in hydroponic solution without Cd also, as previously described for the strain CIAM 1026 (Tsyganov et al., 2004). Thus, the introduction of genetic constructions did not alter the

FIGURE 1 | Nodulated main and lateral roots of wild-type SGE pea (*Pisum sativum*) plants untreated **(A,C,E)** and treated with cadmium chloride **(B,D,F)** at 28 days after inoculation with *Rhizobium leguminosarum* bv. *viciae* strain 3841 **(A,B)**, 3841-PsMT1 **(C,D)**, and 3841-PsMT2 **(E,F)**. Scale bar = 2 mm.

FIGURE 2 | Nodulated main and lateral roots of the mutant SGECd^t pea (*Pisum sativum*) plants untreated **(A,C,E)** and treated with cadmium chloride **(B,D,F)** at 28 days after inoculation with *Rhizobium leguminosarum* bv. *viciae* 3841 **(A,B)**, 3841-PsMT1 **(C,D)**, and 3841-PsMT2 (**E,F**). Scale bar = 2 mm.

ability of modified strains to undergo nodulation. In work by Tsyganov et al. (2005), the ability of the mutant SGECd^t to form nodules resistant to Cd stress upon inoculation with wild-type strain 3841, in contrast to the wild-type SGE, was demonstrated. Yet, surprisingly, transgenic strain 3841-PsMT2 formed pale nodules that may be indicative of their inefficiency.

Expression Analysis

In wild-type nodules, *PsMT1* gene expression was significantly increased (2.4-fold) under the Cd treatment compared with untreated nodules when plants were inoculated with strain 3841 (**Figure 3A**). This gene's expression level in the nodules of the SGECd^t inoculated with strain 3841 remained unchanged, being 2.3-fold lower than in wild-type nodules formed upon inoculation with the same strain (**Figure 3A**). On the contrary, the expression level of the *PsMT2* gene was reduced in nodules formed by strain 3841 on roots of both the wild type and mutant, which may indicate an insignificant role of this gene in detoxification of Cd in the nodules.

Paradoxically, *PsMT1* gene expression did not increase in nodules formed on roots of both the wild type and SGECd^t by strain 3841-PsMT1 carrying the insertion of this gene when compared to strains without this gene (**Figure 3A**). Perhaps this is caused by gene repression due to the introduction of additional copies of the *PsMT1* gene into the rhizobial strain.

In nodules of wild-type plants inoculated with strain 3841-PsMT2, the expression of both *PsMT1* and *PsMT2* genes during the Cd treatment increased 5-fold compared with the untreated control (**Figure 3**). This may indicate general regulatory mechanisms and the relationship between overexpression of the *PsMT1* and *PsMT2* genes in the pea nodules of the SGE line under the influence of Cd.

Yet the expression levels of *PsMT1* and *PsMT2* went unchanged or decreased in nodules formed by any tested strains on roots

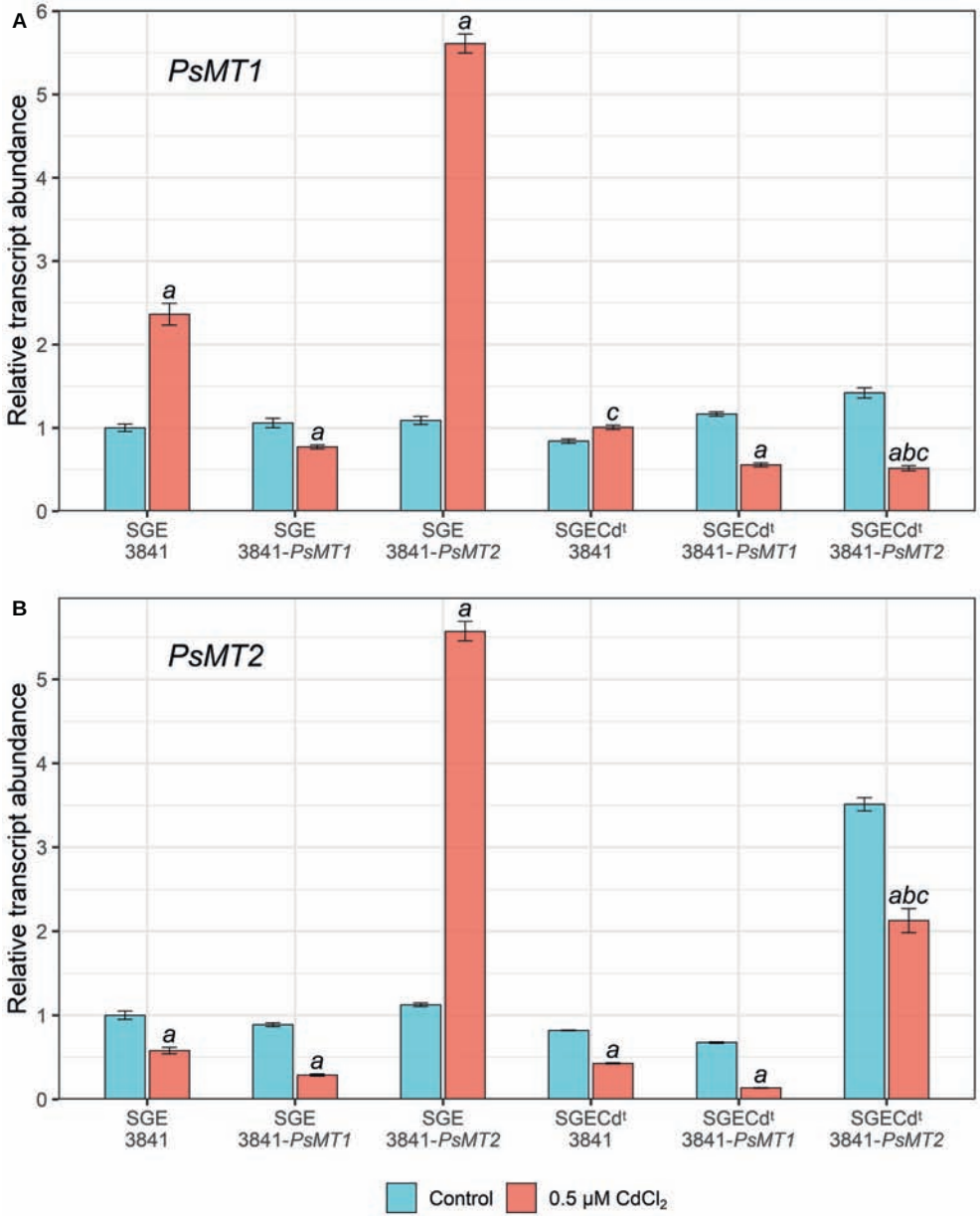

FIGURE 3 | Expression of *PsMT1* **(A)** and *PsMT2* **(B)** genes in the nodules of pea (*Pisum sativum*) plants grown hydroponically without cadmium stress (control) and with the addition of 0.5 μM $CdCl_2$. Letters indicate significant differences (two-way ANOVA, $p \leq 0.05$): *a*, from the control; *b*, of the control SGECd^t from control wild-type plants inoculated with the same strain of *Rhizobium leguminosarum* bv. *viciae*; *c*, of treated SGECd^t from the treated wild type inoculated with the same strain of *R. leguminosarum* bv. *viciae*.

of the mutant SGECd^t. This would correspond to a significantly lower activation of different responses to Cd in this mutant than in the wild type (Tsyganov et al., 2007).

The expression of different genes of plant metallothioneins demonstrates some organ and metal specificity (Joshi et al., 2016). Recently, it was shown that Cu application caused in tomatoes an increase in the expression of the *MT1* and *MT2* genes in the roots, leaves, and fruits. However, Pb treatment led to increased expression of these genes only in leaves. Moreover, with an increase in Pb concentration, the level of *MT1* gene expression decreased (Kisa et al., 2017). Thus, the regulatory mechanism of gene expression of metallothionenins is still far from elucidation.

Previously, we compared the expression levels of genes encoding key Cd detoxification enzymes in 4-week-old nodules formed by strain *R. leguminosarum* bv. *viciae* 3841 in wild-type SGE and mutant SGECd^t exposed to 0.5 μM $CdCl_2$ (Kulayeva and Tsyganov, 2015). These genes were *PsGSH1* (γ-glutamylcysteine synthetase), *PsGSHS* (glutathione synthetase), *PshGSHS* (homoglutathione synthetase), and

PsPCS (phytochelatin synthase). The expression of *PsGSH1* was not altered under Cd exposure in the wild-type nodules, and it was decreased in the mutant SGECd^t. Similarly, expression of *PsGSHS* was reduced in the mutant nodules under the Cd exposure but it increased in wild-type nodules. In contrast to the first two genes, the levels of expression of *PshGSHS* and *PsPCS* were elevated in nodules of both the wild type and the mutant under Cd exposure. However, expression of *PshGSHS* and *PsPCS* increased to a large extent in wild-type nodules, which indicated that (homo)glutathione and phytochelatins are unlikely involved in the elevated Cd tolerance of mutant nodules (Kulayeva and Tsyganov, 2015).

Nodule Histological and Ultrastructural Organization

Histological and Ultrastructural Organization of Cadmium-Treated and Untreated Nodules of the Wild-Type SGE and Mutant SGECd^t Inoculated With *R. leguminosarum* bv. *viciae* Strain 3841

Wild-type SGE (**Figures 4A,B**) and mutant SGECd^t (**Figures 4C,D**) plants inoculated with *R. leguminosarum* bv. *viciae* strain 3841 without Cd exposure formed indeterminate nodules having a typical histological organization (Tsyganov et al., 1998). Ultrastructural organization of the wild-type SGE (**Supplementary Figure S1**) and mutant SGECd^t (data not shown) was also similar. In the nitrogen fixation zone, each infected cell contained symbiosomes with a single differentiated pleiomorphic bacteroid surrounded by a symbiosome membrane (**Supplementary Figure S1A**). In the infection zone, juvenile bacteroids were observed in the narrow layer of cytoplasm (**Supplementary Figure S1B**).

Under the Cd treatment, most of the wild-type nodules showed certain symptoms of cytological damage in the nitrogen fixation zone such as cytoplasm clearing (**Figures 4E,F**), when compared with untreated nodules (**Figures 4A,B**) and Cd-treated nodules of the mutant SGECd^t (**Figures 4G,H**); in addition, an enlarged senescence zone was observed (**Figure 4E**). Nevertheless, some nodules were less affected while others incurred severe structural damage. Electron microscopy revealed the following abnormalities in the Cd-treated nodules of the wild type: polyhydroxybutyrate (PHB) accumulation in the mature bacteroids and destruction of the symbiosome membrane, with lipid peroxidation in the form of electron-dense formations (**Figure 5A**); some infected cells exhibited reduced cytoplasm with clear symptoms of plasmolysis (**Figure 5C**); organelles other than mitochondria and degrading bacteroids were hardly seen; finally, infected cells with destroyed cytoplasm "ghosts" of the bacteroids appeared (**Figure 5E**).

Unlike for the wild type, in the Cd-treated nodules of the mutant SGECd^t exposure to Cd caused less pronounced changes in their ultrastructural organization (**Figures 5B,D,F**). Most of the infected cells showed unchanged bacteroids and a cytoplasm with intact organelles present. In some infected cells, bacteroids with slight PHB accumulation and lipid peroxidation of the symbiosome membranes (**Figure 5D**) were detected. The more pronounced damage from Cd exposure manifested as an expansion of peribacteroid spaces and an irregular shape of the bacteroids (**Figure 5F**).

Histological and Ultrastructural Organization of Cadmium-Treated and Untreated Nodules of the Wild-Type SGE and Mutant SGECd^t Inoculated With *R. leguminosarum* bv. *viciae* Strain 3841-PsMT1

Wild-type SGE and mutant SGECd^t plants inoculated with *R. leguminosarum* bv. *viciae* strain 3841-PsMT1 without exposure to Cd formed nodules having a typical histological and ultrastructural organization (data not shown). Cd-treated nodules of the wild type and mutant SGECd^t formed by the strain 3841-PsMT1 did not cause any marked alterations to their histological organization when compared with nodules not receiving the Cd treatment (**Figures 4I–L**).

Electron microscopy revealed that the main part of infected cells in the nitrogen fixation zone of Cd-treated nodules had a similar ultrastructure in both the wild type and mutant SGECd^t. Infected cells contained well-developed bacteroids (**Figures 6A,B**) and normal infection threads (data not shown). The degenerative changes of infected cells were limited to the presence of an expanded peribacteroid space (**Figure 6C**), irregular shape of bacteroids (**Figure 6D**), damaged symbiosome membranes with lipid peroxidation (**Figures 6A,C**), and PHB accumulation (**Figures 6E,F**). In the rare infected cells, initial symptoms of cytoplasm swelling and clearing (**Figure 6C**), as well as organelle damage, could be observed (**Figures 6E,F**).

Histological and Ultrastructural Organization of Cadmium-Treated and Untreated Nodules of Wild-Type SGE and Mutant SGECd^t Inoculated With *R. leguminosarum* bv. *viciae* Strain 3841-PsMT2

Nodules of wild-type SGE and mutant SGECd^t plants formed by *R. leguminosarum* bv. *viciae* strain 3841-PsMT2 without exposure to Cd showed a typical histological and ultrastructural organization (data not shown). For both the wild type and mutant SGECd^t inoculated with strain 3841-PsMT2, the Cd treatment did not cause the significant alterations to their nodule histological organization (**Figures 4M–P**). By contrast, in the Cd-treated nodules of the mutant SGECd^t an intensive accumulation of starch was evident (**Figures 4O,P**).

Infected cells in the nitrogen fixation zone of both the wild type and mutant SGECd^t nodules under Cd exposure did not differ in their ultrastructural organization. All infected cells contained mature Y-shaped bacteroids (**Figures 7A,B**), and apparently normal infection threads (data not shown). The presence of an expanded peribacteroid space (**Figures 7B–D**), symbiosome membrane destruction (**Figures 7D,E**), lipid peroxidation of symbiosome membranes (**Figures 7A,B**), and PHB accumulation (**Figures 7C,D**) were all observed in most

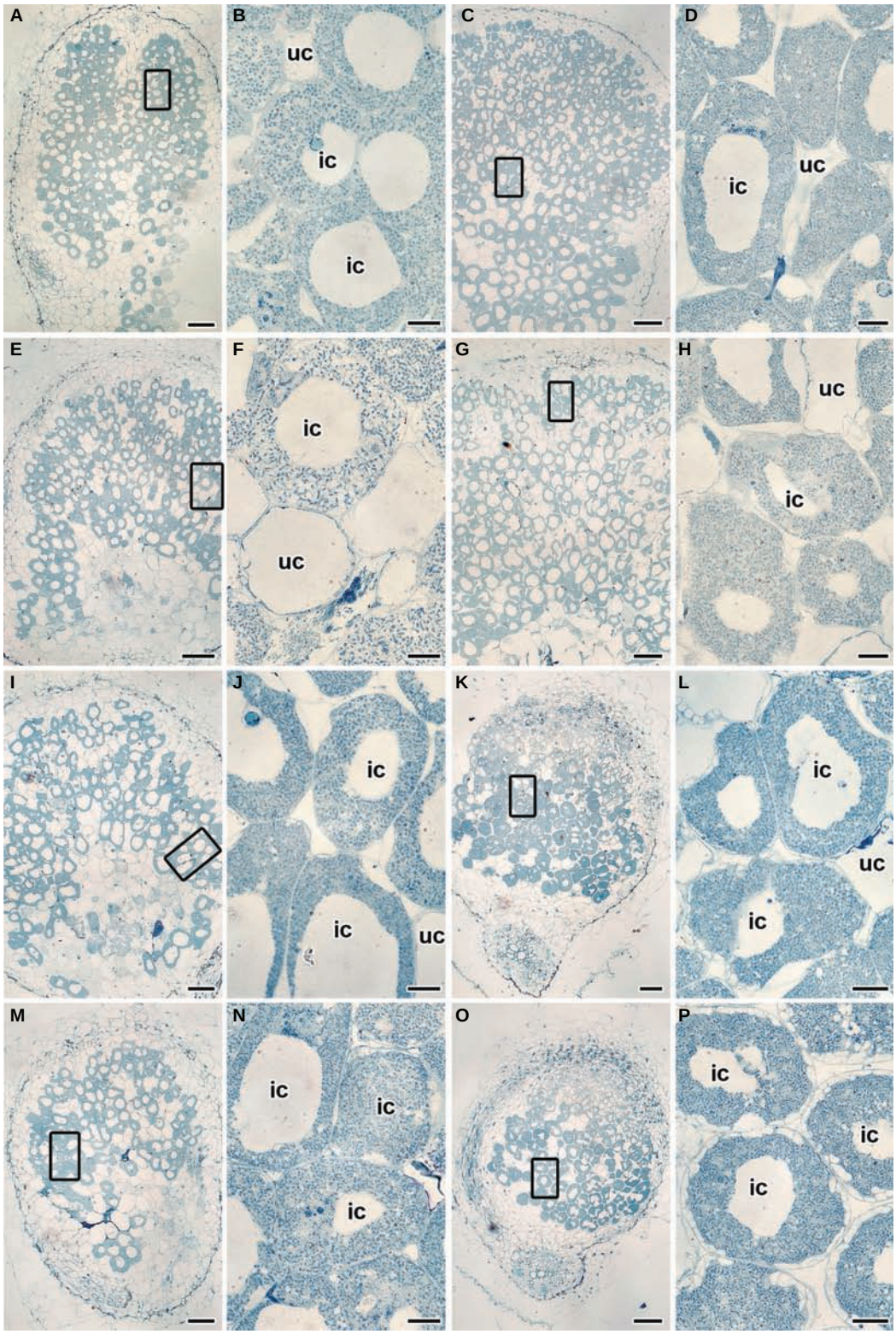

FIGURE 4 | Histological organization of the untreated **(A–D)** and the cadmium-treated **(E–P)** nodules of wild-type SGE **(A,B,E,F,I,J,M,N)** and mutant SGECd^{t} **(C,D,G,H,K,L,O,P)** inoculated with *Rhizobium leguminosarum* bv. *viciae* strain 3841 **(A–H)**, 3841-MT1 **(I–L)** and 3841-MT2 (**M–P**). ic, infected cell; uc, uninfected cell. **(A,C,E,G,I,K,M,O)** Histological organization; **(B,D,F,H,J,L,N,P)** high magnification of the boxed area in **(A,C,E,G,I,K,M,O)**. Scale bar **(A,C,E,G,I,K,M,O)** = 200 μm, **(B,D,F,H,J,L,N,P)** = 20 μm.

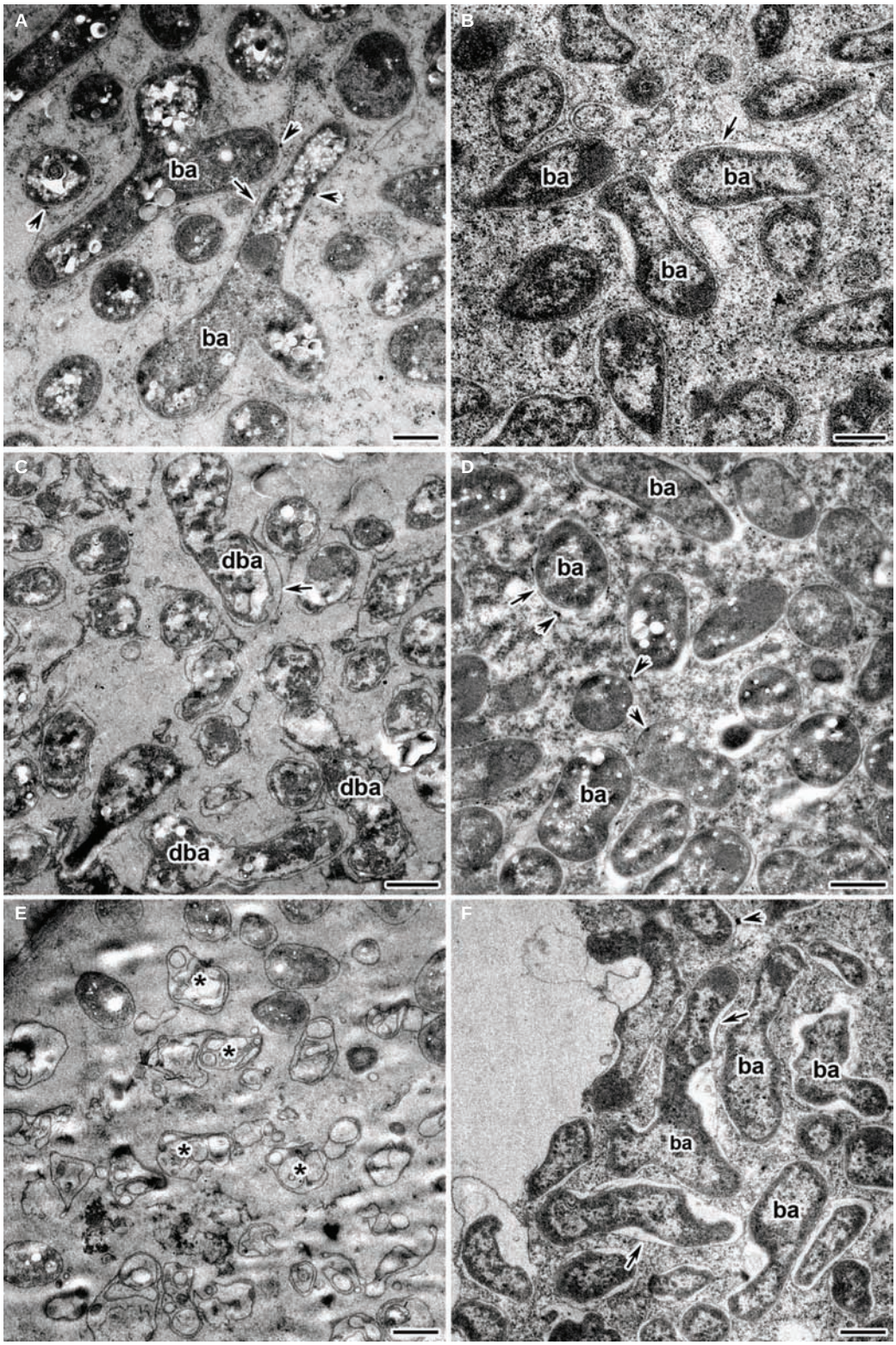

FIGURE 5 | Ultrastructural organization of the cadmium-treated nodules of wild-type SGE **(A,C,E)** and mutant SGECd' **(B,D,F)** inoculated with *Rhizobium leguminosarum* bv. *viciae* strain 3841. ba, bacteroid; dba, degrading bacteroid; arrows indicate the symbiosome membrane; arrowheads indicate the degradation of symbiosome membrane; asterisk used to indicate "ghost" bacteroids. **(A)** Mature bacteroids with polyhydroxybutyrate accumulation, **(B)** normal bacteroids, **(C)** degrading bacteroids, **(D)** bacteroids with polyhydroxybutyrate accumulation, **(E)** "ghost" bacteroids, **(F)** abnormal bacteroids. Scale bar = 500 nm.

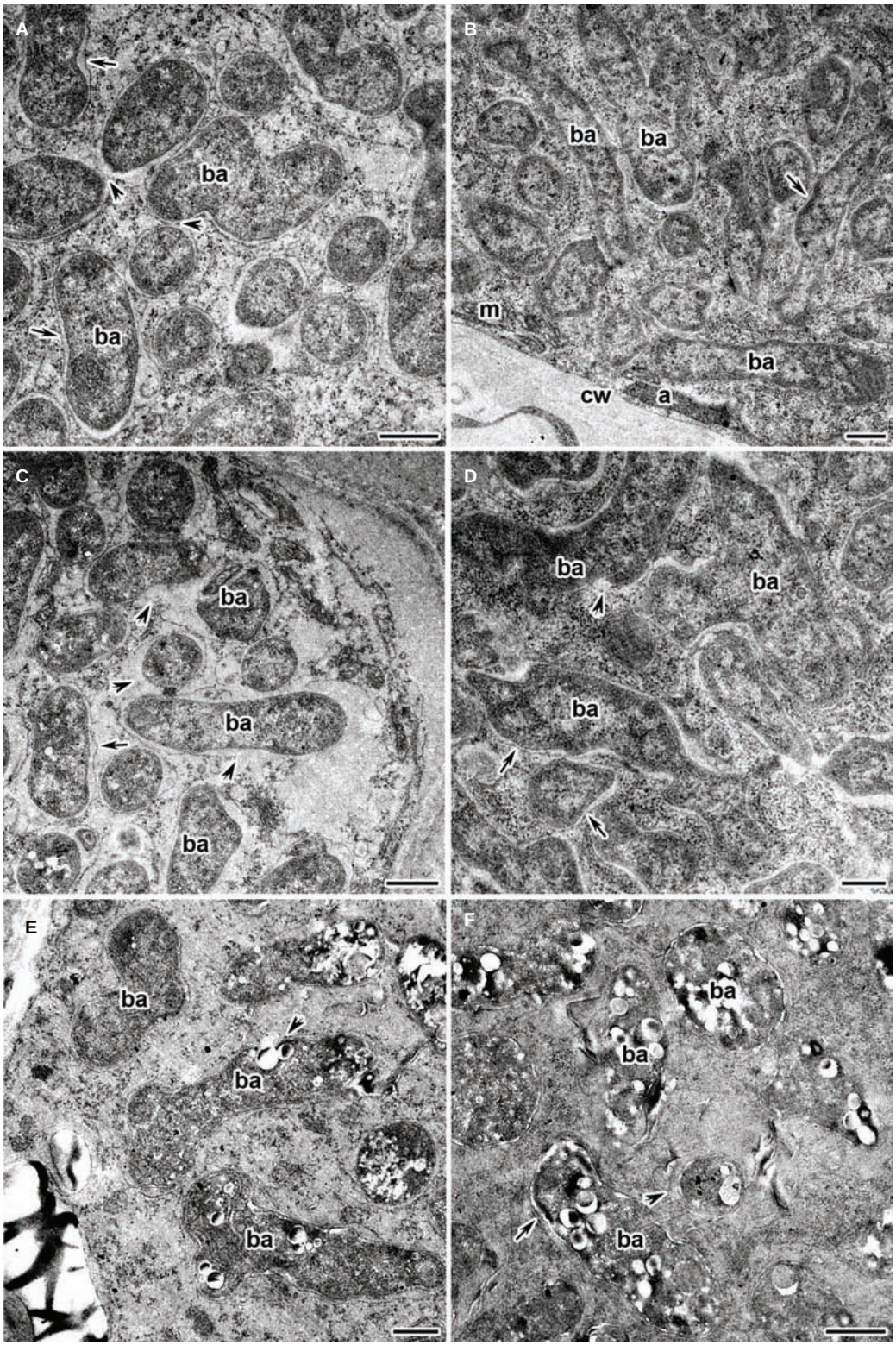

FIGURE 6 | Ultrastructural organization of the cadmium-treated nodules of wild-type SGE **(A,C,E)** and mutant SGECd^t **(B,D,F)** inoculated with *Rhizobium leguminosarum* bv. *viciae* strain 3841-MT1. ba, bacteroid; cw, cell wall; a, amyloplast; m, mitochondrion; arrows indicate the symbiosome membrane; arrowheads indicate the degradation of symbiosome membrane. **(A,B)** Mature bacteroids, **(C)** symbiosomes with partial destruction of symbiosome membranes and cytoplasm swelling, **(D)** abnormal bacteroids, **(E,F)** mature bacteroids with polyhydroxybutyrate accumulation. Scale bar = 500 nm.

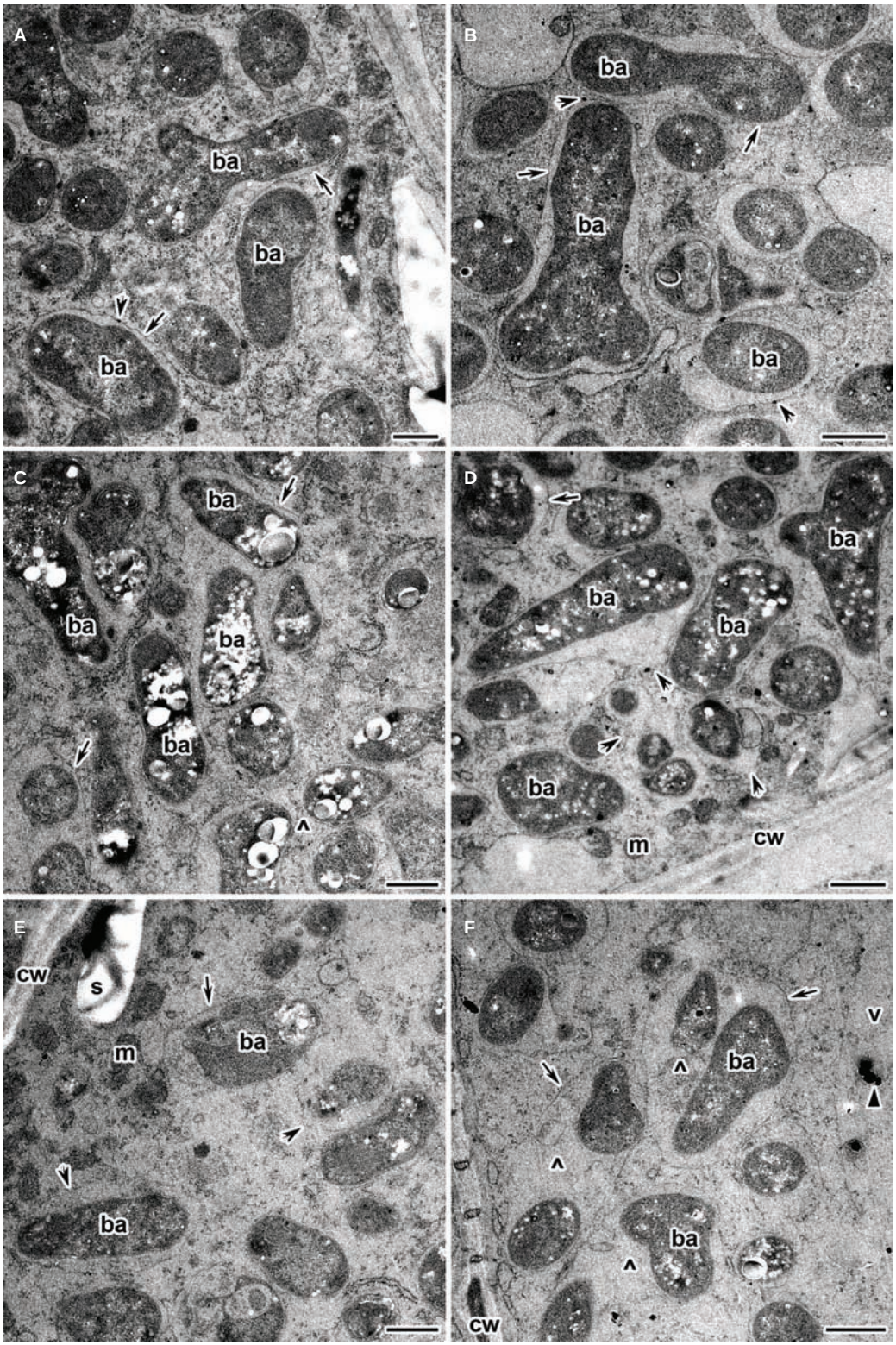

FIGURE 7 | Ultrastructural organization of the cadmium-treated nodules of wild-type SGE **(A,C,E)** and mutant SGECd^t **(B,D,F)** inoculated with *Rhizobium leguminosarum* bv. *viciae* strain 3841-MT2. ba, bacteroid; cw, cell wall; m, mitochondrion; v, vacuole; s, starch granule; ^, "multiple" symbiosome, formed as a result of symbiosome fusion and containing several bacteroids; arrows indicate the symbiosome membrane; arrowheads indicate the degradation of symbiosome membrane; triangle indicates electron dense crystals in the vacuole. **(A,B)** Mature bacteroids, **(C,D)** mature bacteroids with polyhydroxybutyrate accumulation, **(E,F)** symbiosomes with partial destruction of symbiosome membranes and cytoplasm swelling. Scale bar = 500 nm.

of the infected cells of the Cd-treated nodules of both plant genotypes. Some infected cells did show a cleared cytoplasm with initial symptoms of plasmolysis (**Figures 7E,F**). In these cells, bacteroids were released into the vacuole (data not shown), and symbiosomes harbored several bacteroids as a result of symbiosome fusion (**Figures 7C,F**).

Depositions in the Vacuole in the Infected Cells of Cadmium-Treated Nodules of Wild-Type SGE and Mutant SGECd^t Inoculated With *R. leguminosarum* bv. *viciae* Strains 3841, 3841-MT1, and 3841-MT2

An exciting feature revealed by the experiment's Cd treatment were depositions, in the form of electron-dense crystals, in the vacuoles of infected cells in nodules of both plant genotypes when inoculated with *R. leguminosarum* bv. *viciae* strains 3841, 3841-MT1, and 3841-MT2 (**Supplementary Figure S2**). These crystals were never found in both genotypes regardless of the strain used when unexposed to Cd (**Supplementary Figure S1B**). In nodules of the wild-type SGE formed by 3841, such structures in the vacuole were detected in senescent cells with "ghosts" of bacteroids and bacteria released from destroyed infection threads (**Supplementary Figure S2A**). In the nodules of wild-type SGE and mutant SGECd^t plants inoculated with 3841-PsMT1, small electron-dense crystals were observed in conglomerates of destroyed bacteroids and other cell debris (**Supplementary Figures S2C,D**). However, in the nodules of both plant genotypes formed by the strain 3841-MT2, electron-dense crystals in the vacuole occurred in the infected cells with a safe ultrastructural organization (**Supplementary Figure S2E**), as well as in those with initial symptoms of cytoplasm plasmolysis (**Supplementary Figure S2F**).

Recently, the effects of 24-h exposure to 100 μM and 1 mM $CdCl_2$ on the histological and ultrastructural organization of symbiotic nodules of the wild-type SGE and mutant SGECd^t plants inoculated with strain 3841 were studied (Tsyganova et al., 2019). In those wild-type nodules, the Cd treatment caused the formation of an enlarged peribacteroid space in the symbiosomes, along with destruction of the symbiosome membrane and symbiosome fusion, which led to the formation of symbiosomes containing several bacteroids; however, when treated with 1 mM $CdCl_2$, the infected cells underwent cytoplasm clearing and contained destroyed bacteroids. These nodule abnormalities were less pronounced in the mutant SGECd^t (Tsyganova et al., 2019). In *M. sativa* nodules exposed to Cd, evidence for some damaged cells and plasmolysis and destroyed bacteroids were reported, but in some nodules Cd caused less severe degradation, and those infected cells contained bacteroids with an enlarged peribacteroid space and symbiosomes with several bacteroids (Shvaleva et al., 2010). Thus, the observed abnormalities in nodule functioning in our current study are similar to those described before. However, here we also discerned PHB accumulation in the bacteroids. Other work with pea plants demonstrated that PHB accumulation occurs in undifferentiated rhizobia in the infection threads of its nodules but this was absent in bacteroids (Lodwig et al., 2005). By contrast, a recent study showed that PHB accumulation is not restricted to bacteria *per se*, as an analysis of genome sequences identified functional PHB synthase (type III, PhaE PhaC2) in bacteroids (Terpolilli et al., 2016). Moreover, PHB is required for nitrogen fixation by *Azorhizobium caulinodans* in its free-living state and during symbiosis with *Sesbania rostrata* Bremek. & Oberm. (Mandon et al., 1998), but its synthesis may be blocked in bacteroids of other legume species (Cevallos et al., 1996; Aneja and Charles, 1999; Lodwig et al., 2005; Quelas et al., 2013). In other bacteria, apparently PHB may be produced in response to physiological stress. For example, genetic analysis using a phbC mutant strain of *Pseudomonas fluorescens* with host plants revealed that PHB could function as a beneficial microbial compound, one synthesized as the plant adjusts to mitigate cold stress (Stritzler et al., 2018).

We discovered depositions of electron-dense crystals in the vacuoles of infected cells in nodules of both wild type and mutant SGECd^t pea plants formed, by any of the tested strains, under exposure to Cd. However, the nature of these depositions is unclear. Previously, it was shown that Cd is mainly adsorbed by cell walls of the outer cortex and, to a lesser extent, by walls of cells from the infection zone (Sánchez-Pardo et al., 2013). Further studies are necessary to elucidate the nature of these depositions and their long-term effects on the plants.

In the recombinant strains 3841-PsMT1 and 3841-PsMT2 with respective heterologous expression of genes *PsMT1* and *PsMT2* encoding metallothioneins, the negative influence of Cd on nodule development was less pronounced. This result may indicate that metallothioneins have a positive effect on the histological and ultrastructural organization of pea nodules when formed under exposure to Cd in the local environment. Yet, in this respect, strain 3841-PsMT1 clearly had a stronger effect. A more severe alteration of nodule ultrastructure in nodules formed with 3841-PsMT2 on plants of SGECd^t was likely driven by increased Cd accumulation in these nodules. In this variant, at least, the highest Cd content in shoots was observed (see below), and its nodules looked pale while its cells contained many starch granules, a key trait of nodule ineffectiveness (Forrest et al., 1991; Serova et al., 2018).

Cadmium and Nutrient Contents in Plants

Inoculation with strain 3841-PsMT1 increased the shoot (**Figure 8A**) and root (**Figure 8B**) biomass of both untreated and Cd-treated wild-type plants, when compared with those inoculated with strain 3841. But a positive response of mutant SGECd^t to strain 3841-PsMT1 relative to strain 3841 was only found to be significant for roots of Cd-treated plants (**Figure 8B**). Indeed, plants inoculated with strains 3841 and 3841-PsMT2 had a similar biomass for both pea genotypes when grown in the absence or presence of Cd in the nutrient solution (**Figure 8**), and the growth response of the wild type and mutant SGECd^t to the Cd treatment was also similar. In our other work, treatments consisting of 3 μM $CdCl_2$ (Tsyganov et al., 2007) or 4 μM $CdCl_2$ (Belimov et al., 2015a) revealed significant differences between the wild type and mutant SGECd^t plants in terms of their

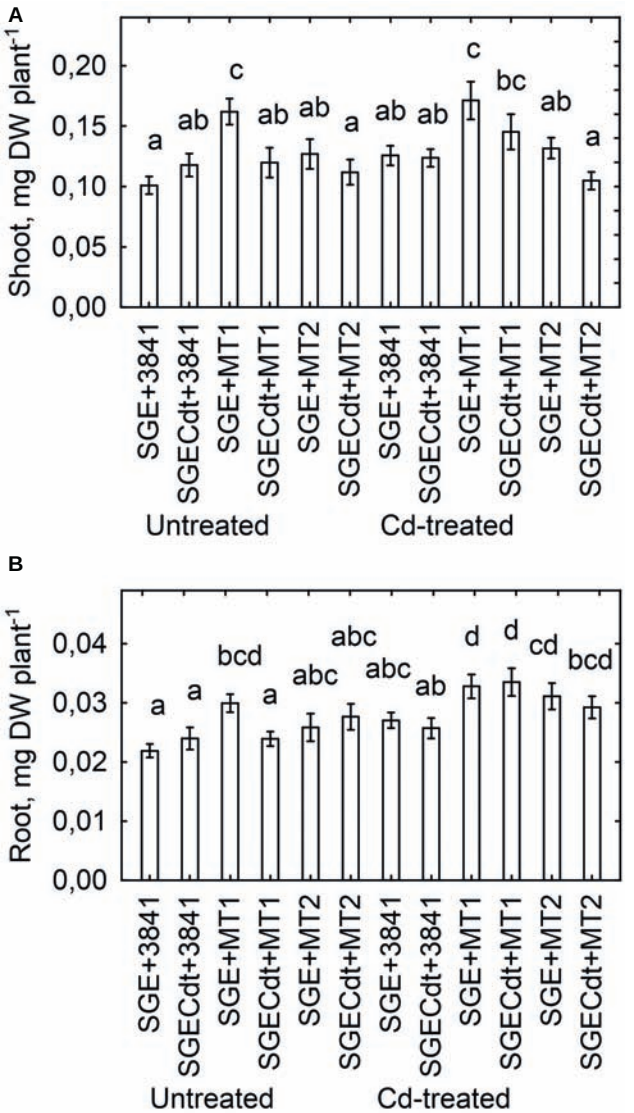

FIGURE 8 | Shoot **(A)** and root **(B)** biomass of pea (*Pisum sativum*) plant genotypes SGE and SGECd^t grown in nutrient solution and inoculated with *Rhizobium leguminosarum* bv. *viciae* strains 3841, 3841-PsMT1 (marked as MT1) or 3841-PsMT2 (marked as MT2), respectively. Vertical bars show standard errors of the means. Different letters show significant differences between the treatments (least significant difference test, $p < 0.05$, $n = 5$). DW denotes dry weight.

biomass production, with the mutant exhibiting greater tolerance to Cd toxicity. But the response of both pea genotypes to 0.5 μM $CdCl_2$ was insignificant, as they had a similar shoot biomass (Kulayeva and Tsyganov, 2015; Belimov et al., 2015b). It is quite likely then that negligible adverse effects of Cd on plant growth and genotypic differences in our current experiment were caused by relatively low Cd concentration in the nutrient solution. Nonetheless, inserting the *PsMT1* gene into nodule bacterium 3841 led to an increased root biomass in both pea genotypes and a greater shoot biomass of SGE grown in the Cd-supplemented solution (**Figure 8**). Yet, strain 3841 with the *PsMT2* gene could only increase the root biomass of Cd-treated SGECd^t.

Strain 3841-PsMT1 decreased the Cd content of shoots in both pea genotypes, whereas strain 3841-PsMT2 had no significant effect upon shoot Cd content (**Figure 9A**). The maximum value for Cd content occurred in shoots of the mutant SGECd^t inoculated with 3841-PsMT2, which significantly differed from that of the wild type inoculated with the parental strain 3841. Although there were no significant genotypic differences within coincident inoculation treatments, a tendency for greater Cd content in the mutant SGECd^t should be mentioned. Previously, under toxic Cd concentrations 3 μM and 4 μM of $CdCl_2$, the mutant SGECd^t accumulated Cd more actively than did its wild-type counterpart (Tsyganov et al., 2007; Belimov et al., 2015a). Those findings suggested the plant-microbe combination based on the plant genotype SGECd^t, with its stronger Cd accumulation capacity, and the genetically modified micro-symbiont carrying *PsMT2* gene would be the most efficient for increasing tissue Cd concentrations. However, in our study here, this combination did not lead to increased accumulation of Cd by shoots because of the relatively low shoot biomass of the mutant SGECd^t (**Figure 8A**). Moreover, there was a negative correlation ($r = -0.91$, $p = 0.013$, $n = 6$) between shoot biomass of Cd-treated plants and their shoot Cd content (**Figure 9B**), suggesting that Cd accumulation by the plants—particularly the mutant SGECd^t—inoculated with 3841-PsMT2 was sufficient to contribute to growth inhibition vis-à-vis those inoculated with strain 3841-PsMT1. The reasons underpinning the opposing effects of 3841-PsMT1 and 3841-PsMT2 on Cd content merit more detailed study. We propose that metallothioneins produced by the bacterial strains differ in their capability for release from bacterial cells, thereby bounding Cd and/or transporting this metal throughout plant tissues, from its root to shoot parts aboveground.

Metallothioneins bind heavy metals through the thiol group of its cysteine residues (Joshi et al., 2016); hence, sulfur (S) is a crucial element for their functioning. As a rule, in our experiment the Cd-treated plants inoculated with strains 3841-PsMT1 or 3841-PsMT2 had a higher shoot S content than those inoculated with strain 3841, in addition to the Cd-untreated plants (**Figure 9C**). However, Cd and S contents of shoots from Cd-treated plants were not significantly correlated ($r = +0.24$, $p = 0.21$, $n = 30$). Therefore, it remains unclear whether metallothioneins participate in a crucial way in Cd translocation from root to shoot. Further, careful measurements of metallothioneins in pea shoots are necessary to robustly test this hypothesis. Nonetheless, the differences we found could be explained by existing differences in organ/tissue-specific expression patterns of the used genes. Indeed, we know that type 1 metallothioneins are mainly expressed in roots, types 2 and 3 in leaves, and type 4 in seeds (Joshi et al., 2016).

Insertion of *PsMT1* and *PsMT2* genes into rhizobia affected the content of nutrient elements in the experimental pea shoots (**Supplementary Table S2**). Compared with strain 3841, inoculation with 3841-PsMT1 decreased the Cu, K, Mo, and P content of shoots in Cd-untreated SGE plants and the B,

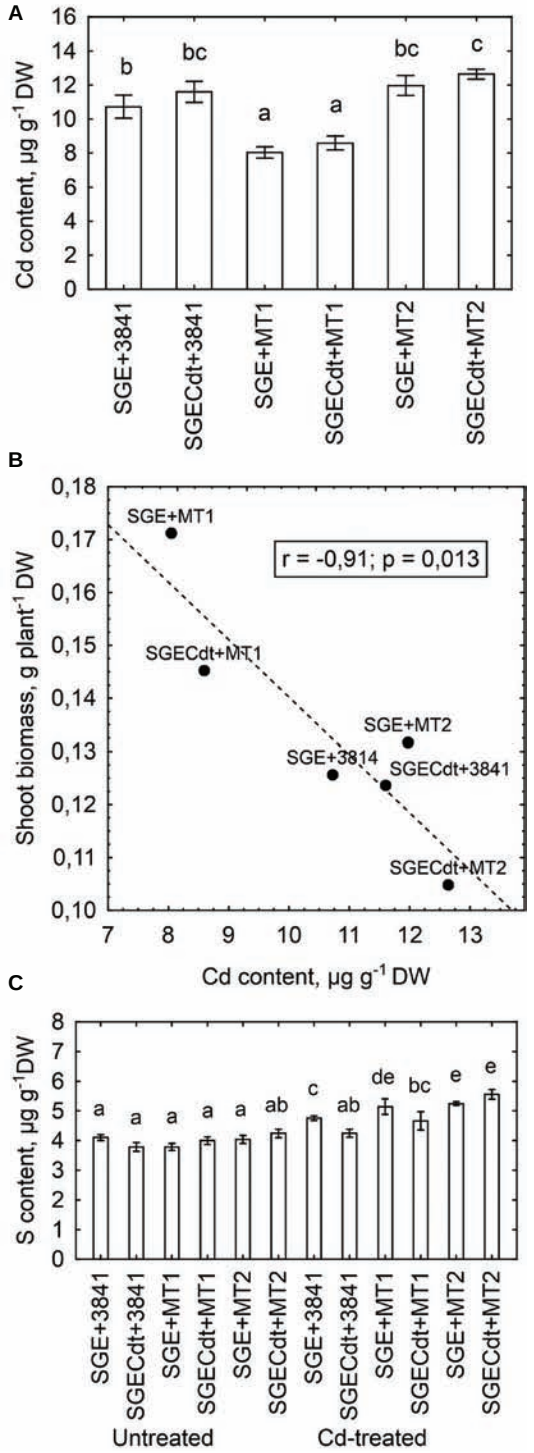

FIGURE 9 | Shoot Cd content in the cadmium-treated pea (*Pisum sativum*) plants **(A)**, and linear regressions between shoot biomass and shoot Cd content **(B)** and shoot S content **(C)** in pea genotypes SGE and SGECd^t grown in nutrient solution and inoculated with *Rhizobium leguminosarum* bv. *viciae* strains 3841, 3841-PsMT1 (marked as MT1) or 3841-PsMT2 (marked as MT2), respectively. Vertical bars show standard errors of the means. Different letters show significant differences between the treatments (least significant difference test, $p<0.05$, $n = 5$). DW denotes dry weight. Fitted linear regression on B is shown by the dashed line.

Fe, K, and Zn content of shoots in Cd-treated SGE plants. The effect of 3841-PsMT1 on nutrients in SGECd^t shoots was generally insignificant with a few exceptions: an increased Ca content and decreased N and Zn content of Cd-treated plants. Generally, the N content was little affected by the inoculations with 3841-PsMT1 or 3841-PsMT2, and the only significant genotypic difference (one of 13%) was detected between the Cd-treated wild type and mutant plants inoculated with 3841-PsMT1. Inoculation with 3841-PsMT2 decreased the K and Mo contents of shoots in Cd-untreated SGE plants and the Co, Fe, and Na content in shoots of Cd-treated SGE plants. However, the response of the mutant SGECd^t to inoculation with 3841-PsMT2 differed significantly from SGE. In particular, the B, Mg, and Mn contents of Cd-untreated plants and B, Co, Cu, K, Mg, Mn, Mo, Na, and Zn contents of Cd-treated plants were all increased. Moreover, differences between Cd-treated SGE and SGECd^t in their tissues' element contents were as a rule significant after inoculation with 3841-PsMT2. These results suggest that strain 3841-PsMT2 improved nutrient uptake by plants, particularly in the case of the Cd-treated SGECd^t mutant. It is known that metallothioneins can bind various elements (Joshi et al., 2016), so it its plausible that uptake of some nutrients was accompanied by 3841-PsMT2. Analysis of averaged values for each inoculation treatment showed that the Cd treatment had a negative effect on B, Cu, Na, Ni, and P contents, but it increased the Mg and Mn contents of SGE and/or SGECd^t plants' shoots (**Supplementary Table S2**). These findings are in line with our previous reports showing Cd affected element composition of the studied pea genotypes as well as better uptake of nutrients by SGECd^t in the presence of toxic Cd concentrations (Tsyganov et al., 2007; Belimov et al., 2016).

CONCLUSION

To our best knowledge, this work is the first example of a legume-rhizobial system developed for Cd phytoremediation in which both partners are genetically modified. Two strains, 3841-PsMT1 and 3841-PsMT2, were constructed and used as rhizobial inoculants of wild-type pea plants and a mutant with a known increased tolerance to Cd. Both strains differ in their effects on plant growth with and without Cd treatment, Cd and nutrient contents in host plant shoots, as well as their nodule histological and ultrastructural organization. The observed differences can be explained by different roles or different organ/tissue expression patterns of the used genes. Positive effects on plant biomass were noticed when the wild-type plants were inoculated with strain 3841-PsMT1. Importantly, this strain also decreased the Cd content of shoots in both pea genotypes and their nodules were able to maintain their organization under exposure to Cd. These features make the 3841-PsMT1 strain an interesting one for inoculating pea plants to increase their biomass and to decrease the Cd concentration in plant tissues. The other strain, 3841-PsMT2, especially in combination with the pea Cd-tolerant mutant, accumulated the highest Cd level among other variants, making it an attractive

candidate for the phytoremediation of Cd-contaminated soil. Still, further experiments are needed to elucidate the required conditions for its possible practical applications.

DATA AVAILABILITY STATEMENT

All datasets generated for this study are included in the article/**Supplementary Material**.

AUTHOR CONTRIBUTIONS

IT designed the experiments. VK and EC obtained the transgenic strains. VK analyzed the plasmid stability. AG and AB analyzed strain tolerance to Cd. AG analyzed growth parameters. TS performed the nodule phenotype analysis. ES, AT, AK, and AG performed the light and electron microscopy. AB performed the elemental analysis. KI, OK, TS, and PK conducted the real-time PCR analysis. AT, AB, and VT analyzed the data and wrote the paper.

FUNDING

This work was supported by the Russian Science Foundation (grant no. 17-76-30016), as was the elemental analysis (grant no. 19-16-00097).

ACKNOWLEDGMENTS

The research was performed using equipment belonging to the Core Centrum "Genomic Technologies, Proteomics and Cell Biology" in All-Russia Research Institute for Agricultural Microbiology. The authors thank Charlesworth Author Services for English editing of a draft of this manuscript.

SUPPLEMENTARY MATERIAL

The Supplementary Material for this article can be found online at: https://www.frontiersin.org/articles/10.3389/fmicb.2020.00015/full#supplementary-material

REFERENCES

Aneja, P., and Charles, T. C. (1999). Poly-3-hydroxybutyrate degradation in *Rhizobium (Sinorhizobium) meliloti*: isolation and characterization of a gene encoding 3-hydroxybutyrate dehydrogenase. *J. Bacteriol.* 181, 849–857. doi: 10.1128/JB.181.3.849-857.1999

Angle, J. S., McGrath, S. P., Chaudri, A. M., Chaney, R. L., and Giller, K. E. (1993). Inoculation effects on legumes grown in soil previously treated with sewage sludge. *Soil Biol. Biochem.* 25, 575–580. doi: 10.1016/0038-0717(93)90196-I

Balestrasse, K. B., Gallego, S. M., and Tomaro, M. L. (2004). Cadmium-induced senescence in nodules of soybean (*Glycine max* L.) plants. *Plant Soil* 262, 373–381. doi: 10.1023/B:PLSO.0000037056.11877.7b

Belimov, A. A., Dodd, I. C., Safronova, V. I., Malkov, N. V., Davies, W. J., and Tikhonovich, I. A. (2015a). The cadmium-tolerant pea (*Pisum sativum* L.) mutant SGECd^t is more sensitive to mercury: assessing plant water relations. *J. Exp. Bot.* 66, 2359–2369. doi: 10.1093/jxb/eru536

Belimov, A. A., Malkov, N. V., Puhalsky, J. V., Safronova, V. I., and Tikhonovich, I. A. (2016). High specificity in response of pea mutant SGECd^t to toxic metals: growth and element composition. *Environ. Exp. Bot.* 128, 91–98. doi: 10.1016/j.envexpbot.2016.04.009

Belimov, A. A., Puhalsky, I. V., Safronova, V. I., Shaposhnikov, A. I., Vishnyakova, M. A., Semenova, E. V., et al. (2015b). Role of plant genotype and soil conditions in symbiotic plant-microbe interactions for adaptation of plants to cadmium-polluted soils. *Water Air Soil Pollut.* 226:264. doi: 10.1007/s11270-015-2537-9

Carpena, R. O., Vázquez, S., Esteban, E., Fernández-Pascual, M., de Felipe, M. R., and Zornoza, P. (2003). Cadmium-stress in white lupin: effects on nodule structure and functioning. *Plant Physiol. Biochem.* 41, 911–919. doi: 10.1016/S0981-9428(03)00136-0

Cevallos, M. A., Encarnación, S., Leija, A., Mora, Y., and Mora, J. (1996). Genetic and physiological characterization of a *Rhizobium etli* mutant strain unable to synthesize poly-beta-hydroxybutyrate. *J. Bacteriol.* 178, 1646–1654. doi: 10.1128/JB.178.6.1646-1654.1996

Chizhevskaya, E., Onishchuk, O., Andronov, E., and Simarov, B. (2011). Use of site-directed mutagenesis to study the functions of gene SMb20332 in the nodule bacteria *Sinorhizobium meliloti*. *Agricult. Biol.* 3, 55–60.

Cobbett, C., and Goldsbrough, P. (2002). Phytochelatins and metallothioneins: roles in heavy metal detoxification and homeostasis. *Annu. Rev. Plant Biol.* 53, 159–182. doi: 10.1146/annurev.arplant.53.100301.135154

Delgadillo, J., Lafuente, A., Doukkali, B., Redondo-Gomez, S., Mateos-Naranjo, E., Caviedes, M. A., et al. (2015). Improving legume nodulation and Cu rhizostabilization using a genetically modified rhizobia. *Environ. Technol.* 36, 1237–1245. doi: 10.1080/09593330.2014.983990

Fagorzi, C., Checcucci, A., DiCenzo, G. C., Debiec-Andrzejewska, K., Dziewit, L., Pini, F., et al. (2018). Harnessing rhizobia to improve heavy-metal phytoremediation by legumes. *Genes* 9:542. doi: 10.3390/genes9110542

Forrest, S. I., Verma, D. P. S., and Dhindsa, R. S. (1991). Starch content and activities of starch-metabolizing enzymes in effective and ineffective root nodules of soybean. *Can. J. Bot.* 69, 697–701. doi: 10.1139/b91-094

Gómez-Sagasti, M. T., and Marino, D. (2015). PGPRs and nitrogen-fixing legumes: a perfect team for efficient Cd phytoremediation? *Front. Plant Sci.* 6:81. doi: 10.3389/fpls.2015.00081

Guo, W.-J., Bundithya, W., and Goldsbrough, P. B. (2003). Characterization of the *Arabidopsis* metallothionein gene family: tissue-specific expression and induction during senescence and in response to copper. *New Phytol.* 159, 369–381. doi: 10.1046/j.1469-8137.2003.00813.x

Hao, X., Taghavi, S., Xie, P., Orbach, M., Alwathnani, H., Rensing, C., et al. (2014). Phytoremediation of heavy and transition metals aided by legume-rhizobia symbiosis. *Int. J. Phytoremediation* 16, 179–202. doi: 10.1080/15226514.2013.773273

Hernandez, L. E., Garate, A., and Carpena-Ruiz, R. (1995). Effect of cadmium on nitrogen fixing pea plants grown in perlite and vermiculite. *J. Plant Nutr.* 18, 287–303. doi: 10.1080/01904169509364902

Humphrey, C. D., and Pittman, F. E. (1974). A simple methylene blue-azure II-basic fuchsin stain for epoxy-embedded tissue sections. *Stain Technol.* 49, 9–14. doi: 10.3109/10520297409116929

Ibekwe, A. M., Angle, J. S., Chaney, R. L., and van Berkum, P. (1996). Zinc and cadmium toxicity to alfalfa and its microsymbiont. *J. Environ. Qual.* 25, 1032–1040. doi: 10.2134/jeq1996.00472425002500050015x

Ike, A., Sriprang, R., Ono, H., Murooka, Y., and Yamashita, M. (2007). Bioremediation of cadmium contaminated soil using symbiosis between leguminous plant and recombinant rhizobia with the *MTL4* and the *PCS* genes. *Chemosphere* 66, 1670–1676. doi: 10.1016/j.chemosphere.2006.07.058

Ivanova, K. A., Tsyganova, A. V., Brewin, N. J., Tikhonovich, I. A., and Tsyganov, V. E. (2015). Induction of host defences by *Rhizobium* during ineffective nodulation of pea (*Pisum sativum* L.) carrying symbiotically defective mutations *sym40* (*PsEFD*), *sym33* (*PsIPD3/PsCYCLOPS*) and *sym42*. *Protoplasma* 252, 1505–1517. doi: 10.1007/s00709-015-0780-y

Joshi, R., Pareek, A., and Singla-Pareek, S. L. (2016). "Plant metallothioneins: classification, distribution, function, and regulation" in *Plant metal interaction: Emerging remediation techniques*. ed. P. Ahmad (Oxford: Elsevier), 239–261.

Kisa, D., Öztürk, L., Doker, S., and Gökçe, İ. (2017). Expression analysis of metallothioneins and mineral contents in tomato (*Lycopersicon esculentum*) under heavy metal stress. *J. Sci. Food Agric.* 97, 1916–1923. doi: 10.1002/jsfa.7995

Kosterin, O. E., and Rozov, S. M. (1993). Mapping of the new mutation *blb* and the problem of integrity of linkage group I. *Pisum Genet.* 25, 27–31.

Kulaeva, O. A., and Tsyganov, V. E. (2011). Molecular-genetic basis of cadmium tolerance and accumulation in higher plants. *Russ. J. Genet. Appl. Res.* 1, 349–360. doi: 10.1134/S2079059711050108

Kulaeva, O. A., and Tsyganov, V. E. (2013). Fine mapping of a *cdt* locus mutation that leads to an increase in the tolerance of pea (*Pisum sativum* L.) to cadmium. *Russ. J. Genet. Appl. Res.* 3, 120–126. doi: 10.1134/S2079059713020020

Kulayeva, O. A., and Tsyganov, V. E. (2015). Gene expression analysis of genes coding key enzymes of cadmium detoxification in garden pea symbiotic nodules. *Russ. J. Genet. Appl. Res.* 5, 479–485. doi: 10.1134/S207905971505007X

Lee, J., Donghwan, S., Won-Yong, S., Inhwan, H., and Youngsook, L. (2004). Arabidopsis metallothioneins 2a and 3 enhance resistance to cadmium when expressed in *Vicia faba* guard cells. *Plant Mol. Biol.* 54, 805–815. doi: 10.1007/s11103-004-0190-6

Lodwig, E. M., Leonard, M., Marroqui, S., Wheeler, T. R., Findlay, K., Downie, J. A., et al. (2005). Role of polyhydroxybutyrate and glycogen as carbon storage compounds in pea and bean bacteroids. *Mol. Plant-Microbe Interact.* 18, 67–74. doi: 10.1094/MPMI-18-0067

Mandon, K., Michel-Reydellet, N., Encarnación, S., Kaminski, P. A., Leija, A., Cevallos, M. A., et al. (1998). Poly-β-hydroxybutyrate turnover in *Azorhizobium caulinodans* is required for growth and affects *nifA* expression. *J. Bacteriol.* 180, 5070–5076. doi: 10.1128/JB.180.19.5070-5076.1998

Marino, D., Damiani, I., Gucciardo, S., Mijangos, I., Pauly, N., and Puppo, A. (2013). Inhibition of nitrogen fixation in symbiotic *Medicago truncatula* upon Cd exposure is a local process involving leghaemoglobin. *J. Exp. Bot.* 64, 5651–5660. doi: 10.1093/jxb/ert334

Neumann, H., Bode-Kirchhoff, A., Madeheim, A., and Wetzel, A. (1998). Toxicity testing of heavy metals with the *Rhizobium*-legume symbiosis: high sensitivity to cadmium and arsenic compounds. *Environ. Sci. Pollut. Res.* 5, 28–36. doi: 10.1007/BF02986371

Onishchuk, O. P., Chizhevskaya, E. P., Kurchak, O. N., Andronov, E. E., and Simarov, B. V. (2015). Identification of new genes of nodule bacteria *Sinorhizobium meliloti* involved in the control of efficiency of symbiosis with alfalfa *Medicago sativa*. *Russ. J. Genet. Appl. Res.* 5, 126–131. doi: 10.1134/S2079059715020070

Pagani, M. A., Tomas, M., Carrillo, J., Bofill, R., Capdevila, M., Atrian, S., et al. (2012). The response of the different soybean metallothionein isoforms to cadmium intoxication. *J. Inorg. Biochem.* 117, 306–315. doi: 10.1016/j.jinorgbio.2012.08.020

Pajuelo, E., Rodriguez-Llorente, I., Lafuente, A., Pérez Palacios, P., Doukkali, B., and Caviedes, M. (2014). Engineering the rhizosphere for the purpose of bioremediation: an overview. *CAB Rev.* 9, 1–17. doi: 10.1079/PAVSNNR20149001

Pérez-Palacios, P., Romero-Aguilar, A., Delgadillo, J., Doukkali, B., Caviedes, M. A., Rodríguez-Llorente, I. D., et al. (2017). Double genetically modified symbiotic system for improved cu phytostabilization in legume roots. *Environ. Sci. Pollut. Res. Int.* 24, 14910–14923. doi: 10.1007/s11356-017-9092-4

Quelas, J. I., Mongiardini, E. J., Pérez-Giménez, J., Parisi, G., and Lodeiro, A. R. (2013). Analysis of two polyhydroxyalkanoate synthases in *Bradyrhizobium japonicum* USDA 110. *J. Bacteriol.* 195, 3145–3155. doi: 10.1128/JB.02203-12

Safronova, V., Piluzza, G., Bullitta, S., and Belimov, A. (2011). "Use of legume-microbe symbioses for phytoremediation of heavy metal polluted soils: advantages and potential problems" in *Handbook of phytoremediation*. ed. I. A. Golubev (New York: Nova Science Pub Inc.), 443–469.

Sánchez-Pardo, B., Carpena, R. O., and Zornoza, P. (2013). Cadmium in white lupin nodules: impact on nitrogen and carbon metabolism. *J. Plant Physiol.* 170, 265–271. doi: 10.1016/j.jplph.2012.10.001

Serova, T. A., Tsyganova, A. V., and Tsyganov, V. E. (2018). Early nodule senescence is activated in symbiotic mutants of pea (*Pisum sativum* L.) forming ineffective nodules blocked at different nodule developmental stages. *Protoplasma* 255, 1443–1459. doi: 10.1007/s00709-018-1246-9

Shvaleva, A., Coba de la Peña, T., Rincón, A., Morcillo, C. N., García de la Torre, V. S., Lucas, M. M., et al. (2010). Flavodoxin overexpression reduces cadmium-induced damage in alfalfa root nodules. *Plant Soil* 326, 109–121. doi: 10.1007/s11104-009-9985-1

Sriprang, R., Hayashi, M., Ono, H., Takagi, M., Hirata, K., and Murooka, Y. (2003). Enhanced accumulation of Cd^{2+} by a *Mesorhizobium* sp. transformed with a gene from *Arabidopsis thaliana* coding for phytochelatin synthase. *Appl. Environ. Microbiol.* 69, 1791–1796. doi: 10.1128/AEM.69.3.1791-1796.2003

Sriprang, R., Hayashi, M., Yamashita, M., Ono, H., Saeki, K., and Murooka, Y. (2002). A novel bioremediation system for heavy metals using the symbiosis between leguminous plant and genetically engineered rhizobia. *J. Biotechnol.* 99, 279–293. doi: 10.1016/S0168-1656(02)00219-5

Sriprang, R., and Murooka, Y. (2007). "Accumulation and detoxification of metals by plants and microbes" in *Environmental bioremediation technologies*. eds. S. N. Singh and R. D. Tripathi (Berlin, Heidelberg: Springer), 77–100.

Stagnari, F., Maggio, A., Galieni, A., and Pisante, M. (2017). Multiple benefits of legumes for agriculture sustainability: an overview. *Chem. Biol. Technol.* 4:2. doi: 10.1186/s40538-016-0085-1

Stritzler, M., Diez Tissera, A., Soto, G., and Ayub, N. (2018). Plant growth-promoting bacterium *Pseudomonas fluorescens* FR1 secrets a novel type of extracellular polyhydroxybutyrate polymerase involved in abiotic stress response in plants. *Biotechnol. Lett.* 40, 1419–1423. doi: 10.1007/s10529-018-2576-6

Teng, Y., Wang, X., Li, L., Li, Z., and Luo, Y. (2015). Rhizobia and their bio-partners as novel drivers for functional remediation in contaminated soils. *Front. Plant Sci.* 6:32. doi: 10.3389/fpls.2015.00032

Terpolilli, J. J., Masakapalli, S. K., Karunakaran, R., Webb, I. U. C., Green, R., Watmough, N. J., et al. (2016). Lipogenesis and redox balance in nitrogen-fixing pea bacteroids. *J. Bacteriol.* 198, 2864–2875. doi: 10.1128/JB.00451-16

Tsyganov, V. E., Belimov, A. A., Borisov, A. Y., Safronova, V. I., Georgi, M., Dietz, K.-J., et al. (2007). A chemically induced new pea (*Pisum sativum*) mutant SGECd^t with increased tolerance to, and accumulation of, cadmium. *Ann. Bot.* 99, 227–237. doi: 10.1093/aob/mcl261

Tsyganov, V. E., Belimov, A. A., Safronova, V. I., Naumkina, T. S., Borisov, A. Y., Dietz, K. J., et al. (2004). "A new pea cadmium tolerant mutant in a unique tool for studying molecular plant-microbe interactions under cadmium stress" in *Biology of plant-microbe interactions: Proceedings of 11th International Congress on IS-MPMI*. eds. I. A. Tikhonovich, B. J. Lugtenberg, and N. A. Provorov (St. Petersburg: International Society for Molecular Plant-Microbe Interactions), 506–509.

Tsyganov, V. E., Kulaeva, O. A., Knox, M. R., Borisov, A. Y., Tikhonovich, I. A., and Ellis, T. H. N. (2013). Using of SSAP analysis for primary localization of mutation *cdt* (*cadmium tolerance*) in pea linkage group VI. *Russ. J. Genet. Appl. Res.* 3, 152–155. doi: 10.1134/S2079059713020081

Tsyganov, V. E., Morzhina, E. V., Stefanov, S. Y., Borisov, A. Y., Lebsky, V. K., and Tikhonovich, I. A. (1998). The pea (*Pisum sativum* L.) genes *sym33* and *sym40* control infection thread formation and root nodule function. *Mol. Gen. Genet.* 259, 491–503. doi: 10.1007/s004380050840

Tsyganov, V. E., Zhernakov, A. I., Khodorenko, A. V., Kisutin, P. Y., Belimov, A. A., Safronova, V. I., et al. (2005). "Mutational analysis to study the role of genetic factors in pea adaptation to stresses during development its symbioses with *Rhizobium* and mycorrhizal fungi" in *Biological nitrogen fixation, sustainable agriculture and the environment*. eds. Y. P. Wang, M. Lin, Z. X. Tian, C. Elmerich, and W. E. Newton (Dordrecht: Springer), 279–281.

Tsyganova, A. V., Kitaeva, A. B., and Tsyganov, V. E. (2018). Cell differentiation in nitrogen-fixing nodules hosting symbiosomes. *Funct. Plant Biol.* 45, 47–57. doi: 10.1071/FP16377

Tsyganova, A. V., Seliverstova, E. V., and Tsyganov, V. E. (2019). Influence of mutation in pea (*Pisum sativum* L.) *cdt* (*cadmium tolerance*) gene on histological and ultrastructural nodule organization. *Ecol. Genet.* 17, 71–80. doi: 10.17816/ecogen17171-80

Tsyganova, A. V., and Tsyganov, V. E. (2018). "Plant genetic control over infection thread development during legume-*Rhizobium* symbiosis" in *Symbiosis*. ed. E. C. Rigobelo (London: IntechOpen), 23–52.

Wang, T. L., Wood, E. A., and Brewin, N. J. (1982). Growth regulators, *Rhizobium* and nodulation in peas. *Planta* 155, 350–355. doi: 10.1007/BF00429464

Zhang, H., Xu, W., Guo, J., He, Z., and Ma, M. (2005). Coordinated responses of phytochelatins and metallothioneins to heavy metals in garlic seedlings. *Plant Sci.* 169, 1059–1065. doi: 10.1016/j.plantsci.2005.07.010

Zimeri, A. M., Dhankher, O. P., McCaig, B., and Meagher, R. B. (2005). The plant MT1 metallothioneins are stabilized by binding cadmiums and are required for cadmium tolerance and accumulation. *Plant Mol. Biol.* 58, 839–855. doi: 10.1007/s11103-005-8268-3

Conflict of Interest: The authors declare that the research was conducted in the absence of any commercial or financial relationships that could be construed as a potential conflict of interest.

Advantages of publishing in Frontiers

OPEN ACCESS
Articles are free to read for greatest visibility and readership

FAST PUBLICATION
Around 90 days from submission to decision

HIGH QUALITY PEER-REVIEW
Rigorous, collaborative, and constructive peer-review

TRANSPARENT PEER-REVIEW
Editors and reviewers acknowledged by name on published articles

Frontiers
Avenue du Tribunal-Fédéral 34
1005 Lausanne | Switzerland

Visit us: www.frontiersin.org
Contact us: info@frontiersin.org | +41 21 510 17 00

REPRODUCIBILITY OF RESEARCH
Support open data and methods to enhance research reproducibility

DIGITAL PUBLISHING
Articles designed for optimal readership across devices

FOLLOW US
@frontiersin

IMPACT METRICS
Advanced article metrics track visibility across digital media

EXTENSIVE PROMOTION
Marketing and promotion of impactful research

LOOP RESEARCH NETWORK
Our network increases your article's readership